UNIVERSIDAD COMPLUTENSE DE MADRID
FACULTAD DE CIENCIAS FÍSICAS
DEPARTAMENTO DE FÍSICA TEÓRICA I

TESIS DOCTORAL

Topological Phases of Matter and Open Quantum Systems

Fases topológicas de la materia y sistemas cuánticos abiertos

MEMORIA PARA OPTAR AL GRADO DE DOCTOR

PRESENTADA POR

Oscar Viyuela García

DIRECTOR

Miguel Ángel Martín-Delgado Alcántara

Madrid, 2017

Topological Phases of Matter and Open Quantum Systems

by

Oscar Viyuela García

under the supervision of

Miguel Ángel Martín-Delgado Alcántara

A thesis submitted to Universidad Complutense de Madrid
for the degree of
Doctor in Physics
Departamento de Física Teórica I (Facultad de Ciencias Físicas)
November 2016

Typeset in LaTeX 2ε.

Fases Topológicas de la Materia y Sistemas Cuánticos Abiertos

por

Oscar Viyuela García

bajo la supervisión de

Miguel Ángel Martín-Delgado Alcántara

Tesis elaborada en la Universidad Complutense de Madrid
para optar al grado de Doctor
Departamento de Física Teórica I (Facultad de Ciencias Físicas)
Noviembre 2016

Acknowledgements

After four years of embarking into the experience of becoming a PhD in Physics, I would like to thank everyone who made this possible. The first person who deserves more credit than anyone is my high-school Physics teacher, Mercedes García, who first showed me how beautiful and challenging science can be. Without your classes I would probably be doing something else. During my Physics degree I had a lot of fun, partly due to the dedication of some very good professors I had: Cristobal, Pepe, Isabel, Juan Manuel, José Luis, M^{a} Jesús, just to name a few without aiming to be exhaustive. Above all, I would like to thank Miguel Ángel Rodríguez. However, a great deal of that fun and unforgettable experiences came from all the friends I made: Rocío, Jorge, Gema, Paula, Loreto, Cristina, Alberto, Ester, Edgar, Javi, Rubén, Keller, Rodrigo, Chechu, Vicky, Sergio, Belén, Fran, Pedro, Samu, just to name a few.

A year after I started the PhD, I happened to find a perfect place to live called Residencia de Estudiantes. I would like to thank the directors Alicia, Pablo and Rosario for their support, and Anabel and Bea for making things easier. I had wonderful discussions and experiences back there while making a lot of friends: Pau, Pepa, Paco, Lola, Elisa, Marco, Ibis, Jose, Ursula, just to name a few. I thank the Ayuntamiento de Madrid for making this happen during three amazing years. I am also grateful to the Department of Theoretical Physics I, at the UCM Physics Faculty; I was always glad to work in that nice environment. There, I had a great time working with many friends, having lunch together, going out every now and then, and celebrating as much as we could. I can only say *gracias* to Santos, David, Héctor, Jose Manuel, Rafa, Arkaitz, Marco, Bea, Vivy, Domingo, Álvaro, Jose Alberto, Prado, Andrés, Santiago, Anmol, Giovanni, Juan Miguel, Miguel, Ricardo, Alejandro, Diego and many more. I would also like to acknowledge support from a FPU MEC grant for four years, and the Spanish MINECO grant FIS2012-33152, MICINN grant FIS2009-10061, the CAM research consortium QUITEMAD S2009-ESP-1594, QUITEMAD+ S2013/ICE-2801, a European Commission PICC: FP7 2007-2013 Grant No. 249958, UCM-BS grant GICC-910758, the U.S. Army Research Office through grant W911NF-14-1-0103 for travel fundings.

Fortunately, I didn't work alone during my PhD. I was part of the GICC group

where I found myself extremely comfortable thanks to Markus, Laura, Alex, Davide, Mª José, Inés, Alberto, Santiago, José María and Hao. Moreover, and most especially, I would like to thank Ángel Rivas. You helped me very much at the beginning, I have learnt a lot from you, and it has been always a pleasure working with you.

I am sincerely grateful to Rosario Fazio for letting me work with his group in Pisa for some months; and to Ignacio Cirac at MPQ, Vlatko Vedral at CQT, Adolfo del Campo and Wojciech Zurek at LANL, Guido Pupillo at Strasbourg, Vignesh Venkataraman at Imperial College and Borja Peropadre at Harvard University for short visits. I was also lucky to work with many collaborators from whom I learned very much. Thanks Davide, Guido, Jiasen, Alberto, Leonardo, Jonathan, Rosario, Davide, Simone, Andreas and Stefan.

Last but not least, I would like to thank my supervisor Miguel Ángel Martín-Delgado. With you I've understood the relevance of communicating effectively ideas to others. Most importantly, I have learnt not to be afraid of topics you may not be familiar with at the beginning. I will always remember your way of stating this idea: *You don't need to know everything, to do something*. Thanks Miguel Ángel for all that.

Por último, quería dedicar esta tesis a mis padres y hermana. Siempre habéis sido un gran apoyo en cualquier decisión que he tomado y nunca podré agradeceros lo suficiente todo que habéis hecho por mi.

Abstract

The growing field of topological orders has been extensively studied both form the communities of condensed matter and quantum simulation. However, very little is known about the fate of topological order in the presence of disturbing effects such as external noise or dissipation. In the first part of this thesis, we start by studying how the edge states of a topological insulator become unstable when interacting with thermal baths. Motivated by these results, we generalise the notion of Chern insulators from the well-known Hamiltonian case to Liouvillian dynamics. We achieve this goal by defining a new topological witness that is still related to the quantum Hall conductivity at finite temperature. The mixed character of edge states is also well captured by our formalism, and explicit models for topological insulators and dissipative channels are considered. Additionally, we find new topological phases that remain quantised at finite temperature. The construction is based on the Uhlmann phase, a geometric quantum phase defined for general density matrices. Using this new tool, we are able to characterise topological insulators and superconductors at finite temperature both in one and two spatial dimensions. From the experimental side, we propose a state-independent protocol to measure the topological Uhlmann phase in the context of quantum simulation.

Symmetry-protected topological orders have traditionally emerged from short-range interactions. It remains very much unknown what the role played by long-range interactions is, within the physics of these topological systems. In the second part of this thesis, we analyse how topological superconducting phases are affected by the inclusion of long-range couplings. Remarkably, we unveil new topological quasi-particles due to long-range interactions, that were absent in short-range models. We also study how topological invariants are modified by the presence of long-range effects.

In the appendix section of the thesis, we explore new numerical methods for driven-dissipative phase transitions. We consider quantum systems with a dissipative term driving the system into a non-equilibrium steady state. The inclusion of short-range fluctuations out-of-equilibrium deeply modifies the shape of the phase-diagram, something never observed in equilibrium thermodynamics.

Publications, Research Visits, Conferences

P1. O. Viyuela, A. Rivas, M.A. Martin-Delgado, *Generalized Toric Codes Coupled to Thermal Baths*, New J. Phys. **14** 033044 (2012).[1]

P2. O. Viyuela, A. Rivas, M.A. Martin-Delgado, *Thermal Instability of Protected End States in a 1-D Topological Insulator*, Phys. Rev. B **86**, 155140 (2012).

P3. A. Rivas, O. Viyuela, M.A. Martin-Delgado, *Density Matrix Topological Insulators*, Phys. Rev. B **88**, 155141 (2013).

P4. O. Viyuela, A. Rivas, M.A. Martin-Delgado, *Uhlmann Phase as a Topological Measure for One-Dimensional Fermion Systems*, Phys. Rev. Lett. **112**, 130401 (2014).

P5. O. Viyuela, A. Rivas, M.A. Martin-Delgado, *2D Density-Matrix Topological Fermionic Phases: Topological Uhlmann Numbers*, Phys. Rev. Lett. **113**, 076408 (2014).

P6. O. Viyuela, A. Rivas, M.A. Martin-Delgado, *Symmetry-protected Topological Phases at Finite Temperature*, 2D Mater. **2** 034006 (2015).

P7. O. Viyuela, D. Vodola, G. Pupillo, M.A. Martin-Delgado, *Topological Massive Dirac Edge Modes and Long-Range Superconducting Hamiltonians*, Phys. Rev. B **94**, 125121 (2016).

P8. J. Jin, A. Biella, O. Viyuela, L. Mazza, J. Keeling, R. Fazio and D. Rossini, *Cluster Mean-Field Approach to the Steady-State Phase Diagram of Dissipative Spin Systems* Phys. Rev. X **6**, 031011 (2016).

P9. O. Viyuela, A. Rivas, S. Gasparinetti, A. Wallraff, S. Filipp and M.A. Martin-Delgado, *Measurement Protocol for the Topological Uhlmann Phase*, arXiv: 1607.08778 (2016) [submitted to PRL].

[1] *IMPACT FACTOR (IF) 2015*: 2D Mater. **IF: 9.611**, Phys. Rev. X **IF: 8.701**, Phys. Rev. Lett. **IF: 7.645**, Phys. Rev. B **IF: 3.718**, New J. Phys. **IF: 3.570**

RV1. Université de Strasbourg (Prof. Guido Pupilo's group), Strasbourg, France, 28 September - 4 November (2015). Invited seminar: "Quantum, Topological and Dissipative".

RV2. Massachusetts University (Prof. Adolfo del Campo's group), Boston, USA, 10 March (2015). Invited seminar: "Quantum, Topological and Dissipative".

RV3. Centre for Integrated Quantum Materials at Harvard University (invited by Dr. Borja Peropadre), Boston, USA, 9 March (2015). Invited seminar: "Quantum, Topological and Dissipative".

RV4. Centre for Quantum Technologies CQT (Prof. Vlatko Vedral's group), Singapore, 30 November - 13 December (2014). Invited seminar: "Quantum, Topological and Dissipative".

RV5. Scuola Normale di Pisa (Prof. Rosario Fazio's group), Italy, 15 September - 30 November (2014). Invited seminar: "Quantum, Topological and Dissipative".

RV6. Los Alamos National Laboratorio (Prof. Wojciech H. Zurek's group), USA, 25-29 March (2012). Invited "Quantum Lunch" seminar: "Topological Insulators meet Dissipation and Decoherence".

RV7. Theory Division (Prof. Ignacio Cirac's group), Max Panck Institut für Quantenoptik, Germany, 23-27 April (2012). Invited seminar: "Thermal Stability of Topological Quantum Memories".

RV8. Controlled Quantum Dynamics Centre (invited by Dr. Vignesh Venkataraman), Imperial College of London, UK, 15 March (2012). Invited seminar: "Thermal Stability of Topological Quantum Memories".

C1. APS March Meeting (**talk**), Baltimore, USA, 2016

C1. Weyl Fermion Workshop (**poster**), Princeton, USA, 2016

C1. APS March Meeting (**talk**), San Antonio, USA, 2015

C2. Quantum Technologies Conference V (**talk**), Krakow, Polland, 2014

C3. 31st Jerusalem Winter School on Theoretical Physics, Jerusalem, Israel, 2014

C4. MPAGs Summer School on Quantum matter (**talk**), Granada, Spain, 2013

C5. 5th Madrid meeting on Cold Atoms (**talk**), Madrid, Spain, 2013

C6. APS March Meeting (**talk**), Baltimore, USA, 2013

C7. Symposium on Topological Quantum Information (**poster**), Benasque, Spain, 2013

C8. Entangle this: Strings, Fields and Atoms, Madrid, Spain, 2012

C9. Quantum Information meets Statistical Mechanics (**poster**), Innsbruck, Austria 2012

C10. Información Cuántica en Espańa (**talk**), Madrid, Spain, 2012

C11. 2nd AQuA Student Congress on Quantum Information & Computation and the 9th Canadian Student conference in Quantum Information (**talk** and **poster**), Waterloo, Canada, 2012

C12. 508. WE-Heraeus-Seminar: Quantum meets Gravity and Metrology (**poster**), Bad Honnef, Germany, 2012

C13. Summer School in Quantum information & Coherence (SUSSP67) (**poster**), Glasgow, UK, 2011

Resumen en español

Título: *Fases Topológicas de la Materia y Sistemas Cuánticos Abiertos*.

Autor: *Oscar Viyuela García.*
Supervisor: *Dr. M. A. Martín-Delgado.*
Departamento de Física Teórica I.
Universidad Complutense de Madrid.

Introducción

Una transición de fase es una transformación entre dos estados de la materia con propiedades físicas diferentes, por ejemplo cuando el agua líquida se convierte en hielo. Tradicionalmente, la física de las transiciones de fase ha sido perfectamente descrita por la teoría de Landau. Esta teoría propone la existencia de un parámetro de orden local que es capaz de distinguir entre dos fases distintas. Además, al atravesar la transición de fase se *rompe* espontáneamente una simetría del sistema.

A partir de los años 80 se empezaron a encontrar un tipo de transiciones de fase que no estaban bien descritas por la teoría de Landau. Estas fases de la materia se denominan **órdenes topológicos** y constituyen el principal objeto de esta tesis doctoral. Para estas transiciones no existe un parámetro de orden local que pueda distinguir entre fases con propiedades físicas distintas. Por el contrario, vienen caracterizadas por un **parámetro de orden global** que es capaz de retener la información topológica del sistema. La otra principal diferencia con respecto a las transiciones de orden, descritas por la teoría de Landau, es el papel que juegan las simetrías. En las transiciones de fase topológicas, cuando se cambia de una fase a otra, no se rompe ninguna simetría. De manera adicional, las fases topológicas de la materia vienen caracterizadas por un conjunto de propiedades distintivas: (1) el estado fundamental está separado por un gap del resto de excitaciones y está degenerado, (2) el sistema presenta **estados gapless localizados en el borde**, (3) las excitaciones son **anyones** con estadística exótica, etc.

Aunque estas fases topológicas están bien entendidas a temperatura cero, se sabe muy poco sobre su comportamiento cuando se entienden como **sistemas cuánticos abiertos**. Dicho con otras palabras, el acoplo inevitable entre el sistema y el

ambiente (que da lugar a efectos de temperatura finita) debe ser tenido en cuenta en la propia definición de orden topológico. Este ha sido uno de los principales objetivos de la presente tesis.

La tesis se encuentra organizada de la siguiente manera. El material presentado en la memoria original se ha dividido en dos partes principales y un apéndice: (A) la **parte** I analiza los sistemas con orden topológico en presencia de ruido y de disipación térmica; (B) en la **parte** II estudiamos el efecto de las interacciones de largo alcance en los superconductores topológicos; (C) el **Apéndice** A versa sobre diversos métodos numéricos para estudiar transiciones de fase disipativas. Dentro de cada parte, hemos incluido diferentes capítulos. Los primeros capítulos de cada parte se dedican a ofrecer una introducción general al campo, y a los diversos métodos y herramientas que se utilizarán más tarde. Los siguientes capítulos contienen las contribuciones originales de esta tesis doctoral, en forma de artículos que han sido publicados en distintas revistas científicas indexadas. Cada uno de estos artículos originales es complementado con una sección preliminar que trata de motivar la necesidad y relevancia de estos trabajos. Estas pequeñas introducciones no son exhaustivas, y se complementan con una extensa bibliografía.

Parte I: Density-matrix Topological Orders

En esta parte de la tesis, hemos estudiado diversos sistemas con órden topológico cuando se encuentran acoplados a un ambiente y se enmarcan dentro de los sistemas cuánticos abiertos. En la publicación **P2**, analizamos las propiedades dinámicas y de estabilidad de un aislante topológico acoplado a un baño térmico. Más tarde, en la publicación **P3**, generalizamos la noción de orden topológico protegido por simetrás para el caso de ecuaciones maestras y superoperadores Liouvillianos. En las publicaciones **P4**, **P5** y **P6**, introducimos una nueva fase cuántica topológica (fase de Uhlmann) que caracteriza aislantes y superconductores topológicos a temperatura finita. En esa misma línea, en la publicacion **P9**, proponemos un protocolo realista para medir esta nueva fase cuántica utilizando un simulador cuántico. Por último, en la publicación **P1**, generalizamos el código tórico de Kitaev (una memoria cuántica topológica) para sistemas de $d > 2$ niveles, y analizamos sus propiedades dinámicas cuando se acopla a baños térmicos.
A continuación se resumen los resultados principales de esta parte de la tesis.

Resultados Principales: Density-matrix Topological Orders

- ✓ Derivamos una ecuación maestra que describe la dinámica de los fermiones (electrones) de un aislante topológico en 1D, cuando se encuentra acoplado a un conjunto de baños térmicos bosónicos.

- ✓ Encontramos un resultado sorprendente: los estados de borde del sistema se

vuelven inestables debido a estos efectos térmicos, y tienen un tiempo de vida finito.

- ✓ Por otra lado, desarrollamos un método para generalizar la noción de aislante topológico para sistemas disipativos.
- ✓ Con este propósito, introducimos el concepto de **Liouvilliano de bandas** como la estructura más apropiada para preservar el orden topológico del sistema. Se puede entender como el contrapunto disipativo a un Hamiltoniano de bandas.
- ✓ Basado en la estructura anterior, construimos un nuevo indicador topológico que denominamos **Chern value**. Con este indicator podemos detectar el orden topológico a temperatura finita para estados cuánticos mezcla generales.
- ✓ De manera reseñable, este nuevo indicator topológico es capaz de detectar la existencia de **estados conductores de tipo mezcla** en el borde, y está a su vez relacionado con la **conductividad Hall cuántica** a temperatura finita.
- ✓ En otro trabajo introducimos la **fase de Uhlmann**, que es una fase geométrica para matrices densidad y la aplicamos a sistemas topológicos en 1D.
- ✓ Demostramos, que para ese tipo de sistemas a temperatura finita, la fase geométrica de Uhlmann adquiere un carácter topológico y únicamente puede estar cuantizada ($\Phi_U = \pi$ topológico no-trivial; $\Phi_U = 0$ trivial).
- ✓ Por debajo de una cierta temperatura crítica T_c la fase de Uhlmann permanece invariante y cuantizada. A T_c hay una transición abrupta, y la fase de Uhlmann se vuelve cero $\Phi_U = 0$ por debajo de esa temperatura. A $T = 0$ recuperamos el diagrama de fases dado por la fase de Berry.
- ✓ En 2D, definimos un nuevo invariante topológico llamado **Uhlmann number**.
- ✓ A temperaturas bajas, el Uhlmann number tiende al Chern number, obteniendo la misma caracterización topológica que a $T = 0$.
- ✓ Utilizando este nuevo formalismo estudiamos diversos modelos bien establecidos como el aislante topológico de Haldane o un superconductor de tipo p-wave que presenta fermiones de Majorana no-abelianos. De manera notable, encontramos que siempre existe una región finita de temperaturas a la que este orden topológico sobrevive.
- ✓ Desde el punto de vista experimental, proponemos un protocolo de medida para la fase de Uhlmann en un simulador cuántico.
- ✓ Efectuando una simulación con ruido e imperfecciones experimentales realistas, demostramos la viabilidad del experimento utilizando una plataforma de **qubits superconductores**.

- ✓ Por último, generalizamos el famoso código tórico de Kitaev (memoria cuántica topológica) para el caso de qudits, o lo que es lo mismo sistemas de espines de d niveles.
- ✓ El código tórico para qudits genera nuevos tipos de excitaciones anyónicas. Estas presentan diferentes estadísticas de braiding con respecto al sistema de qubits.
- ✓ Derivamos una ecuación maestra que da cuenta de la dinámica del código tórico para qudits acoplado a un baño térmico externo.
- ✓ Finalmente mostramos que un código tórico para qutrits ($d = 3$) puede mejorar la estabilidad dinámica de las excitaciones anyónicas.

Parte II: Long-range Topological Superconductivity

En esta segunda parte de la tesis estudiaremos nuevas formas de superconductividad topológica basada en acoplos de largo alcance. La superconductividad se suele definir como la propiedad de ciertos materiales que no muestran resistencia al paso de corriente, por debajo de una cierta temperatura crítica T_c. La teoría BCS da una descripición microscópica de este fenómeno, y explica prácticamente todas las propiedades relacionadas con la superconductividad. Sin embargo, algunos materiales presentan un tipo de superconductividad **no convencional**, que no es capturada por la teoría BCS standard. Los superconductores topológicos aparecen una nueva forma de superconductividad no convencional con una fenomenología de quasipartículas muy exótica. En particular, posee **fermiones de Majorana** desapareados como modos de energía cero localizados en los bordes o vórtices del sistema. En la publicación **P7** estudiamos el efecto de deformaciones hamiltonianas de largo alcance sobre la cadena de Kitaev, un modelo de superconductor topológico en 1D.
A continuación se resumen los resultados principales de esta parte de la tesis.

Resultados principales: Long-range topological superconductivity

- ✓ Introducimos la extensión más general de la cadena de Kitaev incluyendo acoplos de largo alcance.
- ✓ Las deformaciones de los términos de hopping (cinemático) nos permiten incrementar de manera significativa la región del diagrama de fases donde los modos de Majorana aparecen.
- ✓ También analizamos el caso de un pairing superconductor que decae de manera algebraica con la distancia entre fermiones. Si el decaimiento es suficientemente lento encontramos **fermiones de Dirac masivos y no-locales** en el

borde. Estos fermiones son unas nuevas quasipartículas que no están presentes en la cadena de Kitaev estándar.

- ✓ Sorprendentemente encontramos un sector de crossover, donde es posible tener quasipartículas de Majorana y fermiones de Dirac no-locales dependiendo del potencial químico del sistema.
- ✓ Por último, incorporando desorden al sistema comprobamos la robustez de las nuevas quasipartículas de Dirac, debido a su carácter topológico.

Apéndice A: Driven-dissipative phase transitions

En el apéndice de esta tesis introducimos una nueva clase de transiciones de fase cuánticas de **no-equilibrio** producidas por disipación. En los sistemas en equilibrio, las transiciones de fase entre distintos estados de la materia están muy bien entendidas. Sin embargo, las transiciones de fase también pueden tener lugar en situaciones **fuera del equilibrio**. En los sistemas clásicos existen multitud de ejemplos de este tipo: el movimiento de los coches en un atasco, pájaros que muestran un vuelo flocado en grupo, etc. Estas situaciones están relacionadas unas con otras por el hecho de que el orden en el estado estacionario es de origen puramente **dinámico**, y no puede reducirse a propiedades de equilibrio del sistema. En mecánica cuántica, las transiciones de fase fuera del equilibrio pueden ocurrir cuando un sistema interactuante es acoplado a una fuente coherente externa que actúa como ambiente.

En la publicación P8 aplicamos un método numérico, denominado **aproximación de campo medio clusterizado**, con el fin de estudiar transiciones de fase cuánticas disipativas.
A continuación se resumen los resultados principales de esta parte de la tesis.

Resultados Principales: Driven-dissipative phase transitions

- ✓ Estudiamos un sistema magnético de espines 1/2 localizados en una red cuadrada. Las interacciones del sistema están descritas por el model XYZ de Heisenberg. Además consideramos un acoplo externo disipativo que puede voltear los espines.
- ✓ Para estudiar este sistema, extendemos el método de campo medio clusterizado, ampliamente utilizado en sistemas en equilibrio, a un nuevo escenario fuera del equilibrio en el contexto de los sistemas cuánticos abiertos.
- ✓ Al contrario de lo que ocurren en la termodinámica en equilibrio, la inclusión de **fluctuaciones de corto alcance**, a través del método de campo medio clusterizado, cambia profundamente la topología del diagrama de fases de estas transiciones de fase cuánticas disipativas.

- ✓ Combinamos distintos métodos numéricos junto con la aproximación de campo medio clusterizado: redes de tensores y el método de trayectorias cuánticas.
- ✓ Estros resultados podrían ser muy pronto verificados experimentalmente usando novedosas plataformas de **simulación cuántica**, como por ejemplo plataformas de iones atrapados, estados de Rydberg excitados en átomos ultrafríos, y conjuntos de cavidades ópticas y de microondas acopladas.

Conclusions

Los principal objeto de esta tesis han sido el estudio de sistemas con orden topológico y de sistemas cuánticos abiertos. Hemos visto que la conexión entre los dos produce muchas novedades y resultados sorprendentes. Además, la inclusión de efectos de largo alcance en los sistemas topológicos ha sido muy fructífera. Por último, hemo probado que las fluctuaciones de corto alcance tienen un impacto crucial sobre el diagrama de fases de los sistemas cuánticos disipativos, utilizando para ello sofisticados métodos numéricos. La versatilidad de las distintas plataformas de simulación cuántica, unido al enorme interés y dedicación que despiertan los experimentos en materia condensada topológica, nos hacen sentir confiados de que muchos de los nuevos efectos encontrados y detallados a lo largo de esta tesis serán vistos muy pronto en el laboratorio.

Summary in English

Tittle: *Topological Phases of Matter and Open Quantum Systems*.

Author: *Oscar Viyuela García.*
Supervisor: *Dr. M. A. Martín-Delgado.*
Departamento de Física Teórica I.
Universidad Complutense de Madrid.

Introduction

A phase transition is a transformation between two different states of matter with different physical properties (e.g. when liquid water turns into ice). Traditionally, phase transitions in condensed matter have been described using Landau theory. This theory invokes the existence of a local order parameter that distinguishes between two different phases. Additionally, at the phase transition point a symmetry of the system spontaneously breaks.

More recently, there have been phase transitions that do not fit into Landau theory. These phases are called **topological orders** and they constitute the main point of the present thesis. In this case, there is no local order parameter that can distinguish between two different phases with different physical properties. Instead, they are characterised by a **global order parameter**, that is able to retain the topological information of the system. The other main difference with respect to Landau theory is the role that symmetry plays. In topological phase transitions, when traversing from one phase to another, no symmetry is broken. Additionally, topological phases of matter are characterised by a set of remarkable physical properties: (1) the ground state is separated from all excitations by an energy gap and it is **degenerate**, (2) the system host protected **gapless edge states**, (3) quasiparticle excitations are **anyons**, etc.

Although these phases are well-understood at zero temperature, very little was known about their behaviour when the system is consider as an **open quantum system**. In other words, the unavoidable coupling between the system and a thermal environment (finite temperature) needs to be consider into the very definition

of topological order. This has been one of the main objectives of the present thesis as it will be described in what follows.

The thesis is organised in the following way. The material has been divided into two main parts plus an appendix section: (A) **part** I deals with topological order in the presence of noise and thermal dissipation; (B) in **part** II we study the effect of long-range interactions on topological superconductors; (C) **App.** A discuss several state of the art numerical methods for the study of dissipative phase transitions. Within each part, there are several chapters. The first ones try to convey an introduction to the field and the main tools that are going to be used in the following chapters. The rest of the chapters contain original contributions of this thesis. These have been published in well-known international journals as detailed in the list of publications of this thesis. Accordingly, each chapter has an extra introductory section motivating the need and relevance of the work that is presented. These introductions do not intend to be exhaustive and they are complemented with an extensive bibliography.

Part I: Density-matrix Topological Orders

In the first part of the thesis, we have studied systems with topological order when they are coupled to an environment and are considered as open quantum systems. In publication **P2**, we analyse the physics of a topological insulator coupled to a thermal bath. Later, in publication **P3** we generalise the notion of symmetry-protected topological order for master equations and Liouvillian superoperators. In publications **P4**, **P5** and **P6** we introduce a new topological phase (Uhlmann phase) that characterises topological insulators and superconductors at finite temperature; whereas in **P9**, we provide a realistic protocol to measure this new topological quantum phase using a quantum simulator. Lastly, in **P1** we generalise the toric code topological quantum memory for $d-$level systems, and analyse its dynamical properties when coupled to thermal baths.
In what follows we summarise the main results of this part of the thesis.

Main Results: Density-matrix Topological Orders

- ✓ We derive a novel master evolution equation for the fermionic (electrons) degrees of freedom of a 1D topological insulator coupled to an environment made up of bosonic thermal baths.

- ✓ We found a remarkable result: edge states become unstable under thermal effects and they have a finite lifetime.

- ✓ On the other hand, we show a way to generalise the notion of a topological insulator to dissipative systems.

- ✓ For this purpose, we introduce the notion of **band Liouvillian** as the appropriate structure for the dynamics to preserve topological order. It is basically the dissipative counterpart of a band Hamiltonian.
- ✓ We construct a new topological indicator named **density matrix Chern value**, that is able to detect topological order at finite temperature and for general quantum mixed states.
- ✓ Remarkably, this new topological indicator witnesses the existence of **conducting mixed edge states** and is related to the **quantum Hall conductivity** at finite temperature.
- ✓ We introduce the **Uhlmann phase** (a geometric phase for general density matrix) and apply it to topological many-body systems in 1D.
- ✓ We show that when applied to SPT phases at finite temperature, the geometric Uhlmann phase acquires a topological character and it can only be quantised ($\Phi_U = \pi$ topological, $\Phi_U = 0$ trivial).
- ✓ Below a certain temperature T_c, the Uhlmann phase remains unperturbed and quantized . At T_c there is an abrupt transition, and the Uhlmann phase vanishes $\Phi_U = 0$ above that temperature. At zero temperature, it tends to the Berry phase.
- ✓ For 2D, we define a new gauge invariant and quantised topological invariant called the **Uhlmann number**.
- ✓ At very small temperatures, the Uhlmann number tends to the Chern number and we obtain the same topological characterization as at $T = 0$.
- ✓ We apply this new framework to well-established models like the topological insulator Haldane model and the p-wave superconductor that can host non-Abelian Majorana fermions. Remarkably, we always find a finite range of temperatures at which this topological order survives.
- ✓ From an experimental point of view, we propose a novel state-independent **measurement protocol** for the Uhlmann phase using a quantum simulator.
- ✓ By performing a noise simulation and taking into account realistic experimental imperfections, we prove the feasibility of the experiment in state-of-the-art setups of **superconducting qubits**.
- ✓ Finally, we generalise the well-known Kitaev toric code (topological quantum memory) for the case of qudits, i.e. $d-$dimensional spin systems.
- ✓ A Toric code for qudits produces new types of anyonic quasiparticles with different braiding statistics.

- ✓ We derive a master equation that describes the dynamics of a generalised toric code for qudits coupled to an external heat bath.

- ✓ We show that a toric code for qutrits can improve the dynamical stability of anyonic quasiparticle.

Part II: Long-range Topological Superconductivity

In the second part of the thesis, we study novel forms of topological superconductivity based on long-range couplings. Superconductivity is generally defined as a property of certain materials that present exactly zero resistance to the movement of electrons, bellow a certain critical temperature T_c. The BCS theory provides a microscopic description of the phenomenon and explains almost all the general features of superconductivity. However, there are some materials that display an **unconventional** form os superconductivity, that is not capture by standard BCS theory. Topological superconductors are a very new form of unconventional superconductivity with a very exotic quasi-particle phenomena. They posses unpaired **Majorana fermions** as zero-energy modes localised at the edges or vortices of the system. In publication P7, we study the effect of long-range hamiltonian deformations on the Kitaev Majorana chain, a model for a topological superconductor in 1D.
In what follows we summarise the main results of this part of the thesis.

Main Results: Long-range topological superconductivity

- ✓ We propose the most general extension of the Kitaev chain including long-range couplings.

- ✓ Deformation of the hopping terms (kinetic) allows us to significantly increase the region in the phase diagram where Majorana modes are present.

- ✓ We consider pairing amplitudes decaying with a power-law of the distance between fermions. For sufficiently slow decaying pairing terms we find **non-local massive Dirac edge states**. These are new physical quasiparticles that are absent in the standard Kitaev model.

- ✓ Interestingly enough, we find a crossover sector where it is possible to have both Majorana quasiparticles and non-local Dirac quasiparticles depending on the chemical potential of the system.

- ✓ By incorporating static disorder into the system, we show the robustness of the new massive Dirac quasiparticles, due to their topological character.

Appendix A: Driven-dissipative Phase Transitions

In the appendix section, we present a class of **non-equilibrium** quantum phase transitions driven by dissipation. In equilibrium systems, phase transitions between different states of matter are very-well understood. Phase transitions can also occur in **out-of-equilibrium** situations. In classical systems, many examples have been found: moving cars into traffic jams, individual flying birds exhibiting collective flocking, etc. These situations can be related to each other by the fact that the appearance of different steady-state ordering is of purely **dynamical origin** and cannot be reduced to the equilibrium results. In quantum mechanics, phase transitions away from thermal equilibrium may occur when an interacting system is driven by some external coherent source acting as an environment.

In publication **P8**, we apply a numerical technique called **cluster mean-field** approximation in order to study driven-dissipative quantum phase transitions. This method is combined with several others: matrix-product-states, tensor networks and quantum trajectories.
We now summarise the main results of this part of the thesis.

Main Results: Driven-dissipative phase transitions

- ✓ We study a magnetic system of spin-1/2 particles located on a square lattice. The interactions of the system are described by the so-called Heisenberg XYZ model, and we allow for spin-flip transitions associated to some external dissipative coupling.

- ✓ We extend the cluster mean-field method widely used in equilibrium situations, to a new out-of-equilibrium scenario in open quantum systems.

- ✓ Contrary to equilibrium thermodynamics, the inclusion of **short-range fluctuations**, by means of the cluster mean-field method, deeply modifies the steady-state phase-diagram topology of driven-dissipative quantum systems.

- ✓ We combine powerful numerical methods together with the cluster mean-field approach: tensor-networks and quantum trajectories techniques.

- ✓ Our results are amenable to experimental verification using novel **quantum-simulation** platforms like trapped ions, highly excited Rydberg states of ultracold atoms, and arrays of coupled optical or microwave cavities.

Conclusions

Throughout this thesis, we have focused our attention over systems with topological order and open quantum systems. We have seen that the connection of the

two produces many novelties and surprising results. In addition, the inclusion of long-range effects in topological systems has been proven to be very fruitful. Furthermore, we have shown that short-range fluctuations have a dramatic impact on the phase diagram of driven dissipative systems, using sophisticated numerical methods. The versatility of quantum simulation platforms, together with the great effort and interest on topological condensed matter experiments, make us confident that many of the new findings in this thesis will be soon realised in the lab.

Contents

Introduction

At low energies, matter is composed only by three kinds of particles: electrons, protons and neutrons. Nevertheless, these constituents can be arranged in multiple ways such that their behaviour as an ensamble can be completely different from one another. This idea lead to the principle of emergence in condensed matter, very clearly formulated by the Nobel laureate Phil Anderson.

> *The ability to reduce everything to simple fundamental laws does not imply the ability to start from those laws and reconstruct the universe. [...] The behaviour of large and complex aggregates of elementary particles, it turns out, is not to be understood in terms of a simple extrapolation of the properties of a few particles. Instead, at each level of complexity entirely new properties appear, and the understanding of the new behaviours requires research which I think is as fundamental in nature as any other.*
> P. W. Anderson *Science, New Series, Vol.* **177,** *No. 4047 393-396 (1972).*

These words are very illustrative to understand that the collective behaviour of fundamental particles can be very rich and surprising. Emergent phenomena not only occur at the level of fundamental physics, but also collective behaviour has been studied and reported in other disciplines such as Biology [Nov45], Sociology [HYR11], Economics [FM12], etc.

In condensed matter physics, the different manners in which atoms organise themselves through interactions give rise to very different states of matter. Just to name a few examples: solid, liquid and gas; or even more exotic phases like ferromagnetism, superconductivity, superfluidity, Bose-Einstein condensation (BEC), etc. All these states of matter shape the notion of **order** for a many-particle system. We define a **phase of matter** as a particular state in which particles of a many-body system arrange or order themselves, comprising a distinct set of physical properties.

In most cases, **symmetry** [Gro96] plays an essential role to identify and characterise different phases of matter. Two phases may be distinguished from each

other by looking at their symmetries, and the transition between one phase to the another would be accompanied by the breaking or changing of their symmetries.

In 1937 Landau [Lan37] proposed a very general theory to describe transitions between different phases. The theory relies on the identification of a **local order parameter**, i.e., a local property with a finite expectation value in one phase and a vanishing expectation value in the other one. The second fundamental ingredient is the mechanism of **symmetry breaking**. At the phase transition point, a disordered and highly symmetric phase, acquires a non-zero expectation value of the order parameter by reducing or *breaking* the symmetry of the system[2].

Additionally, the theory makes a general assumption: the **free energy**[3] of the system can be expanded in terms of the order parameter. This is possible close to the transition point where the value of the order parameter is small. Based on this idea, phase transitions can be classified [Ehr33, Jae98] according to the lowest derivative of the free energy that is discontinuous at the transition point. The macroscopic theory of Landau describes all continuous[4] phase transitions from the thermally driven paramagnetic-ferromagnetic phase transition to the purely quantum superfluid-BEC one.

The success of this theory was also used by Ginzburg and Landau himself in 1950 to give a macroscopic description of superconductivity [GL50]. This theory, that combines **Landau theory** of second-order phase transitions with a Schrödinger-like wave equation, had a great success in explaining the macroscopic properties of superconductors. Moreover, Abrikosov showed that Ginzburg-Landau theory predicts the division of superconductors into the two categories now referred to as Type I and Type II [Abr57].

According to the modern classification of phase transitions [Sac00], we can stablish two groups:

- **First order phase transitions**

  Transitions between phases with different symmetries cannot occur continuously. For example, when liquid water turns into ice, the inner crystalline structure of the system changes. Hence, for each state of matter the system has either one symmetry or the other, but it cannot have partly one and partly the other. For first order phase transitions, derivatives of the free energy undergo discontinuous changes. The order parameter is also discontinuous at the transition point. Strictly speaking Landau theory is not applicable, since it assumes continuity of the free energy. However, it is usually applied by incorporating appropriate corrections to the effective action. Those are

[2] This is the case for a ferromagnet that breaks spin rotation symmetry and gains a non-zero magnetisation.

[3] The **free energy** is a thermodynamic quantity that measures the amount of work that can be extracted from a system. It can be written as $F = E - TS$ where E is the internal energy of the system, T is the temperature and S is the entropy.

[4] divergences in the second-order or higher-order derivatives of the free energy

higher order terms in the order parameter η which allows for the existence of metastable states (local minimum of the free energy). Transitions between solid, liquid and gas are examples of first order phase transitions. These transitions display a discontinuos change in particle density, proportional to the inverse of the derivative of the free energy with respect to pressure.

- **Continuous phase transitions**

  We have seen that phase transitions between different crystalline structures lead to sudden changes on particle distributions, and the state of the system itself is modified discontinuously. Nevertheless, there are other types of phase transitions involving a change of symmetry whose order parameter does not change discontinuously. A textbook example of this kind [LL00] would be the $BaTiO_3$ compound. At high temperature it has a cubic lattice, but when temperature decreases it changes to a tetragonal lattice. During the process there is no discontinuous change in the state of the system, and the particles rearrange continuously. However, the symmetry of the system changes discontinuously signalling the two different phases. Inside this class of phase transitions there are different subclasses: second order, third order, etc; depending on whether the discontinuity in the free energy appears in the second derivative, the third, etc. There are even infinite-order phase transitions [5].

With the discovery of the Quantum Hall Effect (QHE) [KDP80], it was first noticed that there were continuous phase transitions that could not be explained using Landau theory. The QHE effect belongs to a class of systems called **topological orders** that lie outside Landau theory. The field of topological orders is actually one of the most active in modern condensed matter physics. It comprises several exotic quantum phases such as: topological insulators and superconductors [HK10, QZ10, QZ11], Weyl semimetals [XBA+15, XAB+15, YLS+15], or the fractional QHE [TSG82].

These quantum phases of matter have been largely explored during the last years. However, a theory that incorporates noise, thermal effects, dissipation and long-range interactions has been barely developed. Actually, this is one of the main purposes of the present thesis. We want to shed light upon the field of topological phases of matter when they are subjected to thermal and dissipative effects, or when long-range couplings are considered.

Furthermore, all these phases of matter used to belong exclusively to the realm of condensed matter physics. However, in 1982, Richard Feynman came up with this revolutionary concept of **quantum simulators** [Fey82]. The central idea relies on the main difficulty of traditional condensed matter: sometimes we know fairly

[5] A **Kosterlich-Thouless** [KT73] (also called **infinite order**) phase transition describes a phase transition from a phase with no order where correlation functions decay exponentially with the distance, to a quasi-ordered phase where correlation functions decrease with the distance following a power-law which depends on the temperature. These transitions do not break any symmetry.

well that a certain quantum system is described by set of interactions; however, we don't know how to find a solution exactly. Even if one resorts to numerics, the problem may become intractable for the most advanced computers when the number of particles $N \sim 50$. This is due to the fact that the dimension of the Hilbert space of a quantum many-body system grows exponentially with the number of particles N. The DMRG method [Whi92] has been the traditional strategy for the last two decades to efficiently find the low energy physics of interacting quantum many-body systems in 1D. For fermionic particles, the numerical solution of the dynamics encounters the so-called sign problem [TW05]. This results in an exponential growth of the statistical error and the required simulation time with the number of particles N, eliminating the advantage of quantum Monte Carlo methods [FMNR01]. Thus, considering all these arguments, there is a question that naturally arises:

- *Is there a general way to overcome the intractability of general quantum problems on a classical computer?*

The answer is positive [Llo96], and it is based on the intuition that if we want to solve a quantum many-body problem, it is more convenient to look for a quantum setup instead of a classical one.

> *Let the computer itself be built of quantum mechanical elements which obey quantum mechanical laws.*
> R. Feynman, *Int. J. Theor. Phys. Vol.* **21**, *No. 467 (1982).*

We consider a certain quantum many-body system S_1 that can be effectively described by Hamiltonian H_{S_1}, but whose solution cannot be found exactly. We may encode H_{S_1} on the interactions of a different quantum system H_{S_2} that we can prepare and control in the lab. This analog system S_2 (quantum simulator [GAN14]) evolves in an analog way to the original S_1. But in this case, we can perform very precise measurements and have arbitrary and exquisite control over the quantum simulator S_2, that may not be available in the original system S_1. Summarising, we are replicating the interactions and dynamics of a system on a different platform where controllability can be taken to its best. When we design arbitrary interactions over a system that replicates a different one, that is harder to access, we claim we have performed an **analog quantum simulation** [BDZ08, BN09, Ess10, GLV+93, JBC+98].

Additionally, we could think about a different protocol with the same purpose. We take the unitary evolution of the system S_1 that cannot be solved, we discretise it and reexpress it into a universal set of quantum gates [NC00]. This method is inspired by the field of quantum computing, and it is called **digital quantum simulation** [GAN14].

There are several platforms that are currently being used in order to perform quantum simulations. Let us just name some of the most popular and advanced ones at the moment:

- **Trapped ions** [LBMW03, CZ95, SHR+03, PC04].

  Ions can be trapped using, for instance, magnetic fields generated by simultaneous AC and DC currents. The ions' vibrations can be cooled down and manipulated with high precision using laser fields. More precisely, the quantum states involved are chosen to be some internal states of the ion (for instance the fine or hyperfine structure) together with vibrational modes due to the laser driving. The interplay between these two allows us to perform quantum simulations [SLC+04, BW08] with great single-atom addressability and quantum computations [HHJ+10, LHN+11] with high-fidelity quantum gates.

- **Cold neutral atoms in optical lattices** [LSA+07, BDZ08, JBC+98, JSG+08, KMS+05].

  Counter-propagating laser beams generate standing waves that give rise to spatially periodic polarization patterns called optical lattices. Inside the potential minimums of the optical potential, neutral atoms can be placed. This platform offers great advantages to simulate solid state physics, due to its high controllability [SWE+10] and lack of unwanted defects. The first experiment with a cold atomic gas in an optical lattice simulated the quantum phase transition from a superfluid to a Mott insulator [GME+02]. Since then, a large number of experiments has been successfully carried out including the quantum simulation of topological systems [AAB+13, LDR+16].

- **Circuit Quantum Electrodynamics (QED):** superconducting qubits coupled to microwave photons [MSS01, BHW+04, DWM04, CW08, BGB09, GMS+15, GRSMD08].

  A superconducting qubit is a technology that is formed out of superconducting elements coupled through Josephson junctions [MSS01]. In general, there are two families of superconducting (SC) qubits, depending on whether the charge (charge qubits) or the phase (flux qubits) of the superconducting elements are good quantum numbers. Besides, a high-quality microwave resonator can be coupled to the SC qubits. The situation is analogous to cavity-QED [6], where in this case the SC qubit can be seen as an artificial atom [YN03]. We induce interactions among qubits using the resonator as an "internal bus", similar to the lattice vibrations for an ion trap setup.

All of these different platforms offer several advantages over traditional condensed matter systems: single-site addressability, the possibility to measure the

[6] In cavity-QED an atom is coupled to the electromagnetic field inside a cavity [SZ97].

phase of the wavefunction, ultra precise measurement sensitivity, etc. Nonetheless, the number of constituents of these quantum simulators is still small and great efforts are being made to scale these systems up.

On the other hand, the quantum simulation of **topological physics** is currently one of the most active fields in this area. The possibility to simulate **fictitious gauge fields** [JZ03, LCJ+09, OBS+05] and perform interferometric topological measures [AAB+13, JMD+14, RNC+14, LDR+16] have triggered an increasing amount of experiments and proposals [WGS08, GSN+10, MBG+12, DMMD12, DMMD16, MCLS13, GDD+13]. Additionally, from the point of view of topological quantum computation, several experimental advances have been achieved as well [NMM+14, BKM+14].

Both in quantum simulators and traditional condensed matter, the presence of **finite temperature** and **dissipative effects** is unavoidable. The interaction between our quantum system and its environment is responsible for the transition from purely quantum to *classical* effects [PZ01]. Regarding phase transitions, equilibrium thermodynamic have been the basis for the characterisation of both classical and quantum phases. However, phase transitions out of equilibrium have also been studied [MD99, PSSA09].

Along this thesis, we have explored how all the ingredients presented in this introduction combine together. The thesis is organised as follows. The material has been divided into two main parts plus an appendix section: (A) **part** I deals with topological order in the presence of noise and thermal dissipation; (B) in **part** II we study the effect of long-range interactions on topological superconductors; (C) **App.** A discuss several state of the art numerical methods for the study of dissipative phase transitions.

Each part consists of several chapters, being the first ones a gentle introduction to the theory and tools needed for the understanding of the following chapters. The remaining chapters in each part contain the original material published in peer-reviewed articles. Each paper is supplemented by an introductory section and a summary of the main results. The introductions are in general intended to motivate why the paper is timely and convenient, and what the main questions or problems addressed by each paper are. Bellow, you may find a summary of the content of each chapter.

In **chapter** 1, we give a brief introduction to topological order. We describe the different types of order and their characteristic properties.

In **chapter** 2, we introduce the basic ideas of the theory of open quantum systems. We focus on the derivation of master equations in the weak coupling limit.

In **chapter** 3, we analyse the physics of a topological insulator coupled to a thermal bath. This chapter is based on publication **P2**.

In **chapter** 4, we propose the concept of density-matrix topological oder by defining the notion of topological order from a Liouvillian superoperator. This chapter is based on publication **P3**.

In **chapter** 5, we introduce the Uhlmann phase as a tool to characterise symmetry-protected topological order at finite temperature. In publication **P4** we study the one-dimensional case. Additionally in **P5** we extend the Uhlmann approach to two-dimensional systems. In publication **P6** we give a detailed description of the general Uhmann theory both in $1D$ and $2D$ and analyse a new topological model. Finally, in **P9** we provide a realistic protocol to measure this new topological quantum phase using a quantum simulator.

In **chapter** 6, we generalise a topological quantum memory for the case of qudits ($d-$dimensional quantum bits). We also study the stability of the model when coupled to a thermal bath. This chapter is based on publication **P1**.

In **chapter** 7, we give an introduction to BCS and unconventional topological superconductivity.

In **chapter** 8, we study the effect of long-range hamiltonian deformations on the Kitaev Majorana chain, a model for a topological superconductor in 1D. This chapter is based on publication **P7**.

Finally, in **App.** A we present a class of non-equilibrium quantum phase transitions driven by dissipation. We apply a numerical technique called cluster mean-field approximation in order to study driven-dissipative quantum phase transitions. This method is combined with several others: matrix-product-states, tensor networks and quantum trajectories. This appendix is based on publication **P8**.

Part I

Density-matrix Topological Orders

1

Introduction to Topological Order

Topology is the branch of mathematics that deals with geometrical properties of objects that are insensitive to smooth deformations. Based on this intuitive definition we can argue that a donut belongs to the same topological class as a cup of tea, in the sense that they both have the same number of holes. Mathematically, we say that both objects have the same *genus*. However, a basketball has a different topology than a ring, since they can never be transformed into each other by means of smooth surface deformations. This gives us intuition into why topological properties have some intrinsic robustness with respect to purely geometrical aspects.

The importance of topology in high energy physics [Wit88] was recognised after these ideas became relevant in condensed matter or more generally for low energy physics [Tho98, KT72, KT73, TKNTfd82, Hal83a, NTW85]. However, a paper by Dirac [Dir31] can be considered as a precursor of the role played by topology in Physics. He showed that magnetic monopoles are possible in a quantum theory only if the magnetic charge is an integer times the electric charge of the electron.

Historically, the first known example of topological order in condensed matter was the **integer quantum Hall effect** (IQHE) [KDP80]. At very low temperature, when a 2D electron system (e.g. a MOSFET transistor) is threaded by a strong magnetic field, the **transverse conductivity** σ_{xy} is integer-quantized [NTW85] in units of $\frac{e^2}{h}$[1]. The integer is a topological invariant called the **Chern number**, related to σ_{xy} through the TKNN formula [TKNTfd82]. Along this section, we will describe these topological invariants and show their relation with physical properties of the

[1] Along the paper, h stands for the Planck constant, e is the electron electric charge and c stands for the speed of light.

system. The Chern number is also equal to the number of filled **Landau levels**[2] [LL00] at the **Fermi energy**[3]. In order to understand the relation between the filled Landau levels and the quantum Hall conductance, Laughlin [Lau81] proposed a thought experiment and gave a very intuitive argument. Let us have a 2D Hall bar that we wrap into a loop (taking periodic boundary conditions in one direction), so we get a cylinder. The current along the wrapped direction generates a magnetic flux threading the cylinder. Following Laughlin's calculations, for each quantum flux $\Delta\phi = hc/e$ threading the system, one electron per Landau level is transferred from one edge to the other, leading to the formula for the quantised Hall conductance.

Sometimes, Landau levels are not completely filled, but only a certain fraction of them, with filling factor $\mu = p/q$, where p and q are integer numbers. This produces the famous **fractional quantum Hall effect** (FQHE) that was experimentally realised in 1982 by Nobel laureates Tsui and Störmer [TSG82]. From the theoretical side, Laughlin [Lau83] gave a phenomenological description in terms of a trial wavefunction for the $\mu = 1/q$ states, where q is and odd integer. Haldane [Hal83b] extended the theory for filling factors $\mu \neq 1/q$. It was Halperin [Hal84] in 1984 who conjectured that the quasiparticles given by Laughlin wave functions had unusual particle statistics. Later, Arovas, Schrieffer and Wilczek [ASW84] proved that these quasiparticles were **abelian anyons**[4]. When two of these particles are exchanged, the wavefunction acquires a phase $e^{i\theta}$ with $\theta = \frac{\pi}{q}$. Anyons with non-abelian statistics can be also found in the FQHE [GN91, Wen91, RG00]. A complementary theory for FQH states with different filling factors was proposed using the concept of **composite fermions** [Jai89, HLR93]. The underlaying principle states that particles in the FQHE can be described as IQH states of composite fermions (where magnetic fluxes are attached to electrons). Both the IQHE and the FQHE represent two examples of topological orders that cannot be described using Landau theory.

Therefore, let us understand what are the elements in **Landau theory** [Lan37] of phase transitions that fail to describe topological order. A traditional textbook example for the use of Landau theory describes the phase transition from a paramagnetic (PM) phase to a ferromagnetic (FM) phase of a many-body spin system when temperature decreases. According to Landau theory, these two phases can be distinguished from each other by the expectation value of a **local order parameter** (the magnetisation M). If $T > T_c$ the system behaves as a paramagnet $M = 0$,

[2] In Quantum mechanics, when an electron interacts with a magnetic field, its energy spectrum is discrete. These levels are called **Landau levels**, and can be occupied by electrons with different momentum. The effects associated with Landau levels can only be resolved at small temperatures (small thermal energy) and strong magnetic fields (large energy gaps).

[3] In a system of non-interacting electrons, the **Fermi energy** is defined as the maximum energy that the last occupied state (the one with highest energy) can have. This quantity depends on the material and sets whether a system behaves as a metal or as an insulator/semiconductor.

[4] **Anyons** are excitations with unusual braiding statistics. They are neither bosons nor fermions. Because of these non-trivial braiding statistics they have been proposed as basic elements for Topological Quantum Computation [NSS+08].

whereas for $T < T_c$, the system is a ferromagnet $M = 0$. The critical temperature T_c signals where the phase transition occurs. At that point there is a process called **spontaneous symmetry breaking**, at which the spin rotational symmetry $SO(3)$ in the PM phase spontaneously breaks, and the system becomes FM. This paradigm of a local order parameter characterising the different phases and the symmetry breaking process during the phase transition constitute the main core of Landau theory [Lan37].

Nonetheless, there are other types of phases of matter, that cannot be described using Landau theory. These phases are called **topological orders (TOs)**. In this case, there is no local order parameter that can distinguish between two different phases with different physical properties. Instead, they are characterised by a **global order parameter**, that is able to retain the topological information of the system. The other main difference with respect to Landau theory is the role that symmetry plays. In topological phase transitions, when traversing from one phase to another, no symmetry is broken. The mechanism of spontaneous symmetry breaking is no longer valid. Actually, it is still and open problem whether a Landau-like theory for a topological order parameter can be derived.

On the other hand, topological phases of matter are characterised by a group of remarkable physical properties: the **ground state** is separated from all excitations by an energy gap and may be **degenerate**, they host protected **gapless edge states**, quasiparticle excitations are **anyons**, etc.

Actually, we have very generally defined TOs as phases of matter characterised by a global order parameter, whose phase transitions do not involve symmetry breaking. However, we can further classify TOs in two categories according to the subset of the above physical properties they have:

- **Intrinsic Topological Order (ITO)**:

  These phases of matter have a degenerate ground state, that is isolated by an energy gap to all excitations. They are robust against arbitrary local perturbations. They also posses anyonic quasiparticle excitations with non-trivial braiding statistics. These anyons are a new type of topological quasiparticles that appears in $2D$. They are neither bosons nor fermions. Instead, when we exchange two of these identical anyons, the wavefunction acquires an extra phase $e^{i\theta}$ with $\theta \in (0, \pi)$. More generally the phase could be even non-abelian, which means that after exchanging two identical fermions, the wavefunction is multiplied by a unitary matrix and not just a simple $U(1)$ phase. This opens the possibility to perform universal quantum computations [Kit03, NSS+08]. Examples of intrinsic topological orders are: the FQHE, the toric code [Kit03] and double semion model [FNS+04, LW05], the color codes [BMD06, BMD07], etc. Quantum states with ITO can be also characterised by patterns of long-range entanglement [KP06, LW06, CGW10].

- **Symmetry-protected topological order (SPTO)**:

These phases instead do not have anyonic quasiparticles in the bulk. The non-trivial physics happens at the boundary. Actually, these SPT phases host **protected edge states**, which are isolated from bulk excitations by an energy gap. The edge states are robust against disorder and local perturbations that respect a certain global **protecting symmetry** G (e.g. time-reversal symmetry). Actually, one can classify the different classes of SPT phases according to these discrete symmetries. Moreover, they are short-range entangled phases since they do not have TO in the bulk. Most of these topological phases where found to be associated with the fermion character of particles [HK10, QZ11]. However, bosonic versions of these phases were discovered and they are now all of them understood as symmetry-protected topological orders (SPTOs) [VS13, MKF13, CGLW13].

A detailed analysis of topological phases will be carried out in the next section.

This chapter is organised as follows: In Sec. 1.1, we introduce the notion of symmetry-protected topological order (SPTO). We present a toolkit to analyse the topological phase diagram of these models at zero temperature and discuss the appearance of protected edge states (see also publications **P4**, **P5** and **P6**). In Sec. 1.2, we describe the main features of intrinsic topological orders (ITOs) and their applicability to build topological quantum memories. In particular, we will analyse the basics of the most paradigmatic model for a topological quantum memory called the **toric code** [Kit03] (see publication **P1**).

1.1 Symmetry-protected topological order (SPTO)

In 1988, Haldane [Hal88a] realised that it is possible to obtain a quantum Hall effect for a model with no Landau levels (no net magnetic flux). However, this model still breaks time-reversal (TR) symmetry.

The discovery of **topological insulators** [HK10, QZ10, QZ11] and the rapid development of this whole community started 10 years ago when it was realised that a spin version of the quantum Hall effect was possible [BZ06]. The role of the magnetic field is played by the spin-orbit interaction which does not break TR symmetry. The first experimental proposal [BHZ06] and the first experiment [KWB$^+$07] appear soon thereafter, and the **spin Hall effect** was first meassured in HgTe/CdTe semiconductor quantum wells.

A topological insulator is a material that behaves as a standard insulator in the bulk (band insulator, Mott insulator, Anderson insulator,...); while displaying conducting edge states at the boundary. In the case of the spin Hall effect, they have two counter-propagating conducting states at each edge with spin up and spin down respectively. Due to the conservation of TR symmetry, these states do not

scatter and mix. In Landau theory, the concept of symmetry plays a very important role distinguishing different phases. For the case of SPT phases, symmetry also plays a key role. The focus is not on which symmetries the system breaks, but on which symmetries the system has to preserve to remain stable. SPT phases can be shown to be stable against perturbations that do not break the set of protecting symmetries of the system. Topological insulators belong to the SPT class of topological orders, since their robustness is linked to the preservation of a certain discrete symmetry.

In 2007, a 3D version of topological insulators [FKM07] was first proposed and experimentally realised in a series of experiments [HQW+08, CAC+09, HXW+09, HXQ+09a, HXQ+09b]. These were able to probe: the appearance of **surface Dirac cones**, the spin structure of edge states through ARPES[5] techniques, etc.

Inter-particle interactions can also induce topological insulating phases. **Topological Mott Insulators** [RQHZ08, DMMD12, DMMD16] are a certain kind of Mott insulators[6], whose mean-field phase diagram possesses topological insulating phases. The effect of interactions plays an important role in the topological classification of free fermion systems [FK10]. Very naturally, interactions in SPT phases opened the door for the generalisation of these phases to interacting bosonic systems [CGLW13]. Despite the different particle statistics of fermions and bosons, particle interactions can produce novel states called **bosonic topological insulators** [VS13, MKF13]. From the theoretical point of view, topological insulators can also be described using topological quantum field theory [QHZ08].

The field of topological insulators has attracted a lot of attention during last years. Very recently, it was shown [WTVS11] that for certain 3D materials[7] it is possible to find band structures of the form of a "zero-gap semimetal", for which the valence and conduction band "touch" at a discrete number of crystalline momenta **k** [Bal11]. Some of these band touching points are protected by topology and are called **diabolic points** [Mur07]. The band dispersion relation around these touching points is linear, similar to the massless Dirac fermions observed in graphene. However, as either TR or inversion symmetry has to be broken, the low energy excitations around these diabolic points satisfy the Weyl equation [Wey29], and behave as **Weyl fermions**[8] instead. Weyl semimetal states have been experimentally observed through some of their distinct characteristics: linear band dispersion structure around diabolic points, the presence of surface **Fermi arcs**[9]

[5] Angle-resolved photoemission spectroscopy (ARPES).

[6] A Mott insulator [Mot68] is a type of insulator that is created through strong repulsive interactions between electrons inside a band. These strong their interactions cannot be neglected as in usual solid-state band theory.

[7] For example $R_2Ir_2O_7$ where R stands for a rare-earth element.

[8] **Weyl fermions** satisfy the so-called Weyl equation [Wey29], a two-component Dirac-like equation that was proposed by Hermann Weyl in 1929. The Weyl equation has been used in particle physics to describe the chiral and massless behavior of neutrinos, when their small mass can be neglected.

[9] At the Fermi energy, the states form open arcs whose endpoints are the projection of diabolical

[XBA+15, XAB+15, YLS+15], etc. Simulations of these topological metals in optical lattice have been also proposed [BUGH09]

Inspired by topological insulators, there has been several proposals and experiments to build photonic analogs of SPT phases in **photonics crystals** [LJS14]. The possibility to image robust edge states of light [HMF+13] and measure topological invariants [Haf14, MGF+16] from scattered photons, paves the way for further research to construct robust waveguides with arbitrary shape. **Floquet topological insulators** induced by temporal modulation of a photonic crystal [RZP+13] are recently getting a lot of attention too.

Furthermore, the notion of SPT phases is not restricted to insulating phases. Actually, **superconducting phases** with topological order [SNT06, FK08] are probably the most exciting area within the field of topological orders, due to the appearance of quasiparticles that are **Majorana fermions** [Kit01]. This will be discussed in very much detail in the second part of this thesis (chapter 7).

Lastly, we can classify SPT phases into what is called the **periodic table** of topological insulators and superconductors [Kit09, SRFL08, RSFL09]. This classification is made according to: (a) a set of discrete anti-unitary symmetries (time-reversal TR, particle-hole PH and Chiral C), and (b) the space-time dimension. However, it seems clear that any discrete symmetry should give rise to different topological phases protected by symmetry [CTSR16]. This was first noted by Fu [Fu11] with his proposal for **crystalline topological insulators**, that have already been created in the laboratory [HLL+12, DKD+12]. In addition, **particle interactions** can change the physical properties of the different classes [FK10]. A complete theoretical classification of all possible SPT phases including interactions for $d > 1$ is still missing.

For non-interacting SPT phases a complete topological characterisation can be given by means of the Berry phase, as it will be explained in what follows.

1.1.1 Berry phase

Quantum phases play nowadays a prominent role in modern condensed matter physics. Their importance roots back to the origin of Quantum Mechanics and the role played by the relative phase of a superposition state [GP90] in quantum interference. Recently, quantum phases are being used to produce very powerful computational systems like a quantum computer [NC00, GM02].

The **Aharonov-Bohm (AB) phase** [AB59] is a very special quantum phase since local perturbations leave it unaltered: it is topologically invariant. In classical mechanics we use the concept of **force** to describe the way in which electric or magnetic particles move due to electric or magnetic effects. Forces only depend on the value of the electric field $\mathbf{E}$ or the magnetic field $\mathbf{B}$ and not on the potentials $(V, \mathbf{A})$. Due to the invariance of Maxwell's equations under gauge transformations of the potentials, it has long been thought that these potentials were clearly unphysical,

points onto the surface Brillouin zone.

serving only as a purely mathematical construction to simplify the formulation and calculations. In quantum mechanics, however, potentials and not fields appear at the very heart of Schrödinger's equation. Therefore, the question of whether potentials may have some physical relevance by themselves revived. In 1959, Aharanov and Bohm [AB59] showed that the wave function of a particle acquires a phase, when it traverses regions of the space with a vanishing **B** field but non-zero vector potential $\mathbf{A} = 0$. If a particle in free space winds around a solenoid, it acquires a phase that only depends on the magnetic flux that the close trajectory encircles. But the phase does not depend on the specific path that the particle describes. Equivalently, we say that the phase only depends on the topology of the space.

The **Berry phase** [Ber84] is another special instance of quantum phase, one that is purely geometrical [WS89, Lui06] and independent of dynamical effects during the time evolution of a quantum system. The discovery of this geometric phase by Berry in 1984 is linked to the behaviour of adiabatically driven systems.

Let us consider a system governed by a Hamiltonian $H\big(\mathbf{R}(t)\big)$, where $\mathbf{R}(t)$ is a parameter of the Hamiltonian that varies in time. The evolution of the system under this Hamiltonian is given by the time-dependent Schrödinger equation

$$\frac{d}{dt}|\Psi(t)\rangle = -\frac{\mathrm{i}}{\hbar}H\big(\mathbf{R}(t)\big)|\Psi(t)\rangle, \tag{1.1}$$

where h is the Planck constant. Let the initial state $|\Psi(0)\rangle = |n\big(\mathbf{R}(\mathbf{0})\big)\rangle$ be an eigenstate of $H\big(\mathbf{R}(0)\big)$. If we assume that the evolution is adiabatic, then the state will always remain an eigenstate of the $H\big(\mathbf{R}(t)\big)$, up to some phase factor

$$|\Psi(t)\rangle = \mathrm{e}^{\mathrm{i}\Phi(t)}|n\big(\mathbf{R}(t)\big)\rangle. \tag{1.2}$$

By inserting Eq. (1.2) in Eq. (1.1), we get a differential equation for $\Phi(t)$ that can be integrated straightforwardly

$$\Phi(T) = -\frac{1}{\hbar}\int_0^T E_n\big(\mathbf{R}(t)\big)dt \;+\; \mathrm{i}\int_0^T \langle n\big(\mathbf{R}(t)\big)|\frac{d}{dt}|n\big(\mathbf{R}(t)\big)\rangle dt, \tag{1.3}$$

where T is the final time of the evolution and we set $\Phi(0) = 0$. Using the chain rule

$$\langle n\big(\mathbf{R}(t)\big)|\frac{d}{dt}|n\big(\mathbf{R}(t)\big)\rangle = \frac{d\mathbf{R}(t)}{dt}\cdot\langle n\big(\mathbf{R}\big)|\nabla_{\mathbf{R}}|n\big(\mathbf{R}\big)\rangle, \tag{1.4}$$

we can see that the last term does not really depend on time. Hence, we obtain $\Phi(T) = \Phi_d + \Phi_B$, where

$$\Phi_{\mathrm{d}} = -\frac{1}{\hbar}\int_0^T E_n\big(\mathbf{R}(t)\big)dt \tag{1.5}$$

is called the **dynamical phase** and

$$\Phi_{\mathrm{B}} = \mathrm{i}\oint_C \langle n\big(\mathbf{R}\big)|\nabla_{\mathbf{R}}|n\big(\mathbf{R}\big)\rangle d\mathbf{R} \tag{1.6}$$

is the so-called **Berry phase**, where we have made the choice $|n(\mathbf{R}(T))\rangle = |n(\mathbf{R}(0))\rangle$ for a closed path C in parameter space. The Berry phase Φ_B is a geometric phase that only depends on the geometry of the path $\mathbf{R}(t)$, but not on the speed at which the path is traversed nor on any dynamical details of the driving. It is also independent of the system's energy and it is clearly **gauge invariant**[10]. An easy textbook example for the applicability of this result is a spin precessing due to a slow varying magnetic field. After a periodic driving is completed, the spin picks up a phase that is proportional to the area enclosed by the precession of the spin in the Bloch sphere[11].

It so happens that both the AB phase and the Berry phase are intimately related. When a Berry phase is invariant under deformations of the path traced out by the system during its evolution, it becomes topological as the AB phase. **Topological Berry phases** have also acquired a great relevance in condensed matter systems. The now very active field of topological insulators (TIs) and superconductors (TSCs) [HK10] ultimately owes its topological character to Berry phases associated to the special band structure of these exotic materials.

1.1.2 Topological Band theory: Berry curvature and Chern number

Describing the state of a many-body system in quantum mechanics is an outstanding problem, as the dimension of the Hilbert space grows exponentially with the number of particles N. This is the reason why the Nobel-prize winner Richard Feynman proposed to use a tuneable auxiliary quantum system as a quantum simulator [Fey82].

Despite the great difficulty in solving these systems exactly, this becomes much easier for certain states of matter that can be described using the **band theory** of solids. Here, the energy distribution of electrons tend to group and concentrate over certain available regions (**bands**), while other energies are forbidden (**gaps**). The particular energy distribution of electrons is called **band structure**. The so-called band insulators can be effectively described assuming that electron interactions can be neglected. These systems have a gap between the last band of occupied states (*valence band*) and the first band of unoccupied states (*conduction band*). The **band topology** remains unchanged against perturbations such as particle-interactions that do not close the gap.

A second assumption is that the electron-system is **crystalline** and we can resort to translational invariance. Hence, we can write the Hamiltonian H in momentum space satisfying $H(\mathbf{k}) = H(\mathbf{k} + \mathbf{G})$, where $\mathbf{k}$ is the crystalline momentum, and $\mathbf{G}$

[10] If we choose a different phase for the eigenvectors $|n(\mathbf{R}(t))\rangle \longrightarrow e^{i\alpha(t)}|n(\mathbf{R}(t))\rangle$, the phase Φ_B remains invariant

[11] The Bloch sphere is a geometric and pictorial representation of the pure state space generated by $\{|\uparrow\rangle, |\downarrow\rangle\}$ of a spin 1/2 particle.

is a reciprocal lattice vector [AM76]. The eigenstates also depend on $\mathbf{k}$ and follow Bloch's theorem $|\Psi_n(\mathbf{k})\rangle = e^{i\mathbf{k}\cdot\mathbf{r}}|n(\mathbf{k})\rangle$, where $|n(\mathbf{k})\rangle$ is a cell-periodic eigenstate of $H(\mathbf{k})$. The crystalline momentum $\mathbf{k}$ in the Brillouin Zone (BZ) is equivalent to $\mathbf{k}+\mathbf{G}$, where $\mathbf{G}$ is a reciprocal lattice vector. Thus, the BZ is topologically equivalent to a torus T^d in d spatial dimensions.

The insulating band structure can be understood as a mapping between the BZ torus and the space of Bloch Hamiltonians $H(\mathbf{k})$ with a gap. A complementary tool for the study of SPT phases are the **winding numbers** characterising these mappings [WZ89, Nak03]. This will not be analysed in this section, but more information can be found in the references provided and in publications **P4**, **P5** and **P6**.

In 1989, Zak [Zak89] realised that the characteristic feature for the use of a Berry phase, is that the state of the system depends on a continuous parameter, such that when varied, the system describes a closed path. In band theory, the Berry phase arises very naturally since Bloch states are defined up to some arbitrary phase

$$|n(\mathbf{k})\rangle \quad \longrightarrow \quad e^{i\phi(\mathbf{k})}|n(\mathbf{k})\rangle, \tag{1.7}$$

where the role of the continuous periodic parameter is played by the crystalline momentum $\mathbf{k}$. Thus, we can identify a fiber bundle structure [Nak03]: 1) a manyfold of states defined by $|n(\mathbf{k})\rangle$ and 2) a $U(1)$ fiber associated to the gauge freedom of picking a global phase for the state at each $\mathbf{k}$ point.

From that mathematical point of view, we can construct a connection through a condition for parallel transport of the state $|n(\mathbf{k})\rangle$. A connection is a mathematical object that allows us to transport vectors along a curve and connect states $|n(\mathbf{k})\rangle$ at different momentum $\mathbf{k}$. The condition for Berry parallel transport states that the arbitrary phase $\phi(\mathbf{k})$ at each point should be chosen, such that the distance between $|n(\mathbf{k})\rangle$ and an infinitesimally close $|n(\mathbf{k}+d\mathbf{k})\rangle$ is minimal. This is equivalent to fixing $\langle n(\mathbf{k})||n(\mathbf{k}+d\mathbf{k})\rangle$ to be real. Thus, by Taylor expanding $e^{i\phi(\mathbf{k})}|n(\mathbf{k}+d\mathbf{k})\rangle$ in terms of $d\mathbf{k}$ we get

$$\langle n(\mathbf{k})|n(\mathbf{k}+d\mathbf{k})\rangle = e^{i\phi(\mathbf{k})}\Big[1+\langle n(\mathbf{k})|\nabla_{\mathbf{k}}n(\mathbf{k})\rangle d\mathbf{k} + i d\phi(\mathbf{k}) + O(d\mathbf{k})^2\Big]. \tag{1.8}$$

If we impose this quantity to be real up to first order in $d\mathbf{k}$, we get that the **Berry connection** is given by

$$\mathbf{A}^n_{\mathrm{B}}(\mathbf{k}) \equiv \frac{d\phi(\mathbf{k})}{d\mathbf{k}} = i\langle n(\mathbf{k})|\nabla_{\mathbf{k}}|n(\mathbf{k})\rangle. \tag{1.9}$$

By integrating along a closed loop C that covers the entire BZ we get the **Berry/Zak phase**

$$\Phi^n_{\mathrm{B}} = \oint_C \mathbf{A}^n_{\mathrm{B}}\, d\mathbf{k}. \tag{1.10}$$

Therefore, if we perturb the electron system by quenching $\mathbf{k}$ along the whole BZ, the system acquires a Berry phase Φ_{B}. Note that for the 1D case, the crystalline momentum $k \in (-\pi, \pi)$ is just an scalar, and Φ_{B} is given by a simple line integral.

In 1992, Resta [Res94] showed that the **electric polarisation** is related to the adiabatic charge transport in the system. Therefore, the polarisability can be expressed in terms of the Berry phase across the entire Brillouin Zone [XCN10]. Actually, for inversion invariant systems, the phase is quantised and can only take the values 0 or π depending of whether the system is in a topologically trivial or non-trivial SPT phase respectively. Actually, this is not the only effect linked to the Berry phase in condensed matter. In spatial dimensions higher than one, the topological Berry phase plays a fundamental role in the whole dynamics of Bloch electrons, giving rise to effects such as the quantum Hall conductivity [TKNTfd82], the magnetoelectric effect [QHZ08], etc. Some of these properties will be further analysed in the following sections.

Out of the Berry connection $\mathbf{A}^n_{\mathrm{B}}(\mathbf{k})$ in Eq. (1.9), we can define the associated **Berry curvature**

$$\mathbf{F}^n_{\mu\nu}(\mathbf{k}) = \nabla_{\mathbf{k}} \times \mathbf{A}^n_{\mathrm{B}}(\mathbf{k}). \tag{1.11}$$

In 2D, the integral of the Berry curvature over the BZ gives the so-called **Chern number**[12]

$$c_1 = \frac{1}{2\pi} \int_{\mathrm{BZ}} \mathbf{F}^n_{xy}(\mathbf{k}).d^2\mathbf{k}, \tag{1.12}$$

an integer number that signals whether the associated band structure is topologically non-trivial. A bit later, we will formulate the basic notions of Chern classes and establish why they become important on identifying the topological structure of real physical systems.

First of all, let us understand the relation between the Berry phase and the Chern number defined in Eq. (1.12). This will help us get an intuitive picture of it. By means of the Stokes' theorem, we can identify the Berry phase picked along the closed loop C enclosing the BZ [Eq. (1.10)], with the integral of the curvature over A (the area enclosed by C) [Eq. (1.12)] [Sim83]. As the BZ is a T^2 torus and has no boundary, the integral $\oint_C \mathbf{A}^n_{\mathrm{B}}(\mathbf{k})\, d\mathbf{k}$ would always give zero if $\mathbf{A}^n_{\mathrm{B}}(\mathbf{k})$ is well-defined along the entire BZ.

Is it then impossible to have a non-zero Chern number defined over a T^n (n-dimensional) torus?

The answer is linked to the impossibility of defining a unique vector potential (Berry connection) $\mathbf{A}^n_{\mathrm{B}}(\mathbf{k})$ over the entire BZ when the system lies within a topologically non-trivial phase. Therefore, we need at least two *patches* of $\mathbf{A}^n_{\mathrm{B}}(\mathbf{k})$ associated to different gauge choices of the wavefunctions

$$|n(\mathbf{k})\rangle' = \mathrm{e}^{-\mathrm{i}f(\mathbf{k})}|n(\mathbf{k})\rangle, \tag{1.13}$$

where $f(\mathbf{k})$ is a smooth function over the whole BZ. From this gauge transformation, the Berry connection gets also modified

$$\mathbf{A}^n_{\mathrm{B}}(\mathbf{k})' = \mathbf{A}^n_{\mathrm{B}}(\mathbf{k}) + \nabla_{\mathbf{k}} f(\mathbf{k}). \tag{1.14}$$

[12] Actually, this is strictly speaking the first Chen number, which is the only non-zero Chern class that characterises the fiber bundle in 2D [Nak03].

For simplicity, let us suppose a model where the connection is singular at a single point for a global gauge choice. In that case, two patches are enough to cover the BZ with smooth functions. Thus, we define a connection $\mathbf{A}_1(\mathbf{k})$ over a patch $\mathcal{P}_1$, and $\mathbf{A}_2(\mathbf{k})$ over a patch $\mathcal{P}_2$, where $\mathcal{P}_1 \cup \mathcal{P}_2 = BZ$, and the gauge choices are related by

$$\mathbf{A}_2(\mathbf{k}) = \mathbf{A}_1(\mathbf{k}) + \nabla_{\mathbf{k}} f(\mathbf{k}). \tag{1.15}$$

We can now take Eq. (1.12) and apply **Stokes' theorem**:

$$c_1 = \frac{1}{2\pi} \int_{\mathrm{BZ}} \mathbf{F}^n_{xy}(\mathbf{k}).d^2\mathbf{k} = \frac{1}{2\pi} \int_{\mathcal{P}_1} \nabla_{\mathbf{k}} \times \mathbf{A}_1(\mathbf{k}).d^2\mathbf{k} + \frac{1}{2\pi} \int_{\mathcal{P}_2} \nabla_{\mathbf{k}} \times \mathbf{A}_2(\mathbf{k}).d^2\mathbf{k} = \frac{1}{2\pi} \int_{\partial\mathcal{P}_1} \mathbf{A}_1(\mathbf{k}).d\mathbf{k} + \frac{1}{2\pi} \int_{\partial\mathcal{P}_2} \mathbf{A}_2(\mathbf{k}).d\mathbf{k}. \tag{1.16}$$

The BZ torus has no boundary $\partial T^2_{BZ} = 0$, thus $\partial\mathcal{P}_1 = -\partial\mathcal{P}_2$. Therefore, using Eq. (1.15), we can simplify the Eq. (1.17) even further,

$$c_1 = \frac{1}{2\pi} \int_{\partial\mathcal{P}_2} \Big(\mathbf{A}_2(\mathbf{k}) - \mathbf{A}_1(\mathbf{k})\Big).d\mathbf{k} = \frac{1}{2\pi} \int_{\partial\mathcal{P}_2} \nabla_{\mathbf{k}} f(\mathbf{k}).d\mathbf{k} = n. \tag{1.17}$$

where n is an integer number. The last equality comes from the fact that $|n(\mathbf{k})\rangle$ has to be single valued. Therefore, the winding of the function $f(\mathbf{k})$ along the contour $\partial\mathcal{P}_2$ has to be an integer. Note that by performing a gauge transformation of the wavefunction, we can change the integer if we compute c_1 using the Berry phase formula.This comes from the fact that Φ_B is gauge invariant mod 2π. Therefore, it is generally more convenient to compute the Chern number through the curvature [DMMD14] using Eq. (1.12).

Within this framework, we can now introduce the theory of **Chern classes**. In general, the theory of characteristic classes studies the classification of fiber bundles. A **principal fiber bundle** $\mathcal{P}(\mathcal{M}, \mathcal{F})$, over a base space $\mathcal{M}$ with a typical fiber $\mathcal{F}$ is defined as follows. We consider a total space $\mathcal{E}$ which is a differential manifold, that is projected onto the base space $\mathcal{M}$ according to a surjection[13] $\pi : \mathcal{E} \to \mathcal{M}$, that is called the projection. The inverse image $\pi^{-1}(p) \equiv \mathcal{F}_p$ is called the fiber at $p \in \mathcal{M}$. The fibers $\mathcal{F}_p$ are diffeomorphic to a Lie group called the typical fiber $\mathcal{F} \cong \mathcal{F}_p$.

Interestingly, this is the precise structure that we have introduced when computing the Berry phase. Any quantum mechanical state $|n(\mathbf{k})\rangle \in \mathcal{E}$ belongs to the total Hilbert space $\mathcal{E}$, over which we define a principal fiber bundle $\mathcal{P}(\mathcal{M}, U(1))$. At each point $\mathbf{k}$ of the BZ torus T^n, we can identify a projector $|n(\mathbf{k})\rangle\langle n(\mathbf{k})| \in \mathcal{M}$. The space of projectors (idempotent matrices of trace one) $\mathcal{M}$ represents the base space

[13] A function $f : X \to Y$ is surjective, if every element $y \in Y$ has a corresponding element $x \in X$ such that $f(x) = y$. It is not necessary that x is unique; the function f may map one or more elements of X to the same element from Y.

on which the fiber bundle is built. The quantum state $|n(\mathbf{k})\rangle$ belongs to a $U(1)$ fiber which represents the equivalence class of states $[|n(\mathbf{k})\rangle]$ up to a global phase. Finally, the projection $\pi : \mathcal{E} \to \mathcal{M}$ is defined as $\pi\ g|n(\mathbf{k})\rangle = |n(\mathbf{k})\rangle\langle n(\mathbf{k})|$ where $g \in U(1)$. We have mapped our quantum mechanical problem to a fiber bundle structure and we can now introduce the idea of a Chern class.

Roughly speaking, a characteristic class measures the "twisting" of a principal fibre bundle, and this generates a classification. In summary, a principal fibre bundle $\mathcal{P}(\mathcal{M}, \mathcal{F})$, based on $\mathcal{M}$ with a typical fibre $\mathcal{F}$, can be imagined as a *patchwork*. The topology of the fibre bundle is characterized by the number *patches* that we have to use in order to obtain a well-defined connection over the whole base space $\mathcal{M}$. In particular, if a single connection $\mathbf{A}(\mathbf{k})$ can be defined over the whole base space, then the fiber bundle is trivial. It is therefore intuitive that characteristic classes can generally be expressed in terms of the local connection form A or curvature form F. The **Chern character** is defined as

$$c(F) = \mathrm{Tr}\Big[\exp\ \frac{F}{2\pi}\ \Big] = \frac{dim(\mathcal{M})}{2} + \sum_{j=1} c_j(F), \tag{1.18}$$

where $F = \frac{1}{2}\ \mathbf{F}_{\mu\nu}\ dk^\mu\ \wedge\ dk^\nu$ is the curvature 2-form, and $c_j(F)$ is called the $j-$th Chern character. The integral of $c_j(F)$ over the base space $\mathcal{M}$ is the $j-$th **Chern number**. By considering a $U(1)$ bundle over $\mathcal{M} = T^2$, the only non-zero Chern number is c_1 as given in Eq. (1.12).

The appearance of non-abelian gauge structures in simple quantum mechanical systems was first consider by Wilczek and Zee [WZ84]. Since then, principal fiber bundles associated to non-abelian Lie groups like $SU(n)$ have been extensively studied for their application to real physical situations. In particular, optical lattice simulation of non-abelian gauge fields have been proposed [MBG+12]. They consider non-abelian Lie groups instead of the simplest $U(1)$ case.

1.1.3 Quantum Hall conductivity & Topological edge states

By means of linear response theory, it is possible to prove the relation between the Chern number and the transverse Hall conductivity as originally carried out by Thouless, Kohmoto, Nightingale, and den Nijs in the so-called **TKNN formula** [TKNTfd82]. This is one of the main physical consequence of a system with a topologically non-trivial band structure. A detailed derivation of this formula,

$$\sigma_{xy} = \frac{e^2}{h} c_1, \tag{1.19}$$

can be found in [Gol09, TKNTfd82] based on the so-called Kubo formula[14]. At the same time, Streda also arrived to the quantization of the transverse conductivity

[14]The Kubo formula is an equation based on the linear response of an observable quantity to a time-dependent perturbation, applied to the system.

using linear response theory [Str82].

In this subsection however, we only want to give an intuitive argument proposed by Laughlin [Lau81] to understand why we get quantised charge transfer in the perpendicular direction due to filled Landau levels, and link this to the existence of gapless edge states at the boundary of the system.

We consider a 2D material that is traversed by a magnetic field perpendicular to the plane. Now let us take periodic boundary conditions along the $y-$direction, so the crystalline momentum k_y is a good quantum number. The material will look like a cylinder, with the axis pointing in the $x-$direction. By inserting a magnetic flux $\Delta\phi$ threading the cylinder along x, we generate a current along the wrapped $y-$direction. Note that the direction of this flux is different from the one generated by the magnetic field of the system (radial direction). Following Laughlin's calculations, for each quantum flux $\Delta\phi_0 = h/e$ threading the system, one electron per Landau level is transferred from one edge to the other. If there are n filled Landau levels, n electrons will move, so the total energy transfer is given by

$$\Delta E = n.e.V_x, \tag{1.20}$$

where V_x is the potential difference across the cylinder. On the other hand, the current along the $y-$direction $j_y = \frac{\partial H}{\partial k_y} = \frac{L_y}{2\pi}\frac{\partial H}{\partial \phi}$, where L_y is the length of the circumference of the cylinder. This is so, since the magnetic flux $\Delta\phi$ shifts $k_y \rightarrow k_y + \frac{2\pi\phi}{L_y}$. By taking the expectation value of j_y on the ground state and discretising the formula for j_y, we get that the intensity $I_y = \frac{\Delta E}{\Delta\phi}$. Thus, for each fundamental quantum flux $\Delta\phi_0 = h/e$ we get that the intensity

$$I_y^0 = n\frac{e^2}{h}V_x, \tag{1.21}$$

where we have used Eq. (1.20). Finally, the transverse conductivity can be written as

$$\sigma_{xy} = \frac{I_y^0}{V_x} = n\frac{e^2}{h}, \tag{1.22}$$

where the integer n stands for the number of filled Landau levels.

Additionally, Laughlin argued that the presence of **gapless edge modes** is an inevitable consequence of quantised transverse conductivity in an insulator. The argument works as follows. We know that: (a) the Hall conductivity σ_{xy} is an integer and (b) σ_{xy} cannot change unless the bulk gap closes and reopen again. Therefore, we conclude that the boundary region connecting two insulators with different Hall conductance (for instance a topological insulator and the vacuum) must have a point where the gap closes and opens again. This is equivalent to having an edge mode that crosses the Fermi level. Otherwise the whole space would be gapped, which means that the Hall conductivity should be the same everywhere. In Fig. 1.1 we have depicted a typical energy spectrum of a topological

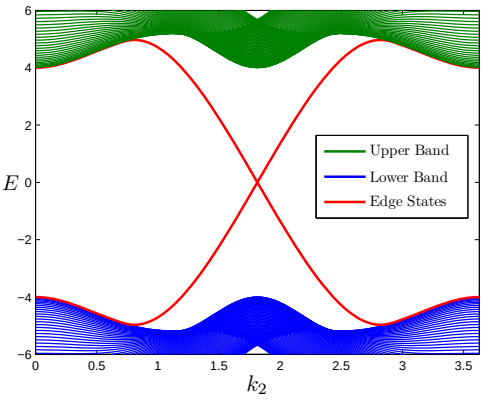

FIGURE 1.1: Energy bands of a topological insulator as a function of momentum in one direction k_2. The red lines correspond to conducting edge state modes. The Fermi energy has been placed at the middle point of the two bands.

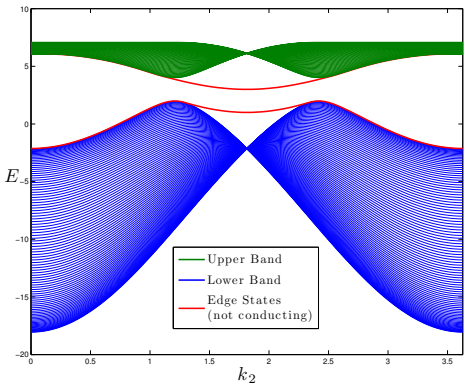

FIGURE 1.2: Energy bands for a trivial insulator as a function of momentum in one direction k_2. The red lines correspond to non-conducting and non-topological edge modes. The transverse Hall conductivity is equal to zero.

insulator. We can see two edge modes crossing the Fermi level from the upper band to the lower band and viceversa. Close to $k = 0$, the energy of the edge states can be linearised as if they were "massless" Dirac fermions. It is essential that the edge states connect the upper and lower bands. A careful analysis of these current-carrying edge states was performed by Halperin [Hal82], studying the robustness of these states in the presence of weak disorder.

On the contrary, in Fig. 1.2 we show the energy dispersion relation for a trivial insulator with edge states. The transverse Hall conductivity is equal to zero, and the edge modes are non-topological. They can be absorbed into the bulk by smooth Hamiltonian deformations.

The study of the fate of edge states when coupled to a thermal reservoir is one the central points studied in publications **P2** and **P3**.

1.2 Intrinsic topological order

In symmetry-protected topological order (SPTO), we have seen that topology is manifested in the physics of the boundary. Inside the bulk, the band structure is similar to the one of a regular insulator [see Fig. (1.1)] and the system is short-range entangled. On the contrary, **Intrinsic Topological Order (ITO)** is a state of matter that is fully topological in the bulk. It has a degenerate ground state and the quasiparticle excitations are anyons with exotic particle statistics [ASW84, Kit03]. Unlike SPT phases, ITO states display long-range entanglement [KP06, LW06, CGW10].

The easiest way to understand this exotic phase, is to focus on a particular

example and review the properties to see how they arise from scratch.

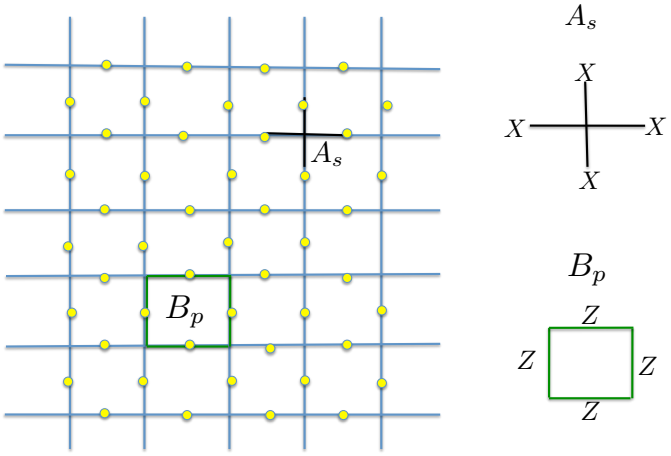

Figure 1.3: Square lattice on the torus. The yellow points represent spins.

1.2.1 Toric Code

The toric code [Kit03] is an exactly solvable model with ITO, originally proposed by Kitaev. It was initially proposed with the idea of performing **fault-tolerant quantum computation**[15]. It turns out that topology provides a very natural scheme to support large error rates on the system, due to the intrinsic robustness of topological properties.

First of all, let us introduce the model and analyse all the elements that defines an intrinsic topological phase. We consider a $k \times k$ square lattice embedded in a T^2-**torus**. At each edge of the lattice, we attach a spin $1/2$, so the total number of spins[16] is $N = 2k^2$. See Fig. 1.3 for a pictorial image. In order to define the interactions between the spins, we construct a particular set of operators A_s and B_p. For each vertex s and each face p,

$$A_s := \prod_{j \in \text{star}(s)} X_j, \qquad B_p := \prod_{j \in \text{boundary}(p)} Z_j, \tag{1.23}$$

where X_j and Z_j are the Pauli matrices acting on the spin at site j. The set of operators A_s and B_p commute with each other since they have either 0 or 2 common edges (see Fig. 1.3). They are also Hermitian and have eigenvalues 1 and -1. Therefore, they constitute an abelian subgroup of the Pauli group of n qubits, named **stabilizer group**.

[15] **Fault-tolerant** means that quantum computation can be done for an arbitrarily long-time, provided that the error rate in the system lies bellow a certain threshold.

[16] Sometimes we refer to spins $1/2$ as **qubits**, since they define two-level systems like the ones for quantum information processing.

Let $\mathcal{H}$ be the Hilbert space of all $n = 2k^2$ qubits. We denote the topological quantum code $\mathcal{C} \subseteq \mathcal{H}$,

$$\mathcal{C} = \Big\{ |\Psi\rangle \in \mathcal{H} : \ A_s|\Psi\rangle = |\Psi\rangle, \ B_p|\Psi\rangle = |\Psi\rangle \text{ for all } s, p \Big\}. \tag{1.24}$$

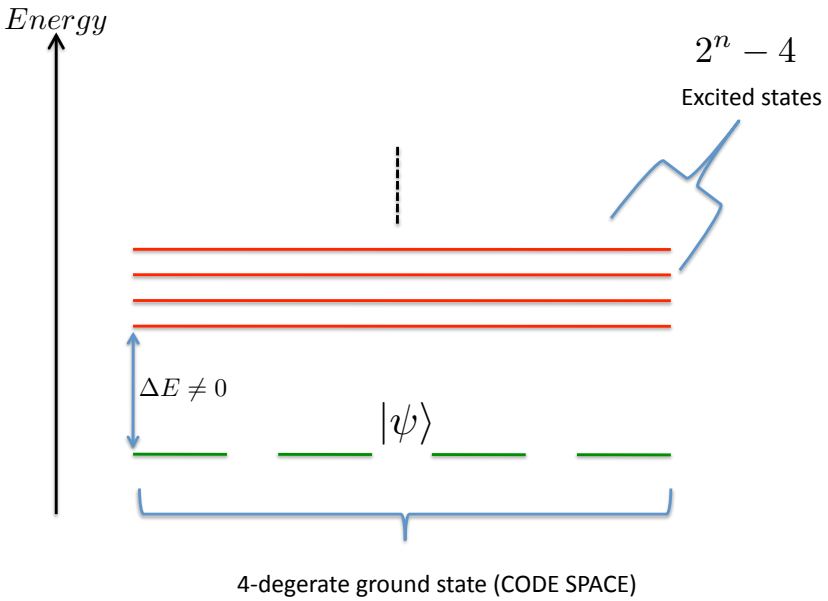

FIGURE 1.4: Schematical spectrum of the Toric Code Hamiltonian. The ground state is the code space $\mathcal{C}$ where we codify our information.

This quantum code is called the **toric code**, and defines the possible states $|\Psi\rangle$ where we can encode and perform protected quantum computation. The operators A_s, B_p are called the **stabilizer operators** of this code, since they leave invariant the code space when acting on it.

So far, we have made a purely mathematical description of a quantum code. In order to set and analyse the physical grounds of the model, we need to construct a Hamiltonian,

$$H^{\text{sys}} := -\sum_s A_s - \sum_p B_p. \tag{1.25}$$

A full diagonalization of this Hamiltonian is possible since operators A_s and B_p commute. In particular, the **ground state** coincides with the protected subspace of the code $\mathcal{C}$. It can be easily checked that the system is **4-fold** degenerate and the excited states are separated by an energy gap $\Delta E \geq 4$ (see figure 1.4). The **ground state degeneracy** d comes from the constraints $\prod_s A_s = 1$ and $\prod_p B_p = 1$, and can be linked to purely topological properties like the genus g (number of holes) of the torus, $d = 2g$. From the point of view of quantum computation, **2 logical qubits** can be codified into the ground state subspace.

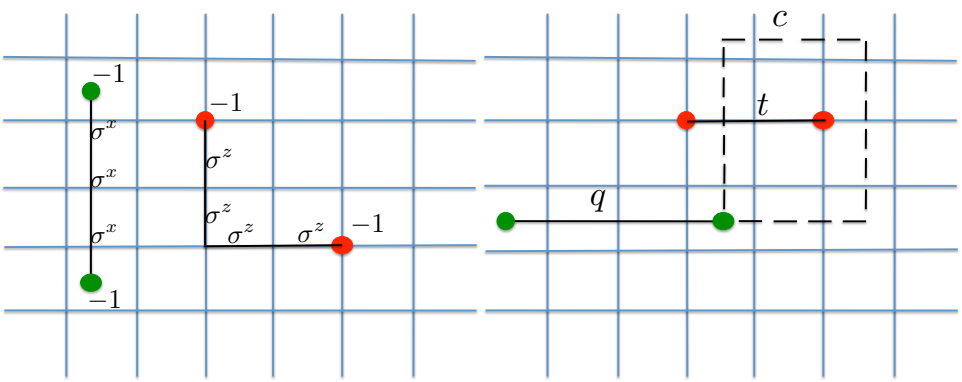

FIGURE 1.5: Anyonic excitations of the model. (a) The end points of the strings correspond to either A_s or B_p plaquette violations, as noted in Eq. (1.26). (b) An anyon of type X (green) moves around an anyon of type Z (red), along path c.

On the other hand, **excitations** come in pairs since they correspond to violations of the plaquette and/or vertex stabilizer operators,

$$A_s|\Psi\rangle_e = -|\Psi\rangle_e, \qquad B_p|\Psi\rangle_e = -|\Psi\rangle_e, \tag{1.26}$$

for a certain number of sites s and/or plaquettes p, and these must comply with the overall constraints $\prod_s A_s = 1$ and $\prod_p B_p = 1$. Thus, excitations are represented by **open strings** on the square lattice [see Fig.1.5(a)] and behave as **anyons**. They are produced by acting with Z_j (*'electric'*) or X_j (*'magnetic'*) Pauli operators onto the ground state subspace, $X_j|\Psi\rangle$ or $Z_{j'}|\Psi\rangle$.

These excitations satisfy anyonic statistics under **braiding** of different anyon types. In Fig.1.5(b) we picture a braiding of an X_j excitation (plaquette violation) around a Z_j excitation (vertex violation) along path c. The movement is induced by the application of Pauli operators on adjacent sites along c. After the braiding is complete, the total wavefunction picks up a $e^{i\pi}$ phase. This process is equivalent to exchanging these particles twice. For bosons or fermions, no phase is picked by the wavefunction after this double exchange of particle excitations is completed, whereas for anyons we have seen that a $e^{i\pi}$ is gained.

We would also like to stress that the toric codes are not the only family of quantum codes that yields topological protection. The most notable instances of topological codes with remarkable properties are on the one hand the **surface codes** [GFG12, FMMC12], and on the other hand the **color codes** [BMD06, BMD07]. Color codes have some important differences with respect to surface codes, namely: (1) they perform quantum computation using only transversal gates, (2) they codify twice as much logical qubits than toric codes giving a certain topology, and (3) they allow for Clifford [NC00] and universal gates depending on the dimension.

An essential feature of Hamiltonian (1.25) is its locality in terms of **four-body interactions**. This is indeed very useful for practical purposes. Another key property is that the Hamiltonian is gapped, which leeds to the initial expectation that

all type of 'errors', i.e. noise-induced excitations will be removed automatically by some relaxation processes. Moreover, it can be shown that this Hamiltonian is robust under local quantum perturbations at zero temperature [BT09]: there would be a level splitting which will vanish as $\exp(-ak)$, where k is the length of the lattice [Kit03].

More generally, one is interested in designing a **stable quantum memory**, i.e. a $N-$particle system which can support at least a single encoded logical qubit for a long time, preferably with this time growing exponentially with N. In Ref. [AFH09], Alicki *et al.* provide a rigorous method to prove thermal instability of the 2D Kitaev model. They derived a master equation that describes the dynamics of the system weakly coupled to a thermal environment.

In publication **P1** we generalise the **Kitaev toric code for qudits** ($d-$dimensional systems), and study the problem of thermal instability within the framework of topological orders to see what novelties we do get by increasing the dimensionality of the spins.

1.2.2 Symmetry-enriched topological order (SETO)

Very recently, a new type of topological order has been studied [LW05, LG12, MR13, EH13], called symmetry-enriched topological order (**SETO**).

Let us consider a system with ITO that is additionally invariant under a certain global symmetry G, as it is the case for SPT phases. The presence of this global symmetry induces **charge fractionalisation** of the anyons. This was shown by Levin and Gu [LG12] for the double semion model (DSM) with a global on-site spin-flip symmetry $G = Z_2$. The DSM is an example of a SETO with excitations that have self-anyonic statistics (unlike the toric code [Kit03] where excitations only behave like anyons under braiding with anyons of different type). In addition, Essin and Hermele [EH13] proposed the **string-flux mechanism** as a method to produce charge fractionalisation of an ITO that is invariant under a certain lattice global symmetry. Actually, it is possible to combine both mechanisms together as it was shown in [OMD16]. These SETO phases also posses protected boundary modes because of the protecting global symmetry G.

Thanks to these works, the mechanism for charge fractionalisation in the FQHE for the Laughlin state with filling factor $\mu = 1/n$, where n is an integer, has been clearly understood. Due to the existence of an ITO with global symmetry $G = U(1)$ (charge conservation), the quasiparticle excitations of the model are Abelian anyons with fractional charge $q = e/n$, where e is the electron electric charge.

Nowadays, SETO constitute an emerging area within the field of topological orders, that will surely produce many novelties in the upcoming years.

2

Introduction to Open Quantum Systems

Since the initial development of quantum theory, it was soon noticed that many of the fascinating properties of quantum mechanics are lost when observing macroscopic objects in nature. The reason behind that fact is the difficulty to isolate quantum systems, that have to be understood as an open system that interacts with an uncontrolled environment [LCD+87, BP07, RH11, CG04, DW08]. In many cases, when a set of particles whose dynamics are governed by quantum mechanics is coupled and interacts with a thermal environment, many quantum properties such as superposition or entanglement [Bal98, GP90] are diminished and eventually vanished.

It is inevitable to consider our quantum system coupled to an environment in order to have a theory that captures those effects. One may even wonder whether it would be possible to have a detailed microscopic description of both the system and environment, so that the quantum theory for closed systems would be enough. Many times this is impossible for two reasons. Firstly, for that statement to be fully correct, we would need the know the specific interaction of our system with the rest of the universe. Even if we restrict ourselves to the most relevant degrees of freedom of the environment, it is not always possible to have a complete microscopic description of the interaction between system and environment. Hence, an effective and probabilistic description is mandatory.

Some other times, a microscopic description of both the system (S) and environment (E) is well known. However, the amount of information that we need to process may be extremely large and intractable, since the environment may have

infinite degrees of freedom or may have a very complicate structure. Therefore, it is very convenient to trace out the degrees of freedom of the environment and to focus on the effective dynamics acting on our system. This idea is depicted in Fig. 2.1.

In the following section, we follow this approach and give a microscopic derivation of the dynamical equations that describe the evolution of an open quantum system. These techniques will be key for the understanding and computation of the many results that are presented along this thesis.

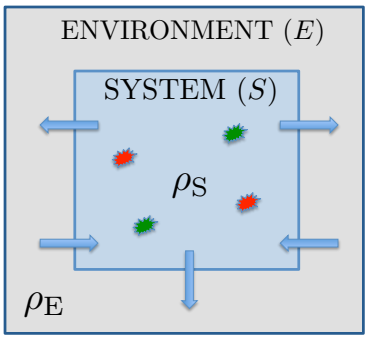

FIGURE 2.1: General situation where a quantum system S interacts with an external environment E. The state of the system ρ_S is affected by the surrounding environment that influences its dynamics, which are no-longer unitary.

2.1 Weak coupling limit

Let us trace out the environmental degrees of freedom and restrict ourselves to the system dynamics. Even in that case, the solution of equations describing the system can be computationally very hard to obtain. Fortunately, it can be sometimes assumed that the our system is moderately well-isolated from the environment and that the coupling between the system and the environment is sufficiently weak. These conditions allow us to derive an effective dynamical equation by using the following reasoning. The total Hamiltonian can be split into three terms

$$H = H_S + H_E + H_I, \tag{2.1}$$

where H_S and H_E are the Hamiltonian of the free system (S) and environment (E) respectively, and the interaction between the two is given by H_I. The state ρ of both system and environment follows the Liouville-von Neumann equation

$$\frac{d}{dt}\rho = -i[H, \rho]. \tag{2.2}$$

It is convenient to perform the derivation in the interaction picture. Hence, we apply the following transformation $\rho_I = U(t)\rho U^\dagger(t)$ and $H_I(t) = U^\dagger(t)H_I U(t)$,

where $U(t) = \mathrm{e}^{-\mathrm{i}(H_S+H_E)t}$. Note that now the interaction Hamiltonian $H_I(t)$ is time-dependent. Inserting these transformations into Eq. (2.2) we get

$$\frac{d}{dt}\rho_I = -\mathrm{i}[H_I(t), \rho_I]. \tag{2.3}$$

We can now formally integrate Eq. (2.3) obtaining

$$\rho_I(t) = \rho_I(0) - \mathrm{i} \int_0^t ds[H_I(s), \rho_I(s)]. \tag{2.4}$$

If we insert this equation into Eq.(2.3) and trace over the environment degrees of freedom, we arrive to the following expression

$$\frac{d}{dt}\rho_S(t) = - \int_0^t ds \mathrm{Tr}_E\{[H_I(t), [H_I(s), \rho_I(s)]]\}, \tag{2.5}$$

where we have used $\rho_S \equiv \mathrm{Tr}_E\{\rho_I\}$ and assumed that the interaction does not generate first order dynamics in the bath, more precisely

$$\mathrm{Tr}_E\{[H_I(t), \rho_I(0)]\} = 0. \tag{2.6}$$

The mean value of the interaction acting on the initial state of the environment equals to zero. Note that Eq.(2.5) still contains the density matrix of both S and E on the right hand side. In order to simplify the equation further, we need to perform a series of approximations. The first one is called the *Born approximation*. This states that the coupling between the system and the environment is sufficiently weak, so the system barely affects the environment. Therefore, we can approximate the state of the joint system at each time t by a tensor product of S and E,

$$\rho_I(t) \approx \rho_S(t) \otimes \rho_E. \tag{2.7}$$

This is justified because of the factorised initial condition $\rho(0) = \rho_S(0) \otimes \rho_E(0)$, and the perturbative approach from the weak coupling limit. However, Eq. (2.7) should be considered as an ansatz to arrive at the correct equation rather than a physical requirement on the evolution [RH11]. If we plug Eq. (2.7) in Eq. (2.5), we obtain

$$\frac{d}{dt}\rho_S(t) = - \int_0^t ds \mathrm{Tr}_E\{[H_I(t), [H_I(s), \rho_S(s) \otimes \rho_E]]\}, \tag{2.8}$$

The second approximation to be performed is called the *Markov approximation*. The state $\rho_S(s)$ that appears in the integrand of Eq. (2.9), is replaced by $\rho_S(t)$,

$$\frac{d}{dt}\rho_S(t) = - \int_0^t ds \mathrm{Tr}_E\{[H_I(t), [H_I(s), \rho_S(t) \otimes \rho_E]]\}. \tag{2.9}$$

This equation is called the Redfield equation [BP07] and is local in time. That means, that the evolution of $\rho_S(t)$ at time t only depends on the value of the state

at that very same time. However, the equation still depends on a particular choice of the initial time ($t = 0$) and therefore it is not yet described by a **dynamical semigroup**. The motivation to look for a dynamical semigroup structure comes from its simplicity, good characterisation and natural properties regarding the system evolution. A dynamical semigroup is a family of quantum maps T_t onto the space of density matrix ρ. The maps have to be completely positive CP and they usually depend on one parameter (time t). They satisfy the semigroup property $T_s T_t = T_{s+t}$. Moreover, the generators of the group are the so-called *Lindblad Superoperators* $\mathcal{L}$, and the semigroup elements can be written as

$$T_t = \mathrm{e}^{\mathcal{L}t}, \tag{2.10}$$

so that by applying the operator to a system density matrix ρ_S and differentiating the equation, the quantum evolution is given by

$$\frac{d}{dt}\rho_S(t) = \mathcal{L}\rho_S(t). \tag{2.11}$$

Hence, with the purpose of obtaining a final equation in the form of Eq. (2.11), we perform a change of variables s by $t - s$ for the integral in Eq. (2.9), and extend the integral to infinity. This can be justified as long as the integrand goes to zero fast enough for $s \gg \tau_E$, where τ_E is the time scale at which correlation functions of environment decay. Equivalently, the approximation is justified if the time-scale at which the system appreciably varies τ_S is large compared to τ_E. The Markovian master equation finally takes this form

$$\frac{d}{dt}\rho_S(t) = -\int_0^\infty ds \mathrm{Tr}_E\{[H_I(t), [H_I(t-s), \rho_S(s) \otimes \rho_E]]\}. \tag{2.12}$$

As we have pointed out before, this equation only makes sense for time-resolutions that are larger than τ_E. In addition, this master equation may not define the generator of a dynamical semigroup [Dav74]. To this end, it is usually performed what is called the *secular or rotating wave approximation RWA*, which basically means averaging over rapid oscillatory terms in Eq. (2.12).

To understand this part, let us first analyse the structure of the interacting Hamiltonian H_I. The most general form of H_I can be written as a sum of operators A acting on the system and operators B acting on the environment,

$$H_I = \sum_\alpha A_\alpha \otimes B_\alpha, \tag{2.13}$$

where A_α and B_α are hermitian. Let us decompose further the interaction into eigenoperators of the system Hamiltonian H_S,

$$A_\alpha(\omega) \equiv \sum_{\epsilon' - \epsilon = \omega} \Pi(\epsilon) A_\alpha \Pi(\epsilon'), \tag{2.14}$$

where $\Pi(\epsilon)$ projects onto the eigenspace defined by the system eigenvalue ϵ of H_S. The sum is extended to all energies ϵ and ϵ'. Because of the form of Eq. (2.14), the following commutation relations are satisfied:

$$\begin{aligned}[H_S, A_\alpha(\omega)] &= -\omega A_\alpha(\omega), \\ [H_S, A_\alpha^\dagger(\omega)] &= +\omega A_\alpha^\dagger(\omega).\end{aligned} \tag{2.15}$$

Thus, the operators $A_\alpha^\dagger(\omega)$ and $A_\alpha(\omega)$ are eigenoperators of H_S with frequencies $\pm\omega$ respectively, and they straightforwardly satisfy that $A_\alpha^\dagger(\omega) = A_\alpha(-\omega)$. In addition they also follow a completeness relation $\sum_\alpha A_\alpha(\omega) = A_\alpha$. Therefore, the interaction Hamiltonian H_I can be written as follows

$$H_I = \sum_{\alpha,\omega} A_\alpha(\omega) \otimes B_\alpha. \tag{2.16}$$

But we are interested in computing H_I in the interaction picture, where $H_I(t) = U^\dagger(t) H_I U(t)$ with $U(t) = e^{-i(H_S+H_E)t}$. Thus, using the commutation relations in Eq. (2.15) and doing some algebra, we get

$$H_I(t) = \sum_{\alpha,\omega} e^{-i\omega t} A_\alpha(\omega) \otimes B_\alpha(t), \tag{2.17}$$

where $B_\alpha(t) = e^{iH_E t} B_\alpha e^{-iH_E t}$. From this, we can understand one of the implications of Eq. (2.6),

$$\langle B_\alpha(t) \rangle_E \equiv \mathrm{Tr}\{B_\alpha(t)\rho_E\} = 0, \tag{2.18}$$

which means that the environment average of $B_\alpha(t)$ is zero. Now, if we substitute Eq. (2.17) into Eq. (2.12), we can simplify the master equation[1]

$$\begin{aligned}\frac{d}{dt}\rho_S(t) = &\int_0^\infty ds \mathrm{Tr}_E\{H_I(t-s)\rho_S(s)\otimes\rho_E H_I(t) - H_I(t)H_I(t-s)\rho_S(s)\otimes\rho_E\} + \text{h.c.} = \\ &= \sum_{\omega,\omega'}\sum_{\alpha,\beta} e^{i(\omega-\omega')t}\Gamma_{\alpha\beta}(\omega)\left(A_\beta(\omega)\rho_S(t)A_\alpha^\dagger(\omega') - A_\alpha^\dagger(\omega')A_\alpha(\omega)\rho_S(t)\right) + \text{h.c.}\end{aligned} \tag{2.19}$$

where $\Gamma_{\alpha\beta}(\omega) \equiv \int_0^\infty ds e^{i\omega s}\langle B_\alpha^\dagger(t) B_\alpha(t-s)\rangle_E$. The most general form of this expression is time-dependent, however if ρ_E conmutes with H_E then it does not depend on time. This is actually the case for the states studied in publications **P1** and **P2**, where the environment is given by a thermal bath, and hence $\rho_E = \frac{e^{H_E/T}}{Z}$ where Z is the partition function.

Let us now perform the final approximation. We define τ_S as the typical time scale related to the system free evolution

$$\tau_S \sim \frac{1}{|\omega - \omega'|}, \tag{2.20}$$

[1] h.c. is the abbreviation for *hermitic conjugate*

for $\omega = \omega'$ typical frequency differences involved. If the relaxation time of the open-system τ_R is large compared to τ_S, then we can neglect terms in Eq. (2.19) that oscillates with frequency differences such that $\omega = \omega'$. This is so, since for a time τ_S when the system will appreciably vary, these terms would have oscillated many times averaging to zero. In quantum optics this is in general well justified and it is called the rotating-wave approximation (RWA). In condensed matter it usually depends, but we can always rely on the weak coupling limit. Roughly speaking, the argument works as follows. If we redefine the interacting Hamiltonian as $H_I \to \alpha H_I$, then if $\alpha \to 0$, the interaction between the system and environment would be very weak and the relaxation time τ_R would be very large. A detailed proof of this argument can be found in [RH11]. Actually, a necessary condition for the weak coupling limit to exist is that the environment E has infinite degrees of freedom. Moreover, a sufficient conditioned was given by Davies [Dav74] and it is related to whether correlation functions in the bath decay sufficiently fast [Dav76].

Returning to the derivation of the master equation, we neglect the fast oscillating terms in Eq. (2.19) obtaining

$$\frac{d}{dt}\rho_S(t) = \sum_{\omega}\sum_{\alpha,\beta}\Gamma_{\alpha\beta}(\omega)\big(A_\beta(\omega)\rho_S(t)A_\alpha^\dagger(\omega) - A_\alpha^\dagger(\omega)A_\alpha(\omega)\rho_S(t)\big) + \text{h.c.} \tag{2.21}$$

It is useful to decompose the environment correlation functions $\Gamma_{\alpha\beta}$ into its real and imaginary parts

$$\Gamma_{\alpha\beta}(\omega) = \frac{1}{2}\gamma_{\alpha\beta}(\omega) + iS_{\alpha\beta}(\omega). \tag{2.22}$$

Using this last equation, we finally arrive to the final form for the master equation,

$$\frac{d}{dt}\rho_S(t) = -i[H_L, \rho_S(t)] + \mathcal{D}\big(\rho_S(t)\big) \tag{2.23}$$

where

$$H_L = \sum_{\omega}\sum_{\alpha,\beta} S_{\alpha\beta}(\omega)A_\alpha^\dagger(\omega)A_\alpha(\omega), \tag{2.24}$$

and

$$\mathcal{D}\big(\rho_S(t)\big) = \sum_{\omega}\sum_{\alpha,\beta}\gamma_{\alpha\beta}(\omega)\ \ A_\beta(\omega)\rho_S(t)A_\alpha^\dagger(\omega) - \frac{1}{2}\{A_\alpha^\dagger(\omega)A_\alpha(\omega)\rho_S(t)\}\ \ . \tag{2.25}$$

The Hamiltonian H_L renormalises the unperturbed energies of H_S due to the coupling between system and environment. From Eqs. (2.15), it follows that $[H_L, H_S] = 0$. The piece given by $\mathcal{D}\big(\rho_S(t)\big)$ is often called **dissipator** and it is the one that accounts for the non-unitary dynamics of the system. Eventually, Eq. (2.23) can be brought into a diagonal form (Lindblad form [Lin76]) by diagonalising the $\gamma_{\alpha\beta}$ matrix.

At this stage, we can identify the form of Eqs. (2.23), (2.24) and (2.25) with the master equations that we derive in publications **P1**, **P2** and **P3** when we try

to understand how the topological properties of our systems change due to the coupling with the environment. Actually in publication **P3**, the very definition of topological properties like the Chern number or the edge states have been studied based on master equations of the form of Eq. (2.23).

Let us make some final comments regarding the applicability of these results. The general approach of the derivation and the standard literature of master equations deals with an environment that is usually uncontrollable and external to the system. Remarkably, thanks to our better understanding of the quantum world and the possibility to control single atoms and photons, we can sometimes construct and design environments that drive the system into a particular state of matter that might be of interest to us and that would be otherwise difficult to prepare by other means [VWIC09, BMS+11, MDP+12].

On the other hand, the theory of open quantum systems has historically been used in the context of quantum optics and few-body physics [RPHP10]. More recently and due to the quick development of quantum simulators, the theory open quantum systems has found applicability in quantum many-body systems [LGL13] and condensed matter [SKCG12, KGI+12].

Within the same spirit, the main goal of this part of the thesis has been to extend the notion of topological orders (well understood at zero temperature and for pure states) to the realm of dissipative systems, governed by a master equation and that are generally described by a density matrix. In **P1** and **P2** we were mainly focused on the study of how topological properties such as the dynamics of anyons, robustness of edge states, etc, change by the coupling of the system to a thermal bath.

On the other hand, in **P3**, **P4**, **P5** we changed the perspective and we ask ourselves whether it is possible to extend the definition of a topological phase of matter for a system with dissipation or at finite temperature. Notably in publication **P9**, we give a protocol to measure a topological phase for an open system, where we assume full control of the environment. In the upcoming sections, the main results of those works will be described in detail.

Finally, in publication **P8** we have used several numerical methods to study **driven-dissipative phase transitions** described by a master equation like Eq. (2.23). This part will be discussed in the appendix section of this thesis.

3

1D Topological Insulator as an open quantum system

3.1 Motivation and background

In the previous section, we have introduced the concept of SPT order. As we have seen, these phases can be classified according to the protecting symmetry that the system preserves [Kit09, SRFL08, RSFL09]. Here, we will focus on a 1D model that has a band insulating phase with chiral symmetry. This topological insulator has a gapped band structure in the bulk characterised by an integer winding number or a topological Berry phase; while it displays zero-energy modes localised at the boundary. The model is called the **Creutz ladder**. In this chapter we try to answer the following question:

- *What happens to the topological properties of a topological insulator (e.g. edge states) when it is coupled to a thermal bath?*

This is a rather relevant question since most studies of topological order and topological phase transitions have focused on the purely quantum regime at zero temperature. There are however some notable exceptions [MRLC13, BMABD13, vNH14, SWY14, DOM15, HCBZ15, LGF16, CDBVN16, DOM14, LRF+16]. In order to address this question, we study the following situation. We need to choose a system (S), a thermal bath (B) and what is going to be the interaction (I) among the two:

i/ The **system (S)** is a model in the $AIII$ chiral-unitary class[1] of topological insulators, called the Creutz ladder [Cre99, Cre01]. The system is constructed as a ladder of spinless fermions that can hop to neighbouring sites with different amplitudes,

$$\begin{aligned} H_{\mathrm{S}} := -\sum_{n=1}^{N} \Big[K \;\; \mathrm{e}^{-\mathrm{i}\theta} a_{n+1}^{\dagger} a_n + \mathrm{e}^{\mathrm{i}\theta} b_{n+1}^{\dagger} b_n \;\; + \\ + K \;\; b_{n+1}^{\dagger} a_n + a_{n+1}^{\dagger} b_n \;\; + M a_n^{\dagger} b_n + \mathrm{h.c.} \Big] , \end{aligned} \tag{3.1}$$

where a_n and b_n are fermionic operators satisfying the anticommutation relations: $\{a_n, a_{n'}^{\dagger}\} = \delta_{n,n'}$, $\{b_n, b_{n'}^{\dagger}\} = \delta_{n,n'}$. K and M are hopping amplitudes, while θ is the magnetic flux per plaquette in natural units. It is known that for $M < 2K$ and open boundary conditions, the system exhibits protected end states [BPAMD09]. In 1D, the conducting edge states of a topological insulator get converted into localised end states at the edge of the system.

Creutz proposed this system as a toy model to understand the chiral modes of the Kaplan-Furman-Shamir [Kap92] domain-wall fermions, widely used in lattice gauge theory simulations. Creutz wanted to shed light upon the *fermion doubling* problem [NN81] in lattice gauge theories to simulate chiral fermions. In particular he studied the chiral nature of the surface modes in high dimensions (inspired by Kaplan's solution [Kap92]) using a toy model in 1D. It was latter noticed [BPAMD09], that this model is in fact a topological insulator in 1D. Interestingly enough, there is a proposal to simulate this model with cold atoms in optical lattices [MBG+12].

ii/ The **bath (B)** is given by a collection of local bosonic baths,

$$H_{\mathrm{B}} := \sum_{n,i} \epsilon_n^i A_n^{i\dagger} A_n^i, \tag{3.2}$$

where A and $A^{\dagger}$ stand for the bath bosonic operators that satisfy the canonical commutation relations $[A_n^i, A_{n'}^{j\dagger}] = \delta_{n,n'}\delta_{i,j}$, $[A_n^i, A_{n'}^j] = 0$. Moreover, the index n denotes the position of the local bath on the CL, and i runs over the bath degrees of freedom.

iii/ The **interaction (I)** between S and B is given by the interacting Hamiltonian H_{I}, which in momentum space (k) reads

$$H_{\mathrm{I}} := \frac{1}{N} \sum_{i,k,k'} g_{kk'}^i (a_k^{\dagger} + b_k^{\dagger})(a_{k'} + b_{k'}) \otimes (A_{k'-k}^{i\dagger} + A_{k-k'}^i). \tag{3.3}$$

[1] The system is invariant under a π rotation with respect to the magnetic field axis. See Fig. 1 of **P2**.

This Hamiltonian describes the interaction between the Creutz Ladder (S) and the thermal baths (B), and it is motivated by the electron-phonon interaction that naturally appears in crystal solids [AM76]. The quantity $g^i_{k,k'}$ regulates the boson-fermion coupling, and it is chosen in such a way that chiral symmetry is preserved. More specifically, the chiral symmetry (also called sublattice symmetry) corresponds to a rotation of π around the magnetic field axis [Cre99, Cre01], which in momentum space swaps the fermion modes a and b, and changes the sign of the momentum k. Thus, we shall assume $g^i_{k,k'} = g^i_{-k,-k'}$ so that the Hamiltonian (3.3) does not break chirality, which is indeed a very natural assumption for this coupling.

Once these three ingredients have been settled, we treat the system as an open quantum system and study its stability from the topological point of view. In publication **P2**, we perform a similar derivation of a master equation, similar to what has been done in the previous chapter 2. We assume weak coupling between S and B and obtain a master equation as given in Eq. (10) of publication **P2**, which is of the form of Eq. (2.2) in chapter 2. The subject of the manuscript is a complete theoretical and numerical analysis of the influence of thermal baths as a source of external noise acting on one-dimensional topological insulators. Let us recall that stable edge states are a defining signature of topological insulators. There is a common believe in the topological insulator community, that the gap defining the topological phase is enough to protect the system against interactions, disorder and even dynamical effects. In what follows, we try to analyse to what extend this belief is true in dissipative systems.

A summary with the main results of **P2** can be found below.

3.2 Outline of the main results

- ✓ We derive a novel master evolution equation for the fermionic (electrons) degrees of freedom of the topological insulator.
- ✓ The electrons play the role of the system degrees of freedom and interact in a natural albeit non-trivial way with the environment made up of bosonic thermal baths.
- ✓ Obtaining a master equation is a central point to study and derive many of the results we find in our work.
- ✓ We compute the "Edge Probability" to find fermions localized at the protected edges of a topological insulator as the system evolves in time (due to the interaction with thermal baths).
- ✓ We can compute lifetimes for the decay of edge states in particular experimental setups and provide figures for these lifetimes.

- ✓ We have found a remarkable result: edge states become unstable under thermal effects and they have a finite lifetime.
- ✓ We have shown that the gap protection does not hold against finite temperature effects: the topological insulator order gets lost regardless of the gap size (see Fig.2 and Fig.4).
- ✓ We have found that the non-equilibrium thermal evolution is able to distinguish between topological and non-topological insulators. We have observed that the existence of topological order strongly influences the system-bath interaction (Fig.2).
- ✓ Notably, the interaction with bosonic thermal baths does not lead this system to the thermal Gibbs state. However, for the low temperature regime we find that both distributions are close to each other.

PHYSICAL REVIEW B **86**, 155140 (2012)

Thermal instability of protected end states in a one-dimensional topological insulator

O. Viyuela, A. Rivas, and M. A. Martin-Delgado
Departamento de Física Teórica I, Universidad Complutense, 28040 Madrid, Spain
(Received 18 July 2012; published 23 October 2012)

We have studied the dynamical thermal effects on the protected end states of a topological insulator (TI) when it is considered as an open quantum system in interaction with a noisy environment at a certain temperature T. As a result, we find that protected end states in a TI become unstable and decay with time. Very remarkably, the interaction with the thermal environment (fermion-boson) respects chiral symmetry, which is the symmetry responsible for the protection (robustness) of the end states in this TI when it is isolated from the environment. Therefore, this mechanism makes end states unstable while preserving their protecting symmetry. Our results have immediate practical implications in recently proposed simulations of TIs using cold atoms in optical lattices. Accordingly, we have computed lifetimes of topological end states for these physical implementations that are useful to make those experiments realistic.

DOI: 10.1103/PhysRevB.86.155140 PACS number(s): 73.20.−r, 03.65.Yz, 11.15.Ha, 37.10.Jk

I. INTRODUCTION

The stability of topological phases of matter, also known as topological orders,[1] against thermal noise has provided several surprising results in the context of topological codes used in topological quantum information.[2,3] However, very little is known about the behavior of a topological insulator (TI) subject to the disturbing thermal effect of its surrounding environment. This is of great relevance if we want to address key questions such as the robustness of TIs to thermal noise, existence of thermalization processes, use of TIs as platforms for quantum computation, etc. Topological insulators have emerged as a new type of quantum phase of matter[4,5] that was predicted theoretically to exist[6–13] and has been discovered experimentally.[14–16] Exploring the possible features and uses of TIs has become a very active interdisciplinary field. For this, knowledge about their stability under nonequilibrium thermal dynamics is crucial in assessing the feasibility of proposals in quantum computation, spintronics, etc.

In this work we present a first-principles calculation to test several thermal effects on a one-dimensional (1D) TI out of equilibrium. In order to achieve these goals, we need first to specify two choices: the type of TI and the type of thermal baths. As for TIs, we work with the Creutz Ladder (CL), which is a paradigmatic example of a quasi-one-dimensional fermion system that exhibits the fundamental properties of TIs;. namely, localized states in the bulk of system and end states in the form of zero-energy modes at the boundary.[17,18] It is a crucial remark that the presence of these end states is independent of whether the system size is finite or infinite. They constitute a clear signature of a TI in the case of the CL. Although the first experimental realizations of TIs are in two dimensions (2D) and three dimensions (3D), the case of 1D TIs also appears in the so-called "periodic table" of TIs.[19–21] Moreover, there are recent proposals to realize TIs in 1D optical lattices,[22,23] and in particular the CL.[24]

As for the environmental quantum noise, we model it in the form of local bosonic thermal baths (see Fig. 1). This is rather natural, but different since usually the bath and system degrees of freedom are taken to be of the same type. Here, we deal with a fermionic system but the bath is made up of bosons. The reason for this choice is inspired by the traditional electron-phonon interaction in crystal solids.[25] The main difference is that our thermal baths are local in order to simplify their study. Moreover, this locality also fits into the traditional scheme of perturbing the global properties of a topological order by means of local external noise, as is natural in topological quantum information. If the CL is realized with optical lattices, then these local baths can be though of as external photons. Therefore, the meaning of the bosonic baths will depend on the specific realization we choose.

A common belief in TI theory is that the gap defining the topological phase is enough to protect the system against interactions, disorder, and even dynamical effects,[26] but the effects of dynamical thermal noise has not been addressed thus far:

(i) We have shown that it does not hold for finite-temperature effects: the TI order gets lost regardless of the gap size (see Figs. 2 and 4).

(ii) Protected end states become unstable when the TI becomes an open quantum system coupled to thermal baths. This is so even when the interaction with the environment respects chiral symmetry, which is responsible for the robustness of end states in the TI [see Eq. (4)]. This is a highly nontrivial effect. It implies that we have found a dynamical thermal mechanism that is relevant to the description of the robustness of end states in TIs. Prior to this work, the robustness of end states in TIs was solely judged on the basis of the protecting symmetries in the isolated system.

(iii) We have observed that the existence of topological order strongly influences the system-bath interaction (Fig. 2). In particular, for our 1D model, the decoherence process remarkably depends whether the system is in a topological phase or not.

(iv) Notably, the interaction with bosonic thermal baths does not lead this system to the thermal state. However, the asymptotic state reached in the low-temperature regime is close to it (see Fig. 3).

Our fundamental result is the derivation of the master equations (10) and (11) for a TI under a bosonic thermal bath from which the thermal instability of the end states is derived along with other relevant consequences.

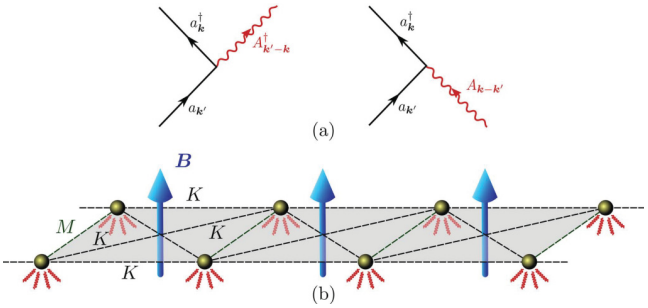

FIG. 1. (Color online) The TI system is pictured in (b) as a ladder of hopping spinless fermions with amplitudes K (horizontal and diagonal) and M (vertical). The fermions are coupled to a magnetic gauge field on the lattice that is perpendicular to the plaquettes. This is a lattice gauge theory known as the Creutz Ladder (CL).[17,18] The wavy lines at each site indicate interaction with thermal bosonic baths. In (a), the interaction vertex of fermions with the bosonic bath is shown.

The total Hamiltonian of the problem considered reads as follows:

$$H = H_{\rm s} + H_{\rm bath} + H_{\rm int}. \tag{1}$$

The first term, $H_{\rm s}$, is the Hamiltonian of the CL,

$$H_{\rm s} := -\sum_{n=1}^{N}[K(e^{-i\theta}a_{n+1}^{\dagger}a_n + e^{i\theta}b_{n+1}^{\dagger}b_n) + K(b_{n+1}^{\dagger}a_n + a_{n+1}^{\dagger}b_n) + Ma_n^{\dagger}b_n + \text{H.c.}], \tag{2}$$

where a_n and b_n are fermionic operators satisfying the anticommutation relations: $\{a_n,a_{n'}^{\dagger}\} = \delta_{n,n'}$, $\{b_n,b_{n'}^{\dagger}\} = \delta_{n,n'}$. K and M are hopping amplitudes, while θ is the magnetic flux per plaquette in natural units. It is known that for $M < 2K$ and open boundary conditions, the system exhibits protected end states[17] that correspond to a TI in 1D.[18]

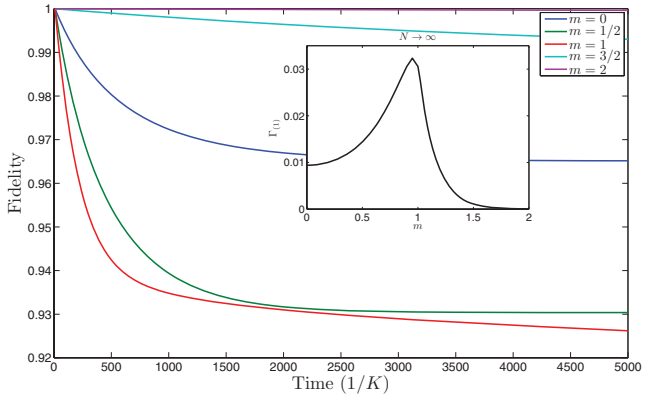

FIG. 2. (Color online) Fidelities for the state of the CL with the initial Fermi sea. Here we have taken $\theta = \pi/2$, $T = 1$ (in units of K, Eq. (2)), and $\omega_c = 3/(2K)$ (of the order of the mean distance between the two bands). We see the fragility of the topological phase ($m < 1$) in comparison with the rest of the cases ($m > 1$). The main plot corresponds to the eight-site CL, and the inset depicts the initial decay rate in the thermodynamic limit (see main text).

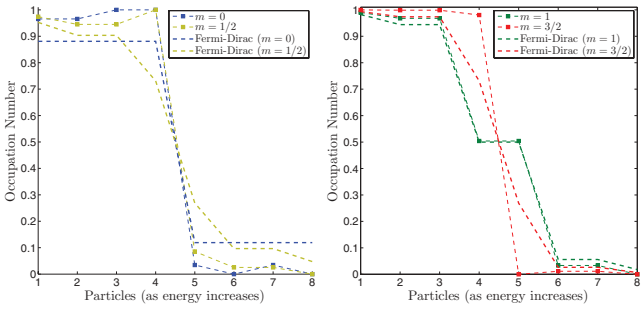

FIG. 3. (Color online) Asymptotic occupation of the fermions for different values of m. The temperature is set to $T = 1$ (in units of K, Eq. (2)). On the left side we have represented some examples which present topological order, on the right side the system is out of the topological phase. Note that on the left side the point 4 is fixed whereas the point 5 is fixed on the right side. For the sake of comparison we have depicted also the Fermi-Dirac distribution which corresponds to the thermal state.

The second term, $H_{\rm bath}$, is the free Hamiltonian of the local baths,

$$H_{\rm bath} := \sum_{n,i}\epsilon_n^i A_n^{i\dagger}A_n^i, \tag{3}$$

where A and $A^{\dagger}$ stand for the bath bosonic operators that satisfy the canonical commutation relations $[A_n^i,A_{n'}^{j\dagger}] = \delta_{n,n'}\delta_{i,j}$, $[A_n^i,A_{n'}^j] = 0$. Moreover, the index n denotes the position of the local bath on the CL, and i runs over the bath degrees of freedom.

Finally, the third term in Eq. (1), $H_{\rm int}$, describes the interaction between the CL and the baths. In momentum space it reads (see Fig. 1)

$$H_{\rm int} := \frac{1}{N}\sum_{i,k,k'} g_{kk'}^i(a_k^{\dagger} + b_k^{\dagger})(a_{k'} + b_{k'}) \otimes \left(A_{k'-k}^{i\dagger} + A_{k-k'}^i\right). \tag{4}$$

The quantity $g_{k,k'}^i$ regulates the boson-fermion coupling, and it is chosen in such a way that chiral symmetry is preserved. More specifically, the chiral symmetry corresponds to a rotation of π around the magnetic field axis,[17] which in momentum space swaps the fermion modes a and b and changes the sign of k (see Fig. 1). Thus, we shall assume $g_{k,k'}^i = g_{-k,-k'}^i$ so that the Hamiltonian (4) does not break chirality, which is indeed a very natural assumption for this coupling. Note that, although the system contains free fermions in a gauge background field, its dynamics is highly nontrivial since the coupling with the bosonic bath involves three-body interactions (see Fig. 1).

II. MASTER EQUATION FOR ONE-DIMENSIONAL TOPOLOGICAL INSULATOR

The evolution of system and bath is given by the Liouville-von Neumann equation, which in the interaction picture reads (unless otherwise stated, natural units $\hbar = k_{\rm B} = 1$ are taken throughout the paper)

$$\frac{d\tilde{\rho}}{dt} = -i[\tilde{H}_{\rm int},\tilde{\rho}], \tag{5}$$

where

$$\tilde{H}_{\rm int} = e^{i(H_{\rm s}+H_{\rm bath})t} H_{\rm int} e^{-i(H_{\rm s}+H_{\rm bath})t} = \frac{1}{N}\sum_{i,k,k'}\sum_{\alpha,\beta=1}^{2} g^i_{kk'}\left(f^{\alpha\dagger}_k h^{\alpha\beta}_{k,k'} e^{i\lambda^{kk'}_{\alpha\beta}t} f^{\beta}_{k'}\right) \otimes\left(e^{i\epsilon^i_{k'-k}t} A^{i\dagger}_{k'-k} + e^{-i\epsilon^i_{k-k'}t} A^i_{k-k'}\right). \quad (6)$$

Here $f^1 := c$ and $f^2 := d$ are the operators which diagonalize the CL Hamiltonian; that is, $H_{\rm s} = \sum_{k\in \rm BZ} \lambda^k_1 c^\dagger_k c_k + \lambda^k_2 d^\dagger_k d_k$ with

$$\lambda^k_{1,2} := 2K[-\cos k\cos\theta \mp \sqrt{\sin^2 k \sin^2\theta + (m+\cos k)^2}] \quad (7)$$

and $m := M/2K$. Moreover, $h^{\alpha\beta}_{k,k'} := F^\alpha_k F^\beta_{k'}$, where

$$F^\alpha_k := \frac{x_k - (-1)^\alpha}{\sqrt{1+x_k^2}}, \quad (8)$$

$$x_k := \frac{\sin k\sin\theta + \sqrt{\sin^2 k\sin^2\theta + (m+\cos k)^2}}{m+\cos k}. \quad (9)$$

Finally, $\lambda^{kk'}_{\alpha\beta} := \lambda^k_\alpha - \lambda^{k'}_\beta$ are Bohr frequencies associated with the eigenvalues of the system Hamiltonian (2) which represent the two energy bands.

By tracing out the bath's degrees of freedom from Eq. (5), we aim at writing a dynamical equation for the CL density matrix, $\rho_{\rm s} = {\rm Tr}_{\rm bath}(\rho)$. Under the natural assumptions of the Born-Markov coupling to the thermal bath (Refs. 27–29 and references therein), we arrive at the following master equation for the TI:

$$\frac{d\rho_{\rm s}}{dt} = -i\,[H_s,\rho_s] + \sum_{\substack{k,k'\\ q,q'}}\sum_{\substack{\alpha,\beta\\ \gamma,\delta=1}}^{2} \Gamma^{kk'qq'}_{\alpha\beta\gamma\delta}\left(f^{\alpha\dagger}_k f^\beta_{k'}\rho_s(t) f^{\gamma\dagger}_q f^\delta_{q'} - \frac{1}{2}\left\{f^{\gamma\dagger}_q f^\delta_{q'} f^{\alpha\dagger}_k f^\beta_{k'},\rho_s(t)\right\}\right), \quad (10)$$

with

$$\Gamma^{kk'qq'}_{\alpha\beta\gamma\delta} = \frac{1}{N^2} 2\pi J\left(\left|\lambda^{qq'}_{\gamma\delta}\right|\right)\left[\Theta\left(\lambda^{qq'}_{\gamma\delta}\right) + \bar{n}\left(\left|\lambda^{qq'}_{\gamma\delta}\right|\right)\right] \times F^\alpha_k F^\beta_{k'} F^\gamma_q F^\delta_{q'} \delta_{\lambda^{k',k}_{\beta\alpha},\lambda^{q,q'}_{\gamma\delta}} \delta_{k'-k,q-q'}. \quad (11)$$

These Γs are the decay rates induced by the dissipative dynamics in our system. Here, $\Theta(\omega)$ denotes the Heaviside step function and $\bar{n}(\omega) = [e^{\omega/T}-1]^{-1}$ is the number of bosons with frequency ω in each local bath; T stands for the bath temperature. For the sake of simplicity we have assumed that $g^i_{k,k'}$ only depends on the difference between k and k', $g^i_{k,k'} \equiv g^i_\epsilon$, where the energy ϵ is related to $k-k'$ through the dispersion relation of the baths (note this is consistent with the chirality-preserving condition $g^i_{k,k'} = g^i_{-k,-k'}$). In such a case, the so-called spectral density of the bath is formally written as $J(\omega) := \sum_i (g^i_\epsilon)^2 \delta(\omega-\epsilon^i)$. For definiteness and as the CL could be realized in an optical lattice setup, we will consider a typical spectral density for a quantum optical 1D system, $J(\omega) = \alpha\omega e^{-\frac{\omega}{\omega_c}}$ where α is a parameter that regulates the interaction strength (typically α will be the fine-structure constant) and ω_c is a cutoff frequency. Furthermore, this "Ohmic" spectral density is widely used in the modeling of condensed matter systems as well.[30]

Despite the apparent complicated structure of $\Gamma^{kk'qq'}_{\alpha\beta\gamma\delta}$ decay rates, the nonvanishing contributions are well understood and both numerical and analytical calculations can be carried out with precision.

III. NONPERTURBATIVE THERMAL DYNAMICS

In this section we analyze the out-of-equilibrium physics described by the master equation (10) in the case of a finite-size CL. This allows us to retrieve nontrivial results about the stability of the topological order and whether it thermalizes, among other properties. In order to study the stability of the system, we may chose different figures of merit. For instance, the fidelity $\mathcal{F}$ of the evolved mixed state of the system $\rho_{\rm s}(t)$ and the initial Fermi sea (FS) for the lower band of the TI represent a measure of how the system remains correlated to its initial state which exhibits a topological order:

$$\mathcal{F}[|{\rm FS}\rangle,\rho_{\rm s}(t)] := \langle {\rm FS}|e^{t\mathcal{L}}(|{\rm FS}\rangle\langle {\rm FS}|)|{\rm FS}\rangle. \quad (12)$$

In fact, if this fidelity remains close to one then it is a strong indication that the topological order is preserved. Figure 2 shows the behavior of the fidelity in a CL of size $N=8$. For some cases the fidelity may remain high, particularly for $m>1$; however, in this case the CL is out of the topological phase.[17,18] On the contrary, if $m<1$ the fidelity may be reduced up to 10% of its initial value.

A complementary criterium for the topological order to persist is given by the evolution of the fermion occupation numbers. Most of fermions escaping from the lower band is a signature that the system no longer keeps the topological order. In Fig. 3 the occupation numbers are plotted for different values of m. The asymptotic occupation (i.e., occupation for sufficiently large times) is close to the Fermi-Dirac statistics, but they do not exactly fit each other. Finally, the existence of end states is a well-defined property that characterizes a TI. If they disappear after the TI is in contact with a thermal bath, we may unequivocally conclude that this type of topological order is lost. As shown in Fig. 4, they are unstable and tend to delocalize along the chain in time. Note that if the bath temperature is small in comparison with the gap of the CL, the system takes a lot of time to delocalize. This fits with the very-well-known argument that TI insulators are stable to perturbations if they present a large gap. However, they always delocalize under thermal noise after some sufficiently large period of time.

Let us see the implications of our thermal evolution analysis on the physical implementations of the Creutz ladder with fermionic atoms in an optical lattice.[24] For that purpose we need two Zeeman sublevels attached to the fermion species a_n and b_n, respectively, laser-assisted tunneling for the transversal and horizontal hopping K, and onsite Raman transitions for the vertical hopping M. The thermal noise can be a model for heating induced by lasers that create the optical trap (due to fluctuating intensity profiles), or any other type of bosonic thermal noise. We take experimental values for $m=0$ and $\theta = \pi/2$ as in Ref. 22: $K \sim 3\hbar$ kHz, gap $\Delta = 12\hbar$ kHz, and bath temperature $T \sim 56$ nK which are currently reachable. We obtain a lifetime for end states $\tau \sim 67$ ms which is much larger

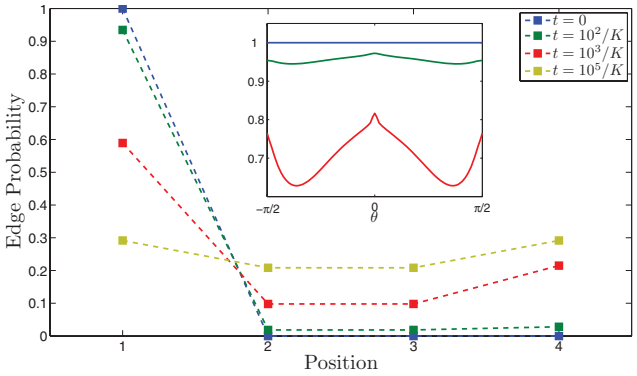

FIG. 4. (Color online) Instability of the topological end states against thermal noise in an eight-site CL (the six-site CL provides the same results). Here, $\theta = \pi/2$ and the bath temperature is $T = 0.04$ (in units of K, Eq. (2)), that is 1% of the CL gap. The x axis represents the longitudinal position on the CL. Thus, at $t = 0$ all fermions are localized at the left end, and as time increases they tend to delocalize along the whole chain. The inset plot depicts the probability that the fermions are in the end for several values of the magnetic flux θ. The decay rate of the end state is smoother at $\theta = 0$ and $\theta = \pi/2$ as the distance between bands increases for these values. Therefore, it is clear that the topological end states are unstable for any value of the magnetic flux. Note that for the decay of a right-end state the result is symmetric because of the chiral symmetry of the interaction (4).

than the typical time for the system dynamics $O(1/K)$. Hence, considering this type of thermal noise, measuring topologically ordered states could be possible within an optical lattice setup.

IV. FIDELITY IN THERMODYNAMIC LIMIT

The evolution of the state can be written up to second order in time as

$$\rho_s(t) = e^{t\mathcal{L}}\rho_s(0) \simeq \left(1 + t\mathcal{L} + \frac{t^2}{2}\mathcal{L}^2 + \cdots\right)\rho_s(0). \quad (13)$$

Using (12), and after several calculations with the master equation (10), we obtain the following result:

$$\mathcal{F}(|\mathrm{FS}\rangle\langle\mathrm{FS}|, \rho_s(t)) \simeq 1 - t\Gamma_{(1)} + \frac{t^2}{2}\left(\Gamma_{(1)}^2 + \Gamma_{(2)}\right), \quad (14)$$

where

$$\Gamma_{(1)} := \sum_{k,q} \Gamma_{2112}^{kqqk}, \quad \Gamma_{(2)} := \sum_{k,q} \Gamma_{2112}^{kqqk}\Gamma_{1221}^{qkkq}. \quad (15)$$

At short times, two rates $\Gamma_{(1)}$ and $\Gamma_{(2)}$ will determine how fast the fidelity of the Fermi sea is lost during its evolution. The initial linear behavior for the lost of fidelity given by $\Gamma_{(1)}$ is patent in Fig. 2 for $N = 8$ as well. Direct processes exciting electrons from one band to the other are dominant in the dissipative evolution, as we might expect. Furthermore, in the inset to Fig. 2, we can see that the initial decay of the Fermi sea's fidelity strongly depends on whether or not the system is in a topological phase $m < 1$. More explicitly, the decay of fidelity increases as we approach the topological crossover point $m = 1$, and then the decay decreases significantly for $m > 1$—out of the topologically ordered regime. This perturbative analysis for the thermodynamic limit is in total agreement with the exact results for $N = 8$ as shown in Fig. 2, and with size $N = 6$ (not shown).

V. CONCLUSIONS

We have derived a master equation describing the dynamical thermal effects of bosonic baths coupled to a one-dimensional TI. As this coupled fermionic-bosonic system is not exactly solvable, our formalism is useful to address relevant thermal effects of TIs in 1D. Let us emphasize that our approach to studying thermal effects on TIs is beyond the standard formalism of assuming that the system is in a thermal state at a certain temperature T. On the contrary, our purpose is to study the out-of-equilibrium dynamics of a TI coupled to a thermal bath. It is this bath which has a well-defined temperature T and disturbs the TI. Very remarkably, the interaction with the thermal environment (fermion-boson) respects chiral symmetry. This symmetry is responsible for the protection (robustness) of the end states in the topological insulator when it is isolated from the environment. Therefore, our mechanism makes end states unstable while preserving their protecting symmetry. In addition, we observed that the dissipative dynamics distinguishes whether the system is in a topological phase or not. We have also shown that thermal noise delocalizes the topological end states into the bulk bands of the TI for sufficiently large times and regardless of the gap size. While this is compatible with the existence of TIs in experiments, this thermal instability will play an important role in detailed control manipulations needed for quantum computation.

ACKNOWLEDGMENTS

We thank the Spanish MICINN grant FIS2009-10061, CAM research consortium QUITEMAD S2009-ESP-1594, European Commission PICC: FP7 2007-2013, Grant No. 249958, UCM-BS Grant No. GICC-910758.

[1] X.-G. Wen, *Quantum Field Theory of Many-Body Systems*, (Oxford Graduate Texts, New York, 2007).
[2] R. Alicki, M. Fannes, and M. Horodecki, J. Phys. A: Math. Theor. **42**, 065303 (2009).
[3] Z. Nussinov and G. Ortiz, Phys. Rev. B **77**, 064302 (2008).
[4] M. Z. Hasan and C. L. Kane, Rev. Mod. Phys. **82**, 3045 (2010).
[5] X.-L. Qi and S.-C. Zhang, Rev. Mod. Phys. **83**, 1057 (2011).
[6] F. D. M. Haldane, Phys. Rev. Lett. **61**, 2015 (1988).
[7] C. L. Kane and E. J. Mele, Phys. Rev. Lett. **95**, 226801 (2005); **95**, 146802 (2005).
[8] B. A. Bernevig and S. C. Zhang, Phys. Rev. Lett. **96**, 106802 (2006).
[9] L. Fu and C. L. Kane, Phys. Rev. B **76**, 045302 (2007).
[10] L. Fu, C. L. Kane, and E. J. Mele, Phys. Rev. Lett. **98**, 106803 (2007).
[11] J. E. Moore and L. Balents, Phys. Rev. B **75**, 121306 (2007).

[12]X.-L. Qi, T. L. Hughes, and S.-C. Zhang, Phys. Rev. B **78**, 195424 (2008).
[13]R. Roy, Phys. Rev. B **79**, 195321 (2009).
[14]M. Konig *et al.*, Science **318**, 766 (2007).
[15]D. Hsieh *et al.*, Nature (London) **452**, 970 (2008).
[16]A. Roth *et al.*, Science **325**, 294 (2009).
[17]M. Creutz, Phys. Rev. Lett. **83**, 2636 (1999).
[18]A. Bermudez, D. Patane, L. Amico, and M. A. Martin-Delgado, Phys. Rev. Lett. **102**, 135702 (2009).
[19]A. P. Schnyder, S. Ryu, A. Furusaki, and A. W W Ludwig, Phys. Rev. B **78**, 195125 (2008).
[20]A. Kitaev, AIP Conf. Proc. **1134**, 22 (2009).
[21]It realizes the symmetry class AIII (chiral unitary).[24]
[22]L.-J. Lang, X. Cai, and S. Chen, Phys. Rev. Lett. **108**, 220401 (2012).
[23]Y. E. Kraus *et al.*, Phys. Rev. Lett. **109**, 106402 (2012).
[24]L. Mazza *et al.*, New J. Phys. **14**, 015007 (2012).
[25]N. W. Ashcroft and N. D. Mermin, *Solid State Physics* (Harcourt College Publishers, Orlando, 1976).
[26]R. C. Hatch, M. Bianchi, D. Guan, S. Bao, J. Mi, B. B. Iversen, L. Nilsson, L. Hornekaer, and P. Hofmann, Phys. Rev. B **83**, 241303(R) (2011).
[27]R. Alicki and K. Lendi, *Quantum Dynamical Semigroups and Applications* (Springer, Berlin, 1987).
[28]H.-P. Breuer and F. Petruccione, *The Theory of Open Quantum Systems* (Oxford University Press, 2002).
[29]A. Rivas and S. F. Huelga, *Open Quantum Systems. An Introduction* (Springer, Heidelberg, 2011).
[30]U. Weiss, *Quantum Dissipative Systems* (World Scientific, Singapore, 2008).

4 Density Matrix Topological Insulators

4.1 Motivation

Although a lot of theory has been done on TIs, very little is known on how to extend topological phases to dissipative systems. In the previous section, we have studied a topological insulator in 1D coupled to thermal baths and hence subjected to external noise. We have analysed the dynamics of this topological system in the presence of dissipation, obtaining the following conclusion: arbitrary interactions with thermal baths can destroy the topological properties that define topological order at zero temperature. This is the case, even if the interaction with the environment preserves the protecting discrete symmetry of the topological insulator (chiral symmetry for the previous case). Similarly, quantum memories based on topological codes have also been shown to be unstable against environmental noise for three or less physical dimensions [AFH09]. This will be discussed in the last chapter (6) of this part of the thesis.

All these facts inspire the following fundamental questions:

- *Is it possible to define topological order in a system with dissipation? Is there a notion of a topological insulating phase for open quantum systems?*

The answer to these questions can be found in publication **P3**. The central idea of the paper is the following: not every dissipative dynamics gives rise to a notion of SPTO for open quantum systems. Actually, the very same thing happens with purely Hamiltonian systems. Not every Hamiltonian help us build topological phases, therefore, not every Liouvillian[1] is well suited to define a dissipative

[1] See chapter 2 for a pedagogical derivation of Liouvillian master equations.

topological phase.

Once we stablish the class of Liouvillians that are good for this purpose, the next steps focus on mimicking the tools that help us define an SPT phase for pure states. Thus, for density matrices, we need to build a connection similar to Berry for pure states (see chapter 1). Similar to the zero temperature case, we have to define a topological witness equivalent to the Chern number and see its relation with the transversed conductivity. Finally, we need to analyse the fate of edge states in the present case.

Very precise answers for all these claims and questions have been given in publication **P3**. A summary of all the results can be found in what follows.

4.2 Outline of the main results

- ✓ We show a way to generalise the notion of a topological insulator to dissipative systems.
- ✓ For this purpose, we introduce the notion of **band Liouvillian** as the appropriate structure for the dynamics to preserve topological order. It is basically the dissipative counterpart of a band Hamiltonian.
- ✓ We construct a new topological indicator named **density matrix Chern value**, that is able to detect topological order at finite temperature and for general quantum mixed states.
- ✓ Remarkably, this new topological indicator witnesses the existence of **conducting mixed edge states**.
- ✓ At finite temperature the quantum Hall conductivity splits into two terms: one corresponding to the density matrix Chern value (topological), and the other accounts for the conduction due to thermal activation of bulk electrons.
- ✓ We apply this general formalism to a two-dimensional graphene [CNGP+09] based model -the so-called Haldane model [Hal88b]- in the presence of thermal dissipation. However, our results are valid for arbitrary dimensions and density matrices.

Density-matrix Chern insulators: Finite-temperature generalization of topological insulators

A. Rivas, O. Viyuela, and M. A. Martin-Delgado
Departamento de Física Teórica I, Universidad Complutense, 28040 Madrid, Spain
(Received 24 January 2013; revised manuscript received 7 June 2013; published 31 October 2013)

Thermal noise can destroy topological insulators (TI). However, we demonstrate how TIs can be made stable in dissipative systems. To that aim, we introduce the notion of band Liouvillian as the dissipative counterpart of band Hamiltonian, and show a method to evaluate the topological order of its steady state. This is based on a generalization of the Chern number valid for general mixed states (referred to as density-matrix Chern value), which witnesses topological order in a system coupled to external noise. Additionally, we study its relation with the electrical conductivity at finite temperature, which is not a topological property. Nonetheless, the density-matrix Chern value represents the part of the conductivity which is topological due to the presence of quantum mixed edge states at finite temperature. To make our formalism concrete, we apply these concepts to the two-dimensional Haldane model in the presence of thermal dissipation, but our results hold for arbitrary dimensions and density matrices.

DOI: 10.1103/PhysRevB.88.155141 PACS number(s): 73.20.At, 03.65.Vf, 03.65.Yz, 73.43.−f

I. INTRODUCTION

Topological insulators have emerged as a new kind of quantum phase of matter,[1–4] which was predicted theoretically to exist and has been discovered experimentally.[5–7] However, the behavior of topological insulators (TIs) subjected to dissipative dynamics has been barely explored. This is inescapable to address questions such as their robustness to thermal noise, which is crucial in assessing the feasibility of these proposals in quantum computation, spintronics, etc.

In a recent work,[8] we have shown that certain one-dimensional topological insulators (TI) lose the topological protection of their edge states when they are coupled to bosonic thermal baths. This is so even when the bath interaction preserves the symmetry that protects the existence of edge states. As a consequence, these edge states decay in time into bulk states of a normal insulator. Thus, a very fundamental question arises: Is it possible to have stable topological insulating states in the presence of a thermal bath? The purpose of this work is to explore this possibility by extending the concept of TI to dissipative systems. Since for dissipative systems quantum states are generally mixed and characterized by a density-matrix operator ρ, we shall refer to these as *density-matrix TIs*.

For usual TIs, the Thouless-Kohmoto-Nightingale–den Nijs (TKNN) invariant[9] provides a characterization of fermionic time-reversal-broken (TRB) topological order in two spatial dimensions. This is done in such a way that the transverse conductivity is written in terms of a topological invariant, the Chern number, which may be related to an adiabatic change of the Hamiltonian in momentum space.[10] However, the extension of this invariant to density matrices is not straightforward.[11] Actually, the problem of generalizing geometric concepts as distances or geometric phases to generally mixed states is highly nontrivial.[12–16] We address this problem and construct an observable that detects the symmetry-protected topological order of a TI even if it is not in a pure but in a general quantum mixed state. Moreover, when this general quantum state is of the form of a Gibbs state, we study the relation between this topological observable and the conductivity, and show that it reduces to the usual notion of TI in the limit of low temperature. However, we stress that the notion of a density-matrix TI is far more general, as we shall see.

The paper is organized as follows. In Sec. II, we introduce the concept of band Liouvillian, which is an appropriate structure for dissipative dynamics in order to preserve topological order. Section III is devoted to construct a topological indicator for density matrices, which plays the same role as the TKNN invariant for pure states. In Sec. IV, we analyze an example of band Liouvillian dynamics for the Haldane model of two-dimensional (2D) TI and, subsequently, in Sec. V, we study its topological properties by using the indicator introduced in Sec. III. Section VI focuses on the behavior of this model under open boundary conditions; this leads to the appearance of mixed edge states in analogy to usual (pure) edge states of a TI in the absence of dissipation. Finally, in Sec. VII, we explain the relation between dissipative topological order and quantum Hall conductivity. Section VIII is devoted to conclusions. In addition, technical details concerning the diagonalization of the Haldane model, derivation of master equations, and its stationary properties are left to Appendixes B, C and D, respectively.

II. BAND LIOUVILLIAN DYNAMICS

The physical problem is defined as follows. Let H_s be the system Hamiltonian representing a certain TI. This could be constructed in an arbitrary spatial dimension, but we shall restrict in what follows to the class of TRB insulators in two spatial dimensions. Furthermore, the TI will be subjected to the action of dissipative effects due to a thermal bath represented by a Hamiltonian H_b. This bath could be general enough so as to comprise fermionic or bosonic degrees of freedom and we assume it is initially in a thermal or Gibbs state at a certain temperature T. The system-bath interaction is described by the Hamiltonian $H_{s\text{-}b}$.

We consider that the state ρ_s of the TI undergoes a time evolution satisfying some Lindblad dynamical equation[17–20] (unless otherwise stated, natural units $\hbar = k_B = 1$ are taken throughout the paper)

$$\frac{d\rho_s}{dt} = \mathcal{L}(\rho_s) = -i[H_s, \rho_s] + \mathcal{D}(\rho_s), \tag{1}$$

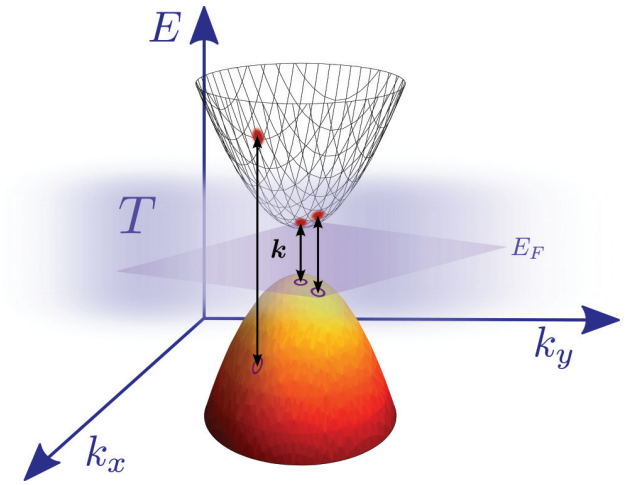

FIG. 1. (Color online) Pictorial image of the action of a band Liouvillian $\mathcal{L} = \sum_{\boldsymbol{k}} \mathcal{L}_{\boldsymbol{k}}$. The vertical lines denote the only possible processes involving the (initially empty) conduction band and (initially filled) valence bands, i.e., those where the momentum $\boldsymbol{k}$ is preserved. The violet fog represents some bath at a certain temperature T which mediates such a process [see Eq. (22)] and the plane indicates the Fermi energy E_F.

where $\mathcal{L}$ is the so-called *Liouvillian* operator, which is composed by a first term representing the Hamiltonian evolution in the absence of system-bath interaction and a second term, the dissipator $\mathcal{D}$, accounting for the effect of the bath dissipation. Concretely, we shall assume that $\mathcal{L}$ is of the Davies type, obtained under the assumption of weak system-bath coupling.[21]

We are interested in searching for sufficient conditions that the Liouvillian dynamics (1) must satisfy in order to preserve the TI phase. In the absence of dissipation, we know that a key ingredient is that the TI Hamiltonian H_{s} is a band Hamiltonian that satisfies the Bloch theorem and can be decomposed as $H_{\mathrm{s}} = \sum_{\boldsymbol{k}\in \mathrm{B.Z.}} H_{\mathrm{s}}(\boldsymbol{k})$ where $\boldsymbol{k}$ denotes a crystalline momentum. Thus, it is natural to restrict our attention to Liouvillian evolutions satisfying a similar condition $\mathcal{L} = \sum_{\boldsymbol{k}\in \mathrm{B.Z.}} \mathcal{L}_{\boldsymbol{k}}$, where each $\mathcal{L}_{\boldsymbol{k}}$ only involves fermionic operators with crystalline momentum $\boldsymbol{k}$; we shall refer to these as *band Liouvillians*. Basically, a Liouvillian of this kind describes processes in such a way that the momenta of the fermions are not changed (up to a vector $\mathbf{G}$ of the reciprocal lattice) (a pictorial image is sketched in Fig. 1). As a consequence, they present invariance under space translations and every $\mathcal{L}_{\boldsymbol{k}}$ satisfies

$$T(\boldsymbol{a})\mathcal{L}_{\boldsymbol{k}}(\rho)T^{\dagger}(\boldsymbol{a}) = \mathcal{L}_{\boldsymbol{k}}[T(\boldsymbol{a})\rho T^{\dagger}(\boldsymbol{a})], \tag{2}$$

where $T(\boldsymbol{a}) = e^{-i\boldsymbol{a}\cdot\hat{\boldsymbol{k}}}$ is the operator that translates a point with coordinate $\boldsymbol{r}$ to the point $\boldsymbol{r} + \boldsymbol{a}$ on the lattice.

An analogy to the Bloch theorem for this kind of Liovillians characterizes its steady states.

Theorem 1. Consider a band Liouvillian $\mathcal{L} = \sum_{\boldsymbol{k}\in \mathrm{B.Z.}} \mathcal{L}_{\boldsymbol{k}}$. If each $\mathcal{L}_{\boldsymbol{k}}$ has a unique stationary state, it has the form

$$\rho_{\mathrm{ss}} = \lambda_0 |0\rangle\langle 0| + \sum_{\boldsymbol{k},\alpha,\beta} \lambda^{\boldsymbol{k}}_{\alpha\beta} |1_{\alpha,\boldsymbol{k}}\rangle\langle 1_{\beta,\boldsymbol{k}}|. \tag{3}$$

Here, α and β denote additional quantum numbers (band indexes, spin indexes, lattice indexes, etc.), and $|1_{\alpha,\boldsymbol{k}}\rangle \equiv |u_{\alpha,\boldsymbol{k}}\rangle$ denotes a particle in the Bloch state with momentum $\boldsymbol{k}$ and additional quantum number α, $T(\boldsymbol{r})|u_{\alpha,\boldsymbol{k}}\rangle = e^{-i\boldsymbol{r}\cdot\boldsymbol{k}}|u_{\alpha,\boldsymbol{k}}\rangle$.

Proof. Consider ρ_{ss} to be the steady state of some $\mathcal{L}_{\boldsymbol{k}}$:

$$\mathcal{L}_{\boldsymbol{k}}(\rho_{\mathrm{ss}}) = 0. \tag{4}$$

By applying the translation operator on both sides and using (2), we obtain

$$\mathcal{L}_{\boldsymbol{k}}[T(\boldsymbol{a})\rho_{\mathrm{ss}}T^{\dagger}(\boldsymbol{a})] = 0. \tag{5}$$

Thus, $\rho'_{\mathrm{ss}} := T(\boldsymbol{a})\rho_{\mathrm{ss}}T^{\dagger}(\boldsymbol{a})$ is also a steady state of the system. Since by assumption ρ_{ss} is unique, $\rho'_{\mathrm{ss}} = \rho_{\mathrm{ss}}$, so that $[T(\boldsymbol{a}), \rho_{\mathrm{ss}}] = 0$ and $T(\boldsymbol{a})$ and ρ_{ss} share the same set of eigenvectors. ■

It is worth noticing that as a difference with the case of pure states, the translational symmetry of a Liovillian does not necessarily imply steady states with well-defined crystalline momentum $\boldsymbol{k}$. They can be a convex mixture of states with different well-defined momenta (3). However, since the subspace with well-defined momentum $\boldsymbol{k}$ is invariant under the action of $\mathcal{L}_{\boldsymbol{k}}$, if the initial state has a well-defined momentum $\boldsymbol{k}$ (for instance, a particle with well-defined momentum in one of the bands of the Hamiltonian), then the steady state under $\mathcal{L}_{\boldsymbol{k}}$ will have well-defined momentum as well:

$$\rho^{\boldsymbol{k}}_{\mathrm{ss}} = \lambda_0 |0\rangle\langle 0| + \sum_{\alpha,\beta} \lambda^{\boldsymbol{k}}_{\alpha\beta} |1_{\alpha,\boldsymbol{k}}\rangle\langle 1_{\beta,\boldsymbol{k}}|. \tag{6}$$

Thus, the steady state ρ_{ss} of the total Liouvillian $\mathcal{L} = \sum_{\boldsymbol{k}\in \mathrm{B.Z.}} \mathcal{L}_{\boldsymbol{k}}$ will be of the form

$$\rho_{\mathrm{ss}} = \bigotimes_{\boldsymbol{k}} \rho^{\boldsymbol{k}}_{\mathrm{ss}}, \quad \rho^{\boldsymbol{k}}_{\mathrm{ss}} := \lambda_0 |0\rangle\langle 0| + \sum_{\alpha,\beta} \lambda^{\boldsymbol{k}}_{\alpha\beta} |1_{\alpha,\boldsymbol{k}}\rangle\langle 1_{\beta,\boldsymbol{k}}|. \tag{7}$$

The coefficients λ_0 and $\lambda^{\boldsymbol{k}}_{\alpha\beta}$ depend on the particular steady state as a result of the dissipative dynamics (1). For instance, if the steady state turns out to be a thermal state density matrix, then they will be given by Gibbs weights (25).

III. CHERN CONNECTIONS FOR DENSITY MATRICES

In order to construct a topological indicator for the generally mixed state ρ_{ss}, we can not use the usual Berry connection as in the formulation of the Chern number because it is defined just for pure states. Regarding density matrices, there is not a unique natural extension of the Berry connection and the Berry phase.[12–16] However, the band Liouvillian structure allows for the construction of a Berry-type connection A^{ρ}_i for the density-matrix steady states, in such a way that the integral of its curvature form F^{ρ}_{ij} gives a topological indicator which we refer to as *density-matrix Chern value*. To construct such an indicator, we use purification, which is a method that allows us to extend quantities defined for pure states to general mixed states.

Generally speaking, for a density matrix ρ acting in a Hilbert space $\mathcal{H}$, a purification $|\Phi^{\rho}\rangle$ is a pure state in an extended Hilbert space $|\Phi^{\rho}\rangle \in \mathcal{H}_A \otimes \mathcal{H}$ such that

$$\rho = \mathrm{Tr}_A(|\Phi^{\rho}\rangle\langle\Phi^{\rho}|). \tag{8}$$

In other words, mixed states can always be seen as pure states of a larger system such that we only have access to partial information of it.

Given some ρ there are infinitely many states $|\Phi^\rho\rangle$ which fulfill (8). Without loss of mathematical generality, we take the ancillary space $\mathcal{H}_A$ to have the same dimension d as $\mathcal{H}$ for the system,[22] then any purification $|\Phi^\rho\rangle$ can be written as

$$|\Phi^\rho\rangle = (U_A \otimes \tilde{\rho})|\Omega\rangle, \tag{9}$$

where U_A is a unitary operator, $\tilde{\rho}\tilde{\rho}^\dagger = \rho$, and

$$|\Omega\rangle := \sum_{\alpha=1}^{d} |v_\alpha\rangle \otimes |v_\alpha\rangle \tag{10}$$

is a (unnormalized) maximally entangled state, with $\{|v_j\rangle\}$ an orthonormal basis of $\mathcal{H}$. From the Schmidt decomposition of $|\Phi^\rho\rangle$ it follows that (9) is the most general form for a purification of ρ.[23]

By using the spectral decomposition of $\rho = \sum_\alpha p_\alpha |\psi_\alpha\rangle\langle\psi_\alpha|$, we may write $\tilde{\rho}$ as

$$\tilde{\rho} = \sum_\alpha \sqrt{p_\alpha}|\psi_\alpha\rangle\langle\varphi_\alpha|, \tag{11}$$

where $\{|\varphi_\alpha\rangle\}$ is also an orthonormal basis which is considered to be arbitrary. Therefore, given some ρ there is a freedom for the choice of U_A and the basis $\{|\varphi_\alpha\rangle\}$ for its purification $|\Phi^\rho\rangle$.

The next theorem is particularly important in the construction of a Berry-type connection for density matrices.

Theorem 2. Consider the steady state of a band Liouvillian (7): we define a Berry-type connection for $\rho_{\rm ss}^{\boldsymbol{k}}$ through one of its purifications $|\Phi_{\boldsymbol{k}}^\rho\rangle$ as

$$A_i^\rho(\boldsymbol{k}) := i\langle\Phi_{\boldsymbol{k}}^\rho|\partial_i\Phi_{\boldsymbol{k}}^\rho\rangle \quad \text{for} \quad \rho_{\rm ss}^{\boldsymbol{k}} = \mathrm{Tr}_A\big(|\Phi_{\boldsymbol{k}}^\rho\rangle\langle\Phi_{\boldsymbol{k}}^\rho|\big). \tag{12}$$

Here, the notation is $\partial_i := \partial_{k_i}$. Under the assumption that U_A and $\{|\varphi_i\rangle\}$ are independent of momentum $\boldsymbol{k}$ of the steady state, the connection (12) is unique and does not depend on the purification. Explicitly, it takes the following form in terms of the spectral decomposition of $\rho_{\rm ss}^{\boldsymbol{k}} = \sum_\alpha p_\alpha^{\boldsymbol{k}}|\psi_{\alpha,\boldsymbol{k}}\rangle\langle\psi_{\alpha,\boldsymbol{k}}|$:

$$A_i^\rho(\boldsymbol{k}) = i\sum_\alpha p_\alpha^{\boldsymbol{k}}\langle\psi_{\alpha,\boldsymbol{k}}|\partial_i\psi_{\alpha,\boldsymbol{k}}\rangle. \tag{13}$$

Proof. Indeed, the general form (9) for a purification of $\rho_{\rm ss}^{\boldsymbol{k}}$ reads as

$$|\Phi_{\boldsymbol{k}}^\rho\rangle = \sum_\alpha \sqrt{p_\alpha^{\boldsymbol{k}}}(U_A \otimes |\psi_{\alpha,\boldsymbol{k}}\rangle\langle\varphi_\alpha|)|\Omega\rangle, \tag{14}$$

where we have used (11). Taking the derivative $\partial_i := \partial_{k_i}$ in (14) and computing the overlap

$$\begin{aligned}\langle\Phi_{\boldsymbol{k}}^\rho|\partial_i\Phi_{\boldsymbol{k}}^\rho\rangle &= \sum_{\alpha,\beta}\sqrt{p_\beta^{\boldsymbol{k}}}\langle\Omega|\Big[\big(\partial_i\sqrt{p_\alpha^{\boldsymbol{k}}}\big)(\mathbb{1}\otimes|\varphi_\beta\rangle\langle\psi_{\beta,\boldsymbol{k}}|\psi_{\alpha,\boldsymbol{k}}\rangle\langle\varphi_\alpha|) \\ &\quad + \sqrt{p_\alpha^{\boldsymbol{k}}}(\mathbb{1}\otimes|\varphi_\beta\rangle\langle\psi_{\beta,\boldsymbol{k}}|\partial_i\psi_{\alpha,\boldsymbol{k}}\rangle\langle\varphi_\alpha|)\Big]|\Omega\rangle.\end{aligned} \tag{15}$$

Since $\langle\Omega|(\mathbb{1}\otimes A)|\Omega\rangle = \mathrm{Tr}(A)$, we obtain

$$A_i^\rho(\boldsymbol{k}) = i\sum_\alpha\sqrt{p_\alpha^{\boldsymbol{k}}}\big(\partial_i\sqrt{p_\alpha^{\boldsymbol{k}}}\big) + p_\alpha^{\boldsymbol{k}}\langle\psi_{\alpha,\boldsymbol{k}}|\partial_i\psi_{\alpha,\boldsymbol{k}}\rangle, \tag{16}$$

which is independent of U_A and $\{|\varphi_i\rangle\}$. Moreover, note that in the pure state case $\rho_{\rm ss}^{\boldsymbol{k}} = |\psi_{\boldsymbol{k}}\rangle\langle\psi_{\boldsymbol{k}}|$ we recover the Berry connection $A_i^\rho(\boldsymbol{k}) = A_i(\boldsymbol{k}) = i\langle\psi_{\boldsymbol{k}}|\partial_i\psi_{\boldsymbol{k}}\rangle$.[24] In addition, the first term on the right-hand side of (16) vanishes by taking into account that $\sum_\alpha p_\alpha^{\boldsymbol{k}} = 1$. Hence, (16) can be simply written as (13). ■

Once this *purified connection* (13) is defined, we may obtain the (Abelian) curvature form through

$$F_{ij}^\rho(\boldsymbol{k}) := \partial_i A_j^\rho(\boldsymbol{k}) - \partial_j A_i^\rho(\boldsymbol{k}), \tag{17}$$

and construct a density-matrix topological indicator $\mathrm{n}_{\rm Ch}^\rho$ associated with the steady state $\rho_{\rm ss}^{\boldsymbol{k}}$ via the first Chern class[25] of this connection:

$$\mathrm{n}_{\rm Ch}^\rho := \frac{1}{4\pi}\mathrm{Tr}\bigg[\int_{\mathrm{T}^2} F_{ij}^\rho(\boldsymbol{k})dk_i\wedge dk_j\bigg]. \tag{18}$$

It is convenient to compute the different contributions that appear in the explicit expression of (17) using (13):

$$F_{ij}^\rho(\boldsymbol{k}) = \sum_\alpha\big[p_\alpha^{\boldsymbol{k}}F_{ij}^\alpha(\boldsymbol{k}) + \big(\partial_i p_\alpha^{\boldsymbol{k}}\big)A_j^\alpha(\boldsymbol{k}) - \big(\partial_j p_\alpha^{\boldsymbol{k}}\big)A_i^\alpha(\boldsymbol{k})\big]. \tag{19}$$

Note that from this equation is not manifestly clear the U(1) gauge invariance of the curvature, but this can be proven by performing a gauge transformation and making use of the property $\sum_\alpha p_\alpha^{\boldsymbol{k}} = 1$. In addition, if N is the dimension of the steady state $\rho_{\rm ss}^{\boldsymbol{k}}$, the curvature is not $\mathrm{U}(1)^N$ gauge invariant, however, that is not the case with the Chern value (18), which is fully invariant. A proof of this fact is given in Appendix A.

Thus, one of the main results of this work is the construction of this object $\mathrm{n}_{\rm Ch}^\rho$, which characterizes the topological structure of insulators in the presence of dissipation. Furthermore, by taking into account Eq. (19), $\mathrm{n}_{\rm Ch}^\rho$ can be written as

$$\begin{aligned}\mathrm{n}_{\rm Ch}^\rho &= \frac{1}{2\pi}\int_{\mathrm{T}^2}F_{12}^\rho(\boldsymbol{k})d^2\boldsymbol{k} \\ &= \frac{1}{2\pi}\sum_\alpha\int_{\mathrm{T}^2}p_\alpha^{\boldsymbol{k}}F_{12}^\alpha(\boldsymbol{k})d^2\boldsymbol{k} \\ &\quad + \frac{1}{2\pi}\sum_\alpha\int_{\mathrm{T}^2}\big[\big(\partial_1 p_\alpha^{\boldsymbol{k}}\big)A_2^\alpha(\boldsymbol{k}) - \big(\partial_2 p_\alpha^{\boldsymbol{k}}\big)A_1^\alpha(\boldsymbol{k})\big]d^2\boldsymbol{k}.\end{aligned} \tag{20}$$

A nonvanishing $\mathrm{n}_{\rm Ch}^\rho$ witnesses a topological nontrivial order present in $\rho_{\rm ss}^{\boldsymbol{k}}$. Since for the pure case the connection (13) becomes the usual Berry connection, if the steady state is a pure Bloch state $\rho_{\rm ss}^{\boldsymbol{k}} = |u_{\alpha,\mathbf{k}}\rangle\langle u_{\alpha,\mathbf{k}}|$, we recover the standard TKNN topological invariant (Chern number).

The density-matrix Chern value $\mathrm{n}_{\rm Ch}^\rho$ [Eq. (20)] has two different terms. The first one is a weighted integration of curvatures for different bands. This term has no topological meaning on its own and it does not distinguish between phases with or without topological order. The second term represents a correction to the value given by the first one that provides the topological character to $\mathrm{n}_{\rm Ch}^\rho$. In addition, both terms have a physical meaning which will be explained in Sec. VII.

The name *Chern value* responds to the fact that despite its topological origin, it may not be an integer for a general mixed state. The reason is very fundamental: the space of density matrices ρ is a convex space, which means that a convex combination of density matrices ρ_1 and ρ_2, $\rho = p_1\rho_1 + p_2\rho_2$ is also a mixed state. Due to the Abelian character of the curvature form F_{ij}^ρ [Eq. (17)], $\mathrm{n}_{\rm Ch}^\rho = p_1\mathrm{n}_{\rm Ch}^{\rho_1} + p_2\mathrm{n}_{\rm Ch}^{\rho_2}$. Therefore, since the weights $p_1, p_2 \in \mathbb{R}$ with $p_1 + p_2 = 1$,

then $n^{\rho}_{\mathrm{Ch}} \in \mathbb{R}$ as well. Nevertheless, this will not be an obstacle to use the Chern value to detect topological properties of insulator states. Note that there are other quantities in the literature which also reflect topological properties but are not integer numbers, for example the Aharonov-Bohm phase (see also Ref. 26). In forthcoming sections, we will apply this formalism to the case of the Haldane model in 2D which is a prototype of TRB topological insulator.[27]

IV. BAND LIOUVILLIAN FOR THE HALDANE MODEL

We can apply our previous formalism to the Haldane model of 2D TI. This is a graphenelike model based on a honeycomb lattice with nearest-neighbor and next-nearest-neighbor couplings. For periodic boundary conditions, the Haldane Hamiltonian in the reciprocal space is given by

$$H_{\mathrm{s}} = \sum_{\boldsymbol{k}\in \mathrm{B.Z.}} (a^{\dagger}_{\boldsymbol{k}}, b^{\dagger}_{\boldsymbol{k}}) H(\boldsymbol{k}) \begin{pmatrix} a_{\boldsymbol{k}} \\ b_{\boldsymbol{k}} \end{pmatrix} = \sum_{\boldsymbol{k}\in \mathrm{B.Z.}} E^{\boldsymbol{k}}_1 c^{\dagger}_{\boldsymbol{k}} c_{\boldsymbol{k}} + E^{\boldsymbol{k}}_2 d^{\dagger}_{\boldsymbol{k}} d_{\boldsymbol{k}}. \tag{21}$$

Here, $a_{\boldsymbol{k}}$ and $b_{\boldsymbol{k}}$ correspond to the two species of fermions associated with the triangular sublattices of a honeycomb lattice, and $c_{\boldsymbol{k}}$ and $d_{\boldsymbol{k}}$ are the fermionic modes which diagonalize the Hamiltonian with eigenvalues $E^{\boldsymbol{k}}_1$ and $E^{\boldsymbol{k}}_2$, respectively. For more details, we refer to Appendix B.

We shall assume a local fermionic bath model, with quadratic coupling of the form

$$H_{\text{s-b}} := \sum_{i,\boldsymbol{r}} g^i \left(a^{\dagger}_{\boldsymbol{r}} \otimes A^i_{\boldsymbol{r}} + a_{\boldsymbol{r}} \otimes A^{i\dagger}_{\boldsymbol{r}} + b^{\dagger}_{\boldsymbol{r}} \otimes B^i_{\boldsymbol{r}} + b_{\boldsymbol{r}} \otimes B^{i\dagger}_{\boldsymbol{r}} \right), \tag{22}$$

where $\boldsymbol{r}$ denotes the point in the sublattices and $A^i_{\boldsymbol{r}}$ and $B^i_{\boldsymbol{r}}$ denote the bath fermion operators coupled with the two species $a_{\boldsymbol{r}}$ and $b_{\boldsymbol{r}}$, respectively. This model could effectively describe situations such as (i) noncontrollable tunneling of electrons between the TI and some surrounding material, (ii) particle losses in simulated topological phases with cold fermionic atoms in optical lattices, or electron transitions to high-energy levels not well described under the tight-binding approximation.

The detailed derivation of the Liouvillian equation (master equation) in the weak coupling limit for this systems is explained in Appendix C; the final result turns out to be

$$\begin{aligned} \frac{d\rho_{\mathrm{s}}(t)}{dt} &= \sum_{\boldsymbol{k}} \mathcal{L}_{\boldsymbol{k}}[\rho_{\mathrm{s}}(t)] \\ &= \sum_{\boldsymbol{k}} \Bigg(-i[H_{\boldsymbol{k}}, \rho_{\mathrm{s}}(t)] + \gamma\left(E^{\boldsymbol{k}}_1\right) \bar{n}_F\left(E^{\boldsymbol{k}}_1\right) \left(c^{\dagger}_{\boldsymbol{k}} \rho_{\mathrm{s}}(t) c_{\boldsymbol{k}} - \frac{1}{2}\{c_{\boldsymbol{k}} c^{\dagger}_{\boldsymbol{k}}, \rho_{\mathrm{s}}(t)\} \right) + \gamma\left(E^{\boldsymbol{k}}_1\right)\left[1 - \bar{n}_F\left(E^{\boldsymbol{k}}_1\right)\right] \left(c_{\boldsymbol{k}} \rho_{\mathrm{s}}(t) c^{\dagger}_{\boldsymbol{k}} - \frac{1}{2}\{c^{\dagger}_{\boldsymbol{k}} c_{\boldsymbol{k}}, \rho_{\mathrm{s}}(t)\} \right) \\ &\quad + \gamma\left(E^{\boldsymbol{k}}_2\right) \bar{n}_F\left(E^{\boldsymbol{k}}_2\right) \left(d^{\dagger}_{\boldsymbol{k}} \rho_{\mathrm{s}}(t) d_{\boldsymbol{k}} - \frac{1}{2}\{d_{\boldsymbol{k}} d^{\dagger}_{\boldsymbol{k}}, \rho_{\mathrm{s}}(t)\} \right) + \gamma\left(E^{\boldsymbol{k}}_2\right)\left[1 - \bar{n}_F\left(E^{\boldsymbol{k}}_2\right)\right] \left(d_{\boldsymbol{k}} \rho_{\mathrm{s}}(t) d^{\dagger}_{\boldsymbol{k}} - \frac{1}{2}\{d^{\dagger}_{\boldsymbol{k}} d_{\boldsymbol{k}}, \rho_{\mathrm{s}}(t)\} \right) \Bigg). \end{aligned} \tag{23}$$

Here,

$$\bar{n}_F(E) := \frac{1}{e^{\beta E} + 1}, \quad \gamma(\omega) := 2\pi J(\omega), \tag{24}$$

where $J(\omega)$ is the bath spectral density.

It is important to emphasize that this Liouvillian (23) fulfills the conditions of a band Liouvillian $\mathcal{L} = \sum_{\boldsymbol{k}\in \mathrm{B.Z.}} \mathcal{L}_{\boldsymbol{k}}$. Moreover, it is quadratic in fermionic operators and its unique steady state is the Gibbs state ($\beta = 1/T$)

$$\rho_{\beta} = \frac{e^{-\beta H_{\mathrm{s}}}}{Z} = \bigotimes_{\boldsymbol{k}} \rho^{\boldsymbol{k}}_{\mathrm{ss}} = \bigotimes_{\boldsymbol{k}} \left(\frac{e^{-\beta E^{\boldsymbol{k}}_1 c^{\dagger}_{\boldsymbol{k}} c_{\boldsymbol{k}}}}{1 + e^{-\beta E^{\boldsymbol{k}}_1}} \right) \left(\frac{e^{-\beta E^{\boldsymbol{k}}_2 d^{\dagger}_{\boldsymbol{k}} d_{\boldsymbol{k}}}}{1 + e^{-\beta E^{\boldsymbol{k}}_2}} \right), \tag{25}$$

that has the form of (7) corresponding to a band Liouvillian. Note that in the limit $T \to 0$, ρ_{β} approaches the Fermi sea where the lower band ($c_{\boldsymbol{k}}$) is fully occupied and the upper band ($d_{\boldsymbol{k}}$) is completely empty (see Appendix D for more details).

V. CHERN VALUE OF THE STEADY STATE

We have obtained that the steady state of the Liouvillian (23) is a product of states $\rho^{\boldsymbol{k}}_{\mathrm{ss}}$ with well-defined momentum. Thus, the (parallel) transport along $\boldsymbol{k}$-*space* of each of these states is well defined and, hence, the state characterization by a density-matrix Chern value (20) is possible.

For the sake of computation, note that $\rho^{\boldsymbol{k}}_{\mathrm{ss}}$ is diagonal in the occupation basis $\rho^{\boldsymbol{k}}_{\mathrm{ss}} = \sum_{n,m\in\{0,1\}} p^{\boldsymbol{k}}_{nm} |m,n\rangle_{\boldsymbol{k}} \langle m,n|$, where

$$\begin{aligned} |00\rangle_{\boldsymbol{k}} &= |0\rangle|0\rangle, \quad |10\rangle_{\boldsymbol{k}} = |u_{c,\boldsymbol{k}}\rangle|0\rangle, \\ |01\rangle_{\boldsymbol{k}} &= |0\rangle|u_{d,\boldsymbol{k}}\rangle, \quad |11\rangle_{\boldsymbol{k}} = |u_{c,\boldsymbol{k}}\rangle|u_{d,\boldsymbol{k}}\rangle. \end{aligned}$$

The vacuum $|0\rangle$ has no particles and does not depend on $\boldsymbol{k}$. If we define the geometric connections for the lower (c) and upper (d) bands

$$A^{\alpha}_i(\boldsymbol{k}) := i\langle u_{\alpha,\boldsymbol{k}} | \partial_i u_{\alpha,\boldsymbol{k}} \rangle, \quad \alpha = c,d \tag{26}$$

then it is possible to express the connection $A^{\rho}_i(\boldsymbol{k})$ in terms of the previous ones (see Appendix D):

$$A^{\rho}_i(\boldsymbol{k}) = \bar{n}_F\left(E^{\boldsymbol{k}}_1\right) A^c_i(\boldsymbol{k}) + \bar{n}_F\left(E^{\boldsymbol{k}}_2\right) A^d_i(\boldsymbol{k}). \tag{27}$$

Note that in the $T \to 0$ limit, we recover the standard Berry connection $A^{\rho}_i(\boldsymbol{k}) \to A^c_i(\boldsymbol{k})$, as the steady state (25) approaches the Fermi sea with the fully occupied lower band.

The Chern value can be now computed by integrating the curvature form of $A^{\rho}_i(\boldsymbol{k})$ [or by using the simplified expression (20)]. The color map in Fig. 2 represents the Chern value for different values of M and ϕ and different bath temperatures.

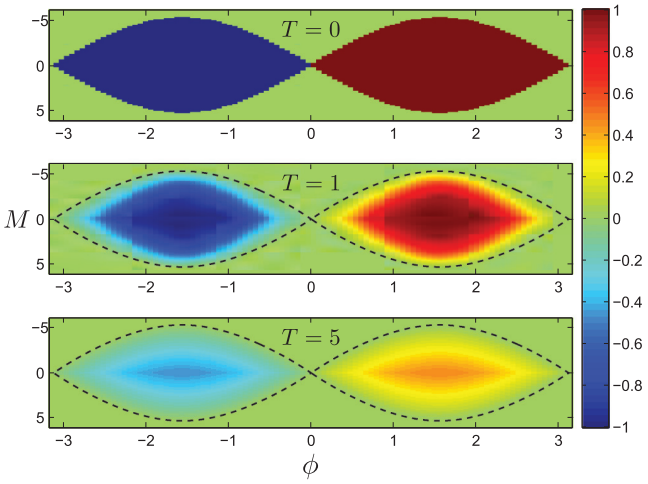

FIG. 2. (Color online) Color map depicting the Chern value in the Haldane model with dissipation, for different values of ϕ, M, and bath temperature T (in units of $t_2 = 1$). As T increases, the Chern value decreases (in absolute value), and for $T = 0$ we recover the phase diagram obtained by Haldane (Ref. 27). The dashed black lines enclose the region displaying topological order at $T = 0$, so that all nonvanishing Chern values are inside of this region for any T. Approximately $T = 1$ and 5 correspond to less than 10% and 50% of the gap, respectively.

Note its nice properties: it is zero for any choice of M and ϕ for all temperatures if it is zero at $T = 0$. This manifests that the topological order can not be created by increasing temperature. Moreover, as T increases, the absolute value of the Chern value decreases, and in the limit of $T \to \infty$ we obtain $\mathrm{n}_{\mathrm{Ch}}^{\rho} \to 0$ for all M and ϕ. This is in agreement with the common intuition that at infinite temperature any kind of order should be spoiled.

VI. MIXED EDGE STATES AND MASTER EQUATION

A physical signature of a TI phase is the existence of gapless (metallic) edge states. Thus, once we have mathematically characterized the phase diagram of the Haldane model under dissipation by means of the density-matrix Chern value, we wonder about the fate of the chiral edge states of the Haldane model at finite temperature.

To that aim, we consider the Haldane model placed on a cylindrical geometry, where we take periodic boundary conditions just along one spatial dimension, say $\boldsymbol{a}_2$. In such a case, the momentum k_2 along the $\boldsymbol{a}_2$ direction is a good quantum number and the Haldane Hamiltonian can be diagonalized obtaining (see Appendix B for more details)

$$H_{\mathrm{s}} = \sum_{k_2 \in \mathrm{B.Z.}} H(k_2) = \sum_{\substack{m \\ k_2 \in \mathrm{B.Z.}}} E_m^{k_2} f_{m,k_2}^{\dagger} f_{m,k_2}. \tag{28}$$

Here, the diagonal modes f_{m,k_2} mix both species of fermions a_{m,k_2} and b_{m,k_2}.

By imposing this geometry also in the interaction Hamiltonian (22), we derive the following dynamical equation for the system (see Appendix C):

$$\begin{aligned}\frac{d\rho_{\mathrm{s}}(t)}{dt} &= \sum_{k_2 \in \mathrm{B.Z.}} \mathcal{L}_{k_2}[\rho_{\mathrm{s}}(t)] \\ &= \sum_{k_2 \in \mathrm{B.Z.}} \Bigg(-i[H(k_2), \rho_{\mathrm{s}}(t)] \\ &\quad + \sum_m \Big(\gamma\big(E_m^{k_2}\big) \bar{n}_F\big(E_m^{k_2}\big) \mathcal{D}_{f_{(m,k_2)}^{\dagger}}[\rho_{\mathrm{s}}(t)] \\ &\quad + \gamma\big(E_m^{k_2}\big)\big[1 - \bar{n}_F\big(E_m^{k_2}\big)\big] \mathcal{D}_{f_{(m,k_2)}}[\rho_{\mathrm{s}}(t)] \Big) \Bigg),\end{aligned} \tag{29}$$

where

$$\mathcal{D}_K[\rho_{\mathrm{s}}(t)] := K \rho_{\mathrm{s}}(t) K^{\dagger} - \tfrac{1}{2}\{K^{\dagger}K, \rho_{\mathrm{s}}(t)\}. \tag{30}$$

Again, the Gibbs state at the same temperature as the bath is the unique steady state of Eq. (29):

$$\rho_{\beta} = \frac{e^{-\beta \sum_{k_2} H(k_2)}}{Z} = \bigotimes_{k_2} \frac{e^{-\beta H(k_2)}}{Z_{k_2}}, \tag{31}$$

with $Z_{k_2} = \mathrm{Tr}\left[e^{-\beta H(k_2)}\right]$. Therefore, as long as the values of M, t_2, and ϕ are such that the system exhibits symmetry-protected topological order (see Fig. 2), two of the modes which diagonalize each $H(k_2)$, say $f_{(L,k_2)}$ and $f_{(R,k_2)}$, correspond to edge states and the Gibbs state is a tensor product in k_2 of states of the form

$$\rho_{\beta}(k_2) = \frac{e^{-\beta H(k_2)}}{Z_{k_2}} = \rho_{\beta}^{\mathrm{L}}(k_2) \otimes \rho_{\beta}^{\mathrm{bulk}}(k_2) \otimes \rho_{\beta}^{\mathrm{R}}(k_2), \tag{32}$$

where

$$\rho_{\beta}^{L,R}(k_2) := \frac{e^{-\beta E_{L,R}(k_2) f_{(L,R,k_2)}^{\dagger} f_{(L,R,k_2)}}}{1 + e^{-\beta E_{L,R}(k_2)}} \tag{33}$$

are Gibbs states of the edge modes. However, as temperature increases (see again Fig. 2), the edge modes in the steady state of the Liouvillian (29) become delocalized along the transverse direction to the edges. Then, the components $\rho^{L,R}(k_2)$ approach to a maximally mixed state with vacuum $|0\rangle$. In such a situation, there is not a way to distinguish the edge from the bulk modes because for all k_2 the occupation along the direction $\boldsymbol{a}_1$ becomes the same and equal to $\frac{1}{2}$. We illustrate this behavior in Fig. 3.

It is worth stressing that in order to study the dissipative effects on the cylindrical Haldane system we must determine how the boundary conditions of the system affect the dissipator operator. To that aim, we need to specify how the dissipator is generated (constructed). In our case, this is the result of the weak interaction of the system with local baths. However, there are also possible scenarios where the dissipator is the effective result of other external interactions (see, for example, Refs. 28–33). Since the process of "opening" or "closing" a system has a physical meaning, we stress that we need to know how the dissipator is physically generated to obtain its "open" and/or "closed" counterpart. Note that a dissipator with periodic boundary conditions may split in different and nonequivalent dissipators once the system is opened along some direction if it is generated in different ways.

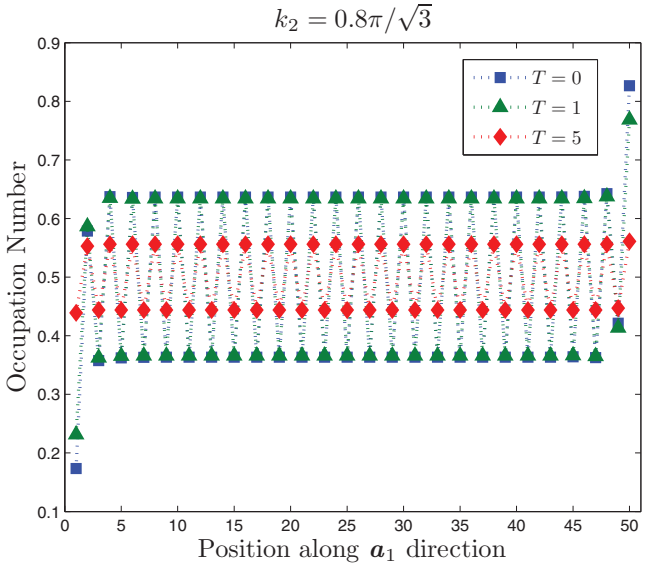

FIG. 3. (Color online) Occupation along the direction $\boldsymbol{a}_1$ for all particles with momentum $k_2 = \frac{4}{5}\frac{\pi}{|\boldsymbol{a}_2|}$, $M = 0$, and $\phi = \pi/2$, for different values of T (in units of $t_2 = 1$). Note the presence of edge states at finite temperature [Eq. (33)] in the positions 1 and 50 along the direction $\boldsymbol{a}_1$. However, as the temperature T significantly increases, the population of the edge modes becomes similar to the population of the bulk modes.

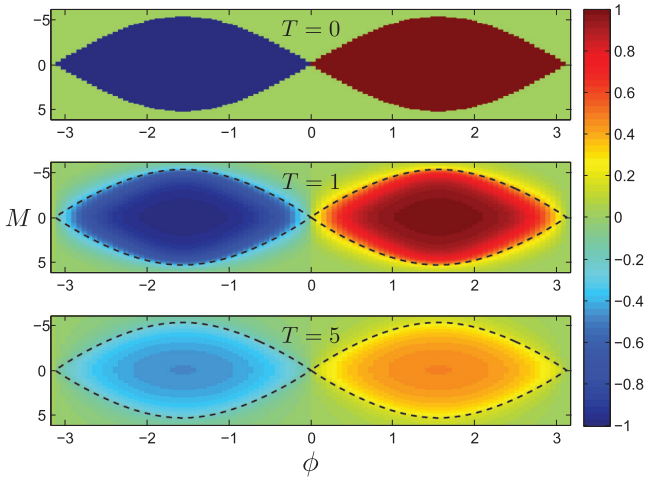

FIG. 4. (Color online) Color map depicting the conductivity Eq. (34) for different values of ϕ, M, and the bath temperature T (in units of $t_2 = 1$). As T increases, the conductivity decreases (in absolute value), and for $T = 0$ we recover the Chern number result (Fig. 2). The dashed black lines enclose the region displaying topological order at $T = 0$. Thus, contrarily to the Chern value, the conductivity is not a topological property for finite T, as it does not vanish for every point outside this region for any T.

VII. QUANTUM HALL CONDUCTIVITY AND CHERN VALUE AT FINITE TEMPERATURE

We can obtain further physical meaning and implications for the density-matrix Chern value (20) by studying the (quantum Hall) transverse conductivity σ_{xy} and its relation to the thermal edge states obtained for the Haldane model. Using the Kubo formula[34] in linear response theory, it is possible to derive an expression for the transverse Hall conductivity at finite temperature[35]:

$$\sigma_{xy}^{\rho} = \frac{e^2}{2\pi h}\sum_{\alpha}\int_{\mathrm{T}^2}\bar{n}_F\left(E_{\alpha}^{\boldsymbol{k}}\right)F_{xy}^{\alpha}(\boldsymbol{k})d^2\boldsymbol{k}. \tag{34}$$

Note that this expression[36] is different from the one obtained for the Chern value (20). Indeed, the conductivity is not topological at finite temperature, as shown in Fig. 4 where nonzero Hall conductivity appears in regions outside the topological regime, in contrast with Fig. 2. Nonetheless, both quantities can be related by means of the following equation:

$$\sigma_{xy}^{\rho} = \frac{e^2}{h}\mathrm{n}_{\mathrm{Ch}}^{\rho} + \frac{e^2}{2\pi h}\sum_{\alpha}\int_{\mathrm{T}^2}\left\{\left[\partial_y\bar{n}_F\left(E_{\alpha}^{\boldsymbol{k}}\right)\right]A_x^{\alpha}(\boldsymbol{k}) - \left[\partial_x\bar{n}_F\left(E_{\alpha}^{\boldsymbol{k}}\right)\right]A_y^{\alpha}(\boldsymbol{k})\right\}d^2\boldsymbol{k}. \tag{35}$$

The second term on the right-hand side of (35) is the same one that appears for the transverse conductivity of a normal insulator with an applied magnetic field (or a pseudomagnetic field as for the Haldane model) at $T \neq 0$. It corresponds to the conduction by thermal activation of excited electrons in the bulk. For instance, for parameters $t_1 = 4, t_2 = 1, \phi = \frac{\pi}{2}$, and $M = 6$ in the Haldane model, this term is the only nonzero contribution to the conductivity, as the system is outside the topological regime, and so $\mathrm{n}_{\mathrm{Ch}}^{\rho} = 0$.

Notwithstanding, the first term on the right-hand side of (35), which is nothing but the Chern value previously defined, represents a contribution due to the topological nature of our system and the presence of conducting edge states. For parameters $t_1 = 4, t_2 = 1, \phi = \frac{\pi}{2}$, and $M = 0$ in the Haldane model, the system is within the topological regime and this new term shows up. Note that at $T = 0$ we recover the well-known TKNN expression for the conductivity:

$$\sigma_{xy}^{\rho} \xrightarrow[T\to 0]{} \frac{e^2}{h}\nu_{\mathrm{Ch}}, \tag{36}$$

where ν_{Ch} denotes the standard Chern number.

VIII. CONCLUSIONS

We have studied topological insulating phases in the presence of dissipation. After introducing the notion of band Liouvillian, we address the characterization of the topological order of its steady states by resorting to the density-matrix Chern value, a topological indicator that is an extension of the Chern number for pure states. The Haldane model of a 2D TI in contact with a thermal bath offers a nice testbed to study these phenomena. More concretely, we compute phase diagrams at finite temperature based on the Chern value, and corroborate that topological order decreases as the bath temperature increases. Thus, from a topologically disordered state it is not possible to induce a topologically ordered phase just by warming the system. However, a topologically ordered state may remain ordered at finite temperature T except at the limit $T \to \infty$. This has to be compared with the previous study[8] where symmetry-protected topological order turned out

to be lost for a dissipative system in the presence of noise not generated by a band Liouvillian. Our results may also have direct application in recent studies regarding dissipation on Majorana fermions in topological superconductors.[29,30,37]

Complementarily, we study the properties of the Haldane model coupled to a thermal bath under cylindrical boundary conditions. We find that the the steady state splits in three different, generally mixed, substates [Eq. (32)]. Two of them are associated with creation or annihilation of fermionic gapless edge modes, and the other one accounts for the same process just in the bulk modes. In the limit $T \to 0$, we recover the properties of the usual Haldane model.

Finally, we examine the relation between the density-matrix Chern value and the conductivity at finite temperature. We show that the latter is a topological property, in contrast to the Chern value. This fact is due to the presence of an extra term which accounts for the conductivity generated by thermal activation of electrons in the bulk, which has not a particular topological meaning and is present in normal insulators. In this regard, provided that the gap between conduction and valence bands is large enough, the Chern value may be approximately estimated by measuring the conductivity, as the thermal activation would be very small. However, recent results[38] suggest that a direct measurement of the density-matrix Chern value could be possible in optical lattice realizations.

ACKNOWLEDGMENTS

We thank A. Dauphin for fruitful discussions. This work has been supported by the Spanish MINECO Grant No. FIS2012-33152, CAM research consortium QUITEMAD S2009-ESP-1594, European Commission PICC: FP7 2007-2013, Grant No. 249958, UCM-BS Grant No. GICC-910758.

APPENDIX A: GAUGE INVARIANCE OF THE DENSITY-MATRIX CHERN VALUE

In this appendix, we provide a proof that the density-matrix Chern value (18) is fully gauge invariant with respect to $\mathrm{U}(1)^N$ transformations of the mixed state. To that aim, consider a $\mathrm{U}(1)^N$ gauge transformation on the eigenstates of $\rho_{\mathrm{ss}}^{\boldsymbol{k}} = \sum_{\alpha=1}^{N} p_\alpha^{\boldsymbol{k}} |\psi_{\alpha,\boldsymbol{k}}\rangle\langle\psi_{\alpha,\boldsymbol{k}}|$:

$$|\psi_{\alpha,\boldsymbol{k}}\rangle \longrightarrow |\tilde{\psi}_{\alpha,\boldsymbol{k}}\rangle = e^{i\phi_{\boldsymbol{k}}^\alpha}|\psi_{\alpha,\boldsymbol{k}}\rangle. \tag{A1}$$

The Berry-type connection (13) and the associated purified curvature (17) transform as

$$\tilde{A}_i^\rho(\boldsymbol{k}) = A_i^\rho(\boldsymbol{k}) - \sum_\alpha p_\alpha^{\boldsymbol{k}} \partial_i \phi_{\boldsymbol{k}}^\alpha, \tag{A2}$$

$$\tilde{F}_{ij}^\rho(\boldsymbol{k}) = F_{ij}^\rho(\boldsymbol{k}) + \sum_\alpha \partial_j\left(p_\alpha^{\boldsymbol{k}} \partial_i \phi_{\boldsymbol{k}}^\alpha\right) - \partial_i\left(p_\alpha^{\boldsymbol{k}} \partial_j \phi_{\boldsymbol{k}}^\alpha\right). \tag{A3}$$

On the other hand, the translational invariance of the lattice imposes that $\rho_{\mathrm{ss}}^{\boldsymbol{k}} = \rho_{\mathrm{ss}}^{\boldsymbol{k}+\boldsymbol{G}}$, where $\boldsymbol{G}$ is a vector in the reciprocal lattice. Then, since the eigenbasis of $\rho_{\mathrm{ss}}^{\boldsymbol{k}}$ is single valued, we conclude that

$$|\psi_{\alpha,\boldsymbol{k}}\rangle = |\psi_{\alpha,\boldsymbol{k}+\boldsymbol{G}}\rangle \tag{A4}$$

independently of the gauge. This implies

$$|\tilde{\psi}_{\alpha,\boldsymbol{k}}\rangle = |\tilde{\psi}_{\alpha,\boldsymbol{k}+\boldsymbol{G}}\rangle \Rightarrow e^{i\phi_{\boldsymbol{k}}^\alpha}|\psi_{\alpha,\boldsymbol{k}}\rangle = e^{i\phi_{\boldsymbol{k}+\boldsymbol{G}}^\alpha}|\psi_{\alpha,\boldsymbol{k}+\boldsymbol{G}}\rangle. \tag{A5}$$

Thus, we obtain that the gauge phase satisfies the relation

$$\phi_{\boldsymbol{k}}^\alpha = \phi_{\boldsymbol{k}+\boldsymbol{G}}^\alpha \,(\mathrm{mod}\, 2\pi). \tag{A6}$$

The Chern value (in 2D for simplicity) is given by

$$\mathrm{n}_{\mathrm{Ch}}^\rho = \frac{1}{2\pi}\int_{\mathrm{T}^2} F_{12}^\rho d^2k. \tag{A7}$$

Performing a $\mathrm{U}(1)^N$ gauge transformation and using (A3),

$$\begin{aligned}\tilde{\mathrm{n}}_{\mathrm{Ch}}^\rho = \frac{1}{2\pi}\int_{\mathrm{T}^2}\tilde{F}_{12}^\rho d^2k &= \mathrm{n}_{\mathrm{Ch}}^\rho + \frac{1}{2\pi}\sum_\alpha\int_{-\pi}^{\pi} dk_1\left[\int_{-\pi}^{\pi} dk_2 \partial_{k_2}\left(p_\alpha^{\boldsymbol{k}}\partial_{k_1}\phi_{\boldsymbol{k}}^\alpha\right)\right] - \frac{1}{2\pi}\int_{-\pi}^{\pi} dk_2\left[\int_{-\pi}^{\pi} dk_1 \partial_{k_1}\left(p_\alpha^{\boldsymbol{k}}\partial_{k_2}\phi_{\boldsymbol{k}}^\alpha\right)\right]\\ &= \mathrm{n}_{\mathrm{Ch}}^\rho + \frac{1}{2\pi}\sum_\alpha\int_{-\pi}^{\pi} dk_1\left[p_\alpha(k_1,k_2=\pi)\partial_{k_1}\phi^\alpha(k_1,k_2=\pi) - p_\alpha(k_1,k_2=-\pi)\partial_{k_1}\phi^\alpha(k_1,k_2=-\pi)\right]\\ &\quad - \frac{1}{2\pi}\sum_\alpha\int_{-\pi}^{\pi} dk_2\left[p_\alpha(k_1=\pi,k_2)\partial_{k_2}\phi^\alpha(k_1=\pi,k_2) - p_\alpha(k_1=-\pi,k_2)\partial_{k_2}\phi^\alpha(k_1=-\pi,k_2)\right],\end{aligned} \tag{A8}$$

where k_1 and k_2 are the two periodic directions along the 2-torus. The weights $p_\alpha^{\boldsymbol{k}}$ are periodic in the B.Z. In particular, for the Gibbs' state, these are functions of the energies of the system. Thus, we have $p_\alpha^{\boldsymbol{k}} = p_\alpha^{\boldsymbol{k}+\boldsymbol{G}}$ and then it follows that

$$\begin{aligned}\tilde{\mathrm{n}}_{\mathrm{Ch}}^\rho = \mathrm{n}_{\mathrm{Ch}}^\rho &+ \frac{1}{2\pi}\sum_\alpha\int_{-\pi}^{\pi} dk_1\left\{p_\alpha(k_1,k_2=\pi)\partial_{k_1}[\phi^\alpha(k_1,k_2=\pi) - \phi^\alpha(k_1,k_2=-\pi)]\right\}\\ &- \frac{1}{2\pi}\sum_\alpha\int_{-\pi}^{\pi} dk_2\left\{p_\alpha(k_1=\pi,k_2)\partial_{k_2}[\phi^\alpha(k_1=\pi,k_2) - \phi^\alpha(k_1=-\pi,k_2)]\right\}.\end{aligned} \tag{A9}$$

At this point, we make use of Eq. (A6) and thus

$$\partial_{k_{x,y}}\left(\phi_{\boldsymbol{k}}^\alpha - \phi_{\boldsymbol{k}+\boldsymbol{G}}^\alpha\right) = 0. \tag{A10}$$

Hence, we can further simplify (A9) using (A10), arriving at the fundamental result

$$\tilde{\mathrm{n}}_{\mathrm{Ch}}^\rho = \mathrm{n}_{\mathrm{Ch}}^\rho. \tag{A11}$$

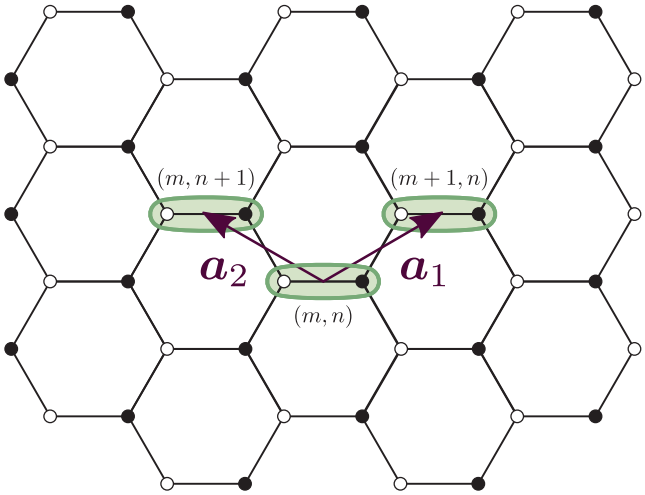

FIG. 5. (Color online) System of coordinates $\{\boldsymbol{a}_1,\boldsymbol{a}_2\}$ taken to write the Haldane Hamiltonian in real space (B1). The solid white and black circles denote fermions a and b, respectively, and the green enclosures highlight the two-site unit cell.

To summarize, the purified Berry curvature is only U(1) gauge invariant, however, the Chern value is $\mathrm{U}(1)^N$ gauge invariant and consequently it can represent a physical observable.

APPENDIX B: HALDANE MODEL GEOMETRIES

In order to write explicitly the Haldane Hamiltonian[27] in real space, we will consider the system of coordinates $\{\boldsymbol{a}_1,\boldsymbol{a}_2\}$ represented in Fig. 5, with $\boldsymbol{a}_1 = \frac{1}{2}(3,\sqrt{3})$ and $\boldsymbol{a}_2 = \frac{1}{2}(-3,\sqrt{3})$ for lattice spacing $a = 1$. We write $a_{(m,n)}$ $(b_{(m,n)})$ for the fermionic operator of kind a (b) in the position $\boldsymbol{r}_{(m,n)} = m\boldsymbol{a}_1 + n\boldsymbol{a}_2$. Then, the Haldane Hamiltonian in real space reads as

$$\begin{aligned} H_{\mathrm{s}} := \sum_{m,n} \Big(& \frac{M}{2}[a^\dagger_{(m,n)}a_{(m,n)} - b^\dagger_{(m,n)}b_{(m,n)}] \\ & + t_1[a^\dagger_{(m,n)}b_{(m,n)} + a^\dagger_{(m+1,n)}b_{(m,n)} + a^\dagger_{(m,n)}b_{(m,n+1)}] \\ & + t_2\big[e^{i\phi}a^\dagger_{(m,n)}a_{(m+1,n+1)} + e^{-i\phi}a^\dagger_{(m,n)}a_{(m+1,n)} \\ & + e^{-i\phi}a^\dagger_{(m,n)}a_{(m,n+1)} + e^{-i\phi}b^\dagger_{(m,n)}b_{(m+1,n+1)} \\ & + e^{i\phi}b^\dagger_{(m,n)}b_{(m+1,n)} + e^{i\phi}b^\dagger_{(m,n)}b_{(m,n+1)}\big] + \mathrm{H.c.}\Big). \end{aligned} \tag{B1}$$

1. Toroidal geometry

By taking periodic boundary conditions in both spatial directions, we may write the Hamiltonian (B1) in the reciprocal space using the Fourier-transformed operators

$$a_{(n,m)} = \frac{1}{\sqrt{N}} \sum_{\boldsymbol{k}\in \mathrm{B.Z.}} e^{i\boldsymbol{k}\cdot\boldsymbol{r}_{(m,n)}} a_{\boldsymbol{k}}, \tag{B2}$$

$$b_{(n,m)} = \frac{1}{\sqrt{N}} \sum_{\boldsymbol{k}\in \mathrm{B.Z.}} e^{i\boldsymbol{k}\cdot\boldsymbol{r}_{(m,n)}} b_{\boldsymbol{k}}, \tag{B3}$$

where B.Z. stands for Brillouin zone which is a hexagon with vertices in the $\boldsymbol{k} = (k_1,k_2)$ points

$$\left(0,\frac{4\pi}{3\sqrt{3}}\right), \left(\frac{2\pi}{3},\frac{2\pi}{3\sqrt{3}}\right), \left(\frac{2\pi}{3},-\frac{2\pi}{3\sqrt{3}}\right), \tag{B4}$$

$$\left(0,-\frac{4\pi}{3\sqrt{3}}\right), \left(-\frac{2\pi}{3},-\frac{2\pi}{3\sqrt{3}}\right), \left(-\frac{2\pi}{3},\frac{2\pi}{3\sqrt{3}}\right), \tag{B5}$$

and N is the total number of two-site unit cells. Thus, the Haldane Hamiltonian is rewritten as

$$H_{\mathrm{s}} = \sum_{\boldsymbol{k}} (a^\dagger_{\boldsymbol{k}}, b^\dagger_{\boldsymbol{k}}) H(\boldsymbol{k}) \begin{pmatrix} a_{\boldsymbol{k}} \\ b_{\boldsymbol{k}} \end{pmatrix}. \tag{B6}$$

Here,

$$\begin{aligned} H_{11}(\boldsymbol{k}) &= M + 2t_2 \sum_i \cos[\phi + (\boldsymbol{k}\cdot\boldsymbol{b}_i)], \\ H_{12}(\boldsymbol{k}) &= H(\boldsymbol{k})^*_{21} = t_1 \sum_i e^{-i\boldsymbol{k}\cdot\boldsymbol{a}_i}, \\ H_{22}(\boldsymbol{k}) &= -M + 2t_2 \sum_i \cos[\phi - (\boldsymbol{k}\cdot\boldsymbol{b}_i)] \end{aligned} \tag{B7}$$

with

$$\boldsymbol{b}_1 = -(3,\sqrt{3})/2, \quad \boldsymbol{b}_2 = (3,-\sqrt{3})/2, \quad \boldsymbol{b}_3 = (0,\sqrt{3}). \tag{B8}$$

By diagonalizing the matrix $H(\boldsymbol{k})$ we obtain

$$H_{\mathrm{s}} = \sum_{\boldsymbol{k}} E^{\boldsymbol{k}}_1 c^\dagger_{\boldsymbol{k}} c_{\boldsymbol{k}} + E^{\boldsymbol{k}}_2 d^\dagger_{\boldsymbol{k}} d_{\boldsymbol{k}}, \tag{B9}$$

where the eigenvalues are given by

$$E^{\boldsymbol{k}}_{1,2} = 2t_2(\cos\phi)\xi_1(\boldsymbol{k}) \mp \sqrt{\Delta(\boldsymbol{k})} \tag{B10}$$

with

$$\begin{aligned} \Delta(\boldsymbol{k}) := {} & M^2 + t_1^2[3 + 2\xi_1(\boldsymbol{k})] \\ & + 4t_2^2(\sin^2\phi)[\xi_2(\boldsymbol{k})]^2 - 4Mt_2(\sin\phi)\xi_2(\boldsymbol{k}), \end{aligned} \tag{B11}$$

and

$$\begin{aligned} \xi_1(\boldsymbol{k}) &:= \sum_i \cos\boldsymbol{k}\cdot\boldsymbol{b}_i = 2\cos\frac{3k_1}{2}\cos\frac{\sqrt{3}k_2}{2} + \cos\sqrt{3}k_2, \\ \xi_2(\boldsymbol{k}) &:= \sum_i \sin\boldsymbol{k}\cdot\boldsymbol{b}_i = -2\cos\frac{3k_1}{2}\sin\frac{\sqrt{3}k_2}{2} + \sin\sqrt{3}k_2. \end{aligned} \tag{B12}$$

The operators $c_{\boldsymbol{k}}$ and $d_{\boldsymbol{k}}$ are related to $a_{\boldsymbol{k}}$ and $b_{\boldsymbol{k}}$ via the canonical transformation

$$\begin{pmatrix} a_{\boldsymbol{k}} \\ b_{\boldsymbol{k}} \end{pmatrix} = \frac{1}{\sqrt{1+|x_{\boldsymbol{k}}|^2}} \begin{pmatrix} x_{\boldsymbol{k}} & 1 \\ -1 & x^*_{\boldsymbol{k}} \end{pmatrix} \begin{pmatrix} c_{\boldsymbol{k}} \\ d_{\boldsymbol{k}} \end{pmatrix}, \tag{B13}$$

where

$$x_{\boldsymbol{k}} := \frac{t_1 \sum_i e^{-i\boldsymbol{k}\cdot\boldsymbol{a}_i}}{M - 2t_2(\sin\phi)\xi_2(\boldsymbol{k}) + \sqrt{\Delta(\boldsymbol{k})}}. \tag{B14}$$

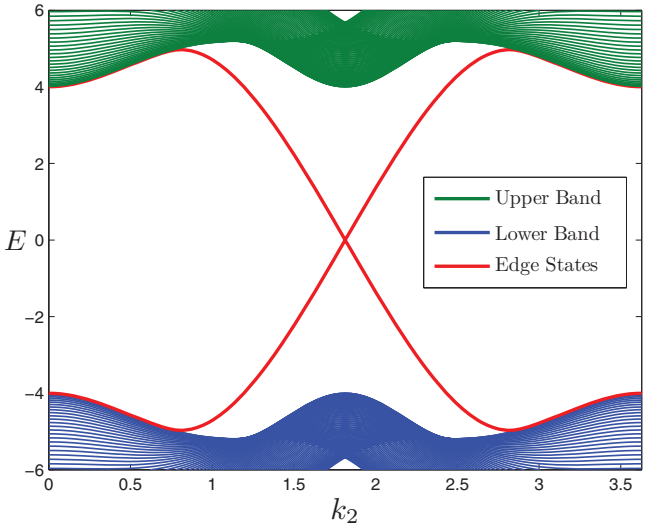

FIG. 6. (Color online) Energy bands of the Hamiltonian (B17) as a function of the momentum k_2. The red lines correspond to the edge-state modes. The rest of the parameters are $M = 0$, $\phi = \pi/2$, and $t_1 = 4$ (in units of $t_2 = 1$).

2. Cylindrical geometry

In this case, we take periodic boundary conditions along the direction $\boldsymbol{a}_2$ and open boundaries along $\boldsymbol{a}_1$, so that we work with a cylindrical configuration. The inverse Fourier transform along the $\boldsymbol{a}_2$ direction of the fermionic operators is given by

$$a_{(m,n)} = \frac{1}{\sqrt{N_2}} \sum_{k_2 \in \text{B.Z.}} e^{ik_2 n|\boldsymbol{a}_2|} a_{(m,k_2)}, \tag{B15}$$

$$b_{(m,n)} = \frac{1}{\sqrt{N_2}} \sum_{k_2 \in \text{B.Z.}} e^{ik_2 n|\boldsymbol{a}_2|} b_{(m,k_2)}, \tag{B16}$$

where the Brillouin zone corresponds to the interval $k_2 \in (-\pi/|\boldsymbol{a}_2|, \pi/|\boldsymbol{a}_2|) = (-\pi/\sqrt{3}, \pi/\sqrt{3})$, and N_2 is the number of two-site basic cells along the direction $\boldsymbol{a}_2$. By using these equations in the Hamiltonian (B1) we obtain

$$\begin{aligned} H_{\text{s}} = \sum_{k_2 \in \text{B.Z.}} \sum_{m} \Bigg(& \left[\frac{M}{2} + t_2 \cos\left(\sqrt{3}k_2 - \phi\right) \right] a^{\dagger}_{(m,k_2)} a_{(m,k_2)} \\ & + \left[-\frac{M}{2} + t_2 \cos(\sqrt{3}k_2 + \phi) \right] b^{\dagger}_{(m,k_2)} b_{(m,k_2)} \\ & + t_1 \left[a^{\dagger}_{(m+1,k_2)} b_{(m,k_2)} + \left(1 + e^{i\sqrt{3}k_2}\right) a^{\dagger}_{(m,k_2)} b_{(m,k_2)} \right] \\ & + t_2 \Big[\left(e^{i(\sqrt{3}k_2 + \phi)} + e^{-i\phi} \right) a^{\dagger}_{(m,k_2)} a_{(m+1,k_2)} \\ & + \left(e^{i(\sqrt{3}k_2 - \phi)} + e^{i\phi} \right) b^{\dagger}_{(m,k_2)} b_{(m+1,k_2)} \Big] + \text{H.c.} \Bigg). \end{aligned} \tag{B17}$$

This Hamiltonian has the structure $H_{\text{s}} = \sum_{k_2 \in \text{B.Z.}} H(k_2)$, therefore we can diagonalize H by diagonalizing each $H(k_2)$. In Fig. 6, we have depicted the behavior of the eigenvalues of $H(k_2)$ as a function of k_2. The red lines connecting the upper and lower bands correspond to the edge-state modes, which are localized on the edges of the direction $\boldsymbol{a}_1$.

APPENDIX C: DERIVATION OF THE MASTER EQUATION FOR THE HALDANE MODEL

In this section, we derive the dynamical equation (master equation) for the Haldane model coupled to a thermal bath. We assume the usual condition of weak system-bath coupling, which is a standard assumption for thermalization.

The total Hamiltonian of the problem considered reads as follows:

$$H := H_{\text{s}} + H_{\text{b}} + H_{\text{s-b}}. \tag{C1}$$

The first term H_{s} is the Haldane Hamiltonian (B1). The second term in (C1), H_{b}, is the free Hamiltonian of the local baths,

$$H_{\text{b}} := \sum_{i,\boldsymbol{r}} \epsilon^i \left(A^{i\dagger}_{\boldsymbol{r}} A^i_{\boldsymbol{r}} + B^{i\dagger}_{\boldsymbol{r}} B^i_{\boldsymbol{r}} \right), \tag{C2}$$

where A and B stand for independent fermionic bath operators that satisfy the canonical anticommutation relations $\{A^i_n, A^{j\dagger}_{n'}\} = \delta_{n,n'}\delta_{i,j}, \{A^i_n, A^j_{n'}\} = 0$ and analogously for B^i_n. The index $\boldsymbol{r}$ denotes the position of the local bath on the lattice and i runs over the bath degrees of freedom. Also, ϵ^i represents the energy of each mode i of the bath which is assumed to be independent of the lattice site. Finally, the third term in (C1), $H_{\text{s-b}}$, is given by

$$H_{\text{s-b}} := \sum_{i,\boldsymbol{r}} g^i \left(a^{\dagger}_{\boldsymbol{r}} \otimes A^i_{\boldsymbol{r}} + a_{\boldsymbol{r}} \otimes A^{i\dagger}_{\boldsymbol{r}} + b^{\dagger}_{\boldsymbol{r}} \otimes B^i_{\boldsymbol{r}} + b_{\boldsymbol{r}} \otimes B^{i\dagger}_{\boldsymbol{r}} \right), \tag{C3}$$

and describes an exchange of fermions between system and bath mediated by a coupling constant g^i which may depend on the specific mode i of the baths.

The total dynamics of system and bath is given by the Liouville–Von Neumann equation

$$\frac{d\rho}{dt} = -i[H, \rho]. \tag{C4}$$

After taking the interaction picture with respect to $H_0 = H_{\text{s}} + H_{\text{b}}$,

$$\frac{d\tilde{\rho}}{dt} = -i[\tilde{H}_{\text{s-b}}, \tilde{\rho}] \quad \text{with} \quad \begin{cases} \tilde{\rho} := e^{iH_0 t} \rho e^{-iH_0 t}, \\ \tilde{H}_{\text{s-b}} := e^{iH_0 t} H_{\text{s-b}} e^{-iH_0 t}. \end{cases} \tag{C5}$$

For small $\tilde{H}_{\text{s-b}}$, the system dynamics is approximately given (see Refs. 17–20) by the equation

$$\frac{d\tilde{\rho}_{\text{s}}}{dt} = -\int_0^{\infty} ds\, \text{Tr}_{\text{b}} \left[\tilde{H}_{\text{s-b}}(t), \left[\tilde{H}_{\text{s-b}}(t-s), \tilde{\rho}_{\text{s}}(t) \otimes \rho^{\beta}_{\text{b}} \right] \right], \tag{C6}$$

where Tr_{b} denotes the trace over the bath degrees of freedom and ρ^{β}_{b} is the initial state of the bath, which we assumed to be the Gibbs state

$$\rho^{\beta}_{\text{b}} := \frac{e^{-\beta H_{\text{b}}}}{Z}. \tag{C7}$$

1. Toroidal geometry

We consider periodic boundary conditions and take Fourier transforms in the Hamiltonian (C1). For the first term we obtain

(B6), for the second we have

$$H_{\mathrm{b}} = \sum_{i,\boldsymbol{k}} \epsilon^i \left(A^{i\dagger}_{\boldsymbol{k}} A^i_{\boldsymbol{k}} + B^{i\dagger}_{\boldsymbol{k}} B^i_{\boldsymbol{k}} \right), \tag{C8}$$

and finally for the interaction term

$$H_{\text{s-b}} = \sum_{i,\boldsymbol{k}} g^i \left(a^\dagger_{\boldsymbol{k}} \otimes A^i_{\boldsymbol{k}} + a_{\boldsymbol{k}} \otimes A^{i\dagger}_{\boldsymbol{k}} + b^\dagger_{\boldsymbol{k}} \otimes B^i_{\boldsymbol{k}} + b_{\boldsymbol{k}} \otimes B^{i\dagger}_{\boldsymbol{k}} \right). \tag{C9}$$

Let us stress again that the strength of the coupling to each mode of the bath is represented by g^i. This, analogously to the energy of each mode ϵ^i, is taken to be independent of the lattice site and of the type of bath A or B, which is rather natural.

In terms of the operators $c_{\boldsymbol{k}}$ and $d_{\boldsymbol{k}}$, the Hamiltonian (C9) reads as

$$H_{\text{s-b}} = \sum_{i,\boldsymbol{k}} g^i \left(c^\dagger_{\boldsymbol{k}} \otimes C^i_{\boldsymbol{k}} + c_{\boldsymbol{k}} \otimes C^{i\dagger}_{\boldsymbol{k}} + d^\dagger_{\boldsymbol{k}} \otimes D^i_{\boldsymbol{k}} + d_{\boldsymbol{k}} \otimes D^{i\dagger}_{\boldsymbol{k}} \right), \tag{C10}$$

where

$$\begin{pmatrix} C^i_{\boldsymbol{k}} \\ D^i_{\boldsymbol{k}} \end{pmatrix} = \frac{1}{\sqrt{1+|x_{\boldsymbol{k}}|^2}} \begin{pmatrix} x^*_{\boldsymbol{k}} & -1 \\ 1 & x_{\boldsymbol{k}} \end{pmatrix} \begin{pmatrix} A^i_{\boldsymbol{k}} \\ B^i_{\boldsymbol{k}} \end{pmatrix} \tag{C11}$$

are new fermionic modes of the bath. Moreover, note that

$$H_{\mathrm{b}} = \sum_{i,\boldsymbol{k}} \epsilon^i \left(C^{i\dagger}_{\boldsymbol{k}} C^i_{\boldsymbol{k}} + D^{i\dagger}_{\boldsymbol{k}} D^i_{\boldsymbol{k}} \right). \tag{C12}$$

Now, it is easy to write $H_{\text{s-b}}$ in the interaction picture and apply the formula (C6), which can be quite simplified by using that

$$\begin{aligned} \mathrm{Tr_b}\left(C^{j\dagger}_{\boldsymbol{k}'} C^i_{\boldsymbol{k}} \rho_\beta \right) &= \mathrm{Tr_b}\left(D^{j\dagger}_{\boldsymbol{k}'} D^i_{\boldsymbol{k}} \rho_\beta \right) = \bar{n}_F(\epsilon^i) \delta_{i,j} \delta_{\boldsymbol{k},\boldsymbol{k}'}, \\ \mathrm{Tr_b}\left(C^j_{\boldsymbol{k}'} C^{i\dagger}_{\boldsymbol{k}} \rho_\beta \right) &= \mathrm{Tr_b}\left(D^j_{\boldsymbol{k}'} D^{i\dagger}_{\boldsymbol{k}} \rho_\beta \right) = [1 - \bar{n}_F(\epsilon^i)] \delta_{i,j} \delta_{\boldsymbol{k},\boldsymbol{k}'}, \\ \mathrm{Tr_b}\left(C^{j\dagger}_{\boldsymbol{k}'} D^i_{\boldsymbol{k}} \rho_\beta \right) &= \mathrm{Tr_b}\left(D^{j\dagger}_{\boldsymbol{k}'} C^i_{\boldsymbol{k}} \rho_\beta \right) = 0. \end{aligned}$$

Here, $\bar{n}_F(E) := \frac{1}{e^{\beta E}+1}$ is the mean number of particles of the Fermi-Dirac distribution, where we have taken the chemical potential μ to be at the origin of the energy. In the continuous limit for the bath degrees of freedom we have

$$\sum_i (g^i)^2 f(\epsilon^i) \longrightarrow \int d\epsilon \, J(\epsilon) f(\epsilon), \tag{C13}$$

for any function $f(\epsilon)$, where $J(\omega)$ is the so-called spectral density of the bath. Thus, the Sokhotsky's identity

$$\int_0^\infty d\tau \, e^{i\omega\tau} = \pi\delta(\omega) + i\,\mathrm{PV}\left(\frac{1}{\omega}\right) \tag{C14}$$

allows us to simplify further the final expression, which after a bit long but straightforward computation reads as

$$\begin{aligned} \frac{d\rho_{\mathrm{s}}(t)}{dt} = \sum_{\boldsymbol{k}} \mathcal{L}_{\boldsymbol{k}}[\rho_{\mathrm{s}}(t)] = \sum_{\boldsymbol{k}} \Bigg(& -i[H_{\boldsymbol{k}}, \rho_{\mathrm{s}}(t)] + \gamma\left(E^{\boldsymbol{k}}_1\right) \bar{n}_F\left(E^{\boldsymbol{k}}_1\right) \left(c^\dagger_{\boldsymbol{k}} \rho_{\mathrm{s}}(t) c_{\boldsymbol{k}} - \frac{1}{2}\{c_{\boldsymbol{k}} c^\dagger_{\boldsymbol{k}}, \rho_{\mathrm{s}}(t)\} \right) \\ & + \gamma\left(E^{\boldsymbol{k}}_1\right) \left[1 - \bar{n}_F\left(E^{\boldsymbol{k}}_1\right)\right] \left(c_{\boldsymbol{k}} \rho_{\mathrm{s}}(t) c^\dagger_{\boldsymbol{k}} - \frac{1}{2}\{c^\dagger_{\boldsymbol{k}} c_{\boldsymbol{k}}, \rho_{\mathrm{s}}(t)\} \right) + \gamma\left(E^{\boldsymbol{k}}_2\right) \bar{n}_F\left(E^{\boldsymbol{k}}_2\right) \left(d^\dagger_{\boldsymbol{k}} \rho_{\mathrm{s}}(t) d_{\boldsymbol{k}} - \frac{1}{2}\{d_{\boldsymbol{k}} d^\dagger_{\boldsymbol{k}}, \rho_{\mathrm{s}}(t)\} \right) \\ & + \gamma\left(E^{\boldsymbol{k}}_2\right) \left[1 - \bar{n}_F\left(E^{\boldsymbol{k}}_2\right)\right] \left(d_{\boldsymbol{k}} \rho_{\mathrm{s}}(t) d^\dagger_{\boldsymbol{k}} - \frac{1}{2}\{d^\dagger_{\boldsymbol{k}} d_{\boldsymbol{k}}, \rho_{\mathrm{s}}(t)\} \right) \Bigg), \end{aligned} \tag{C15}$$

in the Schrödinger picture, where $\gamma(\omega) := 2\pi J(\omega)$. In addition, in this equation we have neglected the imaginary parts of Eq. (C14) because they represent just a small shift of energies which do not affect the dissipative process.[39]

2. Cylindrical geometry

In this case, we take Fourier transform along the direction $\boldsymbol{a}_2$ in (C1). Thus, the Haldane Hamiltonian reads as (B17), the bath Hamiltonian becomes

$$H_{\mathrm{b}} = \sum_{k_2} \sum_{i,m} \epsilon^i \left(A^{i\dagger}_{(m,k_2)} A^i_{(m,k_2)} + B^{i\dagger}_{(m,k_2)} B^i_{(m,k_2)} \right), \tag{C16}$$

and the interaction Hamiltonian

$$\begin{aligned} H_{\text{s-b}} = \sum_{k_2 \in \text{B.Z.}} \sum_{i,m} g^i \Big(& a^\dagger_{(m,k_2)} \otimes A^i_{(m,k_2)} + a_{(m,k_2)} \otimes A^{i\dagger}_{(m,k_2)} \\ & + b^\dagger_{(m,k_2)} \otimes B^i_{(m,k_2)} + b_{(m,k_2)} \otimes B^{i\dagger}_{(m,k_2)} \Big), \end{aligned} \tag{C17}$$

where m runs from 1 to the number of two-site basic cells along the direction $\boldsymbol{a}_1$, N_1.

We may collect the operators a_m and b_m of each site in a new operator c_m where $c_1 := a_1$, $c_2 := b_1$, $c_3 := a_2$, $c_4 := b_2$, and so on. The same can be done for the bath operators A and B with the notation C_m. Then, the interaction Hamiltonian (C17) is written as

$$H_{\text{s-b}} = \sum_{k_2 \in \text{B.Z.}} \sum_{i,m} g^i \left(c^\dagger_{(m,k_2)} \otimes C^i_{(m,k_2)} + c_{(m,k_2)} \otimes C^{i\dagger}_{(m,k_2)} \right), \tag{C18}$$

where now m runs from 1 to $2N_1$.

The diagonal modes $f_{(m,k_2)}$ of $H(k_2) = \sum_m E_m(k_2) f^\dagger_{(m,k_2)} f_{(m,k_2)}$, where $E_m(k_2)$ is depicted in Fig. 6, are related to $c_{(m,k_2)}$ by some unitary transformation

$$c_{(m,k_2)} = \sum_\ell w^{k_2}_{m,\ell} f_{(\ell,k_2)} \quad \text{with} \quad \sum_\ell w^{k_2 *}_{\ell,m} w^{k_2}_{\ell,m'} = \delta_{m,m'}. \tag{C19}$$

By using this equation in (C18) and after a bit of algebra we arrive at

$$H_{\text{s-b}} = \sum_{i,m,k_2} g^i \left(f^\dagger_{(m,k_2)} \otimes F^i_{(m,k_2)} + f_{(m,k_2)} \otimes F^{i\dagger}_{(m,k_2)} \right), \quad \text{(C20)}$$

where

$$F^i_{(m,k_2)} := \sum_\ell w^{k_2 *}_{\ell,m} C^i_{(\ell,k_2)} \quad \text{(C21)}$$

are new fermionic bath modes.

Following the same steps as for the toroidal geometry, it is not difficult to obtain the master equation of the cylindrical array

$$\begin{aligned} \frac{d\rho_{\text{s}}(t)}{dt} = \sum_{k_2 \in \text{B.Z.}} \mathcal{L}_{k_2}[\rho_{\text{s}}(t)] = \sum_{k_2 \in \text{B.Z.}} \Bigg(& -i[H(k_2), \rho_{\text{s}}(t)] \\ & + \sum_m \left(\gamma\left(E^{k_2}_m\right) \bar{n}_F\left(E^{k_2}_m\right) \mathcal{D}_{f^\dagger_{(m,k_2)}}[\rho_{\text{s}}(t)] \right. \\ & \left. + \gamma\left(E^{k_2}_m\right) \left[1 - \bar{n}_F\left(E^{k_2}_m\right)\right] \mathcal{D}_{f_{(m,k_2)}}[\rho_{\text{s}}(t)] \right) \Bigg), \end{aligned} \quad \text{(C22)}$$

where

$$\mathcal{D}_K[\rho_{\text{s}}(t)] := K \rho_{\text{s}}(t) K^\dagger - \tfrac{1}{2}\{K^\dagger K, \rho_{\text{s}}(t)\}. \quad \text{(C23)}$$

APPENDIX D: STEADY STATE FOR THE HALDANE MODEL

1. Toroidal geometry

The steady state of the previous band Liouvillian (C15) is the Gibbs state of the Hamiltonian H_{s},

$$\rho_\beta = \frac{e^{-\beta H_{\text{s}}}}{Z}, \quad \text{(D1)}$$

where $\beta = 1/T$, with T the temperature of the fermionic bath, and $Z = \text{Tr}(e^{-\beta H_{\text{s}}})$ the partition function. To prove this, first note that $[H_{\text{s}}, \rho_\beta] = 0$ so we just need to care about the dissipator in (C15). In addition, since the number operators $c^\dagger_{\boldsymbol{k}} c_{\boldsymbol{k}}$ and $d^\dagger_{\boldsymbol{k}} d_{\boldsymbol{k}}$ commute with $c^\dagger_{\boldsymbol{k}'}, c_{\boldsymbol{k}'}, d^\dagger_{\boldsymbol{k}'}$, and $d_{\boldsymbol{k}'}$ if $\boldsymbol{k} \neq \boldsymbol{k}'$, and we are left only with the part where the crystalline momenta in $\mathcal{L}_{\boldsymbol{k}}$ and $\rho^{\boldsymbol{k}}_{\text{ss}}$ are the same, as the others trivially vanish. Since

$$e^{\beta E} \bar{n}_F(E) = [1 - \bar{n}_F(E)] \quad \text{(D2)}$$

and

$$\rho^{\boldsymbol{k}}_{\text{ss}} = \left(\frac{e^{-\beta E^{\boldsymbol{k}}_1 c^\dagger_{\boldsymbol{k}} c_{\boldsymbol{k}}}}{1 + e^{-\beta E^{\boldsymbol{k}}_1}} \right) \left(\frac{e^{-\beta E^{\boldsymbol{k}}_2 d^\dagger_{\boldsymbol{k}} d_{\boldsymbol{k}}}}{1 + e^{-\beta E^{\boldsymbol{k}}_2}} \right), \quad \text{(D3)}$$

it is easy to prove that

$$\begin{aligned} \mathcal{L}_{\boldsymbol{k}}(\rho^{\boldsymbol{k}}_{\text{ss}}) = & \bar{n}_F(E^{\boldsymbol{k}}_1) \left(c^\dagger_{\boldsymbol{k}} \rho^{\boldsymbol{k}}_{\text{ss}} c_{\boldsymbol{k}} - \frac{1}{2}\{c_{\boldsymbol{k}} c^\dagger_{\boldsymbol{k}}, \rho^{\boldsymbol{k}}_{\text{ss}}\} \right) \\ & + [1 - \bar{n}_F(E^{\boldsymbol{k}}_1)] \left(c_{\boldsymbol{k}} \rho^{\boldsymbol{k}}_{\text{ss}} c^\dagger_{\boldsymbol{k}} - \frac{1}{2}\{c^\dagger_{\boldsymbol{k}} c_{\boldsymbol{k}}, \rho^{\boldsymbol{k}}_{\text{ss}}\} \right) \\ & + \bar{n}_F(E^{\boldsymbol{k}}_2) \left(d^\dagger_{\boldsymbol{k}} \rho^{\boldsymbol{k}}_{\text{ss}} d_{\boldsymbol{k}} - \frac{1}{2}\{d_{\boldsymbol{k}} d^\dagger_{\boldsymbol{k}}, \rho^{\boldsymbol{k}}_{\text{ss}}\} \right) \\ & + [1 - \bar{n}_F(E^{\boldsymbol{k}}_2)] \left(d_{\boldsymbol{k}} \rho^{\boldsymbol{k}}_{\text{ss}} d^\dagger_{\boldsymbol{k}} - \frac{1}{2}\{d^\dagger_{\boldsymbol{k}} d_{\boldsymbol{k}}, \rho^{\boldsymbol{k}}_{\text{ss}}\} \right) = 0. \end{aligned} \quad \text{(D4)}$$

Moreover, the state ρ_β is the unique steady state of (C15) as the interaction Hamiltonian (C3) satisfies the irreducibility condition presented in Ref. 40.

In order to analyze some properties of ρ_β, let us write the density matrix $\rho^{\boldsymbol{k}}_{\text{ss}}$ in the occupation basis of the two bands for a fixed momentum $\boldsymbol{k}$. The basis reads as $|ij\rangle_{\boldsymbol{k}}$, where $i = 0,1$ and $j = 0,1$ stand for the occupation of one-particle state in the lower and upper bands, respectively. Thus, $\rho^{\boldsymbol{k}}_{\text{ss}}$ is a 4×4 diagonal matrix

$$\rho^{\boldsymbol{k}}_{\text{ss}} = \text{diag}\left(p^{\boldsymbol{k}}_{0000}, p^{\boldsymbol{k}}_{1010}, p^{\boldsymbol{k}}_{0101}, p^{\boldsymbol{k}}_{1111} \right) \quad \text{(D5)}$$

with

$$\begin{aligned} p^{\boldsymbol{k}}_{0000} &:= \left[(1 + e^{-\beta E^{\boldsymbol{k}}_1})(1 + e^{-\beta E^{\boldsymbol{k}}_2}) \right]^{-1}, \\ p^{\boldsymbol{k}}_{1010} &:= p^{\boldsymbol{k}}_{0000} e^{-\beta E^{\boldsymbol{k}}_1}, \\ p^{\boldsymbol{k}}_{0101} &:= p^{\boldsymbol{k}}_{0000} e^{-\beta E^{\boldsymbol{k}}_2}, \\ p^{\boldsymbol{k}}_{1111} &:= p^{\boldsymbol{k}}_{0000} e^{-\beta E^{\boldsymbol{k}}_1} e^{-\beta E^{\boldsymbol{k}}_2}. \end{aligned} \quad \text{(D6)}$$

Since we set the origin of energy at $E_0 = 0$ and also took the chemical potential $\mu = 0$ in-between the two bands $E^{\boldsymbol{k}}_1 < 0, E^{\boldsymbol{k}}_2 > 0$. Thus, at the low-temperature limit, the state $\rho^{\boldsymbol{k}}_{\text{ss}} \to |10\rangle_{\boldsymbol{k}}$ as $T \to 0$ K. This means that at $T = 0$ K the lower band is fully occupied and the upper band is completely empty, which is actually what one may expect. At the opposite limit, for $T \to \infty$, the system gets completely mixed, as the four possible states can be equally populated by the environment.

For the sake of clarity, we write the members of the occupation basis as

$$\begin{aligned} |00\rangle_{\boldsymbol{k}} &= |0\rangle|0\rangle, \quad |10\rangle_{\boldsymbol{k}} = |u_{c,\boldsymbol{k}}\rangle|0\rangle, \\ |01\rangle_{\boldsymbol{k}} &= |0\rangle|u_{d,\boldsymbol{k}}\rangle, \quad |11\rangle_{\boldsymbol{k}} = |u_{c,\boldsymbol{k}}\rangle|u_{d,\boldsymbol{k}}\rangle. \end{aligned}$$

Then, by using Eqs. (26) and (13), we obtain (note that the $\partial_i|0\rangle = 0$ as by definition the vacuum has no particles and so it does not depend on $\boldsymbol{k}$)

$$A^\rho_i(\boldsymbol{k}) = p^{\boldsymbol{k}}_{1010} A^c_i(\boldsymbol{k}) + p^{\boldsymbol{k}}_{0101} A^d_i(\boldsymbol{k}) + p^{\boldsymbol{k}}_{1111} \left[A^c_i(\boldsymbol{k}) + A^d_i(\boldsymbol{k}) \right], \quad \text{(D7)}$$

where the Berry connections for the lower c and upper d bands are provided by

$$A^\alpha_i(\boldsymbol{k}) = i \langle u_{\alpha,\boldsymbol{k}} | \partial_i u_{\alpha,\boldsymbol{k}} \rangle, \quad \alpha = c,d. \quad \text{(D8)}$$

Thus, the expressions for $p^{\boldsymbol{k}}_{ijkl}$ given in Eq. (D6) lead to

$$A^\rho_i(\boldsymbol{k}) = \bar{n}_F\left(E^{\boldsymbol{k}}_1\right) A^c_i(\boldsymbol{k}) + \bar{n}_F\left(E^{\boldsymbol{k}}_2\right) A^d_i(\boldsymbol{k}). \quad \text{(D9)}$$

2. Cylindrical geometry

Because of the same reasons as with the toroidal geometry, the master equation on a cylindrical geometry (C22) has a unique steady state, which is the Gibbs state at the same temperature as the bath:

$$\rho_\beta = \frac{e^{-\beta \sum_{k_2} H(k_2)}}{Z} = \bigotimes_{k_2} \frac{e^{-\beta H(k_2)}}{Z_{k_2}}, \quad \text{(D10)}$$

with $Z_{k_2} = \mathrm{Tr}[e^{-\beta H(k_2)}]$. Provided the system exhibits topological order, this state can be split as

$$\rho_\beta(k_2) = \frac{e^{-\beta H(k_2)}}{Z_{k_2}} = \rho_\beta^{\mathrm{L}}(k_2) \otimes \rho_\beta^{\mathrm{bulk}}(k_2) \otimes \rho_\beta^{\mathrm{R}}(k_2), \quad \text{(D11)}$$

where

$$\rho_\beta^{L,R}(k_2) := \frac{e^{-\beta E_{L,R}(k_2) f^\dagger_{(L,R,k_2)} f_{(L,R,k_2)}}}{1 + e^{-\beta E_{L,R}(k_2)}} \quad \text{(D12)}$$

are Gibbs states involving just the gapless edge modes depicted in Fig. 6.

[1] M. Z. Hasan and C. L. Kane, Rev. Mod. Phys. **82**, 3045 (2010).
[2] X.-L. Qi and S.-C. Zhang, Rev. Mod. Phys. **83**, 1057 (2011).
[3] X.-L. Qi and S.-C. Zhang, Phys. Today **63**(1), 33 (2010).
[4] J. E. Moore, Nature (London) **464**, 194 (2010).
[5] M. Konig, S. Wiedmann, C. Brüne, A. Roth, H. Buhmann, L. Molenkamp, X.-L. Qi, and S.-C. Zhang, Science **318**, 766 (2007).
[6] D. Hsieh, D. Qian, L. Wray, Y. Xia, Y. S. Hor, R. J. Cava, and M. Z. Hasan, Nature (London) **452**, 970 (2008).
[7] A. Roth, C. Brüne, H. Buhmann, L. W. Molenkamp, J. Maciejko, X.-L. Qi, and S.-C. Zhang, Science **325**, 294 (2009).
[8] O. Viyuela, A. Rivas, and M. A. Martin-Delgado, Phys. Rev. B **86**, 155140 (2012).
[9] D. J. Thouless, M. Kohmoto, M. P. Nightingale, and M. den Nijs, Phys. Rev. Lett. **49**, 405 (1982); M. Kohmoto, Ann. Phys. (NY) **160**, 343 (1985); Phys. Rev. B **39**, 11943 (1989).
[10] Y. Hatsugai, J. Phys.: Condens. Matter **9**, 2507 (1997).
[11] For some recent works regarding adiabatic transport in open quantum systems, see J. E. Avron, M. Fraas, G. M. Graf, and O. Kenneth, New J. Phys. **13**, 053042 (2011); J. E. Avron, M. Fraas, G. M. Graf, and P. Grech, Commun. Math. Phys. **314**, 163 (2012); J. E. Avron, M. Fraas, and G. M. Graf, J. Stat. Phys. **148**, 800 (2012).
[12] A. Uhlmann, Rep. Math. Phys. **24**, 229 (1986); **36**, 461 (1995).
[13] E. Sjöqvist, A. K. Pati, A. Ekert, J. S. Anandan, M. Ericsson, D. K. L. Oi, and V. Vedral, Phys. Rev. Lett. **85**, 2845 (2000).
[14] S. Filipp and E. Sjöqvist, Phys. Rev. Lett. **90**, 050403 (2003).
[15] M. Ericsson, A. K. Pati, E. Sjöqvist, J. Brännlund, and D. K. L. Oi, Phys. Rev. Lett. **91**, 090405 (2003).
[16] K. Singh, D. M. Tong, K. Basu, J. L. Chen, and J. F. Du, Phys. Rev. A **67**, 032106 (2003).
[17] R. Alicki and K. Lendi, *Quantum Dynamical Semigroups and Applications* (Springer, Berlin, 1987).
[18] C. W. Gardiner and P. Zoller, *Quantum Noise* (Springer, Berlin, 1991).
[19] H.-P. Breuer and F. Petruccione, *The Theory of Open Quantum Systems* (Oxford University Press, Oxford, UK, 2002).
[20] A. Rivas and S. F. Huelga, *Open Quantum Systems. An Introduction* (Springer, Heidelberg, 2011).
[21] E. B. Davies, Commun. Math. Phys. **39**, 91 (1974); Math. Ann. **219**, 147 (1976).
[22] Physically, the ancillary space may represent the thermal bath. However, the dimension of the ancillary space has no physical consequences, it is just restricted to be larger or equal than the dimension of the system's Hilbert space in order to not lose generality.
[23] M. A. Nielsen and I. L. Chuang, *Quantum Computation and Quantum Information* (Cambridge University Press, Cambridge, 2000).
[24] M. V. Berry, Proc. R. Soc. A **392**, 45 (1984).
[25] T. Eguchi, P. B. Gilkey, and A. J. Hanson, Phys. Rep. **66**, 213 (1980).
[26] F. D. M. Haldane, Phys. Rev. Lett. **93**, 206602 (2004).
[27] F. D. M. Haldane, Phys. Rev. Lett. **61**, 2015 (1988).
[28] F. Verstraete, M. M. Wolf, and J. I. Cirac, Nat. Phys. **5**, 633 (2009).
[29] S. Diehl, E. Rico, M. A. Baranov, and P. Zoller, Nat. Phys. **7**, 971 (2011).
[30] C.-E. Bardyn, M. A. Baranov, E. Rico, A. İmamoğlu, P. Zoller, and S. Diehl, Phys. Rev. Lett. **109**, 130402 (2012).
[31] M. Müller, S. Diehl, G. Pupillo, and P. Zoller, Adv. Atom. Mol. Opt. Phys. **61**, 1 (2012).
[32] B. Horstmann, J. I. Cirac, and G. Giedke, Phys. Rev. A **87**, 012108 (2013).
[33] J. Eisert and T. Prosen, arXiv:1012.5013.
[34] R. Kubo, J. Phys. Soc. Jpn. **12**, 570 (1957).
[35] D. Xiao, M.-C. Chang, and Q. Niu, Rev. Mod. Phys. **82**, 1959 (2010).
[36] Note that in this formula we have restored the units e (electron charge) and h (Planck constant) as it is customary in this context.
[37] L. Mazza, M. Rizzi, M. D. Lukin, and J. I. Cirac, arXiv:1212.4778.
[38] M. Atala, M. Aidelsburger, J. T. Barreiro, D. Abanin, T. Kitagawa, E. Demler and I. Bloch, arXiv:1212.0572; D. A. Abanin, T. Kitagawa, I. Bloch, and E. Demler, Phys. Rev. Lett. **110**, 165304 (2013); L. Tarruell, D. Greif, T. Uehlinger, G. Jotzu, and T. Esslinger, Nature (London) **483**, 303 (2012).
[39] A. Rivas, A. D. K. Plato, S. F. Huelga, and M. B. Plenio, New J. Phys. **12**, 113032 (2010).
[40] H. Spohn, Lett. Math. Phys. **2**, 33 (1977).

5

Uhlmann measure in topological systems

In chapter 4, we have provided a very general framework to define a topological insulator as an open quantum system. The previous formalism allows us: (a) to characterise the mixed character of the edge states, (b) to define a new topological witness associated to the topological part of the quantum Hall conductivity at zero temperature, etc. At zero temperature, we have seen that the transverse conductivity of a topological insulator σ_{xy} is integer-quantized [NTW85] in units of $\frac{e^2}{h}$. Actually, the integer is equal to the Chern number as shown in chapter 1. However, we have just seen in publication **P3** that the Chern value (the topological witness we have defined in this dissipative context) is not integer-quantised anymore, and the same applies for the transverse conductivity σ_{xy}. Therefore, there are still two questions remaining:

- *Is it possible to find topological phases that remain QUANTISED even at finite temperature or in the presence of dissipation? Are all quantum properties smoothly degraded at finite temperature?*

In publications **P4**, **P5** and **P6** we show that there are certain topological phases associated to density matrices of SPTOs, that remain quantised for a finite range of temperatures. When considering decoherent effects of the surrounding environment, we have found that the Uhlmann geometric phase provides us with an elegant characterisation of topological regimes of fermion (electron) systems. This phase is a natural generalisation of the Berry phase for general density matrices, based on the Bures metric [Bur69, ACMnT+07, CMnTM+08]. Moreover, the

Uhlmann phase produces a complementary way to extend the notion of symmetry protected topological order at finite temperature. Our topological measure can detect topological regimes both at zero and non-zero temperature for fermion systems with so different physical behavior such as insulators and superconductors in 1D and 2D. This opens the way to future applications for more complicated systems.

Very recently, there has been a proposal [KQM16] relating the critical temperature given by the Uhlmann phase, with that of certain thermodynamic potentials based on Hill thermodynamics [Hil94]. However, a fundamental question remains: how to measure a topological Uhlmann phase in a physical system?

In publication **P9**, we propose a state-independent protocol to measure the topological Uhlmann phase on a quantum simulator experiment, in particular in a platform of superconducting qubits [GAN14]. Recently, there has been an increasing number of experiments performing Digital Quantum simulation of spin [SMO+15] and fermionic [BLK+15] models using transmon qubits [KYG+07]. In addition, the topological Berry/Zak phase has been directly measured with cold atoms in optical lattices [AAB+13] and for a superconducting qubit [LFB+07, SKK+14] through interferometric techniques. Therefore, we feel very confident that the experiment proposed in **P9** will be soon carried out.

5.1 Outline of the main results

Publication P4: Topological Uhlmann phase in 1D

- ✓ We introduce the Uhlmann phase (a geometric phase for general density matrix) and apply it to topological many-body systems.
- ✓ We show that when applied to SPT phases in 1D, the geometric Uhlmann phase acquires a topological character and it can only be quantised ($\Phi_U = \pi$ topological, $\Phi_U = 0$ trivial).
- ✓ In the small temperature limit, the Uhlmann phase witnesses the same topological region as the one given by the winding number of the corresponding Hamiltonian or the Berry phase. Hence it has a well-defined zero temperature limit.
- ✓ As temperature increases, the Uhlmann phase remains unperturbed below a certain temperature T_c, where the system acquires a constant quantum phase in a wide region of the phase diagram witnessing the topological phase (green colored volume in Figs. 2a-c.),
- ✓ At T_c there is a critical transition, and the Uhlmann phase vanishes $\Phi_U = 0$ above that temperature.

- ✓ We find a universal behavior when the coupling constants are such that the models exhibit a flat-band structure (linked to the presence of decoupled edge modes). In that case, the critical temperature of the Uhlmann geometric phase becomes universal regardless of whether the model exhibits insulating or superconducting behavior.
- ✓ We give a geometrical interpretation of T_c along the holonomy.
- ✓ As the Uhlmann phase is a gauge invariant quantity and observable, we give two different methods on how to measure this phase in the context of quantum simulation: 1) purification-based method, 2) using an ancilla qubit. A detail explanation can be found in detail in the Supplementary material of **P4**.

Publication P5: Topological Uhlmann numbers in 2D

- ✓ The Chern number associated to the Uhlmann connection is identically zero, because the associated fiber bundle structure is trivial. However, this is not the only way to introduce topology in a 2D system.
- ✓ We define a new topological invariant called the Uhlmann number, as the winding number associated to the Uhlmann phase of homological cycles along one of the directions of the BZ torus.
- ✓ The Uhlmann number is gauge invariant and it is always integer-quantised.
- ✓ At very small temperatures, the Uhlmann number tends to the Chern number and we obtain the same topological characterization as at $T = 0$.
- ✓ We apply this new framework to well-established models like the topological insulator Haldane model and the p-wave superconductor that can host non-Abelian Majorana fermions. Remarkably, we always find a finite range of temperatures at which this topological order survives.
- ✓ Particularly, we report a model where there is a critical transition between two non-trivial topological phases by the sole effect of the temperature. Thus, we have obtained purely thermal transition between different non-trivial topological regimes for the first time.
- ✓ These new results on stabilizing thermal topological quantum phases in 2D via the observable Uhlmann number may trigger experimental developments in this field and also have direct consequences regarding the thermal stability of Majorana fermions in topological superconductors and topological quantum memories.

Publication P6: Topological Uhlmann theory

- ✓ The initial part of the paper comprises a self-contained explanation of the Uhlmann geometric phase needed to understand the topological properties that it may acquire when applied to topological insulators and superconductors.
- ✓ We explain the fiber bundle structure of the Uhlmann approach from the point of view of amplitudes and purifications of the density matrix.
- ✓ We derive explicitly the Uhlmann connection formula by applying a very natural parallel transport condition inspired by the Berry one.
- ✓ We proof the invariance of the Uhlmann holonomy under general gauge transformations.
- ✓ We study in detail the triviality of the Uhlmann Chern classes associated to the Uhlmann connection.
- ✓ The discontinuous $2\pi-$jump structure of the Uhlmann phase along homological circles in 2D is discussed. This gives an intuitive picture of the quantised and non-zero character of the Uhlmann number in 2D.
- ✓ Finally, we apply the topological Uhlmann theory to another representative model of a topological insulator in two dimensions, the Qi-Wu-Zhang model. We have found a stable symmetry-protected topological (SPT) phase under external thermal fluctuations in two-dimensions. A complete phase diagram for this model is computed.

Publication P9: Measurement Protocol

- ✓ We derive the topological phase diagram according to the Uhlmann phase for a topological qubit in the presence of noise. This is depicted in Fig.1 of the paper.
- ✓ We propose a novel state-independent measurement protocol for the Uhlmann phase, which does not involve prior knowledge of the system state ρ or its mixedness parameter r [see Eq. (1)].
- ✓ Using the same protocol, we can test whether the system is parallely transported in the Uhlmann sense when the holonomy is implemented.
- ✓ We elaborate a gate decomposition of the protocol [see Fig. 2], based on the available set of gates for superconducting qubits experiments.
- ✓ By performing a noise simulation and taking into account realistic experimental imperfections, we prove the feasibility of the experiment in state-of-the-art setups of superconducting qubits [see Fig. 3].

Uhlmann Phase as a Topological Measure for One-Dimensional Fermion Systems

O. Viyuela, A. Rivas, and M. A. Martin-Delgado
Departamento de Física Teórica I, Universidad Complutense, 28040 Madrid, Spain
(Received 2 September 2013; published 2 April 2014)

We introduce the Uhlmann geometric phase as a tool to characterize symmetry-protected topological phases in one-dimensional fermion systems, such as topological insulators and superconductors. Since this phase is formulated for general mixed quantum states, it provides a way to extend topological properties to finite temperature situations. We illustrate these ideas with some paradigmatic models and find that there exists a critical temperature T_c at which the Uhlmann phase goes discontinuously and abruptly to zero. This stands as a borderline between two different topological phases as a function of the temperature. Furthermore, at small temperatures we recover the usual notion of topological phase in fermion systems.

DOI: 10.1103/PhysRevLett.112.130401 PACS numbers: 03.65.Vf, 67.85.-d, 03.65.Yz, 03.67.Mn

Introduction.—Geometric phases have played an essential role in many quantum phenomena since their modern discovery by Berry [1] (see also Refs. [2,3]). An emblematic example is the characterization of the transversal conductivity σ_{xy} in the quantum Hall effect by means of the integral of the Berry curvature over the two-dimensional Brillouin zone (BZ), in units of e^2/h. This is the celebrated TKNN formula [4] that has become a key ingredient in the characterization in the newly emerging field of topological insulators [5,6]. Recently, the experimental measurement of a Berry phase in a one-dimensional optical lattice (Zak phase [7]) simulating the different phases of polyacetylene [8] has opened the way to extend the applications of geometric phases to study topological properties beyond the realm of condensed-matter systems.

A fundamental problem in the theory and applications of geometrical phases is its extension from pure quantum states (Berry) to mixed quantum states described by density matrices. Uhlmann was the first to mathematically address this issue [9] and to provide a satisfactory solution [10–13]. For more than a decade, there has been a renewed interest in studying geometric phases for mixed states and under dissipative evolutions from the point of view of quantum information [14], and more inequivalent definitions have been introduced [15–17]. This has culminated with the first experimental measurement of a geometric phase for mixed quantum states of one system qubit and one ancillary qubit with NMR techniques [18].

In addition, the role played by external dissipative effects and thermal baths in topological insulators and superconductors has attracted much interest both in quantum simulations with different platforms and in condensed matter [19–29]. In this Letter, we show that the Uhlmann geometric phase is endowed with a topological structure when applied to one-dimensional fermion systems. More concretely, (i) we show that the Uhlmann phase allows us to characterize topological insulators and superconductors at both zero and finite temperatures. (ii) We find a finite critical temperature T_c below which the Uhlmann phase is constant and nonvanishing. At T_c there is a discontinuity, and above it the topological behavior ceases to exist. This kind of behavior is very relevant and not present in other formulations. (iii) We study one-dimensional (1D) paradigmatic models such as the Creutz ladder (CL) [30,31], the Majorana chain (MC) [32], and polyacetylene (SSH) [33,34]. A summary of the basic results of this Letter is presented in Table I. Notably, at the limit of zero temperature the Uhlmann phase recovers the usual notion of topological order as given by the Berry phase. Moreover, when the three models are in a flat-band regime the critical temperature is universal [Eq. (15)].

The Uhlmann approach is based on the concept of amplitude. An amplitude for some density matrix ρ is any of the matrices w such that

$$\rho = ww^\dagger. \tag{1}$$

The key idea behind this definition is that the amplitudes form a Hilbert space $\mathcal{H}_w$ with the Hilbert-Schmidt product $(w_1, w_2) \coloneqq \mathrm{Tr}(w_1^\dagger w_2)$. On the contrary, the set of density matrices $\mathcal{Q}$ is not a linear space. From Eq. (1), we see that there is a U(n)-gauge freedom in the choice of the amplitude (n is the dimension of the space): w and wU are amplitudes of the same state for some unitary operator U.

TABLE I. Comparison of Hamiltonian winding number, Berry, and Uhlmann phases for nontrivial topological regimes in the Creutz ladder (CL), Majorana chain (MC), and polyacetylene (SSH) 1D fermion models.

Topological measures in 1D fermion models	CL	MC	SSH
Winding number ($T = 0$)	1	1	1
Berry phase ($T = 0$)	π	π	π
Uhlmann phase ($T < T_c$)	π	π	π
Uhlmann phase ($T > T_c$)	0	0	0

Note the parallelism with the usual U(1)-gauge freedom of pure states, where $|\psi\rangle$ and $e^{i\phi}|\psi\rangle$ represent the same physical state, i.e., the same density matrix given by $|\psi\rangle\langle\psi|$. Thus, the usual gauge freedom can be seen as a particular case of the amplitude U(n)-gauge freedom.

An amplitude is nothing but another way to see the concept of purification. Indeed, by the polar decomposition theorem, we parametrize the possible amplitudes of some density matrix ρ as $w = \sqrt{\rho}U$. Because of the spectral theorem $\rho = \sum_j p_j |\psi_j\rangle\langle\psi_j|$, we have $w = \sum_j \sqrt{p_j}|\psi_j\rangle\langle\psi_j|U$. Let us define the following isomorphism between the spaces $\mathcal{H}_w$ and $\mathcal{H}\otimes\mathcal{H}$: $w = \sum_j \sqrt{p_j}\,|\psi_j\rangle\langle\psi_j|U \longleftrightarrow |w\rangle = \sum_j \sqrt{p_j}\,|\psi_j\rangle \otimes U^{\mathrm{t}}|\psi_j\rangle$ (here the transposition is taken with respect to the eigenbasis of ρ). The property $\rho = ww^\dagger$ is now written as

$$\rho = \mathrm{Tr}_2(|w\rangle\langle w|). \tag{2}$$

Here, Tr_2 denotes the partial trace over the second Hilbert space of $\mathcal{H}\otimes\mathcal{H}$. In other words, any amplitude w of some density matrix ρ can be seen as a pure state $|w\rangle$ of the enlarged space $\mathcal{H}\otimes\mathcal{H}$, with partial trace equal to ρ. Thus, $|w\rangle$ is a purification of ρ.

Let us consider a family of pure states $|\psi_{\boldsymbol{k}}\rangle\langle\psi_{\boldsymbol{k}}|$ and some trajectory in parameter space $\{\boldsymbol{k}(t)\}_{t=0}^1$, such that the initial and final states are the same. This induces a trajectory on the Hilbert space $\mathcal{H}$, $|\psi_{\boldsymbol{k}(t)}\rangle$, and since the path on $\mathcal{Q}$ is closed, the initial and final vectors are equivalent up to some Φ, $|\psi_{\boldsymbol{k}(1)}\rangle = e^{i\Phi}|\psi_{\boldsymbol{k}(0)}\rangle$. Provided the transportation of the vectors in $\mathcal{H}$ is done following the Berry parallel transport condition (i.e., no dynamical phase is accumulated) Φ is the well-known Berry phase Φ_B. This depends only on the geometry of the path and can be written as $\Phi_B = \oint A_B$, where $A_B := i\sum_\mu \langle\psi_{\boldsymbol{k}}|\partial_\mu\psi_{\boldsymbol{k}}\rangle dk_\mu$ is the Berry connection form ($\partial_\mu := \partial/\partial k_\mu$). Similarly, we may have a closed trajectory of not necessarily pure density matrices $\rho_{\boldsymbol{k}}$, which in turn induces a trajectory on the Hilbert space $\mathcal{H}_w$, $w_{\boldsymbol{k}(t)}$. Again, since the path on $\mathcal{Q}$ is closed, the initial and final amplitudes must differ just in some unitary transformation V, $w_{\boldsymbol{k}(1)} = w_{\boldsymbol{k}(0)}V$. Hence, by analogy to the pure state case, Uhlmann defines a parallel transport condition such that V is given by $V = \mathcal{P}e^{\oint A_U}U_0$, where $\mathcal{P}$ stands for the path ordering operator, A_U is the Uhlmann connection form, and U_0 is the gauge taken at $\boldsymbol{k}(0)$. We have illustrated this parallelism between the Berry and Uhlmann approaches in Fig. 1.

The Uhlmann parallel transport condition asserts that for some point $\rho_{\boldsymbol{k}(t)}$ with amplitude $w_{\boldsymbol{k}(t)}$ the amplitude $w_{\boldsymbol{k}(t+dt)}$ of the next point in the trajectory, $\rho_{\boldsymbol{k}(t+dt)}$, is the closest [35] to $w_{\boldsymbol{k}(t)}$ among the possible amplitudes of $\rho_{\boldsymbol{k}(t+dt)}$. With this rule, it is possible to obtain some explicit formulas for A_U. Concretely, in the spectral basis of $\rho_{\boldsymbol{k}} = \sum_j p^j_{\boldsymbol{k}}|\psi^j_{\boldsymbol{k}}\rangle\langle\psi^j_{\boldsymbol{k}}|$, one obtains [12]

$$A_U = \sum_{\mu,i,j}|\psi^i_{\boldsymbol{k}}\rangle \frac{\langle\psi^i_{\boldsymbol{k}}|[(\partial_\mu\sqrt{\rho_{\boldsymbol{k}}}),\sqrt{\rho_{\boldsymbol{k}}}]|\psi^j_{\boldsymbol{k}}\rangle}{p^i_{\boldsymbol{k}}+p^j_{\boldsymbol{k}}}\langle\psi^j_{\boldsymbol{k}}|dk_\mu. \tag{3}$$

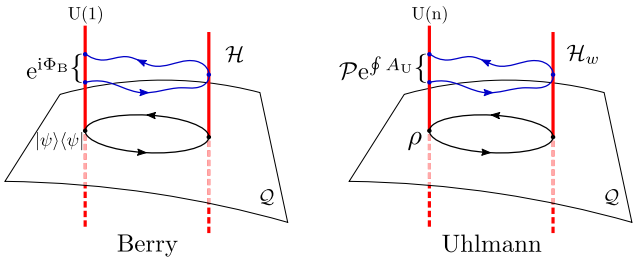

FIG. 1 (color online). Comparison of the Berry and Uhlmann approaches. The usual U(1)-gauge freedom is generalized to the $U(n)$-gauge freedom of the amplitudes in the Uhlmann approach. Thus, according to Berry, after a closed loop in the set $\mathcal{Q}$, a pure state carries a simple phase factor Φ_B. However, for mixed states, the amplitude carries a unitary matrix $\mathcal{P}e^{\oint A_U}$.

Note that this connection form has only zeroes on its diagonal and is skew adjoint so that the Uhlmann connection is special unitary. The Uhlmann geometric phase along a closed trajectory $\{\boldsymbol{k}(t)\}_{t=0}^1$ is defined as

$$\Phi_U := \arg\langle w_{\boldsymbol{k}(0)}|w_{\boldsymbol{k}(1)}\rangle = \arg\mathrm{Tr}[w^\dagger_{\boldsymbol{k}(0)}w_{\boldsymbol{k}(1)}]. \tag{4}$$

By the polar decomposition theorem, we may write $w_{\boldsymbol{k}(0)} = \sqrt{\rho_{\boldsymbol{k}(0)}}U_0$, $w_{\boldsymbol{k}(1)} = \sqrt{\rho_{\boldsymbol{k}(0)}}V$, so that

$$\Phi_U = \arg\mathrm{Tr}[\rho_{\boldsymbol{k}(0)}\mathcal{P}e^{\oint A_U}]. \tag{5}$$

As aforementioned, in this work we shall focus on the Uhlmann phase in 1D fermion models. For such systems, $\boldsymbol{k}\equiv k$ is the one-dimensional crystalline momentum living in a S^1-circle BZ. Thus, because of the nontrivial topology of S^1, geometric phases after a loop in k acquire a topological sense.

Fermionic systems and Uhlmann phase.—Consider two-band Hamiltonians within the spinor representation $\Psi_k = (\hat{a}_k, \hat{b}_k)^{\mathrm{t}}$, where $\hat{a}_k$ and $\hat{b}_k$ stands for two species of fermionic operators. For superconductors, the spinor Ψ_k is constructed out of a Nambu transformation of paired fermions with opposite crystalline momentum [36]. The Hamiltonian is a quadratic form $H = \sum_k \Psi^\dagger_k H_k \Psi_k$, and H_k is a 2×2 matrix

$$H_k = f(k)\mathbb{1} + \frac{\Delta_k}{2}\boldsymbol{n}_k\cdot\boldsymbol{\sigma}. \tag{6}$$

Here, $\boldsymbol{\sigma} = (\sigma_x, \sigma_y, \sigma_z)$ are the Pauli matrices, Δ_k corresponds to the gap of H_k, and $f(k)$ denotes some function of k. The unit vector $\boldsymbol{n}_k = (\sin\theta\cos\phi, \sin\theta\sin\phi, \cos\theta)$ is called the "winding vector" where θ and ϕ are k-dependent spherical coordinates. The band eigenvectors of H_k can be written as

$$|u^k_-\rangle = \begin{pmatrix} -e^{-i\phi(k)}\sin\frac{\theta(k)}{2} \\ \cos\frac{\theta(k)}{2}\end{pmatrix}, \qquad |u^k_+\rangle = \begin{pmatrix} e^{-i\phi(k)}\cos\frac{\theta(k)}{2} \\ \sin\frac{\theta(k)}{2}\end{pmatrix}. \tag{7}$$

If the thermalization process preserves particle number and the Fermi energy is set in the middle of the gap, the equilibrium (thermal) state is given by $\rho_\beta = \prod_k \rho_k^\beta$, with

$$\rho_k^\beta = \frac{e^{-H_k/T}}{\mathrm{Tr}(e^{-H_k/T})} = \frac{1}{2}\left[\mathbb{1} - \tanh\left(\frac{\Delta_k}{2T}\right)\hat{\boldsymbol{n}}_k \cdot \boldsymbol{\sigma}\right], \quad (8)$$

where $T = 1/\beta$ denotes temperature.

By the use of Eq. (7), the Uhlmann connection (3) for ρ_k^β turns out to be

$$A_U^k = m_{12}^k \langle u_-^k | \partial_k u_+^k \rangle |u_-^k\rangle\langle u_+^k| dk + \mathrm{H.c.} \quad (9)$$

where $m_{12}^k := 1 - \mathrm{sech}[\Delta_k/(2T)]$.

Besides, it is well known that discrete symmetries represent a way to classify topological insulators and superconductors [37,38]. Furthermore, for the models considered throughout this Letter, symmetries impose a restriction on the movement of $\boldsymbol{n}_k$ to some plane as a function of k, making only two of its components n_k^i and n_k^j with $i \neq j$ different from zero. Therefore, we have a nontrivial mapping $S^1 \longrightarrow S^1$, characterized by a winding number ω_1. This is defined using the angle α covered by $\boldsymbol{n}_k$ when it winds around the unit circle S^1 and takes the form

$$\omega_1 := \frac{1}{2\pi}\oint d\alpha = \frac{1}{2\pi}\oint \left(\frac{\partial_k n_k^i}{n_k^j}\right) dk, \quad (10)$$

where we have used that $\alpha := \arctan(n_k^i/n_k^j)$.

Moreover, using Eqs. (7) and (10) with (9) and simplifying Eq. (5) we obtain an expression for the Uhlmann phase in terms of ω_1, the temperature, and parameters of the Hamiltonian

$$\Phi_U = \arg\left\{\cos(\pi\omega_1)\cos\left[\oint\left(\frac{\partial_k n_k^i}{2n_k^j}\right)\mathrm{sech}\left(\frac{\Delta_k}{2T}\right)dk\right]\right\}. \quad (11)$$

Particularly, in the limit $T \to 0$,

$$\Phi_U^0 = \arg[\cos(\pi\omega_1)]. \quad (12)$$

Note that for the trivial case $\omega_1 = 0$, the Uhlmann phase is zero as well. However, for nontrivial topological regions $\omega_1 = \pm 1$, we obtain $\Phi_U^0 = \pi$. Thus, the topological order as accounted by Φ_U^0 coincides to the standard notion measured by ω_1. In the following, we compute Φ_U at finite temperature for the three aforementioned models of topological insulators and superconductors.

Creutz ladder.—This model [30] is representative for a topological insulator [24,31] with AIII symmetry [37,38]. It describes the dynamics of spinless electrons moving in a ladder as dictated by the following Hamiltonian:

$$H_{\mathrm{CL}} = -\sum_{n=1}^{L}[R(e^{-i\Theta}a_{n+1}^\dagger a_n + e^{i\Theta}b_{n+1}^\dagger b_n) + R(b_{n+1}^\dagger a_n + a_{n+1}^\dagger b_n) + M a_n^\dagger b_n + \mathrm{H.c.}], \quad (13)$$

where a_n and b_n are fermionic operators associated to the nth site of an upper and lower chain, respectively. The hopping along horizontal and diagonal links is given by $R > 0$ and the vertical one by $M > 0$. In addition, a magnetic flux $\Theta \in [-\pi/2, \pi/2]$ is induced by a perpendicular magnetic field. For nonzero magnetic flux $\Theta \neq 0$ and small vertical hopping $m := M/2R < 1$, the system has localized edge states at the two ends of the open ladder [30]. Interestingly, there exists an experimental proposal for this model with optical lattices [39].

In momentum space, H_{CL} can be written in the form of Eq. (6) with (in units of $2R = 1$)

$$\boldsymbol{n}_k = \frac{2}{\Delta_k}(m + \cos k, 0, \sin\Theta \sin k),$$
$$\Delta_k = 2\sqrt{(m + \cos k)^2 + \sin^2\Theta \sin^2 k}, \quad (14)$$

which in the spinor decomposition made in Eq. (6) implies $\phi = 0, \pi$.

By the means of Eq. (11) we compute the value of the Uhlmann phase (which can only be equal to π or 0) as function of parameters Θ, m, and the temperature T [see Fig. 2(a)]. At $T \to 0$, the topological region coincides with the usual topological phase $\Phi_U^0 = \Phi_B = \pi$ for $m \in [0, 1]$ and $\Theta \in [-(\pi/2), (\pi/2)]$, as expected. However, there exists a critical temperature T_c for any value of the parameters at which the system is not topological in the Uhlmann sense anymore, and Φ_U goes abruptly to zero. The physical meaning of this T_c relies on the existence of some critical momentum k_c splitting the holonomy into two disequivalent topological components according to the value taken by k when performing the closed loop, $\Phi_U(k < k_c) = 0$ and $\Phi_U(k > k_c) = \pi$, respectively. In the trivial topological regime, there is only one component with $\Phi_U = 0$ for every point along the trajectory. Thus, this structure of the Uhlmann amplitudes accounts for a topological kink [40] in the holonomy along the BZ. Further details about the presence or absence with temperature of this topological kink can be seen in the Supplemental Material [41].

Interestingly, at $m = 0$ and $\Theta = \pm(\pi/2)$ (see the arrows in Fig. 2), the edge states become completely decoupled from the system dynamics. When considering periodic boundary conditions, this translates into having *flat bands* in the spectrum. For these flat-band points (FBPs) the critical temperature T_c only depends on the constant value of the gap $\Delta_k = 2$ and can be analytically computed. The result is the same for the three models analyzed in this work,

$$T_c = \frac{1}{\ln(2 + \sqrt{3})}, \quad (15)$$

which is approximately 38% of the gap.

Majorana chain.—Consider a model of spinless fermions with p-wave superconducting pairing, hopping on

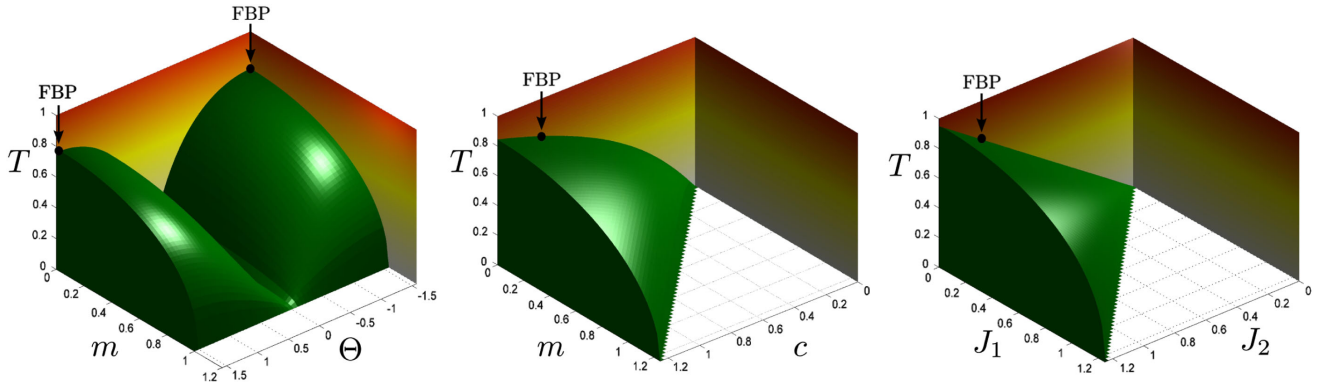

FIG. 2 (color online). Uhlmann topological phases for the CL (a), MC (b), and SSH (c). They are π inside the green volume and zero outside. The FBPs are indicated with an arrow and are universal. Natural units have been taken. In addition, for the CL and the MC we have fixed the horizontal hopping $2R = 1$ and the superconducting pairing $|M| = 1$, respectively.

an L-site one-dimensional chain. The Hamiltonian of this system introduced by Kitaev [32] is

$$H_{\mathrm{MC}} = \sum_{j=1}^{L} \left(-J a_j^\dagger a_{j+1} + M a_j a_{j+1} - \frac{\mu}{2} a_j^\dagger a_j + \mathrm{H.c.} \right), \tag{16}$$

where $\mu > 0$ is the chemical potential, $J > 0$ is the hopping amplitude, the absolute value of $M = |M| e^{i\Theta}$ stands for the superconducting gap, and a_j $(a_j^\dagger)$ are annihilation (creation) fermionic operators.

For convenience, we may redefine new parameters $m := \mu/(2|M|)$ and $c := J/|M|$ and take $\Theta = 0$. It can be shown [32] that the system has nonlocal Majorana modes at the two ends on the chain if $m < c$, which corresponds to nonvanishing ω_1 and Φ_B when taking periodic boundary conditions. Thus, in momentum space, H_{MC} can be written in the form of Eq. (6) using the so-called Nambu spinors $\Psi_k = (a_k, a_{-k}^\dagger)^{\mathrm{t}}$,

$$\begin{aligned} \boldsymbol{n}_k &= \frac{2}{\Delta_k}(0, -\sin k, -m + c\cos k), \\ \Delta_k &= 2\sqrt{(-m + c\cos k)^2 + \sin^2 k}, \end{aligned} \tag{17}$$

in units of $|M| = 1$. This in Eq. (6) implies $\phi = \pm(\pi/2)$.

In analogy to the CL case, we calculate the Uhlmann phase as a function of parameters m, c, and the temperature T [see Fig. 2(b)]. On the one hand, note again that at $T \to 0$ we recover the usual topological phase $\Phi_U^0 = \Phi_B = \pi$ for $m < c$, and on the other hand, there also exists a critical temperature T_c. The FBP corresponds to $m = 0$ and $c = 1$ where the Majorana modes are completely decoupled from the system dynamics. For the FBP, we get the same T_c as before (15) as shown in Fig. 2(b).

Polyacetylene (SSH model).—The following Hamiltonian was introduced in Ref. [34] by Rice and Mele, and it has a topological insulating phase

$$\begin{aligned} H_{\mathrm{SSH}} = &-\sum_n (J_1 a_n^\dagger b_n + J_2 a_n^\dagger b_{n-1} + \mathrm{H.c.}) \\ &+ M \sum_n (a_n^\dagger a_n - b_n^\dagger b_n). \end{aligned} \tag{18}$$

The fermionic operators a_n and b_n act on adjacent sites of a dimerized chain. If the energy imbalance between sites a_n and b_n is $M = 0$, the above Hamiltonian $H \equiv H_{\mathrm{SSH}}$ effectively describes polyacetylene [33], whereas for $M \neq 0$ it can model diatomic polymers [34].

For $M = 0$ and $J_2 > J_1$, there are two edge states at the end of the chain and the system displays topological order, characterized by ω_1 and Φ_B.

In momentum space, H_{SSH} is written in the form of Eq. (6) with

$$\begin{aligned} \boldsymbol{n}_k &= \frac{2}{\Delta_k}(-J_1 - J_2\cos k, J_2 \sin k, 0), \\ \Delta_k &= 2\sqrt{J_1^2 + J_2^2 + 2J_1 J_2 \cos k}, \end{aligned} \tag{19}$$

which in Eq. (6) implies fixing $\theta = \pm(\pi/2)$ for all k.

In Fig. 2(c), we plot Φ_U as a function of the hopping parameters J_1, J_2, and the temperature T. At $T \to 0$, the topological region coincides again with the usual topological phase $\Phi_U^0 = \Phi_B = \pi$ for $J_1 < J_2$, and there exists a critical temperature T_c.

For the FBP, $J_1 = 0$ and $J_2 = 1$, the gap $\Delta_k = 2$ becomes constant and we obtain the same critical temperature as for the other two models; Eq. (15).

Outlook and conclusions.—We have shown that the Uhlmann phase provides us with a way to extend the notion of symmetry-protected topological order in fermion systems beyond the realm of pure states. This comes into

play when studying dissipative effects and particularly thermal baths. When applied to three paradigmatic models of topological insulators and superconductors, it displays a discontinuity in some finite critical temperature T_c, which limits the region with topological behavior. Interestingly enough, a thermal-bulk-edge correspondence with the Uhlmann phase does not exist, and the topology assessed by it does not determine the fate of the edge modes at finite temperature.

Although the analysis has been restricted here to 1D models and some representative examples, we expect that the Uhlmann approach could be extended to higher spacial dimensions and other symmetry classes of topological insulators and superconductors. However, more progress on this line is required.

Finally, let us stress that the Uhlmann phase is an observable [42,43]. Additionally, we analyze possible experimental measurement schemes in the Supplemental Material [41].

We are grateful to the anonymous referee and to Z. Huang for pointing out a correction in a previous version of the manuscript. We thank the Spanish MINECO Grants No. FIS2012-33152 and No. FIS2009-10061, CAM research consortium QUITEMAD S2009-ESP-1594, European Commission PICC: FP7 2007-2013, Grant No. 249958, UCM-BS Grant No. GICC-910758, FPU MEC Grant and Residencia de Estudiantes.

[1] M. V. Berry, Proc. R. Soc. A **392**, 45 (1984).
[2] B. Simon, Phys. Rev. Lett. **51**, 2167 (1983).
[3] A. Shapere and F. Wilczek, *Geometric Phases in Physics* (World Scientific, Singapore, 1989).
[4] D. J. Thouless, M. Kohmoto, M. P. Nightingale, and M. den Nijs, Phys. Rev. Lett. **49**, 405 (1982).
[5] M. Z. Hasan and C. L. Kane, Rev. Mod. Phys. **82**, 3045 (2010).
[6] X.-L. Qi and S.-C. Zhang, Rev. Mod. Phys. **83**, 1057 (2011).
[7] J. Zak, Phys. Rev. Lett. **62**, 2747 (1989).
[8] M. Atala, M. Aidelsburger, J. T. Barreiro, D. Abanin, T. Kitagawa, E. Demler, and I. Bloch, Nat. Phys. **9**, 795 (2013).
[9] A. Uhlmann, Rep. Math. Phys. **24**, 229 (1986).
[10] A. Uhlmann, Ann. Phys. (Berlin) **501**, 63 (1989).
[11] A. Uhlmann, Lett. Math. Phys. **21**, 229 (1991).
[12] M. Hübner, Phys. Lett. A **179**, 226 (1993).
[13] A. Uhlmann, J. Geom. Phys. **18**, 76 (1996).
[14] E. Sjöqvist, A. K. Pati, A. Ekert, J. S. Anandan, M. Ericsson, D. K. L. Oi, and V. Vedral, Phys. Rev. Lett. **85**, 2845 (2000).
[15] R. Bhandari, Phys. Rev. Lett. **89**, 268901 (2002).
[16] J. S. Anandan, E. Sjöqvist, A. K. Pati, A. Ekert, M. Ericsson, D. K. L. Oi, and V. Vedral, Phys. Rev. Lett. **89**, 268902 (2002).
[17] P. B. Slater, Lett. Math. Phys. **60**, 123 (2002).
[18] J. Du, P. Zou, M. Shi, L. C. Kwek, J.-W. Pan, C. H. Oh, A. Ekert, D. K. L. Oi, and M. Ericsson, Phys. Rev. Lett. **91**, 100403 (2003).
[19] M. Müller, S. Diehl, G. Pupillo, and P. Zoller, Adv. At. Mol. Opt. Phys. **61**, 1 (2012).
[20] C.-E. Bardyn, M. A. Baranov, C. V. Kraus, E. Rico, A. İmamoğlu, P. Zoller, and S. Diehl, New J. Phys. **15** 085001 (2013).
[21] C.-E. Bardyn, M. A. Baranov, E. Rico, A. İmamoğlu, P. Zoller, and S. Diehl, Phys. Rev. Lett. **109**, 130402 (2012).
[22] C. V. Kraus, S. Diehl, P. Zoller, and M. A. Baranov, New J. Phys. **14**, 113036 (2012).
[23] L. Mazza, M. Rizzi, M. D. Lukin, and J. I. Cirac, Phys. Rev. B **88**, 205142 (2013).
[24] O. Viyuela, A. Rivas, and M. A. Martin-Delgado, Phys. Rev. B **86**, 155140 (2012).
[25] A. Rivas, O. Viyuela, and M. A. Martin-Delgado, Phys. Rev. B **88**, 155141 (2013).
[26] I. Garate, Phys. Rev. Lett. **110**, 046402 (2013).
[27] L.-J. Lang, X. Cai, and S. Chen, Phys. Rev. Lett. **108**, 220401 (2012).
[28] Y. E. Kraus, Y. Lahini, Z. Ringel, M. Verbin, and O. Zilberberg, Phys. Rev. Lett. **109**, 106402 (2012).
[29] L. Tarruell, D. Greif, T. Uehlinger, G. Jotzu, and T. Esslinger, Nature (London) **483**, 302 (2012).
[30] M. Creutz, Phys. Rev. Lett. **83**, 2636 (1999).
[31] A. Bermudez, D. Patanè, L. Amico, and M. A. Martin-Delgado, Phys. Rev. Lett. **102**, 135702 (2009).
[32] A. Y. Kitaev, Phys. Usp. **44**, 131 (2001).
[33] W. P. Su, J. R. Schrieffer, and A. J. Heeger, Phys. Rev. Lett. **42**, 1698 (1979).
[34] M. J. Rice and E. J. Mele, Phys. Rev. Lett. **49**, 1455 (1982).
[35] In the sense of the Hilbert space distance $\|w_{\boldsymbol{k}(t)} - w_{\boldsymbol{k}(t+dt)}\| = \sqrt{(w_{\boldsymbol{k}(t)} - w_{\boldsymbol{k}(t+dt)}, w_{\boldsymbol{k}(t)} - w_{\boldsymbol{k}(t+dt)})}$.
[36] A. Altland and B. Simons, *Condensed Matter Field Theory* (Cambridge University Press, New York, 2010).
[37] A. P. Schnyder, S. Ryu, A. Furusaki, and A. W. W. Ludwig, Phys. Rev. B **78**, 195125 (2008).
[38] A. Kitaev, AIP Conf. Proc. **1134**, 22 (2009).
[39] L. Mazza, A. Bermudez, N. Goldman, M. Rizzi, M. A. Martin-Delgado, and M. Lewenstein, New J. Phys. **14**, 015007 (2012).
[40] S. Coleman, *Aspects of Symmetry: Selected Erice Lectures* (Cambridge University Press, Cambridge, England, 1985).
[41] See the Supplemental Material at http://link.aps.org/supplemental/10.1103/PhysRevLett.112.130401 for details about the topological meaning of T_c and possible measurements schemes for Φ_U.
[42] M. Ericsson, A. K. Pati, E. Sjöqvist, J. Brännlund, and D. K. L. Oi, Phys. Rev. Lett. **91**, 090405 (2003).
[43] J. Aberg, D. Kult, E. Sjöqvist, and D. K. L. Oi, Phys. Rev. A **75**, 032106 (2007).

Supplementary Material: Uhlmann Phase as a Topological Measure for One-Dimensional Fermion Systems

O. Viyuela, A. Rivas and M.A. Martin-Delgado
Departamento de Física Teórica I, Universidad Complutense, 28040 Madrid, Spain

I. GEOMETRICAL MEANING OF T_c

The appearance of a critical temperature T_c in the Uhlmann phase can be better understood from a very simple model for the behavior of the Uhlmann holonomy in fermion systems.

For the sake of simplicity, let us represent the amplitudes (or purifications) as two-dimensional arrows and the phase between two of them as the angle between their corresponding arrows. In Fig. 1, we sketch different behaviors of the amplitudes (arrows) when they are transported according to the Uhlmann's parallel condition along a closed trajectory embracing the whole Brillouin zone, i.e. from $k=-\pi$ to $k=\pi$, this is left to right on the Fig. 1. We observe several situations:

i) $T=0$ in the trivial topological regime [Fig. 1(a)]. The arrow is transported with constant slope, the initial and final arrows are parallel, so that $\Phi_{\mathrm{U}}^{0}=\Phi_{\mathrm{B}}=0$.

ii) $T=0$ in the non-trivial topological regime [Fig. 1(b)]. The Uhlmann phase remains 0 until some singular point k_c, where the direction of the amplitude is suddenly flipped, and so it remains up to the final point $k=\pi$. Thus, the initial arrow and the final arrow form an angle of π, then $\Phi_{\mathrm{U}}^{0}=\Phi_{\mathrm{B}}=\pi$.

iii) $T_c>T>0$ in a non-trivial topological regime [Fig. 1(c)]. The behavior of the Uhlmann phase follows a similar pattern as before, but now the temperature displaces the position of k_c towards the end of the Brillouin zone.

iv) $T=T_c$ in a non-trivial topological regime [Fig. 1(d)]. The position of k_c reaches the end of the Brillouin zone.

v) $T>T_c$ [Fig. 1(a)]. The temperature is so high that a kink never takes place during the trajectory from $k=-\pi$ to $k=\pi$, hence the arrow does not flip and then the Uhlmann phase vanishes $\Phi_{\mathrm{U}}=0$.

Note that the Uhlmann phase places on equal footing T and the parameters of the Hamiltonian H. Thus, the position of the critical momentum k_c is affected by both H and T.

In summary, as commented in the letter, the existence of a critical temperature T_c is connected to a topological kink structure [1] in the Uhlmann holonomy. More precisely, the variation of temperature produces the presence of absence of a topological kink associated to the physical critical momentum k_c. In fact, there is not a connection between the Uhlmann phase and the presence or absence of edge states. The critical momentum k_c splits the holonomy into two dis-equivalent topological components according to the value taken by k when performing the trajectory. The first component is the region with $k<k_c$ and $\Phi_{\mathrm{U}}=0$, and the second is the region with $k>k_c$ and $\Phi_{\mathrm{U}}=\pi$. Note that these two different components cannot be smoothly connected as for that aim the momentum has to cross the singular point $k=k_c$. In the trivial topological regime $\Phi_{\mathrm{U}}=0$ for every point along the trajectory and there is only one component. The effect of the temperature in the Uhlmann parallel transport can be understood as a displacement of the topological kink along k-space. The critical temperature corresponds to the situation where k_c is at the edge of the Brillouin zone. In other words, T_c determines the admissible amount of noise/disorder such that the Uhlmann holonomy along the Brilluoin zone presents a topological kink structure. For $T>T_c$, the noise is high enough

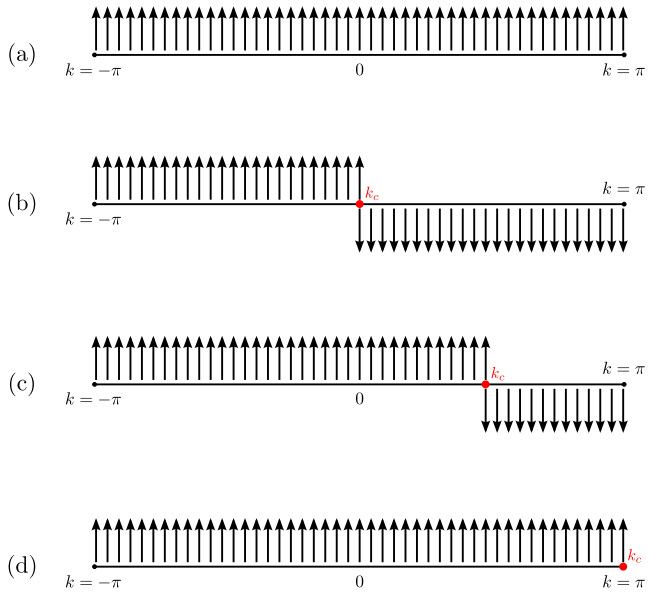

FIG. 1: Schematic plot for the behavior of the Uhlmann phase during the parallel transport from $k=-\pi$ to $k=\pi$ for different situations: $T=0$ and trivial topological regime or $T>T_c$ (a), $T=0$ and nontrivial topological regime (b), $T_c>T>0$ and nontrivial topological regime (c), and $T=T_c$ (d). See comments on the main text of this document.

that the kink is effectively "erased" and the Uhlmann geometric phase becomes trivial.

II. MEASUREMENT OF THE UHLMANN PHASE

As stressed in the letter, the Uhlmann phase is a physical observable. Thus, for the sake of completion we provide here some hints about its measurement in a real experiment. The purpose of this section is to explain how the already existing experimental proposals to measure the Uhlmann phase in the optical domain [2, 3] could be adapted to 1D fermionic systems.

Since the Uhlmann holonomy is defined as a relative phase between amplitudes, in order to measure it we need some auxiliary degree of freedom to construct them from density matrices. We hereby present two different ways for this to be implemented.

A. Purification approach

This method is based on the fact that amplitudes w_k can be seen as pure states $|w_k\rangle$ living in an enlarged Hilbert space $\mathcal{H} = \mathcal{H}_{\rm S} \otimes \mathcal{H}_{\rm A}$ where both system and ancilla Hilbert spaces are of the same dimension [2].

For instance, we may introduce two electrons in the system with the same crystalline momentum k_0 and in the lowest energy band, differing only in a particular non-dynamical degree of freedom. Taking the Creuzt ladder model as an example, the two electrons could differ on their spins ($\uparrow\downarrow$) and be prepared in their ground states. Once this has been done, we may apply the following steps:

1. Prepare an entangled state in the diagonal basis of the two electrons of the following form:

$$|w_{k_0}\rangle = \sqrt{\tfrac{1+r_{k_0}}{2}}|u_-^{\uparrow k_0}\rangle \otimes |u_-^{\downarrow k_0}\rangle + \sqrt{\tfrac{1-r_{k_0}}{2}}|u_+^{\uparrow k_0}\rangle \otimes |u_+^{\downarrow k_0}\rangle, \quad (1)$$

where $r_{k_0} := \tanh \beta \frac{\Delta_{k_0}}{2}$. Let us take for simplicity the flat-band case where $\Delta_k = 2$. Therefore, once the temperature is fixed, r_k is a constant during the holonomy. By taking partial trace with respect to the ancillary electron, the reduced state for the system electron is

$$\rho_{k_0} = {\rm Tr}_{\rm A}(|w_{k_0}\rangle\langle w_{k_0}|) = \frac{1}{2}\Big(\mathbb{1} - r_{k_0}\sigma_z\Big). \quad (2)$$

This corresponds to a thermal state of the system written in the diagonal basis of the system Hamiltonian.

2. Implement the holonomy in $k-$space. For example by applying the unitary operation $V_{k(t)}$ on the ancillary electron. This is determined by imposing the Uhlmann's parallel transport condition on the trajectory $\{k(t)\}_{t=0}^{1}$ such that $k(0) = k_0$ and $k(1) = k_0 + G$, where G stands for the reciprocal lattice vector. This might be achieved using a spin dependent force.

3. Interferometry to measure the relative phase. To retrieve the Uhlmann phase, we make use of

$$\Phi_{\rm U} = \arg\langle w_{k(0)}|w_{k(1)}\rangle. \quad (3)$$

This can be implemented using atom interferometry techniques similar to those in [4]. Another example where the degree of control over fermionic systems is at the highest level can be found in [5].

B. System plus ancillary qubit

A different approach to construct amplitudes was proposed for the optical domain in [3]. The idea is again to enlarge the Hilbert space $\mathcal{H} = \mathcal{H}_{\rm S} \otimes \mathcal{H}_{\rm qubit}$. However, instead of preparing two copies of the system, it is just required an auxiliary two-dimensional quantum system (qubit). Then system and qubit are prepared in a certain mixed state $\hat{\rho}$. It can be shown that the amplitudes associated to the state $\rho_k = w_k w_k^\dagger$ appear in the coherences of this larger state $\hat{\rho}_k$ [3]:

$$\hat{\rho}_k = \frac{1}{2}\rho_k \otimes |0\rangle\langle 0| + \frac{1}{2n}\mathbb{1} \otimes |1\rangle\langle 1| + \frac{1}{2\sqrt{n}} w_k \otimes |0\rangle\langle 1| + \frac{1}{2\sqrt{n}} w_k^\dagger \otimes |1\rangle\langle 0|, \quad (4)$$

where n is the dimension of the system, i.e. the number of bands for the fermion models. Secondly, a protocol can be designed [3] in order to implement the unitary $V_{k(t)}$ on the amplitude and retrieve the Uhlmann phase after the holonomy using again atom interferometric techniques.

Therefore, we can envision possible measurement schemes for the Uhlmann phase in fermionic systems based on what has already been proposed previously for photons in the context of geometric phases for qubits. However, giving a precise experimental proposal for a particular setup would require further analysis which is beyond the scope of this paper.

[1] S. Coleman *Aspects of Symmetry: Selected Erice Lectures* (Cambridge University Press, Cambridge, 1985).

[2] M. Ericsson, A. K. Pati, E. Sjöqvist, J. Brännlund and D. K. L. Oi, Phys. Rev. Lett. **91**, 090405 (2003).

[3] J. Aberg, D. Kult, E. Sjöqvist and D. K. L. Oi, Phys. Rev. A **75**, 032106 (2007).

[4] M. Atala, M. Aidelsburger, J. T. Barreiro, D. Abanin, T. Kitagawa, E. Demler and I. Bloch, Nat. Phys. **9**, 795 (2013).

[5] L. Tarruell, D. Greif, T. Uehlinger, G. Jotzu and T. Esslinger, Nature **483**, 302 (2012).

Two-Dimensional Density-Matrix Topological Fermionic Phases: Topological Uhlmann Numbers

O. Viyuela, A. Rivas, and M. A. Martin-Delgado
Departamento de Física Teórica I, Universidad Complutense, 28040 Madrid, Spain
(Received 30 May 2014; published 13 August 2014)

We construct a topological invariant that classifies density matrices of symmetry-protected topological orders in two-dimensional fermionic systems. As it is constructed out of the previously introduced Uhlmann phase, we refer to it as the topological Uhlmann number n_U. With it, we study thermal topological phases in several two-dimensional models of topological insulators and superconductors, computing phase diagrams where the temperature T is on an equal footing with the coupling constants in the Hamiltonian. Moreover, we find novel thermal-topological transitions between two nontrivial phases in a model with high Chern numbers. At small temperatures we recover the standard topological phases as the Uhlmann number approaches to the Chern number.

DOI: 10.1103/PhysRevLett.113.076408 PACS numbers: 71.10.Pm, 03.65.Vf, 03.65.Yz, 73.43.Nq

Introduction.—Intrinsic topological orders (TOs) [1–4], and symmetry-protected topological orders (SP-TOs), like topological insulators and superconductors in fermionic [5–13], or more recently, bosonic [14–18] systems, have been extensively studied and classified. Although these studies provide a successful picture for quantum systems in pure states, typically the ground state, very little is known about the fate of those topological phases of matter when the system is in a mixed quantum state represented by a density matrix. In fact, the correct understanding of this situation becomes particularly relevant in order to address unavoidable thermal effects on topological phases and nonequilibrium dynamics under dissipation [19].

Over the last few years, there have been some results establishing the absence of stable topological phases subject to thermal effects, like for TOs with spins [20–22], for SP-TOs with spins [23], or SP-TOs with fermions under certain conditions [24]. However, in a recent work [25] we have shown that it is possible to characterize a thermal topological phase for topological insulators and superconductors in one-dimensional systems. This thermal topological phase, classified by Uhlmann holonomies [26,27], is separated from a trivial phase by a critical finite temperature, at which the topological phase abruptly disappears. This result paves the way towards the characterization of SP-TOs with fermions in thermal states, or more general density matrices.

In this paper, we have achieved this goal for two-dimensional fermion systems, either insulating or superconducting. This extension from one to two-dimensional systems is nontrivial in the sense that a direct generalization of the topological invariants for pure states (Chern numbers) to density matrices via the Uhlmann approach leads to trivial results. However, we have succeeded in circumventing this problem and introducing a suitable notion of topological Uhlmann numbers. These are gauge invariant and observable quantities which allows for a classification of topological phases of density matrices in two-dimensional quantum systems. Specifically, we have applied this approach to determine new topological phase diagrams including temperature for three emblematic models of two-dimensional insulators and superconductors. As a result, we have found a thermal topological phase for a two-dimensional chiral p-wave superconductor, which can host vortices with non-Abelian Majorana fermions, and thermal-topological transitions between two nontrivial phases in a model with high Chern numbers.

First of all, let us briefly recall the basic concepts of the Uhlmann approach, the reader may see [25–27] for a more detailed picture. Let $\mathcal{Q}$ denote the convex set of density matrices. For some $\rho \in \mathcal{Q}$, any of the matrices w such that $\rho = ww^\dagger$ is called an amplitude of ρ. The set of amplitudes generates the set $\mathcal{Q}$ via this equation and forms a Hilbert space $\mathcal{H}_w$ with the Hilbert-Schmidt product $(w_1, w_2) \coloneqq \mathrm{Tr}(w_1^\dagger w_2)$. This aims to be the density-matrix analogy to the standard situation where vector states $|\psi\rangle$ span a Hilbert space and generate pure states by the relation $|\psi\rangle\langle\psi|$. Actually, the phase freedom of pure states [U(1)-gauge freedom], is generalized to a U(n)-gauge freedom (n is the dimension of the space), as w and wU are amplitudes of the same density matrix for some unitary operator U.

Now, let $\boldsymbol{k}(t)|_{t=0}^{1}$ define a (closed) trajectory along a family of density matrices parametrized by $\boldsymbol{k}$, $\rho_{\boldsymbol{k}}$. By defining a proper parallel transport condition on the amplitudes $w_{\boldsymbol{k}(t)}$, $\rho_{\boldsymbol{k}(t)} = w_{\boldsymbol{k}(t)} w_{\boldsymbol{k}(t)}^\dagger$, it is possible to define a geometric phase for density matrices via the associated holonomy. More concretely, after the parallel transportation we have $w_{\boldsymbol{k}(1)} = w_{\boldsymbol{k}(0)} V$, with unitary $V = \mathcal{P} e^{\oint A_{\mathrm{U}}}$; where $\mathcal{P}$ stands for the path ordering operator along the trajectory $\boldsymbol{k}(t)|_{t=0}^{1}$, and $A_{\mathrm{U}} = \sum_\mu A_\mu^{\mathrm{U}}(\boldsymbol{k}) dk_\mu$ is the so-called Uhlmann connection form. The geometric phase is defined from the mismatch between the initial point $w_{\boldsymbol{k}(0)}$ and final point $w_{\boldsymbol{k}(1)} = w_{\boldsymbol{k}(0)} V$. Specifically,

$$\Phi_{\mathrm{U}} \coloneqq \arg(w_{\boldsymbol{k}(0)}, w_{\boldsymbol{k}(1)}), \tag{1}$$

which is a gauge-independent quantity [26,27]. In the particular gauge where $w_{\boldsymbol{k}(0)} = \sqrt{\rho_{\boldsymbol{k}(0)}}$, it takes the simple form

$$\Phi_{\mathrm{U}} = \arg(w_{\boldsymbol{k}(0)}, w_{\boldsymbol{k}(1)}) = \arg \mathrm{Tr}\left[\rho_{\boldsymbol{k}(0)} \mathcal{P} \mathrm{e}^{\oint A_{\mathrm{U}}}\right], \tag{2}$$

where the components of the connection are given by [28]

$$A_{\mathrm{U}} = \sum_{\mu,i,j} |\psi^i_{\boldsymbol{k}}\rangle \frac{\langle \psi^i_{\boldsymbol{k}}|[(\partial_\mu \sqrt{\rho_{\boldsymbol{k}}}), \sqrt{\rho_{\boldsymbol{k}}}]|\psi^j_{\boldsymbol{k}}\rangle}{p^i_{\boldsymbol{k}} + p^j_{\boldsymbol{k}}} \langle \psi^j_{\boldsymbol{k}}| dk_\mu, \tag{3}$$

in the spectral basis of $\rho_{\boldsymbol{k}} = \sum_j p^j_{\boldsymbol{k}} |\psi^j_{\boldsymbol{k}}\rangle\langle\psi^j_{\boldsymbol{k}}|$, with $\partial_\mu \coloneqq \partial/\partial k_\mu$.

The phase Φ_{U}, which is experimentally observable [29–31], has a purely geometric meaning in the sense that it depends only on the geometry of the trajectory. Although in general Φ_{U} may change with the starting point of the trajectory $\boldsymbol{k}(0)$, as we shall see, it can be used to construct topological invariants that are independent of this starting point.

At zero temperature, the standard method to define topological invariants in two-dimensional SP-TO systems is by means of Chern numbers. In the simplest scenario, we consider a time-reversal broken two-band system with the Fermi energy between both bands. Then the Chern number is given by

$$\mathrm{Ch} \coloneqq \frac{1}{2\pi} \int_{\mathrm{BZ}} d^2\boldsymbol{k} F_{xy}(\boldsymbol{k}),$$
$$F_{xy}(\boldsymbol{k}) \coloneqq \partial_x A_y(\boldsymbol{k}) - \partial_y A_x(\boldsymbol{k}), \tag{4}$$

where BZ stands for Brillouin zone, $A_j(\boldsymbol{k}) = i\langle u_{\boldsymbol{k}}|\partial_j u_{\boldsymbol{k}}\rangle$ is the Berry connection and $|u_{\boldsymbol{k}}\rangle$ is the eigenvector corresponding to the lower energy band. This number is a topological invariant which only takes on integer values. While this kind of constructions can be extended to higher dimensional systems or systems with time-reversal symmetry [13], when attempting the generalization to density matrices via the Uhlmann connection, one finds the following fundamental obstruction.

Triviality of the Uhlmann Chern number.—The natural way to generalize the Chern number to arbitrary density matrices is to consider the first Chern class associated to the Uhlmann curvature, which is constructed from the Uhlmann connection A_{U} via the standard formula for the non-Abelian case, $F^{\mathrm{U}}_{xy} = \partial_x A^{\mathrm{U}}_y - \partial_y A^{\mathrm{U}}_x + [A^{\mathrm{U}}_x, A^{\mathrm{U}}_y]$. Then, according to the theory of characteristics classes [32,33], the (first) Chern number of the Uhlmann curvature would be given by $\mathrm{Ch}_{\mathrm{U}} \coloneqq (\mathrm{i}/2\pi) \int_{\mathrm{BZ}} d^2\boldsymbol{k} \mathrm{Tr}(F^{\mathrm{U}}_{xy})$; however, this number turns out to be always zero. The reason for this is twofold: on the one hand, the Uhlmann connection belongs to the $\mathfrak{su}(n)$ Lie algebra, so its trace vanishes and so does the trace of its curvature; on the other hand, the Chern number is 0 if there is a smooth gauge defined along the whole BZ [32,33], and this is the case for the Uhlmann $\mathrm{U}(n)$ gauge. We can take the gauge $w_{\boldsymbol{k}} = \sqrt{\rho_{\boldsymbol{k}}}$ which is well defined provided that $\rho_{\boldsymbol{k}}$ is not singular at some crystalline momentum $\boldsymbol{k}$, which is a rather natural condition [34]. Therefore $\mathrm{Ch}_{\mathrm{U}} = 0$ in any case.

This makes not obvious the extension of two-dimensional topological invariants by means of the Uhlmann approach. We hereby show the way to circumvent this obstruction.

Topological Uhlmann numbers.—The fact that Ch_{U} becomes identically zero does not mean that all topological properties of density matrices are trivial. If this assertion were true, we could not claim that systems at $T = 0$ display topological order, as they are just a particular case of generally mixed density matrices. Note that Ch_{U} is not the only topological invariant that we can construct on a torus. Actually, in the Berry case, the Chern number (4) can be rewritten as [35–37]

$$\mathrm{Ch} = \frac{1}{2\pi} \oint dk_x \frac{d\Phi_{\mathrm{B}}(k_x)}{dk_x}, \tag{5}$$

where $\Phi_{\mathrm{B}}(k_x) = \oint dk_y A_y(k_x, k_y)$ is the Berry phase along the k_y nontrivial homological circle of the torus at the point k_x, and $\oint dk_x$ denotes the integration along the k_x nontrivial homological circle. To prove the equality (5), one divides the surface integral (4) in small slices along the k_x direction and applies the Stokes's theorem to each of them [the U(1) gauge, which may be ill defined over the whole BZ, is always well defined in a sufficiently small slice]. Then, in the limit of slices with infinitesimal width, the sum becomes an integral and one immediately obtains Eq. (5). If $\Phi_{\mathrm{B}}(k_x)$ displays some 2π-discontinuous jumps along the k_x circle, we take $\Phi_{\mathrm{B}}(k_x)$ to be a smooth function equal to $\oint dk_y A_y(k_x, k_y)$ mod. 2π in to order to calculate its derivative. Actually, what the Chern number is measuring is the number of those 2π jumps, i.e., the number of windings of $\Phi_{\mathrm{B}}(k_x)$ as the k_x circle is covered. This is clearly a topological invariant, particularly a winding number. It associates every state of the system with an homotopy class of the Berry phase mapping $\Phi_{\mathrm{B}}(k_x): S^1 \to S^1$, between the nontrivial homological circle S^1 and the complex phases $U(1) \cong S^1$.

Remarkably, in contrast to Eq. (4), the equivalent formula (5) allows for a nontrivial generalization to density matrices. To that aim, we proceed by substituting the Berry phase $\Phi_{\mathrm{B}}(k_x)$ by the Uhlmann phase $\Phi_{\mathrm{U}}(k_x)$, Eq. (2), in Eq. (5):

$$\mathrm{n}_{\mathrm{U}} \coloneqq \frac{1}{2\pi} \oint dk_x \frac{d\Phi_{\mathrm{U}}(k_x)}{dk_x}. \tag{6}$$

Analogously to the Berry case, this integer number is a topological invariant which classifies the density matrices of a quantum system according to the homotopy class of the Uhlmann phase mapping, $\Phi_{\mathrm{U}}(k_x): S^1 \to S^1$. Moreover, since for pure states $\Phi_{\mathrm{U}} = \Phi_{\mathrm{B}}$, by computing n_U in a thermal (Gibbs) state, we have that $\mathrm{n}_{\mathrm{U}} \xrightarrow{T\to 0} \mathrm{Ch}$; hence, the

generalization is faithful. Additionally, since Φ_U is an observable, n_U is also an observable. We will refer to this topological invariant n_U as the Uhlmann number.

In what follows, we classify the topological properties of some models of two-band topological insulators and superconductors at finite temperature according to the topological invariant n_U. We shall consider the analogous situation to [25] where the thermalization process preserves the number of particles and the crystalline momentum such as the equilibrium state splits in one-particle Gibbs states $\rho_{\boldsymbol{k}}^{\beta} = \exp[-\beta H(\boldsymbol{k})]/Z$. Here, $H(\boldsymbol{k})$ is the one-particle Hamiltonian represented by a 2×2 matrix in the band indexes. Thus, the total Hamiltonian of these systems is a quadratic form $H_s = \sum_{\boldsymbol{k}\in \mathrm{BZ}} \Psi_{\boldsymbol{k}}^{\dagger} H(\boldsymbol{k}) \Psi_{\boldsymbol{k}}$. In the case of insulators, $\Psi_{\boldsymbol{k}} = (a_{\boldsymbol{k}}, b_{\boldsymbol{k}})^{\mathrm{t}}$, where $a_{\boldsymbol{k}}$ and $b_{\boldsymbol{k}}$ represent two species of fermions, while for superconductors, $\Psi_{\boldsymbol{k}} = (c_{\boldsymbol{k}}, c_{-\boldsymbol{k}}^{\dagger})^{\mathrm{t}}$ is the Nambu spinor for paired fermions with opposite crystalline momentum [13]. We take lattice spacing $a = 1$ throughout the text.

Two-dimensional topological superconductor.—Let us consider the chiral p-wave superconductor [13,38–40]. This system can host vortices with non-Abelian anyonic statistics [40] that are of great relevance in proposals for topological quantum computation [41]. The lattice Hamiltonian for this model is

$$H = \sum_{ij} \Big[-t(c_{i+1,j}^{\dagger} c_{i,j} + c_{i,j+1}^{\dagger} c_{i,j}) - \frac{1}{2}(\mu - 4t) c_{i,j}^{\dagger} c_{i,j} + \Delta(c_{i+1,j}^{\dagger} c_{i,j}^{\dagger} + \mathrm{i} c_{i,j+1}^{\dagger} c_{i,j}^{\dagger}) + \mathrm{H.c.} \Big], \tag{7}$$

where μ is the chemical potential, t is the nearest-neighbor hopping, and Δ is the superconductive pairing.

Without lost of generality, we fix $t = |\Delta| = 1/2$. By means of a Bogoliubov transformation, we obtain the Hamiltonian in the Nambu spinor basis in momentum space,

$$H(\boldsymbol{k}) = -\{\sin(k_y)\sigma_x + \sin(k_x)\sigma_y + [\mu - 2 + \cos(k_x) + \cos(k_y)]\sigma_z\}; \tag{8}$$

here, $\sigma_{x,y,z}$ are the three Pauli matrices.

At $T = 0$, the different topological phases as classified by the Chern number, Eq. (4), are $\mathrm{Ch} = 1$ if $0 < \mu < 2$, $\mathrm{Ch} = -1$ if $2 < \mu < 4$, and $\mathrm{Ch} = 0$ otherwise. For nontrivial regions $\mathrm{Ch} = \pm 1$, the system presents chiral Majorana modes at the edges.

At finite temperature, the different topological phases as classified by the Uhlmann number, Eq. (6), are graphically represented in Fig. 1. The system displays nontrivial topological phases $n_U = \pm 1$ even at nonzero temperature provided it is below a certain critical value T_c, where n_U goes to zero. This critical temperature T_c reaches the maximum value at the middle points $\mu = 1$ and $\mu = 3$ of the topological phases $\mathrm{Ch} = \pm 1$ at $T = 0$. These points are the ones with the highest value of the gap. As expected, in the limit of $T = 0$ we recover the same topological diagram as given by the Chern number.

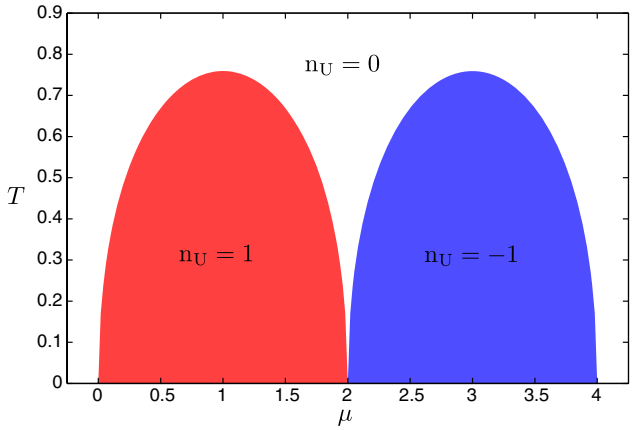

FIG. 1 (color online). Topological Uhlmann phases for the p-wave superconductor model as a function of the chemical potential μ and the temperature T. At $T = 0$, the system has $\mathrm{Ch} = +1$ for $0 < \mu < 2$, $\mathrm{Ch} = -1$ for $2 < \mu < 4$, and $\mathrm{Ch} = 0$ otherwise. As T increases, the nontrivial phases remain up to some critical temperature T_c at which Uhlmann number goes from $n_U = \pm 1$ to $n_U = 0$.

Thus, we see that thermal topological phase transitions are not a unique phenomenon of the one-dimensional case [25] and they may be also found in two-dimensional systems.

Two-dimensional topological insulator with high Chern number.—We consider here the model proposed in [42] that allows us to study two-dimensional topological insulators with high values of the Chern number [43], as in multiband models like the Hofstadter model [44], but still being two-band and analytically solvable.

This system is realized on a triangular lattice of fermionic atoms at each site with an internal orbital degree of freedom. The Hamiltonian is given by

$$H = \sum_{ij} [c_{i+1,j}^{\dagger}(t_1\sigma_x + \mathrm{i}t_3\sigma_z)c_{i,j} + c_{i,j+1}^{\dagger}(t_1\sigma_y + \mathrm{i}t_3\sigma_z)c_{i,j} + c_{i+1,j+1}^{\dagger}(t_2\sigma_z)c_{i,j} + \mathrm{H.c.}]. \tag{9}$$

The Pauli matrices act on the orbital degrees of freedom at each site, which give rise to an orbital dependent nearest-neighbor hopping (t_1, t_2, t_3). In particular, the fermions can gain π or $\pi/2$ phases depending on the initial and final orbital and position state when tunnelling. As in the Haldane model (see below), there is no net magnetic flux in the system, although time-reversal symmetry is broken.

Taking periodic boundary conditions the Hamiltonian in momentum space turns out to be

$$H(\boldsymbol{k}) = 2t_1\cos(k_x)\sigma_x + 2t_1\cos(k_y)\sigma_y + \{2t_2\cos(k_x + k_y) + 2t_3[\sin(k_x) + \sin(k_y)]\}\sigma_z. \tag{10}$$

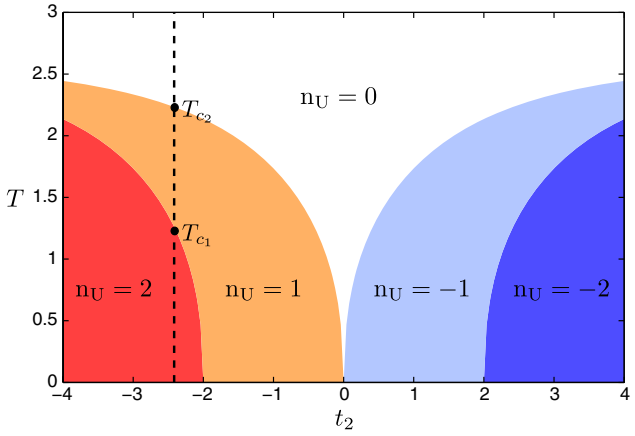

FIG. 2 (color online). Uhlmann topological phase diagram for the model of Eq. (10). The Uhlmann number is plotted for different values of t_2 and T. The dashed line highlights the purely thermal topological transitions between regimes of $n_U = 2$, $n_U = 1$, and $n_U = 0$ by the sole effect of increasing T.

Without loss of generality we take $t_1 = t_3 = 1$. At zero temperature the topological phases as a function of t_2 are

$$\mathrm{Ch} = \begin{cases} +2, & \text{if } t_2 < -2, \\ +1, & \text{if } -2 < t_2 < 0, \\ -1, & \text{if } 0 < t_2 < 2, \\ -2, & \text{if } t_2 > 2. \end{cases} \tag{11}$$

For $T \neq 0$, the topological phase diagram according to Uhlmann number, Eq. (6), is shown in Fig. 2. In this case we obtain two very remarkable and new effects with respect to the previous model. The first one relies on the existence of two critical temperatures T_{c_1} and T_{c_2}. For instance, if at $T = 0$ the system is in a topological phase with $n_U = 2$, we observe that for $T < T_{c_1}$ the same phase is preserved. Then, for $T_{c_1} < T < T_{c_2}$ there is another thermal topological phase with $n_U = 1$. If we now increase the temperature even more, $T > T_{c_2}$, then the topological phase becomes trivial, $n_U = 0$ (see Fig. 2). Hence, there is a critical transition between phases with different (but nonzero) Uhlmann numbers by the sole effect of T. Thus, we have obtained a purely thermal transition between two different nontrivial topological regimes.

Secondly, at zero temperature we see in Eq. (11) that there are only nontrivial topological phases in this model. But, by increasing T, we can always end in a trivial phase with $n_U = 0$. This supports the intuition that at sufficiently high temperatures the order is lost for any system.

Haldane model.—The Haldane model [5] was the first proposal of a two-dimensional lattice of fermions without a constant magnetic field but with quantized Hall conductivity. It is a graphenelike model based on a honeycomb lattice with two different species of fermions (different sublattices), nearest-neighbor hopping t_1, next-nearest-neighbor hopping $t_2 e^{i\phi}$, and a staggered potential m. For periodic boundary conditions the Haldane Hamiltonian in the reciprocal space is

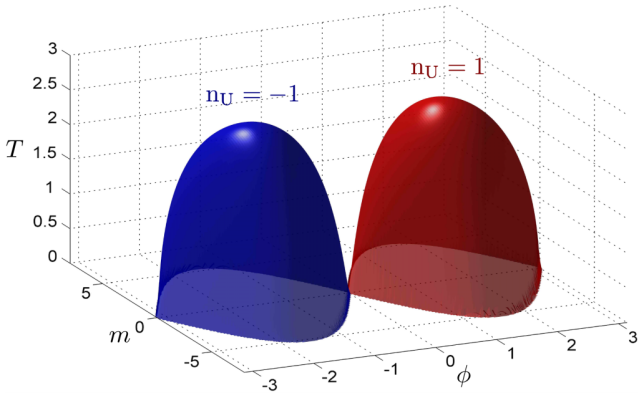

FIG. 3 (color online). Uhlmann topological phase diagram for the Haldane model. Red color represents $n_U = 1$ and blue $n_U = -1$. As we see, at $T = 0$ the two well-known lobes of the Haldane model are obtained, and at a certain finite temperature T_c the system goes to a trivial phase.

$$H(\boldsymbol{k}) = \sum_i \{[2t_2 \cos\phi \cos(\boldsymbol{k}\cdot\boldsymbol{b}_i)]\mathbb{1} + [t_1 \cos(\boldsymbol{k}\cdot\boldsymbol{a}_i)]\sigma_x + [t_1 \sin(\boldsymbol{k}_i\cdot\boldsymbol{a}_i)]\sigma_y + [m - 2t_2 \sin\phi \sin(\boldsymbol{k}_i\cdot\boldsymbol{b}_i)]\sigma_z\}, \tag{12}$$

where $\boldsymbol{a}_i$ are the lattice vectors defining the Bravais lattice and $\boldsymbol{b}_i := \boldsymbol{a}_{i+1} - \boldsymbol{a}_{i-1}$. In particular, we take $t_1 = 4$ and $t_2 = 1$.

At $T = 0$, the system presents topological order for $|m| < 3\sqrt{3}|\sin\phi|$ with Chern number $\mathrm{Ch} = \pm 1$ depending on the sign of m.

The topological phases at finite temperature as a function of m and ϕ are depicted in Fig. 3. The red and blue volumes represent $n_U = 1$ and $n_U = -1$, respectively. Thus, an integer topological invariant ± 1 is retained and a thermal topological phase is present up to some critical temperature T_c where n_U vanishes. Note that at $T = 0$ we recover the well-known phase diagram for the Haldane model [5].

Interestingly enough, the thermal topological properties of this model were first considered in [45]. There, the topological indicator did not show a critical behavior with T but shared the same pattern with m and ϕ as n_U.

Conclusions and outlook.—We have constructed a new topological invariant, the Uhlmann number n_U, that allows us to explore topological phases of fermion systems separated by purely thermal transitions. Notably, we find always a finite range of temperatures at which this topological order survives.

We remark that the existence of critical temperatures seems somehow natural in the Uhlmann approach. For thermal states, it sets on equal footing the temperature and the Hamiltonian parameters. Therefore, if there is a critical behavior as a function of tunnelings and/or staggered potentials, then certainly one should obtain a critical behavior with temperature as well. Moreover, since by increasing T, the quantum coherence properties of any state

are diminished, it is expected that the Uhlmann number decreases by warming the system up.

As explained in [25], measurements of Uhlmann phases and numbers may be affordable by adapting experimental schemes such as [37,46,47], that use interferometric setups for cold atoms in optical lattices. The mapping between Uhlmann amplitudes and pure state vectors in an enlarged Hilbert space should allow for measurements of the Uhlmann phase using an ancillary system.

Based on these results, we envision the possibility of extending the current classification of topological insulators and superconductors on several spatial dimensions [48,49] (also called the "periodic table"), to the case of thermal topological states using the topological Uhlmann numbers introduced here.

We are thankful for the following: the Spanish MINECO Grants No. FIS2012-33152 and No. FIS2009-10061, the CAM research consortium QUITEMAD S2009-ESP-1594, the European Commission PICC: FP7 2007-2013, Grant No. 249958, the UCM-BS Grant No. GICC-910758, and the FPU MEC Grant and Residencia de Estudiantes.

Note added.—Recently we were informed by Z. Huang and D. Arovas about similar extensions of Uhlmann phases to two-dimensional models [50].

[1] X.-G. Wen, *Quantum Field Theory of Many-body Systems* (Oxford University Press, New York, 2004).
[2] X.-G. Wen, Phys. Rev. B **40**, 7387 (1989).
[3] X.-G. Wen and Q. Niu, Phys. Rev. B **41**, 9377 (1990).
[4] D. Arovas, J. R. Schrieffer, and F. Wilczek, Phys. Rev. Lett. **53**, 722 (1984).
[5] F. D. M. Haldane, Phys. Rev. Lett. **61**, 2015 (1988).
[6] C. L. Kane and E. J. Mele, Phys. Rev. Lett. **95**, 226801 (2005).
[7] B. A. Bernevig and S.-C. Zhang, Phys. Rev. Lett. **96**, 106802 (2006).
[8] C. L. Kane and E. J. Mele, Phys. Rev. Lett. **95**, 146802 (2005).
[9] J. E. Moore and L. Balents, Phys. Rev. B **75**, 121306 (2007).
[10] L. Fu, C. L. Kane, and E. J. Mele, Phys. Rev. Lett. **98**, 106803 (2007); X.-L. Qi, T. L. Hughes, and S.-C. Zhang, Phys. Rev. B **78**, 195424 (2008).
[11] M. Z. Hasan and C. L. Kane, Rev. Mod. Phys. **82**, 3045 (2010).
[12] X.-L. Qi and S.-C. Zhang, Rev. Mod. Phys. **83**, 1057 (2011).
[13] B. A. Bernevig and T. L. Hughes, *Topological Insulators and Topological Superconductors* (Princeton University Press, Princeton, NJ, 2013).
[14] A. Vishwanath and T. Senthil, Phys. Rev. X **3**, 011016 (2013).
[15] M. A. Metlitski, C. L. Kane, and M. P. A. Fisher, Phys. Rev. B **88**, 035131 (2013).
[16] T. Senthil, arXiv:1405.4015.
[17] P. Ye and X.-G. Wen, Phys. Rev. B **89**, 045127 (2014).
[18] Z.-X. Liu, Z.-C. Gu, and X.-G. Wen, arXiv:1404.2818.
[19] C.-E. Bardyn, M. A. Baranov, C. V. Kraus, E. Rico, A. İmamoğlu, P. Zoller, and S. Diehl, New J. Phys. **15**, 085001 (2013).
[20] R. Alicki, M. Fannes, and M. Horodecki, J. Phys. A **42**, 065303 (2009).
[21] M. B. Hastings, Phys. Rev. Lett. **107**, 210501 (2011).
[22] Although stable topological phases for standard TOs can be established at high dimensions $D = 4$, 6. R. Alicki, M. Horodecki, P. Horodecki, and R. Horodecki, Open Syst. Inf. Dyn. **17**, 1 (2010); H. Bombin, R. W. Chhajlany, M. Horodecki, and M. A. Martin-Delgado, New J. Phys. **15**, 055023 (2013).
[23] E. P. L. van Nieuwenburg and S. D. Huber, arXiv:1403.2387.
[24] O. Viyuela, A. Rivas, and M. A. Martin-Delgado, Phys. Rev. B **86**, 155140 (2012).
[25] O. Viyuela, A. Rivas, and M. A. Martin-Delgado, Phys. Rev. Lett. **112**, 130401 (2014).
[26] A. Uhlmann, Rep. Math. Phys. **24**, 229 (1986).
[27] A. Uhlmann, Ann. Phys. (Berlin) **501**, 63 (1989).
[28] M. Hübner, Phys. Lett. A **179**, 226 (1993).
[29] M. Ericsson, A. K. Pati, E. Sjöqvist, J. Brännlund, and D. K. L. Oi, Phys. Rev. Lett. **91**, 090405 (2003).
[30] J. Aberg, D. Kult, E. Sjöqvist, and D. K. L. Oi, Phys. Rev. A **75**, 032106 (2007).
[31] J. Zhu, M. Shi, V. Vedral, X. Peng, D. Suter, and J. Du, Europhys. Lett. **94**, 20007 (2011).
[32] T. Eguchi, P. B. Gilkey, and A. J. Hanson, Phys. Rep. **66**, 213 (1980).
[33] M. Nakahara, *Geometry, Topology and Physics* (CRC Press, Bristol, 2003).
[34] This second argument also implies vanishing higher-order Chern numbers for the Uhlmann connection.
[35] R. Resta, Rev. Mod. Phys. **66**, 899 (1994).
[36] D. Xiao, M.-C. Chang, and Q. Niu, Rev. Mod. Phys. **82**, 1959 (2010).
[37] D. A. Abanin, T. Kitagawa, I. Bloch, and E. Demler, Phys. Rev. Lett. **110**, 165304 (2013).
[38] G. E. Volovik, JETP Lett. **70**, 609 (1999).
[39] N. Read and D. Green, Phys. Rev. B **61**, 10267 (2000).
[40] D. A. Ivanov, Phys. Rev. Lett. **86**, 268 (2001).
[41] C. Nayak, S. H. Simon, A. Stern, M. Freedman, and S. Das Sarma, Rev. Mod. Phys. **80**, 1083 (2008).
[42] D. Sticlet, F. Piéchon, J.-N. Fuchs, P. Kalugin, and P. Simon, Phys. Rev. B **85**, 165456 (2012).
[43] See also: S. Yang, Z.-C. Gu, K. Sun, and S. Das Sarma, Phys. Rev. B **86**, 241112(R) (2012).
[44] D. R. Hofstadter, Phys. Rev. B **14**, 2239 (1976).
[45] A. Rivas, O. Viyuela, and M. A. Martin-Delgado, Phys. Rev. B **88**, 155141 (2013).
[46] M. Atala, M. Aidelsburger, J. T. Barreiro, D. Abanin, T. Kitagawa, E. Demler, and I. Bloch, Nat. Phys. **9**, 795 (2013).
[47] F. Grusdt, D. Abanin, and E. Demler, Phys. Rev. A **89**, 043621 (2014).
[48] A. P. Schnyder, S. Ryu, A. Furusaki, and A. W. W. Ludwig, Phys. Rev. B **78**, 195125 (2008).
[49] A. Kitaev, AIP Conf. Proc. **1134**, 22 (2009).
[50] Z. Huang and D. P. Arovas, Phys. Rev. Lett. **113**, 076407 (2014).

Symmetry-protected topological phases at finite temperature

2015 2D Mater. 2 034006

(http://iopscience.iop.org/2053-1583/2/3/034006)

2D Materials

OPEN ACCESS

RECEIVED
17 February 2015

REVISED
2 April 2015

ACCEPTED FOR PUBLICATION
27 April 2015

PUBLISHED
25 June 2015

PAPER

Symmetry-protected topological phases at finite temperature

O Viyuela, A Rivas and M A Martin-Delgado

Departamento de Física Teórica I, Universidad Complutense, 28040 Madrid, Spain

E-mail: mardel@miranda.fis.ucm.es

Keywords: topological insulators, topological superconductors, thermal properties

Abstract

We have applied the recently developed theory of topological Uhlmann numbers to a representative model of a topological insulator in two dimensions, the Qi–Wu–Zhang model. We have found a stable symmetry-protected topological phase under external thermal fluctuations in two dimensions. A complete phase diagram for this model is computed as a function of temperature and coupling constants in the original Hamiltonian. It shows the appearance of large stable phases of matter with topological properties compatible with thermal fluctuations or external noise and the existence of critical lines separating abruptly trivial phases from topological phases. These novel critical temperatures represent thermal topological phase transitions. The initial part of the paper comprises a self-contained explanation of the Uhlmann geometric phase needed to understand the topological properties that it may acquire when applied to topological insulators and superconductors.

1. Introduction

Topological insulators and superconductors [1–9] are novel phases of matter that cannot be described using the standard Gizburg–Landau theory for phase transitions. These novel phases are of great interest for applications in emerging fields such as spintronics, photonics and quantum computing. They have opened an area of new rich physical phenomenology, giving birth to materials that host robust metallic edge states and the possibility for realizing Majorana fermions [10–13], as well as a variety of new exotic particles known as 'anyons' [14–17]. In fact, graphene was the first material proposed to realize a topological insulating phase using a mechanism of spin–orbital coupling between two graphene sheets [2]. Unfortunately, the gap due to this effect in carbon atoms is too small and the quantum spin Hall effect was finally achieved in HgTe quantum wells instead [18, 19]. Very recently, bosonic topological orders have also been proposed [20–24].

Whereas these systems have been extensively studied for the idealized case of zero temperature, the common belief was that these exotic phases are gradually destroyed as the systems are heated up [25, 26]. In [25], it was shown that certain topological properties such as edge states can be destroyed by a thermal bath even when the system–bath interaction respects the protecting symmetry of the topological insulator. It was not until the work in [27] that a topological indicator with a dependence on the temperature of the system was introduced, which was related to the topological part of the quantum Hall conductivity and the degree of mixedness of the edge states due to the dissipative effect. Other attempts to understand the interplay between topological phases and finite temperature [28, 29], nonequilibrium dynamics [30] and dissipation-engineering [31–34] have also been made.

The extension of the notion of symmetry-protected topological (SPT) order for fermions to situations where the system is not in a pure state, but in a quantum mixed state described by a density matrix, has been developed very recently. The first realization of topological fermonic phases in the presence of thermal effects or external noise was proposed in [35]. There a topological invariant remains quantized for a finite range of temperature/noise for the first time in representative examples of topological insulators and superconductors in one dimension (1D). Since then, new advances have been achieved for fermionic phases of matter with SPT order in two-dimensional (2D) systems [36, 37]. The novelty of these works relies on the introduction of two new observables: the Uhlmann phase for wire-shaped systems (1D) [35] and the Uhlmann number for planar ones (2D) [37] as well as a variety of extensions [36], which are able to account for topological order even at

non-zero temperatures. Remarkably, these recent works report purely 'thermal' topological phase transitions between distinct non-trivial topological regions driven solely by temperature, without losing their quantum character. It has also been shown that there always exists a critical temperature above which the topological phase abruptly disappears. The possibility of having several topological thermal critical points has also been discovered as a novel effect [37].

In this way, exotic topological quantum properties can survive even in the presence of dissipative effects and finite temperature, which are the natural conditions in real life experiments. This situation for fermion systems with SPT order is in sharp contrast to some results establishing the absence of stable topological phases subject to thermal effects, such as for topological orders with spins[1] [38–42], for SPT orders with spins [30], or SPT orders with fermions under certain conditions [25]. Therefore, these new results open the way towards the characterization of fermion quantum phases of matter with topological phases protected by symmetry in thermal states, or more general density matrices. Note that other studies on thermal effects and related issues in topological systems have been recently carried out [43–52].

The aim of this paper is to provide a complete and comprehensive derivation of the Uhlmann geometric phase as a tool to characterize SPT orders at finite temperature, performing a detailed analysis of its intrinsic properties. First, we formally derive the expression for the Uhlmann phase as an extension of the Berry phase to the case of quantum mixed states described by density matrices. Later, we apply the formalism to new 2D models for topological insulators with time-reversal broken symmetry that can be characterized using these Uhlmann geometric concepts by the so-called topological Uhlmann numbers [37].

The paper is organized as follows. Section 2 introduces the concept of Uhlmann holonomies, giving a detailed derivation of the Uhlmann parallel transport condition and the geometric Uhlmann phase, by means of amplitudes and purifications of a density matrix. In section 3, the topological Uhlmann phase in 1D is presented and applied to a generic 1D two-band model for a topological insulator or superconductor. In section 4, we derive the topological Uhlmann number for 2D topological systems, discussing some technical issues and using it to characterize an emblematic 2D topological insulator, namely the Qi–Wu–Zhang (QWZ) model [53, 54]. Section 5 is devoted to conclusions.

2. Uhlmann holonomies

Geometric phases have played an essential role in many quantum phenomena since their modern discovery by Berry [55] (see also [56, 57]). An representative example is the description of the quantum Hall effect using the theory of fiber bundles. More concretely, one can relate the transversal conductivity σ_{xy} of the system with the first Chern number Ch as [58, 59],

$$\sigma_{xy} = \mathrm{Ch}\frac{e^2}{h}, \tag{1}$$

where e is the electron charge and h is the Planck constant.

The Chern numbers are topological invariants associated to characteristic classes of complex vector bundles when working on an oriented manifold of even dimension. The first Chern number Ch, which is defined for the 2D case, is just the integral of the Berry curvature over the 2D parameter space, i.e. the Brillouin zone (BZ) in the context of condensed-matter systems. In addition, this topological observable can also be related to the presence of conducting edge states when the system has open boundary conditions.

The standard way to observe the properties and implications that the Berry phase has in solids (the Zak phase [60]), has been through indirect measurements such as the transverse conductivity, or side effects like the presence of conducting edge states at the boundary. However, very recently the first direct experimental measurement of a Berry phase in a cold atom system has been achieved [61–63]. In particular, [61] reports the measurement of the Zak phase in a 1D optical lattice simulating the different phases of polyacetylene, characterizing the topology of the system and observing the quantization of this phase. This paves the way towards the extension of geometric phases to study topological properties beyond the realm of condensed-matter systems [64–67]. Moreover, there have been recent experiments on this context involving the architectures of superconducting qubits [68, 69].

Although these studies provide a successful picture for quantum systems in pure states, typically the ground state, very little is known about the fate of these topological phases of matter when the system is in a mixed quantum state represented by a density matrix.

A fundamental problem in the theory and applications of geometrical phases is the extension from pure quantum states (Berry) to mixed quantum states described by density matrices. Uhlmann was the first to mathematically address this issue [70] and to provide a satisfactory solution [71–74]. For more than a decade, there has been a renewed interest in studying geometric phases for mixed states and under dissipative evolutions from the point of view of quantum information [75–80]. In the rest of this section, we will give a detailed derivation of the Uhlmann geometric phase and the definition of Uhlmann parallel transport. These two key ideas will allow us to later construct two topological observables to distinguish

[1] Although stable topological phases for standard topological orders can be established at high dimensions $D = 4, 6$ [41].

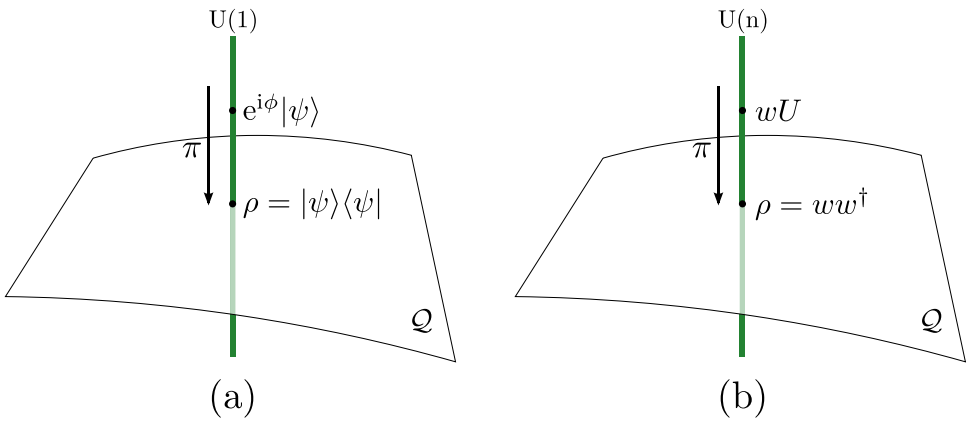

Figure 1. Comparison between the usual fiber bundle of pure states (a) and the fiber bundle proposed by Uhlmann (b) for any density matrix through the concept of amplitude.

different topological phases in condensed-matter systems in both 1D and 2D.

2.1. Amplitudes and purifications

One of the most fundamental problems when applying geometric concepts to the set $\mathcal{Q}$ of density matrices is its nonlinear character. That is, consider some scalars λ_1 and λ_2, for all pairs of density matrices ρ_1 and ρ_2, the linear combination $\lambda_1\rho_1 + \lambda_2\rho_2$ is not another density matrix unless $\lambda_1, \lambda_2 \geqslant 0$ and $\lambda_1 + \lambda_2 = 1$. In the case of pure states $\rho = |\psi\rangle\langle\psi|$, this is not a major issue as we can immediately introduce a Hilbert space formed by the vectors $|\psi\rangle$ so that the quantum state $\rho = |\psi\rangle\langle\psi|$ is the projector on the subspace spanned by $|\psi\rangle$. Then the geometric properties of the Hilbert space can be applied to the vectors $|\psi\rangle$, but keeping in mind that $|\psi\rangle$ and $e^{i\phi}|\psi\rangle$ describe the same physical state $\rho = |\psi\rangle\langle\psi|$. Namely, to work with a Hilbert space we have to pay the price of introducing an additional degree of freedom, the phase of the vectors, such that quantum pure states as seen in the Hilbert space are defined modulo a U(1) phase factor.

The key idea is to realize that an analogous construction is possible for any general density matrix. Specifically, consider a density matrix ρ and define its amplitude as any of the matrices w such that

$$\rho = ww^\dagger. \tag{2}$$

The amplitudes form a Hilbert space $\mathcal{H}_w$ with the Hilbert–Schmidt product $(w_1, w_2) = \mathrm{Tr}(w_1^\dagger w_2)$. From (2), we see that there is a U(n)-gauge freedom in the choice of the amplitude (here n denotes the dimension of the space), since w and wU, where U is a unitary operator, are amplitudes of the same state.

Note the parallelism between the usual U(1) -gauge freedom for pure states, and the U(n)-gauge freedom for the amplitudes, see figure 1. In the case of pure states, one defines a projection map π: $\mathcal{H} \mapsto \mathcal{Q}$:

$$\pi(|\psi\rangle) = |\psi\rangle\langle\psi|, \tag{3}$$

so that $|\psi\rangle$ and $e^{i\phi}|\psi\rangle$ represent the same physical state, i.e. the same density matrix given by the projection map π. In the case of amplitudes, the projection map is analogously defined, π: $\mathcal{H}_w \mapsto \mathcal{Q}$:

$$\pi(w) = ww^\dagger. \tag{4}$$

Thus, the usual gauge freedom for pure states can be seen as a particular case of the amplitude U(n)-gauge freedom for general states.

So far the concept of amplitude seems to be just a mathematical abstraction, however, it also enjoys a nice physical meaning. To see this, consider what is called the 'square root' section of the Uhlmann fiber bundle, which is nothing other than the parametrization $w = \sqrt{\rho}\,U$ for amplitudes of some density matrix ρ (note that this is also called polar decomposition of w, see below). Then by using the spectral decomposition, $\rho = \sum_j p_j\ |\psi_j\rangle\langle\psi_j|$ we have that

$$w = \sum_j \sqrt{p_j}\ \left|\psi_j\right\rangle\left\langle\psi_j\right|\ U. \tag{5}$$

Now we define the following isomorphism between the spaces $\mathcal{H}_w$ and $\mathcal{H} \otimes \mathcal{H}$,

$$\begin{aligned} w &= \sum_j \sqrt{p_j}\ \left|\psi_j\right\rangle\left\langle\psi_j\right|\ U \longleftrightarrow |w\rangle \\ &= \sum_j \sqrt{p_j}\ \left|\psi_j\right\rangle \otimes U^{\mathrm{t}}\left|\psi_j\right\rangle, \end{aligned} \tag{6}$$

where U^{t} denotes the transposition of U taken with respect to the eigenbasis of ρ. Then, the property $\rho = ww^\dagger$ is now written as

$$\rho = \mathrm{Tr}_2(|w\rangle\langle w|). \tag{7}$$

Here, Tr_2 denotes the partial trace over the second Hilbert space of $\mathcal{H} \otimes \mathcal{H}$. In other words, any amplitude w of some density matrix ρ can be seen as a pure state $|w\rangle$ of the enlarged space $\mathcal{H} \otimes \mathcal{H}$ with a partial trace equal to ρ, (7). Thus, it is said that $|w\rangle$ is a purification of ρ. Thanks to this isomorphism between amplitudes and purifications the whole geometric approach by Uhlmann can be written in terms of purifications which are objects with a clear physical meaning. However, we shall keep on developing the

theory and explanations using amplitudes and refer to the purification interpretation when needed.

2.2. Parallel amplitudes

The concept of parallel amplitude is essential to define the Uhlmann parallel transport condition and the holonomy. Given a pair of states ρ_1 and ρ_2, we define two of their amplitudes w_1 and w_2 to be parallel if they minimize the Hilbert space distance in $\mathcal{H}_w$, i.e. $w_1 \parallel w_2$ if

$$\| w_1 - w_2 \|^2 = \min_{\tilde{w}_1, \tilde{w}_2} \| \tilde{w}_1 - \tilde{w}_2 \|^2, \quad \text{with} \quad \rho_1 = \tilde{w}_1 \tilde{w}_1^\dagger,\ \rho_2 = \tilde{w}_2 \tilde{w}_2^\dagger. \tag{8}$$

We may work further on this condition and establish some properties of such w_1 and w_2:

$$\begin{aligned} &\min_{\tilde{w}_1, \tilde{w}_2} \| \tilde{w}_1 - \tilde{w}_2 \|^2 \\ &= \min_{\tilde{w}_1, \tilde{w}_2} \left(\tilde{w}_1 - \tilde{w}_2,\ \tilde{w}_1 - \tilde{w}_2 \right) \\ &= \min_{\tilde{w}_1, \tilde{w}_2} \mathrm{Tr} \left(\tilde{w}_1^\dagger \tilde{w}_1 + \tilde{w}_2^\dagger \tilde{w}_2 - \tilde{w}_1^\dagger \tilde{w}_2 - \tilde{w}_2^\dagger \tilde{w}_1 \right) \\ &= \mathrm{Tr}(\rho_1) + \mathrm{Tr}(\rho_2) - \max_{\tilde{w}_1, \tilde{w}_2} \mathrm{Tr}(\tilde{w}_1^\dagger \tilde{w}_2 + \tilde{w}_2^\dagger \tilde{w}_1) \\ &= 2 - 2 \max_{\tilde{w}_1, \tilde{w}_2} \mathrm{Re} \left[\mathrm{Tr}(\tilde{w}_1^\dagger \tilde{w}_2) \right]. \end{aligned} \tag{9}$$

Since $\mathrm{Re}(x) \leqslant |x|$, it is clear that the condition for the maximum is to chose $\tilde{w}_1$ and $\tilde{w}_2$ such that $\tilde{w}_1^\dagger \tilde{w}_2$ is self-adjoint and positive-definite:

$$\tilde{w}_1^\dagger \tilde{w}_2 = \tilde{w}_2^\dagger \tilde{w}_1 > 0. \tag{10}$$

More explicit expressions may be obtained with the polar decomposition theorem. This theorem states that any operator A (consider it to be finite dimensional for simplicity) can be decomposed as $A = |A| U_A$, where $|A| = \sqrt{AA^\dagger}$ and U_A is a unitary operator [81, 82]. Furthermore for any unitary operator U the following inequality holds

$$\begin{aligned} &\mathrm{Re}[\mathrm{Tr}(AU)] \leqslant |\mathrm{Tr}(AU)| \\ &= |\mathrm{Tr}(|A| U U_A)| \\ &= \left| \mathrm{Tr} \left(\sqrt{|A|}\, \sqrt{|A|}\, U U_A \right) \right| \\ &\leqslant \sqrt{(\mathrm{Tr}\ |A|) \left[\mathrm{Tr} \left(U_A^\dagger U^\dagger\ |A|\ U U_A \right) \right]} \\ &= \mathrm{Tr}|A| \end{aligned} \tag{11}$$

where in the penultimate step we have used the Cauchy–Schwarz inequality $|\mathrm{Tr}(A^\dagger B)|^2 \leqslant \mathrm{Tr}(A^\dagger A)\, \mathrm{Tr}(B^\dagger B)$. Since the equality is reached for $U = U_A^\dagger$, we can write

$$\max_U \mathrm{Re}[\mathrm{Tr}(AU)] = \mathrm{Tr}\ |A|. \tag{12}$$

Now, the polar decomposition theorem on the amplitudes $\tilde{w}_1 = \sqrt{\rho_1} U_1$ and $\tilde{w}_2 = \sqrt{\rho_2} U_2$ jointly with (12) lead to

$$\begin{aligned} &\max_{\tilde{w}_1, \tilde{w}_2} \mathrm{Re} \left[\mathrm{Tr}(\tilde{w}_1^\dagger \tilde{w}_2) \right] \\ &= \max_{U_1, U_2} \mathrm{Re} \left[\mathrm{Tr} \left(U_1^\dagger \sqrt{\rho_1}\, \sqrt{\rho_2}\, U_2 \right) \right] \\ &= \max_{U} \mathrm{Re} \left[\mathrm{Tr} \left(\sqrt{\rho_1}\, \sqrt{\rho_2}\, U \right) \right] \\ &= \mathrm{Tr} \left| \sqrt{\rho_1}\, \sqrt{\rho_2} \right| = \mathrm{Tr} \sqrt{\sqrt{\rho_1} \rho_2 \sqrt{\rho_1}}\,. \end{aligned} \tag{13}$$

Therefore, the Hilbert space distance between two parallel amplitudes w_1 and w_2 is equal to the Bures distance [83] between ρ_1 and ρ_2,

$$\| w_1 - w_2 \|^2 = 2 - 2\mathrm{Tr} \sqrt{\sqrt{\rho_1} \rho_2 \sqrt{\rho_1}}\,, \quad \text{for } w_1 \parallel w_2. \tag{14}$$

Finally, note that the equality in (13) is obtained for $U = U^\dagger_{\sqrt{\rho_1}\sqrt{\rho_2}}$, this is the adjoint of the unitary operator of the polar decomposition of $\sqrt{\rho_1}\sqrt{\rho_2} = |\sqrt{\rho_1}\sqrt{\rho_2}|\, U_{\sqrt{\rho_1}\sqrt{\rho_2}}$. Such a unitary operator is not uniquely defined unless $\sqrt{\rho_1}\sqrt{\rho_2}$ is full rank (and so $\sqrt{\rho_1}$, $\sqrt{\rho_2}$ and $|\sqrt{\rho_1}\sqrt{\rho_2}|$). In such a case, $U_{\sqrt{\rho_1}\sqrt{\rho_2}}$ is given by the equation

$$U_{\sqrt{\rho_1}\sqrt{\rho_2}} = \left| \sqrt{\rho_1}\, \sqrt{\rho_2} \right|^{-1} \sqrt{\rho_1}\, \sqrt{\rho_2}\,. \tag{15}$$

Since from (13) we have $U = U_2 U_1^\dagger = U^\dagger_{\sqrt{\rho_1}\sqrt{\rho_2}}$, by using the unitarity of U and (15) we arrive at

$$U_2 U_1^\dagger = \sqrt{\rho_2^{-1}}\, \sqrt{\rho_1^{-1}}\, \sqrt{\sqrt{\rho_1} \rho_2 \sqrt{\rho_1}}\,. \tag{16}$$

Hence, (16) gives us the relation that the unitaries U_1 and U_2 must satisfy in order to minimize the distance between the associated amplitudes w_1 and w_2, i.e. in order to have $w_1 \| w_2$.

2.3. Uhlmann parallel transport and connection form

Before introducing the Uhlmann holonomy, we need to explain some of its ingredients: the Uhlmann parallel transport condition and the connection form. Consider a trajectory in the density matrix space $\mathcal{Q}$, ρ_r. This induces a trajectory in the space $\mathcal{H}_w$, via the amplitudes w_r, $\rho_r = w_r w_r^\dagger$. Since for a point ρ_r of $\mathcal{Q}$ there are several amplitudes w_r, a unique trajectory on $\mathcal{Q}$ induces multiple trajectories in $\mathcal{H}_w$ depending on which w_r are chosen. To select one of them, we define a parallel transport condition, i.e. for a point ρ_r with some amplitude w_r, we consider the amplitude $w_{r+\mathrm{d}r}$ of the next point of the trajectory, $\rho_{r+\mathrm{d}r}$, to be the closest to w_r according to the Hilbert space distance, so $w_r \| w_{r+\mathrm{d}r}$ in the sense of the previous section, see figure 2. Such a path in $\mathcal{H}_w$ is known as a *parallel lift* of path ρ_r in $\mathcal{Q}$. This is analogous to the Berry parallel transportation, where the U(1) phases of the consecutive state vectors $|\psi_r\rangle$ and $|\psi_{r+\mathrm{d}r}\rangle$ are chosen such that the distance between them $\sqrt{(\langle\psi_r| - \langle\psi_{r+\mathrm{d}r}|)(|\psi_r\rangle - |\psi_{r+\mathrm{d}r}\rangle)}$ is minimal.

Let ρ_{r_0} be the initial state of the trajectory, under the square root section (or equivalently by the polar decomposition theorem) we have $w_{r_0} = \sqrt{\rho_{r_0}}\, U_{r_0}$. For

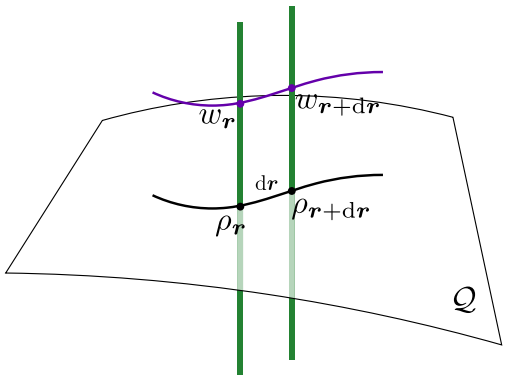

Figure 2. Uhlmann parallel transport condition. The amplitude $w_{\boldsymbol{r}+\mathrm{d}\boldsymbol{r}}$ is the closest amplitude to $w_{\boldsymbol{r}}$ among those in the fiber at $\boldsymbol{r}+\mathrm{d}\boldsymbol{r}$.

the sake of clarity we shall work for the moment on a gauge such that $U_{\boldsymbol{r}_0}=\mathbb{1}$ and we shall refer to this gauge as the 'identity' gauge. At some point $\boldsymbol{r}$ of the trajectory we have $w_{\boldsymbol{r}}=\sqrt{\rho_{\boldsymbol{r}}}V_{\boldsymbol{r}}$, where $V_{\boldsymbol{r}}$ is a unitary (Uhlmann holonomy) constructed from the initial condition $w_{\boldsymbol{r}_0}=\sqrt{\rho_{\boldsymbol{r}_0}}$ by applying the parallel transport rule along the trajectory. The infinitesimal generator $A(\boldsymbol{r})$ of this unitary transformation $V_{\boldsymbol{r}}$ is called the *connection form* of the trajectory. Thus, if $\boldsymbol{r}(t)|_{t=0}^{1}$ is a parametrization of the trajectory $[\boldsymbol{r}(0)\equiv\boldsymbol{r}_0]$, $V_{\boldsymbol{r}}$ is fully determined by the differential problem

$$\begin{cases}\dfrac{\mathrm{d}V_{\boldsymbol{r}(t)}}{\mathrm{d}t}=A[\boldsymbol{r}(t)]\,V_{\boldsymbol{r}(t)},\\ V_{\boldsymbol{r}(0)}=\mathbb{1},\end{cases}\tag{17}$$

whose formal solution can be written independently of the parametrization as

$$V_{\boldsymbol{r}}=\mathcal{P}\mathrm{e}^{\int_{\boldsymbol{r}_0}^{\boldsymbol{r}}A(\boldsymbol{r}')\mathrm{d}\boldsymbol{r}'},\tag{18}$$

where $\mathcal{P}$ is the path ordering operator.

As we shall see, the Uhlmann connection A is not uniquely defined unless the density matrix $\rho_{\boldsymbol{r}}$ is full rank. In order to compute A in such a case, let us rewrite (17) in terms of differentials

$$\mathrm{d}VV^{\dagger}=A,\tag{19}$$

where $A=\sum_i A_i\mathrm{d}r_i$ is understood as a differential one-form. Note that in (17), $A[\boldsymbol{r}(t)]=\sum_i A_i\frac{\mathrm{d}r_i}{\mathrm{d}t}$. Then, consider some full rank density matrix $\rho_1=\rho$ and displace it by an infinitesimal translation $\rho_2=\rho+\mathrm{d}\rho$. The basic condition to compute A is that the corresponding infinitesimally closed amplitudes $w_1=\sqrt{\rho}\,V$ and $w_2=\sqrt{\rho+\mathrm{d}\rho}\,(V+\mathrm{d}V)$ fulfil the parallel transport condition (14). Thus, (16) leads to

$$(V+\mathrm{d}V)V^{\dagger}=\left(\sqrt{\rho}+\mathrm{d}\sqrt{\rho}\right)^{-1}\times\sqrt{\rho^{-1}}\sqrt{\sqrt{\rho}\,(\rho+\mathrm{d}\rho)\,\sqrt{\rho}}\tag{20}$$

where we have used that for an infinitesimal translation $\mathrm{d}\rho$, $\sqrt{\rho+\mathrm{d}\rho}=\sqrt{\rho}+\mathrm{d}\sqrt{\rho}$. Following Hübner [73], we introduce an auxiliary real parameter s multiplying every differential:

$$(V+s\mathrm{d}V)V^{\dagger}=\left(\sqrt{\rho}+s\mathrm{d}\sqrt{\rho}\right)^{-1}\times\sqrt{\rho^{-1}}\sqrt{\sqrt{\rho}\,(\rho+s\mathrm{d}\rho)\,\sqrt{\rho}}\,.\tag{21}$$

The aim of this trick is to expand the above equation around $s=0$ and keep only the first order in s. In order words, we have that

$$\mathbb{1}+s\mathrm{d}VV^{\dagger}=\mathbb{1}+\frac{\mathrm{d}}{\mathrm{d}s}\left[\left(\sqrt{\rho}+s\mathrm{d}\sqrt{\rho}\right)^{-1}\times\sqrt{\rho^{-1}}\sqrt{\sqrt{\rho}\,(\rho+s\mathrm{d}\rho)\,\sqrt{\rho}}\right]\Bigg|_{s=0}s,\tag{22}$$

therefore

$$A=\mathrm{d}VV^{\dagger}=\left[\frac{\mathrm{d}}{\mathrm{d}s}\left(\sqrt{\rho}+s\mathrm{d}\sqrt{\rho}\right)^{-1}\right]\Bigg|_{s=0}\times\sqrt{\rho}+\rho^{-1}\left[\frac{\mathrm{d}}{\mathrm{d}s}\sqrt{\sqrt{\rho}\,(\rho+s\mathrm{d}\rho)\,\sqrt{\rho}}\right]\Bigg|_{s=0}.\tag{23}$$

To give a closed expression for A, we determine its matrix elements with respect to the eigenbasis $\{|\psi_j\rangle\}$ of ρ, which we assume to be diagonalized with eigenvalues $\{p_j\}$. For the first term in (23) we have

$$\begin{aligned}&\left(\sqrt{\rho}+s\mathrm{d}\sqrt{\rho}\right)^{-1}\sqrt{\rho}\\&=\left[\sqrt{\rho}\left(\mathbb{1}+s\sqrt{\rho^{-1}}\,\mathrm{d}\sqrt{\rho}\right)\right]^{-1}\sqrt{\rho}\\&=\left(\mathbb{1}+s\sqrt{\rho^{-1}}\,\mathrm{d}\sqrt{\rho}\right)^{-1}\sqrt{\rho^{-1}}\sqrt{\rho}\\&=\mathbb{1}-s\sqrt{\rho^{-1}}\,\mathrm{d}\sqrt{\rho},\end{aligned}\tag{24}$$

where in the last step the inverse has been taken at first order in s. Hence

$$\left[\frac{\mathrm{d}}{\mathrm{d}s}\left(\sqrt{\rho}+s\mathrm{d}\sqrt{\rho}\right)^{-1}\right]\Bigg|_{s=0}\sqrt{\rho}=-\sqrt{\rho^{-1}}\,\mathrm{d}\sqrt{\rho},\tag{25}$$

and in the eigenbasis of ρ,

$$-\left\langle\psi_i\right|\sqrt{\rho^{-1}}\,\mathrm{d}\sqrt{\rho}\left|\psi_j\right\rangle=-\frac{1}{\sqrt{p_i}}\left\langle\psi_i\right|\mathrm{d}\sqrt{\rho}\left|\psi_j\right\rangle.\tag{26}$$

The second term of (23) is a bit more involved. Define $K(s)\coloneqq\sqrt{\sqrt{\rho}\,(\rho+s\mathrm{d}\rho)\,\sqrt{\rho}}$; we need to compute $\rho^{-1}K'(0)$. By differentiating the square,

$$\begin{aligned}\{[K(s)]^2\}'&=K'(s)K(s)+K(s)K'(s)\\&=\sqrt{\rho}\,\mathrm{d}\rho\sqrt{\rho},\end{aligned}\tag{27}$$

as $K(0)=\rho$ we have

$$K'(0)\rho+\rho K'(0)=\sqrt{\rho}\,\mathrm{d}\rho\sqrt{\rho}.\tag{28}$$

After taking matrix elements in the eigenbasis of ρ,

$$\left(p_i+p_j\right)\left\langle\psi_i\right|K'(0)\left|\psi_j\right\rangle=\sqrt{p_ip_j}\left\langle\psi_i\right|\mathrm{d}\rho\left|\psi_j\right\rangle.\tag{29}$$

Thus, the matrix elements of $\rho^{-1}K'(0)$ are

$$\begin{aligned}&\left\langle\psi_i\right|\rho^{-1}K'(0)\left|\psi_j\right\rangle\\&=\frac{1}{p_i}\left\langle\psi_i\right|K'(0)\left|\psi_j\right\rangle\\&=\frac{\sqrt{p_j}}{\sqrt{p_i}\left(p_i+p_j\right)}\left\langle\psi_i\right|\mathrm{d}\rho\left|\psi_j\right\rangle.\end{aligned}\tag{30}$$

Now, since $\mathrm{d}\rho=\mathrm{d}(\sqrt{\rho}\sqrt{\rho})=(\mathrm{d}\sqrt{\rho})\sqrt{\rho}+\sqrt{\rho}(\mathrm{d}\sqrt{\rho})$, we obtain

$$\begin{aligned}&\left\langle\psi_i\right|\rho^{-1}K'(0)\left|\psi_j\right\rangle\\&=\frac{\sqrt{p_j}\left(\sqrt{p_i}+\sqrt{p_j}\right)}{\sqrt{p_i}\left(p_i+p_j\right)}\left\langle\psi_i\right|\mathrm{d}\sqrt{\rho}\left|\psi_j\right\rangle\end{aligned}\tag{31}$$

and finally the matrix elements of the connection form,

$$\begin{aligned}\left\langle\psi_i\right|A\left|\psi_j\right\rangle&=\left(-\frac{1}{\sqrt{p_i}}+\frac{\sqrt{p_j}\left(\sqrt{p_i}+\sqrt{p_j}\right)}{\sqrt{p_i}\left(p_i+p_j\right)}\right)\\\times\left\langle\psi_i\right|\mathrm{d}\sqrt{\rho}\left|\psi_j\right\rangle&=\frac{\left(\sqrt{p_j}-\sqrt{p_i}\right)}{\left(p_i+p_j\right)}\\&\quad\times\left\langle\psi_i\right|\mathrm{d}\sqrt{\rho}\left|\psi_j\right\rangle.\end{aligned}\tag{32}$$

This can be rewritten in terms of a commutator,

$$A=\sum_{i,j}\left|\psi_i\right\rangle\frac{\left\langle\psi_i\right|\left[\mathrm{d}\sqrt{\rho},\sqrt{\rho}\right]\left|\psi_j\right\rangle}{\left(p_i+p_j\right)}\left\langle\psi_j\right|.\tag{33}$$

Note that this connection form has only zeros on its diagonal and is skew-adjoint, so that the Uhlmann connection is special unitary.

For the particular case of 2×2 density matrices, because of the normalization condition $p_1+p_2=1$, (33) can be written as $A=[\mathrm{d}\sqrt{\rho},\sqrt{\rho}]$. This formula was also obtained by Dittmann and Rudolph [84]. Moreover, expanding in terms of Pauli matrices $\sqrt{\rho}=a_0+\boldsymbol{a}\cdot\boldsymbol{\sigma}$, we may write $A=2\mathrm{i}(\mathrm{d}\boldsymbol{a}\times\boldsymbol{a})\cdot\boldsymbol{\sigma}$ [73].

The result (33) has been obtained under the requirement that ρ is full rank. If this is not the case, for $w_1=w_{\boldsymbol{r}}$ the formula (14) can be fulfilled for several $w_2=w_{\boldsymbol{r}+\mathrm{d}\boldsymbol{r}}$ and there is not a unique solution and so a unique connection. One of these solutions can be obtained from continuity if we have a family of full rank states ρ_λ which approaches the desired non-full rank state as $\lambda\to 0$. Then a connection can be obtained with the formula (33) for ρ_λ, taking the limit $\lambda\to 0$ at the end of the computation. We will come back to this point at the end of the following section.

Once a connection form A is defined, we can construct its associate curvature form via the standard relation,

$$F=\mathrm{d}A+A\wedge A,\tag{34}$$

where $\wedge$ denotes the exterior product and the action of d is understood as the exterior derivative [85]. For the sake of clarity, let us write this equation in components. Expanding $A=\sum_i A_i\mathrm{d}r_i$, we find the usual expression of the field strength,

$$F_{ij}=\partial_iA_j-\partial_jA_i+\left[A_i,A_j\right],\tag{35}$$

where $F=\frac{1}{2}\sum_{i,j}F_{ij}\mathrm{d}r_i\wedge\mathrm{d}r_j$.

This curvature form F allows us to construct the Chern classes of the Uhlmann fiber bundle, which is the standard way to obtain topological invariants. We shall come back to this point in section 4.1.

2.4. Gauge transformations

In the previous subsection we obtained an expression for the Uhlmann connection in the 'identity' gauge, i.e. for the trajectory $\rho_{\boldsymbol{r}}$, we take initially $w_{\boldsymbol{r}(0)}=\sqrt{\rho_{\boldsymbol{r}(0)}}$ and construct the next point of the trajectory in $\mathcal{H}_w$ applying the Uhlmann parallel transport rule, such that $w_{\boldsymbol{r}}=\sqrt{\rho_{\boldsymbol{r}}}V_{\boldsymbol{r}}$ where $V_{\boldsymbol{r}}$ is the Uhlmann holonomy of the trajectory. Now consider a change of gauge by left-multiplying the amplitudes by some $\boldsymbol{r}$-dependent unitary $U_{\boldsymbol{r}}$, $w_{\boldsymbol{r}_0}=\sqrt{\rho_{\boldsymbol{r}_0}}U_{\boldsymbol{r}_0}$, so that $w_{\boldsymbol{r}}=\sqrt{\rho_{\boldsymbol{r}}}U_{\boldsymbol{r}}V_{U,\boldsymbol{r}}$, where $V_{U,\boldsymbol{r}}$ is the Uhlmann holonomy in the new gauge. To compute $V_{U,\boldsymbol{r}}$, we first obtain the connection form in the new gauge.

Similarly to the previous section we have to impose that two infinitesimally closed amplitudes are parallel. Under an infinitesimal displacement $w_1=\sqrt{\rho}UV_U$ changes to $w_2=\sqrt{\rho+\mathrm{d}\rho}\,(U+\mathrm{d}U)(V_U+\mathrm{d}V_U)$, so that according to (16), $w_1\parallel w_2$ if

$$\begin{aligned}&(U+\mathrm{d}U)(V_U+\mathrm{d}V_U)V_U^\dagger U^\dagger\\&=\left(\sqrt{\rho}+\mathrm{d}\sqrt{\rho}\right)^{-1}\sqrt{\rho^{-1}}\sqrt{\sqrt{\rho}\,(\rho+\mathrm{d}\rho)\,\sqrt{\rho}}\,.\end{aligned}\tag{36}$$

From (20) and subsequent equations, the right-hand side is simply $\mathbb{1}+A_{\mathbb{1}}$, where $A_{\mathbb{1}}$ denotes the connection in the 'identity' gauge. Moreover, the left-hand side at first order in differentials is $\mathbb{1}+\mathrm{d}UU^\dagger+U\mathrm{d}V_UV_U^\dagger U^\dagger$, so we obtain,

$$\mathrm{d}UU^\dagger+U\mathrm{d}V_UV_U^\dagger U^\dagger=A_{\mathbb{1}}\tag{37}$$

Since by definition, $A_U=\mathrm{d}V_UV_U^\dagger$ is the connection form in the new gauge, we find the transformation rule

$$A_U=U^\dagger A_{\mathbb{1}}U-U^\dagger\mathrm{d}U.\tag{38}$$

In general, under a change of gauge $U_2=U_1U$ ($w\to wU$), we straightforwardly obtain the transformation law

$$A_{U_2}=U^\dagger A_{U_1}U-U^\dagger\mathrm{d}U.\tag{39}$$

Now we can calculate the holonomy in the new gauge,

$$V_{U,\boldsymbol{r}}=\mathcal{P}\mathrm{e}^{\int_{\boldsymbol{r}_0}^{\boldsymbol{r}}A_U(\boldsymbol{r}')\mathrm{d}\boldsymbol{r}'}.\tag{40}$$

To that aim, consider the parametrization $\boldsymbol{r}(t)|_{t=0}^1$ and compute the t-derivative of $U[\boldsymbol{r}(t)]V_{U,\boldsymbol{r}(t)}U^\dagger[\boldsymbol{r}(0)]$:

$$\frac{\mathrm{d}}{\mathrm{d}t}\left\{U[\boldsymbol{r}(t)]V_{U,\boldsymbol{r}(t)}U^{\dagger}[\boldsymbol{r}(0)]\right\}$$
$$=\frac{\mathrm{d}U[\boldsymbol{r}(t)]}{\mathrm{d}t}V_{U,\boldsymbol{r}(t)}U^{\dagger}[\boldsymbol{r}(0)]$$
$$+U[\boldsymbol{r}(t)]\frac{\mathrm{d}V_{U,\boldsymbol{r}(t)}}{\mathrm{d}t}U[\boldsymbol{r}(0)] \quad (41)$$
$$=\frac{\mathrm{d}U[\boldsymbol{r}(t)]}{\mathrm{d}t}V_{U,\boldsymbol{r}(t)}U^{\dagger}[\boldsymbol{r}(0)]$$
$$+U[\boldsymbol{r}(t)]A_U[\boldsymbol{r}(t)]V_{U,\boldsymbol{r}(t)}U[\boldsymbol{r}(0)] \quad (42)$$
$$=A_{\mathbb{1}}[\boldsymbol{r}(t)]U[\boldsymbol{r}(t)]V_{U,\boldsymbol{r}(t)}U[\boldsymbol{r}(0)], \quad (43)$$

where we have used the definition (40) and introduced the gauge transformation (38). Since $U[\boldsymbol{r}(t)]V_{U,\boldsymbol{r}(t)}U^{\dagger}[\boldsymbol{r}(0)]|_{t=0}=\mathbb{1}$; $\{U[\boldsymbol{r}(t)]V_{U,\boldsymbol{r}(t)}U^{\dagger}[r(0)]\}$ satisfies the same differential problem as $V_{\mathbb{1},\boldsymbol{r}(t)}$, (17), and the uniqueness of the solution implies that:

$$V_{\mathbb{1},\boldsymbol{r}(t)}=U[\boldsymbol{r}(t)]V_{U,\boldsymbol{r}(t)}U^{\dagger}[\boldsymbol{r}(0)]$$
$$\Rightarrow V_{U,\boldsymbol{r}}=U^{\dagger}(\boldsymbol{r})V_{\mathbb{1},\boldsymbol{r}}U(\boldsymbol{r}_0). \quad (44)$$

Therefore, the Uhlmann holonomy of the trajectory is clearly gauge covariant as expected. This is a fundamental requirement in order to define gauge invariant quantities out of this construction.

2.5. Uhlmann geometric phase

Once the concept of Uhlmann holonomy has been presented, it is interesting and convenient to define the gauge invariant quantities associated to it. These are constructed out of the relative phases of the amplitudes that have been parallelly transported. Actually, this is the most important part of the analysis, since we want to relate the mathematical concepts to physical observables that are represented by gauge invariants in the theory.

First of all, consider some trajectory on $\mathcal{Q}$, with initial and final points ρ_0 and ρ_1, respectively. For some initial amplitude w_0, $\rho_0=w_0w_0^{\dagger}$, a parallel lift leads to some amplitude w_1, $\rho_1=w_1w_1^{\dagger}$. The *Uhlmann geometric phase* is defined as

$$\Phi_{\mathrm{U}}:=\arg(w_0,w_1)=\arg\mathrm{Tr}(w_0^{\dagger}w_1), \quad (45)$$

which is a gauge-independent quantity. Indeed, in the identity gauge, $w_0=\sqrt{\rho_0}$ and $w_1=\sqrt{\rho_1}$ we have

$$\Phi_{\mathrm{U}}=\arg\mathrm{Tr}\left(\sqrt{\rho_0}\sqrt{\rho_1}V\right). \quad (46)$$

Under a gauge transformation $w_0\to w_0U_0$, $w_1\to w_1U_1$ and according to (44), $V\to U_1^{\dagger}VU_0$, so $\Phi_{\mathrm{U}}\to\arg\mathrm{Tr}(U_0^{\dagger}\sqrt{\rho_0}\sqrt{\rho_1}U_1U_1^{\dagger}VU_0)=\Phi_{\mathrm{U}}$. Therefore Φ_{U} is gauge invariant.

To better visualize the geometric meaning of Φ_{U}, let us consider the trajectory on $\mathcal{Q}$ to be closed. Then $\rho_0=\rho_1=\rho$ and we have

$$\Phi_{\mathrm{U}}=\arg\mathrm{Tr}(\rho V)$$
$$=\arg\mathrm{Tr}\left(\rho\mathcal{P}\mathrm{e}^{\oint A}\right). \quad (47)$$

In the Uhlmann approach, after a closed trajectory in $\mathcal{Q}$ the amplitude gains an extra geometric $\mathrm{U}(n)-$phase, $\mathcal{P}\mathrm{e}^{\oint A}$. This is the equivalent to the Berry geometric U(1)-phase in this non-abelian approach, see 3. The equation (47) defines a real gauge invariant quantity extracting the non-abelian U(n)-phase which can be understood as the relative phase between w_0 and w_1. Basically, this is because by using the amplitude-purification isomorphism (6), Φ_U can be equivalently written as

$$\Phi_{\mathrm{U}}=\arg\langle w_0|w_1\rangle. \quad (48)$$

This interpretation has in fact suggested some schemes to measure Uhlmann geometric phases [77].

Another important concept needs to be introduced in order to understand the properties of the Uhlmann phase. This is the difference between an *absolute holonomy* and a *pointed holonomy*. The mapping

$$M_U: w\longrightarrow V, \quad (49)$$

is a so-called pointed holonomy. This means that, even if the trajectory in $\mathcal{Q}$ is closed, in general the holonomy depends on the initial point of the path. Nonetheless, we have identified cases in which the pointed holonomy reduces to an *absolute holonomy* becoming independent of the initial point [35, 37]. In addition, it is always true that the mapping

$$\tilde{M}_{\mathrm{U}}: w\longrightarrow \mathrm{spect}(V), \quad (50)$$

where spect(V) stands for the spectrum of the unitary V, is an absolute holonomy.

To conclude this section, consider the case of a pure state trajectory $\rho_{\boldsymbol{r}}=|\psi_{\boldsymbol{r}}\rangle\langle\psi_{\boldsymbol{r}}|$. As we have already pointed out, the Uhlmann connection in this case is not uniquely defined because the state $\rho_{\boldsymbol{r}}$ is not full rank. There are two approaches to overcome this difficulty.

- As aforementioned, a first approach to compute the Uhlmann phase factor in this situation is to consider the connection A^{λ} computed via (33) for a full rank matrix trajectory $\rho_{\boldsymbol{r}}^{\lambda}$ such that $\lim_{\lambda\to0}\rho_{\boldsymbol{r}}^{\lambda}=|\psi_{\boldsymbol{r}}\rangle\langle\psi_{\boldsymbol{r}}|$. Thus, the Uhlmann phase factor is obtained by formula (47) with $V=\lim_{\lambda\to0}\mathcal{P}\mathrm{e}^{\oint A^{\lambda}}$. This is a typical approach when $|\psi_{\boldsymbol{r}}\rangle$ is seen as the ground state of some Hamiltonian and we want to study temperature effects. Then, the family of full rank states will be the Gibbs states which approach the ground state in the zero temperature limit.
- An alternative approach is to look for another solution to the optimization problem (14). For example, consider two pure states, $|\psi_1\rangle$ and $|\psi_2\rangle$, the optimization problem (14) can be easily solved in a gauge with amplitudes of the form of $w_1=|\psi_1\rangle\langle a|\,\mathrm{e}^{\mathrm{i}\phi_1}$, $w_2=|\psi_2\rangle\langle a|\,\mathrm{e}^{\mathrm{i}\phi_2}$ where $|a\rangle$ is some arbitrary $\boldsymbol{r}$-independent vector, and the phases are chosen such that $(\phi_1-\phi_2)=\arg\langle\psi_1|\psi_2\rangle$. This can be directly checked in (14) and also derived from condition (10). Thus, in this

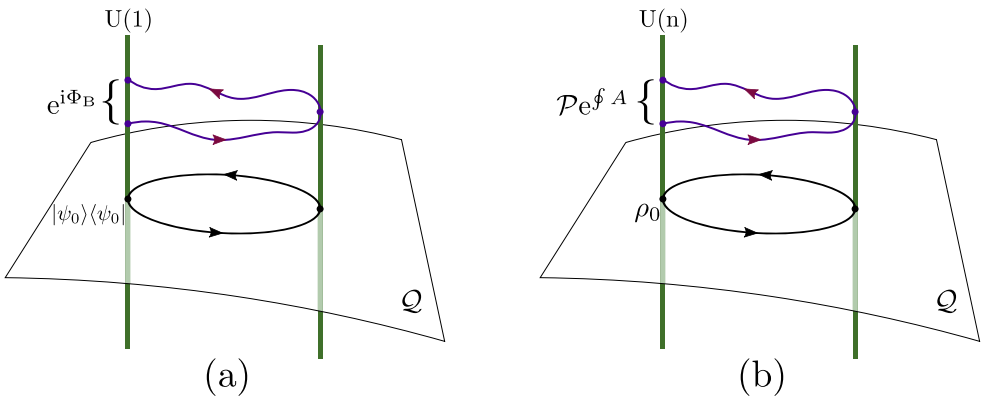

Figure 3. Comparison between Berry and Uhlmann holonomies. In the approach of Berry, valid for pure states (a), after a closed loop on the space $\mathcal{Q}$, the final state vector differs by a phase Φ_B with respect to the initial state vector. In the case of Uhlmann, formulated for density matrices (b), the difference between initial and final amplitude is, in general, the unitary matrix given by $\mathcal{P}e^{\oint A}$.

gauge we can satisfy the parallel transport rule just by varying a U(1) factor, $e^{i\phi}$, extracted from the general U(n) gauge freedom. More concretely, we associate the amplitudes $w_r = |\psi_r\rangle\langle a|\, e^{i\phi(r)}$ with the trajectory $\rho_r = |\psi_r\rangle\langle\psi_r|$. Then we have

$$\begin{aligned} w_r^\dagger (\, w_r + \mathrm{d}w_r) &= |a\rangle\langle a| + e^{-i\phi(r)}\ |a\rangle \\ &\quad \times \langle\psi_r|\ \mathrm{d}\Big(\Big|\psi_r\Big\rangle\langle a|\ e^{i\phi(r)}\Big) \\ &= \Big[1 + \Big\langle\psi_r\Big|\mathrm{d}\psi_r\Big\rangle + i\mathrm{d}\phi(\boldsymbol{r})\Big]|a\rangle\langle a|, \end{aligned} \tag{51}$$

where due to normalization, $\langle\psi_r|\mathrm{d}\psi_r\rangle$ is purely imaginary. The parallel transport law in the form of (10), with $w_1 = w_r$ and $w_2 = w_r + \mathrm{d}w_r$ leads to the condition

$$\mathrm{d}\phi(\boldsymbol{r}) = i\Big\langle\psi_r\Big|\mathrm{d}\psi_r\Big\rangle. \tag{52}$$

If we denote by $|\psi_{r_0}\rangle\langle\psi_{r_0}|$ the initial and final state, we have $w_0 = |\psi_{r_0}\rangle\langle a|\, e^{i\phi(r_0)}$, and the parallel transported final amplitude will be $w_1 = |\psi_{r_0}\rangle\langle a|\, e^{\oint \mathrm{d}\phi(r)} e^{i\phi(r_0)}$, where $e^{\oint \mathrm{d}\phi(r)}$ is the accumulated phase after the parallel translation. Thus, by using (52) the Uhlmann phase factor $\Phi_U = \mathrm{argTr}(w_0^\dagger w_1)$ yields

$$\begin{aligned} \Phi_U &= \mathrm{argTr}\Big[e^{-i\phi(r_0)}\ |a\rangle\Big\langle\psi_{r_0}\Big|\psi_{r_0}\Big\rangle \\ &\quad \times \langle a|\ e^{\oint \mathrm{d}\phi(r)} e^{i\phi(r_0)}\Big] \\ &= i\oint\Big\langle\psi_r\Big|\mathrm{d}\psi_r\Big\rangle \mod 2\pi, \end{aligned} \tag{53}$$

which is nothing other than the usual Berry geometric phase.

Very importantly, since the Uhlmann phase is independent of the gauge, the two approaches must provide the same result. This is going to be crucial in the next section in order to obtain consistent results when taking the limits of zero temperature and pure states.

3. Density-matrix topological insulators and superconductors: topological Uhlmann phase

In this section we will describe how the Uhlmann geometric phase acquires a topological character in certain 1D condensed-matter systems. The problem of combining the study of topological phases with the fact of having mixed states and finite temperature is very relevant and had remained vaguely explored for a long time. In a set of recent papers [25, 27, 35, 37], we tried to deal with this issue and proposed some methods to generalize the notion of SPT order to finite temperature and to systems with dissipation.

The most characteristic feature of a geometric phase, such as the Berry phase, is the fact that it does not depend on properties such as the gauge or the speed at which a given path is traversed but only on the geometry of the path. In the case of closed paths, this is manifested by the fact that the geometric phase only depends on the area enclosed by the trajectory on the manifold defined as the parameter space.

There are cases, however, where the path covered during the holonomy coincides with one of the topologically non-trivial paths of a given manifold. In particular, in condensed matter, we know that due to translational invariance, the *crystalline momentum* $\mathbf{k}$ defines the so-called BZ and characterizes the eigenstates of the system. Then the phase difference picked up by the system when parallelly transported from an initial momentum $\mathbf{k}_0$ to a final one $\mathbf{k}_0 + \mathbf{G}$, where $\mathbf{G}$ is a reciprocal lattice vector, is gauge invariant and a geometric phase as well. This was proven by Zak [60] and the arguments work both in 1D and in higher-dimensional systems. This particular Berry phase is also called the Zak phase. In fact, in 1D systems, Zak [60] showed that the Zak phase is quantized and equal to 0 or π in the presence of inversion symmetry.

On the other hand, the Uhlmann phase was initially proposed as a generalization of the Berry phase to density matrices, but it can also be applied to

condensed-matter systems in the spirit of the Zak phase. This is in fact very fundamental since it deals with the problem of generalizing the notion of topology to systems with dissipation and finite temperature. Indeed, we studied this problem in detail [35] and found that when applied to representative models for topological insulators and superconductors, the Uhlmann phase acquired a topological character and is also quantized to 0 or π depending on whether the system is in a topological phase or not.

Specifically, we consider 1D Hamiltonians with two bands in momentum space. We denote by a and b two different types of fermionic band operators in such a way that in the spinor representation of $\psi_k = (a_k, b_k)^{\mathrm{t}}$ for insulators, while for superconductors $\psi_k = (c_k, c^{\dagger}_{-k})^{\mathrm{t}}$, is the Nambu spinor for paired fermions with opposite crystalline momentum [9]. We take lattice spacing $a = 1$ throughout the text. The Hamiltonian of these systems can be written as

$$H = \sum_k \psi_k^{\dagger} H_k \psi_k, \tag{54}$$

where H is a quadratic form on ψ and H_k is a 2×2 matrix. We aim to study the properties of this Hamiltonian under a displacement in k along a circuit which encloses the whole BZ, which will be the circle S^1.

Note that H_k can be decomposed in the following form

$$H_k = f(k)\mathbb{1} + \frac{\Delta_k}{2}\boldsymbol{n}_k \cdot \boldsymbol{\sigma}. \tag{55}$$

Here, $\boldsymbol{\sigma} = (\sigma_x, \sigma_y, \sigma_z)$ are the Pauli matrices, Δ_k corresponds to the gap of H_k and $f(k)$ denotes some function of k. The unit vector $\boldsymbol{n}_k = (\sin\theta\cos\phi, \sin\theta\sin\phi, \cos\theta)$ is called the *winding vector*, where θ and ϕ are $k-$dependent spherical coordinates.

For a thermalization process preserving particle number, with the Fermi energy set in the middle of the gap, the connection in (33) associated to this equilibrium (thermal) state, $\rho_k^{\beta} = \mathrm{e}^{-\beta H_k} \big/ \mathrm{Tr}\left(\mathrm{e}^{-\beta H_k}\right)$ where $T = 1/\beta$ denotes temperature, is

$$A = m_{12}^k \left\langle u_-^k \middle| \partial_k u_+^k \right\rangle \left| u_-^k \right\rangle \left\langle u_+^k \right| \mathrm{d}k + \mathrm{h.c.} \tag{56}$$

where $m_{12}^k := 1 - \mathrm{sech}\left(\dfrac{\Delta_k}{2\,T}\right)$.

Moreover, making use of the discrete symmetries [86, 87] that restrict the movement of the winding vector $\boldsymbol{n}_k$ as a function of k, only two components n_k^i and n_k^j with $i \neq j$ are non-zero. In order to obtain a simplified expression for the Uhlmann phase, we fix the gauge of the eigenvectors of H_k in (55) in such a way that the off-diagonal overlap $\langle u_-^k \left| \partial_k u_+^k \right\rangle$ and the winding vector components are related in the manner

$$\left\langle u_-^k \middle| \partial_k u_+^k \right\rangle = \frac{\partial_k n_k^i}{2 n_k^j}. \tag{57}$$

Note that as (47) is gauge invariant, we can fix the most convenient gauge to perform the calculation of the Uhlmann phase.

Thus, using (56) with this particular gauge choice and simplifying (47), we obtain a more simplified expression

$$\Phi_{\mathrm{U}} = \arg\left\{ \cos(\pi\omega_1) \cos\left[\oint \left(\frac{\partial_k n_k^i}{2 n_k^j} \right) \times \mathrm{sech}\left(\frac{\Delta_k}{2T} \right) \mathrm{d}k \right] \right\} \tag{58}$$

where $\omega_1 := \dfrac{1}{2\pi} \oint \left(\dfrac{\partial_k n_k^i}{n_k^j} \right) \mathrm{d}k$ is the winding number of $\boldsymbol{n}_k$ [35], a topological indicator characterizing the mapping $S^1 \longrightarrow S^1$, from $k \longrightarrow \boldsymbol{n}_k$.

In the case of being in a trivial phase with $\omega_1 = 0$, the Uhlmann phase is always zero. However, for non-trivial topological regions $\omega_1 = \pm 1$, we can obtain either $\Phi_{\mathrm{U}} = 0$ or $\Phi_{\mathrm{U}} = \pi$ depending on the value of T. Thus, the topological order as accounted by Φ_{U} can also be non-trivial for a range of temperatures $T < T_{\mathrm{c}}$. In [35] we computed the Φ_{U} finite temperature for the three representative models of topological insulators and superconductors, showing this critical effect with temperature represented in different phase diagrams.

On the other hand, the appearance of a critical temperature T_{c} in the Uhlmann phase can be interpreted geometrically in a pictorial and intuitive way. First of all, for the sake of illustration, we can visualize the amplitudes (or purifications) as arrows with fixed length. The angle between two arrows will be given by the relative phase between the corresponding amplitudes. In figure 4, we sketch different situations where the amplitudes (arrows) are transported according to Uhlmann's parallel condition along a closed loop that covers the whole BZ S^1. Here we present a summary of the different behaviors.

1. At $T = 0$ two things may happen. If the system is in a trivial phase, then the arrow is transported always pointing in the same direction, which means that the relative phase between the amplitudes does not change. The initial and final arrows are parallel as in figure 4(b), so that $\Phi_{\mathrm{U}}^0 = \Phi_{\mathrm{B}} = 0$. In the case that the system is in a topological phase, the Uhlmann phase remains 0 (the arrows are parallel) up to a certain critical point k_{c}, when the direction of the arrows is reversed and hence the relative phase between amplitudes is equal to π. This constitutes a *topological kink*. From there, the arrow does not flip anymore until the final point of the path $k_{\mathrm{f}} = 2\pi$ is reached, as in figure 4(a). Thus, the phase $\Phi_{\mathrm{U}}^0 = \Phi_{\mathrm{B}} = \pi$.

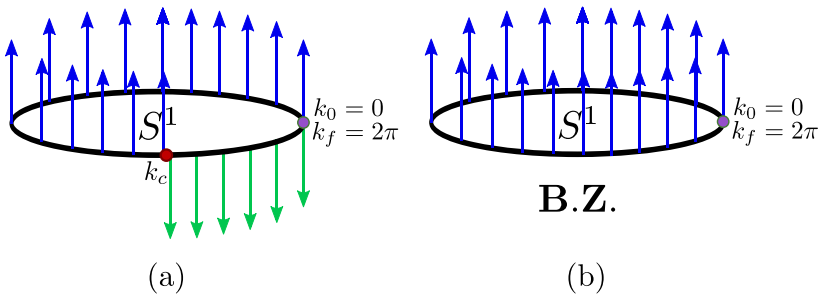

Figure 4. Behavior of the Uhlmann phase during the parallel transport from $k_0 = 0$ to $k_f = 2\pi$. We identify two situations. (a) Non-trivial topology highlighted by the presence of a topological kink at k_c. (b) Trivial order where the topological kink disappears. A detailed explanation of the figure can be found in the text.

2. At $T \neq 0$, we can identify three different possibilities. If the system was in a trivial phase at $T = 0$ then $\Phi_U = 0$, $\forall T$, as we have already proven, being again the case of figure 4(b). If at $T = 0$ the system was in a topological phase, then at finite temperature there are two options. Whenever $T < T_c$, the situation in figure 4(a) is reproduced, the Uhlmann phase remains 0 up to the critical point which is a function of T. From that point, the arrow is reversed and the Uhlmann phase is equal to π until the close path is completed. An increase of temperature shifts the position of k_c towards the end of the BZ. However, if $T > T_c$, then we recover again figure 4(b) with no phase change $\Phi_U = 0$. The position of k_c has already reached the end of the BZ and the topological kink can no longer occur along the path between $k_0 = 0$ and $k_f = 2\pi$.

To conclude, we have derived a connection between the existence of a critical temperature T_c and the presence of a topological kink structure [88] in the Uhlmann holonomy. The same relation can in fact be established with the parameters of the Hamiltonian H, that drives the system out of the topological phase. This is because the Uhlmann phase places on equal footing T and these coupling constants. The reason to call this kink topological is actually well established. The critical momentum k_c divides the holonomy into two different topological sectors according to the value of the final point of the path k_f. The first sector covers the region with $k_f < k_c$ and $\Phi_U = 0$, and the second sector starts when $k_f > k_c$ and $\Phi_U = \pi$. It is clear that these two different sections cannot be smoothly connected without crossing the singular point $k_f = k_c$. In the trivial topological regime $\Phi_U = 0$, however, we can associate every point in the sector with the same class. To be more specific, Φ_U is invariant under changes of the final point of the holonomy $k_f \in (0, k_c)$. The same happens within the other non-trivial topological sector with $\Phi_U = \pi$ once we consider $k_f \in (k_c, 2\pi)$. The effect of the temperature in the Uhlmann parallel transport can be understood as a displacement of the topological kink along k-space. When the temperature reaches the critical value T_c, the critical momentum k_c has been pushed out to the edge of the BZ and the topological kink disappears. The critical temperature T_c can be viewed as the maximum amount of noise/disorder such that the Uhlmann holonomy along the BZ displays a topological kink structure.

4. 2D Uhlmann topological invariants

In the previous section, we have shown that in 1D condensed-matter systems, the Uhlmann geometric phase acquires a topological character when applied to topological insulators and superconductors. In fact, the relation of topological phases for pure states with invariants of SPT order in more than 1D has been extensively studied, in particular see [89, 90]. Nonetheless, the concept of a geometric phase or a topological phase is not at all restricted to 1D and can be defined in higher-dimensional spaces.

The problem of generalizing the Uhlmann phase formalism for 2D cases is not straightforward at all [36, 37]. This has to do with the triviality of the Chern classes associated with the Uhlmann connection of non-singular density matrices, as was first proven in [35]. Different but equivalent ways to solve this problem were proposed in [36, 37]. In [36] an analysis of the spectrum of the whole holonomy matrix was carried out, while in [37] a unique topological invariant called the Uhlmann number was first proposed to characterize the topological order of two-band topological insulators and superconductors at finite temperature in 2D.

In this section we review the theory of topological phases for mixed states in 2D and give a detailed explanation of a particularly useful way to define topological invariants inside the Uhlmann formalism. As a concrete example, we will characterize the topological phase diagram of the QHZ model for a topological insulator at finite temperature.

4.1. Triviality of the Uhlmann Chern classes

At zero temperature, there is a standard way to define topological invariants in 2D SPT order systems out of Chern numbers. In this case, a fiber bundle is formed out from the pure state eigenvectors $|u_{\boldsymbol{k}}\rangle$ corresponding to the lower energy band and the fiber is linked to the U(1) gauge freedom that each eigenvector has. As aforementioned, the first Chern number associated to the first Chern class of fiber bundle can be related to the transverse or quantum Hall conductivity of the system by the so-called TKNN formula (1) [58]. Moreover, the presence of conducting edge states in topological insulators, or Majorana fermions in a topological superconductor, can also be related to the fact of having a topological non-trivial structure in the system.

We shall consider a time-reversal broken two-band system with Fermi energy between both bands. The Chern number is given by

$$\begin{aligned} \mathrm{Ch} &:= \frac{1}{2\pi}\int_{\mathrm{BZ}} \mathrm{d}^2\boldsymbol{k} F_{xy}(\boldsymbol{k}), \\ F_{xy}(\boldsymbol{k}) &:= \partial_x A^{\mathrm{B}}_y(\boldsymbol{k}) - \partial_y A^{\mathrm{B}}_x(\boldsymbol{k}), \end{aligned} \tag{59}$$

where $A^{\mathrm{B}}_j(\boldsymbol{k}) = \mathrm{i}\langle u_{\boldsymbol{k}}|\partial_j u_{\boldsymbol{k}}\rangle$ is the Berry connection and $|u_{\boldsymbol{k}}\rangle$ is the eigenvector corresponding to the lower energy band. This number is a topological invariant which only takes on integer values. While these kinds of constructions can be extended to higher-dimensional systems or systems with time-reversal symmetry [9], when attempting the generalization to density matrices via the Uhlmann connection one finds the following fundamental obstruction.

A natural way to generalize the Chern number to arbitrary density matrices would be to consider the first Chern class associated to the Uhlmann curvature, which is constructed from the Uhlmann connection A via the standard formula for the non-Abelian case, (35),

$$F^{\mathrm{U}}_{xy} = \partial_x A_y - \partial_y A_x + \left[A_x, A_y\right]. \tag{60}$$

Then, using the theory of characteristic classes [85, 91], the (first) Chern number of the Uhlmann curvature would be given by

$$\mathrm{Ch}_{\mathrm{U}} := \frac{\mathrm{i}}{2\pi}\int_{\mathrm{BZ}} \mathrm{d}^2\boldsymbol{k}\ \mathrm{Tr}\left(F^{\mathrm{U}}_{xy}\right). \tag{61}$$

There is, however, a problem with this construction, as Ch_{U} turns out to always be zero. The reason for this is twofold.

1. First of all, the Uhlmann connection belongs to the $\mathfrak{su}(n)$ Lie algebra, so its trace vanishes and so does the trace of its curvature. Hence, using (61), Ch_{U} is zero independently of the associated state ρ_k. This has more to do with the mathematical structure of the Uhlmann construction than with physical properties of ρ_k.
2. On the other hand, the Chern number is 0 as long as there is a smooth gauge defined along the whole BZ [85, 91]. Note that this is the case for the Uhlmann U(n) gauge, as we can always take the gauge $w_{\boldsymbol{k}} = \sqrt{\rho_{\boldsymbol{k}}}$ which is well defined provided that $\rho_{\boldsymbol{k}}$ is not singular at some crystalline momentum $\boldsymbol{k}$. This is a rather natural condition and the usual case in physical situations.

Additionally, the second condition also implies that higher order Chern numbers vanish for the Uhlmann connection. Thus, $\mathrm{Ch}_{\mathrm{U}} = 0$ in any case. This result was first proven in [37].

In conclusion, this obscures the extension of 2D topological invariants by means of the Uhlmann approach. We will show specifically the way to avoid these obstacles and define a proper topological invariant for general density matrices associated to these topological systems.

4.2. Topological Uhlmann numbers

In this section, we explain how to construct single topological invariants associated to density matrices of 2D topological insulators and superconductors. The key tool for this is going to be the topological Uhlmann phase derived previously. The 2D construction as explained here was originally proposed in [37] and also equivalently in [36]. A more detailed derivation and discussion not present in previous works is carried out in the following.

In the previous subsection, we showed that the Chern number associated to the Uhlmann connection was always zero. However, the fact that Ch_{U} becomes identically zero and the associated fiber bundle becomes trivial does not imply that all topological properties of density matrices are trivial. If this assertion were true, we could not claim that systems at $T = 0$ can be topologically ordered, as they are just a particular case of generally mixed density matrices. And, in fact, we see that systems at $T = 0$ display topological order in many fashions (non-zero Chern numbers, topological edge states, Majorana fermions, magnetoelectric effect, ...). The key point in the discussion is that Ch_{U} is not the only topological invariant that we can construct on a torus out of a density matrix.

With that in mind, let us analyze the problem at $T = 0$ from a different perspective. In fact, in the Berry case, the Chern number (59) can be rewritten as [62, 89, 90]

$$\mathrm{Ch} = \frac{1}{2\pi}\oint \mathrm{d}k_x \frac{\mathrm{d}\Phi_{\mathrm{B}}(k_x)}{\mathrm{d}k_x}, \tag{62}$$

where $\Phi_{\mathrm{B}}(k_x) = \oint \mathrm{d}k_y A^{\mathrm{B}}_y(k_x, k_y)$ is the Berry phase along the k_y–nontrivial homological circle of the torus at the point k_x, and $\oint \mathrm{d}k_x$ denotes the integration along the k_x-nontrivial homological circle. See figure 5.

To prove the equality (62) from the general definition of the Chern number, one divides the surface integral in (59) into small slices along the k_x-direction,

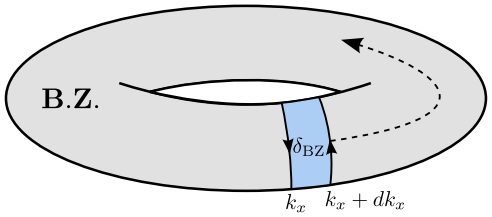

Figure 5. This 2D torus represents the BZ where the crystalline momentum of the system leaves. The figure represents the partition of the torus in infinitesimal slices of width $\mathrm{d}k_x$; computing the Berry (or Uhlmann) phase associated to each slice and integrating the whole homological cycle in k_x, one obtains the Chern number (62) or the Uhlmann number (67), respectively.

$$\frac{1}{2\pi}\int_{\delta_{\mathrm{BZ}}} \mathrm{d}^2\boldsymbol{k} F_{xy}(\boldsymbol{k}), \tag{63}$$

where δ_{BZ} is an infinitesimal element of area that is limited by one k_y-nontrivial homological circle of the torus at the point k_x and another one at the point $k_x + \mathrm{d}k_x$, as shown in figure 5. The U(1)-gauge, which may be ill-defined over the whole BZ, is always well-defined in a sufficiently small slice, so that Stokes' theorem is applicable. Thus,

$$\begin{aligned}\frac{1}{2\pi}\int_{\delta_{\mathrm{BZ}}} \mathrm{d}^2\boldsymbol{k} F_{xy}(\boldsymbol{k}) &= \oint_{\partial\delta_{\mathrm{BZ}}} A^{\mathrm{B}}(\boldsymbol{k})\,\mathrm{d}\boldsymbol{k} \\ &= -\Phi_{\mathrm{B}}(k_x) + \Phi_{\mathrm{B}}(k_x + \mathrm{d}k_x) \\ &= \frac{\partial\Phi_{\mathrm{B}}(k_x)}{\partial k_x}\mathrm{d}k_x.\end{aligned} \tag{64}$$

Then, in the limit of slices with infinitesimal width, summing the slices at both sides of (64) is equivalent to performing the integral and one easily obtains (62).

Note that, (62) indeed provides a lot of information. If $\Phi_{\mathrm{B}}(k_x)$ is a continuous function and $\Phi_{\mathrm{B}}(k_x \to 0) = \Phi_{\mathrm{B}}(k_x \to 2\pi)$, then we trivially obtain $\mathrm{Ch} = 0$. If $\Phi_{\mathrm{B}}(k_x)$ displays some 2π-discontinuous jumps along the k_x circle, then we can always write

$$\Phi_{\mathrm{B}}(k_x) = \mathrm{e}^{\mathrm{i}2\pi\Theta(k_x - k_x^{\mathrm{c}})}\hat{\Phi}_{\mathrm{B}}(k_x), \tag{65}$$

where $\hat{\Phi}_{\mathrm{B}}(k_x)$ is a smooth function equal to $\oint \mathrm{d}k_y A_y^{\mathrm{B}}(k_x, k_y)$ mod. 2π, k_x^{c} is the point at which the discontinuity happens and Θ denotes the Heaviside step function. In this way we can compute the derivative and perform the integration along the k_x − nontrivial homological circle of the torus. In fact, the Chern number is measuring the number of these 2π jumps, which is equivalent to the number of windings of $\Phi_{\mathrm{B}}(k_x)$ as the k_x circle is covered. This is indeed a topological invariant, specifically a winding number, that associates every state of the system with an homotopy class of the Berry phase mapping

$$\Phi_{\mathrm{B}}(k_x)\colon S^1 \to S^1, \tag{66}$$

between the nontrivial homological circle S^1 along k_x and the complex Berry phases $U(1) \cong S^1$.

As we have seen before, (59) does not admit a direct generalization to density matrices, however, the equivalent formula (62) for the Chern number at $T = 0$ and pure states allows for a nontrivial generalization to density matrices. To that aim, we will just replace the Berry phase $\Phi_{\mathrm{B}}(k_x)$ by the Uhlmann phase $\Phi_{\mathrm{U}}(k_x)$, (47), in (62):

$$\mathrm{n_U} := \frac{1}{2\pi}\oint \mathrm{d}k_x \frac{\mathrm{d}\Phi_{\mathrm{U}}(k_x)}{\mathrm{d}k_x}. \tag{67}$$

Note that many of the properties of the Berry case are maintained. This number $\mathrm{n_U}$ is also an integer by the same arguments given previously for the Chern number. If the $\Phi_{\mathrm{U}}(k_x)$ is a continuous function along the k_x circle and $\Phi_{\mathrm{U}}(k_x \to 0) = \Phi_{\mathrm{U}}(k_x \to 2\pi)$, then we trivially obtain $\mathrm{n_U} = 0$. Otherwise, $\mathrm{n_U}$ measures again the number of 2π-discontinuous jumps along the k_x-nontrivial homological circle. It is also trivially gauge invariant, as the Uhlmann phase is gauge invariant already.

This integer number is therefore a topological invariant which classifies the density matrices of a quantum system according to the homotopy class of the Uhlmann phase mapping,

$$\Phi_{\mathrm{U}}(k_x)\colon S^1 \to S^1, \tag{68}$$

between the nontrivial homological circle S^1 along k_x and the complex Uhlmann phases $U(1) \cong S^1$.

Furthermore, the limit at zero temperature is also well-defined. For pure states, the Uhlmann phase coincides with the Berry phase $\Phi_{\mathrm{U}} = \Phi_{\mathrm{B}}$. Thus, if we compute $\mathrm{n_U}$ in a thermal (Gibbs) state, then the following relation is trivially satisfied

$$\mathrm{n_U} \xrightarrow{T\to 0} \mathrm{Ch}, \tag{69}$$

hence, the generalization is faithful.

Additionally, since Φ_{U} is an observable and we even discussed certain general schemes to measure it in different platforms [35], then $\mathrm{n_U}$ is also an observable. We will refer to this topological invariant $\mathrm{n_U}$ as the *Uhlmann number*.

As was shown in [37], the Uhlmann number characterizes representative models for topological insulators and superconductors in 2D. Remarkably, in models with high Chern numbers, one finds novel thermal–topological transitions between two nontrivial phases solely driven by temperature.

In the following, we will analyze a new model for two-band topological insulators at a finite temperature according to the topological invariant $\mathrm{n_U}$.

4.3. QWZ Chern insulator

As an example of the applicability of this method, we present a model for a 2D topological insulator proposed in [53, 54]. Although the model is mathematically simple, it contains the main features of the physics of a Chern insulator.

The model consists of a simple square lattice of spin-1/2 fermions, with spin-dependent nearest-

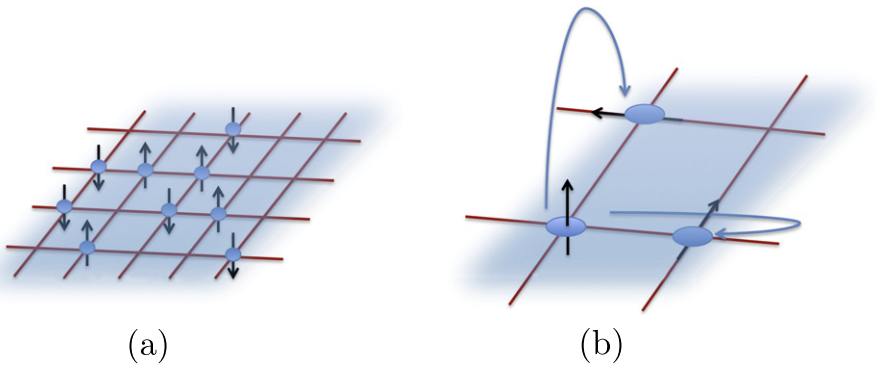

Figure 6. A pictorial image of the QWZ model in real-space is shown here. In (a), we represent the on-site σ_z part of the Hamiltonian interaction, where the arrows represent the spins in the z-direction. In (b), we show an example of the effect of the spin-dependent hopping in the interaction. In particular, $|\uparrow\rangle_z \longrightarrow |\uparrow\rangle_y$ when hopping along the $x-$ axis, but $|\uparrow\rangle_z \longrightarrow |\downarrow\rangle_x$ when hopping along the y-axis.

neighbor hoppings, and an energy imbalance between spin up and down (see figure 6). The Hamiltonian in real space is given by

$$H = \sum_{\vec{r}} \Big[c_{\vec{r}}^{\dagger} \frac{\sigma_z - \mathrm{i}\sigma_x}{2} c_{\vec{r}+\vec{x}} + c_{\vec{r}}^{\dagger} \frac{\sigma_z - \mathrm{i}\sigma_y}{2} c_{\vec{r}+\vec{y}} + \mathrm{h.c.}\Big] + m \sum_{\vec{r}} c_{\vec{r}}^{\dagger} \sigma_z c_{\vec{r}} \tag{70}$$

where $c_{\vec{r}}^{\dagger}$, $c_{\vec{r}}$ are fermionic creation and annihilation operators and $\vec{x}$ and $\vec{y}$ are unitary vectors along the x- and y-directions, respectively. The Pauli matrices $\sigma_{x,y,z}$ act on the spin-1/2 degree of freedom. The model describes the quantum anomalous Hall effect. The σ_x and σ_y terms appear due to strong spin–orbit coupling and the σ_z part represents some ferromagnetic polarization. It has been shown to be realizable in $Hg_{1-x}Mn_xTe/Cd_{1-x}Mn_xTe$ quantum wells with a proper amount of Mn spin polarization [92].

In figure 6 we sketch the dynamics of the system for a certain spin orientation as an example. Figure 6(a) represents the on-site σ_z part and figure 6(b) shows the hopping mechanism for a certain spin state in order to visualise the dynamics. When a fermion with spin up in the $z-$direction hops along the x-direction, then $|\uparrow\rangle_z \longrightarrow |\uparrow\rangle_y$. If it hops along the y-direction, then $|\uparrow\rangle_z \longrightarrow |\downarrow\rangle_x$, as shown in figure 6(b).

Taking periodic boundary conditions the Hamiltonian in momentum space reads

$$H(\boldsymbol{k}) = \sin(k_x)\sigma_x + \sin\big(k_y\big)\sigma_y + \Big[m + \cos(k_x) + \cos\big(k_y\big)\Big]\sigma_z, \tag{71}$$

where m is some energy imbalance between two atoms of different species.

At $T = 0$, the different topological phases as classified by the Chern number, (59), are:

$$\mathrm{Ch} = \begin{cases} +1, & \text{if } -2 < m < 0, \\ -1, & \text{if } 0 < m < 2, \\ 0, & \text{if otherwise.} \end{cases} \tag{72}$$

For nontrivial regions $\mathrm{Ch} = \pm 1$, the system presents metallic edge states at the boundary. Indeed, the conductivity of these edge states is given by the Chern number $\sigma_{\mathrm{Edge}} = \dfrac{e^2}{h}\mathrm{Ch}$.

The different topological phases as classified by the Uhlmann number, (67), are graphically represented in figure 7 at finite temperature. The system displays nontrivial topological phases $\mathrm{n_U} = \pm 1$ even at nonzero temperature, provided it is below a certain critical value T_c, where $\mathrm{n_U}$ goes to zero. This critical temperature T_c reaches its maximum at the points $m = \pm 1$ within the topological phases $\mathrm{Ch} = \pm 1$ at $T = 0$. These points are associated with the highest value of the gap. This matches the common intuition that the resilience of topological order has to do with the ratio between the gap and the temperature, and the larger the gap, the more stable it is. As expected, in the limit of $T = 0$ we recover the same topological diagram as given by the Chern number.

In fact, we can understand the discontinuity in the Uhlmann number when crossing different topological regions even better by looking at figure 8. We show $\Phi_{\mathrm{U}}(k_x)$ for different topological sectors. Namely, we have set $m = -1$ which is a topological region at $T = 0$. At low temperatures we see that there is still a jump in the phase at a certain critical momentum $k_c = 0$, which accounts for $\mathrm{n_U} = 1$. However, in the same figure we can see what happens at higher temperatures where the jump disappears, the Uhlmann phase is a continuous function of k_x and hence, $\mathrm{n_U} = 0$. This supports the previous explanation that the topological Uhlmann number accounts for the number of discontinuous jumps of the Uhlmann phase in momentum space.

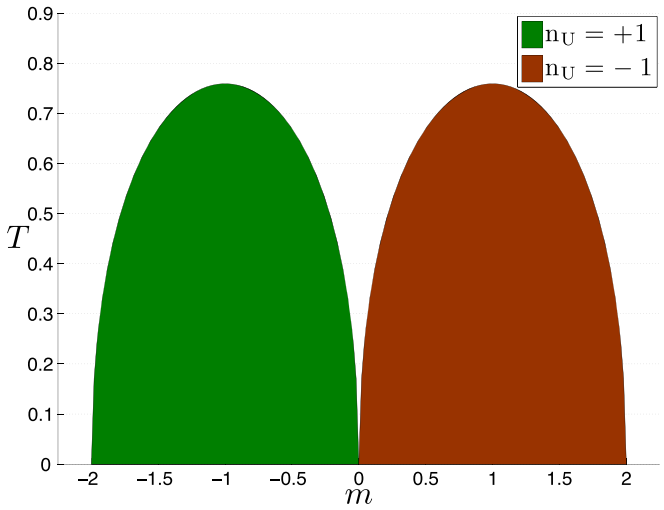

Figure 7. Topological phase diagram given by the Uhlmann number for the QWZ model. Varying both the energy imbalance m and the temperature T we can go from a topological region to a trivial one. Note that n_U remains quantized everywhere. If we fix m and vary the temperature T, there is always a critical point where n_U goes discontinuously and abruptly to zero.

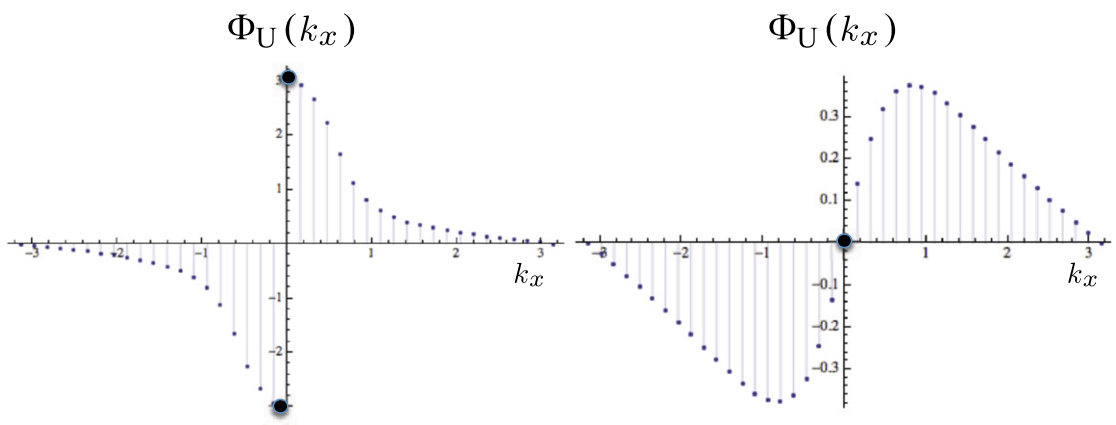

Figure 8. We represent $\Phi_U(k_x)$ in the QWZ model for $m = -1$. In the left panel, we set $T = 0.1$ and observe a discontinuous jump in the phase which is responsible for the robustness of the topological phase at finite temperature. In the right panel, we take a higher temperature $T = 1.2$ where the system is no longer topological and the discontinuity in the phase disappears.

Thus, we see that thermal topological phase transitions are not a unique phenomenon of the 1D case [35] and they are also found in 2D systems.

5. Conclusions

In this paper we have characterized a new representative model for a topological insulator, the QWZ model introduced in [53, 54] using the topological Uhlmann number introduced in [37] in order to find a stable SPT phase under external thermal fluctuations in 2D. This was originally discovered in representative examples of topological insulators and superconductors in 1D [37], which later lead to higher-dimensional constructions [36, 37]. A complete phase diagram of the topological Uhlmann number as a function of the parameters of the Hamiltonian in the QWZ and as a function of the temperature of the system is shown in figure 7. We clearly see stable thermal topological phases in large regions of the phase diagram where the topological invariant remains quantized and critical temperatures where the system jumps onto a trivial phase with zero value for the topological Uhlmann number.

In order to apply our newly developed topological invariant [37] to the topological insulator in 2D given by the QWZ model, we have presented a self-contained explanation of the theory of geometric phases in quantum mixed states represented by density matrices and how they may account for new topological effects under certain conditions. Thus, we have introduced the main concepts and results of the Uhlmann geometric theory. We have used the Uhlmann geometric phase as a tool to characterize SPT systems such as topological insulators and superconductors at finite

temperature. The Uhlmann phase acquires a topological character in these situations, remaining quantized even for a finite range of temperatures. In fact, when computed for a thermal state of generic two-band models in 1D, the complicated expression of the Uhlmann phase simplifies significantly and can be related to the winding number of the Hamiltonian and the temperature of the system. It also has a well-defined limit at $T = 0$, tending to the Berry/Zak phase, which makes the theory consistent and dependable.

Moreover, we have presented how this tool can be generalized to 2D systems in a detailed fashion. The topological invariant in this case is the topological Uhlmann number, which generalizes the Chern number for symmetry-protected time-reversal-broken topological insulators and superconductors in 2D. In fact, with these results, we may think of the possibility of extending the current classification of topological insulators and superconductors on several spatial dimensions [86, 87] (also called the 'periodic table'), to the situation of thermal SPT states with fermions using topological Uhlmann numbers.

Let us emphasize that the existence of critical temperatures seems quite natural in the Uhlmann approach. We find that for thermal states, this approach sets on equal footing the temperature and the coupling constants in the original Hamiltonian. Therefore, if there is a critical behavior as a function of tunnelings and/or staggered potentials, then one should obtain a critical behavior with temperature as well. Moreover, since by raising the temperature T, the quantum coherence properties of any state are affected, it is quite natural that the Uhlmann number decreases by warming the system up.

Beyond the scope of this paper is the possible adaptation of the Uhlmann formalism to explore interacting topological phases at finite temperature. They include not only bosonic/spin topological phases but also interacting fermionic SPT phases that have been recently proposed and classified [93–95] based on group cohomology and supercohomology theory, and response field theory corresponding to a non-trivial fiber bundle of the symmetry group [96, 97]. In this regard, the application of topological Uhlmann invariants to more complicated models and higher dimensions may lead to novel thermal topological transitions and new effects.

Acknowledgments

We thank the Spanish MINECO grant FIS2012–33152, FIS2009–10061, CAM research consortium QUITEMAD+S2013/ICE-2801, European Commission PICC: FP7 2007–2013 grant No. 249958, UCM-BS grant GICC-910758, FPU MEC grant and Residencia de Estudiantes.

References

[1] Haldane F D M 1988 *Phys. Rev. Lett.* **61** 2015
[2] Kane C L and Mele E J 2005 *Phys. Rev. Lett.* **95** 226801
[3] Bernevig B A and Zhang S-C 2006 *Phys. Rev. Lett.* **96** 106802
[4] Kane C L and Mele E J 2005 *Phys. Rev. Lett.* **95** 146802
[5] Moore J E and Balents L 2007 *Phys. Rev.* B **75** 121306
[6] Fu L, Kane C L and Mele E J 2007 *Phys. Rev. Lett.* **98** 106803
[7] Hasan M Z and Kane C L 2010 *Rev. Mod. Phys.* **82** 3045
[8] Qi X-L and Zhang S-C 2011 *Rev. Mod. Phys.* **83** 1057
[9] Bernevig B A and Hughes T L 2013 *Topological Insulators and Topological Superconductors* (Princeton, NJ: Princeton University Press)
[10] Kitaev A Y 2001 *Phys.-Usp* **44** 131
[11] Volovik G E 1999 *JETP Lett.* **70** 609
[12] Read N and Green D 2000 *Phys. Rev.* B **61** 10267
[13] Ivanov D A 2001 *Phys. Rev. Lett.* **86** 268
[14] Leinaas J M and Myrheim J 1977 *Nuovo Cimento* B **37** 1
[15] Wilczek F 1982 *Phys. Rev. Lett.* **49** 957
[16] Arovas D P, Schrieffer J R and Wilczek F 1984 *Phys. Rev. Lett.* **53** 772
[17] Nayak C, Simon S H, Stern A, Freedman M and das Sarma S 2008 *Rev. Mod. Phys.* **80** 1083
[18] Bernevig B A, Hughes T L and Zhang S-C 2006 *Science* **314** 1757
[19] König M, Wiedmann S, Brüne C, Roth A, Buhmann H, Molenkamp L W, Qi X-L and Zhang S C 2007 *Science* **318** 766
[20] Vishwanath A and Senthil T 2013 *Phys. Rev.* X **3** 011016
[21] Metlitski M A, Kane C L and Fisher M P A 2013 *Phys. Rev.* B **88** 035131
[22] Senthil T 2014 arXiv: 1405.4015
[23] Ye P and Wen X-G 2014 *Phys. Rev.* B **89** 045127
[24] Liu Z-X, Gu Z-C and Wen X-G 2014 *Phys. Rev. Lett.* **113** 267206
[25] Viyuela O, Rivas A and Martin-Delgado M A 2012 *Phys. Rev.* B **86** 155140
[26] Mazza L, Rizzi M, Lukin M D and Cirac J I 2013 *Phys. Rev.* B **88** 205142
[27] Rivas A, Viyuela O and Martin-Delgado M A 2013 *Phys. Rev.* B **88** 155141
[28] Garate I 2013 *Phys. Rev. Lett.* **110** 046402
[29] Saha K and Garate I 2014 *Phys. Rev.* B **89** 205103
[30] van Nieuwenburg E P L and Huber S D 2014 *Phys. Rev.* B **90** 075141
[31] Bardyn C-E, Baranov M A, Rico E, Imamoglu A, Zoller P and Diehl S 2012 *Phys. Rev. Lett.* **109** 130402
[32] Kraus C V, Diehl S, Zoller P and Baranov M A 2012 *New J. Phys.* **14** 113036
[33] Bardyn C-E, Baranov M A, Kraus C V, Rico E, İmamoğlu A, Zoller P and Diehl S 2013 *New J. Phys.* **15** 085001
[34] Budich J C, Zoller P and Diehl S 2015 *Phys. Rev.* A **91** 042117
[35] Viyuela O, Rivas A and Martin-Delgado M A 2014 *Phys. Rev. Lett.* **112** 130401
[36] Huang Z and Arovas D P 2014 *Phys. Rev. Lett.* **113** 076407
[37] Viyuela O, Rivas A and Martin-Delgado M A 2014 *Phys. Rev. Lett.* **113** 076408
[38] Alicki R, Fannes M and Horodecki M 2009 *J. Phys. A: Math. Theor.* **42** 065303
[39] Nussinov Z and Ortiz G 2009 *Proc. Natl Acad. Sci.* **106** 16944
[40] Hastings M B 2011 *Phys. Rev. Lett.* **107** 210501
[41] Alicki R, Horodecki M, Horodecki P and Horodecki R 2010 *Open Syst. Inf. Dyn.* **17** 1
Bombin H, Chhajlany R W, Horodecki M and Martin-Delgado M A 2013 *New J. Phys.* **15** 055023
[42] Viyuela O, Rivas A and Martin-Delgado M A 2012 *New J. Phys.* **14** 033044
[43] Albert V V and Jiang L 2014 *Phys. Rev.* A **89** 022118
[44] Khoury A Z and Oxman L E 2014 *Phys. Rev.* A **89** 032106
[45] Dauphin A, Müller M and Martin-Delgado M A 2014 *New J. Phys.* **16** 073016
[46] Shen H Z, Wang W and Yi X X 2014 *Sci. Rep.* **4** 6455
[47] Dehghani H, Oka T and Mitra A 2014 *Phys. Rev.* B **90** 195429

[48] Sirker J, Maiti M, Konstantinidis N P and Sedlmayr N 2014 *J. Stat. Mech.* P10032
[49] Ho S-H, Chao S-P, Chou C-H and Lin F-L 2014 *New J. Phys.* **16** 113062
[50] Patrascu A T 2014 arXiv:1411.4475
[51] Yang X-C, Zhang D-W, Xu P, Yu Y and Zhu S-L 2015 *Phys. Rev.* A **91** 022303
[52] Budich J C and Diehl S 2015 *Phys. Rev.* B **91** 165140
[53] Qi X-L, Wu Y-S and Zhang S-C 2006 *Phys. Rev.* B **74** 045125
[54] Qi X-L, Hughes T and Zhang S-C 2008 *Phys. Rev.* B **78** 195424
[55] Berry M V 1984 *Proc. R. Soc.* A **392** 45
[56] Simon B 1983 *Phys. Rev. Lett.* **51** 2167
[57] Shapere A and Wilczek F 1989 *Geometric Phases in Physics* (Singapore: World Scientific)
[58] Thouless D J, Kohmoto M, Nightingale M P and den Nijs M 1982 *Phys. Rev. Lett.* **49** 405
Kohmoto M 1985 *Ann. Phys. NY* **160** 343
Kohmoto M 1989 *Phys. Rev.* B **39** 11943
[59] Hatsugai Y 1997 *J. Phys.: Condens. Matter* **9** 2507
[60] Zak J 1989 *Phys. Rev. Lett.* **62** 2747
[61] Atala M, Aidelsburger M, Barreiro J T, Abanin D, Kitagawa T, Demler E and Bloch I 2013 *Nat. Phys.* **9** 795
[62] Abanin D A, Kitagawa T, Bloch I and Demler E 2013 *Phys. Rev. Lett.* **110** 165304
[63] Grusdt F, Abanin D and Demler E 2014 *Phys. Rev.* A **89** 043621
[64] Tarruell L, Greif D, Uehlinger T, Jotzu G and Esslinger T 2012 *Nature* **483** 302
[65] Jotzu G, Messer M, Desbuquois R, Lebrat M, Uehlinger T, Greif D and Esslinger T 2014 *Nature* **515** 237
[66] Duca L, Li T, Reitter M, Bloch I, Schleier-Smith M and Schneider U 2015 *Science* **347** 288
[67] Aidelsburger M, Lohse M, Schweizer C, Atala M, Barreiro J T, Nascimbène S, Cooper N R, Bloch I and Goldman N 2015 *Nat. Phys.* **11** 162
[68] Schroer M D, Kolodrubetz M H, Kindel W F, Sandberg M, Gao J, Vissers M R, Pappas D P, Polkovnikov A and Lehnert K W 2014 *Phys. Rev. Lett.* **113** 050402
[69] Roushan P *et al* 2014 *Nature* **515** 241
[70] Uhlmann A 1986 *Rep. Math. Phys.* **24** 229
[71] Uhlmann A 1989 *Ann. Phys.* **46** 63
[72] Uhlmann A 1991 *Lett. Math. Phys.* **21** 229
[73] Hübner M 1993 *Phys. Lett.* A **179** 226
[74] Uhlmann A 1995 *Rep. Math. Phys.* **36** 461
[75] Sjöqvist E, Pati A K, Ekert A, Anandan J S, Ericsson M, Oi D K L and Vedral V 2000 *Phys. Rev. Lett.* **85** 2845
[76] Anandan J S, Sjöqvist E, Pati A K, Ekert A, Ericsson M, Oi D K L and Vedral V 2002 *Phys. Rev. Lett.* **89** 268902
[77] Ericsson M, Pati A K, Sjoöqvist E, Brännlund J and Oi D K L 2003 *Phys. Rev. Lett.* **91** 090405
Tidström J and Sjöqvist E 2003 *Phys. Rev.* A **67** 032110
[78] Du J, Zou P, Shi M, Kwek L C, Pan J-W, Oh C H, Ekert A, Oi D K L and Ericsson M 2003 *Phys. Rev. Lett.* **91** 100403
[79] Aberg J, Kult D, Sjöqvist E and Oi D K L 2007 *Phys. Rev.* A **75** 032106
[80] Zhu J, Shi M, Vedral V, Peng X, Suter D and Du J 2011 *EPL* **94** 20007
[81] See for example Nielsen M A and Chuang I L 2000 *Quantum Computation and Quantum Information* (Cambridge: Cambridge University Press)
[82] Galindo A and Martin-Delgado M A 2002 *Rev. Mod. Phys.* **74** 347
[83] Bures D 1969 *Trans. Am. Math. Soc.* **135** 199
[84] Dittmann J and Rudolph G 1992 *J. Geom. Phys.* **10** 93
[85] Nakahara M 2003 *Geometry, Topology and Physics* (Bristol: CRC Press)
[86] Schnyder A P, Ryu S, Furusaki A and Ludwig A W W 2008 *Phys. Rev.* B **78** 195125
[87] Kitaev A 2009 *AIP Conf. Proc.* **1134** 22
[88] Coleman S 1985 *Aspects of Symmetry: Selected Erice Lectures* (Cambridge: Cambridge University Press)
[89] Resta R 1994 *Rev. Mod. Phys.* **66** 899
[90] Xiao D, Chang M-C and Niu Q 2010 *Rev. Mod. Phys.* **82** 1959
[91] Eguchi T, Gilkey P B and Hanson A J 1980 *Phys. Rep.* **66** 213
[92] Liu C-X, Qi X-L, Dai X, Fang Z and Zhang S-C 2008 *Phys. Rev. Lett.* **101** 146802
[93] Gu Z-C and Wen X-G 2009 *Phys. Rev.* B **80** 155131
[94] Chen X, Gu Z-C, Liu Z-X and Wen X-G 2012 *Science* **338** 1604–6
[95] Guand Z-C and Wen X-G 2014 *Phys. Rev.* B **90** 115141
[96] Cheng M and Gu Z-C 2014 *Phys. Rev. Lett.* **112** 141602
[97] Wang J C, Gu Z-C and Wen X-G 2015 *Phys. Rev. Lett.* **114** 031601

A Measurement Protocol for the Topological Uhlmann Phase

O. Viyuela[1], A. Rivas[1], S. Gasparinetti[2], A. Wallraff[2], S. Filipp[3] and M.A. Martin-Delgado[1]
1. Departamento de Física Teórica I, Universidad Complutense, 28040 Madrid, Spain
2. Department of Physics, ETH Zurich, CH-8093 Zurich, Switzerland
3. IBM Research - Zurich, 8803 Rueschlikon, Switzerland

Topological insulators and superconductors at finite temperature can be characterised by the topological Uhlmann phase. However, the direct experimental measurement in condensed matter systems has remained elusive. We explicitly demonstrate that the topological Uhlmann phase can be measured with the help of ancilla states in systems of entangled qubits that simulate a topological insulator. We propose a novel state-independent measurement protocol which does not involve prior knowledge of the system state. With this construction, otherwise unobservable phases carrying topological information about the system become accessible. This enables the measurement of a complete phase diagram including environmental effects. We explicitly consider a realization of our scheme using a circuit of superconducting qubits. This measurement scheme is extendible to interacting particles and topological models with a large number of bands.

PACS numbers: 42.50.Dv,85.25.-j,03.65.Vf

1. Introduction.— The search for topological phases in condensed matter [1–6] has triggered an experimental race to detect and measure topological phenomena in a wide variety of quantum simulation experiments [7–12]. In quantum simulators the phase of the wave function can be accessed directly, opening a whole new way to measure topological properties [7, 9, 13] beyond the realm of traditional condensed matter. These quantum phases are very fragile, but when controlled and mastered, they can produce very powerful computational systems like a quantum computer [14, 15]. The Berry phase [16] is a special instance of quantum phase, one that is purely geometrical [17] and independent of dynamical effects during the time evolution of a quantum system. When it is invariant under deformations of the path traced out by the system during its evolution, it becomes topological. Topological Berry phases have also acquired a great relevance in condensed matter systems. The now very active field of topological insulators (TIs) and superconductors (TSCs) [1] ultimately owes its topological character to Berry phases [18] associated to the special band structure of these exotic materials.

However, when a TI or a TSC is open to an environment that can cause external noise like thermal fluctuations, these quantum phases are very fragile [19–28] and may not even be well-defined. These phases of matter are very relevant since they are based on the Berry phase acquired by a pure state. The fragility problem has been successfully solved for one-dimensional systems [30] and extended to two-dimensions later [31–33]. The key concept behind this theoretical characterisation is the notion of *Uhlmann phase* [34–38], a natural extension of the Berry phase for density matrices.

Although the topological Uhlmann phase is gauge invariant and thus in principle observable, a fundamental question remains: how to measure a topological Uhlmann phase in a physical system? In this work we address this challenge by: 1) proposing a new protocol to measure experimentally this topological phase, and 2) computing the topological phase diagram for qubits with an arbitrary noise parameter r [see Eq. (S1)], described by Hamiltonian (3). To this end, we employ an ancillary system as a part of the measurement apparatus, in such a way that by encoding the temperature (or mixedness) of the system in the entanglement with that ancilla, the Uhlmann phase appears as a relative phase that can be

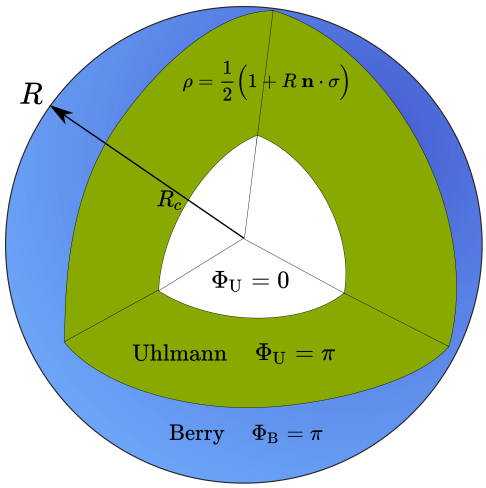

FIG. 1: Topological measures for a single qubit in a mixed state $\rho = (1-r)|1\rangle\langle 1| + r|0\rangle\langle 0| = \frac{1}{2}\left(\mathbb{1} + R\,\mathbf{n}\cdot\sigma\right)$ in the Bloch sphere representation. The mixedness parameter r between states $|1\rangle$ and $|0\rangle$ is encoded into the degree of mixedness $R = |2r-1|$. We compute the Berry Φ_B and Uhlmann Φ_U phases for non-trivial topological regimes. If $r \notin \{1, 0\}$ or equivalently $R < 1$, then only Φ_U is well defined and highlights a non-trivial topological phase ($\Phi_U = \pi$), provided that $R > R_c = |1 - 2r_{c1,c2}|$. Here, R_c denotes the critical amount of noise that the system can withstand while remaining topological.

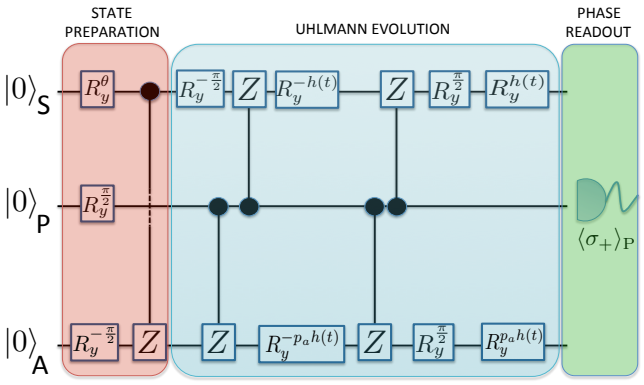

FIG. 2: Circuit diagram to measure the topological Uhlmann phase, e.g., with superconducting circuits as explained in the text. The circuit represents the decomposition of the bi-local unitary evolution $U_S(t) \otimes U_A(t)$ into elementary single and two-qubit gates [42]. The gate R_y^{θ} represents a single qubit rotation about the y-axis for an angle θ, and Z stands for a controlled-phase gate.

determined by interferometric techniques. The difficulty with this type of measurement is that it requires a high level of control, beyond the reach of condensed matter experiments. On the contrary, this situation is specially well-suited for a quantum simulation scenario realised, for example, with superconducting qubits [39–41]. A summary and a comparison with pure state topological measures are shown in Fig 1.

This approach leads naturally to construct a state independent protocol that detects whether a given mixed state is topological in the Uhlmann sense (see Fig. 2). Our proposal also provides a novel quantum simulation of the AIII class [43, 44] of topological insulators (those with chiral symmetry) in the presence of disturbing external noise. Other cases of two-dimensional TIs, TSCs and interacting systems can also be achieved by appropriate modifications mentioned in the conclusions.

2. Topological Uhlmann phase for qubits.— We briefly present the main ideas of the Uhlmann approach for a qubit that simulates two-band models of TIs and TSCs. Let $\theta(t)|_{t=0}^{1}$ define a closed trajectory along a family of single qubit density matrices parametrised by θ,

$$\rho_\theta = (1-r)|1_\theta\rangle\langle 1_\theta| + r|0_\theta\rangle\langle 0_\theta|, \tag{1}$$

where r stands for the mixedness parameter between the θ dependent "ground" state $|1_\theta\rangle$ and the "excited" state $|0_\theta\rangle$, e.g. that of a transmon qubit [45]. Note that ρ_θ can be treated as a pure state $|\Psi_\theta\rangle$ in an enlarged Hilbert space $\mathcal{H} = \mathcal{H}_S \otimes \mathcal{H}_A$, where S stands for system and A for the ancilla degrees of freedom. A second transmon can be used to realise the ancilla. This process is called purification, and satisfies the constraint $\rho_\theta = \mathrm{Tr}_A\Big(|\Psi_\theta\rangle\langle\Psi_\theta|\Big)$, where Tr_A takes the partial trace over the ancilla. The set of purifications $|\Psi_\theta\rangle$ generates the family of density matrices ρ_θ.

The evolution of the purification (system qubit S and ancilla qubit A) can be written as

$$\begin{aligned}|\Psi_{\theta(t)}\rangle = &\sqrt{r}U_S(t)\,|0\rangle_S \otimes U_A(t)\,|0\rangle_A + \\ &+ \sqrt{1-r}U_S(t)\,|1\rangle_S \otimes U_A(t)\,|1\rangle_A\,,\end{aligned} \tag{2}$$

where $|0\rangle = \begin{pmatrix}1\\0\end{pmatrix}$ and $|1\rangle = \begin{pmatrix}0\\1\end{pmatrix}$ is the standard qubit basis, and $U_S(t)$ and $U_A(t)$ are unitary matrices determined by the system Hamiltonian and the Uhlmann parallel transport condition. Namely, parallel transport requires that the distance between two infinitesimally closed purifications $\||\Psi_{\theta(t+dt)}\rangle - |\Psi_{\theta(t)}\rangle\|^2$ reaches a minimum value [34]. Physically, this condition ensures that the outcome quantum phase will be purely geometrical and without dynamical contributions. This is actually a source of robustness, since variations on the transport velocity will not change the resulting phase. To form the state in Eq. (S21), entanglement between two superconducting qubits can be created, for instance, via their common coupling to a microwave cavity [46].

Next, we consider the Hamiltonian of a topological insulator in the AIII chiral-unitary class [43, 44]

$$\begin{aligned}H_\theta &= \frac{G_\theta}{2}\boldsymbol{n}_\theta \cdot \boldsymbol{\sigma},\\ \boldsymbol{n}_\theta &= \frac{2}{G_\theta}(\sin\theta, 0, M+\cos\theta),\\ G_\theta &= 2\sqrt{1+M^2+2M\cos\theta}.\end{aligned} \tag{3}$$

where G_θ stands for the two-level gap, and $\boldsymbol{n}_\theta$ is a unit vector called winding vector [30]. The parameter θ can be varied in time, and it will play the role of the crystalline momentum in topological insulators and superconductors [1]. When invoking the rotating wave approximation this model describes, e.g. the dynamics of a driven transmon qubit [11, 13]. The detuning $\Delta = 2\big(\cos\theta + M\big)$ is parametrised in terms of the crystalline momentum θ and a hopping amplitude M, whereas the coupling strength between the qubit and the incident microwave field is given by $\Omega = 2\sin\theta$.

For pure states in those topological materials ($r \in \{0,1\}$), non-trivial topology can be witnessed by the winding number. This is defined as the angle swept out by $\boldsymbol{n}_\theta$ as θ varies from 0 to 2π, namely,

$$\omega_1 := \frac{1}{2\pi}\oint\left(\frac{\partial_\theta n_\theta^x}{n_\theta^z}\right)d\theta. \tag{4}$$

Then, using Eq. (3) and Eq. (S29), the system is topological ($\omega_1 = 1$) when the hopping amplitude is less than unity ($M < 1$) and trivial ($\omega_1 = 0$) if $M > 1$. In fact, the topological phase diagram coincides with the one given by the Berry phase acquired by the ground state $|1\rangle_\theta$ (or the excited state $|0\rangle_\theta$) of Hamiltonian (3) when θ varies from 0 to 2π, (see Sec. III of the SM [47]).

The computation of the evolutions $U_{\rm S}$ and $U_{\rm A}$ in Eq. (S21) for Hamiltonian (3), yields the following form

$$U_{\rm S}(t) = {\rm e}^{-{\rm i}\int_0^t h(t')dt'\boldsymbol{\sigma}_y}, \quad U_{\rm A}(t) = {\rm e}^{-{\rm i}p_a\int_0^t h(t')dt'\boldsymbol{\sigma}_y}, \quad (5)$$

with $h(t) := \frac{\partial_t n_t^x}{2n_t^z}$. The unitary $U_{\rm S}$ implements the eigenstate transport $|1_\theta\rangle = U_{\rm S}|1\rangle$ and $|0_\theta\rangle = U_{\rm S}|0\rangle$, and $U_{\rm A} = (U_{\rm S})^{p_a}$ with $p_a \in [0,1]$ defined as the ancillary weight. When $p_a = p_r := 2\sqrt{r(1-r)}$, the purification precisely follows Uhlmann parallel transport. For more details, see Sec. I and II of the SM [47].

Now, from Eq. (S21) it is possible to define the relative phase $\Phi_{\rm M}$ between the initial $|\Psi_{\theta(0)}\rangle$ and the final state, i.e. $|\Psi_{\theta(t_{\rm f})}\rangle$. For Hamiltonian (3), density matrix (S1) and purification (S21), we find

$$\begin{aligned}\Phi_{\rm M} &:= \arg\left[\langle\Psi_{\theta(0)}|\Psi_{\theta(t_{\rm f})}\rangle\right] = \quad (6)\\ &= \arg\Big[\cos\left(I_{\rm f}\right)\cos\left(p_a I_{\rm f}\right) + p_r\sin\left(I_{\rm f}\right)\sin\left(p_a I_{\rm f}\right)\Big],\end{aligned}$$

where $I_{\rm f} := \int_0^{t_{\rm f}} h(t')dt'$. In particular, if $p_a = p_r$, the relative phase $\Phi_{\rm M}$ is called the Uhlmann phase $\Phi_{\rm U}$. This phase is a gauge independent quantity [34], defined through the parallel transport of the purification $|\Psi_\theta\rangle$. It also characterises topological order of density matrices [30–33], (see Sec. III of the SM [47]).

For a closed path $t_{\rm f} = 1$, the integral $I_{\rm f} = \pi\omega_1 = \Phi_B$ is precisely the topological Berry phase. In that case the Uhlmann phase simplifies to

$$\Phi_{\rm U} = \arg\{\cos[(1-2p_r)\pi\omega_1]\}. \quad (7)$$

From this, we can deduce the topological properties of these topological materials in the presence of external noise, as measured by the parameter r [Eq. (S1)]. This is depicted in Fig. 1. Namely, if $M > 1$ then $\omega_1 = 0$, and $\Phi_{\rm U} = 0$ for every mixedness parameter r. If $M < 1$ then $\omega_1 = 1$ and hence $\Phi_{\rm U} = \arg[-\cos(2\pi\sqrt{r(1-r)})]$. If the state is pure ($r = 0$), then $\Phi_{\rm U}^0 = \pi$, recovering the same topological phase given by the winding number and the Berry phase. However, for $r \neq 0$ there are critical values of the mixedness r_c at which $p_r = 0.5$, and the Uhlmann phase, according to Eq. (7), jumps from π to zero (see Fig. 1). The first $r_{c1} = \frac{1}{4}(2-\sqrt{3})$ signals the mixedness at which the system loses the topological character of the ground state. Moreover, there exists another $r_{c2} = 1 - r_{c1}$ at which the system becomes topological again due to the topological character of the excited state ($r \to 1$). Actually, $p_r(r = r_c) = 0.5$ implies that whenever the state satisfies $p_r < 0.5$, the system is topological in the Uhlmann sense, as long as $M < 1$. The new reentrance in the topological phase at r_{c2} was absent in previous works [30–32].

3. State-independent protocol.— The application of $U_{\rm S}(t)$ and $U_{\rm A}(t)$ with $p_a = p_r$ to the purification $|\Psi_{\theta(t)}\rangle$ implements the Uhlmann parallel transport and hence $\Phi_{\rm M} = \Phi_{\rm U}$. However, this would imply knowing the mixedness parameter r of the state beforehand, which is not always possible. Hence, we modify the previous protocol to measure the topological Uhlmann phase without prior knowledge of the state ρ and its mixedness parameter r in the following way.

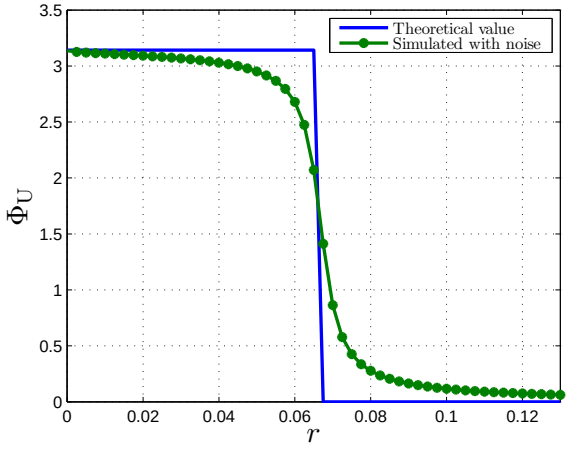

FIG. 3: Comparison between the theoretical value of the Uhlmann phase $\Phi_{\rm U}$ and a realistic noise simulation, as a function of the mixedness r. We have taken into account experimental imperfections such as finite coherence time or residual interactions. The topological transition is clearly appreciable also in the presence of noise. Details can be found in Sec. IV of the SM [47].

Firstly, we assume a linear variation $\theta(t) = v_s t$, fix $v_s = 2\pi$ and consider open holonomies $\frac{1}{2} < t_{\rm f} < 1$ covering more than half of the complete path. No previous knowledge of the state is assumed to perform the evolution. Hence, the ancillary weight p_a might be different than the unknown weight p_r in Eq. (S21), but still satisfying $0 \leq p_a \leq 1$. From Eq. (S24), the overlap $\langle\Psi_{\theta=0}|\Psi_{\theta=2\pi t_{\rm f}}\rangle$ is always real and thus the phase $\Phi_{\rm M}$ has to be 0 or π, depending on both the weight p_r associated to the state ρ_θ [Eq. (S1)] and the ancillary weight p_a.

There is an intuitive reason why we can get topological information out of a phase that is associated to a path that covers more than half of the non-trivial topological loop. Indeed, $h(t)$ is symmetric around $t = \frac{1}{2}$. Then, once we have covered half of the path, we know about the topology of the whole system thanks to this symmetry. Therefore, even an open path for $\frac{1}{2} < t_{\rm f} < 1$ can be considered global.

Using Eq. (S24), we compute the value of p_a^c (where the superindex c stands for critical) at which $\Phi_{\rm M}$ goes abruptly from π to 0 as a function of p_r and $I_{\rm f}$,

$$p_a^c = \frac{-1}{I_{\rm f}}\arctan\Big(\frac{1}{p_r\tan\left(I_{\rm f}\right)}\Big), \quad (8)$$

which is a monotonically decreasing function of p_r.

At this point, we are in position to deduce the topological

properties for the open quantum system without a priori knowledge of its density matrix:
(a) For the trivial case $M > 1$, there is no critical value p_a^c since $\Phi_{\rm M} = 0$ – equivalent to the Uhlmann phase $\Phi_{\rm U}$ – for every p_r and p_a.
(b) For the case $M < 1$ and $\frac{1}{2} < t_{\rm f} < 1$, we compute the critical weight $p_{\rm T} := p_a^c(p_r = 0.5)$ at which $\Phi_{\rm M}$ goes to zero at the topological frontier $p_r = 0.5$. A given state is topological if $p_r < 0.5$, and not topological if $p_r > 0.5$. Therefore, applying the gates $U_{\rm S}$ and $U_{\rm A}$ with $p_a = p_{\rm T}$ may give either

i) $\Phi_{\rm M}(p_{\rm T}) = 0$ implying $p_a^c < p_{\rm T}$ and hence $p_r > 0.5$, as p_a^c always decreases with p_r. Thus, the system is in a trivial phase.

ii) $\Phi_{\rm M}(p_{\rm T}) = \pi$ implying $p_a^c > p_{\rm T}$, thus $p_r < 0.5$. The system is in a non-trivial topological phase.

Therefore we have been able to map the phase $\Phi_{\rm M}(p_{\rm T})$ to the topological Uhlmann phase $\Phi_{\rm U}$. A more detailed explanation is given in Sec. III of the SM [47].

Finally, in order to experimentally measure the Uhlmann phase, we need to include an extra third qubit acting as a probe P. The measurement protocol is described in Fig. 2:

Step 1. Following Eq. (S24), we prepare the initial state $|\Psi_{\theta=0}\rangle \otimes |0\rangle_{\rm P}$ (red block of Fig. 2) using single qubit rotations R_y^θ about the y-axis for an angle θ and a two-qubit entangling gate, e.g. a controlled phase gate for frequency-tunable transmons [48].

Step 2. We apply the bi-local unitary $U_{\rm S}(t) \otimes U_{\rm A}(t)$ on $S \otimes A$ conditional to the state of the probe P. This is accomplished by single qubit rotations about an angle determined by $h(t)$ and p_a (blue block of Fig. 2), and two-qubit controlled-phase gates. As a consequence the 3 qubits $\{{\rm S}, {\rm A}, {\rm P}\}$ are in the superposition

$$|\Phi\rangle_{\rm SAP} = \frac{1}{\sqrt{2}}\big(|\Psi_{\theta=0}\rangle \otimes |0\rangle_P + |\Psi_{\theta=2\pi t_{\rm f}}\rangle \otimes |1\rangle_P\big). \quad (9)$$

Step 3. After the holonomic evolution has been completed, we read out $\Phi_{\rm M}$ from the state of the probe qubit. Tracing out the system and ancilla in Eq. (9), the reduced state for the probe qubit is

$$\rho_{\rm P} = \frac{1}{2}\Big(\mathbb{1} + {\rm Re}(\langle\Psi_{\theta=0}|\Psi_{\theta=2\pi}\rangle)\boldsymbol{\sigma}_x + {\rm Im}(\langle\Psi_{\theta=0}|\Psi_{\theta=2\pi}\rangle)\boldsymbol{\sigma}_y\Big). \quad (10)$$

Thus, by measuring the expectation values $\langle\boldsymbol{\sigma}_x\rangle$ and $\langle\boldsymbol{\sigma}_y\rangle$ (green block of Fig. 2), we can retrieve $\Phi_{\rm M}$ in the form of

$$\begin{aligned}\Phi_{\rm M} &= \arg\left[\langle\boldsymbol{\sigma}_x\rangle + {\rm i}\langle\boldsymbol{\sigma}_y\rangle\right] = \\ &= \arg\left[\langle\Psi_{\theta=0}|U_{\rm S}(t_{\rm f}) \otimes U_{\rm A}(t_{\rm f})|\Psi_{\theta=0}\rangle\right],\end{aligned} \quad (11)$$

Complementary, if we set $p_a = p_r$ we are also able to test the Uhlmann parallel transport condition by measuring $\Phi_{\rm M}$ at each step along the holonomy.

Under realistic experimental conditions, decoherence and dissipation will adversely affect the measured topological Uhlmann phase. We have thus included a realistic noise simulation based on modest assumptions on the coherence of three transmon qubits. With typical gate durations of 25 and 45 ns for single and two-qubit gates, relaxation times of $T_1 \approx 5\mu$s and coherence times of $T_2 \approx 3\mu$s [49], we clearly observe a phase jump of π for the Uhlmann phase as shown in Fig. 3. More details about the simulation are given in the supplementary material [47].

5. Conclusions and Outlook.— We have devised an explicit protocol to perform a realistic measurement of the Uhlmann phase in topological insulators and superconductors implementable in a minimal quantum simulator with 3 superconducting qubits. In particular, we exploit the quantum simulator to realize a controlled coupling of the system to an environment represented by the ancilla degree of freedom. The proposed state-independent protocol allows us to classify states of topological systems according to the Uhlmann measure. Interestingly, some thermodynamical connections to the topological Uhlmann phase have been recently addressed [50].

An increase of experimental resources such us the number of qubits, the speed and fidelity of the quantum gates, etc. would allow us to study novel topological phenomena with superconducting qubits. In particular, by including interactions in the model Hamiltonian we could test different new features: quantum simulations of thermal topological transitions in 2D TIs and TSCs, the interplay between noise and interactions inside a topological phase, etc. These new effects could be achieved since a system with more interacting qubits can be mapped onto models for interacting fermions with spin [12]. Further details can be found in Sec. V of the SM [47]. Although such a proposal would be experimentally more demanding, it represents a clear outlook when the controllability of more qubits and the possibility of performing more gates with high fidelity would be at hand.

M.A.MD., A.R. and O.V. thank the Spanish MINECO grant FIS2012-33152, the CAM research consortium QUITEMAD+ S2013/ICE-2801, the U.S. Army Research Office through grant W911NF-14-1-0103, FPU MEC Grant and Residencia de Estudiantes. S.G., A.W. and S.F. acknowledge support by the Swiss National Science Foundation (SNF, Project 150046).

[1] M. Z. Hasan and C. L. Kane, Rev. Mod. Phys. **82**, 3045 (2010); X.-L. Qi and S.-C. Zhang, Rev. Mod. Phys. **83**, 1057 (2011); B. A. Bernevig and T. L. Hughes, *Topological Insulators and Topological Superconductors* (Princeton University Press, New Jersey, 2013); *and references therein*

[2] B. A. Bernevig, T. L. Hughes, S-C Zhang, Science **314**, 5806 1757-1761 (2006).

[3] M. Koenig et al. Science **318**, 5851 766-770 (2007).
[4] T. H. Hsieh, H. Lin, J. Liu, W. Duan, A. Bansil and L. Fu, Nature Communications **3**, 982 (2012).
[5] P. Dziawa et al. Nature Materials **11**, 1023-1027 (2012).
[6] S. Xu et al. Science **349**, 6248 613-617 (2015).
[7] M. Atala, M. Aidelsburger, J. T. Barreiro, D. Abanin, T. Kitagawa, E. Demler and I. Bloch, Nat. Phys. **9**, 795 (2013).
[8] G. Jotzu, M. Messer, R. Desbuquois, M. Lebrat, T. Uehlinger, D. Greif, T. Esslinger, Nature **515**, 237-240 (2014)
[9] L. Duca, T. Li, M. Reitter, I. Bloch, M. Schleier-Smith, U. Schneider, Science **347**, 288 (2015).
[10] T. Li, L. Duca, M. Reitter, F. Grusdt, E. Demler, M. Endres, M. Schleier-Smith, I. Bloch, U. Schneider, Science **352**, 1094 (2016).
[11] M. D. Schroer et al. Phys. Rev. Lett. **113**, 050402 (2014).
[12] P. Roushan et al. Nature **515**, 241–244 (2014).
[13] P. J. Leek et al. Science **318** 5858 1889-1892 (2007).
[14] M. A. Nielsen and I. L. Chuang, *Quantum Computation and Quantum Information* (Cambridge University Press, Cambridge, 2000).
[15] A. Galindo and M.A. Martin-Delgado, Rev. Mod. Phys. **74** 347-423, (2002).
[16] M. V. Berry, Proc. R. Soc. A **392**, 45 (1984).
[17] A. Shapere and F. Wilczek, *Geometric Phases in Physics* (World Scientific, Singapore, 1989).
[18] J. Zak, Phys. Rev. Lett. **62**, 2747 (1989).
[19] O. Viyuela, A. Rivas and M. A. Martin-Delgado, Phys. Rev. B **86**, 155140 (2012).
[20] A. Rivas, O. Viyuela and M. A. Martin-Delgado, Phys. Rev. B **88**, 155141 (2013).
[21] L. Mazza, M. Rizzi, M. D. Lukin and J. I. Cirac, Phys. Rev. B **88**, 205142 (2013).
[22] C.-E. Bardyn, M. A. Baranov, C. V. Kraus, E. Rico, A. Imamoglu, P. Zoller, S. Diehl, New J. Phys. **15** (2013).
[23] E. P. L. van Nieuwenburg and S. D. Huber, Phys. Rev. B **90**, 075141 (2014).
[24] H. Z. Shen, W. Wang, X. X. Yi, Scientific Reports **4**, 6455 (2014).
[25] H. Dehghani, T. Oka, and A. Mitra, Phys. Rev. B **90**, 195429 (2014).
[26] Y. Hu, Z. Cai, M. Baranov, and P. Zoller, Phys. Rev. B **92**, 165118 (2015).
[27] D. Linzner, F. Grusdt, M. Fleischhauer, arXiv: 1605.00756 (2016).
[28] P. W. Claeys, S. De Baerdemacker, and D. Van Neck, Phys. Rev. B **93**, 220503(R) (2016).
[29] F. Lemini, D. Rossini, R. Fazio, S. Diehl, and L. Mazza, Phys. Rev. B **93**, 115113 (2016).
[30] O. Viyuela, A. Rivas and M. A. Martin-Delgado, Phys. Rev. Lett **112**, 130401 (2014).
[31] O. Viyuela, A. Rivas and M. A. Martin-Delgado, Phys. Rev. Lett **113**, 076408 (2014).
[32] Z. Huang and D. P. Arovas, Phys. Rev. Lett. **113**, 076407 (2014).
[33] O. Viyuela, A. Rivas and M. A. Martin-Delgado, 2D Mater. **2** 034006 (2015).
[34] A. Uhlmann, Rep. Math. Phys. **24**, 229 (1986).
[35] E. Sjöqvist, A. K. Pati, A. Ekert, J. S. Anandan, M. Ericsson, D. K. L. Oi and V. Vedral, Phys. Rev. Lett. **85**, 2845 (2000).
[36] M. Ericsson, A. K. Pati, E. Sjöqvist, J. Brännlund and D. K. L. Oi, Phys. Rev. Lett. **91**, 090405 (2003).
[37] J. Åberg, D. Kult, E. Sjöqvist, and D. K. L. Oi, Phys. Rev. A **75**, 032106 (2007).
[38] J. Zhu, M. Shi, V. Vedral, X. Peng, D. Suter and J. Du, EPL **94** 20007 (2011).
[39] R. J. Schoelkopf and S. M. Girvin, Nature, **451**, 664-669 (2008).
[40] R. Barends *et al*, Nature communications, **6**, 7654 (2015).
[41] Y. Salathé, M. Mondal, M. Oppliger, J. Heinsoo, P. Kurpiers, A. Potocnik, A. Mezzacapo, U. Las Heras, L. Lamata, E. Solano, S. Filipp, and A. Wallraff, Phys. Rev. X, **5**, 021027 (2015).
[42] A. Galindo and M.A. Martin-Delgado, Rev. Mod. Phys. **74** 347-423, (2002).
[43] A. P. Schnyder, S. Ryu, A. Furusaki and A. W. W. Ludwig, Phys. Rev. B **78**, 195125 (2008).
[44] A. Kitaev, AIP Conf. Proc. **1134**, 22 (2009).
[45] J. Koch, T. M. Yu, J. Gambetta, A. A. Houck, D. I. Schuster, J. Majer, A. Blais, M. H. Devoret, S. M. Girvin, and R. J. Schoelkopf, Phys. Rev. A **76**, 042319 (2007).
[46] A. Blais, J. Gambetta, A. Wallraff, D. I. Schuster, S. M. Girvin, M. H. Devoret, and R. J. Schoelkopf, Phys. Rev. A **75**, 032329 (2007).
[47] Supplementary Material.
[48] F. W. Strauch, P. R. Johnson, A. J. Dragt, C. J. Lobb, J. R. Anderson, and F. C. Wellstood, Phys. Rev. Lett. **91**, 167005 (2003).
[49] L. Steffen *et al*. Nature, **500**, 319 (2013).
[50] S.N. Kempkes, A. Quelle, C. Morais Smith, arXiv: 1607.03373 (2016).

SUPPLEMENTARY MATERIAL

I. Uhlmann phase for qubit systems

The Uhlmann phase extends the notion of the geometric Berry phase from pure quantum states (Berry) to mixed quantum states described by density matrices. Uhlmann was first to study this problem from a rigorous mathematical perspective [1] and to find a satisfactory solution [2–5].

Let $\theta(t)|_{t=0}^{1}$ define a trajectory along a family of single qubit density matrices parametrised by θ,

$$\rho_\theta = (1-r)|1_\theta\rangle\langle 1_\theta| + r|0_\theta\rangle\langle 0_\theta|, \tag{S1}$$

where r stands for the degree of mixedness between the ground state $|1_\theta\rangle$ and the excited state $|0_\theta\rangle$. Note that ρ_θ can always be viewed as a pure state $|\Psi_\theta\rangle$ in an enlarged Hilbert space $\mathcal{H} = \mathcal{H}_{\rm S}\otimes\mathcal{H}_{\rm A}$, where S stands for system and A for the ancilla degrees of freedom. This process is called purification, and satisfies the constraint $\rho_\theta = {\rm Tr}_{\rm A}\Big(|\Psi_\theta\rangle\langle\Psi_\theta|\Big)$. The set of purifications $|\Psi_\theta\rangle$ generates the family of density matrices ρ_θ. This aims to be the density-matrix analog to the standard situation where vector states $|\psi\rangle$ span a Hilbert space and generate pure states by the relation $\rho = |\psi\rangle\langle\psi|$. Actually, the phase freedom of pure states, U(1)-gauge freedom, is generalised to a U(n)-gauge freedom (n is the dimension of the density matrix). This occurs since $|\Psi_\theta\rangle$ and $V_{\rm A}^{\rm t}|\Psi_\theta\rangle$ are purifications of the same density matrix for some unitary operator $V_{\rm A}^{\rm t}$ acting on the ancilla degrees of freedom. The superindex t denotes the transposition with respect to the standard qubit basis. If the trajectory defined by $\theta(t)$ is closed $\rho_{\theta(1)} = \rho_{\theta(0)}$, the initial and final purifications must differ just in some unitary transformation $V_{\rm A}^{\rm t}$, $|\Psi_{\theta(1)}\rangle = V_{\rm A}^{\rm t}|\Psi_{\theta(0)}\rangle$. Hence, by analogy to the pure state case, Uhlmann defines a parallel transport condition such that $V_{\rm A}$ is constructed by imposing that the distance between two infinitesimally closed purifications, $\|\Psi_{\theta(t+dt)}\rangle - |\Psi_{\theta(t)}\rangle\|^2$, reaches its minimum value. Then it is possible to write

$$V_{\rm A} = \mathcal{P}{\rm e}^{\int A_{\rm U}}, \tag{S2}$$

where $\mathcal{P}$ stands for the path ordering operator along the trajectory $\theta(t)|_{t=0}^{1}$, and $A_{\rm U}$ is the so-called Uhlmann connection form [1, 6, 7].

The Uhlmann geometric phase is defined from the mismatch between the initial point $|\Psi_{\theta(0)}\rangle$ and the final point after the parallel transportation, i.e. $|\Psi_{\theta(1)}\rangle$,

$$\Phi_{\rm U} := \arg\left[\langle\Psi_{\theta=0}|\Psi_{\theta=1}\rangle\right] = \arg{\rm Tr}\left[\rho_{\theta(0)}V_{\rm A}\right] \tag{S3}$$

This phase is a gauge independent quantity [1–3], that comes from the parallel transport of the purification $|\Psi_\theta\rangle$. The most explicit formula for the Uhlmann connection was given by Hübner [4],

$$A_{\rm U} = \sum_{\theta,i,j}|\psi_\theta^i\rangle\frac{\langle\psi_\theta^i|\left[(\partial_\theta\sqrt{\rho_\theta}),\sqrt{\rho_\theta}\right]|\psi_\theta^j\rangle}{p_\theta^i+p_\theta^j}\langle\psi_\theta^j|d\theta, \tag{S4}$$

in the spectral basis of $\rho_\theta = \sum_j p_\theta^j|\psi_\theta^j\rangle\langle\psi_\theta^j|$. The parameter θ may play the role of the crystalline momentum in condensed matter systems.

The derivative of the square-root of the density matrix with respect to the transport parameter θ is given by

$$\begin{aligned}\partial_\theta\sqrt{\rho_\theta} &= \sqrt{(1-r)}\big(|\partial_\theta 1_\theta\rangle\langle 1_\theta| + |1_\theta\rangle\langle\partial_\theta 1_\theta|\big) + \\ &+ \sqrt{r}\big(|\partial_\theta 0_\theta\rangle\langle 0_\theta| + |0_\theta\rangle\langle\partial_\theta 0_\theta|\big).\end{aligned} \tag{S5}$$

We can simplify the connection $A_{\rm U}$ in (S4), for density matrix (S1) and Hamiltonian (3) in the main text. We substitute Eq. (S5) in Eq. (S4), and take into account that the summation indices in Eq. (S4) only runs over the states $|1_\theta\rangle$ and $|0_\theta\rangle$, obtaining

$$\begin{aligned}A_{\rm U} = \Big[&(1-p_r)\langle 1|\partial_\theta 0_\theta\rangle\ |0_\theta\rangle\langle 1_\theta| \\ &+ (1-p_r)\langle 0_\theta|\partial_\theta 1_\theta\rangle\ |0_\theta\rangle\langle 1_\theta|\Big]d\theta,\end{aligned} \tag{S6}$$

where $p_r = 2\sqrt{r(1-r)}$.

For computational purposes, we fix the gauge for the eigenstates of the system Hamiltonian [Eq. (3) of the main text] such that,

$$|0_\theta\rangle = \frac{1}{\sqrt{1+g^2(\theta,M)}}\begin{pmatrix}1\\ g(\theta,M)\end{pmatrix}, \tag{S7}$$

$$|1_\theta\rangle = \frac{1}{\sqrt{1+g^2(\theta,M)}}\begin{pmatrix}g(\theta,M)\\ -1\end{pmatrix}, \tag{S8}$$

where

$$g(\theta,M) := \frac{\sin\theta}{M+\cos\theta+\sqrt{1+M^2+2M\cos\theta}}. \tag{S9}$$

From Eq. (S7) and Eq. (S8), we compute

$$\begin{aligned}\langle 0_\theta|\partial_\theta 1_\theta\rangle = \frac{\partial_\theta n_\theta^x}{2n_\theta^z} &= \frac{1+M\cos\theta}{2+2M^2+4M\cos\theta}, \\ |0_\theta\rangle\langle 1_\theta| - |1_\theta\rangle\langle 0_\theta| &= \begin{pmatrix}0 & -1\\ 1 & 0\end{pmatrix},\end{aligned} \tag{S10}$$

where n_θ^i is the $i-$th component of the winding vector. Finally, we insert Eqs. (S10) in Eq. (S6) and obtain

$$A_{\rm U} = -{\rm i}(1-p_r)\frac{\partial_\theta n_\theta^x}{2n_\theta^z}\boldsymbol{\sigma}_y d\theta. \tag{S11}$$

As the connection in Eq. (S11) commutes for different values of θ, we can drop the path ordering that appears

in the expression for the Uhlmann unitary [Eq. (S2)], and get the simplified equation

$$V_{\rm A}(\theta) = {\rm e}^{-{\rm i}(1-p_r)\int_0^\theta \frac{\partial_{\theta'} n^x_{\theta'}}{2n^z_{\theta'}}\boldsymbol{\sigma}_y d\theta'}. \tag{S12}$$

Lastly, we substitute Eq. (S12) and Eq. (S1) in Eq. (S3) to compute the Uhlmann phase

$$\Phi_{\rm U} = \arg\left\{\cos\left[\frac{1-2p_r}{2}\int_0^\theta\left(\frac{\partial_{\theta'} n^x_{\theta'}}{n^z_{\theta'}}\right)d\theta'\right]\right\}. \tag{S13}$$

II. Holonomic time evolution

At this stage, we would like to physically implement the holonomy that has been mathematically described in the previous section. For that purpose, we express the parallel transport generated by parameter θ, as a unitary time evolution over system and ancilla $U_{\rm S}\otimes U_{\rm A}$ where the control-parameter is varied in time $\theta(t)$. The system unitary evolution $U_{\rm S}$ is defined through the relations

$$|0\rangle_{\theta(t)} := U_{\rm S}(t)|0\rangle, \quad |1\rangle_{\theta(t)} := U_{\rm S}(t)|1\rangle, \tag{S14}$$

where $|0\rangle = \begin{pmatrix}1\\0\end{pmatrix}$ and $|1\rangle = \begin{pmatrix}0\\1\end{pmatrix}$ is the standard qubit basis. Using the eigenstate equations (S7) and (S8), $U_{\rm S}(\theta)$ is obtained straightforwardly,

$$U_{\rm S}(t) = \frac{1}{\sqrt{1+g^2[\theta(t),M]}}\begin{pmatrix}1 & -g[\theta(t),M]\\ g[\theta(t),M] & 1\end{pmatrix}, \tag{S15}$$

where $g(\theta,M)$ was defined in Eq. (S9).

At this point Eq. (S15) can be expressed as the exponential of a Hamiltonian using the following relations

$$U_{\rm S}(t) \;=\; {\rm e}^{-{\rm i}\int_0^t h(t')dt'}, \tag{S16}$$

$$h(t) \;=\; {\rm i}\left(\frac{d\theta}{dt}\right)\big[\partial_\theta U_{\rm S}(\theta)\big]U^\dagger_{\rm S}(\theta). \tag{S17}$$

We substitute Eq. (S15) into Eq. (S17), arriving at

$$h(t) = \left(\frac{d\theta}{dt}\right)\frac{\partial_{\theta(t)} n^x_{\theta(t)}}{2n^z_{\theta(t)}}\boldsymbol{\sigma}_y, \tag{S18}$$

where we have used Eq. (S10) as well.

The unitary for the ancilla qubit $U_{\rm A}$ is determined by combining: 1) the transport of the eigenstates $|0(1)_\theta\rangle$ through $U_{\rm S}(t)$ and 2) the Uhlmann correction $V_{\rm A}[\theta(t)]$, for the purification as a whole to be parallely transported [Eq. (S12)]; hence,

$$U_{\rm A}(t) = [U^\dagger_{\rm S}(t)V_U(t)]^{\rm t}. \tag{S19}$$

Here, the superindex t denotes the transposition with respect to the standard qubit basis. Further simplifications of Eq. (S19) using Eq. (S18) and Eq. (S12) lead to

$$U_{\rm A}(t) = {\rm e}^{-{\rm i}p_a\int_0^t h(t')dt'}, \tag{S20}$$

with $p_a = p_r$.

III. State-independent phase mapping to the Uhlmann phase

Let us know consider open holonomies [open trajectories given by $\theta(t)$] with the following constraints:

1. We fix a linear ramp $\theta(t) = v_s t$ and units $v_s = 2\pi$.
2. We consider holonomic open paths satisfying $\frac{1}{2} < t_{\rm f} < 1$.
3. Although the Uhlmann parallel transport condition implies $p_a = p_r$, let us consider a more general evolution for the ancilla qubit $p_a \neq p_r$. The ancilla weight p_a can be different than p_r, but still satisfying $0 \leq p_a \leq 1$.

The evolution of the purification (system qubit S and ancilla qubit A) can be written as

$$\begin{aligned}|\Psi_{\theta(t)}\rangle = \sqrt{r}U_{\rm S}(t)\,|0\rangle_{\rm S}\otimes U_{\rm A}(t)\,|0\rangle_{\rm A} + \\ + \sqrt{1-r}U_{\rm S}(t)\,|1\rangle_{\rm S}\otimes U_{\rm A}(t)\,|1\rangle_{\rm A}\,,\end{aligned} \tag{S21}$$

where $U_{\rm S}(t)$ and $U_{\rm A}(t)$ were given in Eq. (S17) and Eq. (S20) respectively.

To shorten the notation, we define $I_{\rm f} := \int_0^{t_{\rm f}} h(t')dt'$ and perform the integration for Hamiltonian (3) in the main text,

$$\begin{aligned}I_{\rm f} = \;& \frac{1}{4}\Big\{t_{\rm f} + 2\arctan\left[\frac{(1+M)\cot(t_{\rm f}/2)}{M-1}\right] + \\ & + \pi{\rm sgn}(1-M)\Big\}, \quad \text{if} \;\; 0 < t_{\rm f} < 1.\end{aligned} \tag{S22}$$

Now we compute the state $|\Psi_{\theta(t_{\rm f})}\rangle$ at the end of the holonomy

$$\begin{aligned}|\Psi_{\theta(t_{\rm f})}\rangle \;=\; & \sqrt{r}\Big(\cos(I_{\rm f})\,|0\rangle_{\rm S} - \sin(I_{\rm f})\,|1\rangle_{\rm S}\Big)\otimes \\ & \otimes\;\Big(\cos(p_a I_{\rm f})\,|0\rangle_{\rm A} - \sin(p_a I_{\rm f})\,|1\rangle_{\rm A}\Big) + \\ & +\;\sqrt{1-r}\Big(\sin(I_{\rm f})\,|0\rangle_{\rm S} + \cos(I_{\rm f})\,|1\rangle_{\rm S}\Big)\otimes \\ & \otimes\;\Big(\sin(p_a I_{\rm f})\,|0\rangle_{\rm A} + \cos(p_a I_{\rm f})\,|1\rangle_{\rm A}\Big) = \\ & =\;\sqrt{r}\Big(\cos(I_{\rm f})\cos(p_a I_{\rm f})\,|0\rangle_{\rm S}\otimes|0\rangle_{\rm A} + \\ & +\;\sin(I_{\rm f})\sin(p_a I_{\rm f})\,|1\rangle_{\rm S}\otimes|1\rangle_{\rm A} - \\ & -\;\sin(I_{\rm f})\cos(p_a I_{\rm f})\,|1\rangle_{\rm S}\otimes|0\rangle_{\rm A} - \\ & -\;\cos(I_{\rm f})\sin(p_a I_{\rm f})\,|0\rangle_{\rm S}\otimes|1\rangle_{\rm A}\Big) + \\ & +\;\sqrt{1-r}\Big(\sin(I_{\rm f})\sin(p_a I_{\rm f})\,|0\rangle_{\rm S}\otimes|0\rangle_{\rm A} + \\ & +\;\cos(I_{\rm f})\cos(p_a I_{\rm f})\,|1\rangle_{\rm S}\otimes|1\rangle_{\rm A} + \\ & +\;\cos(I_{\rm f})\sin(p_a I_{\rm f})\,|1\rangle_{\rm S}\otimes|0\rangle_{\rm A} + \\ & +\;\sin(I_{\rm f})\cos(p_a I_{\rm f})\,|0\rangle_{\rm S}\otimes|1\rangle_{\rm A}\Big).\end{aligned} \tag{S23}$$

We can associate a phase mismatch $\Phi_{\rm M}$ between the initial $|\Psi_{\theta(0)}\rangle$ and the final state, i.e. $|\Psi_{\theta(t_{\rm f})}\rangle$. This is

given by $\Phi_{\rm M} := \arg\left[\langle\Psi_{\theta=0}|\Psi_{\theta=t_{\rm f}}\rangle\right]$. After a straightforward calculation using Eq. (S23),

$$\Phi_{\rm M} = \arg\Big[\cos\left(I_{\rm f}\right)\cos\left(p_a I_{\rm f}\right) + p_r \sin\left(I_{\rm f}\right)\sin\left(p_a I_{\rm f}\right)\Big]. \tag{S24}$$

This phase generally depends both on the weight associated to the state (p_r) and the one applied to the circuit (p_a). Moreover, the overlap $\langle\Psi_{\theta=0}|\Psi_{\theta=t_{\rm f}}\rangle$ is always real and hence the argument gives $\Phi_{\rm M} = 0, \pi$. In addition, for $p_a = p_r$ the phase mismatch $\Phi_{\rm M} = \Phi_{\rm U}$.

Let us now consider an ancillary weight $p_a \neq p_r$. From Eq. (S24) we can find the value $p_a = p_a^c$ (where the superindex c stands for critical) at which $\Phi_{\rm M}$ goes abruptly from π to 0 as a function of p_r and $I_{\rm f}$,

$$p_a^c = \frac{-1}{I_{\rm f}} \arctan\Big(\frac{1}{p_r \tan\left(I_{\rm f}\right)}\Big). \tag{S25}$$

If we set $\frac{1}{2} < t_{\rm f} < 1$, then p_a^c is a monotonically decreasing function of p_r,

$$\frac{\partial p_a^c}{\partial p_r} = \frac{\tan\left(I_{\rm f}\right)}{I_{\rm f}[1 + p_r^2 \tan^2\left(I_{\rm f}\right)]} < 0. \tag{S26}$$

If $M > 1$, then $-\pi/2 < I_{\rm f} < \pi/2$, which from Eq. (S24) implies that $\Phi_{\rm M} = 0$ for any value of p_r and p_a. Hence, for the trivial case $M > 1$, there is no critical value p_a^c and $\Phi_{\rm M} = 0$ always. This maps $\Phi_{\rm M}$ to the Uhlmann phase $\Phi_{\rm U}$ at least for this case. On the contrary, if $M < 1$, then $\pi/2 < I_{\rm f} < \pi$ which implies that $\tan\left(I_{\rm f}\right) < 0$. As $0 < p_r < 1$, then $-\arctan\Big(\frac{1}{p_r \tan\left(I_{\rm f}\right)}\Big) < \pi/2$. Thus, from Eq. (S24), there is always a solution $0 < p_a^c < 1$ for any p_r of the state. As discussed in the main text, the state ρ_θ in Eq. (S1) is topological in the Uhlmann sense $\Phi_{\rm U} = \pi$, only if $M < 1$ and $p_r < 0.5$.

Next, we compute the associated critical value of p_a for the particular case of $p_r = 0.5$, defined as

$$p_{\rm T} := p_a^c(p_r = 0.5) = \frac{-1}{I_{\rm f}} \arctan\Big(\frac{2}{\tan\left(I_{\rm f}\right)}\Big). \tag{S27}$$

Note that the true p_r of the system is unknown as we have assumed no knowledge of the state. But if $p_r > 0.5$, then its associated critical value [from Eq. (S25)] is $p_a^c < p_{\rm T}$. This means that applying $U_{\rm A}$ with $p_a = p_{\rm T}$ and measuring the associated phase $\Phi_{\rm M}$ we can extract the following conclusions:

- If we measure $\Phi_{\rm M}(p_{\rm T}) = 0$, the system is within a trivial phase ($\Phi_{\rm U} = 0$). Because this implies $p_a^c < p_{\rm T}$ and hence $p_r > 0.5$ ($\Phi_{\rm U} = 0$), as we have proven that p_a^c always decreases with p_r.

- If we measure $\Phi_{\rm M}(p_{\rm T}) = \pi$, the system is in a topological phase ($\Phi_{\rm U} = \pi$). Because in that case $p_a^c > p_{\rm T}$ and then $p_r < 0.5$ ($\Phi_{\rm U} = \pi$).

Hence, we have been able to map $\Phi_{\rm M}(p_{\rm T})$ to the Uhlmann phase $\Phi_{\rm U}$. However, this mapping only works iff $\pi/2 < I_{\rm f} < \pi$ which only occurs for $M < 1$ and covering more than half of the path $\frac{1}{2} < t_{\rm f} < 1$. Therefore, in order to test if the system is topological or not, we just have to follow the following protocol:

1. We prepare the initial state $|\Psi_{\theta=0}\rangle \otimes |0\rangle_{\rm P}$. The state $|\Psi_{\theta(t)}\rangle$ is given in Eq. (S21) and P is an extra probe qubit. This qubit is needed to measure the phase $\Phi_{\rm M}$.

2. We set the length of the evolution $t_{\rm f}$ and apply the bi-local unitary $U_{\rm S}(t) \otimes U_{\rm A}(t)$ on $S \otimes A$ conditional to the state of the probe P. The ancilla evolution $U_{\rm A}(t)$ is carried out taking the ancilla weight $p_a = p_{\rm T}$.

3. After the holonomic evolution has been completed, we read out $\Phi_{\rm M}$ from the state of the probe qubit by measuring the argument of the expectation value of $\langle\boldsymbol{\sigma}_x\rangle_{\rm P} + {\rm i}\langle\boldsymbol{\sigma}_y\rangle_{\rm P}$.

Finally, we explain why covering at least half of the entire non-trivial path allows us to access topological information, i.e. global. The Hamiltonian of the single-qubit system Eq. (S28) is the circuit QED analog of a topological insulator in the AIII chiral-unitary class,

$$H_\theta = \frac{G_\theta}{2} \boldsymbol{n}_\theta \cdot \boldsymbol{\sigma}, \tag{S28}$$

where G_θ stands for the two-level gap, and $\boldsymbol{n}_\theta$ is the winding vector. Both quantities have been defined in Eq. (3) of the main text.

For this model, there is a restriction on the movement of of the winding vector $\boldsymbol{n}_\theta$ from the sphere S^2 to the to the circle S^1 on the $xz-$plane. Hence, only two of its components n_θ^x and n_θ^z are different from zero. Therefore, there is a mapping from the family of Hamiltonians H_θ on the parameter $\theta \in S^1$ onto the winding vectors $\boldsymbol{n}_\theta \in S^1$. This mapping $S^1 \longrightarrow S^1$ is characterized by a winding number ω_1. This is a topological invariant defined as the angle swept by $\boldsymbol{n}_\theta$ when the parameter θ is tuned from 0 to 2π,

$$\omega_1 := \frac{1}{2\pi}\oint d\alpha = \frac{1}{2\pi}\oint \Big(\frac{\partial_\theta n_\theta^x}{n_\theta^z}\Big) d\theta, \tag{S29}$$

where we have used that $\alpha := \arctan\left(n_\theta^x / n_\theta^z\right)$. For this model, if the parameter $M < 1$ the system is topological ($\omega_1 = 1$) and if $M > 1$ the system is in trivial phase ($\omega_1 = 0$). The integral $I_{\rm f}$ defined in Eq. (S22) equals the area covered by the winding vector when θ is varied. Actually, if the loop is closed ($t_{\rm f} = 1$), then $I_{\rm f} = \pi\omega_1$. Moreover, $h(t)$ in Eq. (S18) is symmetric around $t = \frac{1}{2}$. So basically when half of the path has been traversed, the information about the whole topology of the system is unveiled. Therefore, an open path that covers more

than half of the non-trivial topological loop ($\frac{1}{2} < t_{\rm f} < 1$) can be considered global and we can get topological information from the phase $\Phi_{\rm M}$.

IV. Noise simulation

We have analyzed the detrimental effect of experimental noise in the proposed measurement scheme. We have modeled this by means of some Liouvillian term $\mathcal{L}_{\rm noise}$, so that the Liouvillian $\mathcal{L}_0$, accounting for the idealized dynamics, is in fact substituted by $\mathcal{L}_0 + \mathcal{L}_{\rm noise}$. Specifically, if some gate is performed during a time τ via some Hamiltonian H_0, i.e. $U_{\rm gate} = e^{-iH_0\tau}$, we substitute

$$e^{-iH_0\tau}\rho e^{iH_0\tau} \equiv e^{\mathcal{L}_0\tau}\rho \to e^{(\mathcal{L}_0+\mathcal{L}_{\rm noise})\tau}\rho. \qquad \text{(S30)}$$

This noise Liouvillian includes typical sources of imperfections: a) some residual ZZ coupling during a C-Phase gate, $H_{\rm ZZ} = J\boldsymbol{\sigma}_z\boldsymbol{\sigma}_z$; b) spontaneous emission and dephasing terms $\mathcal{L}_-(\rho) = \gamma_-(\sigma_-\rho\sigma_+ - \frac{1}{2}\{\sigma_+\sigma_-,\rho\})$ and $\mathcal{L}_z(\rho) = \gamma_z(\boldsymbol{\sigma}_z\rho\boldsymbol{\sigma}_z - \rho)$, respectively.

We have accommodated the values of γ_- and γ_z to the characteristic longitudinal and transverse relaxation times of $T_1 \sim 5$ μs and $T_2 \sim 3$ μs. The residual ZZ strength has been taken to be about $J \sim 0.5$ MHz [8]. In addition, we consider $\tau_{2\pi} \sim 25$ ns and $\tau_{\rm CP} \sim 45$ ns as characteristic times for a 2π-rotation on a single qubit and the C-Phase gate (see Fig. 2 of the main text), respectively. Waiting times of 5 ns after a single qubit gate and 40 ns after a C-Phase gate are also included.

In Fig. 3 of the main text, we show the result of the simulation including noise in the determination of the topological Uhlmann phase $\Phi_{\rm U}$. We plot the value of the measured Uhlmann phase as a function of the purity of the state r for $M < 1$. Despite the noise, the topological transition is clearly noticed.

V. Interacting Systems: New Effects

The protocol to measure the topological Uhlmann phase deals with single-qubit Hamiltonians [Eq. (3) in the main text]. These can be mapped to free-fermion topological insulators. We may identify the ramp parameter θ with the crystalline momentum in the Brillouin zone k.

Nonetheless, more complicated Hamiltonians involving more qubits could be considered in a more general setup. Actually, it has been shown in [9] that an $L-$qubit interacting system can be mapped onto two types of systems that will be discussed in what follows.

On the one hand, a system of 2 qubits can be mapped to a system of two interacting fermions with spin 1/2. Therefore, an Uhlmann experiment for interacting 2-qubit Hamiltonians would be the first experimental measurement of a topological phase associated to an interacting system in a mixed state. It would be very interesting to analyse how the interacting term counteracts or enhance the effect that noise produces in the system.

On the other hand, there is a complementary mapping from a many-body interacting spin system to Haldane-like models [10] with 2^L bands. These are free-fermion models but the fact of having more bands opens the possibility of having higher topological quantum numbers. From the point of view of the Uhlmann theory of symmetry-protected topological order at finite temperature, one can clearly envision the possibility of testing topological transitions between non-trivial topological phases solely driven by noise or temperature. This is an effect that only appears in systems with high topological numbers as shown in [11].

[1] A. Uhlmann, Rep. Math. Phys. **24**, 229 (1986).
[2] A. Uhlmann, Ann. Phys. (Leipzig) **46**, 63 (1989).
[3] A. Uhlmann, Lett. Math. Phys. **21**, 229 (1991).
[4] M. Hübner, Phys. Lett. A **179**, 226 (1993).
[5] A. Uhlmann, J. Geom. Phys. **18**, 76 (1996).
[6] O. Viyuela, A. Rivas and M. A. Martin-Delgado, Phys. Rev. Lett **112**, 130401 (2014).
[7] O. Viyuela, A. Rivas and M. A. Martin-Delgado, 2D Mater. **2** 034006 (2015).
[8] L. Steffen *et al.* Nature, **500**, 319 (2013).
[9] P. Roushan et al. Nature **515**, 241–244 (2014).
[10] F. D. M. Haldane, Phys. Rev. Lett. **61**, 2015 (1988).
[11] O. Viyuela, A. Rivas and M. A. Martin-Delgado, Phys. Rev. Lett **113**, 076408 (2014).

6

Topological Quantum memories at finite temperature

6.1 Motivation

At the end of chapter 1, we have introduced the Kitaev toric code as an example of intrinsic topological order (ITO) displaying a degenerate ground state and quasi-particles with anyonic statistics. This model was originally proposed by Kitaev [Kit03] in the context of **fault-tolerant quantum computation**. Fault-tolerance means that quantum computation can be performed for an arbitrarily long-time, provided that the error rate in the system lies bellow a certain threshold. It turns out that topological systems provide a very natural scheme to support large error rates on the system, due to the intrinsic robustness of topological properties.

In the Kitaev model [Kit03], the information is stored within the degenerate ground state subspace. The Hamiltonian is gapped, which leads to the initial expectation that all type of 'errors', i.e. noise-induced excitations, will be removed automatically by some relaxation processes [NO08]. Moreover, it can be shown that this Hamiltonian is robust under local quantum perturbations at zero temperature [BT09]: there would be a level splitting which will vanish as $\exp(-ak)$, where k is the length of the lattice [Kit03].

Quantum error correction has opened the possibility of correcting errors **actively** on a quantum memory. Outstandingly, small instances of topological quantum codes have been already constructed in the lab. A fully-protected logical qubit has been encoded [NMM+14] on a platform of ion traps, based on the color code [BMD06, BMD07]. A small instance of the surface code [GFG12, FMMC12] has also

been achieved [BKM+14] using superconducting quantum circuits.

An alternative and even more attractive playground goes in the direction of constructing a quantum memory with minimal active support. Actually, **passive protection schemes** lie at the heart of functional classical technology (e.g. transistors, ferromagnetic hard disks, etc). Therefore, one would be interested in designing a **stable quantum memory**, i.e. a $N-$particle system which can support at least a single encoded logical qubit for a long time, preferably with this time growing exponentially with N. Unfortunately, Alicki *et al.* [AFH09] provided a rigorous method showing thermal instability of the 2D Kitaev model. They achieved this by deriving a master equation that describes the dynamics of the system weakly coupled to a thermal environment. Soon after that, the same authors [AHHH10] proved that a 4D version of the toric code is thermally stable below a certain critical temperature T_c. Additionally, no-go theorems for certain types of 2D and 3D topological quantum memories have been proven [BT09, Has11, Yos11], but the question of whether it is possible to find a passively thermally stable topological quantum memory in 2D and 3D remains open [BRWCMD13, BLP+14].

In publication **P1**, we generalise the **Kitaev toric code for qudits** ($d-$dimensional systems) and study the problem of thermal instability within the framework of topological orders. We focus on the novelties we do get by increasing the dimensionality of the spins.

6.2 Outline of the main results

- ✓ We generalise the well-known Kitaev toric code for the case of qudits, i.e. $d-$dimensional spin systems.
- ✓ A Toric code for qudits produces new types of anyonic quasiparticles with different braiding statistics.
- ✓ By increasing the dimension of the logic unit from 2 to d, we enlarge the number of possible topological charges.
- ✓ We derive a master equation that describes the dynamics of a generalised toric code for qudits coupled to an external heat bath.
- ✓ We show that this new system also thermalises, making the system unstable under thermal perturbations.
- ✓ However, we show that a toric code for qutrits can improve the dynamical stability of anyonic quasiparticle.
- ✓ Therefore, increasing the dimensionality of the logic unit may help improve the lifetimes of topological quantum memories.

Generalized toric codes coupled to thermal baths

2012 New J. Phys. 14 033044

(http://iopscience.iop.org/1367-2630/14/3/033044)

New Journal of Physics
The open-access journal for physics

Generalized toric codes coupled to thermal baths

O Viyuela[1], **A Rivas and M A Martin-Delgado**
Departamento de Física Teórica I, Universidad Complutense,
28040 Madrid, Spain
E-mail: oviyuela@fis.ucm.es

New Journal of Physics **14** (2012) 033044 (32pp)
Received 15 December 2011
Published 30 March 2012
Online at http://www.njp.org/
doi:10.1088/1367-2630/14/3/033044

Abstract. We have studied the dynamics of a generalized toric code based on qudits at finite temperature by finding the master equation coupling the code's degrees of freedom to a thermal bath. We find that in the case of qutrits, new types of anyons and thermal processes appear that are forbidden for qubits. These include creation, annihilation and diffusion throughout the system code. It is possible to solve the master equation in a short-time regime and find expressions for the decay rates as a function of the dimension d of the qudits. While we provide an explicit proof that the system relaxes to the Gibbs state for arbitrary qudits, we also prove that above a certain crossover temperature the qutrits' initial decay rate is smaller than the original case for qubits. Surprisingly, this behavior only happens for qutrits and not for other qudits with $d > 3$.

[1] Author to whom any correspondence should be addressed.

Contents

1. Introduction

It is known that the fragility of quantum states in the presence of interaction with an environment represents the main challenge for the large-scale implementation of quantum information devices in quantum computation and communication. Quantum error correction is the theoretical method that was devised to protect a quantum memory or communication channel from external noise [1–8]. In these quantum error correction schemes, to improve the stability of quantum information processing, the logical qubits should be implemented in many-particle systems, typically N physical spins per logical qubit. This is the quantum version of the classical method based on encoding information by repetition or redundancy of logical bits in terms of physical bits [9, 10]. The logical qubits should be stable objects with efficient methods of state preparation, measurements and application of gates. By *efficiency* we mean a certain scaling behavior, e.g. the lifetime of a logical qubit should grow with N.

In order to implement fault-tolerant methods for quantum information processing, we need to find a physical system with good enough properties to accomplish this protection from a noisy environment and decoherence. One promising candidate is topological orders in strongly correlated systems. Here, the ground state is a degenerate manifold of states whose degeneracy depends on the topological properties of a certain lattice of qubits embedded into a surface with nontrivial topology [11]. Many-body interacting terms in a Hamiltonian are responsible for the existence of this topological degeneracy. The logical qubits are stored in global properties of the system represented by nontrivial homological cycles of the surface. In these topological codes,

the property of locality in error detection and correction is of great importance both theoretically and for practical implementations [12–14]. It is also possible to generalize these topological codes for units of quantum information based on multilevel systems known as qudits, i.e. d-level systems [15–18], and study their local stability [19]. An alternative scheme to manipulate topological quantum information is based not in the ground-state properties of the system but in its excitations [11]. These are non-Abelian anyons that can implement universal gates for quantum information [20]. However, being within the framework of topological codes based on ground state properties, it is possible to formulate new surface codes known as topological color codes (TCCs) [21] such that they have enhanced quantum computational capabilities while preserving nice locality properties [21–23]. TCCs in two-dimensional (2D) surfaces allow for the implementation of quantum gates in the whole Clifford group. This makes possible quantum teleportation, distillation of entanglement and dense coding in a fully topological scenario. Moreover, with TCCs in 3D spatial manifolds it is possible to implement the quantum gate $\pi/8$, thereby allowing for universal quantum computation [24, 25]. Very nice applications of topological surface codes can be seen in other fields [26, 27].

Acting externally on topological codes, in order to cure the system from external noise and decoherence, produces benefits from the locality properties of these codes. Namely, a very important figure of merit is the error threshold of the topological code, i.e. the critical value of the external noise below which it is possible to perform quantum operations with arbitrary accuracy and time. For toric codes with qubits, the error threshold is very good, about 11% [12]. This value is obtained by mapping the process of error correction to a classical Ising model on a 2D lattice with random bonds. Interestingly enough, this type of mapping can be made more general and applied to TCCs yielding the same error threshold [28] while maintaining enhanced quantum capabilities [29, 30]. These results have been confirmed using different types of computation methods [31–35]. It is also possible to carry out certain computations by changing the code geometry over time, something called 'code deformation' [12, 36, 37] that allows us to perform quantum computation in a different way. A more general type of code can be constructed with quantum lattice gauge theories based on quantum link models [38].

In this paper, we adopt a different approach than external protection of topological codes. Hence, instead of performing active error correction, we just rely on the robustness of a Hamiltonian that has a gap above the ground state manifold where the quantum information is stored. Thus, we leave the system to interact with the surrounding environment and study the fate of the topological order under these circumstances. This source of noise is inescapable: the microscopic interactions of the physical spins with thermal particles or excitations of the local environment. The analogous situation for classical information processing is well understood, but the existence of a similar mechanism for quantum information is still an open problem. The quantum theory of open systems provides a natural framework for studying stability in the presence of thermal noise. The particularly simple properties of Kitaev's model allow us to apply Davies' theory, namely the dynamics of a quantum system weakly interacting with a heat bath in the Born–Markov approximation [39–46]. There have also been some related studies regarding thermal effects on adiabatic quantum computation [47, 48].

The first indication that the toric code for qubits in 2D spatial dimensions is unstable against thermal noise was shown in [12]. Further analytical and quantitative arguments of thermal instability were given in [49]. Later, a rigorous proof of this fact has been established using the theory of quantum open systems [50, 51]. Subsequently, other investigations have been conducted for Abelian models, non-Abelian models, TCCs [52–56], etc. Remarkably

enough, while with qubits in 2D lattice models the topological protection is lost under the action of thermal fluctuations [57], it is however possible to set up a fully fledged topological quantum computation using certain types of TCCs in higher-dimensional lattices [58]. Under these conditions, it is possible to prove that self-correcting quantum computation, including state preparation, quantum gates and measurement can be carried out in the presence of the disturbing thermal noise. Additionally, note that thermal noise does not always turn out to be detrimental in quantum information, even for systems without topological order [59, 60].

In this work, we extend those results regarding the thermal effects on generalized toric codes constructed out of qudits. Here in we summarize briefly some of our main results.

1. We formulate the dynamics of a generalized toric code based on qudits at finite temperature. To this end, we find the master equation coupling the qudits of the system code to a thermal bath.
2. We study and classify the different types of thermal processes that may occur when the anyonic excitations are created, annihilated or diffused throughout the system. In particular, we find that for qutrits new types of anyons and thermal processes appear that are forbidden for qubits.
3. The master equation is too involved so as to yield an explicit expression for the decay rate of the topological order initially present in the code. However, in a short-time regime it is possible to solve it and find expressions for the decay rates as a function of the dimension d of the qudits. Interestingly enough, we find that the decay rate for qutrits presents a crossover temperature T_c that is absent for any other qudits.
4. We can give an explicit proof that for long enough times, the non-local order parameter representing the topological order in the system decays to zero.

This paper is organized as follows. In section 2, we review the formulation of the master equation of the 2D Kitaev code for qubits in order to establish the notation and the necessary tools to study thermal effects in more general toric codes. We also introduce a non-local order parameter and study the fate of topological orders for two different regimes: the short-time regime and the long-time regime. In section 3, we find the master equation describing topological qutrits coupled to a thermal bath. This allows us to see new energy processes for the anyonic excitations that are not present when the toric code is made up of qubits. Likewise, the short-time regime has a different behavior that can be seen in the initial decay rate of the topological order. In particular, we can define a crossover temperature for qutrits where the decay rate is better than that with other qudits. Section 4 presents the conclusions. See appendix A for the evolution of the order parameter for qutrits and appendix B for a proof of the irreducibility of the computational representation of the d-Pauli group needed to study the master equation in the long-time regime.

2. Thermal stability of the Kitaev two-dimensional (2D) model

We shall not dwell upon the details of Kitaev's toric code [4]; however, we will introduce the basic ideas to understand how to apply a thermal stability analysis to it, as well as to establish the notation and methods. We will consider a $k \times k$ square lattice embedded in a 2-torus. Let us

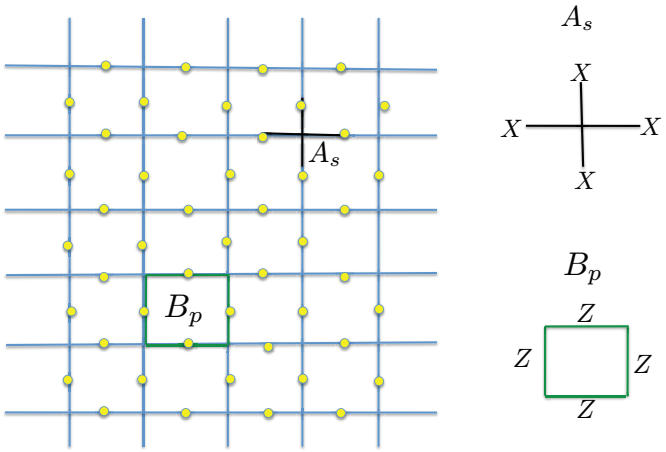

Figure 1. Square lattice on the torus. The yellow points represent qubits.

attach a qubit, such as a spin 1/2, to each edge of the lattice. So we have $N = 2k^2$ qubits. For each vertex s and each face p, we denote the stabilizer operators in the following form:

$$A_s := \prod_{j \in \text{star}(s)} X_j, \quad B_p := \prod_{j \in \text{boundary}(p)} Z_j, \tag{1}$$

where X_j and Z_j are the Pauli matrices applied to the qubit on site j. A_s and B_p commute among each other for they have either 0 or 2 common edges. They are also Hermitian and have eigenvalues 1 and -1 (see figure 1). Therefore, they constitute an Abelian subgroup of the Pauli group of n qubits that is a stabilizer group.

Let $\mathcal{H}$ be the Hilbert space of all $n = 2k^2$ qubits and define the topological quantum code or protected subspace $\mathcal{C} \subseteq \mathcal{H}$ as follows:

$$\mathcal{C} = \left\{ |\Psi\rangle \in \mathcal{H} : \ A_s|\Psi\rangle = |\Psi\rangle, \ B_p|\Psi\rangle = |\Psi\rangle \text{ for all } s, p \right\}. \tag{2}$$

This construction defines a quantum code called the *toric code*. The operators A_s and B_p are the *stabilizer operators* of this code, i.e. operators that leave trivially invariant the code space. As we want to analyze the physical properties of this code, in particular the thermal properties of the topological order, it is convenient to define its associated Hamiltonian in the form

$$H^{\text{sys}} := -\sum_s A_s - \sum_p B_p. \tag{3}$$

Complete diagonalization of this Hamiltonian is possible since operators A_s, B_p commute. In particular, the ground state coincides with the protected subspace of the code $\mathcal{C}$; it is fourfold degenerate (see figure 2). All excited states are separated by an energy gap $\Delta E \geqslant 4$. This is due to the fact that the difference between the eigenvalues of $A_s(B_p)$ is equal to 2. Excitations come in pairs since they correspond to violations of the plaquette and/or vertex stabilizer operators and these must comply with the overall constraints $\prod_s A_s = 1$ and $\prod_p B_p = 1$. Thus, excitations are represented as open strings in the direct or the dual lattice of the original square lattice.

An essential feature of this Hamiltonian is its locality in terms of four-body interactions, very useful for practical purposes. Another key property is that this Hamiltonian model is gapped, which led to the initial expectation that all types of 'errors', i.e. noise-induced excitations, will be removed automatically by some relaxation processes. Of course, this

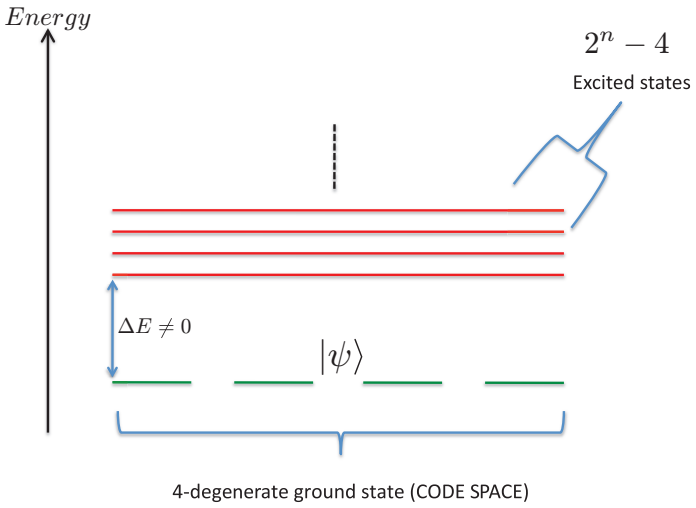

Figure 2. Schematic spectrum of the toric code Hamiltonian. The ground state is the code space $\mathcal{C}$ where we codify our information.

requires cooling, i.e. some coupling to a thermal bath with low temperature (in addition to the Hamiltonian (3)), as we shall describe later on. It can be shown that this Hamiltonian is robust under local quantum perturbations at zero temperature [57]: there would be a level splitting that will vanish as $\exp(-ak)$, where k is the length of the lattice [4].

Due to this unavoidable coupling to a thermal bath, our system is subject to thermal errors as well. These can be seen as violations on the plaquette and vertex conditions $A_s|\Psi\rangle = |\Psi\rangle$, $B_p|\Psi\rangle = |\Psi\rangle$. Moreover, A_s and B_p are unitary, and also Hermitian in the case of qubits. Therefore, violations on the plaquette and/or vertex condition are given by

$$A_s|\Psi\rangle = -|\Psi\rangle, \quad B_p|\Psi\rangle = -|\Psi\rangle, \tag{4}$$

for a certain number of sites s and/or plaquettes p.

These violations cost energy to our system, thereby becoming excitations. As long as they always come in pairs (to satisfy the conditions $\prod_s A_s = 1$ and $\prod_p B_p = 1$), they can be seen (pictorially) as string operators with plaquette or vertex violations at the ends.

Errors on the system can be expressed in terms of operators σ^x, σ^z or products among themselves. These operators act on each edge j where the physical qubits are placed. We use the notation σ^x for a Pauli operator of type X when it refers to an error, i.e. a bump operator acting due to the coupling to the thermal bath. Likewise with σ^z. It is just a matter of notation to distinguish when we have an operator that defines our stabilizer operators in A_s, B_p and when we have an error acting on the system. To see what effect they produce, we will see how the ground state changes by applying these $\sigma^{x,z}$. We will see that this corresponds to the creation, annihilation and movement of a pair of excitations, which from now on we shall refer to as *anyons*. These are called anyons since their wave function picks up a different phase than fermions or bosons when we exchange the end-particles of string operators of x-type with z-type. According to this notation, when we apply a bump operator from the thermal bath, it will

act on the ground state of the system as follows:

$$\sigma_j^z|\Psi\rangle, \tag{5}$$

where $|\Psi\rangle$ is the ground state of the system where our information is encoded. This means that the physical qubit at the edge j has been bumped. The energy cost will be $\Delta E = 4$ in energy units of the system corresponding to the definition of H^{sys}.

As a first step, one is interested in designing a stable quantum memory, i.e. an N-particle system that can support at least a single encoded logical qubit for a long time, preferably with this time growing exponentially with N. This is the notion of stability we shall refer to from now on. In the paper by Alicki *et al* [50], they provide a rigorous method to prove thermal instability of the 2D Kitaev model and obtain a master equation that describes the dynamics of the system weakly coupled to a thermal environment. We will study the problem of thermal instability within the framework of topological orders obtaining complementary and interesting results.

2.1. Davies' formalism

Let us consider a small and finite system that is coupled to one or more heat baths at the same inverse temperature $\beta = (k_{\text{B}}T)^{-1}$, leading to the total Hamiltonian

$$H = H^{\text{sys}} + H^{\text{bath}} + V \quad \text{with} \quad V = \sum_{\alpha} S_\alpha \otimes f_\alpha. \tag{6}$$

Here H^{sys} represents the Hamiltonian of the system where the quantum information is encoded and which we want to protect from the external thermal noise. H^{bath} is the bath Hamiltonian, i.e. it describes the internal dynamics of the bath that is out of our control. Finally, V represents the coupling between the system and the thermal bath. S_α and f_α are operators that act on the system and bath, respectively. Both the coupling operators S_α and f_α are assumed to be Hermitian (without loss of generality [41]).

In the weak-coupling regime that we shall assume throughout this work, the Fourier transform $\hat{g}_\alpha$ of the auto-correlation function of f_α plays an important role, as it describes the rate at which the coupling is able to transfer energy between the bath and the system [39–42]. Often a minimal coupling to the bath is chosen, minimal in the sense that the interaction part of the Hamiltonian is as simple as possible but still addresses all energy levels of the system Hamiltonian in order to have an ergodic reduced dynamics. This last condition is ensured if [41, 43–46]

$$\{S_\alpha, H^{\text{sys}}\}' = \mathbb{C}\mathbb{1}, \tag{7}$$

i.e. no system operator apart from those proportional to the identity commutes with all the S_α and H^{sys}.

The weak-coupling limit [39–42] results in a Markovian evolution for the system given in the Heisenberg picture by the master equation

$$\frac{\mathrm{d}X}{\mathrm{d}t} = \mathcal{G}(X) := \mathrm{i}\delta(X) + \mathcal{L}(X). \tag{8}$$

The generator of the evolution $\mathcal{G}(X)$ is a sum of two terms: the first is a usual Liouville–von Neumann term as in the quantum mechanics of closed systems, while the second

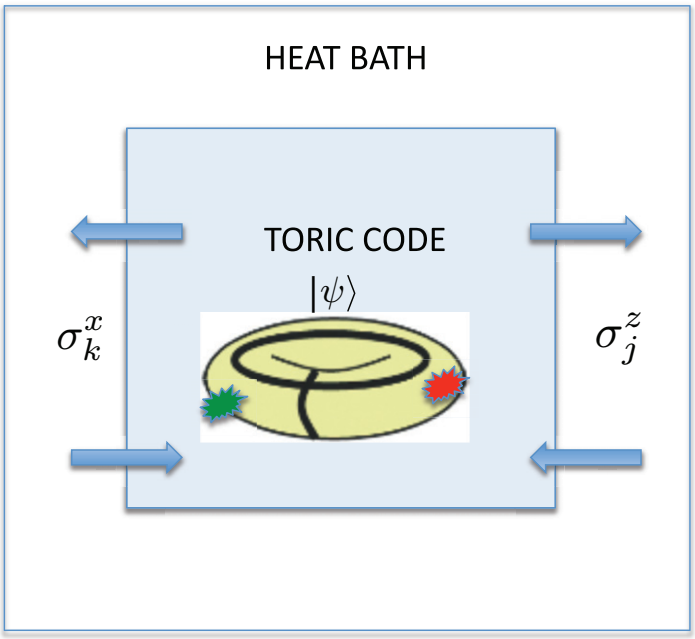

Figure 3. Toric code coupled to a heat bath. Outgoing arrows in the upper part of the figure mean information flowing from the system to the bath, and ingoing arrows in the lower part mean information flowing from the bath to the system.

is a particular type of the Kossakowski–Lindblad generator:

$$\delta(X) = [H^{\mathrm{sys}}, X], \tag{9}$$

$$\mathcal{L}(X) = \sum_{\alpha} \sum_{\omega \geqslant 0} \mathcal{L}_{\alpha\,\omega}(X) \tag{10}$$

$$= \sum_{\alpha} \sum_{\omega \geqslant 0} \hat{g}_{\alpha}(\omega) \left\{ (S_{\alpha}(\omega))^{\dagger} \, [X,\ S_{\alpha}(\omega)] + \left[(S_{\alpha}(\omega))^{\dagger},\ X \right] S_{\alpha}(\omega) \right.$$
$$\left. \mathrm{e}^{-\beta\omega} \, S_{\alpha}(\omega) \, \left[X,\ (S_{\alpha}(\omega))^{\dagger} \right] + \mathrm{e}^{-\beta\omega} \, [S_{\alpha}(\omega),\ X] \, (S_{\alpha}(\omega))^{\dagger} \right\}. \tag{11}$$

Here the $S_{\alpha}(\omega)$ are the Fourier components of S_{α} as it evolves under the system Hamiltonian

$$\mathrm{e}^{\mathrm{i}t H^{\mathrm{sys}}} \, S_{\alpha} \, \mathrm{e}^{-\mathrm{i}t H^{\mathrm{sys}}} = \sum_{\omega} S_{\alpha}(\omega) \, \mathrm{e}^{-\mathrm{i}\omega t}, \tag{12}$$

where the ωs are the Bohr frequencies of the system Hamiltonian ($\hbar\omega = E_1 - E_2$, for two energy levels E_1 and E_2).

In addition, the temperature of the environment appears in (11) through β, and this generator is the so-called Davies' generator [39] or the Born–Markov generator in the quantum optics literature.

2.2. Master equation for the 2D Kitaev model with qubits

Given the simplicity of Kitaev's model, we can apply Davies' theory for studying its stability in the presence of thermal noise. This is represented pictorially in figure 3.

The interaction Hamiltonian is assumed to be local and associated with σ^x and σ^z errors:

$$V = \sum_j \sigma_j^x \otimes f_j^x + \sigma_j^z \otimes f_j^z, \tag{13}$$

where f_j^x and f_j^z are associated with two different baths. Thus, first of all, we need to compute the Fourier transform of the system operators $e^{itH^{sys}}\sigma_j^x e^{-itH^{sys}}$ and $e^{itH^{sys}}\sigma_j^z e^{-itH^{sys}}$ in order to define the dynamical operators of the system. Here $H^{sys} := H_0 = -\sum_s A_s - \sum_p B_p$, with $[A_s, B_p] = 0$, $[A_s, \sigma_j^z] = 0$ and $[B_p, \sigma_j^x] = 0$. Thus, stabilizers A_s only play a role in the Fourier transform of σ_j^x and B_p only in σ_j^z. By computing this Fourier transform, we obtain the dynamical operators of the system due to the coupling to the thermal bath. With $\Delta = 4$ denoting the gap of the Toric code Hamiltonian, then the expressions for these operators $S_\alpha(\omega)$ that appear in equation (11) are as follows [50].

1. Operators associated with σ_j^x errors:

$$\begin{aligned} S_j^x(0) &:= b_j^0 = \sigma_j^x R_j^0, \\ S_j^x(\Delta) &:= b_j = \sigma_j^x R_j^+, \\ S_j^x(-\Delta) &:= b_j^\dagger = \sigma_j^x R_j^-, \end{aligned} \tag{14}$$

   with $R_j^0 := \frac{1}{2}(1 - B_p B_{p'})$ and $R_j^\pm := \frac{1}{4}(1 \mp B_p)(1 \mp B_{p'})$ being orthogonal projectors.
2. Operators associated with σ_j^z errors:

$$S_j^z(0) := a_j^0 = \sigma_j^z P_j^0, \tag{15}$$

$$S_j^z(\Delta) := a_j = \sigma_j^z P_j^+, \tag{16}$$

$$S_j^z(-\Delta) := a_j^\dagger = \sigma_j^z P_j^-$$

   and the projectors: $P_j^0 := \frac{1}{2}(1 - A_s A_{s'})$ and $P_j^\pm := \frac{1}{4}(1 \mp A_s)(1 \mp A_{s'})$.

These operators have a nice interpretation in terms of anyonic properties of the system.

1. $a_j^\dagger (b_j^\dagger)$ creates a pair of anyons of z-type (x-type) on the lattice at position j. See figure 4.
2. $a_j (b_j)$ annihilates a pair of anyons of z-type (x-type) on the lattice at position j. See figure 5.
3. $a_j^0 (b_j^0)$ moves a pair of anyons of z-type (x-type) on the lattice. See figure 6.

Thus, the dissipator of the master equation $\mathcal{L}(X)$ for the system is

$$\begin{aligned} \mathcal{L}(X) &= \mathcal{L}^z(X) + \mathcal{L}^x(X), \\ \mathcal{L}^x(X) &= \sum_j \frac{1}{2} R(4)\{(-b_j^\dagger b_j X - X b_j^\dagger b_j + b_j^\dagger X b_j) + e^{-4\beta}(-b_j b_j^\dagger X - X b_j b_j^\dagger \\ &\quad + b_j X b_j^\dagger\} - \tfrac{1}{2} R(0)[b_j^0, [b_j^0, X]], \\ \mathcal{L}^z(X) &= \sum_j \frac{1}{2} R(4)\{(-a_j^\dagger a_j X - X a_j^\dagger a_j + a_j^\dagger X a_j) + e^{-4\beta}(-a_j a_j^\dagger X - X a_j a_j^\dagger \\ &\quad + a_j X a_j^\dagger\} - \tfrac{1}{2} R(0)[a_j^0, [a_j^0, X]], \end{aligned}$$

where $R(4)$ and $R(0)$ are the exchange rates between the system and the bath associated with each Bohr frequency, namely $\omega = 0, 4$, assuming units of $J = 1$.

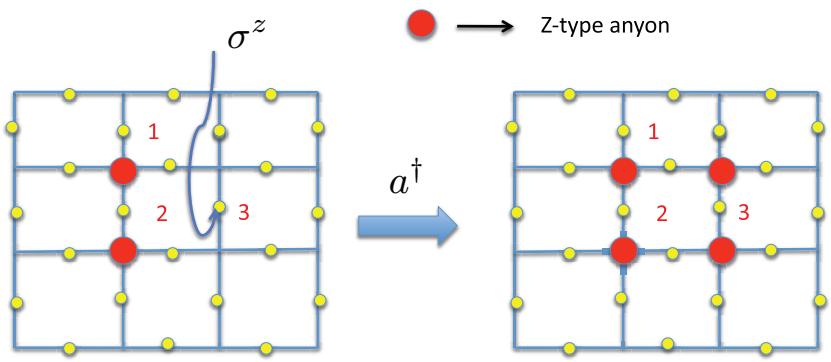

Figure 4. Dynamics induced by the heat bath on the toric code. Creation of a new pair of anyons. Energy increases by $\Delta E = 4$.

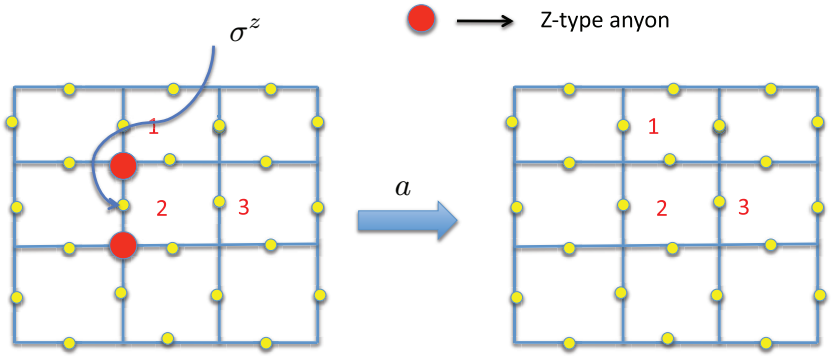

Figure 5. Dynamics induced by the heat bath on the toric code. Annihilation of a pair of anyons. Energy goes down by $\Delta E = 4$.

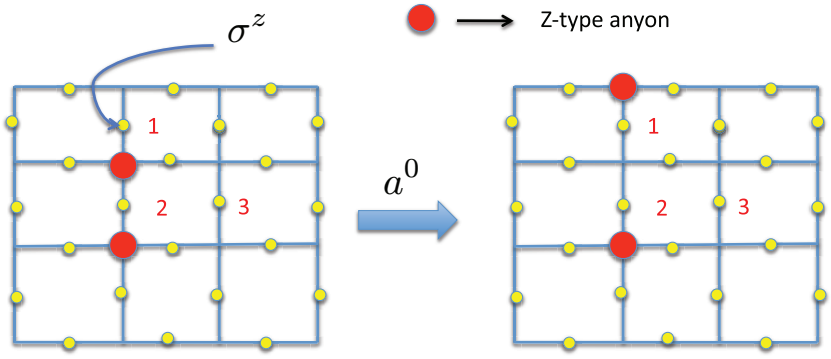

Figure 6. Dynamics induced by the heat bath on the toric code. Pure decoherence by moving an anyon with no energy change.

2.3. Topological order

We shall study the evolution of the expectation value $\langle \mathrm{GS}| X_c |\mathrm{GS}\rangle$ as a simple order parameter, where X_c is the tensor product of σ^x Pauli operators along one non-contractible loop on the surface of the torus and $|\mathrm{GS}\rangle$ denotes a generic ground state of the system Hamiltonian.

This ground state is a superposition of the degenerate states in the ground state manifold of $H^{\rm sys}$, namely $\mathcal{C}$. This gives us a sufficient measure of the topological order of the system [49]. If this quantity falls to zero during the time evolution for every element of $\mathcal{C}$, there is not a global and self-protected way to encode quantum information. The evolution of the operator $X_{\rm c}$ is given by equation (47),

$$\frac{{\rm d}X_{\rm c}(t)}{{\rm d}t} = {\rm i}\delta[X_{\rm c}(t)] + \mathcal{L}[X_{\rm c}(t)].$$

In order to simplify the computation, we remove the free evolution by performing the transformation

$$\tilde{X}_{\rm c}(t) = {\rm e}^{-{\rm i}H^{\rm sys}t} X_{\rm c}(t) {\rm e}^{{\rm i}H^{\rm sys}t}. \tag{17}$$

Since the dissipator is invariant under this transformation, we obtain

$$\frac{{\rm d}\tilde{X}_{\rm c}(t)}{{\rm d}t} = \mathcal{L}[\tilde{X}_{\rm c}(t)]. \tag{18}$$

Interestingly, for the expectation value we obtain $\langle {\rm GS}|\, X_{\rm c}(t)\, |{\rm GS}\rangle = \langle {\rm GS}|\, \tilde{X}_{\rm c}(t)\, |{\rm GS}\rangle$, as $|{\rm GS}\rangle$ is an eigenstate of $H^{\rm sys}$.

Taking into account expressions (14) and (15), the action of the dissipators on $X_{\rm c}$ can be simplified to

$$\mathcal{L}_x(X_{\rm c}) = -\frac{1}{2}\sum_j R(\Delta)\left([R_+^j,[R_+^j,X_{\rm c}]] + {\rm e}^{-\Delta\beta}[R_-^j,[R_-^j,X_{\rm c}]]\right) + R(0)[R_0^j,[R_0^j,X_{\rm c}]] \tag{19}$$

and

$$\begin{aligned}\mathcal{L}_z(X_{\rm c}) = \sum_j & R(\Delta)[P_+^j\sigma_j^z X_{\rm c}\sigma_j^z P_+^j - P_+^j X_{\rm c} + {\rm e}^{-\Delta\beta}(P_-^j\sigma_j^z X_{\rm c}\sigma_j^z P_-^j - P_-^j X_{\rm c})] \\ & + R(0)[P_0^j\sigma_j^z X_{\rm c}\sigma_j^z P_0^j - P_0^j X_{\rm c}],\end{aligned}$$

where we have used the fact that $[P_{\pm,0}^j, X_{\rm c}] = 0$ for every j, as these projectors are only functions of vertex operators. However, the same assertion is not true for $R_{\pm,0}^j$ in general. If $j \notin c$, i.e. j does not belong to the path where $X_{\rm c}$ is acting on, every element commutes with each other and their contribution is zero. On the other hand, if $j \in c$, as $\sigma_j^z\sigma_j^x\sigma_j^z = -\sigma_j^x$, the string operator yields $\sigma_j^z X_{\rm c}\sigma_j^z = -X_{\rm c}$. Therefore, simplifying we obtain

$$\mathcal{L}_z(X_{\rm c}) = -\frac{\Delta}{2}|c|X_{\rm c}\{R(\Delta)[P_+^j + {\rm e}^{-\Delta\beta}P_-^j] + R(0)P_0^j\}, \tag{20}$$

where $|c|$ is the number of points in the path c.

2.4. Short-time regime

The solution to the master equation (18) is formally written as $\tilde{X}_{\rm c}(t) = {\rm e}^{\mathcal{L}(t)}X_{\rm c}$. However, this expression is too involved to be computed analytically except for short and long times to be specified hereby. In the first case, at lowest order we have

$$\tilde{X}_{\rm c}(t) \simeq (1 + t\mathcal{L})X_{\rm c}. \tag{21}$$

The evolution of $\langle \mathrm{GS}|\, X_c(t)\, |\mathrm{GS}\rangle$ is given by

$$\langle \tilde{X}_c(t)\rangle \simeq [1 - 2t|c|R(\Delta)e^{-\Delta\beta}]\langle X_c(0)\rangle. \tag{22}$$

To arrive at this equation, we have used the fact that for all j:

$$\begin{aligned} P^j_{+,0}\,|\mathrm{GS}\rangle &= 0, \\ P^j_{-}\,|\mathrm{GS}\rangle &= |\mathrm{GS}\rangle\,, \\ R^j_{+,0}\,|\mathrm{GS}\rangle &= 0, \\ R^j_{-}\,|\mathrm{GS}\rangle &= |\mathrm{GS}\rangle\,. \end{aligned}$$

Thus, the contribution of $\mathcal{L}_x$ is zero:

$$\begin{aligned} \langle \mathrm{GS}|\, \mathcal{L}_x(X_c)\, |\mathrm{GS}\rangle &= -\frac{1}{2}\sum_j R(\Delta)e^{-\Delta\beta}\, \langle \mathrm{GS}|\, [R^j_-, [R^j_-, X_c]]\, |\mathrm{GS}\rangle \\ &= -\frac{1}{2}\sum_j R(\Delta)e^{-\Delta\beta}\left(\langle \mathrm{GS}|[R^j_-, X_c]|\mathrm{GS}\rangle - \langle \mathrm{GS}|[R^j_-, X_c]|\mathrm{GS}\rangle\right) = 0, \end{aligned} \tag{23}$$

whereas for $\mathcal{L}_z$, we have

$$\mathcal{L}_z(X_c) = -\frac{\Delta}{2}|c|R(\Delta)e^{-\Delta\beta}\, \langle \mathrm{GS}|\, X_c|\mathrm{GS}\rangle. \tag{24}$$

Finally, as $\langle \mathrm{GS}|\, X_c(t)\, |\mathrm{GS}\rangle = \langle \mathrm{GS}|\, \tilde{X}_c(t)\, |\mathrm{GS}\rangle$, the desired equation valid at short times is

$$\langle X_c(t)\rangle \simeq \left[1 - \frac{\Delta}{2}t|c|R(\Delta)e^{-\Delta\beta}\right]\langle X_c(0)\rangle, \tag{25}$$

with $\Delta = 4$.

It is important to remark that $R(0)$ does not appear in the initial decay rate, as long as short times are concerned. The diffusion of anyons is a second-order process in time as it requires first the creation of a pair of anyons with $R(\Delta)$, and later free diffusion with $R(0)$.

2.5. Long-time regime

On the other hand, in order to analyze the thermal properties for long times, we write the Davies generator in the Schrödinger picture through the relation $\mathrm{Tr}[\mathcal{L}^\dagger(\rho)X] = \mathrm{Tr}[\rho\mathcal{L}(X)]$ for any X and ρ. It is a well-known result [39–42] that the Gibbs state is a stationary state for $\mathcal{L}^\dagger$,

$$\mathcal{L}^\dagger(\rho_\beta) = 0, \tag{26}$$

where $\rho_\beta = e^{-\beta H^{\mathrm{sys}}}/Z$, β is the same to the inverse temperature as the surrounding bath, and $Z := \mathrm{Tr}(e^{-\beta H^{\mathrm{sys}}})$ is the system partition function. To guarantee that any initial state of the system relaxes to ρ_β, we can resort to condition (7). In our case this follows from Schur's lemma as $S_\alpha = \sigma^x_j, \sigma^z_j$ and $\{\mathbb{1}, \sigma^x, \sigma^z, \sigma^x\sigma^z\}$ form an irreducible representation of the Pauli group.

Thus $\langle \mathrm{GS}|\, X_c(t)\, |\mathrm{GS}\rangle \simeq \mathrm{Tr}[X_c\rho_\beta]$ for large t, and we have $\mathrm{Tr}[X_c\rho_\beta] = 0$. This is simply due to the fact that ρ_β is diagonal in any of the possible eigenbases of H^{sys}, and it is not difficult to choose one such that X_c vanish on diagonal elements,

$$\mathrm{Tr}[X_c\rho_\beta] = \frac{1}{Z}\sum_i \mathrm{e}^{-\beta\lambda_i}\, \langle\psi_i|\, X_c\, |\psi_i\rangle = 0, \tag{27}$$

for some eigenbases $\{|\psi_i\rangle\}$ of H_0, Kitaev's Hamiltonian.

In conclusion, whatever the initial value of the order parameter $\langle X_c(0)\rangle$, it decays to zero during the time evolution of the system, provided that the temperature is finite. The decay rate at short times is equal to $\frac{\Delta}{2}|c|R(\Delta)\mathrm{e}^{-\Delta\beta}$. Note the detrimental effect of the factor $|c|$: the larger size of the system, the higher the decay rate. In order to keep the order parameter above a certain finite value such that $\langle X_c(0)\rangle \neq 0$, this decay rate must decrease, which is not the case when increasing the system size.

3. The Kitaev 2D model for qudits

In this section, we consider again a 2D toric code, but instead of assuming that we have a two-level system on each site, we will consider that particles arranged on the torus have d accessible levels. We will first derive a general theory for *qudits* and then consider the case $d = 3$ (qutrits). A qutrit can be represented, for instance, as a particle of spin 1 or a three-level system in an atom, etc.

This problem is very interesting since qutrits have certain advantages with respect to qubits.

1. Qutrits have a larger capacity for information storage.
2. Quantum channels are more robust for qutrits. For example, Bell inequalities are proved with more accurate bounds. This is relevant for quantum key distribution.
3. Entanglement quantum distillation is more efficient with qutrits than with qubits [61].
4. Qutrit logic gates [62] are also capable of providing universal quantum computation, i.e. the necessary computational power to construct all possible logic gates [8].

To build a system like that, we will try to choose the Hamiltonian and the operators acting on the system in the same way as before. Previously, for two-level systems, we have considered the Pauli matrix algebra to be the basis of operators in our system. Now, we have to use a proper generalization for dimension d. As $\mathrm{i}XZ = Y$ gives the second Pauli matrix, it is enough to consider X and Z in this generalization to quantum states with d multilevels. However, the generalization of Pauli matrices to dimension d is not unique[2]. Thus, we shall select the most important properties of Pauli matrices of dimension 2 for our purpose of quantum error correction.

In $d = 2$, we defined a basis: $|0\rangle$, $|1\rangle$ in the Fock space of each particle. They are defined as the eingenstates of the Z Pauli matrix. And the X Pauli matrix takes $|0\rangle$ to $|1\rangle$ and vice versa.

$$X = \begin{pmatrix} 0 & 1 \\ 1 & 0 \end{pmatrix}, \quad Z = \begin{pmatrix} 1 & 0 \\ 0 & -1 \end{pmatrix},$$

[2] Indeed, there are different generalizations for the operators X and Z. What makes simple the generalization of the toric code to higher dimensions is to keep the action of X and Z on the computational basis to be analogous to the case of qubits. This implies a specific structure for the anticommutation rule, namely $XZ = \omega ZX$, where ω is a primitive d-root of unity. Note, for instance, that another common generalization of X and Z, based on the generators of the Lie algebra $\mathfrak{su}(d)$, does not fulfill these anticommutation relations.

$$Z|0\rangle = +|0\rangle, \quad Z|1\rangle = -|1\rangle,$$
$$X|0\rangle = +|1\rangle, \quad X|1\rangle = |0\rangle.$$

The key important properties of these matrices for doing error correction are the following.

- They satisfy a cyclic condition (i.e. applying twice Z or X Pauli matrices is the identity), i.e. they are unitary.
- They anticommute, which means $XZ = -ZX$.

Those are the properties that are generalized to the d-dimensional case. Hermiticity is not taken into account as a basic ingredient, as we can always add the Hermitian conjugate obtaining a Hermitian operator, e.g. $\tilde{Z} = Z + Z^{\dagger}$, then $\tilde{Z}$ is Hermitian. Now we consider a basis for the particle Fock space: $|0\rangle, |1\rangle, \ldots, |d-1\rangle$, which will be the eingenvectors of the generalized Z matrix with a certain eingenvalue. We define X as the operator which takes the state $|0\rangle$ to $|1\rangle$, then $|1\rangle$ to $|2\rangle$ and so on. We will also ask for a cyclic condition as in the previous case:

$$X^d = \mathbb{1}, \quad Z^d = \mathbb{1}. \tag{28}$$

All these requirements can be cast on to the following defining relations:

$$Z|0\rangle = +|0\rangle, \quad Z|1\rangle = \omega|1\rangle, \quad \boldsymbol{Z}|2\rangle = \omega^2|2\rangle, \ldots, \quad Z|d-1\rangle = \omega^{d-1}|d-1\rangle;$$
$$X|0\rangle = +|1\rangle, \quad X|1\rangle = |2\rangle, \ldots, \quad X|d-1\rangle = |0\rangle. \tag{29}$$

Looking at equation (29) we can deduce the meaning of operators X and Z. X is the displacement operator in the computational basis (i.e. in the Fock space basis of the physical qudits). Z is the dual operator of X under a discrete Fourier transform. In other words, Z is diagonal in the computational basis and its eingenvalues are the weights of the Fourier transform. Thus, X plays the role of the displacement operator and Z is the dual operator on a system with discrete states of qudits [8].

Due to the cyclic condition (28) of Z ($Z^d = \mathbb{1}$), we have the relation $\omega^d = 1$ where, in general, ω is a complex number. This implies that ω is a primitive d-root of unity,

$$\omega = \mathrm{e}^{\mathrm{i}(2\pi/d)}. \tag{30}$$

Additionally, we can easily verify that $ZX = \omega XZ$, as follows from equation (29).

We have already the algebra of operators that we are going to use in order to built the stabilizer operators on this qudit toric code. The problem is that if we construct the vertex and plaquette operators as before, namely,

$$A_s = \prod_{j \in \mathrm{star}(s)} X_j, \quad B_p = \prod_{j \in \mathrm{boundary}(p)} Z_j, \tag{31}$$

then $[A_s, B_p] \neq 0$ for all s and p. They commute with each other provided that they do not share any common edge, but that is not the case if they share two. This happens because in this case the operators X and Z are no longer Hermitian.

As shown in figure 7, we have

$$[A_s, B_p] = [X_1X_2X_3X_4, Z_3Z_4Z_5Z_6] = (1-\omega^2)A_sB_p, \tag{32}$$

which does no vanish for dimension $d > 2$, $(1-\omega^2) \neq 0$. The case of $d = 2$ is a very special case with $\omega = -1$ and therefore $(1-\omega^2) = 0$. This happens because for $d = 2$, X and Z are

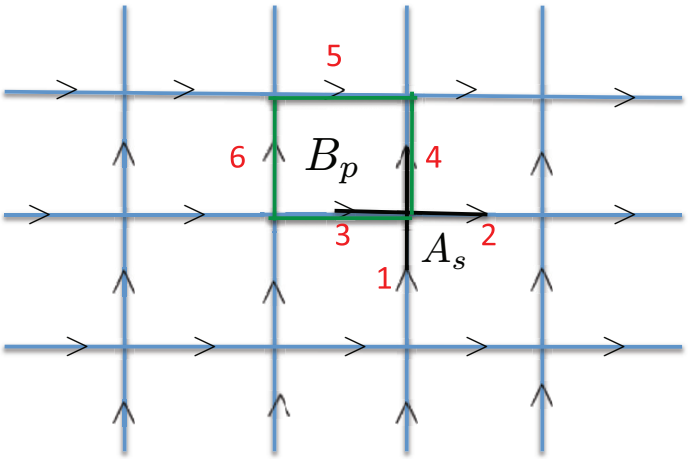

Figure 7. New lattice for qudits showing vertex A_s and plaquette B_p operators: orientation of the lattice is necessary.

Hermitian operators. We need to think of another way to define our operators to have the same commutation rules as before, and this leads to defining an orientation on the lattice. This is shown in figure 7. Defining an orientation on the lattice is a direct consequence of the non-Hermiticity of operators X and Z.

Using the orientation of the lattice, we define the stabilizer operators in the following way. To build the vertex operators A_s we assign an operator X or X^{-1} depending on the arrows of the edges of the lattice. If an arrow is pointing towards the vertex j, we will use X_j^{-1} to build A_s, and if the arrow is pointing out another vertex, we use X_j. For plaquette operators B_p, Z_k is taken if the arrow is pointing clockwise and Z_k^{-1} for anti-clockwise, as shown in figure 7. To see now that we obtain the correct commutation rule, we look again at figure 7 and check,

$$[A_s, B_p] = [X_1^{-1}X_2X_3^{-1}X_4, Z_3^{-1}Z_6Z_5Z_3^{-1}] = (1-\omega\omega^{-1})A_sB_p = 0. \tag{33}$$

Then, the Hamiltonian could be written as follows:

$$H_{aux} := -\sum_s A_s - \sum_p B_p. \tag{34}$$

Although, according to the definition of A_s and B_p, this operator is unitary, it is important to note that the operators A_s and B_p are no longer Hermitian, so H_{aux} is no longer Hermitian. However, we may redefine the Hamiltonian in the following way:

$$H^{sys} := \tfrac{1}{2}(H_{aux} + H_{aux}^{\dagger}), \tag{35}$$

where H^{sys} is Hermitian now. The effect that $H_{aux}^{\dagger}$ has in the system is a redefinition of the orientation on the lattice. So we have a superposition of a lattice orientated in the way of figure 7 (arrows up and right) and another with arrows down and left. Nevertheless, one can always think in terms of H_{aux} for the pictorial image and then use H^{sys} to compute energies and derive equations.

3.1. The anyon model

The theory developed above was done for the general case of qudits. From now on and to be concrete concerning thermal effects, we will focus on the case where $d = 3$ (qutrits).

Later on we will be able to extract conclusions for qudits as well. There are still many important aspects to be studied about this model and its coupling to a thermal bath. We need to compute the energy gap of the Hamiltonian, i.e. the energy difference between the ground state where the code lies and the excited states which represent the errors. It is also important to calculate the anyon statistics, as long as they are associated with the excitations of a topological system with qutrits.

At $d = 3$, the phase factors are $\omega = e^{i(2\pi/3)}$, $\omega^2 = e^{i(4\pi/3)}$, $\omega^3 = 1$. We will see, for this particular case, how excitations can be created, moved and annihilated. This will give us the properties of the anyon model that is going to be associated with the group $\mathbb{Z}_3$.

As before, we use a notation in which $\sigma_j^z = Z_j$ and $\sigma_j^x = X_j$, except that we use the symbol σ to denote errors acting on the system, i.e. bump operators acting because of the coupling to the thermal bath, whereas we shall use X, Z for the Hamiltonian interactions defined by the vertex and plaquette operators of H^{sys}.

Errors on the system can be expressed in terms of operators σ^x, σ^z or products containing them, and acting on each edge j where the qutrits are placed. And the same goes for σ^z. To see what effect these errors have on the system, we will see how the ground state changes by applying $\sigma^{x,z}$. We will see that this corresponds to processes in which anyons are created, annihilated or moved throughout the torus.

Let us see what happens when we bump a qutrit in a position j from the outside and then act with the Hamiltonian H_{aux},

$$H_{\text{aux}}\sigma_j^z|\psi\rangle.$$

Note that every operator of the Hamiltonian commutes with this σ_j^z except two A_s operators which share a *leg* with this qubit j. But, contrary to the case of $d = 2$, there is an orientation defined on the lattice. So, for instance, if an error (σ_j^z) occurs in a certain vertical edge, one of these A_s (the one below) is defined with an X_j, thus:

$$A_s\sigma_j^z\,|\psi\rangle = \omega^{-1}\sigma_j^z A_s\,|\psi\rangle = \omega^2\sigma_j^z\,|\psi\rangle\,, \tag{36}$$

but the $A_{s'}$ above the edge is defined with X_j^{-1}, then:

$$A_{s'}\sigma_j^z\,|\psi\rangle = \omega\sigma_j^z A_{s'}\,|\psi\rangle = \omega\sigma_j^z\,|\psi\rangle\,. \tag{37}$$

Hence, we have two violations of the vertex condition, one with charge ω and the other with ω^2. This is one of the two types of anyons that we will have in this system, and we shall denote it as an ω^2–ω anyon. It is important to point out that these are only labels to classify the excitations based on the violations of the operator A_s (and B_p). In principle, we could classify anyons based on the violation of stabilizers A_s^{-1} (and B_p^{-1}) that appears in $H_{\text{aux}}^\dagger$. It is just a matter of labeling; the physics is the same.

Now we can act with σ_j^z again and obtain the other anyon type called ω–ω^2. Actually, they could be considered as the same anyon type as before but with opposite orientation. However, it is convenient to define them as two types of anyons as they will have different braiding properties. Moving anyons of the same type around each other will be different from the case of having anyons of different types. Likewise, it will be necessary to have anyons of different types in order to have fusion of anyons without annihilation. We shall explain this in the next subsection in more detail.

Note that acting twice with σ_j^z is equivalent to acting with $(\sigma_j^z)^{-1}$. Thus, although every error can be expressed in terms of X and Z operators, it will be useful to think sometimes as if

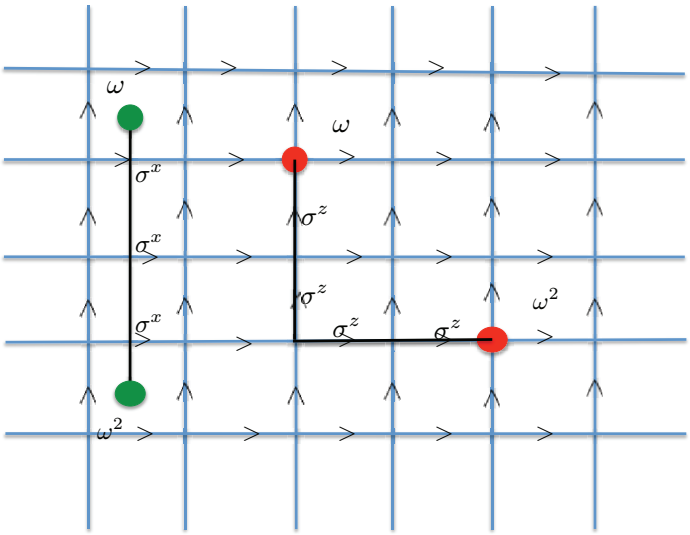

Figure 8. Anyons of type x (red) on the direct lattice. Anyons of type x (green) on the dual lattice.

we act with either X, Z or X^{-1}, Z^{-1}. All these arguments are exactly the same in the case of B_p operators and σ^x errors. Therefore, we have four types of anyons, two of plaquette type and two of vertex type.

Let us study now the braiding of the anyons. We will consider two chains of different types: plaquette anyon and vertex anyon (as in figure 8). In this case, we get something remarkably different from the $d = 2$ case. Now it is not the same to let one anyon remain still and move the other around it as it is to do it the other way around. Thus, let us move particles around each other. For example, let us move an x-type particle around a z-type particle (see figure 9). Then,

$$|\Psi_{\text{initial}}\rangle = S^z(t)\,|\psi^x(q)\rangle, \quad |\Psi_{\text{final}}\rangle = S^x(c)\,S^z(t)\,|\psi^x(q)\rangle = \omega^2|\Psi_{\text{initial}}\rangle,$$

because $S^x(c)$ and $S^z(t)$ cross each other on just one qutrit satisfying the relation

$$XZ = \omega^2 ZX$$

and $S^x(c)|\psi^x(q)\rangle = |\psi^x(q)\rangle$. We see that the global wave function, i.e. the state of the entire system, acquires the phase factor ω^2. Nonetheless, if the operation is the opposite, i.e. if we move a z-type particle around a x-type particle, then

$$|\Psi_{\text{initial}}\rangle = S^x(q)\,|\psi^z(t)\rangle, \quad |\Psi_{\text{final}}\rangle = S^z(c)\,S^x(q)\,|\psi^z(t)\rangle = \omega|\Psi_{\text{initial}}\rangle,$$

since $S^x(q)$ and $S^z(c)$ cross each other just on one qutrit again satisfying the relation

$$ZX = \omega XZ \tag{38}$$

and $S^z(c)|\psi^z(t)\rangle = |\psi^z(t)\rangle$. We see that the global wave function acquires now the phase factor ω.

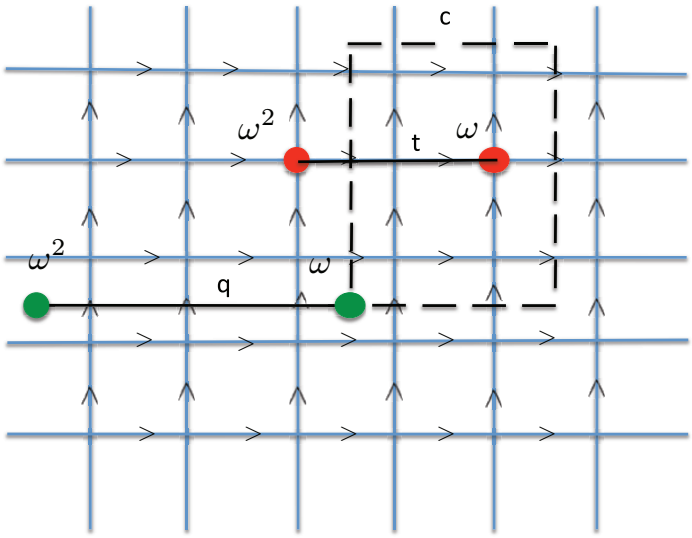

Figure 9. Anyons of type Z (red) on the direct lattice attached to a string t. Anyons of type x (green) on the dual lattice associated with a string q. The x-type particle moves around a z-type particle on a closed string c.

Thus, we arrive at a very important novelty for qutrits that is different from the case when we dealt with qubits in two aspects.

1. The phase that the anyon picks up is different from -1.
2. The phase depends on the orientation in which the braiding close path is traversed.

3.2. New anyon energy processes

First of all, let us look at the gap of the Hamiltonian. We will reach our first excited state by applying a σ^z or σ^x operator to the ground state. Let us see what is the energy difference between the ground state and the first excited state. Remember that $2H^{\text{sys}} = H_{\text{aux}} + H_{\text{aux}}^{\dagger}$. We denote by P and S the number of plaquette and vertex operators, respectively, with $P + S = N$ being the number of qutrits in the lattice, and $\{l, l'\}$ are the adjacent vertices of the site of a qutrit j:

$$H|\psi\rangle = \frac{1}{2}\left\{-\sum_{\text{s}} A_{\text{s}} - \sum_{\text{p}} B_{\text{p}} + \text{h.c.}\right\}|\psi\rangle = -(P+S)|\psi\rangle\,, \tag{39}$$

$$H\sigma_j^z|\psi\rangle = \frac{1}{2}\left\{-\sum_{\text{s}} A_{\text{s}} - \sum_{\text{p}} B_{\text{p}} + \text{h.c.}\right\}\sigma_j^z|\psi\rangle = -(P+S-2)\sigma_j^z|\psi\rangle - \frac{1}{2}(A_l\sigma_j^z|\psi\rangle$$

$$-A_{l'}\sigma_j^z|\psi\rangle + A_l^{\dagger}\sigma_j^z|\psi\rangle - A_{l'}^{\dagger}\sigma_j^z|\psi\rangle) = -(P+S-2)\sigma_j^z|\psi\rangle - \omega^2\sigma_j^z|\psi\rangle - \omega\sigma_j^z A_{l'}^{\dagger}|\psi\rangle$$

$$= -(P+S-2+\omega+\omega^2)\sigma_j^z|\psi\rangle = -\left(P+S-2+2\cos\frac{2\pi}{3}\right)\sigma_j^z|\psi\rangle$$

$$= -(P+S-3)\sigma_j^z|\psi\rangle\,.$$

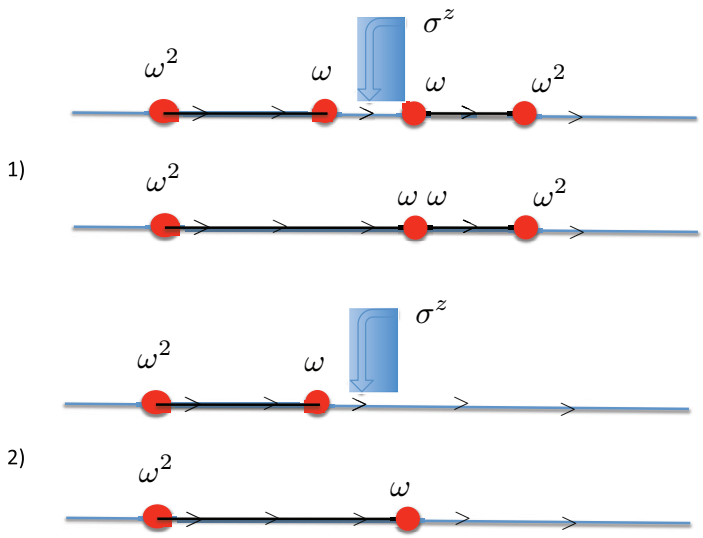

Figure 10. (1) Fusion of anyons (ending tied, not annihilated). (2) Movement of an anyon. We plot just one dimension as long as the rest of the lattice is irrelevant, i.e. the process is the same everywhere.

Thus, the energy difference is

$$\Delta E = 3.$$

The action of σ^x produces the same energy increment but we have to do the commutation with the operators B_p.

This calculation can be easily extended to the case of *qudits* with arbitrary d, obtaining the gap equation

$$\Delta E = \Delta_d = 2\left(1 - \cos\frac{2\pi}{d}\right). \tag{40}$$

Note that there is a reduction of the energy gap for $d = 3$ in comparison with the case of qubits, where it was 4. It is also important to point out that if we act again on the same bond of the lattice with $(\sigma^z)^{-1}$, there would be an energy reduction of the same amount of energy. Moreover, if at the endpoint of an anyon ω — ω^2 we act with σ^z, we obtain the same pair of anyons again, and the same energy, but longer (see figure 10.(2)). In this process, the energy is preserved, $\Delta E = 0$. This means that there is no energy exchange between the thermal bath and the system. We can understand the process as a diffusion of the anyon with no energy cost. In analogy to the case $d = 2$, this is what is called moving an anyon. It is also important to remark that for qutrits, all processes that involve moving a simple pair of anyons still have no energy cost.

Until now, there is a complete analogy with the case of $d = 2$. But we are going to see now a process that only occurs at $d > 2$. Imagine that there have been two excitations on the system, and two anyons of opposite orientation have been created. Moreover, they are separated by just one vertex operator. The situation is plotted in figure 10.(1).

Imagine that we act now with a σ^z on the bond, which is error-free, that links the anyons ω^2—ω and ω—ω^2 (opposite orientation). Let us analyze the energy process.

$$H\left|\psi'\right\rangle = -\frac{1}{2}\left(-\sum_{\mathrm{s}} A_{\mathrm{s}} - \sum_{\mathrm{p}} B_{\mathrm{p}}\right)\left|\psi'\right\rangle + \mathrm{h.c.} = -(P+S-6)\left|\psi\right\rangle,$$

$$H\sigma_j^z\left|\psi'\right\rangle = -\frac{1}{2}\left(-\sum_{\mathrm{s}} A_{\mathrm{s}} - \sum_{\mathrm{p}} B_{\mathrm{p}}\right)\sigma_j^z\left|\psi'\right\rangle + \mathrm{h.c.} = -\frac{1}{2}(P+S-\omega-\omega-\omega^2\omega^2)\sigma^z\left|\psi'\right\rangle$$

$$-\frac{1}{2}(P+S-\omega^2-\omega^2-\omega\omega)\sigma^z\left|\psi'\right\rangle = -\left(P+S-6+\frac{3}{2}\right)\sigma^z\left|\psi'\right\rangle, \tag{41}$$

so the energy difference is

$$\Delta E = -3/2.$$

What has occurred is that two anyons have been tied together, but not annihilated. This process lowers the energy of the system by a smaller amount than the process of annihilation. If in this situation we would act with a $(\sigma_j^z)^{-1}$ on the point where the two pairs of anyons are tied together, the two anyons would split apart, and this process would cost energy $\Delta E = 3/2$. This could be analyzed exactly the same way with σ^x errors and B_{p} operators.

It is remarkable that this phenomenon cannot happen at $d = 2$, as at $d = 2$ the product $\omega\omega = (-1)(-1) = 1$. Therefore, $d = 3$ is the first nontrivial case to have processes like these in a toric code with qudits.

3.3. Master equation for topological qutrits

As we have seen, all these processes are generated by the action of operators σ^z, $(\sigma^z)^2$ and σ^x, $(\sigma^x)^2$; as in this case, the square of the Pauli operators is their Hermitian conjugate. Nevertheless, the energy exchange depends on the situation of the system when we bump it with the thermal bath from outside. Before writing the master equation that describes the dynamics of the system, it will be useful to distinguish between these situations by local projectors. The answer to the question whether this is possible or not in this case is not trivial. However, we show that it is possible to classify into groups of processes that have the same energy gain from the bath. Furthermore, they could be distinguished by certain projection operators that only involve two adjacent vertex or plaquette operators.

We arrive at the following classification:

1——1	$P^j_{++} = 4\mathcal{A}^{(1)}_{\alpha=+1}(s)\mathcal{A}^{(1)}_{\alpha=-1}(s)\mathcal{A}^{(1)}_{\alpha=+1}(s')\mathcal{A}^{(1)}_{\alpha=-1}(s)$
ω——1	$P^j_{+(1)} = 8\mathcal{A}^{(2)}_{\alpha=0}(s,s')\mathcal{A}^{(2)}_{\alpha=+1}(s,s')\Delta\mathcal{A}(s,s')\Delta\mathcal{A}^{\dagger}(s,s')\mathcal{A}^{(1)}_{\alpha=-1}(s)\mathcal{A}^{\dagger(1)}_{\alpha=-1}(s)$
1——ω	$P^j_{+(2)} = 8\mathcal{A}^{(2)}_{\alpha=0}(s,s')\mathcal{A}^{(2)}_{\alpha=+1}(s,s')\Delta\mathcal{A}(s,s')\Delta\mathcal{A}^{\dagger}(s,s')\mathcal{A}^{(1)}_{\alpha=-1}(s)\mathcal{A}^{\dagger(1)}_{\alpha=-1}(s)$
ω^2——1	$P^j_{0(1)} = 8\mathcal{A}^{(2)}_{\alpha=0}(s,s')\mathcal{A}^{(2)}_{\alpha=-1}(s,s')\Delta\mathcal{A}(s,s')\Delta\mathcal{A}^{\dagger}(s,s')\mathcal{A}^{(1)}_{\alpha=+1}(s')\mathcal{A}^{\dagger(1)}_{\alpha=+1}(s')$
1——ω^2	$P^j_{0(2)} = 8\mathcal{A}^{(2)}_{\alpha=0}(s,s')\mathcal{A}^{(2)}_{\alpha=-1}(s,s')\Delta\mathcal{A}(s,s')\Delta\mathcal{A}^{\dagger}(s,s')\mathcal{A}^{(1)}_{\alpha=+1}(s)\mathcal{A}^{\dagger(1)}_{\alpha=+1}(s)$
ω——ω	$P^j_{0(3)} = 8\mathcal{A}^{(2)}_{\alpha=0}(s,s')\mathcal{A}^{(2)}_{\alpha=-1}(s,s')\mathcal{A}^{(1)}_{\alpha=+1}(s)\mathcal{A}^{\dagger(1)}_{\alpha=+1}(s)\mathcal{A}^{(1)}_{\alpha=+1}(s')\mathcal{A}^{\dagger(1)}_{\alpha=+1}(s')$

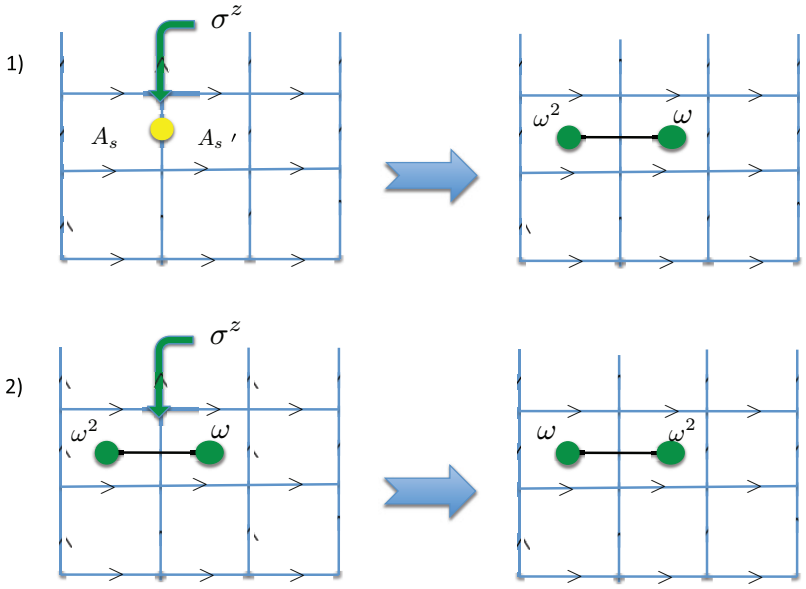

Figure 11. (1) Initial state 1—1 $\Rightarrow$ Final state ω^2—ω. (2) Initial state ω^2—$\omega \Rightarrow$ Final state ω—ω^2. This is an example of what happens to the topological charges when there is a bump from the thermal bath outside. The first one the energy gain is $\Delta E = 3$. The second one $\Delta E = 0$.

ω^2——ω	$P^j_{-(1)} = 8\mathcal{A}^{(2)}_{\alpha=+1}(s,s')\mathcal{A}^{(2)}_{\alpha=-1}(s,s')\Delta\mathcal{A}(s,s')\Delta\mathcal{A}^{\dagger}(s,s')\mathcal{A}^{(1)}_{\alpha=+1}(s')\mathcal{A}^{\dagger(1)}_{\alpha=+1}(s')$
ω——ω^2	$P^j_{-(2)} = 8\mathcal{A}^{(2)}_{\alpha=+1}(s,s')\mathcal{A}^{(2)}_{\alpha=-1}(s,s')\Delta\mathcal{A}(s,s')\Delta\mathcal{A}^{\dagger}(s,s')\mathcal{A}^{(1)}_{\alpha=+1}(s)\mathcal{A}^{\dagger(1)}_{\alpha=+1}(s)$
ω^2——ω^2	$P^j_{--} = 8\mathcal{A}^{(2)}_{\alpha=0}(s,s')\mathcal{A}^{(2)}_{\alpha=+1}(s,s')\mathcal{A}^{(1)}_{\alpha=-1}(s)\mathcal{A}^{\dagger(1)}_{\alpha=-1}(s)\mathcal{A}^{(1)}_{\alpha=-1}(s')\mathcal{A}^{\dagger(1)}_{\alpha=-1}(s')$

(42)

In this table, we have represented all combinations of two adjacent topological charges. In the first column, we depict a representation of the different types of anyons, with two topological charges attached at their ends and linked by a dash. Correspondingly, all these anyons have an intrinsic orientation. At the left side of the dash there is the eigenvalue of the operator A_s and at the right side, the eigenvalue of the adjacent operator A'_s. A physical qutrit j would be in the middle of the dash (see the example in figure 11). In the second column, we write the projector that gives 1 for that situation and 0 for the others.

Here we have defined the following operators in order to simplify the notation:

$$\mathcal{A}^{(1)}_{\alpha=0,+1,-1}(s) := (1-\omega^{\alpha}A_s),$$

$$\mathcal{A}^{(2)}_{\alpha=0,+1,-1}(s,s') := (1-\omega^{\alpha}A_sA'_s),$$

$$\Delta\mathcal{A}(s,s') := \mathcal{A}^{(1)}_{\alpha=0}(s') - \mathcal{A}^{(1)}_{\alpha=0}(s),$$

where s and s' are the two vertexes surrounding the qutrit j. The index α takes values on the exponent of the phases ω that appear from the braiding processes. These projectors tell us which

charges of the system surround a certain qutrit. That is why they are local projectors. Moreover, it is easy to verify that they form a set of orthogonal projectors:

$$\sum_{\alpha} P_{\alpha}^{j} = \mathbb{1},$$

$$P_{\alpha}^{j} = P_{\alpha}^{j\dagger},$$

$$(P_{\alpha}^{j})^2 = P_{\alpha}^{j}.$$

As we have already explained, we classify the situation of the system in terms of the charges according to the eingenvalues of the operators A_s associated with the part of the Hamiltonian H_{aux}. One could do the same thing for A_s^{-1}, but the situation of the system will be the same independently of the label we assign them. So these projectors can discriminate perfectly between eigenstates of the Hamiltonian H^{sys}.

Now, given a certain state of the system $|\psi'\rangle$, by applying these projectors we can figure out which situation we have. This means that if an operator σ^z or σ^x (or their Hermitian conjugate) is going to act on our system, we will know which energy process is bound to happen. Based on this, and studying the different situations that we can encounter, one can define a set of operators that tells us whether an anyon has been moved, created, annihilated or fused when we apply the generalized Pauli operators (as we did in figure 10). This is done by analyzing the initial and the final state after the action of a bump operator and seeing which would be the energy after and before the process, as shown in figure 11. Therefore, we have:

$$\begin{aligned}
a_j^{(1)\dagger} &:= \sigma_j^z P_{++}^j + (\sigma_j^z)^{-1} P_{++}^j, \\
a_j^{(1)} &:= (\sigma_j^z)^{-1} P_{-(1)}^j + \sigma_j^z P_{-(2)}^j, \\
a_j^{(2)\dagger} &:= (\sigma_j^z)^{-1} P_{+(1)}^j + \sigma_j^z P_{+(2)}^j + \sigma_j^z P_{0(1)}^j (\sigma_j^z)^{-1} P_{0(2)}^j, \\
a_j^{(2)} &:= (\sigma_j^z)^{-1} P_{0(3)}^j + \sigma_j^z P_{0(3)}^j + \sigma_j^z P_{--}^j + (\sigma_j^z)^{-1} P_{--}^j, \\
a_j^{0} &:= \sigma_j^z P_{+(1)}^j + (\sigma_j^z)^{-1} P_{+(2)}^j + \sigma_j^z P_{0(2)}^j (\sigma_j^z)^{-1} P_{0(1)}^j + \sigma_j^z P_{-(1)}^j + (\sigma_j^z)^{-1} P_{-(2)}^j.
\end{aligned} \tag{43}$$

Here the upper indices of operators a_j are related to the energy cost of the process.

- $a_j^{(1)\dagger}$ creates a pair of anyons of z-type and $a_j^{(1)}$ annihilates it. The energy cost is $\Delta E = 3$.
- $a_j^{(2)\dagger}$ and $a_j^{(2)}$ are related to the process of fusion or separation, respectively, of anyons as in figure 10.(1) and also to the process of creation (and annihilation) of a pair of anyons tied to a previous pair. The energy cost is $\Delta E = \frac{3}{2}$.
- a_j^0 moves anyons and also it can invert the orientation of a pair of anyons (as in figure 11.(2). There is no energy cost in these processes.

For the plaquette operators B_p we proceed in the same way, obtaining a similar result. The corresponding local projectors that we denote as R_j are built analogously just by changing A_s for B_p, where p and p' are the adjacent plaquettes to the qutrit j. Then the operators that

describe the analogous process for x-type anyons are

$$\begin{aligned}
b_j^{(1)\dagger} &:= \sigma_j^x R_{++}^j + (\sigma_j^x)^{-1} R_{++}^j, \\
b_j^{(1)} &:= (\sigma_j^x)^{-1} R_{-(1)}^j + \sigma_j^x R_{-(2)}^j, \\
b_j^{(2)\dagger} &:= (\sigma_j^x)^{-1} R_{+(1)}^j + \sigma_j^x R_{+(2)}^j + \sigma_j^x R_{0(1)}^j (\sigma_j^x)^{-1} R_{0(2)}^j, \\
b_j^{(2)} &:= (\sigma_j^x)^{-1} R_{0(3)}^j + \sigma_j^x R_{0(3)}^j + \sigma_j^x R_{--}^j + (\sigma_j^x)^{-1} R_{--}^j, \\
b_j^0 &:= \sigma_j^x R_{+(1)}^j + (\sigma_j^x)^{-1} R_{+(2)}^j + \sigma_j^x R_{0(2)}^j (\sigma_j^x)^{-1} R_{0(1)}^j + \sigma_j^x R_{-(1)}^j + (\sigma_j^x)^{-1} R_{-(2)}^j.
\end{aligned} \tag{44}$$

Some of these operators are associated with more than one projector, unlike for qubits. That is because for three-level systems, the possibilities for different excitation scenarios have grown significantly.

As we have seen in the previous section, these operators arise naturally as the Fourier transform of the interaction Hamiltonian when a thermal bath is weakly coupled with our system,

$$\mathrm{e}^{\mathrm{i}tH^{\mathrm{sys}}} S_\alpha \, \mathrm{e}^{-\mathrm{i}tH^{\mathrm{sys}}} = \sum_\omega S_\alpha(\omega) \, \mathrm{e}^{-\mathrm{i}\omega t}. \tag{45}$$

In this case, the interaction Hamiltonian will be of the form

$$V = \sum_\alpha S_\alpha \otimes f_\alpha = \sum_j \sigma_j^z \otimes f_j^z + (\sigma_j^z)^{-1} \otimes (f_j^z)^\dagger + \sigma_j^x \otimes f_j^x + (\sigma_j^x)^{-1} \otimes (f_j^x)^\dagger, \tag{46}$$

and it is quite important to remark that there are only three Bohr frequencies this time, $\omega = 0, \pm\frac{3}{2}, \pm 3$.

We can check that the dynamical operators obtained are indeed compatible with this interaction potential as $\sum_\alpha S_\alpha = \sum_\alpha S_\alpha(\omega)$. In our case, it is trivial to check:

$$\begin{aligned}
\sigma_j^z + (\sigma_j^z)^{-1} &= \sum_n a_j^n, \\
\sigma_j^x + (\sigma_j^x)^{-1} &= \sum_n b_j^n,
\end{aligned}$$

with $n = 0, 1, 2$, using equations (44) and (45).

Moreover, $[H, a^n] \propto a^n$, based on the fact that H^{sys} is made of stabilizers, which at most introduces a phase when they are applied to states $a^i |\phi\rangle$. Thus, $A_{\mathrm{s}}(B_{\mathrm{p}}) a^i |\phi\rangle \propto a^i |\phi\rangle$ and $a^i A_{\mathrm{s}}(B_{\mathrm{p}}) |\phi\rangle \propto a^i |\phi\rangle$; therefore $[H, a^i] \propto a^i$, $\forall a^i$ a dynamical operator of our system. With this proviso, the Davies generator turns out to be given by

$$\frac{\mathrm{d}X}{\mathrm{d}t} = \mathcal{G}(X) = \mathrm{i}\delta(X) + \mathcal{L}(X), \tag{47}$$

with

$$\delta(X) = [H^{\rm sys}, X] = \tfrac{1}{2}[H_{\rm aux} + H_{\rm aux}^{\dagger}, X],$$

$$\mathcal{L}(X) = \mathcal{L}^{z}(X) + \mathcal{L}^{x}(X),$$

$$\begin{aligned}\mathcal{L}^{x}(X) = \sum_j \frac{1}{2} R(3)\{&(-b_j^{(1)\dagger} b_j^{(1)} X - X b_j^{(1)\dagger} b_j^{(1)} + 2 b_j^{(1)\dagger} X b_j^{(1)}) + {\rm e}^{-3\beta}(-b_j^{(1)} b_j^{(1)\dagger} X - X b_j^{(1)} b_j^{(1)\dagger} \\ &+2 b_j^{(1)} X b_j^{(1)\dagger})\} + \tfrac{1}{2} R(3/2)\{(-b_j^{(2)\dagger} b_j^{(2)} X - X b_j^{(2)\dagger} b_j^{(2)} + 2 b_j^{(2)\dagger} X b_j^{(2)}) \\ &+{\rm e}^{-\frac{3}{2}\beta}(-b_j^{(2)} b_j^{(2)\dagger} X - X b_j^{(2)} b_j^{(2)\dagger} + 2 b_j^{(2)} X b_j^{(2)\dagger})\} - \tfrac{1}{2} R(0)[b_j^0, [b_j^0, X]], \\ \mathcal{L}^{z}(X) = \sum_j \tfrac{1}{2} R(3)\{&(-a_j^{(1)\dagger} a_j^{(1)} X - X a_j^{(1)\dagger} a_j^{(1)} + 2 a_j^{(1)\dagger} X a_j^{(1)}) + {\rm e}^{-3\beta}(-a_j^{(1)} a_j^{(1)\dagger} X - X a_j^{(1)} a_j^{(1)\dagger} \\ &+2 a_j^{(1)} X a_j^{(1)\dagger})\} + \tfrac{1}{2} R(3/2)\{(-a_j^{(2)\dagger} a_j^{(2)} X - X a_j^{(2)\dagger} a_j^{(2)} + 2 a_j^{(2)\dagger} X a_j^{(2)}) \\ &+{\rm e}^{-\frac{3}{2}\beta}(-a_j^{(2)} a_j^{(2)\dagger} X - X a_j^{(2)} a_j^{(2)\dagger} + 2 a_j^{(2)} X a_j^{(2)\dagger})\} - \tfrac{1}{2} R(0)[a_j^0, [a_j^0, X]]. \end{aligned} \tag{48}$$

3.4. Topological order

Similarly to the case of qubits, we will study the evolution of the expectation value $\langle {\rm GS}|\, X_{\rm c}\, |{\rm GS}\rangle$, where $X_{\rm c}$ is the tensor product of σ^x generalized Pauli operators ($d = 3$) along a non-contractible loop, and $|{\rm GS}\rangle$ denotes a certain ground state in the stabilizer subspace; namely, a superposition of the degenerate states in the ground state manifold of $H^{\rm sys}$.

In the weak-coupling limit, the master equation that describes the dynamics of this quantity is

$$\frac{{\rm d}X_{\rm c}(t)}{{\rm d}t} = {\rm i}[H^{\rm sys}, X_{\rm c}(t)] + \mathcal{L}[X_{\rm c}(t)]. \tag{49}$$

In order to simplify the calculation, we remove the free evolution part of the equation

$$\tilde{X}_{\rm c}(t) = {\rm e}^{-{\rm i}H^{\rm sys}t} X_{\rm c}(t) {\rm e}^{{\rm i}H^{\rm sys}t} \implies \frac{{\rm d}\tilde{X}_{\rm c}(t)}{{\rm d}t} = \mathcal{L}[\tilde{X}_{\rm c}(t)], \tag{50}$$

both the dissipator $\mathcal{L}$ and the mean value $\langle {\rm GS}|\, X_{\rm c}\, |{\rm GS}\rangle$ being invariant under this transformation.

3.5. Short-time regime

In the short-time regime, we can approximate $\tilde{X}_{\rm c}(t) \simeq (1 + t\mathcal{L})X_{\rm c}$; here we denote $X_{\rm c} := X_{\rm c}(0)$. Thus, the evolution of $\langle {\rm GS}|\, X_{\rm c}(t)\, |{\rm GS}\rangle$ is

$$\langle \tilde{X}_{\rm c}(t)\rangle \simeq \langle {\rm GS}|\, X_{\rm c}\, |{\rm GS}\rangle + t\, \langle {\rm GS}|\, \mathcal{L}(X_{\rm c}) |{\rm GS}\rangle. \tag{51}$$

We need to calculate $\langle {\rm GS}|\, \mathcal{L}(X_{\rm c})\, |{\rm GS}\rangle$, with $\mathcal{L}(X_{\rm c}) = \mathcal{L}^{x}(X_{\rm c}) + \mathcal{L}^{z}(X_{\rm c})$. This calculation is done in appendix A, obtaining

$$\langle {\rm GS}|\, \mathcal{L}(X_{\rm c})\, |{\rm GS}\rangle = -\frac{\Delta}{2} R(\Delta) {\rm e}^{-\Delta\beta} |c|\, \langle {\rm GS}|\, X_{\rm c} |{\rm GS}\rangle. \tag{52}$$

Hence, we can define $\Gamma := \frac{\Delta}{2} R(\Delta) {\rm e}^{-\Delta\beta} |c|$ as the initial decay rate of the system. For qutrits, $\Delta = 3$, while for qubits (see equation (25)) we have obtained an analogous expression but with $\Delta = 4$ instead.

This result can be generalized for the case of *qudits* with arbitrary d. We have already seen that, at short times, only the creation of anyons contributes to the decay of topological order. The free diffusion of anyons and the fusion processes among them will not appear as they are second order processes in time. However, as we increase d there are more types of anyons with different energies. Moreover, a pair of anyons should always be compatible with the conditions $\prod_s A_s = 1$ and $\prod_p B_p = 1$. That means that the possible types of anyons with different energies are of the form $\omega^n - \omega^{d-n}$ with $n = 1, \ldots, \lfloor \frac{d}{2} \rfloor$, and respective energies $\Delta_n = 2(1 - \cos \frac{2\pi n}{d})$. Note that $n = 1$ refers to the lowest energy pair of anyons, i.e. the energy gap of the Hamiltonian. Thus, the initial decay rate has to be the sum of all these contributions:

$$\Gamma_d = \sum_{n=1}^{\lfloor \frac{d}{2} \rfloor} \frac{\Delta_n}{2} |c| R(\Delta_n) \mathrm{e}^{-\Delta_n \beta}. \tag{53}$$

It is important to point out that in the case of qudits, an analogous expression for the interaction with the environment to (13) involves $S_\alpha = \sigma^x, (\sigma^x)^2, \ldots, (\sigma^x)^{d-1}, \sigma^z, (\sigma^z)^2, \ldots, (\sigma^z)^{d-1}$. All nontrivial powers of σ^x and σ^z are included to allow for excitations of physical *qudits* from one level to another, at first order in time.

Using equation (53) it will be possible to establish a crossover temperature T_c as the limit for which the initial decay rate Γ will be larger for qubits than for qudits. For the sake of comparison, we take $R(\Delta_n)$ the same for qubits and qudits. This is reasonable since Δ_n are of the same order, and $R(\Delta_n)$ are the Fourier transforms of the bath coupling that induces the excitations on the physical qudits. Thus, we set up the condition $\Gamma_d(T_c) := \Gamma_2(T_c)$. Using equation (53) we arrive at the following expression:

$$4 = \sum_{n=1}^{\lfloor \frac{d}{2} \rfloor} \Delta_n \mathrm{e}^{-(\Delta_n - 4)\beta} > \sum_{n=1}^{\lfloor \frac{d}{2} \rfloor} \Delta_n, \tag{54}$$

as $\Delta_n < 4$ for $d > 2$, $\forall n$. Therefore, this equation only has a solution for such values of d satisfying $\sum_{n=1}^{\lfloor \frac{d}{2} \rfloor} \Delta_n < 4$. But, this is only true for $d = 3$. Thus, there exists only such a T_c for *qutrits*. For other values of d, the initial decay rate for qudits will always be larger than for qubits. This happens as $\sum_n \Delta_n$ increases almost linearly with d, and $d = 3$ is the only case when this quantity is smaller than 4, i.e. the gap in the case of qubits. Let us now compute T_c for qutrits:

$$3E_0 \, \mathrm{e}^{-3E_0\beta_c} = 4E_0 \, \mathrm{e}^{-4E_0\beta_c}, \tag{55}$$

with E_0 being the natural energy unit of the system. This leads to the following crossover temperature:

$$T_c = \frac{E_0}{k_B \ln \frac{4}{3}}. \tag{56}$$

The meaning of this temperature is the following. Above this temperature T_c, the initial decay rate for qutrits is smaller than that for qubits, something that makes qutrits better in this comparison. For $E_0 \sim 100\,\mathrm{kHz}$ used in the proposal of a Rydberg quantum simulator [63] for the operators of the 2D toric code, we obtain an estimate of $T_c \sim 20\,\mu\mathrm{K}$.

In addition, it could be computed a T_c comparing systems with d odd and $(d-1)$ even. There is always a temperature above which the system of *qudits* with d odd has a lower initial decay rate than the previous $(d-1)$ even.

It is also important to point out that Γ is only the initial decay rate. It is possible that the dynamics of anyons, with free diffusion, etc, play an important role in the loss of topological order. Beyond short times, our conjecture is that the new processes that appear in the case of qutrits, i.e. fusion of anyons that end tied up, will be an obstacle to the free diffusion of anyons. This would represent an improvement for the stability of the generalized toric code in some intermediate time regime for this is the cause of the loss of topological order in the system.

3.6. Long-time regime

Now we want to study the master equation (49) in the opposite time regime. We are interested in the fate of the non-local order parameter we are using to describe the topological order in a system of qudits in a generalized toric code. We conjecture that the final state will be given by a thermal Gibbs state. To show that our observable for the order parameter $\langle X_c \rangle$ approaches the expectation value of X_c in the Gibbs state for times long enough, we resort again to the condition (7). In the generalized case, it reads as

$$\{\sigma_x, \sigma_x^2, \ldots, \sigma_x^{d-1}, \sigma_z, \sigma_x^2, \ldots, \sigma_z^{d-1}\}' = \mathbb{C}\mathbb{1}, \quad \text{for any } d. \tag{57}$$

This is due to the fact that if some generic operator, say A, commutes with every element of the set $\{\sigma_x, \sigma_x^2, \ldots, \sigma_x^{d-1}, \sigma_z, \sigma_x^2, \ldots, \sigma_z^{d-1}\}$, so does it with every element of the d-Pauli group. This follows from the Jacobi identity and the fact that $\sigma_z\sigma_x = \omega\sigma_x\sigma_z$. Therefore, given the irreducibility of the computational representation of the d-Pauli group (the technical details of this proof are given in appendix B), the condition (57) holds.

With this result, we may obtain the behavior in the long-time regime

$$\langle X_c(t \to \infty) \rangle = \mathrm{Tr}(X_c \rho(t \to \infty)) = \frac{1}{Z} \sum_i \mathrm{e}^{-\beta\lambda_i} \langle \psi_i | X_c | \psi_i \rangle = 0, \tag{58}$$

which implies that the topological order is also destroyed for qudits in the generalized toric code when times of interaction with a thermal bath are long enough.

Now, let us summarize and combine the results for both time regimes, i.e. short- and long-time behaviours. We have proved that at short times the global order parameter we are considering behaves as

$$\langle X_c(t) \rangle_\beta = \mathrm{e}^{-\Gamma t} \langle X_c(0) \rangle, \tag{59}$$

with $\Gamma = \frac{\Delta}{2} R(\Delta) \mathrm{e}^{-\Delta\beta} |c|$ and $\Delta = 3$ for qutrits. We have also shown that there exits a crossover temperature T_c above which the initial decay rate for qutrits is smaller than for qubits. Furthermore, we have shown this event only occurs in the case of qutrits, as for other values of d, the initial decay rate is always larger than for qubits. On the other hand, far from this initial short-time regime, the topological order of the system decays to zero for long enough times.

4. Conclusions

We have introduced the basic concepts of the 2D Kitaev model for *qubits* as well as a generalization of the code for *qudits*, i.e. d-level systems with the main purpose of studying its decoherence properties due to thermal effects. To this end, we have coupled these systems to thermal baths in order to study the thermal stability within a quantum open system's formalism, namely Davies' theory.

The generalization of the toric code leads to new physics. Indeed, we have specialized for the case of *qutrits* and obtained very interesting results. First of all, new Abelian anyons have arisen with novel braiding properties, i.e. new statistics by exchange of particles. For instance, let us move a pair of anyons around another pair that stays still. We would pick up a different phase, letting the first pair remain still and moving the other one around. Furthermore, new energy processes appear which are forbidden for *qubits*, $d = 3$ being the first nontrivial system where these new processes can be observed. Moreover, we present a master equation that describes the dynamics of any observable of the system coupled to a thermal bath, giving a complete description of the problem.

We have proposed a new way to study thermal stability regarding the loss of topological order in the system. At short times, the system starts losing its order with a certain decay rate that we are able to compute explicitly. We have checked that the system relaxes to the thermal state for any value of d, as expected. However, we have proved that above a certain crossover temperature, the initial decay rate for *qutrits* is smaller than in the original case for *qubits*. Surprisingly, this behavior only happens with *qutrits* and not with other *qudits* with $d > 3$.

It would be very interesting to be able to generalize this study further to other topological codes [64–70] coupled to thermal baths by deriving appropriate master equations for them. Other challenges in this direction are to study thermal effects with non-Abelian topological codes [71–77], higher-dimensional codes [12, 78–88] and systems with topological order based on two-body interactions [89–92], instead of many-body interactions in the Hamiltonian. This would facilitate the physical simulation of these topological quantum models [63, 93–99].

Acknowledgments

We acknowledge support from the Spanish MICINN grant no. FIS2009-10061, the CAM research consortium QUITEMAD S2009-ESP-1594, the European Commission PICC: FP7 2007-2013, grant no. 249958 and UCM-BS grant no. GICC-910758.

Appendix A. Evolution of the order parameter for qutrits

In order to compute $\langle \mathrm{GS}|\, \mathcal{L}(X_\mathrm{c})|\mathrm{GS}\rangle$ (with $\mathcal{L}(X_\mathrm{c}) = \mathcal{L}^x(X_\mathrm{c}) + \mathcal{L}^z(X_\mathrm{c})$), we need the expressions for the system operators that appear in equation (48) which were defined previously in equations (44) and (45). These operators are expressed in terms of some orthogonal projectors whose definition is given in equation (42). However, there are only two projectors that are relevant here, namely

$$P^j_{++}\,|\mathrm{GS}\rangle = |\mathrm{GS}\rangle \quad \text{and} \quad R^j_{++}\,|\mathrm{GS}\rangle = |\mathrm{GS}\rangle\,, \tag{A.1}$$

as the rest of them vanish when acting on the ground state. Remember that P^j are the projectors associated with the stabilizers A_s and R^j with stabilizers B_p. Moreover, we have

$$b^{(1)}_j|\mathrm{GS}\rangle = 0, \quad b^{(2)}_j|\mathrm{GS}\rangle = 0, \quad b^{(2)\dagger}_j|\mathrm{GS}\rangle = 0, \quad b^{(0)}_j|\mathrm{GS}\rangle = 0. \tag{A.2}$$

Thus, after doing some simplifications on equation (48):

$$\begin{aligned}\langle \mathrm{GS}|\mathcal{L}_x(X_\mathrm{c})|\mathrm{GS}\rangle &= \frac{R(\Delta)}{2}\mathrm{e}^{-\Delta\beta}\sum_j \langle \mathrm{GS}|(2b^{(1)}_j X_c b^{(1)\dagger}_j - b^{(1)}_j b^{(1)\dagger}_j X_\mathrm{c} - X_c b^{(1)}_j b^{(1)\dagger}_j)|\mathrm{GS}\rangle \\ &= 2|c|\,\langle \mathrm{GS}|\,(\sigma^x_j + (\sigma^x_j)^{-1})X_\mathrm{c}\,|\mathrm{GS}\rangle = 0,\end{aligned} \tag{A.3}$$

as $X_c |\mathrm{GS}\rangle \propto |\mathrm{GS}\rangle$ but $\sigma_j^x |\mathrm{GS}\rangle$ is orthogonal to $|\mathrm{GS}\rangle$, and we have used the fact that $[P_{\pm,0}^j, X_c] = 0$ for every j, as these projectors are only functions of vertex operators. This is not true for $R_{\pm,0}^j$ if $j \in c$, i.e. j belongs to the path where X_c is acting on. In that case, since $\sigma_j^z \sigma_j^x (\sigma_j^z)^{-1} = \omega \sigma_j^x$, we obtain $\sigma_j^z X_c (\sigma_j^z)^{-1} = \omega X_c$ for the string operator. In addition, by making use of

$$a_j^{(1)} |\mathrm{GS}\rangle = 0, \quad a_j^{(2)} |\mathrm{GS}\rangle = 0, \quad a_j^{(2)\dagger} |\mathrm{GS}\rangle = 0, \quad a_j^{(0)} |\mathrm{GS}\rangle = 0, \tag{A.4}$$

the result for $\langle \mathrm{GS}| \mathcal{L}_z(X_c) |\mathrm{GS}\rangle$ turns out to be

$$\begin{aligned}
\langle \mathrm{GS}| \mathcal{D}_z(X_c) |\mathrm{GS}\rangle &= \frac{R(\Delta)}{2} \mathrm{e}^{-\Delta\beta} \sum_j \langle \mathrm{GS}| (2 a_j^{(1)} X_c a_j^{(1)\dagger} - a_j^{(1)} a_j^{(1)\dagger} X_c - X_c a_j^{(1)} a_j^{(1)\dagger}) |\mathrm{GS}\rangle \\
&= \frac{R(3)}{2} \mathrm{e}^{-3\beta} \sum_j \langle \mathrm{GS}| (\sigma_j^z + (\sigma_j^z)^{-1}) X_c (\sigma_j^z + (\sigma_j^z)^{-1}) |\mathrm{GS}\rangle - \langle \mathrm{GS}| P_{++}^j X_c |\mathrm{GS}\rangle \\
&\quad - \frac{1}{2} \langle \mathrm{GS}| P_{++}^j (\sigma_j^z + (\sigma_j^z)^{-1}) P_{++}^j X_c |\mathrm{GS}\rangle - \langle \mathrm{GS}| X_c P_{++}^j |\mathrm{GS}\rangle \\
&\quad - \langle \mathrm{GS}| X_c P_{++}^j (\sigma_j^z + (\sigma_j^z)^{-1}) P_{++}^j |\mathrm{GS}\rangle \\
&= \frac{R(3)}{2} \mathrm{e}^{-3\beta} \sum_j \delta_{j \notin c} (\langle \mathrm{GS}| (2 + \sigma_j^z + (\sigma_j^z)^{-1}) X_c |\mathrm{GS}\rangle - \langle \mathrm{GS}| X_c |\mathrm{GS}\rangle \\
&\quad - \frac{1}{2} \langle \mathrm{GS}| (\sigma_j^z + (\sigma_j^z)^{-1}) X_c |\mathrm{GS}\rangle - \langle \mathrm{GS}| X_c |\mathrm{GS}\rangle \\
&\quad - \frac{1}{2} \langle \mathrm{GS}| (\sigma_j^z + (\sigma_j^z)^{-1}) X_c |\mathrm{GS}\rangle) \\
&\quad + \delta_{j \in c} (\langle \mathrm{GS}| (\sigma_j^z + (\sigma_j^z)^{-1}) (\omega^2 \sigma_j^z + \omega (\sigma_j^z)^{-1}) X_c |\mathrm{GS}\rangle - 2 \langle \mathrm{GS}| X_c |\mathrm{GS}\rangle \\
&\quad - \langle \mathrm{GS}| (\sigma_j^z + (\sigma_j^z)^{-1}) X_c |\mathrm{GS}\rangle) = -\frac{3}{2} R(3) \mathrm{e}^{-3\beta |c|} \langle \mathrm{GS}| X_c |\mathrm{GS}\rangle \\
&= -\frac{\Delta}{2} R(\Delta) \mathrm{e}^{-\Delta\beta |c|} \langle \mathrm{GS}| X_c |\mathrm{GS}\rangle ,
\end{aligned}$$

where $|c|$ is the number of points in the path c.

Appendix B. Irreducibility of the computational representation of the *d*-Pauli group

The d-Pauli group is generated by products of σ_x and σ_y such that $\sigma_x^d = \sigma_z^d = \mathbb{1}$ and $\sigma_z \sigma_x = \omega \sigma_x \sigma_z$, where ω is a primitive d-root of unity. Its order is d^3, which is a direct consequence that any element of the group can be written as $\omega^n \sigma_x^m \sigma_z^k$ for some n, m and k.

We take the representation of the d-Pauli group when acting on the computational basis:

$$\sigma_x |n\rangle = |n+1\rangle \mod d, \tag{B.1}$$

$$\sigma_z |n\rangle = \omega^n |n\rangle, \tag{B.2}$$

and we want to show that this representation is irreducible. We proceed by computing the character χ of every one of its elements, which is given by the trace of the matrices. Using the computational basis when taking the trace, from the above relations, $\chi(\sigma_x^m) = 0$ for $m \in \{1, \ldots, d-1\}$. Similarly $\chi(\sigma_z^m) = 0$ for $m \in \{1, \ldots, d-1\}$ as the sum of the roots of unity

vanishes. On the other hand, because $\sigma_z\sigma_x = \omega\sigma_x\sigma_z$ and the cyclic property of the trace, we conclude that the character of every element of the form $\sigma_x^m\sigma_z^k$ is zero for any representation. The rest of the terms are proportional to the identity $\omega^n\mathbb{1}$, and so $\chi(\omega^n\mathbb{1}) = \omega^n d$.

The irreducibility criterion asserts [9, 100] that a representation of a group G is irreducible if and only if the scalar product of characters is the identity, that is

$$(\chi, \chi) = \frac{1}{|G|}\sum_{g\in G}\chi^*(g)\chi(g) = 1, \tag{B.3}$$

where $|G|$ is the order of the group. For the computational representation of the d-Pauli group we have

$$(\chi, \chi) = \frac{1}{d^3}\sum_{n=0}^{d-1}(\omega^n d)^*\omega^n d = \frac{1}{d}\sum_{n=0}^{d-1}|\omega|^n = 1, \tag{B.4}$$

thus, the representation is irreducible.

References

[1] Shor P W 1995 Scheme for reducing decoherence in quantum computer memory *Phys. Rev.* A **52** R2493

[2] Steane A M 1996 Error correcting codes in quantum theory *Phys. Rev. Lett.* **77** 793

[3] Calderbank A R and Shor P W 1996 Good quantum error-correcting codes exist *Phys. Rev.* A **54** 1098–5

[4] Yu A 1997 Kitaev quantum computations: algorithms and error correction *Russ. Math. Surv.* **52** 1191

[5] Gottesman D 1996 Class of quantum error-correcting codes saturating the quantum hamming bound *Phys. Rev.* A **54** 1862–8

[6] Calderbank A R, Rains E M, Shor P M and Sloane N J A 1997 Quantum error correction and orthogonal geometry *Phys. Rev. Lett.* **78** 405

[7] Preskill J 1998 Reliable quantum computers *Proc. R. Soc.* A **454** 385–410

[8] Gottesman D 1998 Fault-tolerant quantum computation with higher-dimensional systems *Proc. 1st NASA Int. Conf. on Quantum Computing and Quantum Communications (QCQC) (Palm Springs, CA)* ed C Williams (New York: Springer) pp 302–13
Gottesman D 1999 *Chaos Solitons Fractals* **10** 1749–58

[9] Nielsen M A and Chuang I L 2000 *Quantum Computation and Quantum Information* (Cambridge: Cambridge University Press)

[10] Galindo A and Martin-Delgado M A 2002 Information and computation: classical and quantum aspects *Rev. Mod. Phys.* **74** 347–423

[11] Kitaev Yu A 2003 Fault-tolerant quantum computation by anyons *Ann. Phys.* **303** 2–30

[12] Dennis E, Kitaev A, Landahl A and Preskill J 2002 Topological quantum memory *J. Math. Phys.* **43** 4452–505

[13] Bombin H and Martin-Delgado M A 2007 Optimal resources for topological 2D stabilizer codes: comparative study *Phys. Rev.* A **76** 012305

[14] Kovalev A A, Dumer I and Pryadko L P 2011 Design of additive quantum codes via the code-word-stabilized framework *Phys. Rev.* A **84** 062319

[15] Bombin H and Martin-Delgado M A 2007 Homological error correction: classical and quantum codes *J. Math. Phys.* **48** 052105

[16] Bullock S S and Brennen G K 2007 Qudit surface codes and gauge theory with finite cyclic groups *J. Phys. A: Math. Theor.* **40** 3481

[17] Albuquerque C D, Palazzo R Jr and Silva E B 2009 Topological quantum codes on compact surfaces with genus $g \geqslant 2$ *J. Math. Phys.* **50** 023513

[18] Anderson J T 2011 Homological stabilizer codes arXiv:1107.3502

[19] Bravyi S, Hastings M B and Michalakis S 2010 Topological quantum order: stability under local perturbations *J. Math. Phys.* **51** 093512
[20] Nayak C, Simon S H, Stern A, Freedman M and Sarma S D 2008 Non-Abelian anyons and topological quantum computation *Rev. Mod. Phys.* **80** 1083–159
[21] Bombin H and Martin-Delgado M A 2006 Topological quantum distillation *Phys. Rev. Lett.* **97** 180501
[22] Fowler A G 2011 Two-dimensional color-code quantum computation *Phys. Rev.* A **83** 042310
[23] Sarvepalli P and Raussendorf R 2011 Efficient decoding of topological color codes arXiv:1111.0831
[24] Bombin H and Martin-Delgado M A 2007 Topological computation without braiding *Phys. Rev. Lett.* **98** 160502
[25] Bombin H and Martin-Delgado M A 2007 Exact topological quantum order in $D = 3$ and beyond: branyons and brane-net condensates *Phys. Rev.* B **75** 075103
[26] Ocko S A, Xie Chen, Bei Zeng, Beni Yoshida, Zhengfeng Ji, Ruskai M B and Chuang I L 2011 Quantum codes give counterexamples to the unique preimage conjecture of the N-representability problem *Phys. Rev. Lett.* **106** 110501
[27] Nussinov Z, Ortiz G and Cobanera E 2011 Effective and exact holographies from symmetries and dualities arXiv:1110.2179
[28] Katzgraber H G, Bombin H and Martin-Delgado M A 2009 Error threshold for color codes and random three-body Ising models *Phys. Rev. Lett.* **103** 090501
[29] Katzgraber H G, Bombin H, Andrist R S and Martin-Delgado M A 2010 Topological color codes on Union Jack lattices: a stable implementation of the whole Clifford group *Phys. Rev.* A **81** 012319
[30] Andrist R S, Katzgraber H G, Bombin H and Martin-Delgado M A 2011 Tricolored lattice gauge theory with randomness: fault tolerance in topological color codes *New J. Phys.* **13** 083006
[31] Ohzeki M 2009 Accuracy thresholds of topological color codes on the hexagonal and square-octagonal lattices *Phys. Rev.* E **80** 011141
[32] Ohzeki M and Nishimori H 2009 Analytical evidence for the absence of spin glass transition on self-dual lattices *J. Phys. A: Math. Theor.* **42** 332001
[33] Wang D S, Fowler A G, Hill C D and Hollenberg L C L 2009 Graphical algorithms and threshold error rates for the 2d colour code, arXiv:0907.1708
[34] Fowler A G, Wang D S and Hollenberg L C L 2010 Surface code quantum error correction incorporating accurate error propagation, arXiv:1004.0255
[35] Landahl A J, Anderson J T and Rice P R 2011 Fault-tolerant quantum computing with color codes arXiv:1108.5738
[36] Raussendorf R, Harrington J and Goyal K 2007 Topological fault-tolerance in cluster state quantum computation *New J. Phys.* **9** 199
[37] Bombin H and Martin-Delgado M A 2009 Quantum measurements and gates by code deformation *J. Phys. A: Math. Theor.* **42** 095302
[38] Chandrasekharan S and Wiese U-J 1997 Quantum link models: a discrete approach to gauge theories *Nucl. Phys.* B **492** p 455–71
[39] Davies E B 1974 Markovian master equations *Commun. Math. Phys.* **39** 91–110
[40] Alicki R and Lendi L 2007 *Quantum Dynamical Semigroups and Applications* (Berlin: Springer)
[41] Rivas A and Huelga S F 2011 *Open Quantum Systems. An Introduction* (Heidelberg: Springer)
[42] Breuer H-P and Petruccione F 2002 *The Theory of Open Quantum Systems* (Oxford: Oxford University Press)
[43] Frigerio A 1978 Stationary states of quantum dynamical semigroups *Commun. Math. Phys.* **63** 269
[44] Spohn H 1976 Approach to equilibrium for completely positive dynamical semigroups of N-level systems *Rep. Math. Phys.* **10** 189
Spohn H 1976 Approach to equilibrium for completely positive dynamical semigroups of N-level systems *Rep. Math. Phys.* **10** 189
[45] Spohn H 1977 An algebraic condition for the approach to equilibrium of an open N-level system *Lett. Math. Phys.* **2** 33

[46] Spohn H 1980 Kinetic equations from Hamiltonian dynamics: Markovian limits *Rev. Mod. Phys.* **52** 569
[47] Sarandy M S and Lidar D A 2005 Adiabatic quantum computation in open systems *Phys. Rev. Lett.* **95** 250503
[48] Ashhab S, Johansson J R and Nori F 2006 Decoherence in a scalable adiabatic quantum computer *Phys. Rev.* A **74** 052330
[49] Nussinov Z and Ortiz G 2008 Autocorrelations and thermal fragility of anyonic loops in topologically quantum ordered systems *Phys. Rev.* B **77** 064302
[50] Alicki R, Fannes M and Horodecki M 2009 On thermalization in Kitaev's 2D model *J. Phys. A: Math. Theor.* **42** 065303
[51] Alicki R and Fannes M 2009 Decay of fidelity in terms of correlation functions *Phys. Rev.* A **79** 012316
[52] Iblisdir S, Perez-Garcia D, Aguado M and Pachos J 2010 Thermal states of anyonic systems *Nucl. Phys.* B **829** 401–24
[53] Iblisdir S, Perez-Garcia D, Aguado M and Pachos J 2009 Scaling law for topologically ordered systems at finite temperature *Phys. Rev.* B **79** 134303
[54] Kargarian M 2009 Finite-temperature topological order in two-dimensional topological color codes *Phys. Rev.* A **80** 012321
[55] Karimipour V 2009 Complete characterization of the spectrum of the Kitaev model on spin ladders *Phys. Rev.* B **79** 214435
[56] Kim I H 2011 Stability of topologically invariant order parameters at finite temperature arXiv:1109.3496
[57] Bravyi S and Terhal B 2009 A no-go theorem for a two-dimensional self-correcting quantum memory based on stabilizer codes *New J. Phys.* **11** 043029
[58] Bombin H, Chhajlany R W, Horodecki M and Martin-Delgado M A 2008 Self-correcting quantum computers arXiv:0907.5228
[59] Plenio M B and Huelga S F 2002 Entangled light from white noise *Phys. Rev. Lett.* **88** 197901
[60] Huelga S F and Plenio M B 2007 Stochastic Resonance phenomena in quantum many-body systems *Phys. Rev. Lett.* **98** 170601
[61] Bombin H and Martin-Delgado M A 2005 Entanglement distillation protocols and number theory *Phys. Rev.* A **72** 032313
[62] Di Y-M and Wei H-R 2011 Elementary gates for ternary quantum logic circuit arXiv:1105.5485
[63] Weimer H, Müller M, Lesanovsky I, Zoller P and Büchler H P 2010 A Rydberg quantum simulator *Nature Phys.* **6** 382–8
[64] Tu H-H, Zhang G-M, Xiang T, Liu Z-X and Ng T-K 2009 Topologically distinct classes of valence-bond solid states with their parent Hamiltonians *Phys. Rev.* B **80** 014401
[65] Bombin H 2010 Topological subsystem codes *Phys. Rev.* A **81** 032301
[66] Suchara M, Bravyi S and Terhal B 2011 Constructions and noise threshold of topological subsystem codes *J. Phys. A: Math. Theor.* **44** 155301
[67] Yu S, Chen Q and Oh C H 2007 Graphical quantum error-correcting codes arXiv:0709.1780
[68] Dan H, Weidong T, Meisheng Z, Qing C, Sixia Y and Oh C H 2008 Graphical nonbinary quantum error-correcting codes *Phys. Rev.* A **78** 012306
[69] Rico E and Briegel H J 2008 2D multipartite valence bond states in quantum anti-ferromagnets *Ann. Phys.* **323** p 2115–31
[70] Bravyi S, Terhal B M and Leemhuis B 2010 Majorana fermion codes *New J. Phys.* **12** 083039
[71] Bombin H and Martin-Delgado M A A 2008 Family of non-abelian kitaev models on a lattice: topological confinement and condensation *Phys. Rev.* B **78** 115421
[72] Bombin H and Martin-Delgado M A 2008 Nested topological order arXiv:0803.4299
[73] Bais F A and Slingerland J K 2009 Condensate-induced transitions between topologically ordered phases *Phys. Rev.* B **79** 045316
[74] Buerschaper O and Aguado M 2009 Mapping Kitaev's quantum double lattice models to Levin and Wen's string-net models *Phys. Rev.* B **80** 155136
[75] Beigi S, Shor P W and Whalen D 2011 The quantum double model with boundary: condensations and symmetries *Commun. Math. Phys.* **306** 663–94

[76] Burnell F J, Simon S H and Slingerland J K 2011 Condensation of achiral simple currents in topological lattice models: Hamiltonian study of topological symmetry breaking *Phys. Rev.* B **84** 125434
[77] Bonzom V and Livine E R 2011 A new Hamiltonian for the topological BF phase with spinor networks arXiv:1110.3272
[78] Alicki R, Horodecki M, Horodecki P and Horodecki R 2008 On thermal stability of topological qubit in Kitaev's 4D model arXiv:0811.0033
[79] Si T and Yu Y 2007 Exactly soluble spin-1/2 models on three-dimensional lattices and non-Abelian statistics of closed string excitations, arXiv:0709.1302
[80] Si T and Yu Y 2008 Anyonic loops in three-dimensional spin liquid and chiral spin liquid *Nucl. Phys.* B **803** 428–49
[81] Mandal S and Surendran N 2009 Exactly solvable Kitaev model in three dimensions *Phys. Rev.* B **79** 024426
[82] Mandal S and Surendran N 2011 Topological excitations in three dimensional Kitaev model arXiv:1101.3718
[83] Bravyi S, Leemhuis B and Terhal B M 2011 Topological order in an exactly solvable 3D spin model *Ann. Phys.* **326** 839–66
[84] Haah J 2011 Local stabilizer codes in three dimensions without string logical operators *Phys. Rev.* A **83** 042330
[85] Kim I H 2011 Local non–Calderbank–Shor–Steane quantum error-correcting code on a three-dimensional lattice *Phys. Rev.* A **83** 052308
[86] Grover T, Turner A M and Vishwanath A 2011 Entanglement entropy of gapped phases and topological order in three dimensions arXiv:1108.4038
[87] Bacon D 2006 Operator quantum error-correcting subsystems for self-correcting quantum memories *Phys. Rev.* A **73** 012340
[88] Tsomokos D I, Ashhab S and Nori F 2010 Using superconducting qubit circuits to engineer exotic lattice systems *Phys. Rev.* A **82** 052311
[89] Bombin H, Kargarian M and Martin-Delgado M A 2009 Interacting anyonic fermions in a two-body color code model *Phys. Rev.* B **80** 075111
[90] Kargarian M, Bombin H and Martin-Delgado M A 2010 Topological color codes and two-body quantum lattice Hamiltonians *New J. Phys.* **12** 025018
[91] Sun K-W and Chen Q-H 2009 Quantum phase transition of the one-dimensional transverse-field compass model *Phys. Rev.* B **80** 174417
[92] Yang S, Zhou D L and Sun C P 2007 Mosaic spin models with topological order *Phys. Rev.* B **76** 180404
[93] Müller M, Hammerer K, Zhou Y L, Roos C F and Zoller P 2011 Simulating open quantum systems: from many-body interactions to stabilizer pumping *New J. Phys.* **13** 085007
[94] Weimer H, Müller Büchler H P and Lesanovsky I 2011 Digital quantum simulation with Rydberg atoms arXiv:1104.3081
[95] Gao W-B, Fowler A G, Raussendorf R, Yao X-C, Lu H, Xu P, Lu C-Y, Peng C-Z, Deng Y, Chen Z-B and Pan J-W 2009 Experimental demonstration of topological error correction arXiv:0905.1542
[96] Levy J E, Ganti A, Phillips C A, Hamlet B R, Landahl A J, Gurrieri T M, Carr R D and Carroll M S 2009 The impact of classical electronics constraints on a solid-state logical qubit memory arXiv:0904.0003
[97] Albuquerque A F, Katzgraber H G, Troyer M and Blatter G 2008 Engineering exotic phases for topologically protected quantum computation by emulating quantum dimer models *Phys. Rev.* B **78** 014503
[98] Brennen G K, Aguado M and Cirac J I 2009 Simulations of quantum double models *New J. Phys.* **11** 053009
[99] Mazza L, Rizzi M, Lewenstein M and Cirac J I 2010 Emerging bosons with three-body interactions from spin-1 atoms in optical lattices *Phys. Rev.* A **82** 043629
[100] Jansen L and Boon H 1967 *Theory of Finite Groups. Application in Physics* (Amsterdam: North-Holland)

Part II

Long-range Topological Superconductivity

7

Introduction to superconductivity

Superconductivity [Tin04, AM76, Kit63, AGD75, Ann04] is generally defined as a property of certain materials that present exactly **zero resistance** to the movement of electrons, below a certain critical temperature T_c. It was first discovered by Onnes in Leiden in 1917 [Onn11]. He showed that at very low temperatures[1], the resistance of mercury drops to zero. Superconductivity can also be viewed as a paradigmatic example of how purely quantum properties operate at the macroscopic level. A finite fraction of electrons do truly condensate into a *superfluid* macrostate, that extends all over the system.

There is another equally surprising experimental property that was observed a few years latter by Meissner and Ochsenfeld [MO33], the so-called **Meissner effect**. This accounts for the screening of a magnetic field by a superconductor, i.e. the superconductor expels the magnetic field from its interior[2]. A direct consequence of this effect is the existence of persisting electric currents that compensate the applied external magnetic field.

From the theoretical side, after a first trial by Gorter and Casimir [GC34], the first phenomenological description of superconductivity was **London theory**. It was proposed by brothers Fritz and Heinz London in 1935 [LL35], based on simple arguments using Newton's second law and Faraday's law. A major achievement of the theory is the capability to explain the Meissner effect.

The next big leap in the theory of superconductivity didn't arrive until 1950, when Ginzburg and Landau [GL50] gave a macroscopic description of the phenomena. Their theory combines Landau theory of second-order phase transitions

[1] at liquid Helium temperatures, i.e. around 4K.

[2] Sometimes this effect is also referred to as **perfect diamagnetism**.

with a Schrödinger-like wave equation, and had a great success in explaining the macroscopic properties of superconductors. They proposed the existence of an effective wave function that corresponds to the local density of condensed electrons, which they treat as an order parameter. Lately, Abrikosov showed that **Ginzburg-Landau theory** predicts the division of superconductors into two categories now referred as Type I and Type II [Abr57].

Despite those successful trials, a microscopic description of the physical mechanism behind superconductivity was still missing. The first hint shedding light over this problem came from the experimental side. Maxwell [Max50] and independently Reynolds *et al.* [RSWN50] realised that the critical temperature T_c for superconductivity depends on the isotope mass M_{I} of the sample. This is called the **isotope effect**, $T_c \sim 1/M_{\mathrm{I}}^{\delta}$, where δ is a certain exponent. With the exception of several transition group elements, for most of superconductors $\delta = 1/2$. There is a direct implication of this effect. If T_c depends on M_{I}, it means that phonons (created by lattice vibrations) have to play an essential role in the physical mechanism that explains superconductivity. Actually, the coupling constant g_{e-p} that describes **electron-phonon interaction** explicitly depends on M_{I} through a power-law with exponent $\delta = 1/2$ [Kit63].

Based on this idea, Cooper [Coo56] showed that an arbitrarily small attraction between two electrons, placed right above the Fermi surface, induces a bound state with a lower energy than the Fermi energy. The state that is formed out of the two paired electrons is commonly called **Cooper pair**. Actually, the argument that favours the formation of a Cooper pair works even if the mediating interaction is different from electron-phonon interaction. This aspect will become important when we will try to explain unconventional superconductivity in the next chapter. Anyhow, when Cooper published his paper, he was clearly influenced by the isotope effect and the interaction between electrons and lattice vibrations[3].

Finally, the microscopic **BCS theory** of superconductivity was proposed by Bardeen, Cooper and Schrieffer in 1957 [BCS57]. They proposed a variational ansazt for the many-body wave function which is basically a condensate of Cooper pairs. The ansatz was later found to be exact in the dense limit of pairs. Moreover, it predicts extremely well most properties of superconductors. In the following section we will present a brief introduction to this theory.

7.1 BCS superconductivity

The BCS theory is a beautiful example of how a simple (but non-trivial) theory is able to explain with precision the essential effects linked to superconductivity. In this chapter, we do not intend to give a complete and self-contained derivation of

[3]Cooper (1956): *"Consider a pair of electrons which interact above a quiescent Fermi sphere, with an interaction of the kind that might be expected due to the phonon and the screened Coulomb fields. If there is a net attraction between the electrons, it turns out that they can form a bound state..."*

BCS theory[4]; but to explain its main ingredients and to show what we can learn in order to describe topological superconductors later on. The BCS theory is based on 3 key ideas:

1. The direct interaction between two electrons is repulsive. However, inside a solid, the effective force between electrons can sometimes be attractive when it is mediated by lattice phonons. This is due to the screening that positively-charged ions produce on the electron-electron repulsive interaction.

2. Above the Fermi surface, if one puts two electrons, they tend to form a bound state below the Fermi energy of a free electron gas. This statement holds no matter how weak the attractive force is [Coo56].

3. Schrieffer showed that actually all electrons near the Fermi surface tend to form Cooper pairs. Moreover, there is a **gap**[5] linked to the breaking up of a Cooper pair into two free electrons. This is one of the main reasons that make superconductivity possible, the robustness under scattering processes of Cooper pairs.

Remarkably, BCS theory provides a microscopic description of the phenomenon, that goes far beyond the previous theory proposed by Ginzburg and Landau. BCS explains almost all the general features of superconductivity. It predicts the existence of a critical temperature T_c for the superconductive transition to occur. But it also predicts the dependence of T_c with the Debye temperature of the metal and the coupling strength of the electron-phonon interaction (which in the standard theory is assumed to be small). In the light of BCS, the effective wave function in Ginzburg-Landau theory represents the centre-of-mass distribution of Cooper pairs.

Let us now give the main hints for the microscopic derivation of BCS theory. The total Hamiltonian for the electrons, phonons and the interaction among them is given by

$$H = H_0 + H_{\mathrm{I}} = \sum_{k,s} \epsilon_k a^\dagger_{k,s} a_{k,s} + \sum_q \omega_q b^\dagger_q b_q + \mathrm{i}D \sum_{k,q,s} a^\dagger_{k+q,s} a_{k,s} (b_q - b^\dagger_{-q}), \tag{7.1}$$

where the index k/q is the crystalline momentum, $s = \uparrow, \downarrow$ stands for spin up or down, a_j ($a^\dagger_j$) are annihilation (creation) fermionic operators (electrons), and b_j ($b^\dagger_j$) are annihilation (creation) bosonic operators (phonons). The coupling constant D mediates an indirect interaction between two electrons. One of the electrons

[4] A detailed and pedagogical description of BCS theory can be found in Refs. [Tin04, AM76, Kit63, Ann04].

[5] There are several ways to observe the energy **gap** in the excitation spectrum of a superconductor. For instance, the threshold in frequency for absorbing light gives a value for the energy gap. Another method is to measure the electron tunneling current. No current will flow until the applied voltage exceeds the energy gap $V > \Delta E$.

polarises the lattice while the other electron interacts with this polarisation. At the end of the day, we can derive an effective interaction between two electrons a mediated by phonons b.

As explained in [Kit63] in great detail, it is possible to perform a canonical transformation over Hamiltonian (7.1), trace out the bosonic degrees of freedom and keep terms up to $O(D^2)$ (assuming the interaction is weak enough). Then, the interacting part of H can be written as

$$H_{\mathrm{I}} = D^2 \sum_{\substack{k,k,q \\ s,s'}} \frac{\omega_q}{(\epsilon_k - \epsilon_{k-q})^2 - \omega_q^2} a^\dagger_{k+q,s} a^\dagger_{k'-q,s'} a_{k',s'} a_{k,s}. \tag{7.2}$$

As we can see from Eq. (7.2), the interaction is attractive as long as $|\epsilon_{k\pm q} - \epsilon_k| < \omega_q$. But even within the attractive sector, the interaction is screened by Coulomb repulsion between electrons. However, we can confidently assume that the attraction is dominant around the Fermi energy

$$\epsilon_{\mathrm{F}} - \omega_{\mathrm{D}} < \epsilon_k, \epsilon_{k\pm q} < \epsilon_{\mathrm{F}} + \omega_{\mathrm{D}} \,, \tag{7.3}$$

where ω_{D} is the **Debye energy**[6]. The repulsive region in Eq. (7.2) can be safely neglected, and the attractive coupling can be taken as a constant for simplicity,

$$H_{\mathrm{I}} = -V \sum_{\substack{k,k,q \\ s,s'}} a^\dagger_{k+q,s} a^\dagger_{k'-q,s'} a_{k',s'} a_{k,s}. \tag{7.4}$$

where the sum is over all values of k, k', q, s and s' with the restriction that the electron energies involved are all within the range $\pm\omega_{\mathrm{D}}$ of the Fermi surface.

In addition, the formation of a Cooper pair $(k, -k)$ whose center of mass momentum is zero ($K_{\mathrm{CM}} = 0$) minimises the energy of the pair. Regarding the spin part of the wave function, it can be either in a **spin singlet** ($s \otimes s' = 0$) or a **spin triplet** ($s \otimes s' = 1$) state. Superconductors described by BCS theory form spin singlet Cooper pairs. On the other hand, those phases described by spin triplet states are known as **unconventional superconductors** and they will be described in the next section.

Taking into account the previous assumptions, we restrict Eq. (7.2) to electron pairs $(k, -k)$ and spin singlet channel,

$$H = \sum_{k,s} \epsilon_k a^\dagger_{k,s} a_{k,s} - V \sum_{k,k} a^\dagger_{k\uparrow} a^\dagger_{-k\downarrow} a_{-k'\downarrow} a_{k'\uparrow}. \tag{7.5}$$

Although we have very much simplified the original Hamiltonian (7.1), the interaction in Eq. (7.8) is still quartic in fermionic operators and cannot be solved exactly. In order to overcome this problem, Bardeen, Cooper and Schrieffer [BCS57]

[6] Roughly speaking, the **Debye energy** gives the maximum phonon frequency of oscillation in the low temperature limit.

proposed the following variational ansatz for the ground state,

$$|\Psi_{\text{BCS}}\rangle = \prod_k \; u_k + v_k a^\dagger_{k\uparrow} a^\dagger_{-k\downarrow} \; |0\rangle, \tag{7.6}$$

where $|0\rangle$ is the state with no electrons at the Fermi surface, and the parameters u_k and v_k ($|u_k|^2 + |v_k|^2 = 1$) have to be determined by energy minimisation (variational method). Actually, Eq. (7.6) describes a coherent state of Cooper pairs with a lower energy than the Fermi energy of a free electron gas.

Equivalently, one can find that $|\Psi_{\text{BCS}}\rangle$ is also the mean field ground state solution of H. The mean field is performed assuming a non-vanishing off-diagonal expectation value $\langle a_{-k\downarrow} a_{k\uparrow}\rangle$, for which the **superconducting gap** Δ is given by

$$\Delta = V \sum_k \langle a_{-k\downarrow} a_{k\uparrow}\rangle. \tag{7.7}$$

After some straightforward calculations [Tin04, AM76, Kit63, Ann04], the mean-field Hamiltonian (up to some zero point energy offsets) casts the form

$$H_{\text{mf}} = \sum_{k,s} \epsilon_k a^\dagger_{k,s} a_{k,s} - \sum_k \left(\Delta a^\dagger_{k\uparrow} a^\dagger_{-k\downarrow} + \Delta^* a_{-k\downarrow} a_{k\uparrow}\right). \tag{7.8}$$

One can study the quasiparticles excitation spectra applying a **Bogoliuvov-Valatin transformation**[7] to Hamiltonian (7.8),

$$H_{\text{mf}} = \sum_k E_k \;\; c^\dagger_{k\uparrow} c_{k\uparrow} + c^\dagger_{-k\downarrow} c_{-k\downarrow} \tag{7.9}$$

where $E_k = \sqrt{\epsilon_k^2 + \Delta^2}$ and the operators

$$\begin{aligned} c_{k\uparrow} &= u_k^* a_{k\uparrow} - v_k^* a^\dagger_{-k\downarrow} \;\; , \\ c^\dagger_{-k\downarrow} &= v_k a_{k\uparrow} + u_k a^\dagger_{-k\downarrow} \;\; , \end{aligned} \tag{7.10}$$

satisfy the canonical fermionic anticonmutation relations as well. The new quasiparticles created and annihilated by these operators are not found in the BCS ground state given in Eq. (7.6). We can easily check that

$$\begin{aligned} c_{k\uparrow}|\Psi_{\text{BCS}}\rangle &= 0 \; , \\ c_{-k\downarrow}|\Psi_{\text{BCS}}\rangle &= 0 \; . \end{aligned} \tag{7.11}$$

Thus, the BCS ground state is the vacuum for these **Bogoliuvov quasi-particles**. At finite temperature T, the occupation number of these modes will be given by the Fermi-Dirac distribution instead. Finally, the superconducting gap Δ can be

[7] A canonical transformation that diagonalises the Hamiltonian and preserve the anticommutation rules of the original operators.

determined by a self-consistent equation. The computation of this quantity can be found in the literature [Kit63], although it is not of particular interest for the purpose of this thesis.

Summarising, we have derived a mean-field Hamiltonian [Eq. (7.8)] that is able to describe the main features of superconductivity. From Eq. (7.6), we can see that the ground state of this Hamiltonian is given by a condensate of Cooper pairs of electrons with opposite crystalline momentum $(k, -k)$ forming a spin singlet. The Bogoliuvov quasiparticles [Eq. (7.10)] represent the excitations of the system. In BCS theory, the pairing terms $\Delta a^{\dagger}_{k\uparrow} a^{\dagger}_{-k\downarrow}$ arise from electron-phonon interactions [Eq. (7.2)]. This term breaks the $U(1)$ gauge symmetry of Hamiltonian (7.8) linked to charge conservation.

In the next section, we will consider different (unconventional) forms of superconducting pairing, that are not captured by standard BCS theory. That will form the basis to define topological superconductors.

7.2 Unconventional and topological superconductivity

The majority of superconducting materials that were known until the 70's were described by an attractive interaction among electrons mediated by phonons. According to BCS, the interacting channel is the most symmetric one ($l = 0$ or s-wave) and spin singlet. In these superconductors, the electron-phonon interaction overcomes Coulomb repulsion through the retardation effect[8]. However, in several transition metals where electrons are tight to atomic orbitals, **Coulomb interaction** dominates over the attractive electron-phonon coupling and novel mechanisms are needed to explain superconductivity.

The first example that could not be fitted into the BCS paradigm was the A and B phases of superfluid ^3He discovered by Osheroff, Richardson and Lee [ORL72] in 1972. In ^3He, Cooper pairs of fermionic atoms are characterised by p-wave ($l = 1$) pairing and a spin-triplet state. The pairing mechanism is of non-phononic nature, and it is mediated by Van der Waals and spin fluctuation interactions [Leg75]. The later discovery of **high-temperature superconductivity** in cuprate compounds [BM86] definitely popularised the field of unconventional superconductivity.

With this increasing interest in the field, there has been mainly two different lines of research. The first approach focuses on understanding the microscopic mechanism that leads to more exotic forms of pairing than in standard BCS theory. The second approach is concerned with the new **quasi-particle** phenomena the appears in these systems, in the spirit of Eq. (7.10).

The field of **topological superconductors** follows this second path [BAB13]. They have received a lot of attention since they produce novel quasi-particles

[8] Conduction electrons are not well localised within atomic orbitals in a normal metal, and they move much faster than the ions, behaving basically as free particles.

that behave as **Majorana fermions**[9] [Wil09]. Topological superconductors have been shown to be realisable by means of proximity effect of a normal superconductor to a topological insulator [FK08], in graphene [SJLA+15], etc. Actually, there has been recent groundbreaking experiments [MZF+12, DYH+12, DRM+12, NPDL+14, AHM+16, SZH+16] providing strong evidence for the presence of Majorana fermions, and thus topological superconductors.

From now on, we suppose that there exists some source of underlaying pairing mechanism that can be well described using a **mean-field** formulation. Therefore, we are interested in non-interacting quasi-particles *dressed* by a background pairing potential. We will not analyse additional effects that may arise from a self-contained microscopic description of every element of the problem.

The first theoretical proposal of a topological superconductor, displaying Majorana fermions as **zero-energy modes** at the boundary, was done by Kitaev [Kit01]. In what follows, we will analyse the simple but non-trivial model that he proposed. We will show how these new quasi-particles arise, and the reason to call these systems topological.

Consider a model of spin-polarised fermions hopping on a L-site one-dimensional chain, with ***p*-wave superconducting pairing**. The Hamiltonian of this system introduced by Kitaev [Kit01] is

$$H_{\mathrm{MC}} = \sum_{j=1}^{L} \; -J a_j^\dagger a_{j+1} + M a_j a_{j+1} - \tfrac{\mu}{2} a_j^\dagger a_j + \mathrm{h.c.} \quad , \tag{7.12}$$

where μ is the chemical potential, $J > 0$ is the hopping amplitude, the absolute value of $M = |M|\mathrm{e}^{\mathrm{i}\theta}$ stands for the superconducting gap, and a_j ($a_j^\dagger$) are annihilation (creation) fermionic operators. Note the analogy of this Hamiltonian to the BCS one in Eq. (7.8) in chapter 7. Both are quadratic Hamiltonians with aa and $a^\dagger a^\dagger$ terms, where the $U(1)$ charge conservation symmetry has been broken to Z_2 (fermion parity conservation). The symmetry of the pairing term in Eq. (7.12) is of p-wave type, different from Eq. (7.8) (s-wave). This becomes clear by writing the pairing term $M a_j a_{j+1}$ in Fourier space $M \sin(k) a_k a_{-k}$, which is and odd function (p-wave) of k. On the contrary, in BCS theory, the pairing potential is even (s-wave).

The model in Eq. (7.12) can effectively reproduce a semiconductor nano-wire in the vicinity of an s-wave superconductor [MZF+12], where the p-wave pairing is

[9] A **Majorana fermion** is a fermionic particle that is its own antiparticle. It was originally proposed by Ettore Majorana [Maj08] in 1937, while looking for real solutions of the Dirac equation. There is however a difference between the original Majorana fermion proposed in the context of particle physics and the quasi-particle that appears in condensed matter. In particle physics, a Majorana fermion follows Dirac statistics, the same as electrons and other usual Dirac fermions. In condensed matter, Majorana fermions follow non-abelian anyonic statistics, although they satisfy the fermionic anticommutation relations and they are their own anti-particle too. In order to state that difference with respect to particle physics, they are often called **Majorana zero modes**, as they appear as mid-gap zero energy states.

induced by **proximity effect**. It is now convenient to express Hamiltonian (7.12) in terms of Majorana fermion operators

$$\begin{aligned} c_{2j-1} &= \frac{1}{\sqrt{2}} \left(e^{-\frac{i\theta}{2}} a_j^\dagger + e^{\frac{i\theta}{2}} a_j \right) , \\ c_{2j} &= \frac{i}{\sqrt{2}} \left(e^{-\frac{i\theta}{2}} a_j^\dagger - e^{\frac{i\theta}{2}} a_j \right) , \end{aligned} \tag{7.13}$$

satisfying the Majorana anticommutation relation $\{c_i, c_j\} = \delta_{ij}$ and $c_j^\dagger = c_j$. Majorana fermions in these systems usually pair locally in such a way that they constitute an ordinary Dirac fermion. However, for open boundary conditions, and particular values of the coupling constants (J, M and μ), two Majorana fermions at the boundary remain unpaired. These transformations are the equivalent ones to the Bogoliuvov-Valatin transformations introduced in chapter 7 in Eq. (7.10). For simplicity, let us take $\theta = 0$ and $|M| = J$. This model belongs to the **BDI symmetry class**[10] and can also be realised by coupling a topological insulator in the chiral-unitary AIII class to a normal s-wave superconductor [HWC+14]. We now express Hamiltonian (7.12) in the Majorana basis (7.13), obtaining

$$H = iJ \sum_{j=1}^{L-1} c_{2j} c_{2j+1} - i\mu \sum_{j=1}^{L} c_{2j-1} c_{2j}, \tag{7.14}$$

Let us first study the two limiting cases. If $J = 0$, then each Majorana pairs locally with another Majorana within the same site. This is the standard topologically trivial phase. We now focus on the opposite limit, where $J = 0$ but $\mu = 0$. In that case, each Majorana couples with another Majorana belonging to a neighbouring site. However, the Majorana operators at the edges c_1 and c_{2N} do not appear in the Hamiltonian, being zero energy modes. They are decoupled from the dynamics. These Majorana zero modes (MZMs) are **topologically protected** and represent a hallmark of topological order in the system. A pictorial image is shown in Fig. 7.1. Actually, as long as $|\mu| < J$ the system remains in the topological phase, and the two Majoranas are exponentially localised at the ends of the chain.

But a question remains: *Why is this superconducting phase called topological?*

In what follows, we elaborate on the answer to this pertinent question. Along the first part of this thesis, we have seen simple models for topological insulators that can be characterised by a two-band Hamiltonian separated by a gap. The mathematical description relies on the fact that in momentum space, the Hamiltonian of a topological insulator can be written in an spinor basis such that

$$H = \sum_k \Psi_k^\dagger H_k \Psi_k, \tag{7.15}$$

[10] Hamiltonians that belong to the **BDI symmetry class** of topological superconductors [RSFL09, Kit09] are invariant under particle-hole, time-reversal and chiral symmetry transformations. Additionally, they conserve the **fermion parity**, which is the total number of fermions modulo 2.

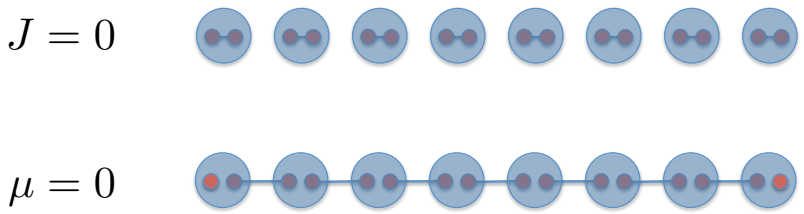

FIGURE 7.1: The big blue dots stand for the original Dirac fermions. Red dots stand for Majorana operators as defined in Eq. (7.13). (a) The first chain represents the trivial superconductor where Majorana fermions pair locally into a standard Dirac Fermion. (b) The second chain is a topological superconductor where the Majoranas pair between adjacent sites. The two Majoranas at the edge remain unpaired and decoupled from the dynamics.

where $\Psi_k = \left(a_k, b_k\right)^{\mathrm{t}}$ is the spinor, $\{a_k, b_k\}$ stand for two different fermion species, and H_k is a 2×2 matrix. The diagonalisation of H_k yields the ground state of the system, that corresponds to the lower band eigenvector $|u\rangle_k$ (valence band). The upper band eigenvector $|v\rangle_k$ represents the excitations to the conduction band. The two bands are well separated by an energy gap, which turns the system into an insulator. As we have shown in chapter 1, the **Berry phase** Φ_{B} picked up by $|u\rangle_k$ along the holonomy covering the entire BZ, acquires a topological and quantised character. It helps us distinguish between trivial and non-trivial topological phases, also highlighted by the presence of edge states.

For topological superconductors, an analogous situation occurs. The Hamiltonian in Eq. (7.12) can be written in momentum space as $H = \sum_k \Psi_k^\dagger H_k \Psi_k$ (similar to Eq. (7.15)). However, $\Psi_k = \left(a_k, a_{-k}^\dagger\right)^{\mathrm{t}}$ stands for the **Nambu-spinor** basis of paired fermions [AS10]. The system also has a gap that represents the cost of creating a Bogoliuvov quasi-particle. The Berry phase Φ_{B} picked up by the ground state $|GS\rangle_k$ along the holonomy covering the entire BZ also classifies the topology of the system. In the particular case of Hamiltonian (7.14) for the Kitaev chain, there is a trivial phase ($\Phi_{\mathrm{B}} = 0$) with no edge states, and a non-trivial topological phase ($\Phi_{\mathrm{B}} = \pi$) linked to the **unpaired MZMs** at the edges.

In the next chapter, based on publication **P7**, we include long-range deformations in the hopping and pairing terms of Eq. (7.12), and study how the topological phase diagram is modified. Moreover, we prove that new topological quasiparticles are created: **non-local massive Dirac fermions**.

8 Long-range Kitaev chain

8.1 Motivation

More than 70 years ago, Peierls [E23, E35] and Landau [Lan37, LL00] showed that no classical (finite temperature) second order phase transition can occur in 1D with **short range interactions**, due to the absence of long-range order and spontaneous symmetry breaking. For instance, this occurs with the classical Ising model in 1D [Isi25]. The idea behind the absence of a FM phase transition is that the energy cost to create an excitation is independent of the length of a magnetic domain; however, the entropy grows logarithmically with the length of the chain.

Nevertheless, these arguments are only valid as long as purely short range interactions are considered. In 1969, Dyson proposed a modified Ising model with a pairwise coupling, that decreases algebraically with the distance between spins [Dys69a, Dys69b]. Because of **long-range interaction**, he demonstrated that depending on the power-law decaying exponent, the model can display phase transitions and long-range order even in 1D.

The previous example illustrates that the inclusion of long-range interactions can qualitatively modify the phase diagram of a system, with respect to purely short-range interacting terms. It may happen that long-range effects lead to drastic changes and not only to a mere reshaping of the phases that already exited for purely short-range interactions. A detail and comprehensive discussion on the role of long-range interactions in statistical mechanics can be found in [Muk09].

With that motivation, we will try to answer the following question:

- *What happens when we consider long-range effects in topological superconductors?*

To this end, we consider the 1D Kitaev chain [Kit01] and study the result of incorporating **long-range couplings** [VLE+14] (hopping and pairing deformations of Eq. (7.12)) in the spirit of the pioneering work by Dyson [Dys69a, Dys69b]. Despite the simplicity of this topological superconductor model, it produces many novelties with respect to the standard short-range version [Kit01].

8.2 Outline of the main results

- ✓ We propose the most general extension of the Kitaev chain including long-range couplings.
- ✓ Deformation of the hopping terms (kinetic) allows us to significantly increase the region in the phase diagram where Majorana modes are present (Fig. 1 of the paper).
- ✓ This Hamiltonian may be realisable in simulations of topological superconductors using cold atoms in optical lattices. Here, the penetration length of the hopping can be tuned by changing the optical depth of the lattice.
- ✓ We consider pairing amplitudes decaying with a power-law of the distance between fermions. For sufficiently slow decaying pairing terms we find non-local massive Dirac edge states. These are new physical quasiparticles that are absent in the standard Kitaev model.
- ✓ An immediate consequence of these new topological massive Dirac edge states is the appearance of a new platform for topological quantum computation based on Dirac particles.
- ✓ We present the complete phase diagram of the model based on analytical and numerical methods (Fig. 3 of the paper).
- ✓ The topological structure of the winding number is changed by the long-range, although it is still able to discriminate between different topological phases.
- ✓ Interestingly enough, we find a crossover sector where it is possible to have both Majorana quasiparticles and non-local Dirac quasiparticles depending on the chemical potential of the system.
- ✓ In the SM of the paper, we have shown how to analytically construct the new edge modes in the presence of long-range.
- ✓ We have shown by means of finite size scaling, that the non-local Dirac modes remain massive in the thermodynamic limit. Thus proving, that this is not a finite size effect but a purely long-range one.

✓ By incorporating static disorder into the system, we show the robustness of the new massive Dirac quasiparticles, due to their topological character.

Topological massive Dirac edge modes and long-range superconducting Hamiltonians

O. Viyuela,[1] D. Vodola,[2] G. Pupillo,[2] and M. A. Martin-Delgado[1]
[1]*Departamento de Física Teórica I, Universidad Complutense, 28040 Madrid, Spain*
[2]*icFRC, IPCMS (UMR 7504) and ISIS (UMR 7006), Université de Strasbourg and CNRS, 67000 Strasbourg, France*
(Received 26 November 2015; published 13 September 2016)

We discover novel topological effects in the one-dimensional Kitaev chain modified by long-range Hamiltonian deformations in the hopping and pairing terms. This class of models display symmetry-protected topological order measured by the Berry/Zak phase of the lower-band eigenvector and the winding number of the Hamiltonians. For exponentially decaying hopping amplitudes, the topological sector can be significantly augmented as the penetration length increases, something experimentally achievable. For power-law decaying superconducting pairings, the massless Majorana modes at the edges get paired together into a massive nonlocal Dirac fermion localized at both edges of the chain: a new topological quasiparticle that we call topological massive Dirac fermion. This topological phase has fractional topological numbers as a consequence of the long-range couplings. Possible applications to current experimental setups and topological quantum computation are also discussed.

DOI: 10.1103/PhysRevB.94.125121

I. INTRODUCTION

The quest for the experimental realization of topological superconductors has turned out to be far more elusive than for their insulating counterparts. Simple models for topological superconductors have been proposed [1,2], but yet their unambiguous implementation is challenging in condensed matter or with quantum simulations. Here we address the issue as to whether those simple models [3,4] are in fact very specific in hosting their long sought-after topological properties. Quite on the contrary, we find that these properties can not only be generic with respect to natural extensions of the model-Hamiltonian terms, but also that Hamiltonian deformations can give rise to unconventional topological edge-mode physics that is novel *per se* and for applications in topological quantum computation.

The appearance of topological superconductors is having a strong impact [5–10] in condensed matter physics and quantum simulators. A tremendous effort is now directed at the experimental demonstration of existing topological models and at the development of new ones that may be easier to realize. What makes a topological superconductor interesting is the presence of Majorana modes as zero-energy localized modes at the edges or boundaries of the material. These modes lie within the superconducting gap and are rather exotic since Majorana fermions are their own antiparticles (holes). Standard (nontopological) superconductors do not exhibit such modes in their energy spectrum. Thus, topological superconductors represent new physics: Majorana modes are topologically protected against local perturbations disturbing the system and cannot be removed unless a topological phase transition occurs. This robustness makes them useful for storing and manipulating quantum information in a topological quantum computer.

In this paper we focus on the Kitaev chain model and propose novel modifications of the basic Hamiltonian, in order to enrich the appearance of Majorana physics (see Fig. 1) and even new topological excitations (see Fig. 2, Fig. 3). These modifications come in two ways: (i) exponentially decaying kinetic terms and (ii) long-range (LR) interaction terms. They produce novel beneficial topological effects and new unconventional topological physics, respectively. In case (ii), we propose a hopping deformation that allows us to significantly increase the region in the phase diagram where Majorana zero modes (MZMs) are present. Interestingly enough, this modification may result in a realistic description for cold atoms in optical lattices. In case (ii), we study the topological properties of another complementary modification of the Kitaev model based on long-range pairing terms decaying algebraically with a certain exponent α. We discover novel topological effects not found in any simple model before (see Fig. 2): for $\alpha < 1$ the model suffers a major qualitative change manifested in the absence of MZMs that are transmuted onto Dirac modes, which are massive nonlocal edge states. These new edge states are topologically protected against perturbations that do not break fermion parity nor particle-hole symmetry. These modes appear as midgap superconducting states that cannot be absorbed into bulk states. These topological massive Dirac edge states are new physical quasiparticles that are absent in the standard Kitaev model. They represent a new unconventional topological phase.

II. LONG-RANGE DEFORMATIONS OF SUPERCONDUCTING HAMILTONIANS

We consider a model of spinless fermions on an L-site one-dimensional chain, with p-wave superconducting pairing and a hopping term. The Hamiltonian of the system is

$$H = \sum_{j=1}^{L}\left(-J\sum_{l=1}^{L-1}\frac{1}{r_{l,\xi}}a_j^\dagger a_{j+l} + M\sum_{l=1}^{L-1}\frac{1}{R_{l\alpha}}a_j a_{j+l} - \frac{\mu}{2}\left(a_j^\dagger a_j - \frac{1}{2}\right) + \text{H.c.}\right), \tag{1}$$

where μ is the chemical potential, $J > 0$ is the hopping amplitude, the absolute value of $M = |M|e^{i\Theta}$ stands for the superconducting gap, $a_j(a_j^\dagger)$ are annihilation (creation) fermionic operators. The Hamiltonian deformations are $r_{l,\xi}, R_{l,\alpha}$. They are generic functions of an integer distance l, and parameters ξ and α, respectively. The total number of fermions modulo 2 is called the fermion parity and it is a conserved quantity for all

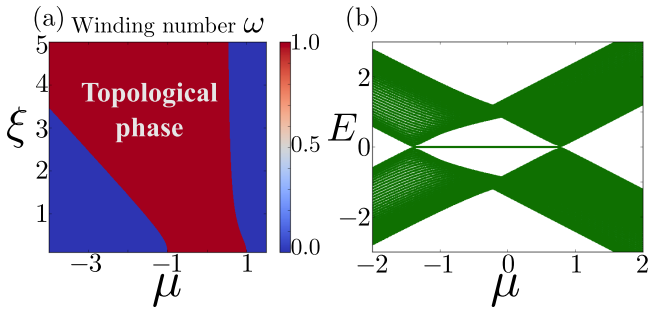

FIG. 1. (a) Topological phase diagram for the Kitaev chain with exponentially decaying hopping. As the penetration length ξ increases, the topological phase ($\Phi_B = \pi\omega = \pi$) gets enlarged. For $\xi \to 0$ we recover the well-known Majorana chain with nearest-neighbour hopping only. (b) Energy spectrum for $\xi = 0.8$. The region with MZMs $\mu \in (-1,1)$ in the original model has been augmented in one to one correspondence with a nontrivial Berry phase and winding number.

models in (1). Considering only nearest-neighbors hopping and pairing, we recover the famous model introduced by Kitaev [4]. This model is topological displaying MZMs at the edges like in Fig. 2(a). In the topological phase, the ground state of the Kitaev model is twofold degenerate: a bulk of with even fermion parity, while populating the two Majorana modes at the edges amounts to a single ordinary fermion and odd parity. The conservation of fermion parity and the nonlocal character of the unpaired Majoranas at the edges make the system an ideal candidate for a topological qubit out of the twofold degenerate ground state [11,12].

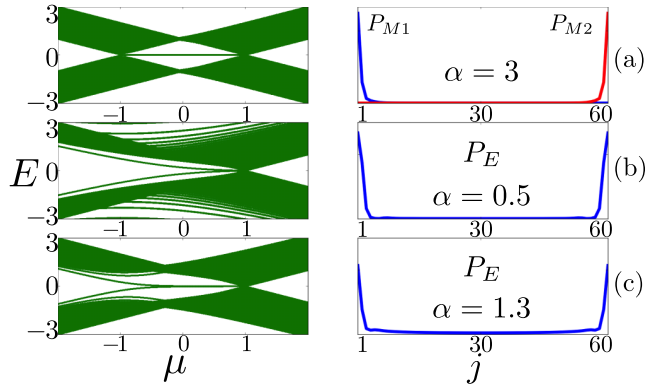

FIG. 2. Left: We plot the spectrum for the Kitaev chain with long-range decaying pairing, for $L = 60$ sites. On the right-hand side we show the probability distribution P_E of the edge modes for different topological phases. (a) Majorana sector with $\alpha = 3$. We can see MZMs for $\mu \in [-1,1]$ localised at the edges of the chain, as plotted on the right-hand side for $\mu = -0.5$ (P_{M1} and P_{M2}). Notice that each Majorana mode is decoupled, represented with different colors. (b) Massive Dirac sector with $\alpha = 0.5$. Within the new topological phase ($\mu < 1$), there are topological massive Dirac fermions localised at both edges at the same time, as shown on the right-hand side for $\mu = -1.5$. (c) Crossover sector with $\alpha = 1.3$. There are both MZMs and massive Dirac fermions depending on the value of μ. We plot the probability for a massive Dirac fermion at $\mu = -1.2$.

Without loss of generality, we may fix the pairing amplitude to be real and $M = J = \frac{1}{2}$. Assuming periodic boundary conditions, we can diagonalize the Hamiltonian deformations (1) in Fourier space and in the Nambu-spinor basis representing paired fermions [13]: $H = \frac{1}{2}\sum_k \Psi_k^\dagger H_k \Psi_k$, where $\Psi_k = (a_k, a_{-k}^\dagger)^t$ and H_k is of the form $H_k = E_k \boldsymbol{n}_k \cdot \boldsymbol{\sigma}$. The energy dispersion relation is given by E_k, $\boldsymbol{\sigma}$ is the Pauli matrix vector and $\boldsymbol{n}_k$ is a unit vector called winding vector. Explicitly,

$$\boldsymbol{n}_k = -\frac{1}{E_k}(0, f_\alpha(k), \mu + g_\beta(k)),$$
$$E_k = \sqrt{(\mu + g_\xi(k))^2 + f_\alpha^2(k)}, \tag{2}$$

with

$$g_\xi(k) = \sum_{l=1}^{L-1} \frac{\cos(k\cdot l)}{r_{l,\xi}} \text{ and } f_\alpha(k) = \sum_{l=1}^{L-1} \frac{\sin(k\cdot l)}{R_{l,\alpha}}. \tag{3}$$

Particular instances of the functions $r_{l,\xi}$ and $R_{l,\alpha}$ have been considered in Refs. [14,15], where long-range deformations of the Kitaev chain were first considered.

These models (2) belong to the BDI symmetry class of topological insulators and superconductors [16,17], with particle-hole, time-reversal, and chiral symmetry. The inclusion of long-range effects do not break these symmetries, nor the conservation of fermion parity. This is an important condition for the topological character of the original short-range model to be preserved. These symmetries impose a restriction on the movement of the winding vector $\boldsymbol{n}_k$ from the sphere S^2 to the circle S^1 on the yz plane. Thus, we have a mapping from the reduced Hamiltonians H_k on the Brillouin zone $k \in S^1$ onto the winding vectors $\boldsymbol{n}_k \in S^1$. This mapping $S^1 \longrightarrow S^1$ is characterized by a winding number ω, a topological invariant defined as the angle swept by $\boldsymbol{n}_k$ when the crystalline momentum k is varied across the whole Brillouin zone (BZ) from $-\pi$ to $+\pi$,

$$\omega := \frac{1}{2\pi}\oint d\theta = \frac{1}{2\pi}\oint \left(\frac{\partial_k n_k^z}{n_k^y}\right) dk, \tag{4}$$

where we have used that $\theta := \arctan(n_k^z/n_k^y)$.

As a complementary tool in 1D systems, we can use the Berry/Zak phase [18–20] to characterize topological order. When the system is adiabatically transported from a certain crystalline momentum k_0 up to $k_0 + G$, where G is a reciprocal lattice vector, the eigenstate of the lower band of the system $|u_k^-\rangle$ picks up a topological Berry phase given by

$$\Phi_B = \oint A_B(k) dk. \tag{5}$$

The Berry connection $A_B(k) = i\langle u_k^-|\partial_k u_k^-\rangle$ connects by means of a parallel transport two infinitesimally close points on the manifold defined by $|u_k^-\rangle$ in k space. For the standard Kitaev chain [4], the resulting gauge-invariant phase Φ_B is quantized (0 or π) due to the particle-hole symmetry that characterizes distinct topological phases in one-to-one correspondence with the winding number [21].

III. AUGMENTED TOPOLOGICAL PHASES INDUCED BY EXPONENTIALLY DECAYING HOPPINGS

This remarkable effect is obtained choosing nearest-neighbor pairing, i.e., $R_{1,\alpha} = 1$ and $R_{l>1,\alpha} = \infty$ and $r_{l,\xi} = e^{\frac{(l-1)}{\xi}}$, where ξ is the penetration length of the exponentially decaying hopping terms. This Hamiltonian may be realizable in simulations of topological superconductors using cold atoms in optical lattices [22–24], where the exponential decay of the hopping terms with distance can be tuned, e.g., by varying the depth of the lattice potentials [25].

In Fig. 1 we plot the complete phase diagram by computing the winding number and the topological Berry phase from Eqs. (4) and (5). For $\xi \to 0$ we recover the usual Kitaev chain. The system is topological for $\mu \in [-1,1]$, displaying MZMs at the edges. Interestingly enough, when we increase the penetration length ξ, the region where we observe MZMs is augmented. In fact, this widening effect is purely due to the hopping deformation since we find that including an exponentially decaying pairing deformation does not change the topological phases. In the thermodynamic limit $L \to \infty$, the phase separation between the trivial and nontrivial topological phases can be computed analytically from Eq. (2), obtaining

$$\mu_{c1} = \frac{e^{\frac{1}{\xi}}}{1 + e^{\frac{1}{\xi}}}, \quad \mu_{c2} = \frac{e^{\frac{1}{\xi}}}{1 - e^{\frac{1}{\xi}}}. \tag{6}$$

Thus, increasing the penetration length of the deformed hopping, we can arbitrarily enlarge the topologically nontrivial sector (see Fig. 1). Although symmetry-protected topological order is usually associated with local interactions, we have shown that nonlocal terms can favor the formation of a topological phase. Related studies for the Kitaev chain with long-distance hopping were carried out [26] and qualitatively similar effects have been recently observed in Ref. [27] for the spin-1 long-range Haldane model [28].

IV. UNCONVENTIONAL TOPOLOGICAL SUPERCONDUCTIVITY WITH DIRAC TOPOLOGICAL MASSIVE STATES

Long-range deformations may not only enlarge topological phases but also produce new types of topological phases. To this end, let us now consider pairing terms that decay algebraically with a power-law exponent α, and no deformation of the hopping terms. That is, $r_{1,\xi} = 1, r_{l>1,\xi} = \infty$ and $R_{\alpha,l} = l^{\alpha}$.

In the thermodynamic limit $L \to \infty$, the function $f_\alpha(k)$ in Eq. (3) is divergent at $k = 0$ for $\alpha < 1$. This function defines the long-range pairing and appears in the energy dispersion relation and the winding vector of Eq. (2). Thus, the dispersion relation and the group velocity also become divergent at $k = 0$ if $\alpha < 1$. Nevertheless, ω [Eq. (4)] and Φ_B [Eq. (5)] are still integrable. Moreover, it is not possible to gauge away the divergence from $k = 0$ by means of a gauge transformation, as in the ordinary Kitaev chain. Therefore, the divergence behaves as a topological singularity. A detailed discussion of this effect at $k = 0$ on the topological indicators is carried out in Sec. I of the Supplemental Material [29]. According to the behavior of $f_\alpha(k)$ at $k = 0$, we find three different topological sectors depending on the exponent α:

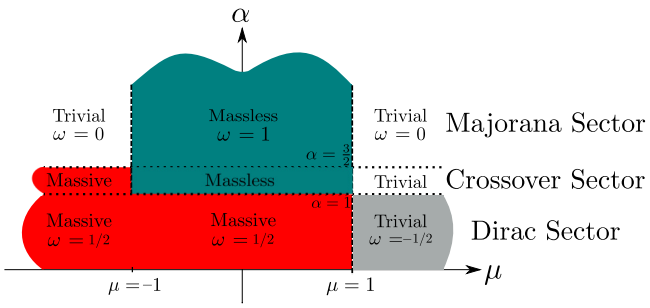

FIG. 3. Topological phase diagram for the Kitaev chain with long-range pairing. The wavy lines at the border of certain phases indicate that they extend endlessly. Fractional topological numbers highlight the appearance of an unconventional topological phase with massive nonlocal Dirac edge states. The topological characterisation of the crossover sector is discussed in the main text and the Supplemental Material [29].

(i) Majorana sector [$\alpha > 3/2$]

This sector is topologically equivalent to the one of the short-range Kitaev chain [4]: For $|\mu| > 1$, the phase is topologically trivial and we do not find MZMs. In the region $\mu \in (-1,1)$, we find that MZMs are always present [see Fig. 2(a)]. The function $f_\alpha(k)$ is not divergent and we can compute the winding number ω of Eq. (4) and the Berry phase Φ_B of Eq. (5) obtaining $\Phi_B = \pi\omega = \pi$. The lower-band eigenvector $|u_k^-\rangle$, thus, shows a $U(1)$ phase discontinuity at $k = 0$. The corresponding topological phase is depicted in blue in the phase diagram of Fig. 3.

(ii) Massive Dirac sector [$\alpha < 1$]

An unconventional topological phase appears for sufficiently slow decaying pairing. As an example, in Fig. 2(b) we see for $\alpha = 1/2$ two clearly different phases as a function of μ. For $\mu > 1$ the system is in a trivial phase, with no edge states. However, for $\mu < 1$ the system has a topological massive Dirac fermion at the edges, as shown in the wave function plot in Fig. 2(b). The two Majorana modes at the two distant edges have paired up onto a single massive Dirac fermion. Notice that the fermion is highly nonlocal and its nature is deeply rooted in the long-range/nonlocal character of the pairing term (see Sec. III of the Supplemental Material [29] for details). We notice that if we had considered imaginary pairing amplitudes within D symmetry class (particle-hole symmetric), the nonlocal massive Dirac fermions would persist. This topological quasiparticle is still protected by fermion parity: the ground state has still even parity, whereas the first excited state populates this nonlocal massive fermion and has odd parity. One cannot induce a transition between these two states without violating the fermion parity conservation of the Hamiltonian, and applying a nonlocal operation is needed. Moreover, the subspace of these two edge states is still protected by the bulk gap from bulk excitations. The conservation of fermion parity and the nonlocal character of the massive Dirac fermion make these two states ideal to define a topological qubit using two copies of the Kitaev chain [30–33]. Further details are detoured to Sec.V of the Supplemental Material. Additionally, in Sec. II of the Supplemental Material [29], by means of finite-size

scaling we show that the mass of the Dirac fermion stays finite in the thermodynamic limit for $\mu < 1$ and $\alpha < 1$. This way we can prove that the effect is purely topological and caused by the long-range deformation.

When we close the chain, the edge states disappear as we may expect for a topological effect. Despite the long-range pairing coupling, the system still belongs to the BDI symmetry class [16,17], since no discrete symmetry has been broken. The winding number ω can still be formally defined using Eq. (4). However, the topological singularity at $k = 0$ deeply modifies the value of ω. For the trivial phase $\mu > 1$, the winding number is $\omega = -1/2$, whereas for the new unconventional topological phase is $\omega = +1/2$ if $\mu < 1$. The semi-integer character of ω is associated to the integrable divergence at $k = 0$, which modifies the continuous mapping $S^1 \longrightarrow S^1$. Notwithstanding, in this region there is still a jump of one unit between the two topologically different phases, $\Delta\omega = \omega_{\text{top}} - \omega_{\text{trivial}} = 1$ (see Fig. 3). Moreover, the topological indicators take on the same value within the whole phase until the bulk gap closes at $\mu = 1$, giving rise to a topological phase transition, and the new massive topological edge states disappear. Therefore, we can still establish a bulk-edge correspondence.

There is a novelty in this case regarding the parallel transport for the Berry phase. Namely, at $k = 0$ the adiabatic condition breaks down since both the energy dispersion relation E_k and the quasiparticle group velocity $\partial_k E_k$ diverge. Moreover, the singularity at $k = 0$ of the lower-band eigenvector $|u_k^-\rangle$, cannot be removed by a simple gauge transformation as it is not just a $U(1)$ phase difference, but a phase shift unitary jump,

$$|u^-_{k\to 0^+}\rangle = \mathrm{e}^{\mathrm{i}\pi P_\pm}|u^-_{k\to 0^-}\rangle, \tag{7}$$

where $P_\pm = \frac{1}{2}(\mathbb{1} \pm \sigma_z)$. More explicitly,

$$\mathrm{e}^{\mathrm{i}\pi P_-} = \begin{pmatrix} 1 & 0 \\ 0 & \mathrm{e}^{\mathrm{i}\pi} \end{pmatrix}, \quad \mathrm{e}^{\mathrm{i}\pi P_+} = \begin{pmatrix} \mathrm{e}^{\mathrm{i}\pi} & 0 \\ 0 & 1 \end{pmatrix}. \tag{8}$$

The difference in sign $\pm$ of the projector $P_\pm$ depends on the topological regime. For $\mu > 1$, the system is in a trivial phase with no edge states and the long-range singularity of $|u_k^-\rangle$ at $k = 0$ is given by $\mathrm{e}^{\mathrm{i}\pi P_-}$. On the other hand for $\mu < 1$, the system is in a topological phase with massive and nonlocal edge states. The singularity of $|u_k^-\rangle$ at $k = 0$ in that case is given by $\mathrm{e}^{\mathrm{i}\pi P_+}$.

(iii) Crossover sector [$\alpha \in (1,3/2)$]

This is a crossover region between sectors (i) and (ii). Within this sector, there are massless Majorana edge states for $-1 < \mu < 1$ like in sector (i), but for $\mu < -1$ the edge states become massive like in sector (ii). This is shown through finite-size scaling in Sec. II and III of the Supplemental Material [29]. The intuition behind this result is that the gap closes in the thermodynamic limit at $\mu = -1$ also for $\alpha \in (1, \frac{3}{2})$. The dispersion relation E_k is no longer divergent, however its derivative $\partial_k E_k$ (the group velocity) is still singular at $k = 0$ and the structure of the topological singularity changes accordingly. The winding number is not able to capture the mixed character of this sector. However, as detailed in Sec. I of the Supplemental Material [29], we can clearly see that the behavior of the winding vector and the lower-band eigenstate is different from the other two sectors.

In Fig. 3, we present a complete phase diagram summarizing the different topological phases of the model as a function of μ and α.

V. OUTLOOK AND CONCLUSIONS

We have found that finite-range and long-range extensions of the one-dimensional Kitaev chain can be used as a resource for enhancing existing topological properties and for unveiling new topological effects. In particular, for long-range pairing deformations, we observe nonlocal massive Dirac fermions characterized by fractional topological numbers. Hamiltonians with long-range pairing and hopping may be realized in Shiba chains as recently proposed in Refs. [34,35], where edge states can be detected, e.g., by scanning tunneling spectroscopy [36]. Alternatively, next-nearest neighbor hopping may be harnessed in atomic and molecular setups [23], where massive edge modes should be observable via a combination of spectroscopic techniques and single-site addressing [37,38]. The extension of existing models for qubits, constructed by topologically protected gapped modes, may boost the search for long-range deformations in more complicated topological models with symmetry-protected or even intrinsic topological order.

ACKNOWLEDGMENTS

M.A.M-D. and O.V. thank the Spanish MINECO Grant FIS2012-33152, the CAM research consortium QUITEMAD+ S2013/ICE-2801, the U.S. Army Research Office through Grant W911NF-14-1-0103, FPU MECD Grant and Residencia de Estudiantes. G.P. and D.V. acknowledge support by the ERC-St Grant ColdSIM (No. 307688), EOARD, UdS via Labex NIE, ANR via BLUSHIELD and IdEX, RYSQ.

[1] M. Z. Hasan and C. L. Kane, Rev. Mod. Phys. **82**, 3045 (2010).
[2] X.-L. Qi and S.-C. Zhang, Rev. Mod. Phys. **83**, 1057 (2011).
[3] N. Read and D. Green, Phys. Rev. B **61**, 10267 (2000).
[4] A. Y. Kitaev, Phys.-Usp. **44**, 131 (2001).
[5] V. Mourik, K. Zuo, S. M. Frolov, S. R. Plissard, E. P. A. M. Bakkers, and L. P. Kouwenhoven, Science **336**, 1003 (2012).
[6] M. T. Deng, C. L. Yu, G. Y. Huang, M. Larsson, P. Caroff, and H. Q. Xu, Nano Lett. **12**, 6414 (2012).
[7] A. Das, Y. Ronen, Y. Most, Y. Oreg, M. Heiblum and H. Shtrikman, Nat. Phys. **8**, 887 (2012).
[8] S. Nadj-Perge, I. K. Drozdov, J. Li, H. Chen, S. Jeon, J. Seo, A. H. MacDonald, B. A. Bernevig, and A. Yazdani, Science **346**, 602 (2014).

[9] H.-H. Sun, K.-W. Zhang, L.-H. Hu, C. Li, G.-Y. Wang, H.-Y. Ma, Z.-A. Xu, C.-L. Gao, D.-D. Guan, Y.-Y. Li, C. Liu, D. Qian, Y. Zhou, L. Fu, S.-C. Li, F.-C. Zhang, and J.-F. Jia, Phys. Rev. Lett. **116**, 257003 (2016).
[10] S. M. Albrecht, A. P. Higginbotham, M. Madsen, F. Kuemmeth, T. S. Jespersen, J. Nygard, P. Krogstrup and C. M. Marcus, Nature (London) **531**, 206 (2016).
[11] C. Nayak, S. H. Simon, A. Stern, M. Freedman, and S. D. Sarma, Rev. Mod. Phys. **80**, 1083 (2010).
[12] B. M. Terhal, Rev. Mod. Phys. **87**, 307 (2015).
[13] A. Altland and B. Simons, *Condensed Matter Field Theory* (Cambridge University Press, New York, 2010).
[14] D. Vodola, L. Lepori, E. Ercolessi, A. V. Gorshkov, and G. Pupillo, Phys. Rev. Lett. **113**, 156402 (2014).
[15] D. Vodola, L. Lepori, E. Ercolessi, and G. Pupillo, New J. Phys. **18**, 015001 (2016).
[16] A. P. Schnyder, S. Ryu, A. Furusaki, and A. W. W. Ludwig, Phys. Rev. B **78**, 195125 (2008).
[17] A. Kitaev, in *Advances in Theoretical Physics: Landau Memorial Conference*, edited by V. Lebedev and M. Feigel'man, AIP Conf. Proc. No. 1134 (AIP, New York, 2009), p. 22.
[18] M. V. Berry, Proc. R. Soc. A **392**, 45 (1984).
[19] B. Simon, Phys. Rev. Lett. **51**, 2167 (1983).
[20] J. Zak, Phys. Rev. Lett. **62**, 2747 (1989).
[21] O. Viyuela, A. Rivas, and M. A. Martin-Delgado, Phys. Rev. Lett. **112**, 130401 (2014).
[22] P. Massignan, A. Sanpera, and M. Lewenstein, Phys. Rev. A **81**, 031607(R) (2010).
[23] L. Jiang, T. Kitagawa, J. Alicea, A. R. Akhmerov, D. Pekker, G. Refael, J. I. Cirac, E. Demler, M. D. Lukin, and P. Zoller, Phys. Rev. Lett. **106**, 220402 (2011).
[24] A. Bühler, N. Lang, C. V. Kraus, G. Möller, S. D. Huber and H. P. Büchler, Nature Commun. **5**, 4504 (2014).
[25] I. Bloch, J. Dalibard, and W. Zwerger, Rev. Mod. Phys. **80**, 885 (2008).
[26] W. DeGottardi, M. Thakurathi, S. Vishveshwara, and D. Sen, Phys. Rev. B **88**, 165111 (2013).
[27] Z.-X. Gong, M. F. Maghrebi, A. Hu, M. Foss-Feig, P. Richerme, C. Monroe, and A. V. Gorshkov, Phys. Rev. B **93**, 205115 (2016).
[28] Z.-X. Gong, M. F. Maghrebi, A. Hu, M. L. Wall, M. Foss-Feig, and A. V. Gorshkov, Phys. Rev. B **93**, 041102 (2016).
[29] See Supplemental Material at http://link.aps.org/supplemental/10.1103/PhysRevB.94.125121 for details on the winding vector, the analytical structure of the edge states, the finite-size scaling of the edge mass gap, the robustness of the massive Dirac edge states against disorder, and the construction of a topological qubit within the massive Dirac phase.
[30] S. Das Sarma, M. Freedman, and C. Nayak, npj Quantum Information **1**, 15001 (2015).
[31] S. B. Bravyi, A. Y. Kitaev, Ann. Phys. (NY), **298**, 210 (2002).
[32] J. Alicea, Y. Oreg, G. Refael, F. von Oppen and M. P. A. Fisher, Nat. Phys. **7**, 412 (2011).
[33] C. V. Kraus, P. Zoller, and M. A. Baranov, Phys. Rev. Lett. **111**, 203001 (2013).
[34] F. Pientka, L. I. Glazman, and F. von Oppen, Phys. Rev. B **88**, 155420 (2013).
[35] F. Pientka, L. I. Glazman, and F. von Oppen, Phys. Rev. B **89**, 180505(R) (2014).
[36] A. Yazdani, B. A. Jones, C. P. Lutz, M. F. Crommie, and D. M. Eigler, Science **275**, 1767 (1997).
[37] W. S. Bakr, J. I. Gillen, A. Peng, S. Fölling, and M. Greiner, Nature (London) **462**, 74 (2009).
[38] J. F. Sherson, C. Weitenberg, M. Endres, M. Cheneau, I. Bloch, and S. Kuhr, Nature (London) **467**, 68 (2010).

SUPPLEMENTARY MATERIAL

I. Winding vector and Berry phase in the presence of a Topological Singularity

In the thermodynamic limit $L \to \infty$, the function $f_\alpha(k)$ in (3) tends to

$$f_\alpha(k) = \frac{\mathrm{i}}{2}\Big(\mathrm{Li}_\alpha(\mathrm{e}^{-\mathrm{i}k}) - \mathrm{Li}_\alpha(\mathrm{e}^{\mathrm{i}k})\Big). \tag{S1}$$

where $\mathrm{Li}_\alpha(\mathrm{e}^{\mathrm{i}k})$ is a polylogarithmic function. This function defines the long-range pairing and is divergent at $k = 0$ for $\alpha < 1$. As a consequence, the energy gap in (2) diverges if $\alpha < 1$, and the particle group velocity $v_g = \partial_k E_k$ diverges for $\alpha < 3/2$ at $k = 0$. In line with this, we can trace the effect of this divergence over the winding vector and the topological phases within the different topological sectors:

i/ Majorana Sector [$\alpha > 3/2$]— There is no topological singularity in this sector. The winding number and the Berry phase can be computed using (4) and (5). We find the same topological indicators and the same type of edge states physics as for the short range Kitaev model ($\alpha \to \infty$). In Fig. S1 we plot the winding vector for $L = 201$ sites and for different values of the chemical potential μ belonging to different topological regimes. We can see that for trivial regions $|\mu| > 1$, the winding vector winds back and forth and never covers the entire S^1 circle. On the other hand, when the system is within a topological phase $\mu \in (-1, 1)$, the winding vector winds around S^1 completely. The lower band eigenvector $\left|u_k^-\right\rangle$ can always be chosen to be periodic. If the system is in the trivial phase, $\left|u_k^-\right\rangle$ is also continuous, whereas inside the topological phase, there is a $U(1)$ phase discontinuity at $k = 0$, i.e.,

$$\left|u^-_{k\to 0^+}\right\rangle = \mathrm{e}^{\mathrm{i}\pi}\left|u^-_{k\to 0^-}\right\rangle. \tag{S2}$$

This phase shift can be gauged away from $k = 0$, and it represents the Berry phase gained by the system after an adiabatic transport from a certain crystalline momentum k_0 up to $k_0 + G$, where G is a reciprocal lattice vector.

ii/ Massive Dirac Sector [$\alpha < 1$]— The topological singularity at $k = 0$ makes the winding vector ill-defined at that point, although its contribution to the winding number can still be integrated. In Fig. S2 we plot the winding vector for $L = 301$ sites and for different values of μ. In particular, for $\mu > 1$ the winding vector covers the entire lower half of the S^1 circle, explaining the value $\omega = -1/2$ of the winding number. On the contrary, for $\mu < 1$, the winding vector just covers the entire upper half of S^1 as shown in the figure. The function $f_\alpha(k)$ at $k = 0$ diverges as

$$f_\alpha(k \to 0^-) \longrightarrow -\infty\ ,\ f_\alpha(k \to 0^+) \longrightarrow \infty. \tag{S3}$$

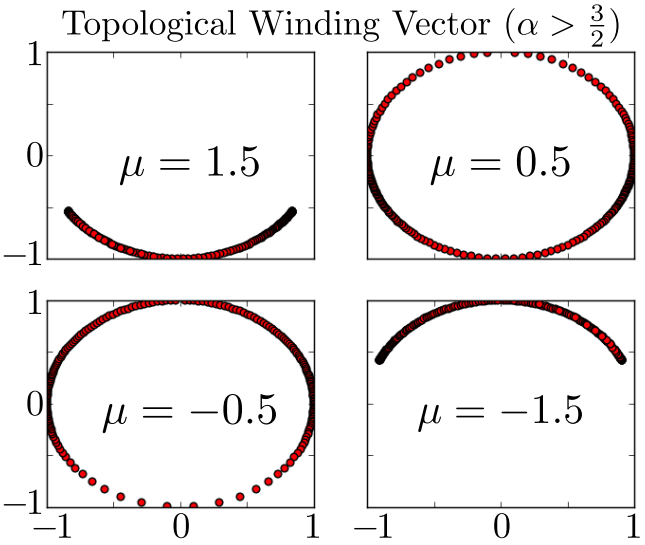

FIG. S1: Trajectories of the winding vector for different regions within the Majorana sector, for $L = 201$ sites and $\alpha = 3$. The red spots represent the movement of the winding vector along the unit circle S^1. As we see, for $\mu > 1$ and $\mu < -1$, the vector never winds around the whole S^1, just moving back and forth twice. However, if $\mu \in (-1, 1)$ the vector winds around S^1. The darker regions highlight a larger density of points.

Hence, in the transition from $k < 0$ to $k > 0$, the winding vector skips the entire lower part of the S^1 circle because of the topological singularity at $k = 0$. This explains the value of the winding vector $\omega = +1/2$ in this new topological phase. Complementary, the adiabatic condition breaks down at $k = 0$ as the quasi-particle group velocity diverges. Therefore, we can no longer say that the system picks up a $U(1)$ phase after a close loop in momentum space. Actually, the singularity at $k = 0$ of the lower band eigenvector $\left|u_k^-\right\rangle$, cannot be removed by a simple gauge transformation as it is not just a $U(1)$ phase difference, but a phase shift unitary jump,

$$\left|u^-_{k\to 0^+}\right\rangle = \mathrm{e}^{\mathrm{i}\pi P_\pm}\left|u^-_{k\to 0^-}\right\rangle, \tag{S4}$$

where $P_\pm = \frac{1}{2}\big(\mathbb{1} \pm \sigma_z\big)$. More explicitly,

$$\mathrm{e}^{\mathrm{i}\pi P_-} = \begin{pmatrix} 1 & 0 \\ 0 & \mathrm{e}^{\mathrm{i}\pi} \end{pmatrix},\quad \mathrm{e}^{\mathrm{i}\pi P_+} = \begin{pmatrix} \mathrm{e}^{\mathrm{i}\pi} & 0 \\ 0 & 1 \end{pmatrix}. \tag{S5}$$

The difference in sign $\pm$ of the projector $P_\pm$ depends on the topological sector. For $\mu > 1$, the system is in a trivial phase with no edge states and the singularity of the eigenstate at $k = 0$ is given by $\mathrm{e}^{\mathrm{i}\pi P_-}$. On the other hand for $\mu < 1$, the system is in a topological phase with massive and non-local edge states. The singularity of the eigenstate at $k = 0$ in that case is given by $\mathrm{e}^{\mathrm{i}\pi P_+}$.

iii/ Crossover Sector [$\alpha \in (1, 3/2)$]— This is a crossover region between the previous two sectors i/ and ii/. In this case, the structure of the topological singularity at $k = 0$

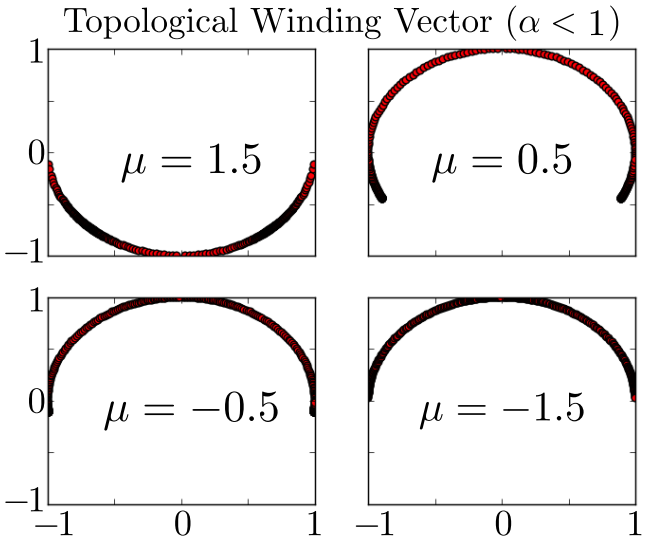

FIG. S2: Trajectories of the winding vector for different regions within the massive Dirac sector, for $L = 301$ sites and $\alpha = 0.5$. The red spots represent the movement of the winding vector along the unit circle S^1. For $\mu > 1$, the winding vector covers the lower half of S^1. However, if $\mu < 1$ the vector covers only the upper half of the circle. The darker regions highlight a larger density of points.

has changed. The components of the winding vector are continuous, but their derivatives diverge. Therefore, the population of points close to $k = 0$ is extremely dispersive. The winding vector does not cover the entire south pole sector due to the divergence in the derivatives of its components in the thermodynamic limit. Hence, the behaviour of the winding vector is different than in the other two previous sectors i/ and ii/. This might be linked to the mixed character of the sector with the presence of MZMs ($-1 < \mu < 1$) and massive Dirac fermions ($\mu < -1$). Regarding the lower band eigenvector, it is continuous but its derivative is still divergent at $k = 0$ breaking the adiabatic condition.

II. Edge mass gap finite-size scaling

In Sec. IV of the main text, we claimed that the pairing of the MZMs into a massive non-local Dirac fermion cannot be explained as a simple interaction between the Majorana fermions at the edges due to a finite size effect. Actually, its nature is deeply rooted into the long-range/non-local character of the pairing deformation of the Kitaev chain. The absence of a degenerate zero energy subspace avoids a wave function superposition to localise a single Majorana mode at one edge only. On the contrary, the two edges are inevitably coupled to each other, pairing to a non-local massive Dirac mode as shown in Fig. 2.

In order to proof this claim more rigorously, we have computed the mass of the edge states through a finite-size scaling for different values of the decaying exponent α and the chemical potential μ.

In Fig. S3(a) we perform a finite-size scaling for the masses of the MZMs for the Majorana sector. Within the topological sector $\mu \in (-1, 1)$, the edge mass gap clearly goes to zero with L as we expected. In Fig. S3(b) we perform the same finite-size scaling analysis for the massive Dirac sector. In this case, there are edge states for $\mu < 1$. As we can see, the masses of the edge states depend on both μ and α, and go to a finite value even in the thermodynamic limit. This proves that the topological nature of the non-local massive Dirac fermions purely comes from the long-range deformation of the original Kitaev Hamiltonian and not from a finite size effect.

On the other hand, Fig. S3(c) and Fig. S3(d) show the finite-size scaling for the edge mass gap within the crossover sector. Although there are edge states all over $\mu < 1$, they can be either massive or massless depending on the chemical potential μ. If $-1 < \mu < 1$ the edge states are massless as shown in Fig. S3(c), whereas for $\mu < -1$ the edge states become massive as shown in Fig. S3(d). Hence, this sector displays a mixed character between a Majorana and a massive Dirac phase.

Lastly, we have investigated the edge properties of the model by studying the wavefunction probability density $|\psi(0)|^2$ for the lowest-energy single-particle eigenstate at one of the edges. Fig. S4 shows $|\psi(0)|^2$ for different μ as a function of α. The results can be summarised as follows: i/ for $\mu > 1$ (purple line) there are no edge states regardless of α. ii/ If $-1 < \mu < 1$ (blue line) there is always a finite edge-state density. In addition, from Fig. S3 we obtain that if $\alpha > 1$ the edge states are massless, whereas if $\alpha < 1$ they are massive. iii/ If $\mu < -1$ (green line) there are edge states if $\alpha < \frac{3}{2}$. Then, from Fig. S3 we conclude that they are always massive in this case. Actually, we can even monitor how one of the Dirac bulk states gets transmuted into a non-local massive Dirac edge mode by lowering α.

The results are in complete agreement with Fig.3 from the main text and the finite size scaling analysis in Fig. S3.

III. Analytical Structure of the Edge States

We take the Hamiltonian defined in Eq. (1) of the main text, where only long-range pairing terms are considered. For the parameter choice $\theta = 0$ and $J = |M| = \frac{1}{2}$ assumed along the paper, we can separate the short-range and long-range contributions:

$$H := H_{SR} + H_{\mu} + H_{LR}, \tag{S6}$$

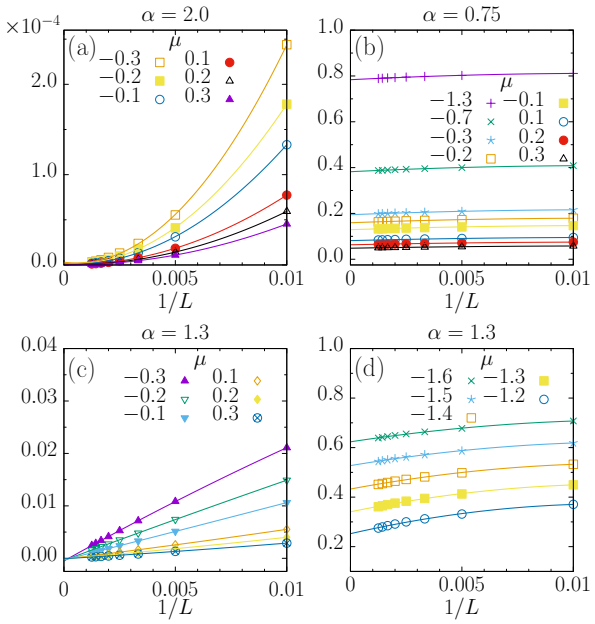

FIG. S3: Finite size scaling of the edge mass gap for different values of the exponent α and the chemical potential μ. In (a) we plot the case for $\alpha = 2.0$ belonging to the Majorana sector. The edge mass gap closes with L for every μ within the topological phase. In (b) we take $\alpha = 0.75$ in the massive Dirac sector. For $\mu < 1$ the edge mass gap tends to a finite value in the thermodynamic limit. In (c) and (d) we perform the finite-size scaling for $\alpha = 1.3$ within the crossover sector. If $-1 < \mu < 1$ (c), there are massless edge states. If $\mu < -1$ (d), there are massive edge states up to our numerical precision.

where

$$
\begin{aligned}
H_{SR} &:= \sum_{j=1}^{L} \left(-a_j^\dagger a_{j+1} + a_j a_{j+1} + \text{h.c}\right), \\
H_{\mu} &:= -\mu \sum_{j=1}^{L} \left(a_j^\dagger a_j - \frac{1}{2}\right), \\
H_{LR} &:= \sum_{j=1}^{L} \sum_{l=2}^{L-j} \frac{1}{R_{l,\alpha}} a_j a_{j+l} + \text{h.c} \qquad \text{(S7)}
\end{aligned}
$$

In order to uncover the different topological phases of the model, we will rewrite this Hamiltonian in terms of Majorana operators

$$
c_j = \tfrac{1}{\sqrt{2}}\left(a_j^\dagger + a_j\right), \qquad d_j = \tfrac{\mathrm{i}}{\sqrt{2}}\left(a_j^\dagger - a_j\right), \qquad \text{(S8)}
$$

satisfying the fermionic anticommutation relation $\{c_i, c_j\} = \delta_{ij}$, but also the Majorana condition $c_j^\dagger = c_j$ and the same for d_j.

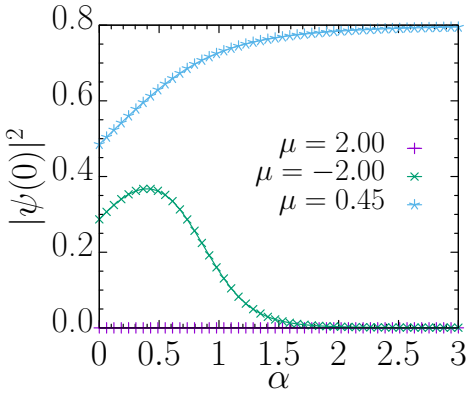

FIG. S4: We plot the wavefunction probability density $|\psi(0)|^2$ for the lowest-energy eigenstate at one of the edges for different μ as a function of α: i/ $\mu > 1$ (purple line) there are no edge states regardless of α. ii/ $-1 < \mu < 1$ (blue line) there is always a finite edge-state density. iii/ $\mu < -1$ (green line) there are edge states if $\alpha \lesssim \frac{3}{2}$.

Substituting Eq.(S8) in Eq.(S7), we get

$$
\begin{aligned}
H_{SR} &= \mathrm{i} \sum_{j=1}^{L-1} d_j c_{j+1}, \\
H_{\mu} &= -\mathrm{i}\mu \sum_{j=1}^{L} c_j d_j, \\
H_{LR} &= \frac{\mathrm{i}}{2} \sum_{j=1}^{L} \sum_{l=2}^{L-j} \frac{1}{R_{l,\alpha}} \Big(d_j c_{j+l} + c_j d_{j+l}\Big). \qquad \text{(S9)}
\end{aligned}
$$

Short-range Kitaev chain

Let us first consider the purely short-range Kitaev chain with a chemical potential. Majorana fermions usually pair locally in such a way that they constitute a regular Dirac fermion. However, for open boundary conditions and certain values of the coupling constants, two Majorana fermions at the boundary remain unpaired. The Majorana operators at the edges c_1 and d_N do not appear in the short-range Hamiltonian H_{SR}, hence, if we set $\mu = 0$ they become zero energy modes (see Fig. 1(b) in the main text) as they decouple from the dynamics. These MZMs are topologically protected and represent a hallmark of topological order in the system.

Note that if $\mu \neq 0$, then c_1 and d_N do appear in $H_{\text{SR}} + H_\mu$, however we will show that these modes have an exponentially small energy and are exponentially localised at the edges. Hence, in the thermodynamic limit they become exact zero energy modes.

In order to prove this, we will elaborate on an ansatz method [1] in order to construct the edge modes ana-

lytically for the short-range Kitaev chain. A fermionic zero mode Ψ is an operator that commutes with the Hamiltonian: $[H, \Psi] = 0$, anticommutes with $(-1)^F$, i.e. $\{(-1)^F, H\} = 0$ and it is conveniently normalised. The second property guarantees that the operator Ψ maps the odd and even parity sectors. The first one instead imposes the condition for a zero energy mode, based on the Heisenberg equation $\frac{d\Psi}{dt} = -\mathrm{i}[H, \Psi]$.

First of all, we note that the fermionic mode constructed out of the two unpaired Majoranas c_1 and d_N, namely,

$$\tilde{a}_{\mathrm{E}} = \frac{1}{\sqrt{2}}(c_1 + \mathrm{i}d_N), \tag{S10}$$

clearly commutes with $H_{\mathrm{SR}} + H_\mu$ for $\mu = 0$, $[H_{\mathrm{SR}} + H_\mu, \tilde{a}_{\mathrm{E}}] = 0$. Moreover, $\tilde{a}_{\mathrm{E}}$ destroys a fermionic mode in the system, thereby mapping the even and odd parity sectors. For $\mu \neq 0$ instead, the fermionic operator $\tilde{a}_{\mathrm{E}}$ does not conmute with H, however, the new edge mode can still be determined.

Let us propose an ansatz wavefunction for the modified left Majorana mode Φ_{left}. We know that $\Phi_{\mathrm{left}}(\mu = 0) = c_1$ and the Hamiltonians defined in Eq. (S9), H_{SR}, H_μ, H_{LR} have only mixing terms $c_i d_j$. Hence, the most general ansatz would be:

$$\Phi_{\mathrm{left}} = \sum_{j=1}^{L} m_j c_j \tag{S11}$$

where c_j are Majorana operators and m_j are real coefficients to be determined. Namely,

$$[H_{SR} + H_\mu, \Phi_{\mathrm{left}}] = \mathrm{i}\sum_{j=1}^{L-1}\Big(m_{j+1} + \mu m_j\Big)d_j \ + \mu m_L d_L, \tag{S12}$$

where we have used the anticonmuting properties of the Majorana operators,

$$[d_k c_j, c_l] = \delta_{j,l} d_k, \quad \text{and} \quad [c_j d_k, c_l] = -\delta_{j,l} d_k. \tag{S13}$$

If we want to make Φ_{left} a MZM, then we should impose the commutator in Eq. (S12) to be zero. Hence,

$$m_{j+1} + \mu m_j = 0 \quad \forall j = 1, ..., L-1. \tag{S14}$$

Note that the coefficient accompanying d_L will be determined with the $L-1$ previous equations. For continuity with the $\mu = 0$, we take $m_1 = 1$ up to normalisation of the final wavefunction. It is now very easy to see that the solution to the recursive equation (S14) is

$$m_j = (-\mu)^{j-1} \quad \forall j = 2, ..., L. \tag{S15}$$

Thus,

$$\Phi_{\mathrm{left}} = c_1 - \mu c_2 + \mu^2 c_3 - \mu^3 c_4 + ... \tag{S16}$$

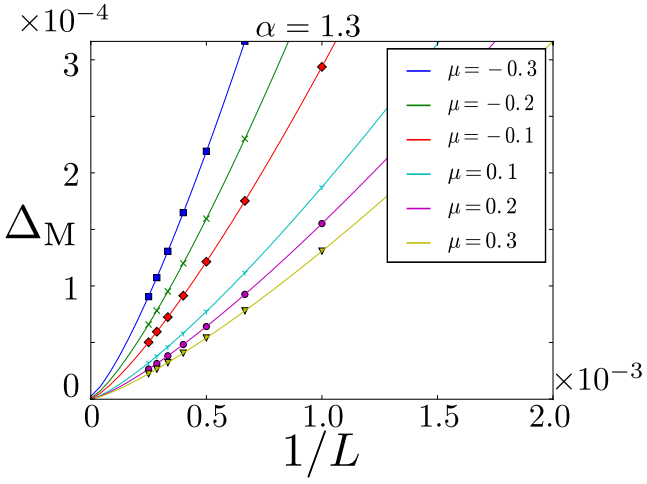

FIG. S5: Finite size scaling of the mass indicator Δ_M within the crossover sector, $\alpha \in (\frac{3}{2}, 1)$, for the massless phase ($-1 < \mu < 1$) where we expect MZMs. As we can see, Δ_M goes to zero when L increases.

and

$$[H_{SR} + H_\mu, \Phi_{\mathrm{left}}] = \mu m_L d_L = \mu(-\mu)^{L-1} d_L. \tag{S17}$$

The same equation holds for the right edge Majorana mode,

$$\Phi_{\mathrm{right}} = d_L - \mu d_{L-1} + \mu^2 d_{L-2} - \mu^3 d_{L-3} + ... \tag{S18}$$

Hence, the two new Majorana (almost) zero modes localised around the left and right edges for $|\mu| < 1$, can be combined into a Dirac fermionic edge mode, $\Psi_{\mathrm{E}} = \frac{1}{\sqrt{2}}\Big(\Phi_{\mathrm{left}} + \mathrm{i}\Phi_{\mathrm{right}}\Big)$. This edge fermion doesn't commute exactly with $H_{\mathrm{SR}} + H_\mu$,

$$[H_{SR} + H_\mu, \Psi_{\mathrm{E}}] = \mu(-\mu)^{L-1}\frac{1}{\sqrt{2}}(c_1 + \mathrm{i}d_L). \tag{S19}$$

However, this coefficient is exponentially small in L as long as $|\mu| < 1$. Hence, in the thermodynamic limit $L \to \infty$, the fermionic mode Ψ_{E} commutes with the Hamiltonian, satisfying the condition to be a zero energy mode, and the new Majorana fermionic operators Φ_{left} and Φ_{right} are unpaired.

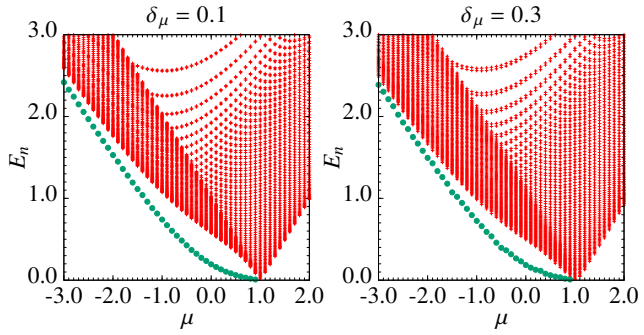

FIG. S6: The plot shows the energy spectrum of the Hamiltonian with long-rang pairing Eq. (1) of the main text and a random chemical potential term Eq. (S25) as a function of the chemical potential μ for two values of the disorder strength δ_μ. The states plotted in green are separated by a finite gap from the band of bulk states plotted in red.

Kitaev chain with long-range couplings.

Let us now include the long-range deformations given by H_{LR},

$$\begin{aligned}&[H_{LR},\Phi_{\text{left}}]=\\&=\frac{\mathrm{i}}{2}\sum_{j=1}^{L}\sum_{l=2}^{L-j}\sum_{k=1}^{L}\frac{m_k}{R_{l,\alpha}}\Big([d_jc_{j+l},c_k]+[c_jd_{j+l},c_k]\Big)=\\&=\frac{\mathrm{i}}{2}\Big(\sum_{j=1}^{L-2}\sum_{l=2}^{L-j}\frac{m_{j+l}}{R_{l,\alpha}}d_j-\sum_{j=1}^{L-2}\sum_{l=2}^{L-j}\frac{m_j}{R_{l,\alpha}}d_{j+l}\Big).\end{aligned}\tag{S20}$$

The commutator of total Hamiltonian, $H=H_{SR}+H_\mu+H_{LR}$, can be regrouped into a similar fashion as for the short-range case, but with more complicated contributions,

$$\begin{aligned}[H,\Phi_{\text{left}}]=\mathrm{i}\sum_{j=1}^{L-1}\Big(m_{j+1}+\mu m_j+\sum_{l=2}^{L-j}\frac{m_{j+l}}{2R_{l,\alpha}}-\\-\sum_{k=1}^{j-2}\frac{m_k}{2R_{j-k,\alpha}}\Big)d_j+\mathrm{i}\Big(\mu m_L-\sum_{k=1}^{L-2}\frac{m_k}{2R_{L-k,\alpha}}\Big)d_L.\end{aligned}\tag{S21}$$

Proceeding as in the previous section, we now impose all the coefficients accompanying the operators d_j to be zero, except the one coming from d_L, which will be automatically determined by these equations. Then, if the coefficient accompanying d_L goes to zero as L increases, we can claim that we still have unpaired Majorana modes. Otherwise, a massive non-local Dirac mode will appear.

Therefore, we need to solve the following discrete equation:

$$m_{j+1}+\mu m_j+\sum_{l=2}^{L-j}\frac{m_{j+l}}{2R_{l,\alpha}}-\sum_{k=1}^{j-2}\frac{m_k}{2R_{j-k,\alpha}}=0,\quad\forall j=1,...,L-1\tag{S22}$$

Note that the first sum only contributes from $j=3$ and the last sum only runs up to $j=L-2$. Once we solve Eq. (S22), the edge mass indicator of the system is determined from Eq. (S21), by computing

$$\Delta_M:=\mu m_L-\sum_{k=1}^{L-2}\frac{m_k}{2R_{L-k,\alpha}}\tag{S23}$$

Note that Δ_M is not exactly the edge mass gap, however, it distinguishes the region where we have MZM or when they turn into a non-local massive Dirac fermion, $[H,\Psi_{\text{E}}]=\Delta_M\frac{1}{\sqrt{2}}(c_1+\mathrm{i}d_L)$. If Δ_M goes to zero as L increases, then we will certainly have a MZM. Note the analogy with the short-range case with a non-zero chemical potential μ.

Although a complete analytical solution might be involved, this process can be easily programmed in a computer as a set of linear equations. In Fig. S5, we compute the finite-size scaling of Δ_M within the crossover sector for $-1<\mu<1$ where we expect MZMs. Up to our numerical precision, Δ_M goes to zero in perfect accordance with the phase diagram of Fig. 3 in the main text and the finite-size scaling for the energy of the edge modes in Fig. S3.

Before concluding, we would like to give an intuitive picture to explain the mechanism that pairs MZMs non-locally via the long-range coupling. At first sight, one might think that long-range interactions would couple every Majorana fermion with each other, mixing them all. However, c_1 and d_N commute with $H_{SR}=\mathrm{i}\sum_{j=1}^{L-1}d_jc_{j+1}$, and the long-range Hamiltonian H_{LR} only couples the two of them together (up to exponential and algebraic tails). This can be indeed inferred from the commutator of $\tilde{a}_{\text{E}}=\frac{1}{\sqrt{2}}(c_1+\mathrm{i}d_N)$ and H_{LR}:

$$[H_{LR},\tilde{a}_{\text{E}}]=-\frac{1}{2R_{L-1,\alpha}}\tilde{a}_{\text{E}}-\sum_{j=2}^{L-2}\frac{1}{2R_{L-j,\alpha}}\tilde{a}_j,\tag{S24}$$

where $\tilde{a}_j=\frac{1}{\sqrt{2}}(c_j+\mathrm{i}d_{L+1-j})$ are new bulk fermionic modes, and the edge Majoranas c_1 and d_N only appear in $\tilde{a}_E$.

Actually, a complementary way to construct the new fermionic edge mode Ψ_{E} is by incorporating corrections, term by term, to $\tilde{a}_{\text{E}}$ that cancel the contribution coming from $\tilde{a}_j$ in Eq. (S24) up to a higher order. However, this method is even more involved than the one we have proposed along this section.

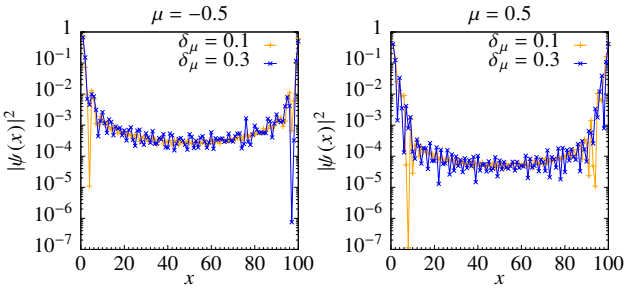

FIG. S7: Spatial probability distribution $|\psi(x)|^2$ for the massive Dirac edge mode for different chemical potentials μ and disorder strengths δ_μ. The wave functions are localised at the ends of the chain, even in the presence of a disordered potential.

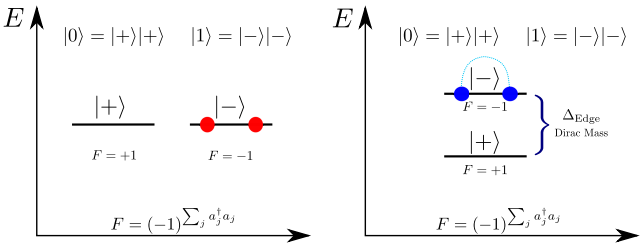

FIG. S8: At the l.h.s. we have depicted the construction of a qubit within the even parity sector for the short-range case. The two level system $|+\rangle, |-\rangle$ represent whether the two MZMs at the edge are populated or not. At the r.h.s. we can see a similar scheme for a qubit in the even parity sector within the Dirac phase. The only difference comes at level of the states $|+\rangle, |-\rangle$, representing whether the non-local massive Dirac fermion is populated or not.

IV. Robustness of the massive Dirac edge states to disorder

In this Section we show that the massive Dirac states are robust against the presence of a disordered potential. To this end, we add a random chemical potential

$$H_{\delta_\mu} = \sum_i \epsilon_i a_i^\dagger a_i \tag{S25}$$

to the Hamiltonian (1) of the main text with only long-range pairing terms. The coefficients $\epsilon_i \in [-\delta_\mu, \delta_\mu]$ are chosen from a random uniform distribution with zero mean value and width $2\delta_\mu$.

Figure S6 shows the energy spectrum E_n (averaged over 100 disorder realizations) of the total Hamiltonian $H + H_{\delta_\mu}$ for $\alpha = 0.5$ in the massive Dirac sector for two values of δ_μ. It is possible to see that, when $\mu < 1$, one state (plotted in green) is separated by a finite gap from the band of the bulk states (plotted in red). This state is still an edge state as Fig. S7 shows. There we plot the spatial distribution $|\psi(x)|^2$ of the wave function of the mode lying outside the band of the bulk states for two values of δ_μ and μ for a system of $L = 100$ sites. Even in the presence of a random potential term, this state is a Dirac massive edge state as it is always localised at the ends of the chain.

V. Topological Quantum Memory

As stated in the main text, it is possible to define a topological qubit using the new non-local massive Dirac fermions. In the short-range Kitaev chain, the topological protection of the unpaired Majoranas is related to the conservation of fermion parity and the gap isolating the MZMs from the bulk states. We want to stress that these same features also hold true for non-local massive Dirac fermions.

As depicted in Fig. S8, we can still define even and odd parity states $\{|+\rangle, |-\rangle\}$, respectively. These two states have different fermion parity F, physically depending on whether we populate the non-local Dirac fermion or not:

$$\tilde{a}_{\rm E} |+\rangle = 0, \qquad |-\rangle = \tilde{a}_{\rm E}^\dagger |+\rangle . \tag{S26}$$

The fact that the effective two level system is gapped is irrelevant in that respect. Additionally, as we show in Fig. S6, this effective two level system is separated from the bulk eigenstates by an energy gap and it is robust against disorder perturbations. Using these states, we can define a qubit using two copies of the Kitaev chain. The reason behind is the impossibility to have a qubit without a definite fermion parity [2, 3]. Therefore, the qubit can be defined either in the even or odd parity sector. As shown in Fig. S8 of the SM, we define a qubit with even fermion parity, as $|0\rangle = |+\rangle|+\rangle$ and $|1\rangle = |-\rangle|-\rangle$.

Furthermore, proposals to perform topological quantum gates with Majorana fermions based on their braiding properties have been recently proposed [4, 5]. All the physical operations needed can be written in terms of fermionic degrees of freedom, involving on-and-off switchings of the different coupling constants. For the present case with long-range couplings, a more detailed analysis in order to elaborate a concrete proposal would be required. This is out of the scope of the present work but it is left as an outlook of the paper.

[1] P. Fendly, J. Stat. Mech. P11020 (2012).
[2] C. Nayak, S. H. Simon, A. Stern, M. Freedman, and S. Das Sarma, Rev. Mod. Phys. **80**, 1083 (2008).
[3] S. Das Sarma, M. Freedman, C. Nayak, npj Quantum Information **1**, 15001 (2015).
[4] J. Alicea,Y. Oreg, G. Refael, F. von Oppen and M. P. A. Fisher, Nat. Phys. **7**, 412–417 (2011).
[5] C. V. Kraus, P. Zoller, M. A. Baranov, Phys. Rev. Lett. **111**, 203001 (2013).

A

APPENDIX: Driven-Dissipative Phase Transitions

A.1 Dissipative Phase transitions

In **equilibrium systems**, phase transitions between different states of matter (e.g., that between liquid water and ice) are very-well understood. As we saw in the introduction of this thesis, Landau theory [Lan37] characterises phase transitions by defining a local order parameter, i.e., a local property with a finite expectation value in one phase and a vanishing expectation value in the other one. In most cases, symmetry [Gro96] also plays an essential role to identify different phases of matter, and usually a symmetry-breaking process is involved. Nonetheless, there are some other phases of matter that cannot be characterised by a local order parameter and symmetry breaking. Instead, they are described by a global order parameter associated to a topological invariant. These are the so-called topological phase transitions, which have been the centre of attention of this thesis.

When they are at equilibrium, topological and non-topological phase transitions have been extensively studied in the literature: at zero temperature, or when the system arrives to thermal equilibrium with the bath. The theory of equilibrium phase transitions shows that apparently distinct physical systems undergo transitions in the same way; invoking renormalisation group (RG) arguments [Wil75], details on small length scales do not matter.

Phase transitions can also occur in **out-of-equilibrium** situations. In classical systems, many examples have been found: moving cars into traffic jams, individual flying birds exhibiting collective flocking, etc. These situations can be related to

each other by the fact that the appearance of different steady-state ordering is of purely dynamical origin and cannot be reduced to the equilibrium results.

In quantum mechanics, phase transitions away from thermal equilibrium may occur when an interacting system is driven by some external coherent source acting as an environment. Due to this external driving, the environment takes the system into a steady state. If the Hamiltonian and the dissipative dynamics do not commute, the steady state may change abruptly by varying the different coupling constants involved. A sudden change in the static properties[1] of the system may happen, e.g. the spin polarisation. This leads to the so-called **driven-dissipative phase transitions (DDPT)**.

In the field of statistical mechanics at equilibrium, there several toy models that capture the physics of a wide range of physical systems. These models can even be classified within different universality classes [Sac00], according to their behaviour close to the phase transitions point. On the contrary, only a few models for DDPT have been analysed. The main difficulty relies on the exponential growth of the Hilbert space dimension of a many-body system, which leads to density matrices of dimension $d^N \times d^N$ (where d is the dimension of the local degrees of freedom, e.g., a spin, and N is the number of particles)[2].

Therefore, approximated methods are needed in order to tackle with a formidable problem like this one. Nowadays, the amount of analytical and numerical tools available to study dissipative phase transitions in open quantum systems is highly limited. Remarkable examples are: the use of mean-field approximations [DTM+10, KGI+12, LGL13], Keldysh formalism [SBD16], Matrix product operators [JNK13], etc.

In this appendix section, we will describe several of these tools and propose new ones (yet never used for dissipative phase transitions). The power and combination of these different methods allow us to find new features of these transitions that had not been previously observed, namely the key role of short-range fluctuations in DDPT.

A.1.1 Matrix product operators

The first numerical method that we present is based on the ideas of **Density Matrix Renormalization Group (DMRG)** [Sch05]. This method was introduced by Steve White in 1992 [Whi92].

The success of DMRG and its generalisations relies on the fact that certain

[1] There are other studies [LvHGmcuuG13] that characterise DDPT using purely dynamical observables based on time correlations, or spin-spin correlations [PSSA09].

[2] This problem has already been explained in more detail in chapter 2, when introducing the theory of open quantum systems.

many-body states in 1D systems can be accurately described in terms of the so-called **matrix product states (MPS)**, i.e. a states of the form

$$|\psi\rangle = \sum_{s_1,\ldots,s_N}^{d} \mathrm{Tr}\left(A_1^{s_1}\ldots A_N^{s_N}\right)|s_1,\ldots,s_N\rangle. \tag{A.1}$$

The coefficients describing the state $|\psi\rangle$ are given in terms of the matrices A_n, whose dimension is bounded by a certain number χ, and d is the dimension of the local Hilbert space associated to the physical sites (e.g. spins).

DMRG can be understood in essence as an iterative variational method: given a fixed bond dimension χ, it computes the matrices A_n whose state $|\psi\rangle$ minimises the energy.

More than a decade later, Guifré Vidal developed the **Time-Evolving Block Decimation (TEBD)** method [Vid03, Vid04] to implement real time evolution of Matrix Product States. In other words, it gives a particular receipe to update the matrices A_n as a function of time. Subsequently, a new method was devised to compute real time evolution within the DMRG formalism [FW05]. More recently, new proposals have been put forward to extend the method to 2D and 3D, extending the definition of Matrix Product States into the more general framework of **Tensor Networks** [CV09].

Although these methods were initially proposed to deal with Hamiltonian systems and pure states, the extension of TEBD to open systems is possible [ZV04, VGRC04]. With this method, dissipative systems governed by master equations can be efficiently simulated [VGRC04], provided that entanglement does not grow very much and spatial correlations decay exponentially. For simplicity, we will focus on interacting spins although the method can also be applied to bosonic and fermionic systems.

A generic many-body mixed state on a L-site lattice can be written as

$$\rho = \sum_{\vec{i},\vec{j}} C_{i_1\cdots i_L, j_1\cdots j_L}|i_1\cdots i_L\rangle\langle j_1\cdots j_L|, \tag{A.2}$$

where we define $\vec{i} = \{i_1\ldots i_L\}$. The density matrix ρ can be recast in the super-operator language $|\rho\rangle$ as an MPS [Eq. (A.3)] in the enlarged Hilbert space of dimension $d^L \otimes d^L$, where d is the dimension of the onsite Hilbert space,

$$|\rho\rangle = \sum_{\vec{i},\vec{j}} C_{i_1\cdots i_L, j_1\cdots j_L}||i_1\cdots i_L,\, j_1\cdots j_L\rangle\rangle, \tag{A.3}$$

where the super-ket $||i_1\cdots i_L,\, j_1\cdots j_L\rangle\rangle = \bigotimes_{a=1}^{L}|i_a\rangle\langle j_a|$ is used in order to deal with the super-operator formalism, i.e. with linear operators acting on vector spaces of linear operators.

We can use the singular value decomposition (SVD) or equivalently the Schmidt decomposition [GM02] to write the tensor $C_{i_1\cdots i_L, j_1\cdots j_L}$ in Eq. (A.2) in terms of a

product of local tensors associated to each site i. We start by computing the SVD of $|\rho\rangle$ into the first spin and the $N-1$ remaining ones,

$$|\rho\rangle = \sum_{\alpha_1} \lambda^{[1]}_{\alpha_1} ||\Phi^{[1]}_{\alpha_1}\rangle\rangle ||\Phi^{[2\ldots N]}_{\alpha_1}\rangle\rangle = \sum_{i_1 j_1} \sum_{\alpha_1} \Gamma^{[1]i_1,j_1}_{1,\alpha_1} \lambda^{[1]}_{\alpha_1} ||i_1 j_1\rangle\rangle ||\Phi^{[2\ldots N]}_{\alpha_1}\rangle\rangle, \tag{A.4}$$

where each Schmidt vector $||\Phi^{[1]}_{\alpha_1}\rangle\rangle = \sum_{i_1 j_1} ||i_1 j_1 \Gamma^{[1]i_1,j_1}_{1,\alpha_1}\rangle\rangle$ has been expanded into the basis vector $||i_1 j_1\rangle\rangle$, and $\lambda^{[1]}_{\alpha_1}$ are the corresponding Schmidt coefficients. For every interaction, the maximum Schmidt rank is limited by χ, which sets the dimension of the tensors $\Gamma^{[n]i_n,j_n}_{\alpha,\alpha'}$. We now proceed with site 2 of the chain. We expand the Schmidt vector $||\Phi^{[2\ldots N]}_{\alpha_1}\rangle\rangle$ into the local basis of the second spin $||i_2 j_2\rangle\rangle$,

$$||\Phi^{[2\ldots N]}_{\alpha_1}\rangle\rangle = \sum_{i_2 j_2} ||i_2 j_2\rangle\rangle ||\tau^{[3\ldots N]}_{\alpha_1 i_2 j_2}\rangle\rangle, \tag{A.5}$$

and project $||\tau^{[3\ldots N]}_{\alpha_1 i_2 j_2}\rangle\rangle$ onto the at most χ Schmidt vectors $\{||\Phi^{[3\ldots N]}_{\alpha_2}\rangle\rangle\}^{\chi}_{\alpha_2=1}$ with their corresponding Schmidt coefficients $\lambda^{[2]}_{\alpha_2}$,

$$||\tau^{[3\ldots N]}_{\alpha_1 i_2 j_2}\rangle\rangle = \sum_{\alpha_2} \Gamma^{[2]i_2,j_2}_{\alpha_1,\alpha_2} \lambda^{[2]}_{\alpha_2} ||\Phi^{[3\ldots N]}_{\alpha_2}\rangle\rangle. \tag{A.6}$$

Now, if we substitute Eq. (A.6) in Eq. (A.5), and this last equation into Eq. (A.4), we obtain

$$|\rho\rangle = \sum_{i_1 i_2 j_1 j_2} \sum_{\alpha_1 \alpha_2} \Gamma^{[1]i_1,j_1}_{1,\alpha_1} \lambda^{[1]}_{\alpha_1} \Gamma^{[2]i_2,j_2}_{\alpha_1,\alpha_2} \lambda^{[2]}_{\alpha_2} ||i_1 i_2 j_1 j_2\rangle\rangle ||\Phi^{[3\ldots N]}_{\alpha_2}\rangle\rangle. \tag{A.7}$$

By iterating this process for all sites [Vid03], we finally arrive to the MPO representation of the state

$$|\rho_{\mathrm{MPO}}\rangle = \sum_{\vec{i},\vec{j}=1}^{d} \sum_{\vec{\alpha}=1}^{\chi} (\Gamma^{[1]i_1,j_1}_{1,\alpha_1} \lambda^{[1]}_{\alpha_1}) (\Gamma^{[2]i_2,j_2}_{\alpha_1,\alpha_2} \lambda^{[2]}_{\alpha_2}) \ldots (\lambda^{[L-1]}_{\alpha_{L-1}} \Gamma^{[L]i_L,j_L}_{\alpha_{L-1},1}) ||i_1 \cdots i_L, j_1 \cdots j_L\rangle\rangle . \tag{A.8}$$

The bond-link dimension χ of the MPO (A.8) can be kept under a given threshold by cutting the smallest singular values. Hence, it is proportional to the amount of quantum correlations between the system sites, that can be encoded in $|\rho_{\mathrm{MPO}}\rangle$. Starting from $\chi = 1$ (separable state) and increasing χ, quantum correlations can be taken into account at increasing distance.

At this stage, the TEBD scheme can be naturally embedded in the Ansatz given in Eq. (A.8), by performing a Suzuki-Trotter decomposition [HS05] of the Liouvillian super-operator $\mathcal{L}_{\#}$ of a Lindblad master equation

$$\frac{d}{dt}|\rho_{\mathrm{MPO}}\rangle(t) = \mathcal{L}_{\#}|\rho_{\mathrm{MPO}}\rangle. \tag{A.9}$$

For a one-dimensional system with only local and nearest-neighbour interactions,

$$\mathcal{L}_{\#} = \sum_{i\in\text{odd}} \mathcal{L}^{i}_{\#} + \mathcal{L}^{i,i+1}_{\#} + \sum_{i\in\text{even}} \mathcal{L}^{i}_{\#} + \mathcal{L}^{i,i+1}_{\#} = \mathcal{L}_{\#\text{odd}} + \mathcal{L}_{\#\text{even}} \ , \tag{A.10}$$

where $\mathcal{L}^{i}_{\#}$ are linear operators acting on a local site i, and on the r.h.s equality we have divided the lattice into even and odd sites. This division is useful since all terms inside $\mathcal{L}_{\#\text{odd}}(\mathcal{L}_{\#\text{even}})$ commute with each other. Thus, performing a Suzuki-Trotter decomposition, the evolution of $|\rho_{\text{MPO}}\rangle$ at each time $t+dt$ can be written as

$$\begin{aligned} |\rho_{\text{MPO}}\rangle(t+dt) &= \mathrm{e}^{\mathcal{L}_{\#}dt}|\rho_{\text{MPO}}\rangle(t) = \\ &= \prod_{i\in\text{odd}} \mathrm{e}^{\mathcal{L}^{i}_{\#\text{odd}}\frac{dt}{2}} \prod_{i\in\text{odd}} \mathrm{e}^{\mathcal{L}^{i}_{\#\text{even}}dt} \prod_{i\in\text{odd}} \mathrm{e}^{\mathcal{L}^{i}_{\#\text{odd}}\frac{dt}{2}} |\rho_{\text{MPO}}\rangle(t) + O(dt^3). \end{aligned} \tag{A.11}$$

Fortunately, updating the description (A.11) of $|\rho_{\text{MPO}}\rangle$ at time $t+dt$ involves a product of local $\mathcal{L}^{n}_{\#}$ and nearest-neighbour $\mathcal{L}^{n,n+1}_{\#}$ operators acting on site n. Thus, they only change the local tensor $\Gamma^{[n]}\lambda^{[n]}\Gamma^{[n+1]}$, whose associated computational cost is of $O(\chi^2)$ basic operations.

Finally, we are mainly interested in computing stationary state properties of the system. The time needed to reach the steady-state is of the order of the inverse of the Lindbladian gap[3]. Close to a phase transition point, the gap necessarily goes to zero and the method is not very well-suited, due to the unavoidable growth of the computational time needed to reach the steady state. The same problem appears in closed systems when finding the ground state of a certain configuration, using imaginary time evolution. Finally, one should also pay attention to the stability of the resulting steady state solution with respect to the bond dimension χ. If the MPO is faithfully capturing most of the correlations present in the system, the steady state solution should not vary by increasing χ.

A.1.2 Quantum trajectories

The method of **quantum trajectories (QT)** [DCM92] describes a protocol to numerically simulate dissipative dynamics. It was initially used in quantum optics as a technique to compute the time evolution of a density matrix following a Lindblad master equation[4]. It was first introduced [DCM92] as a Monte Carlo method to study laser cooling.

Instead of addressing directly the master equation, we solve the dynamics as a **stochastic average** over individual trajectories, which can be numerically evolved in time as pure states. We only perform a stochastic evolution protocol over a pure state vector of size 2^L (L spins-1/2), instead of a density matrix $\rho(t)$ of dimension

[3] The Lindbladian gap is given by the non-zero eigenvalue with the smallest real part of the Liouville super-operator in Eq. (A.10).

[4] In chapter 2 we explained the structure and the main properties of a Lindblad master equation.

$2^L \times 2^L$. The QT approach requires to manipulate $N \times 2^L$ elements, N being the number of trajectories. Typically, $N \ll 2^L$ is sufficient to get reliable results (small statistical errors).

The QT protocol [Dal14] works as follows. Let us consider a interacting spin-1/2 chain, governed by a Lindblad master equation

$$\frac{\partial \rho}{\partial t} = -\frac{i}{\hbar}[\hat{H}, \rho] + \sum_j \mathcal{L}_j[\rho]\,. \tag{A.12}$$

The first term in the r.h.s. describes the coherent unitary time evolution (ruled by the system Hamiltonian $\hat{H}$). The second term, corresponding to a sum of local Lindbladian superoperators $\mathcal{L}_j[\rho]$, takes into account the coupling to the external environment. In particular, we assume the following form

$$\sum_j \mathcal{L}_j[\rho] = \gamma \sum_j \left[\hat{\sigma}_j^- \rho\, \hat{\sigma}_j^+ - \frac{1}{2}\left\{ \hat{\sigma}_j^+ \hat{\sigma}_j^-, \rho \right\} \right], \tag{A.13}$$

where γ is the dissipative rate that tends to flip all spins down, $\hat{\sigma}_j^\alpha$ ($\alpha = x, y, z$) denote the Pauli matrices on the j-th site of the system, and $\hat{\sigma}_j^\pm = \frac{1}{2}\ \hat{\sigma}_j^x \pm \mathrm{i}\hat{\sigma}_j^y$ stand for the corresponding raising and lowering operators along the z axis.

The unitary time evolution part of Eq. (2.23), together with the anti-commutator term in Eq. (2.25), can be regarded as if the evolution were performed by means of an effective non-Hermitian Hamiltonian $\hat{H}_{\text{eff}} = \hat{H} + i\hat{K}$, with $\hat{K} = -\frac{\gamma}{2}\sum_j \hat{\sigma}_j^+ \hat{\sigma}_j^-$. The remaining term in Eq. (A.13) originates the so-called **quantum jumps**. If the density matrix at some reference time t_0 is given by the pure state $\rho(t_0) = |\psi_0\rangle\langle\psi_0|$, after an infinitesimal amount of time δt, it will evolve into the statistical mixture of pure states $\{|\tilde{\psi}_0\rangle, |\tilde{\psi}_j\rangle\}_{j=1,\ldots,L}$ (the tilde indicates states at time $t_0 + \delta t$) [Dal14],

$$\rho(t_0 + \delta t) = \ 1 - \sum_j \mathrm{d}p_j\ \ |\tilde{\psi}_0\rangle\langle\tilde{\psi}_0| + \sum_j \mathrm{d}p_j |\tilde{\psi}_j\rangle\langle\tilde{\psi}_j|\,, \tag{A.14}$$

where $\mathrm{d}p_j = \gamma^2 \langle\psi_0|\hat{\sigma}_j^+\hat{\sigma}_j^-|\psi_0\rangle$ and

$$|\tilde{\psi}_0\rangle = \frac{e^{-i\hat{H}_{\text{eff}}\delta t}|\psi_0\rangle}{\sqrt{1 - \sum_j \mathrm{d}p_j}}\,, \quad |\tilde{\psi}_j\rangle = \frac{\hat{\sigma}_j^-|\psi_0\rangle}{\|\hat{\sigma}_j^-|\psi_0\rangle\|}\,. \tag{A.15}$$

Therefore, if we prepare an initial pure state $|\psi_0\rangle$ at time t_0:

1. With probability $\mathrm{d}p_j$, the state evolves or "jumps" to state $|\tilde{\psi}_j\rangle$ at time δt.
2. With probability $1 - \sum_j \mathrm{d}p_j$, there are no jumps and the state $|\psi_0\rangle$ unitarily evolves according to $\hat{H}_{\text{eff}}$. The state at time δt would be $|\tilde{\psi}_0\rangle$.

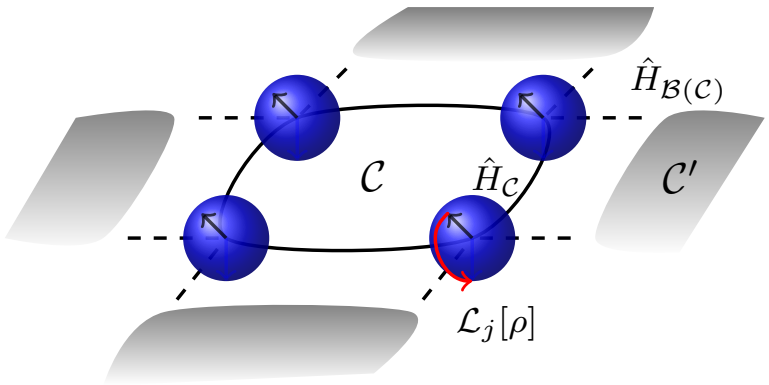

Figure A.1: Sketch of the cluster mean-field approach in a dissipative system of interacting spin-1/2 particles. The figure refers to 2×2 cluster on a two-dimensional square lattice.

Assuming there is a single steady state $\rho_{\rm SS}$ for Eq. (A.12),

$$\mathrm{Tr}(\hat{O}\rho_{\rm SS}) = \lim_{T\to\infty} \frac{1}{T} \int_{T_0}^{T_0+T} \langle\psi(t)|\hat{O}|\psi(t)\rangle \mathrm{d}t\,, \tag{A.16}$$

for any observable $\hat{O}$ and for a sufficiently long waiting time T_0 [DCM92]. In practical situations, one usually takes T_0 to be the typical time-scale to relax to the steady state (about the inverse of the Lindbladian gap). The state $|\psi(t)\rangle$ is stochastically chosen among those in Eq. (A.15), according to the statistical mixture (A.14), after iterating the above algorithm for $(T - T_0)/\delta t$ times. The time interval δt has to be much smaller than the relevant dynamical time scales. If the trajectory is randomly chosen, it is possible to compute the asymptotic average for a single trajectory; however, Eq. (A.16) is only exact at $T \to \infty$. Therefore, we can speed up the convergence of Eq. (A.15) for a sufficiently large T, by averaging over different trajectories.

A.1.3 Cluster mean-field approximation

Mean-field theory is a very useful and extended approximation to deal with hard-to-solve many-body problems in physics. The main idea of this method can be summarised in the following way: mean-field theory transforms an interacting many-body system into a single-particle problem, embedded inside a background field generated by the other particles. In other words, if we focus on a single-particle of the system, the effect of all interactions among particles can be averaged out into a background field.

This is actually a very crude approximation, since we are neglecting fluctuations at all orders by considering only a uniform background field. **Mean-field theory** is based on the assumption that fluctuations around the average value of the order

parameter are small enough to be neglected. For low dimensional equilibrium systems, specially close to a phase transition point, fluctuations become important and mean field theory may give qualitatively wrong predictions. Dimensionality plays a big role in determining whether a mean-field approach will work for any particular problem. Generally, the larger the dimension the more accurate the mean-field approximation becomes. Notorious examples where mean-field gives qualitatively good predictions are the BCS theory of superconductivity [BCS57], liquid crystals [WA58], magnetic models in large spatial dimensions [SV87], etc. For the the 2D Ising model [Ons44], mean-field theory correctly predicts the existence of a phase transition, despite not yielding the correct critical exponents.

On the other hand, one of the most famous examples where mean-field theory completely fails is the 1D Ising model [Isi25]. This classical spin model is exactly solvable and has no phase transition. However, mean-field theory predicts a paramagnetic (PM) to ferromagnetic (FM) phase transition at some critical temperature T_c. As the model is exactly solvable, there is no doubt that the mean-field result is wrong. A complementary way to show the absence of a phase transition within the mean-field philosophy can be done by incorporating short-range fluctuations [Yam09]. This method is referred to in the literature as **cluster mean-field**.

Let us consider the Hamiltonian of a 2D spin model with nearest-neighbour interactions $\hat{H} = \sum_{\langle i,j\rangle} \hat{h}_{ij}$. We isolate a given subset $\mathcal{C}$ of contiguous lattice sites (**cluster**), from the rest of the lattice forming the system [see Fig. A.1]. The decoupled cluster mean-field (CMF) Hamiltonian with respect to the cluster can be written as

$$\hat{H}_{\text{CMF}} = \hat{H}_{\mathcal{C}} + \hat{H}_{\mathcal{B}(\mathcal{C})}\,, \tag{A.17}$$

where

$$\hat{H}_{\mathcal{C}} = \sum_{\langle i,j\rangle | i,j\in\mathcal{C}} \hat{h}_{ij} \tag{A.18}$$

faithfully describes the interactions inside the cluster, while

$$\hat{H}_{\mathcal{B}(\mathcal{C})} = \sum_{j\in\mathcal{B}(\mathcal{C})} \mathbf{B}_j^{\text{eff}} \cdot \hat{\boldsymbol{\sigma}}_j \tag{A.19}$$

effectively represents the mean-field interactions of the cluster $\mathcal{C}$ with its neighbors [$\hat{\boldsymbol{\sigma}}_j = (\hat{\sigma}_j^x, \hat{\sigma}_j^y, \hat{\sigma}_j^z)$]. The sum is restricted to boundary sites $\mathcal{B}(\mathcal{C})$ of the cluster. The parameter $\mathbf{B}_j^{\text{eff}} = (B_j^x, B_j^y, B_j^z)$ in Eq. (A.19) is related to the average magnetisation of the neighboring spins of i belonging to the cluster $\mathcal{C}'$ adjacent to $\mathcal{C}$. The effective field needs to be computed self-consistently.

In **equilibrium** systems, the self-consistency determination of the average magnetisation usually relies on the **free-energy minimisation**, based on the Gibbs-Bogolyubov inequality [Oku71]. We will give some intuition for this variational method. Let us consider a Hamiltonian

$$H = H_0 + H_1, \tag{A.20}$$

that can be divided into an easy solvable part H_0 and a more difficult (probably non-solvable) part H_1. We now replace H by a trial Hamiltonian

$$\hat{H} = H_0 + \langle H_1 \rangle_0 \,, \tag{A.21}$$

where $\langle\ \rangle_0$ stands for the average over the canonical ensemble defined by H_0. By averaging H_1, the resulting Hamiltonian $\hat{H}$ can be solved. It is clear that $\langle H \rangle_0 = \langle \hat{H} \rangle_0$, which implies [Oku71] that the following inequality holds $F \leq \hat{F}$, where $\hat{F}$ is the free energy for $\hat{H}$. By minimising $\hat{F}$ with respect to the mean-field parameters (e.g. the magnetisation), we obtain the self-consistency equations for those same parameters. In general, the approximation of Hamiltonian H by $\hat{H}$ tends to be better, the larger the spatial dimension is.

For **non-equilibrium** systems, the situation is quite different. Once the mean-field or cluster mean-field approximation in the Liouvillian has been performed, the spin magnetisation (or any other local observable) is determined **dynamically**. We compute the steady state value of the magnetisation by dynamically solving the master equation (e.g. Eq. (A.12)). During the evolution, the value of $\mathbf{B}_j^{\text{eff}}$ is hence determined self-consistently in time. The full problem is eventually simplified into the evolution of the density matrix ρ_c of the cluster in the presence of a time-dependent effective field $\mathbf{B}_j^{\text{eff}}(t)$.

Finally, in order to improve the accuracy of the method and to have a reliable scaling of the correlations, clusters of sufficiently large dimensions need to be considered. For small clusters a direct integration of the cluster master equation is feasible, while larger clusters can be faithfully treated by combining the cluster mean-field approach with quantum trajectories and tensor-network techniques.

This new method for self-consistency determination of the mean-field $\mathbf{B}_j^{\text{eff}}(t)$ is a crucial difference between equilibrium and non-equilibrium systems. Actually, this is the fundamental reason why me may expect qualitatively different behaviour from the inclusion of short-range fluctuations in non-equilibrium situations.

As commented before, the cluster mean-field (CMF) method can be combined with quantum trajectories (QT) techniques. For each time evolving quantum trajectory, one finds the corresponding mean fields for each site j inside the considered cluster. The mean field $\mathbf{B}_j^{\text{eff}}$ that appears in the effective Hamiltonian in Eq. (A.19), to be used in the master equation for the cluster density matrix, is obtained by averaging over all the N trajectories. For 1D dissipative many-body systems, it is also possible to combine CMF with the master-equation dynamics simulated by means of the TEBD scheme using MPOs. The only novel ingredient is provided by the mean fields computed at the two edge sites of the chain. These can be easily evaluated self-consistently in time within the TEBD scheme.

A.2 Outline of the main results

- ✓ We study a magnetic system of spin-1/2 particles located on a two-dimensional square lattice. The interactions of the system are described by the so-called Heisenberg XYZ model, and we allow for spin-flip transitions associated to some external dissipative coupling.
- ✓ The unitary dynamics induced by the Hamiltonian (XYZ model) compete with the dissipative ones generated by a Lindbladian (spin flips), thus giving rise to non-equilibrium effects.
- ✓ We extend the cluster mean-field method widely used in equilibrium situations, to a new out-of-equilibrium scenario in open quantum systems.
- ✓ Contrary to equilibrium thermodynamics, the inclusion of short-range fluctuations, by means of the cluster mean-field method, deeply modifies the steady-state phase-diagram topology of driven-dissipative quantum systems.
- ✓ We combine powerful numerical methods together with the cluster mean-field approach. Namely, we employ tensor-networks (like matrix-product operators) and quantum trajectories techniques.
- ✓ For standard single-site mean-field, where correlations are completely neglected, the system displays a ferromagnetic (FM) phase. However, when short-range correlations are taken into account, they produce a reentrance of the paramagnetic (PM) phase that changes the topology of the single-site mean-field phase diagram.
- ✓ We perform a stability analysis showing the robustness of these results against perturbations.
- ✓ Our results are amenable to experimental verification using novel quantum-simulation platforms like trapped ions, highly excited Rydberg states of ultracold atoms, and arrays of coupled optical or microwave cavities.

Cluster Mean-Field Approach to the Steady-State Phase Diagram of Dissipative Spin Systems

Jiasen Jin,[1] Alberto Biella,[2,3] Oscar Viyuela,[4] Leonardo Mazza,[5,2,3] Jonathan Keeling,[6,3] Rosario Fazio,[7,2,3] and Davide Rossini[2,3]

[1]*School of Physics and Optoelectronic Engineering, Dalian University of Technology, 116024 Dalian, China*

[2]*NEST, Scuola Normale Superiore and Istituto Nanoscienze-CNR, I-56126 Pisa, Italy*

[3]*Kavli Institute for Theoretical Physics, University of California, Santa Barbara, California 93106, USA*

[4]*Departamento de Física Teórica I, Universidad Complutense, 28040 Madrid, Spain*

[5]*Département de Physique, Ecole Normale Supérieure/PSL Research University, CNRS, 24 rue Lhomond, F-75005 Paris, France*

[6]*SUPA, School of Physics and Astronomy, University of St. Andrews, St. Andrews KY16 9SS, United Kingdom*

[7]*ICTP, Strada Costiera 11, 34151 Trieste, Italy*

(Received 22 February 2016; revised manuscript received 20 May 2016; published 27 July 2016)

We show that short-range correlations have a dramatic impact on the steady-state phase diagram of quantum driven-dissipative systems. This effect, never observed in equilibrium, follows from the fact that ordering in the steady state is of dynamical origin, and is established only at very long times, whereas in thermodynamic equilibrium it arises from the properties of the (free) energy. To this end, by combining the cluster methods extensively used in equilibrium phase transitions to quantum trajectories and tensor-network techniques, we extend them to nonequilibrium phase transitions in dissipative many-body systems. We analyze in detail a model of spin-$1/2$ on a lattice interacting through an XYZ Hamiltonian, each of them coupled to an independent environment that induces incoherent spin flips. In the steady-state phase diagram derived from our cluster approach, the location of the phase boundaries and even its topology radically change, introducing reentrance of the paramagnetic phase as compared to the single-site mean field where correlations are neglected. Furthermore, a stability analysis of the cluster mean field indicates a susceptibility towards a possible incommensurate ordering, not present if short-range correlations are ignored.

DOI: 10.1103/PhysRevX.6.031011

Subject Areas: Condensed Matter Physics, Statistical Physics

I. INTRODUCTION

In thermodynamic equilibrium, a transition to a state with a spontaneous broken symmetry can be induced by a change in the external conditions (such as temperature or pressure) or in the control parameters (such as an external applied field). The most widely studied examples are for systems at nonzero temperature, in the framework of classical phase transitions [1]. Here, equilibrium thermal fluctuations are responsible for the critical behavior associated with the discontinuous change of the thermodynamic properties of the system. Transitions may also occur at zero temperature, as a function of some coupling constant [2]; in that case, since there are no thermal fluctuations, quantum fluctuations play a prominent role. For many decades, the study of phase transitions and critical phenomena has attracted the attention of a multitude of scientists from the most diverse fields of investigations: Phase transitions are present at all energy scales, in cosmology and high-energy physics, as well as in condensed matter.

Moving away from the thermodynamic equilibrium, collective phenomena and ordering also appear in open systems, upon tuning the rate of transitions caused by the environment [3]. For example, they emerge in most diverse situations [4] ranging from the synchronous flashing of fireflies [5] to the evolution of financial markets [6]. The classical statistical mechanics of such driven systems (including traffic models, active matter, and flocking) has attracted increased attention over the years; see, e.g., Refs. [7,8]. Such interest is in part due to the remarkable possibility of achieving ordered states that are not possible in equilibrium systems, displaying, for example, long-range order in two-dimensional flocking [9], something forbidden by the Mermin-Wagner theorem [10] in equilibrium.

Thanks to the recent impressing experimental progresses (see, e.g., Refs. [11–13]), the investigation of nonequilibrium properties of driven-dissipative systems has entered the quantum world. Rydberg atoms in optical lattices [14],

systems of trapped ions [14], exciton-polariton condensates [15], cold atoms in cavities [16], and arrays of coupled QED cavities [17,18] are probably the most intensively investigated experimental platforms in relation to this aim. The predicted steady-state phase diagram of these driven-dissipative systems becomes incredibly rich, displaying a variety of phenomena. Just as for classical statistical mechanics, phases, which are not possible in an equilibrium phase diagram, may appear [19]. The steady state itself need not be time independent, and the system may end up in a limit cycle [20–24]. Renormalization-group (RG) calculations using the Keldysh formalism have been performed [25]; in some cases, the universality class of the transitions may be modified both by the presence of the external environment and by nonequilibrium effects [26,27]. A judicious engineering of the system-bath couplings can lead to nontrivial many-body states in the stationary regime [28,29]. The field of dissipative many-body open systems embraces a much wider class of problems, ranging from transport to relaxation dynamics to quantum information processing (just to mention a few examples). A more comprehensive panorama of the recent literature can also be found in Refs. [30–49] and citations therein.

In condensed matter systems, most notably in Josephson junction arrays, the impact of an external bath on the phase diagram and the relative critical properties have been thoroughly studied over the last 20 years; see, e.g., Refs. [50–53]. In all of those studies, the system and the bath were in an overall equilibrium situation at a given (possibly zero) temperature. In quantum driven-dissipative systems, such as the one considered here, nonequilibrium conditions and the flow of energy through the system play a major role.

Our work focuses on an important aspect of the physics of many-body open systems: the determination of the steady-state phase diagram. We consider systems in which the coupling to the environment leads to a Markovian dynamics. In these cases, the evolution of the corresponding density matrix $\rho(t)$ obeys the Lindblad equation

$$\frac{\partial \rho}{\partial t} = -\frac{i}{\hbar}[\hat{H}, \rho] + \sum_j \mathcal{L}_j[\rho]. \tag{1}$$

The first term in the rhs describes the coherent unitary time evolution (ruled by the system Hamiltonian $\hat{H}$). The second term, corresponding to a sum of Lindbladian superoperators $\mathcal{L}_j[\rho]$, takes into account the coupling to the external bath(s). The steady-state phase diagram is obtained by looking at the long-time limit ($t \to \infty$) of the solution to Eq. (1) and computing appropriate averages $\langle \hat{O} \rangle = \mathrm{Tr}[\hat{O}\rho_{t\to\infty}] \equiv \mathrm{Tr}[\hat{O}\rho_{\mathrm{SS}}]$ of local observables $\hat{O}$, in order to determine the (possible) existence of phases with broken symmetries (space, time, spin, …) [54].

Nearly all the results obtained so far on the phase diagram (with the notable exception of the works based on Keldysh RG mentioned above) rely on the (single-site) mean-field approximation, where all the correlations are ignored. Very little is known beyond that limit about the interplay between many-body correlations and dissipation, although there are some contributions in this direction [55–57]. While quasi-exact numerical methods exist for open one-dimensional (1D) systems, unfortunately no true phase transitions are expected to occur in that context. Beyond one dimension, such methods are much harder to apply. However, it is well known that the mean-field decoupling, while important to grasp the salient features of the system, is not at all accurate in locating the phase boundaries.

An improvement in the determination of the phase diagram can be obtained by a systematic inclusion of short-range correlations (up to a given cluster size). In equilibrium, this has been achieved within the cluster mean-field approximation [58–60] and using linked cluster expansions [61]. In the cluster mean-field approach, the accuracy of the diagram is obviously related to the size of the considered cluster. Even though it is still mean field in nature, a suitable scheme that combines it with finite-size scaling may, in principle, allow us to extract nonclassical critical exponents [62]. In higher dimensions (above the lower critical one) where one expects spontaneous symmetry breaking, cluster methods lead only to quantitative corrections (a mere shift) to the mean-field predictions. These corrections become smaller on increasing the dimensionality.

For equilibrium phase transitions, the topology of the phase diagram is well captured at the mean-field level, and the short-range fluctuations considered by cluster methods only lead to shifts in the location of the transition lines or points. Normally, they do not cut an ordered phase into two separate parts, divided by a disordered region. The possibility to have a radical change of topology is, however, permitted out of equilibrium, where the spontaneous breaking of symmetry is of pure dynamical nature: Terms that are formally irrelevant in the RG sense can nonetheless modify the flow of RG-relevant terms, so as to move a point in parameter space from one side to the other side of a phase boundary. Such a scenario is rarely, if ever, seen in equilibrium.

We demonstrate that the above picture is indeed verified in the open many-body context, and ordering with a nontrivial spatial pattern may emerge (see Fig. 1). The most natural way to show this is to include correlations through a cluster mean-field analysis which, to the best of our knowledge, has never been systematically applied in the open many-body context. Although the general strategy is the same as for equilibrium systems, there are several peculiarities emerging in this scenario, which need to be carefully addressed. The steady-state solution typically

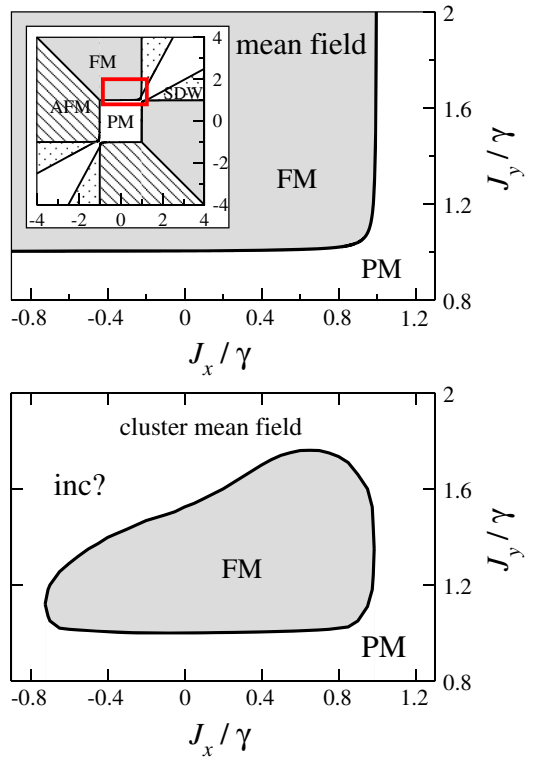

FIG. 1. A sketch of the phase diagram of the model defined by Eqs. (2) and (3), for $J_z = 1$. The single-site mean field as worked out in Ref. [19] would predict the emergence of different phases: paramagnetic (PM), ferromagnetic (FM), antiferromagnetic (AFM), and spin-density-wave (SDW) phases (inset to the top panel). Here, we focus on the region highlighted by the red box, which displays a transition from PM to FM states (magnified in the top panel). A proper inclusion of short-range correlations (through the cluster mean field) shrinks the ferromagnetic region to a small "island," thus suppressing the order at large couplings and hinting at a possible incommensurate (inc) ordering (bottom panel).

needs to be obtained dynamically via Eq. (1) (and not through a solution of a self-consistent equation [63]). To increase the cluster size, we introduce a new approach that combines the cluster mean field with quantum trajectories [64] and with matrix-product operators [65,66].

We apply our technique to a spin-1/2 XYZ model with relaxation (as previously studied by Lee *et al.* [19]) and show that the short-range correlations captured by the cluster approach can have a dramatic effect on the phase diagram. This last point is exemplified in Fig. 1 (which summarizes one of our main results). A mean-field analysis predicts a transition from a paramagnet to a ferromagnet (upper panel) in the whole region of large couplings $J_y > J_y^c$. The lower panel sketches the outcome of the cluster analysis. The ferromagnetic regime has shrunk to a finite region disappearing in the limit of large couplings. For an equilibrium system, such behavior would be very strange: Large coupling strengths increase the tendency toward ferromagnetic order, yet here we find that the ordered state is destroyed by strong couplings. Furthermore, indications from a stability analysis hint at a different type of ordering at large values of J_y.

The paper is organized as follows. In the next section, we define the spin-1/2 model with nearest-neighbor XYZ interactions coupled to a local bath, which will be considered in the following. We then introduce the cluster mean-field approach to driven-dissipative systems and show how to combine it with quantum trajectories (Sec. III B) and with the matrix-product-operator (Sec. III C) formalism. We see this method at work by looking at the steady-state phase diagram and comparing its rich features with those pointed out in Ref. [19] at the single-site mean-field level. Specifically, in Sec. IV, we discuss how the location of the transition lines is qualitatively changed in the cluster approach. Our aim is to highlight the key role of short-range correlations in driven-dissipative systems. For this purpose, we concentrate on a specific region of the diagram where a paramagnetic-to-ferromagnetic transition takes place. In one dimension (Sec. IV A), the cluster approach with appropriate scaling restores the absence of symmetry breaking. While the one-dimensional results presented here are as expected, we believe they are, however, useful as a benchmark of the numerical methods employed in the rest of this paper. Surprises appear in the two-dimensional case (Sec. IV B), where a ferromagnetic phase is possible. Including cluster correlations gives rise to a phase diagram that is radically different from what was derived within a single-site mean field. The extent of the ferromagnetic region becomes finite. The nature of such transitions is discussed in Sec. IV C, where a stability analysis around the mean-field solution is performed. The finite extent of the ordered phase appears to persist in higher-dimensional systems (Sec. IV D), even though the mean field progressively becomes, as expected, more accurate. The underlying dynamical mechanism responsible for such dramatic modifications in the phase diagram will be discussed in Sec. IV E, where we provide a more physical intuition of the results obtained in this work. Finally, in Sec. V, we conclude with a brief summary of our results.

II. THE MODEL

We consider a spin-1/2 lattice system whose coherent internal dynamics is governed by an anisotropic XYZ-Heisenberg Hamiltonian,

$$\hat{H} = \sum_{\langle i,j\rangle} h_{ij} = \sum_{\langle i,j\rangle} (J_x \hat{\sigma}_i^x \hat{\sigma}_j^x + J_y \hat{\sigma}_i^y \hat{\sigma}_j^y + J_z \hat{\sigma}_i^z \hat{\sigma}_j^z), \quad (2)$$

with $\hat{\sigma}_j^\alpha$ ($\alpha = x, y, z$) denoting the Pauli matrices on the jth site of the system. The Lindbladian for this model reads

$$\sum_j \mathcal{L}_j[\rho] = \gamma \sum_j \left[\hat{\sigma}_j^- \rho \hat{\sigma}_j^+ - \frac{1}{2}\{\hat{\sigma}_j^+ \hat{\sigma}_j^-, \rho\} \right], \tag{3}$$

where γ is the rate of the dissipative processes that tend to flip all the spins down independently [$\hat{\sigma}_j^{\pm} = \frac{1}{2}(\hat{\sigma}_j^x \pm \hat{\sigma}_j^y)$ stand for the corresponding raising and lowering operators along the z axis]. In the rest of the paper, we set $\hbar = 1$ and work in units of γ. The (single-site) mean-field phase diagram of the model defined in Eqs. (2) and (3) has been worked out in Ref. [19]; for orientation, we summarize the main results of this analysis here.

It is important to remark that an in-plane XY anisotropy ($J_x \neq J_y$) is fundamental to counteract the dissipative spin flips along the orthogonal direction [19]. In the case in which $J_x = J_y$, Eq. (2) reduces to an XXZ Heisenberg model. Since this latter conserves the global magnetization along the z axis, the steady-state solution $\rho_{\rm SS}$ of Eq. (1) would trivially coincide with the pure product state having all the spins aligned and pointing down along the z direction. This corresponds to a paramagnetic state where the dissipation is dominant, and such that $\langle \hat{\sigma}_j^x \rangle_{\rm SS} = \langle \hat{\sigma}_j^y \rangle_{\rm SS} = 0$ and $\langle \hat{\sigma}_j^z \rangle_{\rm SS} = -1$, where $\langle \hat{O} \rangle_{\rm SS} = {\rm Tr}(\hat{O}\rho_{\rm SS})$ denotes the expectation value of a given observable $\hat{O}$ on the steady state.

The steady-state phase diagram presented in Ref. [19] is particularly rich and includes, for strongly anisotropic spin-spin interactions, ferromagnetic, antiferromagnetic, spin-density-wave, and staggered-XY states. Hereafter, we concentrate on the regime of parameters J_x, $J_y \geq 1$ and $J_z = 1$, where the single-site mean field predicts a single ferromagnetic (FM) to paramagnetic (PM) phase transition. Indeed, by changing the various coupling constants, the PM phase may become unstable and the system can acquire a finite magnetization along the xy plane ($\langle \hat{\sigma}_j^x \rangle_{\rm SS}, \langle \hat{\sigma}_j^y \rangle_{\rm SS} \neq 0$), thus entering a FM phase. This fact is associated with the spontaneous breaking of the $\mathbb{Z}_2$ symmetry, which is present in the model and corresponds to a π rotation along the z axis ($\hat{\sigma}^x \to -\hat{\sigma}^x$, $\hat{\sigma}^y \to -\hat{\sigma}^y$). The picture changes dramatically when local correlations are included.

As already mentioned in the Introduction, in an open system the stationary state may also break time-translational invariance (the steady state is time periodic) [20–24]. Our numerics suggests that a time-independent solution exists for all parameters we study, and so we will not consider this last case and instead concentrate on stationary time-independent solutions. This corresponds to the stationary point of Eq. (1), $\partial_t \rho_{\rm SS} = 0$, irrespective of the initial condition. In the remainder of the paper, we always implicitly refer to this occurrence.

III. METHODS

Solving Eq. (1) for a many-body system is a formidable task, even from a numerical point of view. The exponential increase of the Hilbert space makes a direct integration of the master equation unfeasible already for relatively small system sizes. Indeed, one needs to manipulate a density matrix of dimensions $2^L \times 2^L$, which becomes a computationally intractable task already for quite a small number of sites ($L \gtrsim 10$). In order to access systems as large as possible and to perform finite-size scaling up to reasonable sizes, we employ a combination of strategies.

In this section, we discuss how to use cluster mean-field methods for driven-dissipative systems; these will be employed to determine the phase diagram of the model defined by Eqs. (2) and (3). In order to keep the notation as simple as possible, we describe the cluster approach in the spin-1/2 language for nearest-neighbor Hamiltonians. A straightforward extension of our formalism allows us to consider generic short-range Hamiltonians of the form $\hat{H} = \sum_i \hat{h}_i^{(0)} + \sum_{\langle i,j \rangle} \hat{h}_{ij}^{(1)} + \sum_{\langle\langle i,j \rangle\rangle} \hat{h}_{ij}^{(2)} + \cdots$ (with the various terms including on-site, nearest-neighbor, next nearest-neighbor, …, couplings, respectively) and a generic dissipator containing more than one Lindblad operator on each site.

A. Cluster mean field

Let us isolate a given subset $\mathcal{C}$ of contiguous lattice sites, hereafter called cluster, from the rest of the lattice forming the system (which is supposed to be at the thermodynamic limit). This is pictorially shown in Fig. 2. The decoupled cluster mean-field (CMF) Hamiltonian with respect to the cluster can be written as

$$\hat{H}_{\rm CMF} = \hat{H}_{\mathcal{C}} + \hat{H}_{\mathcal{B}(\mathcal{C})}, \tag{4}$$

where

$$\hat{H}_{\mathcal{C}} = \sum_{\langle i,j \rangle | i,j \in \mathcal{C}} \hat{h}_{ij} \tag{5}$$

faithfully describes the interactions inside the cluster, while

$$\hat{H}_{\mathcal{B}(\mathcal{C})} = \sum_{j \in \mathcal{B}(\mathcal{C})} \mathbf{B}_j^{\rm eff} \cdot \hat{\boldsymbol{\sigma}}_j \tag{6}$$

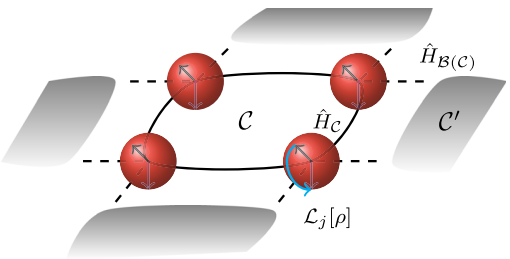

FIG. 2. Sketch of the cluster mean-field approach in a dissipative system of interacting spin-1/2 particles. The figure refers to a 2×2 cluster on a two-dimensional square lattice.

effectively represents the mean-field interactions of the cluster $\mathcal{C}$ with its neighbors [$\hat{\boldsymbol{\sigma}}_j = (\hat{\sigma}_j^x, \hat{\sigma}_j^y, \hat{\sigma}_j^z)$]. The sum is restricted to the sites on the boundary $\mathcal{B}(\mathcal{C})$ of the cluster. The parameter $\mathbf{B}_j^{\text{eff}} = (B_j^x, B_j^y, B_j^z)$ in Eq. (6) is related to the average magnetization of the neighboring spins of i belonging to the cluster $\mathcal{C}'$ adjacent to $\mathcal{C}$. The effective field needs to be computed self-consistently in time.

This reduced description arises from a factorized Ansatz for the global density matrix

$$\rho_{\text{CMF}} = \bigotimes_{\mathcal{C}} \rho_{\mathcal{C}}, \tag{7}$$

where $\rho_{\mathcal{C}}$ is the density matrix of the $\mathcal{C}$th cluster. Inserting such Ansatz into Eq. (1) and exploiting the translational invariance with respect to the cluster periodicity ($\rho_{\mathcal{C}} = \rho_{\mathcal{C}'}$, $\forall \mathcal{C}, \mathcal{C}'$), we get an effective master equation of the form

$$\frac{\partial \rho_{\mathcal{C}}}{\partial t} = -\frac{i}{\hbar}[\hat{H}_{\text{CMF}}, \rho_{\mathcal{C}}] + \sum_{j \in \mathcal{C}} \mathcal{L}_j[\rho_{\mathcal{C}}]. \tag{8}$$

We recall that the standard mean-field treatment derives from assuming that the cluster is formed by a single site.

The mean-field approach represents a crude approximation for a many-body interacting system since all the correlations are effectively neglected. The decoupling on a larger structure described above partially overcomes this problem: The idea is that interactions among the sites inside a cluster are treated exactly [see Eq. (5)], while those among neighboring clusters are treated at the mean-field level [see Eq. (6)]. As a consequence, short-range correlations inside the cluster are safely taken into account. The full problem is eventually simplified into the evolution of the density matrix $\rho_{\mathcal{C}}$ of the cluster in the presence of a time-dependent effective field $\mathbf{B}_j^{\text{eff}}(t)$.

So far, what we discussed equally applies to any cluster mean-field approximation, either classical or quantum. The only nontrivial modification in the present case is that one has to study the evolution of Eq. (8) in the presence of a time-dependent field that has to be determined self-consistently. In order to improve its accuracy and to have a reliable scaling of the correlations, clusters of sufficiently large dimensions need to be considered. For small clusters, a direct integration of the cluster master equation is feasible, while larger clusters can be faithfully treated by combining the above explained approach with specific techniques designed to deal with open systems. Specifically, we integrate the cluster mean-field approximation together with quantum trajectories and with tensor-network approaches. The idea and procedure is straightforward, but some practical details need to be stated explicitly. We present such details in the next sections.

B. Quantum trajectories

There is a simple procedure that allows us to avoid simulating the mixed time evolution of the full master equation (1) [which would need to store and evolve a $2^L \times 2^L$ matrix $\rho(t)$]. Indeed, it can be shown that one can equivalently perform a stochastic evolution protocol of a pure state vector of size 2^L, according to the quantum-trajectory (QT) approach [64] [which requires one to manipulate $N \times 2^L$ elements, N being the number of trajectories (typically $N \ll 2^L$ is sufficient to get reliable results)]. The unitary time evolution part of Eq. (1), together with the anticommutator term in Eq. (3), can be regarded as if the evolution were performed by means of an effective non-Hermitian Hamiltonian $\hat{H}_{\text{eff}} = \hat{H} + i\hat{K}$, with $\hat{K} = -(\gamma/2)\sum_j \hat{\sigma}_j^+ \hat{\sigma}_j^-$. The remaining term in Eq. (3) gives rise to the so-called quantum jumps. It can be shown that, if the density matrix at some reference time t_0 is given by the pure state $\rho(t_0) = |\psi_0\rangle\langle\psi_0|$, after an infinitesimal amount of time δt, it will evolve into the statistical mixture of the pure states $\{|\tilde{\psi}_0\rangle, |\tilde{\psi}_j\rangle\}_{j=1,\ldots,L}$ (the tilde indicates states at time $t_0 + \delta t$):

$$\rho(t_0 + \delta t) = \left(1 - \sum_j \mathrm{d}p_j\right)|\tilde{\psi}_0\rangle\langle\tilde{\psi}_0| + \sum_j \mathrm{d}p_j |\tilde{\psi}_j\rangle\langle\tilde{\psi}_j|, \tag{9}$$

where $\mathrm{d}p_j = \gamma\langle\psi_0|\hat{\sigma}_j^+\hat{\sigma}_j^-|\psi_0\rangle$ and

$$|\tilde{\psi}_0\rangle = \frac{e^{-i\hat{H}_{\text{eff}}\delta t}|\psi_0\rangle}{\sqrt{1 - \sum_j \mathrm{d}p_j}}, \qquad |\tilde{\psi}_j\rangle = \frac{\hat{\sigma}_j^-|\psi_0\rangle}{\|\hat{\sigma}_j^-|\psi_0\rangle\|}. \tag{10}$$

Therefore, with probability $\mathrm{d}p_j$ a jump to the state $|\tilde{\psi}_j\rangle$ occurs, while with probability $1 - \sum_j \mathrm{d}p_j$, there are no jumps and the system evolves according to $\hat{H}_{\text{eff}}$. Assuming that there exists a single steady state ρ_{SS} for Eq. (1), one has [64]

$$\mathrm{Tr}(\hat{O}\rho_{\text{SS}}) = \lim_{T\to\infty} \frac{1}{T}\int_{T_0}^{T_0+T} \langle\psi(t)|\hat{O}|\psi(t)\rangle \mathrm{d}t, \tag{11}$$

for any observable $\hat{O}$ and reference time T_0. The state $|\psi(t)\rangle$ is stochastically chosen among those in Eq. (10), according to the statistical mixture (9), after iterating the above algorithm for $(t - t_0)/\delta t$ times, where the time interval δt has to be much smaller than the relevant dynamical time scales.

It is possible to combine the QT method with the above-described CMF approach at the cost of some moderate modifications. In order to do that, it is necessary to perform a simulation of a sufficiently large number N of trajectories in parallel. For each trajectory k, the mean-field expectation value $\langle\hat{\boldsymbol{\sigma}}_j(t)\rangle_k \equiv {}_k\langle\psi(t)|\hat{\boldsymbol{\sigma}}_j|\psi(t)\rangle_k$ on each site j of the

considered cluster $\mathcal{C}$ is computed iteratively in time. The average over all the trajectories gives the correct mean field at time t,

$$\mathbf{B}_j^{\text{eff}}(t) = \frac{1}{N}\sum_{k=1}^{N}\langle\hat{\boldsymbol{\sigma}}_j(t)\rangle_k, \tag{12}$$

which has to be self-consistently used to describe effective interactions between adjacent clusters [see Eq. (6)]. Note that this approach corresponds to performing the stochastic unraveling of the cluster mean-field theory. Such an approach is different from performing a cluster mean-field decoupling of a stochastic unraveling of the original equation (i.e., each trajectory would evolve according to *its own* mean field).

Eventually, one gets an effective non-Hermitian cluster mean-field Hamiltonian

$$\hat{H}_{\text{eff,CMF}} = (\hat{H}_{\mathcal{C}} + i\hat{K}_{\mathcal{C}}) + \hat{H}_{\mathcal{B}(C)}, \tag{13}$$

which, together with the possibility of having quantum jumps, governs the time evolution of each trajectory for the next time step, as in Eqs. (9) and (10). The idea of this combined approach is schematically depicted in Fig. 3 and turns out to be effective to deal with clusters containing $L \gtrsim 10$ sites.

C. Matrix product operators

Quantum trajectories are not the only method that can be fruitfully combined to cluster mean-field techniques.

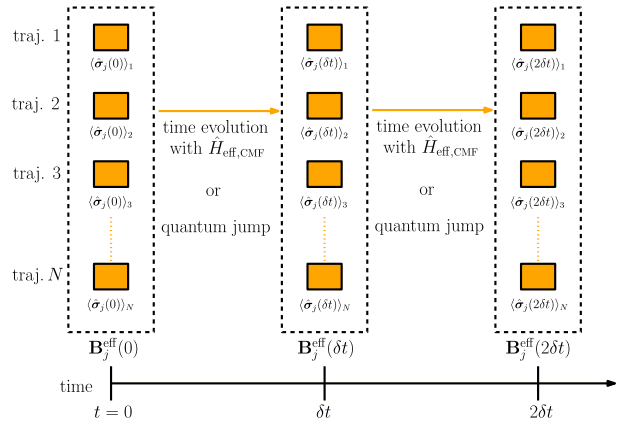

FIG. 3. Quantum trajectories combined with the mean-field or cluster mean-field method. Colored boxes along a given line stand for the time-evolved state of the kth trajectory, which is stochastically chosen among the set of pure states $\{|\psi_0(t)\rangle_k, |\psi_j(t)\rangle_k\}$ according to Eq. (9). For each of those states, one finds the corresponding mean fields on each site j inside the considered cluster, $\langle\hat{\boldsymbol{\sigma}}_j(t)\rangle_k$. The mean field $\mathbf{B}_j^{\text{eff}}(t)$ parametrizing the effective Hamiltonian in Eq. (13), to be used in the master equation for the cluster density matrix, is obtained by averaging over all the N trajectories.

Tensor networks are also ideally suited to this aim. Below, we consider matrix product operators (MPO) that work very well for 1D systems. It would be highly desirable to also have tensor-network approaches in higher dimensions. We believe that in combination with the cluster mean field, this will represent a significant step forward in an accurate analysis of this class of nonequilibrium critical points.

For 1D systems, the long-time limit of Eq. (1) can be faithfully addressed using a MPO Ansatz for the density matrix [65,66]. The solution ρ_{SS} is reached dynamically by following the time evolution according to Eq. (1), using an algorithm based on the time-evolving block decimation (TEBD) scheme [67] adapted to open systems.

The starting point is based on the fact that a generic many-body mixed state on an L-site lattice, $\rho = \sum_{\vec{i},\vec{j}} C_{i_1\ldots i_L, j_1\ldots j_L}|i_1\ldots i_L\rangle\langle j_1\ldots j_L|$ (we defined $\vec{i} = \{i_1\ldots i_L\}$), can be written as a matrix product state in the enlarged Hilbert space of dimension $d^L \otimes d^L$, where d is the dimension of the on-site Hilbert space. By means of repeated singular-value decompositions of the tensor $C_{i_1\cdots i_L, j_1\cdots j_L}$, it is possible to obtain

$$\rho_{\text{MPO}} = \sum_{\vec{i},\vec{j}=1}^{d}\sum_{\vec{\alpha}=1}^{\chi}(\Gamma_{1,\alpha_1}^{[1]i_1,j_1}\lambda_{\alpha_1}^{[1]})(\Gamma_{\alpha_1,\alpha_2}^{[2]i_2,j_2}\lambda_{\alpha_2}^{[2]})\ldots \times(\lambda_{\alpha_{L-1}}^{[L-1]}\Gamma_{\alpha_{L-1},1}^{[L]i_L,j_L})\|i_1\ldots i_L, j_1\ldots j_L\rangle\rangle, \tag{14}$$

where the super-ket $\|i_1\ldots i_L, j_1\ldots j_L\rangle\rangle = \otimes_{a=1}^{L}|i_a\rangle\langle j_a|$ is used in order to deal with the superoperator formalism, i.e., with linear operators acting on vector spaces of linear operators. The bond-link dimension χ of the MPO (14) can be kept under a given threshold by cutting the smallest singular values and is proportional to the amount of quantum correlations between the system sites that can be encoded in ρ_{MPO}. Starting from $\chi = 1$ (separable state) and increasing χ, quantum correlations can be taken into account at increasing distance.

The TEBD scheme can be naturally embedded in the Ansatz given in Eq. (14), by performing a Trotter decomposition of the Liouvillian superoperator [67] which describes the master equation (1) [this can be easily handled for Hamiltonian and Lindbladian equations written as sums of local terms, as in Eqs. (2) and (3)]. In the case of translationally invariant systems, it is even possible to adopt an infinite version of the TEBD (the i-TEBD), using the same approach that has been successfully applied to pure states [68]. Indeed, this can be generalized to encompass arbitrary 1D evolution operators that can be expressed as a (translationally invariant) tensor network [69]. The TEBD method has been proven to be very effective in many different open 1D quantum systems, such as coupled cavity arrays [44,70], Bose-Hubbard chains with bond dissipation [71], and driven or dissipative spin systems [72]. Alternative approaches based on the variational search of

the Liouvillian superoperator [73,74] or on the local purification of the density matrix [75] have been proposed recently.

The description of 1D dissipative many-body systems in terms of MPO and the search for the steady state by time evolving the Liouvillian superoperator can be combined with the CMF approach in a natural way (see Fig. 4 for a sketch of the idea). We consider a linear cluster of L sites with open boundary conditions (OBC); its master-equation dynamics can be simulated by means of the TEBD scheme. The only novel ingredient is provided by the mean fields that have to be applied only at the two edge sites of the chain (the leftmost and the rightmost site). These can be easily evaluated in a self-consistent way in time, by computing the average expectation values:

$$\mathbf{B}_1^{\mathrm{eff}}(t) = \mathrm{Tr}[\hat{\boldsymbol{\sigma}}_L \rho(t)], \qquad \mathbf{B}_L^{\mathrm{eff}}(t) = \mathrm{Tr}[\hat{\boldsymbol{\sigma}}_1 \rho(t)], \tag{15}$$

respectively, on site 1 and site L of the chain, at regular time intervals, as outlined above for the other methods. Such fields are inserted in the effective Hamiltonian (6), which is used to build up the Liouvillian operator for the time evolution up to the next iterative step.

As mentioned at the beginning of this subsection, the extension of all these ideas to two-dimensional systems would be very intriguing. For example, one could think to combine the cluster mean-field approach with MPOs using a mapping of the lattice to a one-dimensional structure with long-range interactions, through an appropriate wiring-up strategy. This method has already been successfully employed in the context of equilibrium

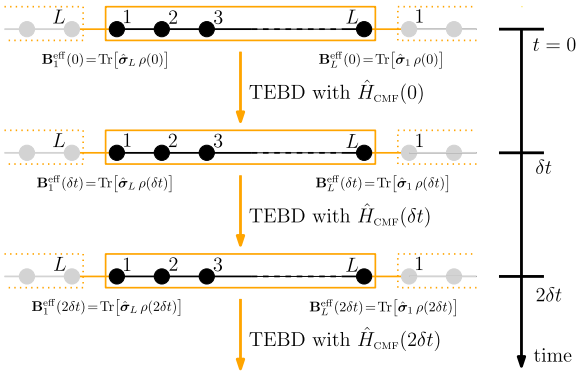

FIG. 4. One-dimensional TEBD scheme for 1D systems with open boundaries, combined with the cluster mean-field method. Circles denote the sites of the lattice. The many-body state corresponding to the OBC cluster made up of L black circles inside the orange box is written in a MPO representation and evolved in time with the TEBD scheme. The cluster is coupled to the rest of the system (gray circles) through the mean field at the edges. At regular small time intervals, the mean fields $\mathbf{B}_1^{\mathrm{eff}}(t) = \mathrm{Tr}[\hat{\boldsymbol{\sigma}}_L\rho(t)]$ on the leftmost site and $\mathbf{B}_L^{\mathrm{eff}}(t) = \mathrm{Tr}[\hat{\boldsymbol{\sigma}}_1\rho(t)]$ on the rightmost site are self-consistently evaluated and used to construct the Hamiltonian for the next TEBD iteration.

systems, where impressive results on wide strips have been obtained (see, e.g., Ref. [76]). In higher dimensions, these methods suffer from problems related to the computational cost of the tensor network contraction [77], which is common to all planar structures. The presence of dissipation could help reduce the amount of correlations in the steady state, so it might be possible that relatively good accuracies will be reached even with small bond links.

IV. RESULTS

Let us now put into practice the methods outlined above and study the PM-FM dissipative phase transition of the interacting spin model described by Eqs. (1)–(3). As detailed in Sec. II, this is associated with a $\mathbb{Z}_2$-symmetry-breaking mechanism, whose location in the phase diagram we would like to accurately unveil.

The full phase diagram at the single-site MF level has already been obtained in Ref. [19]. By writing the mean-field equations of motion for the magnetization along the different axes, it is possible to analytically evaluate the critical point separating the PM from the FM phase. For fixed values of J_x, J_z, it is located at

$$J_y^c = J_z - \frac{1}{16 z^2 (J_x - J_z)}, \tag{16}$$

where z is the coordination number of the lattice, i.e., the number of nearest neighbors of each lattice site. As in any single-site mean field, the only effect of the system's dimensionality enters through the integer z. From the theory of critical phenomena, we know that the role of dimensionality is crucial, particularly in low dimensions. Below, we show that, under a more careful treatment of the short-range correlations, the cluster mean field produces important qualitative and quantitative changes to the phase diagram. In the following subsections, we address the cases of increasing dimensionality. In one-dimensional systems, where we do not expect any phase transition, the cluster mean field, together with quantum trajectories and MPO, allows us to recover this result.

A. One dimension

The 1D case represents the most suitable situation to benchmark our methods. Here, due to the reduced dimensionality (the system has a coordination number $z = 2$), the MF predictions are known to fail, and no symmetry-breaking mechanism should occur (as already stated in Ref. [19]). Using a combination of strategies as described in Sec. III, we numerically verify the absence of symmetry breaking, thus gaining confidence on how accurate our methods can be for driven-dissipative systems.

We are able to perform a direct integration of the master equation (1) for systems with up to $L = 9$ spins, by employing a standard fourth-order Runge-Kutta (RK)

method, without applying consistent MF terms at the boundaries. For larger systems, with $10 \leq L \leq 16$, we use the quantum trajectory approach (the time evolution of each trajectory is computed by means of a fourth-order RK method) obtaining reliable results already with a number of trajectories not exceeding $N = 500$, for all the values of the parameters we have probed. For even larger clusters ($L \lesssim 40$), we resort to a MPO approach combined with the cluster mean field.

In order to check for the (possible) existence of an ordered FM phase, we calculate the steady-state ferromagnetic spin-structure factor $S^{xx}_{\rm SS}(k=0)$, where

$$S^{xx}_{\rm SS}(k) = \frac{1}{L^2}\sum_{j,l=1}^{L} e^{-ik(j-l)}\langle\sigma^x_j\sigma^x_l\rangle_{\rm SS}. \tag{17}$$

A nonzero value of $S^{xx}_{\rm SS}(0)$ indicates the stabilization of a FM ordering in the thermodynamic limit. We do not look directly at the order parameter $\langle\sigma^x_j\rangle_{\rm SS}$ since we are studying finite-size systems and the $\mathbb{Z}_2$ symmetry may not spontaneously break [78].

In Fig. 5, we show the behavior of $S^{xx}_{\rm SS}(0)$ for small systems ($L \leq 16$) with open boundary conditions, for fixed values of $J_x = 0.9$, $J_z = 1$ and varying J_y (analogous results are obtained by taking different values of $-1 \leq J_x \leq 1$). Data have been obtained with RK and with QT approaches. According to Eq. (16), the MF approach predicts a critical point at $J^c_y = 37/32 \approx 1.156$ separating a

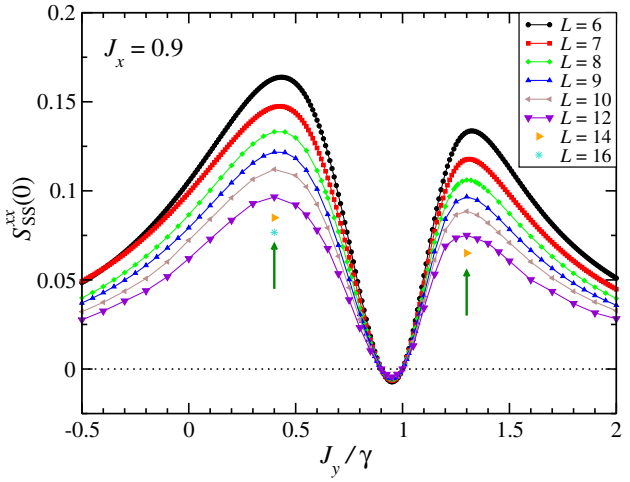

FIG. 5. Ferromagnetic spin-structure factor along the x direction, in a 1D setup, as a function of J_y. The various curves and symbols stand for different system sizes from $L = 6$ to $L = 16$, as indicated in the plot. The two arrows point at the positions of the two peaks ($J_y = 0.4$ and $J_y = 1.3$), for which we provide a finite-size scaling (Fig. 6) and an analysis of the two-point correlation functions (Fig. 7). Here, we have set $J_x = 0.9$ and $J_z = 1$, and we work in units of γ. Note that for $J_y = 0.9$ and $J_y = 1$, the spin structure factor is rigorously zero.

PM (for $J_y < J^c_y$) from a FM region (for $J_y > J^c_y$). In striking contrast with this, our numerics displays a decrease of the xx correlations with the system size. We also observe a nonmonotonic behavior with J_y, and the fact that $S^{xx}_{\rm SS}(0)$ vanishes for $J_y = 0.9$ and $J_y = 1$. This result can be explained as follows. For $J_x = J_y$, the Hamiltonian (2) conserves the magnetization along z. Since the dissipative spin-flip processes occur along the same direction, it is clear that they cannot be counteracted by the unitary dynamics, so the steady state is a pure product state, having all the spins aligned and pointing down along the z direction, making the xx and yy correlations vanishing at any distance. On the contrary, for $J_y = J_z$, the total magnetization along the x axis is conserved by the Hamiltonian. In this case, because of the different privileged axis with respect to the dissipation process, the steady state is not a product state. The correlators are generally different from zero; however, the spin-structure factor of Eq. (17) at $k = 0$ sums to zero. It is worth noticing that, on the contrary, $S^{yy}_{\rm SS}(k=0)$ is not affected by the Hamiltonian symmetry and is different from zero (not shown).

Coming back to the data in Fig. 5 on the spin-structure factor $S^{xx}_{\rm SS}(k=0)$, we can pinpoint the emergence of two peaks at $J_y \approx 0.4$ and 1.3. Before commenting on the behavior of the spin-structure factor in proximity of such peaks, let us analyze in more detail their dependence on L by performing a finite-size scaling of our data. This dependence is provided in Fig. 6. Black data sets correspond to those in Fig. 5. We observe a systematic drop of the correlations with L for both peaks, which can be nicely fit with a power law,

$$S^{xx}_{\rm SS}(0) \sim \kappa L^{-\alpha}, \tag{18}$$

where the exponent α depends on the value of J_y as indicated in the various panels.

We were able to reach longer sizes by employing a MPO approach for considerably larger chain lengths ($L \leq 40$). We applied a cluster mean field at the edges of the chain, in order to better mimic the thermodynamic limit. The results obtained with this method are displayed in Fig. 6 by the blue sets of data, and they qualitatively agree with the previous results without a mean field (black data). In particular, an analogous power-law behavior (18) emerges. Notice that, in correspondence to the peak that is a remnant of the ferromagnetic phase ($J_y = 1.3$), a nonmonotonic behavior in the combined MPO-CMF approach emerges. This has to be ascribed to the mean-field corrections that become very effective for very short clusters.

Further evidence of the remnants of the $\mathbb{Z}_2$-symmetry breaking predicted at the mean-field level is provided by analyzing the two-point correlation functions $\langle\sigma^x_j\sigma^x_{j+r}\rangle_{\rm SS}$ as a function of the distance r. Figure 7 shows results for parameters corresponding to the two distinct phases

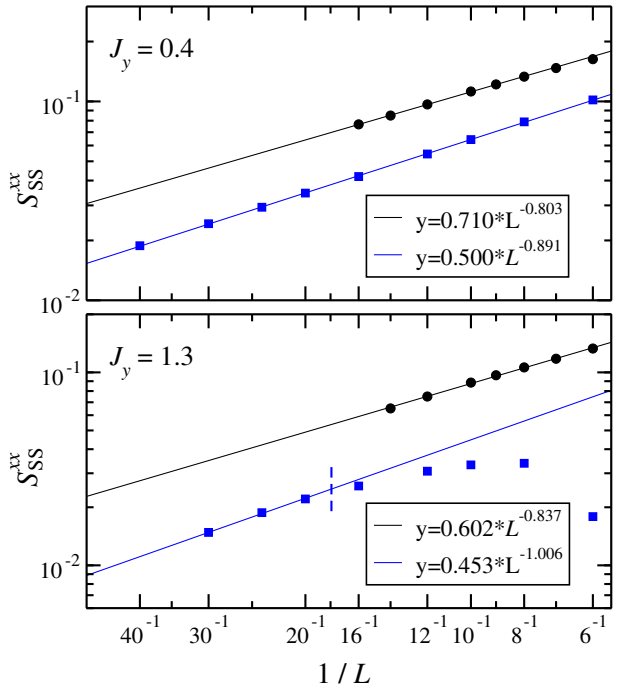

FIG. 6. Scaling of $S^{xx}_{SS}(0)$ as a function of the inverse system size L, for two values of J_y in proximity of the peaks (see the arrows in Fig. 5). The symbols denote the numerical data, while the continuous lines are power-law fits performed for the data points to the left of the vertical dashed line. The black sets correspond to those of Fig. 5, obtained by simulating a small system with RK and QT approaches. The blue sets have been obtained with MPO simulations, where the CMF has been applied to the two edges. The other parameters are set as in Fig. 5.

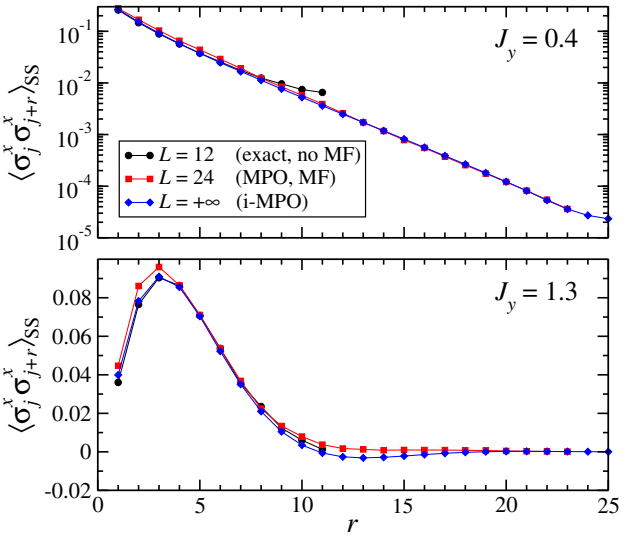

FIG. 7. Spatial decay of the correlation functions $\langle \sigma^x_j \sigma^x_{j+r} \rangle_{SS}$ with the distance r. Correlators have been chosen in a symmetric way with respect to the center of the chain. In the upper panel, $J_y = 0.4$ (left peak in Fig. 5), while in the lower panel, $J_y = 1.3$ (right peak in Fig. 5). The various data sets correspond to different system sizes: Results for $L = 12$ have been obtained for systems with PBC by means of RK integration or the QT approach to the master equation; those for $L = 24$ are, with MPO, used to simulate OBC and combined with the CMF; the thermodynamic limit $L \to \infty$ (diamonds-solid blue lines) has been addressed with a translationally invariant i-MPO method. The other parameter values are set as in Fig. 5.

predicted by the mean-field theory. In particular, we observe that, in the cases where the symmetry is not broken in the MF, correlations of the order parameter exhibit a clear exponential decay with the distance, as one can recognize in the upper panel ($J_y = 0.4$). This is evident already at very small sizes $L \sim 12$. A more intriguing situation occurs in the case where the MF would predict a symmetry-broken phase (see the lower panel for $J_y = 1.3$). In such case, an instability of the PM phase at short lengths emerges, in the sense that a bump in the correlators clearly emerges at $r \lesssim 10$ and the exponential suppression of correlations is not immediately visible. Longer sizes are needed to observe the absence of quasi-long-range correlations.

To corroborate our analysis, we also performed simulations by directly addressing the thermodynamic limit. We employed a TEBD numerical approach based on a translationally invariant Ansatz for the MPO [69]. Here, the mean field need not be used. The results are in perfect agreement with those obtained with the cluster mean field, thus validating our approach. In all the cases that we considered, we clearly see an emergence of exponential decay at large distances, thus signaling the absence of ferromagnetic order in any parameter range. Remarkably, the data obtained with MPO simulations (both in the finite and the infinite case) converge with a relatively small bond-link dimension ($\chi \leq 120$).

B. Two dimensions

We now proceed with the discussion of the model in a two-dimensional square lattice ($z = 4$). Here, there is no chance to solve Eq. (1) exactly for any thermodynamically relevant system size; therefore, we resort to approximate techniques combined with a CMF approach. In this framework, we are able to highlight a number of significant modifications to the steady-state phase diagram predicted by the single-site MF. Clearly, such differences must arise from taking into account the effect of short-range correlations inside the cluster. The shape of the considered clusters always respects the square-lattice geometry (i.e., they have a number of sites $L = \ell \times \ell$). With the numerical capabilities at our disposal, we are able to deal with clusters up to size $\ell = 4$. The $\ell \leq 3$ data have been computed by numerically integrating the time evolution of the cluster master equation with a standard RK method. In order to address the case $\ell = 4$, we employed the quantum trajectories approach explained in Sec. III B.

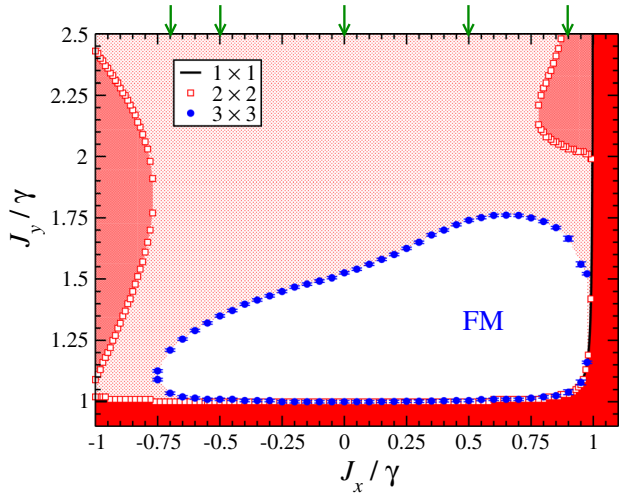

FIG. 8. Two-dimensional cluster mean-field phase diagram in the $J_x - J_y$ plane (with fixed $J_z = 1$). The single-site MF (1×1) predicts a ferromagnetic steady state in the top left region with respect to the black curve. The extent of this region appears to be very fragile to a more accurate cluster mean-field treatment. At the 2×2 level (red squares), the boundaries of the two phases are slightly deformed, while with a 3×3 analysis, the FM phase shrinks down to a region of finite size (blue circles). The darkest color filling indicates the region that is PM in all simulations, while the lightest indicates that which is FM in all cases. The FM region shrinks with increasing cluster size, as indicated by the varying shades of color but, as discussed in the text, appears to converge with increasing cluster size. The five arrows denote the cuts along different values of J_x, which will be analyzed in detail in Figs. 9 and 10.

Our main result is reported in Fig. 8, which displays the phase diagram in a region of the parameter space where the MF analysis would predict the occurrence of a $\mathbb{Z}_2$-symmetry-breaking mechanism. It is immediately visible that, under a CMF treatment of the system, the extent of the FM phase is drastically reduced. Specifically, we contrast the single-site MF predictions (black line) with the results obtained using a 3×3 cluster size (blue circles). On the one side, the single-site MF analysis predicts a symmetry-broken phase in a large and extended portion of the phase space [fixing $J_z = 1$, for $-1 \lesssim J_x \lesssim 1$, the ferromagnet extends for any $J_y \gtrsim 1$ according to Eq. (16), and disappears only in the asymptotic limit $J_y \to \infty$]. On the other side, the latter analysis indicates a tendency to confine the FM phase into a finite-size region in the parameter phase, which is surrounded by the PM phase, thus modifying the topology of the diagram.

Our CMF numerics shows that the disappearance of the ordered phase at large J_y is accompanied by the progressive shrinkage of the Bloch vector for the single-site density matrix, by increasing the coupling strength. This effect can already be seen from the Bloch equations of the single-site MF [19], which predict a saturation of the spins in the limit of infinite coupling—see Eqs. (20) and (21), and analogously for $[M^y_{\rm SS}]_{\rm MF}$. It is however important to remark that, even though the left and upper boundaries of the FM phase shrink with the cluster size while the right and bottom ones are almost unaffected, our results support the existence of a finite region for the symmetry-broken phase even in the thermodynamic limit $\ell \to \infty$, as we will detail below. Since the calculations with large clusters are very demanding, we considered few (representative) couplings. Our analysis performed with clusters of size up to 4×4 indicates that the ferromagnet will survive in the limit $\ell \to \infty$, for fixed $J_x = 0.9$ and for $1.04 \lesssim J_y \lesssim 1.4$ (see Fig. 10). We expect that for other values of J_x, the behavior will be similar.

Before commenting on the scaling with the cluster size, let us point out the fact that the CMF data for $\ell = 2$ (red squares in Fig. 8) evidence an intermediate situation. Indeed, taking into account only nearest-neighbor interactions, the extent of the FM phase is slightly reduced as compared to the single-site MF, yet it is not sufficient to confine the symmetry-broken phase into a finite-size region surrounded by the PM phase. Nonetheless, after a more careful analysis of the magnitude of the order parameter, we are able to detect a clear tendency toward a topological modification of the diagram. Specifically, we fixed several values of the coupling J_x, while varying J_y, and investigated the FM-PM phase transition by looking at the steady-state on-site magnetization along the x axis:

$$M^x_{\rm SS} = \frac{1}{\ell^2} \sum_{j=1}^{\ell^2} \langle \sigma^x_j \rangle_{\rm SS}, \tag{19}$$

so as to explore the phase diagram of Fig. 8 along certain vertical cuts. Notice that we do not need to calculate the correlators $S^{xx}_{\rm SS}(0)$ of Eq. (17) as we did in the 1D geometry since the self-adaptive mean-field method automatically breaks the symmetry in the FM phase.

The different panels of Fig. 9 refer to four values of J_x, as indicated by the first four green arrows on the left in Fig. 8, and they display $M^x_{\rm SS}$ as a function of J_y, for different cluster sizes ℓ. The 1×1 MF data (black lines) can be found by working out the steady-state limit of the MF Bloch equations for the magnetization [19], giving the following result:

$$[M^x_{\rm SS}]_{\rm MF} = \pm \sqrt{2[M^z_{\rm SS}]_{\rm MF}([M^z_{\rm SS}]_{\rm MF} + 1)\frac{J_y - J_z}{J_x - J_y}}, \tag{20}$$

with

$$[M^z_{\rm SS}]_{\rm MF} = -\frac{1}{4z}\sqrt{\frac{1}{(J_z - J_x)(J_y - J_z)}}. \tag{21}$$

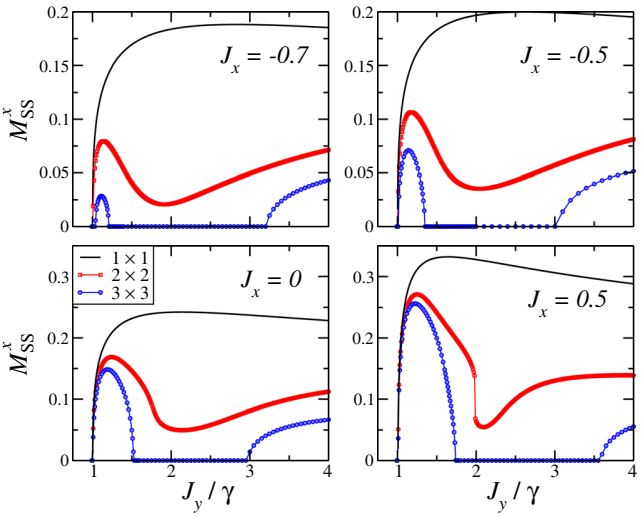

FIG. 9. Cluster mean-field analysis of the ferromagnetic order parameter in two dimensions, for four different vertical cuts of Fig. 8, at constant J_x (the corresponding values of J_x are indicated in the various panels). The various data sets denote different sizes of the clusters, up to $\ell = 3$.

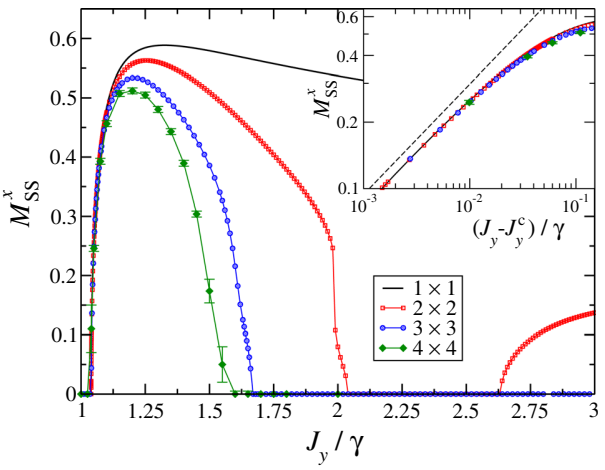

FIG. 10. Same analysis as in Fig. 9, but for $J_x = 0.9$. In the inset, we show the rescaled data close to the left phase transition; the straight dashed line denotes a square-root behavior as in Eq. (22) and is plotted as a guide to the eye.

These curves exhibit a finite magnetization for all $J_y \gtrsim 1$, with a maximum at a given value of J_y (dependent of J_x), and they eventually go to zero in the limit $J_y \to +\infty$. This vanishing order at strong coupling is similar to the absence of ordering on resonance in the Dicke model [12] and the suppression of ordering in the degenerate limit of the Rabi model [24]. The nonmonotonicity of M^x_{SS} as a function of J_y also emerges in the CMF analysis: The 2×2 data signal a strong suppression of the order parameter for $J_y \sim 2$, which, however, remains finite. Going further with a 3×3 cluster, we see the sharp disappearance of the FM in an intermediate extended region where $M^x_{SS} = 0$ (for $1.5 \lesssim J_y \lesssim 3$, depending on the value of J_x, the system is not ferromagnetically ordered along x or y). The revival of the FM phase at large values of J_y ($J_y \gtrsim 3$) is outside the parameter range of Fig. 8. We analyze this feature later in Sec. IV C.

Let us now have a closer look at the vertical cut of Fig. 8 for $J_x = 0.9$; the magnetization is shown in Fig. 10 for clusters up to $\ell = 4$. Both for the 3×3 and the 4×4 CMF analysis, we do not see any reappearance of the FM ordering at large J_y (we numerically checked this statement up to $J_y = 10$). The symmetry-broken phase is confined to a finite-size region that shrinks with increasing ℓ. While the left boundary is basically unaffected by the role of correlations ($J_y^{c(\mathrm{left})} \approx 1.04 \pm 0.01$), the right boundary is strongly sensitive to ℓ. Our simulations indicate a transition point $J_y^{c(\mathrm{right})} \approx 2.04 \pm 0.005, 1.67 \pm 0.01, 1.57 \pm 0.03$, for clusters, respectively, with $\ell = 2, 3, 4$. A scaling with ℓ of these data for the right boundary indicates a behavior that is compatible with $J_y^{c(\mathrm{right})} \approx 1.40 + 2.54\ell^{-2}$, and thus which supports the existence of the FM phase in the limit of large cluster size $\ell \to \infty$, for $1.04 \lesssim J_y \lesssim 1.40$. In the data for $\ell = 2$, a discontinuity of M^x_{SS} seems to appear immediately before the right transition point (at $J_y \approx 2$), which requires a further analysis (a similar behavior is observed in the lower right panel of Fig. 9, for $J_y = 0.5$). We will return to this point in Sec. IV C.

We also checked that, close to the transition, our numerics predicts a growth of the order parameter that is well approximated by

$$M^x_{SS} \sim m\sqrt{J_y - J^c_y}, \tag{22}$$

as displayed in the inset of Fig. 10, around the left critical point $J_y^{c(\mathrm{left})}$. We repeated a similar analysis for other vertical (fixed J_y) and horizontal (fixed J_x) cuts and obtained qualitatively analogous results. This evidences the fact that the CMF remains a mean-field analysis and leads to the same critical exponents as those of its single-site version. In order to get the correct exponents, one would need a more careful finite-size analysis [62], which requires slightly larger values of ℓ and is unfortunately out of reach for the present computational capabilities.

The stability of the symmetry-broken phase for $J_y^{c(\mathrm{left})} < J_y < J_y^{c(\mathrm{right})}$ up to 4×4 clusters is corroborated by the behavior of the correlation functions $\langle \sigma^x_j \sigma^x_{j+r} \rangle_{SS}$ and $\langle \sigma^y_j \sigma^y_{j+r} \rangle_{SS}$ with the distance r, as reported in Fig. 11 for three different values of J_y. As discussed in Sec. IV A for the 1D case, in the parameter region where we predict a PM, the correlators decay exponentially with r (black data set at $J_y = 1$). On the opposite side, the point at $J_y = 1.2$ (red data) displays a marked distance independence of correlations with the distance, thus signaling the presence

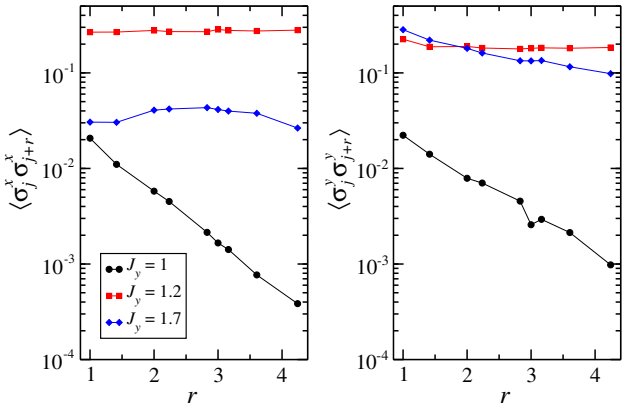

FIG. 11. The two-point xx (left panel) and yy (right panel) correlations as a function of the distance r in a two-dimensional square-lattice geometry. The calculations have been performed on a square lattice of size $\ell = 4$, while the point j has been chosen to be at one of the corners of the more-square cluster. The three sets of data refer to different values of J_y according to the legend: two inside the PM phase ($J_y = 1$ and $J_y = 1.7$) and one inside the FM phase ($J_y = 1.2$). We fixed $J_x = 0.9$, $J_z = 1$.

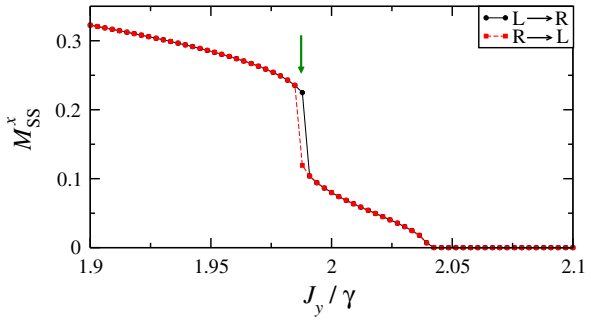

FIG. 12. Magnification of the 2×2 CMF analysis for $J_x = 0.9$, close to $J_y = 2$ (see the red data in Fig. 10). The two sets are calculated by sweeping both from upward and downward J_y values, where the initial conditions for each point are based on the previous one, with a small offset. This evidences the presence of a first-order jump within the ordered phase for $J_y \approx 1.985$ (green arrow), followed by a second-order transition to the normal state, for $J_y^{c(\mathrm{right})} \approx 2.04$.

of a FM phase (notice that this point lies well inside the closed region in Fig. 8). The case $J_y = 1.7$ (blue data) shows a subtler behavior and corresponds to a point for which the single-site and the 2×2 mean-field analysis would predict a symmetry-broken phase, contrary to our $\ell \geq 3$ CMF calculations which display no evidence of this type. The reminiscence of a kind of quasiordering at short distances is indeed forecast by a slow decay of correlations. While we are not able to see a clear exponential decay with r, because of our limited numerical capabilities, we expect that this would be visible for clusters appreciably longer than $\ell = 4$. Nonetheless, we stress that xx correlations here are 1 order of magnitude smaller than in the FM point.

A sketch of the phase diagram summarizing all our results is provided in Fig. 1.

C. Two dimensions—stability analysis

As anticipated in the previous subsection, the 2×2 analysis reveals a discontinuity of the order parameter inside the first FM phase, very close to the transition point $J_y^{c(\mathrm{right})}$ to the disordered phase. Such a jump, between two symmetry-broken states, is known as a metamagnetic transition. The jump is visible for certain values of J_x and seems to vanish quickly with increasing cluster size (already for $\ell = 3$, it is barely recognizable from our data). On the one hand, the latter observation suggests that this jump could be an artifact of the CMF analysis. On the other hand, a deeper investigation is required to understand its origins.

To highlight the existence of this feature, in Fig. 12 we show a magnification of the relevant parameter region of Fig. 10. We only consider the 2×2 case since this is the situation where it is mostly relevant. We observe the presence of a first-order phase transition within the first ordered phase, where the order parameter exhibits a discontinuity. This is corroborated by a bistability effect: Specifically, we calculated the magnetization M_{SS}^x starting from different initial states, and we observed a slight difference in proximity to the jump, as is visible from the figure [79].

At this point, we perform a linear stability analysis, in order to check whether and how the system becomes unstable in correspondence to the jump. We start from the CMF factorization Ansatz given in Eq. (7), where each cluster density matrix ρ_C obeys the mean-field master equation (8). The stability analysis is performed directly on the factorized density matrix, as detailed in Ref. [33]. Let us first rewrite the equation of motion for a single cluster, say the nth one, in the superoperator formalism as

$$\partial_t \|\rho_n\rangle\rangle = \mathcal{M}_0 \|\rho_n\rangle\rangle + \sum_j (\mathcal{E}_j \cdot \|\rho_{n+\mathbf{e_j}}\rangle\rangle)\mathcal{M}_j \|\rho_n\rangle\rangle, \qquad (23)$$

where we omitted the index $_c$. Here, $\|\rho_n\rangle\rangle$ denotes a super ket, i.e., a vectorized form of the density matrix, and $\mathcal{M}_i$ denote superoperators. In this equation, $\mathcal{M}_0$ represents all the on-cluster terms, while $\mathcal{M}_j$ is the on-cluster part of an off-cluster term and $\mathcal{E}_j$ the corresponding off-cluster expectation. For example, in the term $J_x \langle\sigma_N^x\rangle \sigma_1^x$, we have $\mathcal{M}_j = -iJ_x \|\sigma_1^x\rangle\rangle$, and $\mathcal{E}_j = \mathcal{E}[\sigma_N^x]$ is the superoperator form of the expectation. Moreover, $\mathbf{e_j}$ is the direction to the neighboring cluster involved.

When performing linear stability analysis, we expand the fluctuations in terms of plane waves

$$\|\rho_n\rangle\rangle = \|\rho_0\rangle\rangle + \sum_{\mathbf{k}} e^{i\mathbf{k}\cdot\mathbf{r_n}} \|\delta\rho_{\mathbf{k}}\rangle\rangle \tag{24}$$

so that the resulting equation of motion for $\|\delta\rho_{\mathbf{k}}\rangle\rangle$ is

$$\partial_t \|\delta\rho_{\mathbf{k}}\rangle\rangle = \left[\mathcal{M}^0 + \sum_j (\mathcal{E}_j \cdot \|\rho_0\rangle\rangle)\mathcal{M}_j\right] \|\delta\rho_{\mathbf{k}}\rangle\rangle + \sum_j e^{i\mathbf{k}\cdot\mathbf{e_j}} \mathcal{M}_j \|\rho_0\rangle\rangle (\mathcal{E}_j \cdot \|\delta\rho_{\mathbf{k}}\rangle\rangle). \tag{25}$$

The last term is a sum of rank-one matrices (since $\mathcal{M}_j\|\rho_0\rangle\rangle$ is a vector, like $\mathcal{E}_j$). Thus, we obtain

$$\partial_t \|\delta\rho_{\mathbf{k}}\rangle\rangle = \left[\mathcal{M}^{0,\mathrm{eff}} + \sum_{\mathbf{e}} e^{i\mathbf{k}\cdot\mathbf{e}} \mathcal{M}^{1,\mathbf{e}}\right] \|\delta\rho_{\mathbf{k}}\rangle\rangle, \tag{26}$$

where in the second part, we have grouped terms with the same vector $\mathbf{e}$ together, as these all get the same $\mathbf{k}$-dependent factor. We then numerically compute the eigenvalues of the effective superoperator in Eq. (26) for each value of $\mathbf{k} = (k_x, k_y)$. The most unstable eigenvalue is the one with the largest positive real part. Since for an $\ell \times \ell$ cluster the vectors $\mathbf{e_j}$ must be ℓ times the elementary lattice vectors, the range of lattice momenta coming from the $\ell \times \ell$ cluster stability analysis are restricted to the first Brillouin zone of the superlattice, $|k_j| < \pi/\ell$.

In Fig. 13, we plot the real part of the most unstable eigenvalue as a function of the momentum k_x and the coupling J_y (for fixed $J_x = 0.9$). We notice that the jump inside the FM phase occurs when there is an instability at finite k, around $|\mathbf{k}| = \pi/4$. This suggests that the finite cluster size is responsible for the particular metamagnetic transition seen, and it explains why the extent of the ordered phase reduces as larger clusters (capable of describing such short-range fluctuations) are used. The transition to the normal state also occurs from a finite-momentum instability, at small $|\mathbf{k}|$. We also see an incommensurate finite-momentum instability at the rebirth of the FM phase, for large J_y, thus signaling that the reappearance of the ordered phase is probably an artifact of the translationally invariant CMF Ansatz. Finally, we checked that the dispersion is almost isotropic in k_x, k_y.

D. Three- and four-dimensional systems

For completeness, we also consider the case of higher dimensions. Although not relevant for direct experimental realizations, it helps in completing the picture achieved so far; it may also be possible to study (finite-sized) four-dimensional systems by using synthetic dimensions as proposed recently by Ozawa *et al.* [80]. Mean-field results are expected to improve their validity by increasing the coordination number z in the lattice. It is therefore tempting to investigate systems in higher dimensionality by means of CMF techniques. Obviously, on increasing d, our ability in considering larger clusters drastically decreases. We checked the dependence on d of the PM-FM transition by means of a mean-field analysis with clusters of size $L = 2^d$. In these cases, we looked again at the average on-site magnetization along the x axis. The results are displayed in Fig. 14.

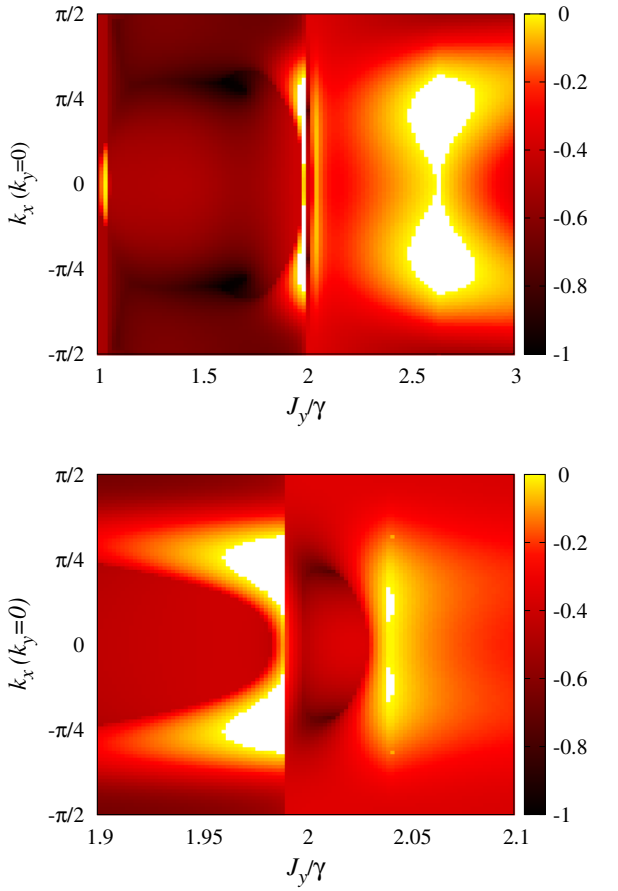

FIG. 13. Upper panel: Real part of the most unstable eigenvalue (negative is stable) as a function of J_y and k_x (for $k_y = 0$). The parameters are set as in Fig. 10. Lower panel: High-resolution plot with the same range of J_y as in Fig. 12, corresponding to upward trace.

Naturally, the extent of the symmetry-broken phase region is increasing with the dimensionality, as is apparent from Fig. 14 (even though the value of the order parameter does not necessarily become larger). This supports the common wisdom of the validity of a single-site mean field in high dimensions. What is surprising from Fig. 14 is that even the four-dimensional system shows a critical value of J_y beyond which the phase is paramagnetic. This result is in sharp contrast with the mean-field result that does not capture this second critical point. Our limited analysis up to four dimensions and for very small clusters does not allow us to draw conclusions in determining how or if the second critical point moves in higher dimensions. It is, however, an interesting point to be understood.

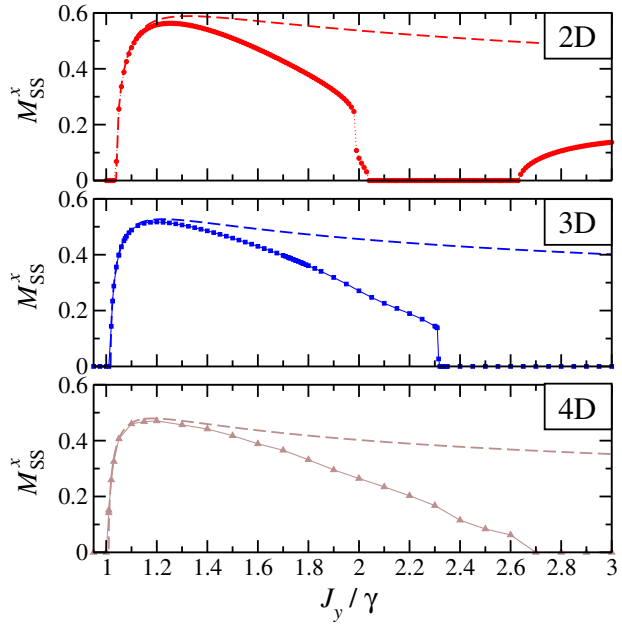

FIG. 14. Cluster mean-field analysis of the ferromagnetic order parameter for a system defined on a square lattice geometry in different dimensionalities. The upper panel refers to 2D ($z = 4$), the middle one to 3D ($z = 6$), and the lower one to 4D ($z = 8$). Dashed lines denote the MF predictions, while symbols and continuous curves are the results of numerical simulations, with clusters of size $L = 2^D$ (D being the system dimensionality).

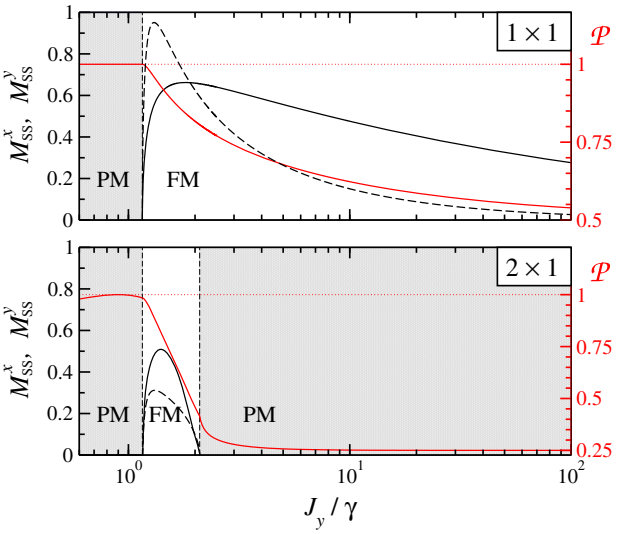

FIG. 15. Magnetization along the x (solid black line) and y (dashed black line) directions and purity $\mathcal{P} = \mathrm{Tr}[\rho^2_{SS}]$ (solid red line) as a function of J_y, for fixed $J_x = 0.9$, $J_z = 1$. The single-site MF (1×1, top panel) predicts a PM phase for $J_y < J^c_y$ and a FM phase for $J_y > J^c_y$. On the contrary, according to a CMF analysis (2×1, lower panel), the FM phase shrinks down to a finite region $J^c_y = J^{c(\mathrm{left})}_y < J_y < J^{c(\mathrm{right})}_y$ allowing the reentrance of a PM phase for $J_y > J^{c(\mathrm{right})}_y$.

E. Short-range correlations and Lindblad dynamics: Origin of the reentrant paramagnetic phase

As discussed in detail in Sec. IV B, our calculations show that, on improving the Ansatz for the steady-state density matrix by including short-range correlations, the critical points may shift from $J_y = +\infty$ to a finite value of J_y. This situation may appear as counterintuitive. It is indeed unlikely to occur at equilibrium, where the inclusion of short-range fluctuations may only lead to a shift of the boundary position of the order of the energy fluctuations inside the cluster [$O(zJ_y)$ in this case]. In this section, we want to explain the mechanism responsible for this behavior. This will also help us to elucidate the nature of the PM phase observed at large J_y within the CMF approach and, consequently, the reentrance to a disordered phase. To this aim, it is sufficient to compare the single-site with the 2×1 (two-site) cluster cases. We consider this minimal cluster dimension for simplicity, since taking larger clusters would not add new ingredients to the understanding of the mechanism.

First, it is important to stress that, already at the single-site MF, a steady state with vanishing spontaneous magnetization in all the directions is predicted in the limit $J_y \to +\infty$. As shown in the top panel of Fig. 15 (for fixed $J_x = 0.9$ and $J_z = 1$), two phases emerge: a PM for $J_y < J^c_y$ and a FM for $J_y > J^c_y$, with magnetization along y (or equivalently along x) initially increasing but then decreasing asymptotically toward zero as J_y is increased. This phenomenon is related to the progressive deterioration of the purity of the steady-state density matrix, $\mathcal{P} = \mathrm{Tr}[\rho^2_{SS}]$, for $J_y > J^c_y$. This comes as a consequence of the out-of-equilibrium nature of the steady state resulting from the interplay of driving and dissipation and cannot occur at equilibrium, where an increasing coupling typically stabilizes the ordering. A similar kind of behavior can be seen in a driven two-level system [81,82], where increasing driving enhances the population but suppresses the purity of the system, leading to a suppression of the homodyne amplitude $|\langle\sigma^-\rangle|$ and of the purity when driven on resonance. We see that $\mathcal{P} = 1$ in the PM phase, and then it decreases toward its minimal value ($\mathcal{P} = 1/2$ in the case of a single-site cluster) as J_y is increased beyond the critical value J^c_y. This suggests the fact that the disordered phase detected for $J_y < J^c_y$ is different in nature compared to the one reached in the large-J_y limit for the cluster mean-field simulation. The former is due to the stabilization of a fully polarized one along the z direction, which coincides with the single-site MF solution for any $J_y < J^c_y$ (while it is the exact solution to the problem only for $J_x = J_y$). The latter PM phase is a consequence of the fact that the steady state for $J_y \to +\infty$ is fully mixed.

What is the effect of including short-range correlations? In order to understand this point, let us consider in more

detail the smallest cluster where this feature can be observed, namely, a 2×1 plaquette. As shown in the lower panel of Fig. 15, the FM phase now shrinks to a finite region going from $J_y^{c(\mathrm{left})}$ to $J_y^{c(\mathrm{right})}$, so the PM for $J_y \to +\infty$ stabilizes over an extended region $J_y > J_y^{c(\mathrm{right})}$. The steady-state purity indicates a nearly pure state in the left PM region, $J_y < J_y^{c(\mathrm{left})}$, that has to be contrasted with a nearly fully mixed state in the right PM region, $J_y > J_y^{c(\mathrm{right})}$ (the minimal value for a two-site cluster is $\mathcal{P} = 1/4$). Thus, the exact inclusion of the nearest-neighbor correlations allows for the reentrance of a PM phase for $J_y > J_y^{c(\mathrm{right})}$. At the single-site MF level, such a PM phase appears only in the limiting case $J_y \to +\infty$ and then is never detectable for any finite value of the couplings. We remark that decreasing the purity, and the consequent reduction of the magnetizations, as J_y is increased is a common nonequilibrium feature of the two Ansätze (1×1 and 2×1). While in the 1×1 case the purity reduction is not enough to kill the FM order, in the 2×1 plaquette, this reduction of purity is more prominent and the latter phenomenon (suppression of magnetization) occurs.

The equations of motion in the Heisenberg picture for magnetization $\langle \sigma_j^\beta \rangle$ ($\beta = x, y, z$) are

$$\partial_t \langle \sigma_j^\beta \rangle = -2 \sum_{\alpha=x,y,z} J_\alpha \epsilon_{\alpha\beta\gamma} [\langle \sigma_j^\gamma \rangle \langle \sigma_{j+1}^\alpha \rangle + \langle \sigma_j^\gamma \sigma_{j+1}^\alpha \rangle] - \frac{\gamma}{2} [\langle \sigma_j^\beta \rangle + \delta_{\beta z} (\langle \sigma_j^\beta \rangle + 2)], \tag{27}$$

where $\epsilon_{\alpha\beta\gamma}$ is the Levi-Civita symbol and $\delta_{\alpha\beta}$ is the Kronecker delta. The steady-state density matrix in the 2×1 plaquette for $J_y > J_y^{c(\mathrm{right})}$ can be analytically computed and is *almost* fully mixed. Therefore, it can be written as $\rho_{\mathrm{SS}}^{[2+1]} \approx \rho^{[1]} \otimes \rho^{[2]}$. The two-point spin correlator appearing in Eq. (27) can thus be decomposed as

$$\langle \sigma_j^\gamma \sigma_{j+1}^\alpha \rangle = \langle \sigma_j^\gamma \rangle \langle \sigma_{j+1}^\alpha \rangle + \langle \Sigma_{j,j+1}^{\gamma,\alpha} \rangle, \tag{28}$$

where $|\langle \Sigma_{j,j+1}^{\gamma,\alpha} \rangle| \ll 1$. Inserting this expression into Eq. (27) and exploiting translational invariance, we get

$$\partial_t \langle \sigma_j^\beta \rangle = \mathcal{L}_{[1\times1]}^\beta - 2 \sum_\alpha J_\alpha \epsilon_{\alpha\beta\gamma} \langle \Sigma_{j,j+1}^{\gamma,\alpha} \rangle, \tag{29}$$

where $\mathcal{L}_{[1\times1]}^\beta$ are the terms one would get from the single-site MF. Equation (29) shows that spin-spin correlations correct the single-site MF equations of motion only through the small term $\langle \Sigma_{j,j+1}^{\gamma,\alpha} \rangle$. On the other hand, we know that, for $J_y > J_y^{c(\mathrm{right})}$, the steady-state properties can change dramatically when considering a single site or a plaquette as a cluster: In the former case, one gets a ferromagnet, while in the latter case, one gets a paramagnet. Spin-spin correlations, even if very weak, cannot be neglected and drastically modify the structure of the density matrix at long times. These conspire with the dynamically induced reduction of purity at large J_y, already visible for the single-site mean field, to suppress the ordering altogether. This is the key to understanding the dramatic changes in the phase boundaries we presented in the previous sections.

We believe that the mechanism is generic and should be relevant for other driven-dissipative models as well.

V. CONCLUSIONS

In this work, we introduced a cluster mean-field approach combined with quantum trajectories and tensor-network techniques to the study of the steady-state phase diagram in driven-dissipative systems. This approach allowed us to analyze the effect of short-range correlations. The result is somewhat unexpected. The whole structure of the phase diagram is radically modified, in clear opposition to what typically happens in equilibrium phase transitions. In particular, we observed that the location of critical points may shift from infinite to finite values of the system parameters. The reason underlying this behavior is related to the fact that, differently from equilibrium, spontaneous symmetry breaking is of pure dynamical nature and is not determined through a free-energy analysis. It is already known that in dissipative systems, energy-minimizing ferromagnetic phases may be destabilized and replaced by incommensurate or antiferromagnetic order. Such behavior has been extensively studied in classical pattern-forming systems [4], including examples such as active matter and flocking [7–9]. As such, short-range correlations can be expected to play a much greater role in dissipative than in equilibrium systems. Accordingly, the topology of the phase diagram can significantly change. This appears clearly in Fig. 1, where the results from the single-site and the cluster mean-field analysis are compared. Furthermore, the cluster method hints at ordering with a nontrivial spatial pattern, a possibility that is not detected within the single-site mean-field Ansatz.

The results that we highlighted here are amenable to an experimental verification. As discussed in Ref. [19], the model considered in this paper can be implemented using trapped ions. Moreover, by changing external controls, it is possible to explore the phase diagram, thus allowing us to check the results of the present work. Besides the examined system, we think that cluster approaches may be powerful in the general context of driven-dissipative systems, ranging from Rydberg atoms in optical lattices to cavity or optomechanical arrays. Our findings point out the importance of the interplay between short-range fluctuations and dissipation in the physics emerging in such devices.

All the present analysis has been performed by considering a static mean field. It would be of great interest to extend these calculations so as to also include self-energy

corrections as in the dynamical mean field, already extended to nonequilibrium for the single-site case [83].

Finally, we believe that a very interesting development, left for the future, is the determination of the non-Landau critical exponents. When successful, this will be an important step to also establish the power of cluster techniques in many-body open systems. On this perspective, the combination of our approach with the corner space renormalization method developed in Ref. [55] looks promising, and some encouraging results have already been obtained [84].

The research data supporting this publication can be accessed Ref. [85].

ACKNOWLEDGMENTS

We warmly thank I. Carusotto, C. Ciuti, M. Fleischhauer, S. Gopalakrishnan, M. Hafezi, and T. Lee for useful discussions. A. B., L. M., J. K., R. F., and D. R. acknowledge the Kavli Institute for Theoretical Physics, University of California, Santa Barbara (USA) for the hospitality and support during the completion of this work. This research was supported in part by the Italian MIUR via FIRB Project No. RBFR12NLNA, by the EU integrated projects SIQS, QUIC, by the National Science Foundation under Grant No. NSF PHY11-25915, and by the National Research Foundation, Prime Ministers Office, Singapore under its Competitive Research Programme (CRP-QSYNC Award No. NRF-CRP14-2014-02). O. V. acknowledges support from the Spanish MINECO Grant No. FIS2012-33152, the CAM research consortium QUITEMAD+, the U.S. Army Research Office through Grant No. W911NF-14-1-0103, the FPU MEC Grant, and Residencia de Estudiantes. J. K. acknowledges support from the EPSRC program "TOPNES" (EP/I031014/1). J. J. was supported by the National Natural Science Foundation of China under Grants No. 11547119 and No. 11305021, by the Fundamental Research Funds for the Central Universities, No. DUT15RC(3)034, and by Natural Science Foundation of Liaoning Province, No. 2015020110. L. M. is supported by LabEX ENS-ICFP: ANR-10-LABX-0010/ANR-10-IDEX-0001-02 PSL*.

[1] N. Goldenfeld, *Lectures on Phase Transitions and the Renormalization Group* (Addison Wesley, New York, 1992).
[2] S. Sachdev, *Quantum Phase Transitions* (Cambridge University Press, Cambridge, England, 2000).
[3] U. Weiss, *Quantum Dissipative Systems* (World Scientific, Singapore, 2008).
[4] M. C. Cross and P. C. Hohenberg, *Pattern Formation Outside of Equilibrium*, Rev. Mod. Phys. **65**, 851 (1993).
[5] S. Strogatz, *Sync: The Emerging Science of Spontaneous Order* (Hyperion Press, New York, 2003).
[6] R. N. Mantegna and H. E. Stanley, *Introduction to Econophysics: Correlations and Complexity in Finance* (Cambridge University Press, Cambridge, England, 2000).
[7] T. Vicsek and A. Zafeiris, *Collective Motion*, Phys. Rep. **517**, 71 (2012).
[8] B. Schmittmann and R. K. P. Zia, in *Statistical Mechanics of Driven Diffusive Systems*, Vol. 17: Phase Transitions and Critical Phenomena, edited by C. Domb and J. L. Lebowitz (Academic Press, London, 1995).
[9] J. Toner and Y. Tu, *Flocks, Herds, and Schools: A Quantitative Theory of Flocking*, Phys. Rev. E **58**, 4828 (1998).
[10] N. D. Mermin and H. Wagner, *Absence of Ferromagnetism or Antiferromagnetism in One- or Two-Dimensional Isotropic Heisenberg Models*, Phys. Rev. Lett. **17**, 1133 (1966).
[11] J. Kasprzak, M. Richard, S. Kundermann, A. Baas, P. Jeambrun, J. M. J. Keeling, F. M. Marchetti, M. H. Szymanska, R. André, J. L. Staehli, V. Savona, P. B. Littlewood, B. Deveaud, and Le Si Dang, *Bose-Einstein Condensation of Exciton Polaritons*, Nature (London) **443**, 409 (2006).
[12] K. Baumann, C. Guerlin, F. Brennecke, and T. Esslinger, *Dicke Quantum Phase Transition with a Superfluid Gas in an Optical Cavity*, Nature (London) **464**, 1301 (2010).
[13] N. Syassen, D. M. Bauer, M. Lettner, T. Volz, D. Dietze, J. J. García-Ripoll, J. I. Cirac, G. Rempe, and S. Dürr, *Strong Dissipation Inhibits Losses and Induces Correlations in Cold Molecular Gases*, Science **320**, 1329 (2008).
[14] M. Müller, S. Diehl, G. Pupillo, and P. Zoller, *Engineered Open Systems and Quantum Simulations with Atoms and Ions*, Adv. At. Mol. Opt. Phys. **61**, 1 (2012).
[15] I. Carusotto and C. Ciuti, *Quantum Fluids of Light*, Rev. Mod. Phys. **85**, 299 (2013).
[16] H. Ritsch, P. Domokos, F. Brennecke, and T. Esslinger, *Cold Atoms in Cavity-Generated Dynamical Optical Potentials*, Rev. Mod. Phys. **85**, 553 (2013).
[17] A. A. Houck, H. E. Türeci, and J. Koch, *On-Chip Quantum Simulation with Superconducting Circuits*, Nat. Phys. **8**, 292 (2012).
[18] A. Tomadin and R. Fazio, *Many-Body Phenomena in QED-Cavity Arrays*, J. Opt. Soc. Am. B **27**, A130 (2010).
[19] T. E. Lee, S. Gopalakrishnan, and M. D. Lukin, *Unconventional Magnetism via Optical Pumping of Interacting Spin Systems*, Phys. Rev. Lett. **110**, 257204 (2013).
[20] T. E. Lee, H. Häffner, and M. C. Cross, *Antiferromagnetic Phase Transition in a Nonequilibrium Lattice of Rydberg Atoms*, Phys. Rev. A **84**, 031402 (2011).
[21] J. Jin, D. Rossini, R. Fazio, M. Leib, and M. J. Hartmann, *Photon Solid Phases in Driven Arrays of Nonlinearly Coupled Cavities*, Phys. Rev. Lett. **110**, 163605 (2013).
[22] M. Ludwig and F. Marquardt, *Quantum Many-Body Dynamics in Optomechanical Arrays*, Phys. Rev. Lett. **111**, 073603 (2013).
[23] C.-K. Chan, T. E. Lee, and S. Gopalakrishnan, *Limit-Cycle Phase in Driven-Dissipative Spin Systems*, Phys. Rev. A **91**, 051601 (2015).
[24] M. Schiró, C. Joshi, M. Bordyuh, R. Fazio, J. Keeling, and H. E. Türeci, *Exotic Attractors of the Non-equilibrium Rabi-Hubbard Model*, Phys. Rev. Lett. **116**, 143603 (2016).
[25] L. M. Sieberer, S. D. Huber, E. Altman, and S. Diehl, *Dynamical Critical Phenomena in Driven-Dissipative Systems*, Phys. Rev. Lett. **110**, 195301 (2013).

[26] E. G. Dalla Torre, E. Demler, T. Giamarchi, and E. Altman, *Dynamics and Universality in Noise-Driven Dissipative Systems*, Phys. Rev. B **85**, 184302 (2012).
[27] J. Marino and S. Diehl, *Driven Markovian Quantum Criticality*, Phys. Rev. Lett. **116**, 070407 (2016).
[28] S. Diehl, A. Micheli, A. Kantian, B. Kraus, H. P. Büchler, and P. Zoller, *Quantum States and Phases in Driven Open Quantum Systems with Cold Atoms*, Nat. Phys. **4**, 878 (2008).
[29] F. Verstraete, M. M. Wolf, and J. I. Cirac, *Quantum Computation and Quantum-State Engineering Driven by Dissipation*, Nat. Phys. **5**, 633 (2009).
[30] S. Diehl, A. Tomadin, A. Micheli, R. Fazio, and P. Zoller, *Dynamical Phase Transitions and Instabilities in Open Atomic Many-Body Systems*, Phys. Rev. Lett. **105**, 015702 (2010).
[31] A. Tomadin, V. Giovannetti, R. Fazio, D. Gerace, I. Carusotto, H. E. Türeci, and A. Imamoglu, *Signatures of the Superfluid-Insulator Phase Transition in Laser-Driven Dissipative Nonlinear Cavity Arrays*, Phys. Rev. A **81**, 061801 (2010).
[32] F. Nissen, S. Schmidt, M. Biondi, G. Blatter, H. E. Türeci, and J. Keeling, *Nonequilibrium Dynamics of Coupled Qubit-Cavity Arrays*, Phys. Rev. Lett. **108**, 233603 (2012).
[33] A. Le Boité, G. Orso, and C. Ciuti, *Steady-State Phases and Tunneling-Induced Instabilities in the Driven Dissipative Bose-Hubbard Model*, Phys. Rev. Lett. **110**, 233601 (2013); *Bose-Hubbard Model: Relation between Driven-Dissipative Steady States and Equilibrium Quantum Phases*, **90**, 063821 (2014).
[34] J. Jin, D. Rossini, M. Leib, M. J. Hartmann, and R. Fazio, *Steady-State Phase Diagram of a Driven QED-Cavity Array with Cross-Kerr Nonlinearities*, Phys. Rev. A **90**, 023827 (2014).
[35] I. Lesanovsky, B. Olmos, and J. P. Garrahan, *Thermalization in a Coherently Driven Ensemble of Two-Level Systems*, Phys. Rev. Lett. **105**, 100603 (2010); B. Olmos, I. Lesanovsky, and J. P. Garrahan, *Facilitated Spin Models of Dissipative Quantum Glasses*, Phys. Rev. Lett. **109**, 020403 (2012).
[36] M. J. Hartmann, *Polariton Crystallization in Driven Arrays of Lossy Nonlinear Resonators*, Phys. Rev. Lett. **104**, 113601 (2010).
[37] T. Grujic, S. R. Clark, D. Jaksch, and D. G. Angelakis, *Non-equilibrium Many-Body Effects in Driven Nonlinear Resonator Arrays*, New J. Phys. **14**, 103025 (2012).
[38] I. Carusotto, D. Gerace, H. E. Türeci, S. De Liberato, C. Ciuti, and A. Imamoğlu, *Fermionized Photons in an Array of Driven Dissipative Nonlinear Cavities*, Phys. Rev. Lett. **103**, 033601 (2009).
[39] R. O. Umucalilar and I. Carusotto, *Fractional Quantum Hall States of Photons in an Array of Dissipative Coupled Cavities*, Phys. Rev. Lett. **108**, 206809 (2012).
[40] A. J. Daley, *Quantum Trajectories and Open Many-Body Quantum Systems*, Adv. Phys. **63**, 77 (2014).
[41] M. Hoening, W. Abdussalam, M. Fleischhauer, and T. Pohl, *Antiferromagnetic Long-Range Order in Dissipative Rydberg Lattices*, Phys. Rev. A **90**, 021603(R) (2014).
[42] M. Höning, D. Muth, D. Petrosyan, and M. Fleischhauer, *Steady-State Crystallization of Rydberg Excitations in an Optically Driven Lattice Gas*, Phys. Rev. A **87**, 023401 (2013).
[43] D. Petrosyan, M. Höning, and M. Fleischhauer, *Spatial Correlations of Rydberg Excitations in Optically Driven Atomic Ensembles*, Phys. Rev. A **87**, 053414 (2013).
[44] A. Biella, L. Mazza, I. Carusotto, D. Rossini, and R. Fazio, *Photon Transport in a Dissipative Chain of Nonlinear Cavities*, Phys. Rev. A **91**, 053815 (2015).
[45] M. F. Maghrebi and A. V. Gorshkov, *Nonequilibrium Many-Body Steady States via Keldysh Formalism*, Phys. Rev. B **93**, 014307 (2016).
[46] E. Ilievski and T. Prosen, *Exact Steady State Manifold of a Boundary Driven Spin-1 Lai-Sutherland Chain*, Nucl. Phys. **B882**, 485 (2014).
[47] T. Prosen, *Exact Nonequilibrium Steady State of an Open Hubbard Chain*, Phys. Rev. Lett. **112**, 030603 (2014).
[48] N. Šibalić, C. G. Wade, C. S. Adams, K. J. Weatherill, and T. Pohl, *Driven-Dissipative Many-Body Systems with Mixed Power-Law Interactions: Bistabilities and Temperature-Driven Non-equilibrium Phase Transitions*, arXiv:1512.02123.
[49] R. M. Wilson, K. W. Mahmud, A. Hu, A. V. Gorshkov, M. Hafezi, and M. Foss-Feig, *Collective Phases of Strongly Interacting Cavity Photons*, arXiv:1601.06857.
[50] S. Chakravarty, G.-L. Ingold, S. Kivelson, and A. Luther, *Onset of Global Phase Coherence in Josephson-Junction Arrays: A Dissipative Phase Transition*, Phys. Rev. Lett. **56**, 2303 (1986).
[51] S. E. Korshunov, *Phase Diagram of a Chain of Dissipative Josephson Junctions*, Europhys. Lett. **9**, 107 (1989).
[52] P. A. Bobbert, R. Fazio, G. Schön, and A. D. Zaikin, *Phase Transitions in Dissipative Josephson Chains: Monte Carlo Results and Response Functions*, Phys. Rev. B **45**, 2294 (1992).
[53] G. Refael, E. Demler, Y. Oreg, and D. S. Fisher, *Superconductor-to-Normal Transitions in Dissipative Chains of Mesoscopic Grains and Nanowires*, Phys. Rev. B **75**, 014522 (2007).
[54] We do not take into account the possibility that the steady state is of topological nature [see, for example, M. Roncaglia, M. Rizzi, and J. I. Cirac, *Pfaffian State Generation by Strong Three-Body Dissipation*, Phys. Rev. Lett. **104**, 096803 (2010); C.-E. Bardyn, M. A. Baranov, C. V. Kraus, E. Rico, A. Imamoğlu, P. Zoller, and S. Diehl, *Topology by Dissipation*, New J. Phys. **15**, 085001 (2013); F. Iemini, D. Rossini, R. Fazio, S. Diehl, and L. Mazza, *Dissipative Topological Superconductors in Number-Conserving Systems*, Phys. Rev. B **93**, 115113 (2016)]. The cases we analyze assume the only spontaneous symmetry breaking can occur in the steady state.
[55] S. Finazzi, A. Le Boité, F. Storme, A. Baksic, and C. Ciuti, *Corner-Space Renormalization Method for Driven-Dissipative Two-Dimensional Correlated Systems*, Phys. Rev. Lett. **115**, 080604 (2015).
[56] P. Degenfeld-Schonburg and M. J. Hartmann, *Self-Consistent Projection Operator Theory for Quantum Many-Body Systems*, Phys. Rev. B **89**, 245108 (2014).

[57] H. Weimer, *Variational Principle for Steady States of Dissipative Quantum Many-Body Systems*, Phys. Rev. Lett. **114**, 040402 (2015).

[58] H. A. Bethe, *Statistical Theory of Superlattices*, Proc. R. Soc. A **150**, 552 (1935).

[59] R. Kikuchi, *A Theory of Cooperative Phenomena*, Phys. Rev. **81**, 988 (1951).

[60] T. Oguchi, *A Theory of Antiferromagnetism, II*, Prog. Theor. Phys. **13**, 148 (1955).

[61] J. Oitmaa, C. Hamer, and W. Zheng, *Series Expansion Methods for Strongly Interacting Lattice Models* (Cambridge University Press, Cambridge, England, 2006).

[62] M. Suzuki, *Statistical Mechanical Theory of Cooperative Phenomena. I. General Theory of Fluctuations, Coherent Anomalies and Scaling Exponents with Simple Applications to Critical Phenomena*, J. Phys. Soc. Jpn. **55**, 4205 (1986).

[63] In principle, it is even possible to proceed as for the Hamiltonian case and determine a self-consistent solution for the dark state of the Liouvillian operator on the corresponding cluster (instead of the ground state of the cluster Hamiltonian). The computational effort is, however, huge because of the size of the Liouvillian (e.g., in a system composed of L spins, it is a $4^L \times 4^L$ non-Hermitian matrix).

[64] J. Dalibard, Y. Castin, and K. Mølmer, *Wave-Function Approach to Dissipative Processes in Quantum Optics*, Phys. Rev. Lett. **68**, 580 (1992); K. Mølmer, Y. Castin, and J. Dalibard, *Monte Carlo Wave-Function Method in Quantum Optics*, J. Opt. Soc. Am. B **10**, 524 (1993).

[65] F. Verstraete, J. J. García-Ripoll, and J. I. Cirac, *Matrix Product Density Operators: Simulation of Finite-Temperature and Dissipative Systems*, Phys. Rev. Lett. **93**, 207204 (2004).

[66] M. Zwolak and G. Vidal, *Mixed-State Dynamics in One-Dimensional Quantum Lattice Systems: A Time-Dependent Superoperator Renormalization Algorithm*, Phys. Rev. Lett. **93**, 207205 (2004).

[67] G. Vidal, *Efficient Classical Simulation of Slightly Entangled Quantum Computations*, Phys. Rev. Lett. **91**, 147902 (2003); *Efficient Simulation of One-Dimensional Quantum Many-Body Systems*, Phys. Rev. Lett. **93**, 040502 (2004).

[68] G. Vidal, *Classical Simulation of Infinite-Size Quantum Lattice Systems in One Spatial Dimension*, Phys. Rev. Lett. **98**, 070201 (2007).

[69] R. Orús and G. Vidal, *Infinite Time-Evolving Block Decimation Algorithm Beyond Unitary Evolution*, Phys. Rev. B **78**, 155117 (2008).

[70] M. Biondi, E. P. L. van Nieuwenburg, G. Blatter, S. D. Huber, and S. Schmidt, *Incompressible Polaritons in a Flat Band*, Phys. Rev. Lett. **115**, 143601 (2015).

[71] L. Bonnes, D. Charrier, and A. M. Läuchli, *Dynamical and Steady-State Properties of a Bose-Hubbard Chain with Bond Dissipation: A Study Based on Matrix Product Operators*, Phys. Rev. A **90**, 033612 (2014).

[72] C. Joshi, F. Nissen, and J. Keeling, *Quantum Correlations in the One-Dimensional Driven Dissipative XY Model*, Phys. Rev. A **88**, 063835 (2013).

[73] J. Cui, J. I. Cirac, and M. C. Bañuls, *Variational Matrix Product Operators for the Steady State of Dissipative Quantum Systems*, Phys. Rev. Lett. **114**, 220601 (2015).

[74] E. Mascarenhas, H. Flayac, and V. Savona, *Matrix-Product-Operator Approach to the Nonequilibrium Steady State of Driven-Dissipative Quantum Arrays*, Phys. Rev. A **92**, 022116 (2015).

[75] A. H. Werner, D. Jaschke, P. Silvi, M. Kliesch, T. Calarco, J. Eisert, and S. Montangero, *Positive Tensor Network Approach for Simulating Open Quantum Many-Body Systems*, Phys. Rev. Lett. **116**, 237201 (2016).

[76] S. Yan, D. A. Huse, and S. R. White, *Spin-Liquid Ground State of the $S = 1/2$ Kagome Heisenberg Antiferromagnet*, Science **332**, 1173 (2011).

[77] R. Orús, *A Practical Introduction to Tensor Networks: Matrix Product States and Projected Entangled Pair States*, Ann. Phys. (Amsterdam) **349**, 117 (2014).

[78] We also tried to break the symmetry by adding a small external magnetic field along the x axis and then extrapolating the value of the spontaneous magnetization by calculating the zero-field susceptibility. However, the results we obtained are less clean than those found by the analysis of the two-point correlations in Eq. (17).

[79] Note, however, that our code introduces a small perturbation to the state before each new parameter value (to destabilize the normal state); thus, the real bistability region will be larger than shown.

[80] T. Ozawa, H. M. Price, N. Goldman, O. Zilberberg, and I. Carusotto, *Synthetic Dimensions in Integrated Photonics: From Optical Isolation to Four-Dimensional Quantum Hall Physics*, Phys. Rev. A **93**, 043827 (2016).

[81] L. Tian and H. J. Carmichael, *Quantum Trajectory Simulations of Two-State Behavior in an Optical Cavity Containing One Atom*, Phys. Rev. A **46**, R6801 (1992).

[82] L. S. Bishop, J. M. Chow, J. Koch, A. A. Houck, M. H. Devoret, E. Thuneberg, S. M. Girvin, and R. J. Schoelkopf, *Nonlinear Response of the Vacuum Rabi Resonance*, Nat. Phys. **5**, 105 (2009).

[83] E. Arrigoni, M. Knap, and W. von der Linden, *Nonequilibrium Dynamical Mean Field Theory: An Auxiliary Quantum Master Equation Approach*, Phys. Rev. Lett. **110**, 086403 (2013).

[84] R. Rota, F. Storme, and C. Ciuti (private communication).

[85] DOI: 10.17630/c4e587d0-1e3b-464f-bfa9-6ada5b2d99c0.

Conclusions

In this thesis we have studied a wide range of relevant phenomena associated to topological orders and open quantum systems. The results presented in this thesis have been covered in a series of publications [P1 - P9] where they are explained and discussed in detail. The content of this thesis has been distributed over two parts and an appendix section.

In the first part I, we have analysed to what extent topological phases of matter can be characterised when they are considered as open quantum systems. When we focus on symmetry-protected topological orders (SPTOs) like topological insulators and superconductors, the following results are found. Initially, we have derived a novel master evolution equation for the electrons of a topological insulator in 1D when they are coupled to thermal baths. We have found a remarkable result: edge states become unstable under thermal effects and they have a finite lifetime. This is so, regardless of whether the interaction with the bath respects the protecting symmetry of the topological insulator (in our case chiral symmetry). The usual gap protection does not hold against finite temperature effects: the topological insulator order gets lost regardless of the gap size, although their lifetime increases.

Next, we have constructed a scheme to generalise the idea of a topological insulator to dissipative systems. With this line, we have introduced the notion of band Liouvillian (the dissipative counterpart of a band Hamiltonian) as a fundamental ingredient for the topological order to be preserved. We have constructed a new topological invariant (the density matrix Chern value) that is able to detect topological order at finite temperature and for general quantum mixed states. The Chern value can be related to the mixed character of the edge states, and accounts for the topological contribution to the quantum Hall conductivity at finite temperature. As an example, we have analysed a 2D model for a topological insulator -the Haldane model- in the presence of thermal dissipation.

Finally, we have wondered whether quantised topological phases can exist even at finite temperature and in the presence of dissipation. For this very ambitious purpose, we have introduced the Uhlmann phase (a geometric phase for general density matrix) in topological systems. We showed that when applied to topological insulators and superconductors in 1D the geometric Uhlmann phase acquires a topological and quantised character. Based on this phase, we have constructed another topological invariant valid for 2D systems called Uhlmann number. At zero temperature, the Uhlmann phase witnesses the same topological sector as the

one given by the winding number of the corresponding Hamiltonian or the Berry phase, and the Uhlmann number tends to the Chern number. As temperature increases, the Uhlmann phase/number remains quantised and different from zero below a certain temperature T_c, above which it vanishes. In 2D, we have reported a model where there is a critical transition between two non-trivial topological phases solely driven by temperature. Furthermore, we have discussed several options to measure this new topological phase, but in particular we have proposed a state-independent protocol to measure the topological Uhlmann phase in the context of quantum simulation. In particular, we have shown the feasibility of the protocol for a superconducting qubit setup considering realistic experimental imperfections and noise effects.

We have also studied intrinsic topological orders as open quantum systems from the perspective of topological quantum memories. We have derived a master equation that describes the dynamics of a generalised toric code for qudits coupled to an external heat bath. Interestingly, a toric code for qudits produces new types of anyonic quasiparticles with different braiding statistics. Moreover, we have proven that the system is unstable under thermal perturbations, similar to what happens for the qubit version of the code. However, we have shown that a toric code for qutrits can improve the dynamical stability of anyonic quasiparticles.

In the second part II, we have dealt with long-range extensions of topological superconductors. In particular, we have proposed the most general extension of the 1D Kitaev chain including long-range couplings. Through this procedure we have found two very surprising and even counterintuitive effects. Firstly, we considered finite-range deformation of the hopping (kinetic) amplitudes. By increasing the penetration length of the hopping we have significantly increased the region in the phase diagram where Majorana modes appear. Secondly, for sufficiently slow-decaying pairing terms we have found a new topological quasiparticle that we called non-local massive Dirac fermion, that is localised at both edges of the chain at the same time. By means of finite size scaling, we have shown that there is an edge gap even in the thermodynamic limit. Moreover, we have incorporated static disorder into the system to prove the robustness of the new massive Dirac quasiparticles due to their topological character. All these interesting results provide further evidence of the relevance of topological effects within the field of unconventional superconductivity.

In the appendix section A, we have presented different numerical methods to deal with driven-dissipative quantum phase transitions. We have applied the cluster mean-field method widely used in equilibrium situations, to a new out-of-equilibrium scenario in open quantum systems. In particular, we have studied the XYZ Heisenberg model of interacting spins on a 2D square lattice subjected to dissipative effects. Remarkably, we have shown that the inclusion of short-range

fluctuations deeply modifies the steady-state phase-diagram topology of driven-dissipative quantum systems, contrarily to what happens in equilibrium thermodynamics.

As a final remark, we can clearly envision that the results presented in this thesis shed light upon the fields of topological orders and open quantum systems. Furthermore, we have shown that the combination of the two leads to surprising and novel results. Throughout this thesis, we have also proposed realistic implementations and experimental proposals to test these effects. The versatility of quantum simulation platforms, together with the great effort and interest on topological condensed matter experiments, make us confident that many of the new findings in this thesis will be soon realised in the lab.

References

[AAB+13] Marcos Atala, Monika Aidelsburger, Julio T. Barreiro, Dmitry Abanin, Takuya Kitagawa, Eugene Demler, and Immanuel Bloch, *Direct measurement of the Zak phase in topological Bloch bands*, Nat Phys **9** (2013), no. 12, 795–800.

[AB59] Y. Aharonov and D. Bohm, *Significance of Electromagnetic Potentials in the Quantum Theory*, Physical Review **115** (1959), 485–491.

[Abr57] A. A. Abrikosov, *On the Magnetic properties of superconductors of the second group*, Sov. Phys. JETP **5** (1957), 1174–1182, [Zh. Eksp. Teor. Fiz.32,1442(1957)].

[ACMnT+07] K. M. R. Audenaert, J. Calsamiglia, R. Muñoz Tapia, E. Bagan, Ll. Masanes, A. Acin, and F. Verstraete, *Discriminating States: The Quantum Chernoff Bound*, Phys. Rev. Lett. **98** (2007), 160501.

[AFH09] R Alicki, M Fannes, and M Horodecki, *On thermalization in Kitaev's 2D model*, Journal of Physics A: Mathematical and Theoretical **42** (2009), no. 6, 065303.

[AGD75] A.A. Abrikosov, L.P. Gorkov, and I.E. Dzyaloshinski, *Methods of quantum field theory in statistical physics*, Dover Publications, 1975.

[AHHH10] R. Alicki, M. Horodecki, P. Horodecki, and R. Horodecki, *On Thermal Stability of Topological Qubit in Kitaev's 4D Model*, Open Systems & amp; Information Dynamics **17** (2010), no. 01, 1–20.

[AHM+16] S. M. Albrecht, A. P. Higginbotham, M. Madsen, F. Kuemmeth, T. S. Jespersen, J. Nygård, P. Krogstrup, and C. M. Marcus, *Exponential protection of zero modes in Majorana islands*, Nature **531** (2016), no. 7593, 206–209.

[AM76] Neil W. Ashcroft and N. David Mermin, *Solid state physics*, Brooks Cole, 1976.

[Ann04] J.F. Annett, *Superconductivity, Superfluids and Condensates*, Oxford Master Series in Physics, OUP Oxford, 2004.

[AS10] A. Altland and B. Simons, *Condensed Matter Field Theory*, Cambridge University Press, 2010.

[ASW84] D. Arovas, J. R. Schrieffer, and F. Wilczek, *Fractional Statistics and the Quantum Hall Effect*, Physical Review Letters **53** (1984), 722–723.

[BAB13] Taylor L. Hughes B. Andrei Bernevig, *Topological Insulators and Topological Superconductors*, Princeton University Press, 2013.

[Bal98] L.E. Ballentine, *Quantum Mechanics: A Modern Development*, World Scientific, 1998.

[Bal11] Leon Balents, *Viewpoint: Weyl electrons kiss*, Physics **4** (2011) (en).

[BCS57] J. Bardeen, L. N. Cooper, and J. R. Schrieffer, *Theory of Superconductivity*, Phys. Rev. **108** (1957), 1175–1204.

[BDZ08] I. Bloch, J. Dalibard, and W. Zwerger, *Many-body physics with ultracold gases*, Reviews of Modern Physics **80** (2008), 885–964.

[Ber84] M. V. Berry, *Quantal Phase Factors Accompanying Adiabatic Changes*, Royal Society of London Proceedings Series A **392** (1984), 45–57.

[BGB09] M. Boissonneault, J. M. Gambetta, and A. Blais, *Dispersive regime of circuit QED: Photon-dependent qubit dephasing and relaxation rates*, Phys. Rev. A **79** (2009), 013819.

[BHW+04] A. Blais, R.-S. Huang, A. Wallraff, S. M. Girvin, and R. J. Schoelkopf, *Cavity quantum electrodynamics for superconducting electrical circuits: An architecture for quantum computation*, Phys. Rev. A **69** (2004), 062320.

[BHZ06] B. A. Bernevig, T. L. Hughes, and S.-C. Zhang, *Quantum Spin Hall Effect and Topological Phase Transition in HgTe Quantum Wells*, Science **314** (2006), 1757.

[BKM+14] R. Barends, J. Kelly, A. Megrant, A. Veitia, D. Sank, E. Jeffrey, T. C. White, J. Mutus, A. G. Fowler, B. Campbell, Y. Chen, Z. Chen, B. Chiaro, A. Dunsworth, C. Neill, P. O'Malley, P. Roushan, A. Vainsencher, J. Wenner, A. N. Korotkov, A. N. Cleland, and John M. Martinis, *Superconducting quantum circuits at the surface code threshold for fault tolerance*, Nature **508** (2014), no. 7497, 500–503.

[BLK+15] R. Barends, L. Lamata, J. Kelly, L. Garcia-Alvarez, A. G. Fowler, A Megrant, E Jeffrey, T. C. White, D. Sank, J. Y. Mutus, B. Campbell, Yu Chen, Z. Chen, B. Chiaro, A. Dunsworth, I. C. Hoi, C. Neill, P. J. J. O'Malley, C. Quintana, P. Roushan, A. Vainsencher, J. Wenner, E. Solano, and John M. Martinis, *Digital quantum simulation of fermionic models with a superconducting circuit*, Nat Commun **6** (2015).

[BLP+14] B. J. Brown, D. Loss, J. K. Pachos, C. N. Self, and J. R. Wootton, *Quantum Memories at Finite Temperature*, ArXiv e-prints (2014).

[BM86] J. G. Bednorz and K. A. Müller, *Possible high T_c superconductivity in the $Ba - La - Cu - O$ system*, Zeitschrift für Physik B Condensed Matter **64** (1986), no. 2, 189–193.

[BMABD13] C.-E. Bardyn, E. Rico A. İmamoğlu P. Zoller M. A. Baranov, C. V. Kraus, and S. Diehl, *Topology by dissipation*, New Journal of Physics **15** (2013), no. 8, 085001.

[BMD06] H. Bombin and M. A. Martin-Delgado, *Topological Quantum Distillation*, Phys. Rev. Lett. **97** (2006), 180501.

[BMD07] H. Bombin and M. A. Martin-Delgado, *Topological Computation without Braiding*, Phys. Rev. Lett. **98** (2007), 160502.

[BMS+11] Julio T. Barreiro, Markus Muller, Philipp Schindler, Daniel Nigg, Thomas Monz, Michael Chwalla, Markus Hennrich, Christian F. Roos, Peter Zoller, and Rainer Blatt, *An open-system quantum simulator with trapped ions*, Nature **470** (2011), no. 7335, 486–491.

[BN09] I. Buluta and F. Nori, *Quantum Simulators*, Science **326** (2009), 108–.

[BP07] H.P. Breuer and F. Petruccione, *The Theory of Open Quantum Systems*, OUP Oxford, 2007.

[BPAMD09] A. Bermudez, D. Patanè, L. Amico, and M. A. Martin-Delgado, *Topology-Induced Anomalous Defect Production by Crossing a Quantum Critical Point*, Phys. Rev. Lett. **102** (2009), 135702.

[BRWCMD13] H Bombin, M. Horodecki R. W. Chhajlany, and M. A. Martin-Delgado, *Self-correcting quantum computers*, New Journal of Physics **15** (2013), no. 5, 055023.

[BT09] Sergey Bravyi and Barbara Terhal, *A no-go theorem for a two-dimensional self-correcting quantum memory based on stabilizer codes*, New Journal of Physics **11** (2009), no. 4, 043029.

[BUGH09] D. Bercioux, D. F. Urban, H. Grabert, and W. Häusler, *Massless Dirac-Weyl fermions in a T_3 optical lattice*, Physical Review A **80** (2009), 063603.

[Bur69] Donald Bures, *An Extension of Kakutani's Theorem on Infinite Product Measures to the Tensor Product of Semifinite w^*-Algebras*, Transactions of the American Mathematical Society **135** (1969), 199–212.

[BW08] Rainer Blatt and David Wineland, *Entangled states of trapped atomic ions*, Nature **453** (2008), no. 7198, 1008–1015.

[BZ06] B. A. Bernevig and S.-C. Zhang, *Quantum Spin Hall Effect*, Physical Review Letters **96** (2006), no. 10, 106802.

[CAC+09] Y. L. Chen, J. G. Analytis, J.-H. Chu, Z. K. Liu, S.-K. Mo, X. L. Qi, H. J. Zhang, D. H. Lu, X. Dai, Z. Fang, S. C. Zhang, I. R. Fisher, Z. Hussain, and Z.-X. Shen, *Experimental Realization of a Three-Dimensional Topological Insulator, Bi2Te3*, Science **325** (2009), no. 5937, 178–181.

[CDBVN16] Pieter W. Claeys, Stijn De Baerdemacker, and Dimitri Van Neck, *Read-Green resonances in a topological superconductor coupled to a bath*, Phys. Rev. B **93** (2016), 220503.

[CG04] Peter Zoller Crispin Gardiner, *Quantum noise: A Handbook of Markovian and Non-Markovian Quantum Stochastic Methods with Applications to Quantum Optics*, 2nd enlarged ed ed., Springer series in synergetics, Springer, 2004.

[CGLW13] Xie Chen, Zheng-Cheng Gu, Zheng-Xin Liu, and Xiao-Gang Wen, *Symmetry protected topological orders and the group cohomology of their symmetry group*, Phys. Rev. B **87** (2013), 155114.

[CGW10] Xie Chen, Zheng-Cheng Gu, and Xiao-Gang Wen, *Local unitary transformation, long-range quantum entanglement, wave function renormalization, and topological order*, Phys. Rev. B **82** (2010), 155138.

[CMnTM+08] J. Calsamiglia, R. Muñoz Tapia, Ll. Masanes, A. Acin, and E. Bagan, *Quantum Chernoff bound as a measure of distinguishability between density matrices: Application to qubit and Gaussian states*, Phys. Rev. A **77** (2008), 032311.

[CNGP+09] A. H. Castro Neto, F. Guinea, N. M. R. Peres, K. S. Novoselov, and A. K. Geim, *The electronic properties of graphene*, Rev. Mod. Phys. **81** (2009), 109–162.

[Coo56] Leon N. Cooper, *Bound Electron Pairs in a Degenerate Fermi Gas*, Phys. Rev. **104** (1956), 1189–1190.

[Cre99] M. Creutz, *End States, Ladder Compounds, and Domain-Wall Fermions*, Physical Review Letters **83** (1999), 2636–2639.

[Cre01] M. Creutz, *Aspects of chiral symmetry and the lattice*, Reviews of Modern Physics **73** (2001), 119–150.

[CTSR16] Ching-Kai Chiu, Jeffrey C. Y. Teo, Andreas P. Schnyder, and Shinsei Ryu, *Classification of topological quantum matter with symmetries*, Rev. Mod. Phys. **88** (2016), 035005.

[CV09] J Ignacio Cirac and Frank Verstraete, *Renormalization and tensor product states in spin chains and lattices*, Journal of Physics A: Mathematical and Theoretical **42** (2009), no. 50, 504004.

[CW08] John Clarke and Frank K. Wilhelm, *Superconducting quantum bits*, Nature **453** (2008), no. 7198, 1031–1042.

[CZ95] J. I. Cirac and P. Zoller, *Quantum Computations with Cold Trapped Ions*, Phys. Rev. Lett. **74** (1995), 4091–4094.

[Dal14] Andrew J. Daley, *Quantum trajectories and open many-body quantum systems*, Advances in Physics **63** (2014), no. 2, 77–149.

[Dav74] E. B. Davies, *Markovian master equations*, Comm. Math. Phys. **39** (1974), no. 2, 91–110.

[Dav76] E. B. Davies, *Quantum Theory of Open Systems*, Academic Press, 1976.

[DCM92] Jean Dalibard, Yvan Castin, and Klaus Mølmer, *Wave-function approach to dissipative processes in quantum optics*, Phys. Rev. Lett. **68** (1992), 580–583.

[Dir31] P. A. M. Dirac, *Quantised Singularities in the Electromagnetic Field*, Proceedings of the Royal Society of London A: Mathematical, Physical and Engineering Sciences **133** (1931), no. 821, 60–72.

[DKD+12] P. Dziawa, B. J. Kowalski, K. Dybko, R. Buczko, A. Szczerbakow, M. Szot, E. Łusakowska, T. Balasubramanian, B. M. Wojek, M. H. Berntsen, O. Tjernberg, and T. Story, *Topological crystalline insulator states in $Pb_{1-x}Sn_xSe$*, Nat. Mater. **11** (2012), no. 12, 1023–1027.

[DMMD12] A. Dauphin, M. Müller, and M. A. Martin-Delgado, *Rydberg-atom quantum simulation and Chern-number characterization of a topological Mott insulator*, Phys. Rev. A **86** (2012), 053618.

[DMMD14] A Dauphin, M Müller, and M A Martin-Delgado, *Efficient algorithm to compute the Berry conductivity*, New Journal of Physics **16** (2014), no. 7, 073016.

[DMMD16] A. Dauphin, M. Müller, and M. A. Martin-Delgado, *Quantum simulation of a topological Mott insulator with Rydberg atoms in a Lieb lattice*, Phys. Rev. A **93** (2016), 043611.

[DOM14] Hossein Dehghani, Takashi Oka, and Aditi Mitra, *Dissipative Floquet topological systems*, Phys. Rev. B **90** (2014), 195429.

[DOM15] Hossein Dehghani, Takashi Oka, and Aditi Mitra, *Out-of-equilibrium electrons and the Hall conductance of a Floquet topological insulator*, Phys. Rev. B **91** (2015), 155422.

[DRM+12] Anindya Das, Yuval Ronen, Yonatan Most, Yuval Oreg, Moty Heiblum, and Hadas Shtrikman, *Zero-bias peaks and splitting in an Al-InAs nanowire topological superconductor as a signature of Majorana fermions*, Nat. Phys. **8** (2012), no. 12, 887–895.

[DTM+10] Sebastian Diehl, Andrea Tomadin, Andrea Micheli, Rosario Fazio, and Peter Zoller, *Dynamical Phase Transitions and Instabilities in Open Atomic Many-Body Systems*, Phys. Rev. Lett. **105** (2010), 015702.

[DW08] Gerard J. Milburn D.F. Walls, *Quantum Optics*, 2nd ed ed., Springer, 2008.

[DWM04] M. H. Devoret, A. Wallraff, and J. M. Martinis, *Superconducting Qubits: A Short Review*, arXiv: cond-mat/0411174 (2004).

[DYH+12] M. T. Deng, C. L. Yu, G. Y. Huang, M. Larsson, P. Caroff, and H. Q. Xu, *Anomalous Zero-Bias Conductance Peak in a Nb − −InSb Nanowire − −Nb Hybrid Device*, Nano Letters **12** (2012), no. 12, 6414–6419, PMID: 23181691.

[Dys69a] Freeman J. Dyson, *Existence of a phase-transition in a one-dimensional Ising ferromagnet*, Comm. Math. Phys. **12** (1969), no. 2, 91–107.

[Dys69b] Freeman J. Dyson, *Non-existence of spontaneous magnetization in a one-dimensional Ising ferromagnet*, Comm. Math. Phys. **12** (1969), no. 3, 212–215.

[E23] Peirls R E, Helv. Phys. Acta **7** (1923), no. 81.

[E35] Peierls R E, *Some properties of solids*, Ann. Inst. Henri Poincaré **5** (1935), no. 177.

[EH13] A. M. Essin and M. Hermele, *Classifying fractionalization: Symmetry classification of gapped Z_2 spin liquids in two dimensions*, Phys. Rev. B **87** (2013), 104406.

[Ehr33] P.. Ehrenfest, *Phase changes in the ordinary and extended sense classified according to the corresponding singularities of the thermodynamic potential.*, Proceedings of the Academy of Science, Amsterdam, **36** (1933), 153–157.

[Ess10] T. Esslinger, *Fermi-Hubbard physics with atoms in an optical lattice*, ArXiv e-prints (2010).

[Fey82] R. P. Feynman, *Simulating Physics with Computers*, International Journal of Theoretical Physics **21** (1982), 467–488.

[FK08] L. Fu and C. L. Kane, *Superconducting Proximity Effect and Majorana Fermions at the Surface of a Topological Insulator*, Physical Review Letters **100** (2008), no. 9, 096407.

[FK10] Lukasz Fidkowski and Alexei Kitaev, *Effects of interactions on the topological classification of free fermion systems*, Phys. Rev. B **81** (2010), 134509.

[FKM07] L. Fu, C. L. Kane, and E. J. Mele, *Topological Insulators in Three Dimensions*, Physical Review Letters **98** (2007), no. 10, 106803.

[FM12] John Foster and J. Stan Metcalfe, *Economic emergence: An evolutionary economic perspective*, Journal of Economic Behavior & Organization **82** (2012), no. 2–3, 420 – 432, Emergence in Economics.

[FMMC12] Austin G. Fowler, Matteo Mariantoni, John M. Martinis, and Andrew N. Cleland, *Surface codes: Towards practical large-scale quantum computation*, Phys. Rev. A **86** (2012), 032324.

[FMNR01] W. M. C. Foulkes, L. Mitas, R. J. Needs, and G. Rajagopal, *Quantum Monte Carlo simulations of solids*, Rev. Mod. Phys. **73** (2001), 33–83.

[FNS+04] Michael Freedman, Chetan Nayak, Kirill Shtengel, Kevin Walker, and Zhenghan Wang, *A class of P, T-invariant topological phases of interacting electrons*, Annals of Physics **310** (2004), no. 2, 428–492.

[Fu11] Liang Fu, *Topological Crystalline Insulators*, Phys. Rev. Lett. **106** (2011), 106802.

[FW05] Adrian E. Feiguin and Steven R. White, *Time-step targeting methods for real-time dynamics using the density matrix renormalization group*, Phys. Rev. B **72** (2005), 020404.

[GAN14] I. M. Georgescu, S. Ashhab, and Franco Nori, *Quantum simulation*, Rev. Mod. Phys. **86** (2014), 153–185.

[GC34] C.J Gorter and H Casimir, *On supraconductivity I*, Physica **1** (1934), no. 1, 306 – 320.

[GDD+13] Nathan Goldman, Jean Dalibard, Alexandre Dauphin, Fabrice Gerbier, Maciej Lewenstein, Peter Zoller, and Ian B. Spielman, *Direct imaging of topological edge states in cold-atom systems*, Proceedings of the National Academy of Sciences **110** (2013), no. 17, 6736–6741.

[GFG12] Joydip Ghosh, Austin G. Fowler, and Michael R. Geller, *Surface code with decoherence: An analysis of three superconducting architectures*, Phys. Rev. A **86** (2012), 062318.

[GL50] V. L. Ginzburg and L. D. Landau, *On the Theory of Superconductivity*, Zh. Eksp. Teor. Fiz. **20** (1950), 1064–1082.

[GLV+93] G. Grynberg, B. Lounis, P. Verkerk, J.-Y. Courtois, and C. Salomon, *Quantized motion of cold cesium atoms in two- and three-dimensional optical potentials*, Physical Review Letters **70** (1993), 2249–2252.

[GM02] A. Galindo and M. A. Martín-Delgado, *Information and computation: Classical and quantum aspects*, Reviews of Modern Physics **74** (2002), 347–423.

[GME+02] M. Greiner, O. Mandel, T. Esslinger, T. W. Hänsch, and I. Bloch, *Quantum phase transition from a superfluid to a Mott insulator in a gas of ultracold atoms*, Nature **415** (2002), 39–44.

[GMS+15] Michael R. Geller, John M. Martinis, Andrew T. Sornborger, Phillip C. Stancil, Emily J. Pritchett, Hao You, and Andrei Galiautdinov, *Universal quantum simulation with prethreshold superconducting qubits: Single-excitation subspace method*, Phys. Rev. A **91** (2015), 062309.

[GN91] Moore G. and Read N., *Nonabelions in the fractional quantum hall effect*, Nuclear Physics B **360** (1991), no. 2, 362 – 396.

[Gol09] N. Goldman, *Quantum transport and phase transitions in lattices subjected to external gauge fields*, Ph.D. thesis, Université libre de Bruxelles, Faculté des Sciences – Physique, Bruxelles., 2009.

[GP90] A. Galindo and P. Pascual, *Quantum mechanics I*, Quantum Mechanics, Springer-Verlag, 1990.

[Gro96] D. J. Gross, *The Role of Symmetry in Fundamental Physics*, Proceedings of the National Academy of Science **93** (1996), 14256–14259.

[GRSMD08] Juan José García-Ripoll, Enrique Solano, and Miguel Angel Martin-Delgado, *Quantum simulation of Anderson and Kondo lattices with superconducting qubits*, Phys. Rev. B **77** (2008), 024522.

[GSN+10] N. Goldman, I. Satija, P. Nikolic, A. Bermudez, M. A. Martin-Delgado, M. Lewenstein, and I. B. Spielman, *Realistic Time-Reversal Invariant Topological Insulators with Neutral Atoms*, Phys. Rev. Lett. **105** (2010), 255302.

[Haf14] M Hafezi, *Measuring Topological Invariants in Photonic Systems*, Phys. Rev. Lett. **112** (2014), 210405.

[Hal82] B. I. Halperin, *Quantized Hall conductance, current-carrying edge states, and the existence of extended states in a two-dimensional disordered potential*, Physical Review B **25** (1982), 2185–2190.

[Hal83a] F. D. M. Haldane, *Nonlinear Field Theory of Large-Spin Heisenberg Antiferromagnets: Semiclassically Quantized Solitons of the One-Dimensional Easy-Axis Néel State*, Phys. Rev. Lett. **50** (1983), 1153–1156.

[Hal83b] F. D. M. Haldane, *Fractional Quantization of the Hall Effect: A Hierarchy of Incompressible Quantum Fluid States*, Phys. Rev. Lett. **51** (1983), 605–608.

[Hal84] Bertrand I Halperin, *Statistics of quasiparticles and the hierarchy of fractional quantized Hall states*, Physical Review Letters **52** (1984), no. 18, 1583.

[Hal88a] F. D. M. Haldane, *Model for a quantum Hall effect without Landau levels: Condensed-matter realization of the parity anomaly*, Physical Review Letters **61** (1988), 2015–2018.

[Hal88b] F. D. M. Haldane, *Model for a Quantum Hall Effect without Landau Levels: Condensed-Matter Realization of the "Parity Anomaly"*, Phys. Rev. Lett. **61** (1988), 2015–2018.

[Has11] Matthew B. Hastings, *Topological Order at Nonzero Temperature*, Phys. Rev. Lett. **107** (2011), 210501.

[HCBZ15] Ying Hu, Zi Cai, Mikhail A. Baranov, and Peter Zoller, *Majorana fermions in noisy Kitaev wires*, Phys. Rev. B **92** (2015), 165118.

[HHJ+10] D. Hanneke, J. P. Home, J. D. Jost, J. M. Amini, D. Leibfried, and D. J. Wineland, *Realization of a programmable two-qubit quantum processor*, Nat Phys **6** (2010), no. 1, 13–16.

[Hil94] T.L. Hill, *Thermodynamics of Small Systems*, Dover Phoenix editions, Dover Publications, 1994.

[HK10] M. Z. Hasan and C. L. Kane, *Colloquium : Topological insulators*, Rev. Mod. Phys. **82** (2010), 3045–3067.

[HLL+12] Timothy H. Hsieh, Hsin Lin, Junwei Liu, Wenhui Duan, Arun Bansil, and Liang Fu, *Topological crystalline insulators in the SnTe material class*, Nat Commun **3** (2012), 982.

[HLR93] Bertrand I Halperin, Patrick A Lee, and Nicholas Read, *Theory of the half-filled Landau level*, Physical Review B **47** (1993), no. 12, 7312.

[HMF+13] M Hafezi, S Mittal, J Fan, A Migdall, and J M Taylor, *Imaging topological edge states in silicon photonics*, Nature Photonics **7** (2013), 1001 – 1005.

[HQW+08] D. Hsieh, D. Qian, L. Wray, Y. Xia, Y. S. Hor, R. J. Cava, and M. Z. Hasan, *A topological Dirac insulator in a quantum spin Hall phase*, Nature **452** (2008), 970–974.

[HS05] Naomichi Hatano and Masuo Suzuki, *Finding Exponential Product Formulas of Higher Orders*, pp. 37–68, Springer Berlin Heidelberg, Berlin, Heidelberg, 2005.

[HWC+14] James J. He, Jiansheng Wu, Ting-Pong Choy, Xiong-Jun Liu, Y. Tanaka, and K. T. Law, *Correlated spin currents generated by resonant-crossed Andreev reflections in topological superconductors*, Nat Commun **5** (2014).

[HXQ+09a] D. Hsieh, Y. Xia, D. Qian, L. Wray, J. H. Dil, F. Meier, J. Osterwalder, L. Patthey, J. G. Checkelsky, N. P. Ong, A. V. Fedorov, H. Lin, A. Bansil, D. Grauer, Y. S. Hor, R. J. Cava, and M. Z. Hasan, *A tunable topological insulator in the spin helical Dirac transport regime*, Nature **460** (2009), 1101–1105.

[HXQ+09b] D. Hsieh, Y. Xia, D. Qian, L. Wray, F. Meier, J. H. Dil, J. Osterwalder, L. Patthey, A. V. Fedorov, H. Lin, A. Bansil, D. Grauer, Y. S. Hor, R. J. Cava, and M. Z. Hasan, *Observation of Time-Reversal-Protected Single-Dirac-Cone Topological-Insulator States in Bi_2Te_3 and Sb_2Te_3*, Physical Review Letters **103** (2009), no. 14, 146401.

[HXW+09] D. Hsieh, Y. Xia, L. Wray, D. Qian, A. Pal, J. H. Dil, J. Osterwalder, F. Meier, G. Bihlmayer, C. L. Kane, Y. S. Hor, R. J. Cava, and M. Z. Hasan, *Observation of Unconventional Quantum Spin Textures in Topological Insulators*, Science **323** (2009), 919–.

[HYR11] Dirk Helbing, Wenjian Yu, and Heiko Rauhut, *Self-Organization and Emergence in Social Systems: Modeling the Coevolution of Social Environments and Cooperative Behavior*, The Journal of Mathematical Sociology **35** (2011), no. 1-3, 177–208.

[Isi25] E. Ising, *Beitrag zur Theorie des Ferromagnetismus*, Zeitschrift fur Physik **31** (1925), 253–258.

[Jae98] Gregg Jaeger, *The Ehrenfest Classification of Phase Transitions: Introduction and Evolution*, Archive for History of Exact Sciences **53** (1998), no. 1, 51–81.

[Jai89] J. K. Jain, *Composite-fermion approach for the fractional quantum Hall effect*, Phys. Rev. Lett. **63** (1989), 199–202.

[JBC+98] D. Jaksch, C. Bruder, J. I. Cirac, C. W. Gardiner, and P. Zoller, *Cold Bosonic Atoms in Optical Lattices*, Physical Review Letters **81** (1998), 3108–3111.

[JMD+14] Gregor Jotzu, Michael Messer, Remi Desbuquois, Martin Lebrat, Thomas Uehlinger, Daniel Greif, and Tilman Esslinger, *Experimental realization of the topological Haldane model with ultracold fermions*, Nature **515** (2014), no. 7526, 237–240.

[JNK13] Chaitanya Joshi, Felix Nissen, and Jonathan Keeling, *Quantum correlations in the one-dimensional driven dissipative XY model*, Phys. Rev. A **88** (2013), 063835.

[JSG+08] R. Jördens, N. Strohmaier, K. Günter, H. Moritz, and T. Esslinger, *A Mott insulator of fermionic atoms in an optical lattice*, Nature **455** (2008), 204–207.

[JZ03] D. Jaksch and P. Zoller, *Creation of effective magnetic fields in optical lattices: the Hofstadter butterfly for cold neutral atoms*, New Journal of Physics **5** (2003), 56.

[Kap92] D. B. Kaplan, *A method for simulating chiral fermions on the lattice*, Physics Letters B **288** (1992), 342–347.

[KDP80] K. V. Klitzing, G. Dorda, and M. Pepper, *New Method for High-Accuracy Determination of the Fine-Structure Constant Based on Quantized Hall Resistance*, Physical Review Letters **45** (1980), 494–497.

[KGI+12] E. M. Kessler, G. Giedke, A. Imamoglu, S. F. Yelin, M. D. Lukin, and J. I. Cirac, *Dissipative phase transition in a central spin system*, Phys. Rev. A **86** (2012), 012116.

[Kit63] C. Kittel, *Quantum theory of solids*, Wiley, 1963.

[Kit01] A. Y. Kitaev, *Unpaired Majorana fermions in quantum wires*, Physics Uspekhi **44** (2001), 131.

[Kit03] A. Y. Kitaev, *Fault-tolerant quantum computation by anyons*, Annals of Physics **303** (2003), 2–30.

[Kit09] A. Kitaev, *Periodic table for topological insulators and superconductors*, American Institute of Physics Conference Series (V. Lebedev and M. Feigel'Man, ed.), American Institute of Physics Conference Series, vol. 1134, May 2009, pp. 22–30.

[KMS+05] M. Köhl, H. Moritz, T. Stöferle, K. Günter, and T. Esslinger, *Fermionic Atoms in a Three Dimensional Optical Lattice: Observing Fermi Surfaces, Dynamics, and Interactions*, Physical Review Letters **94** (2005), no. 8, 080403.

[KP06] Alexei Kitaev and John Preskill, *Topological Entanglement Entropy*, Phys. Rev. Lett. **96** (2006), 110404.

[KQM16] S. N. Kempkes, A. Quelle, and C. Morais Smith, *Universalities of thermodynamic signatures in topological phases*, arXiv: 1607.03373 (2016).

[KT72] J M Kosterlitz and D J Thouless, *Long range order and metastability in two dimensional solids and superfluids. (Application of dislocation theory)*, Journal of Physics C: Solid State Physics **5** (1972), no. 11, L124.

[KT73] J M Kosterlitz and D J Thouless, *Ordering, metastability and phase transitions in two-dimensional systems*, Journal of Physics C: Solid State Physics **6** (1973), no. 7, 1181.

[KWB+07] M. König, S. Wiedmann, C. Brüne, A. Roth, H. Buhmann, L. W. Molenkamp, X.-L. Qi, and S.-C. VERY IMPORTANT!!! Zhang, *Quantum Spin Hall Insulator State in HgTe Quantum Wells*, Science **318** (2007), 766.

[KYG+07] Jens Koch, Terri M. Yu, Jay Gambetta, A. A. Houck, D. I. Schuster, J. Majer, Alexandre Blais, M. H. Devoret, S. M. Girvin, and R. J. Schoelkopf, *Charge-insensitive qubit design derived from the Cooper pair box*, Phys. Rev. A **76** (2007), 042319.

[Lan37] L. D. Landau, *On the theory of phase transitions*, Zh. Eksp. Teor. Fiz. (Journal of Experimental and Theoretical Physics) **7** (1937), 19–32.

[Lau81] R. B. Laughlin, *Quantized Hall conductivity in two dimensions*, Physical Review B **23** (1981), 5632–5633.

[Lau83] R. B. Laughlin, *Anomalous quantum Hall effect - An incompressible quantum fluid with fractionally charged excitations*, Physical Review Letters **50** (1983), 1395–1398.

[LBMW03] D. Leibfried, R. Blatt, C. Monroe, and D. Wineland, *Quantum dynamics of single trapped ions*, Reviews of Modern Physics **75** (2003), 281–324.

[LCD+87] A. J. Leggett, S. Chakravarty, A. T. Dorsey, Matthew P. A. Fisher, Anupam Garg, and W. Zwerger, *Dynamics of the dissipative two-state system*, Rev. Mod. Phys. **59** (1987), 1–85.

[LCJ+09] Y.-J. Lin, R. L. Compton, K. Jiménez-García, J. V. Porto, and I. B. Spielman, *Synthetic magnetic fields for ultracold neutral atoms*, Nature **462** (2009), 628–632.

[LDR+16] Tracy Li, Lucia Duca, Martin Reitter, Fabian Grusdt, Eugene Demler, Manuel Endres, Monika Schleier-Smith, Immanuel Bloch, and Ulrich Schneider, *Bloch state tomography using Wilson lines*, Science **352** (2016), no. 6289, 1094–1097.

[Leg75] Anthony J. Leggett, *A theoretical description of the new phases of liquid ^{3}He*, Rev. Mod. Phys. **47** (1975), 331–414.

[LFB+07] P. J. Leek, J. M. Fink, A. Blais, R. Bianchetti, M. Göppl, J. M. Gambetta, D. I. Schuster, L. Frunzio, R. J. Schoelkopf, and A. Wallraff, *Observation of Berry's Phase in a Solid-State Qubit*, Science **318** (2007), no. 5858, 1889–1892.

[LG12] Michael Levin and Zheng-Cheng Gu, *Braiding statistics approach to symmetry-protected topological phases*, Phys. Rev. B **86** (2012), 115109.

[LGF16] D. Linzner, F. Grusdt, and M. Fleischhauer, *Thouless pumping and reservoir-induced topological order in interacting open spin chains*, arXiv: 1605.00756 (2016).

[LGL13] Tony E. Lee, Sarang Gopalakrishnan, and Mikhail D. Lukin, *Unconventional Magnetism via Optical Pumping of Interacting Spin Systems*, Phys. Rev. Lett. **110** (2013), 257204.

[LHN+11] B. P. Lanyon, C. Hempel, D. Nigg, M. Müller, R. Gerritsma, F. Zähringer, P. Schindler, J. T. Barreiro, M. Rambach, G. Kirchmair, M. Hennrich, P. Zoller, R. Blatt, and C. F. Roos, *Universal Digital Quantum Simulation with Trapped Ions*, Science **334** (2011), no. 6052, 57–61.

[Lin76] G. Lindblad, *On the generators of quantum dynamical semigroups*, Communications in Mathematical Physics **48** (1976), no. 2, 119–130.

[LJS14] Ling Lu, John D Joannopoulos, and Marin Soljacic, *Topological photonics*, Nat Photon **8** (2014), no. 11, 821–829.

[LL35] F. London and H. London, *The Electromagnetic Equations of the Supraconductor*, Proceedings of the Royal Society of London A: Mathematical, Physical and Engineering Sciences **149** (1935), no. 866, 71–88.

[LL00] L. D. Landau and E. M. Lifshitz, *Statistical Physics*, Butterworth-Heinemann, 2000.

[Llo96] S. Lloyd, *Universal Quantum Simulators*, Science **273** (1996), 1073–1078.

[LRF+16] Fernando Lemini, Davide Rossini, Rosario Fazio, Sebastian Diehl, and Leonardo Mazza, *Dissipative topological superconductors in number-conserving systems*, Phys. Rev. B **93** (2016), 115113.

[LSA+07] M. Lewenstein, A. Sanpera, V. Ahufinger, B. Damski, A. Sen, and U. Sen, *Ultracold atomic gases in optical lattices: mimicking condensed matter physics and beyond*, Advances in Physics **56** (2007), 243–379.

[Lui06] Alfredo Luis, *Geometric phase in a flat space for electromagnetic scalar waves*, Opt. Lett. **31** (2006), no. 16, 2471–2473.

[LvHGmcuuG13] Igor Lesanovsky, Merlijn van Horssen, Mǎd ălin Guţă, and Juan P. Garrahan, *Characterization of Dynamical Phase Transitions in Quantum Jump Trajectories Beyond the Properties of the Stationary State*, Phys. Rev. Lett. **110** (2013), 150401.

[LW05] Michael A. Levin and Xiao-Gang Wen, *String-net condensation: A physical mechanism for topological phases*, Phys. Rev. B **71** (2005), 045110.

[LW06] Michael Levin and Xiao-Gang Wen, *Detecting Topological Order in a Ground State Wave Function*, Phys. Rev. Lett. **96** (2006), 110405.

[Maj08] Ettore Majorana, *Teoria simmetrica dell'elettrone e del positrone*, Il Nuovo Cimento (1924-1942) **14** (2008), no. 4, 171–184.

[Max50] Emanuel Maxwell, *Isotope Effect in the Superconductivity of Mercury*, Phys. Rev. **78** (1950), 477–477.

[MBG+12] Leonardo Mazza, Alejandro Bermudez, Nathan Goldman, Matteo Rizzi, Miguel Angel Martin-Delgado, and Maciej Lewenstein, *An optical-lattice-based quantum simulator for relativistic field theories and topological insulators*, New Journal of Physics **14** (2012), no. 1, 015007.

[MCLS13] A. Mezzacapo, J. Casanova, L. Lamata, and E. Solano, *Topological qubits with Majorana fermions in trapped ions*, New Journal of Physics **15** (2013), no. 3, 033005.

[MD99] J. Marro and R. Dickman, *Nonequilibrium Phase Transitions in Lattice Models*, Cambridge University Press, 1999.

[MDP+12] Markus Müller, Sebastian Diehl, Guido Pupillo, Peter Zoller, Ennio Arimondo Paul Berman, and Chun Lin, *Engineered Open Systems and Quantum Simulations with Atoms and Ions*, vol. Volume 61, pp. 1–80, Academic Press, 2012.

[MGF+16] Sunil Mittal, Sriram Ganeshan, Jingyun Fan, Abolhassan Vaezi, and Mohammad Hafezi, *Measurement of topological invariants in a 2D photonic system*, Nat Photon **10** (2016), no. 3, 180–183.

[MKF13] Max A. Metlitski, C. L. Kane, and Matthew P. A. Fisher, *Bosonic topological insulator in three dimensions and the statistical Witten effect*, Phys. Rev. B **88** (2013), 035131.

[MO33] W. Meissner and R. Ochsenfeld, *Ein neuer Effekt bei Eintritt der Supraleitfähigkeit*, Naturwissenschaften **21** (1933), no. 44, 787–788.

[Mot68] N. F. Mott, *Metal-Insulator Transition*, Reviews of Modern Physics **40** (1968), 677–683.

[MR13] Andrej Mesaros and Ying Ran, *Classification of symmetry enriched topological phases with exactly solvable models*, Phys. Rev. B **87** (2013), 155115.

[MRLC13] L. Mazza, M. Rizzi, M. D. Lukin, and J. I. Cirac, *Robustness of quantum memories based on Majorana zero modes*, Phys. Rev. B **88** (2013), 205142.

[MSS01] Yuriy Makhlin, Gerd Schön, and Alexander Shnirman, *Quantum-state engineering with Josephson-junction devices*, Rev. Mod. Phys. **73** (2001), 357–400.

[Muk09] D. Mukamel, *Notes on the Statistical Mechanics of Systems with Long-Range Interactions*, arXiv: 0905.1457 (2009).

[Mur07] Shuichi Murakami, *Phase transition between the quantum spin Hall and insulator phases in 3D: emergence of a topological gapless phase*, New Journal of Physics **9** (2007), no. 9, 356.

[MZF+12] V. Mourik, K. Zuo, S. M. Frolov, S. R. Plissard, E. P. A. M. Bakkers, and L. P. Kouwenhoven, *Signatures of Majorana Fermions in Hybrid Superconductor-Semiconductor Nanowire Devices*, Science **336** (2012), no. 6084, 1003–1007.

[Nak03] Mikio Nakahara, *Geometry, Topology and Physics*, IOP, Graduate student series in physics, June 2003.

[NC00] M.A Nielsen and I.L. Chuang, *Quantum Computation and Quantum Information*, Cambridge University Press, 2000.

[NMM+14] D. Nigg, M. Müller, E. A. Martinez, P. Schindler, M. Hennrich, T. Monz, M. A. Martin-Delgado, and R. Blatt, *Quantum computations on a topologically encoded qubit*, Science **345** (2014), no. 6194, 302–305.

[NN81] H.B. Nielsen and M. Ninomiya, *A no-go theorem for regularizing chiral fermions*, Physics Letters B **105** (1981), no. 2, 219 – 223.

[NO08] Zohar Nussinov and Gerardo Ortiz, *Autocorrelations and thermal fragility of anyonic loops in topologically quantum ordered systems*, Phys. Rev. B **77** (2008), 064302.

[Nov45] Alex B. Novikoff, *The Concept of Integrative Levels and Biology*, Science **101** (1945), no. 2618, 209–215.

[NPDL+14] Stevan Nadj-Perge, Ilya K. Drozdov, Jian Li, Hua Chen, Sangjun Jeon, Jungpil Seo, Allan H. MacDonald, B. Andrei Bernevig, and Ali Yazdani, *Observation of Majorana fermions in ferromagnetic atomic chains on a superconductor*, Science **346** (2014), no. 6209, 602–607.

[NSS+08] C. Nayak, S. H. Simon, A. Stern, M. Freedman, and S. Das Sarma, *Non-Abelian anyons and topological quantum computation*, Reviews of Modern Physics **80** (2008), 1083–1159.

[NTW85] Q. Niu, D. J. Thouless, and Y.-S. Wu, *Quantized Hall conductance as a topological invariant*, Physical Review B **31** (1985), 3372–3377.

[OBS+05] K. Osterloh, M. Baig, L. Santos, P. Zoller, and M. Lewenstein, *Cold Atoms in Non-Abelian Gauge Potentials: From the Hofstadter "Moth" to Lattice Gauge Theory*, Physical Review Letters **95** (2005), no. 1, 010403.

[Oku71] Susumu Okubo, *Some General Inequalities in Quantum Statistical Mechanics*, Journal of Mathematical Physics **12** (1971), no. 7, 1123–1128.

[OMD16] L. Ortiz and M. A. Martin-Delgado, *Bilayer Double Semion Model with $\mathbb{Z}_2 \times \mathbb{Z}_2$ Symmetry-Protected Topological Order*.

[Onn11] H. K. Onnes, *The resistance of pure mercury at helium temperatures*, Commun. Phys. Lab. Univ. Leiden **12** (1911), 120+.

[Ons44] Lars Onsager, *Crystal Statistics. I. A Two-Dimensional Model with an Order-Disorder Transition*, Phys. Rev. **65** (1944), 117–149.

[ORL72] D. D. Osheroff, R. C. Richardson, and D. M. Lee, *Evidence for a New Phase of Solid He^3*, Phys. Rev. Lett. **28** (1972), 885–888.

[PC04] D. Porras and J. I. Cirac, *Effective Quantum Spin Systems with Trapped Ions*, Physical Review Letters **92** (2004), no. 20, 207901.

[PSSA09] Dario Patanè, Alessandro Silva, Fernando Sols, and Luigi Amico, *Thermalization Dynamics Close to a Quantum Phase Transition*, Phys. Rev. Lett. **102** (2009), 245701.

[PZ01] J. P. Paz and W. H. Zurek, *Environment-Induced Decoherence and the Transition from Quantum to Classical*, pp. 533–614, Springer Berlin Heidelberg, Berlin, Heidelberg, 2001.

[QHZ08] X.-L. Qi, T. L. Hughes, and S.-C. Zhang, *Topological field theory of time-reversal invariant insulators*, Physical Rview B **78** (2008), no. 19, 195424.

[QZ10] X.-L. Qi and S.-C. Zhang, *The quantum spin Hall effect and topological insulators*, Physics Today **63** (2010), 010000.

[QZ11] Xiao-Liang Qi and Shou-Cheng Zhang, *Topological insulators and superconductors*, Rev. Mod. Phys. **83** (2011), 1057–1110.

[Res94] R. Resta, *Macroscopic polarization in crystalline dielectrics: the geometric phase approach*, Reviews of Modern Physics **66** (1994), 899–915.

[RG00] N. Read and D. Green, *Paired states of fermions in two dimensions with breaking of parity and time-reversal symmetries and the fractional quantum Hall effect*, Physical Review B **61** (2000), 10267–10297.

[RH11] Á. Rivas and S.F. Huelga, *Open Quantum Systems: An Introduction*, SpringerBriefs in Physics, Springer Berlin Heidelberg, 2011.

[RNC+14] P. Roushan, C. Neill, Yu Chen, M. Kolodrubetz, C. Quintana, N. Leung, M. Fang, R. Barends, B. Campbell, Z. Chen, B. Chiaro, A. Dunsworth, E. Jeffrey, J. Kelly, A. Megrant, J. Mutus, P. J. J. O'Malley, D. Sank, A. Vainsencher, J. Wenner, T. White, A. Polkovnikov, A. N. Cleland, and J. M. Martinis, *Observation of topological transitions in interacting quantum circuits*, Nature **515** (2014), no. 7526, 241–244.

[RPHP10] Ángel Rivas, A Douglas K Plato, Susana F Huelga, and Martin B Plenio, *Markovian master equations: a critical study*, New Journal of Physics **12** (2010), no. 11, 113032.

[RQHZ08] S. Raghu, X.-L. Qi, C. Honerkamp, and S.-C. Zhang, *Topological Mott Insulators*, Physical Review Letters **100** (2008), no. 15, 156401.

[RSFL09] S. Ryu, A. Schnyder, A. Furusaki, and A. Ludwig, *Classification of topological insulators and superconductors in three spatial dimensions*, APS Meeting Abstracts (2009), 33012.

[RSWN50] C. A. Reynolds, B. Serin, W. H. Wright, and L. B. Nesbitt, *Superconductivity of Isotopes of Mercury*, Phys. Rev. **78** (1950), 487–487.

[RZP+13] Mikael C. Rechtsman, Julia M. Zeuner, Yonatan Plotnik, Yaakov Lumer, Daniel Podolsky, Felix Dreisow, Stefan Nolte, Mordechai Segev, and Alexander Szameit, *Photonic Floquet topological insulators*, Nature **496** (2013), no. 7444, 196–200.

[Sac00] Subir Sachdev, *Quantum Phase Transitions*, Cambridge University Press, January 2000.

[SBD16] L M Sieberer, M Buchhold, and S Diehl, *Keldysh field theory for driven open quantum systems*, Reports on Progress in Physics **79** (2016), no. 9, 096001.

[Sch05] U. Schollwöck, *The density-matrix renormalization group*, Reviews of Modern Physics **77** (2005), 259–315.

[SHR+03] F. Schmidt-Kaler, H. Häffner, M. Riebe, S. Gulde, G. P. T. Lancaster, T. Deuschle, C. Becher, C. F. Roos, J. Eschner, and R. Blatt, *Realization of the Cirac-Zoller controlled-NOT quantum gate*, Nature **422** (2003), 408–411.

[Sim83] B. Simon, *Holonomy, the Quantum Adiabatic Theorem, and Berry's Phase*, Physical Review Letters **51** (1983), 2167–2170.

[SJLA+15] P. San-Jose, J. L. Lado, R. Aguado, F. Guinea, and J. Fernández-Rossier, *Majorana Zero Modes in Graphene*, Phys. Rev. X **5** (2015), 041042.

[SKCG12] M. J. A. Schuetz, E. M. Kessler, J. I. Cirac, and G. Giedke, *Superradiance-like electron transport through a quantum dot*, Phys. Rev. B **86** (2012), 085322.

[SKK+14] M. D. Schroer, M. H. Kolodrubetz, W. F. Kindel, M. Sandberg, J. Gao, M. R. Vissers, D. P. Pappas, Anatoli Polkovnikov, and K. W. Lehnert, *Measuring a Topological Transition in an Artificial Spin-1/2 System*, Phys. Rev. Lett. **113** (2014), 050402.

[SLC+04] T. Schaetz, D. Leibfried, J. Chiaverini, M.D. Barrett, J. Britton, B. DeMarco, W.M. Itano, J.D. Jost, C. Langer, and D.J. Wineland, *Towards a scalable quantum computer/simulator based on trapped ions*, Applied Physics B **79** (2004), no. 8, 979–986.

[SMO+15] Y. Salathé, M. Mondal, M. Oppliger, J. Heinsoo, P. Kurpiers, A. Potočnik, A. Mezzacapo, U. Las Heras, L. Lamata, E. Solano, S. Filipp, and A. Wallraff, *Digital Quantum Simulation of Spin Models with Circuit Quantum Electrodynamics*, Phys. Rev. X **5** (2015), 021027.

[SNT06] S. D. Sarma, C. Nayak, and S. Tewari, *Proposal to stabilize and detect half-quantum vortices in strontium ruthenate thin films: Non-Abelian braiding statistics of vortices in a $p_x + ip_y$ superconductor*, Physical Review B **73** (2006), no. 22, 220502–+.

[SRFL08] Andreas P. Schnyder, Shinsei Ryu, Akira Furusaki, and Andreas W. W. Ludwig, *Classification of topological insulators and superconductors in three spatial dimensions*, Phys. Rev. B **78** (2008), 195125.

[Str82] P Streda, *Quantised Hall effect in a two-dimensional periodic potential*, Journal of Physics C: Solid State Physics **15** (1982), no. 36, L1299.

[SV87] E. Sanchez-Velasco, *A finite-size scaling study of the 4D Ising model*, Journal of Physics A: Mathematical and General **20** (1987), no. 14, 5033.

[SWE+10] J. F. Sherson, C. Weitenberg, M. Endres, M. Cheneau, I. Bloch, and S. Kuhr, *Single-Atom Resolved Fluorescence Imaging of an Atomic Mott Insulator*, ArXiv e-prints (2010).

[SWY14] H. Z. Shen, W. Wang, and X. X. Yi, *Hall conductance and topological invariant for open systems*, Scientific Reports **4** (2014), 6455 EP –.

[SZ97] M.O. Scully and M.S. Zubairy, *Quantum Optics*, Cambridge University Press, 1997.

[SZH+16] Hao-Hua Sun, Kai-Wen Zhang, Lun-Hui Hu, Chuang Li, Guan-Yong Wang, Hai-Yang Ma, Zhu-An Xu, Chun-Lei Gao, Dan-Dan Guan, Yao-Yi Li, Canhua Liu, Dong Qian, Yi Zhou, Liang Fu, Shao-Chun Li, Fu-Chun Zhang, and Jin-Feng Jia, *Majorana Zero Mode Detected with Spin Selective Andreev Reflection in the Vortex of a Topological Superconductor*, Phys. Rev. Lett. **116** (2016), 257003.

[Tho98] D.J. Thouless, *Topological Quantum Numbers in Nonrelativistic Physics*, World Scientific, 1998.

[Tin04] M. Tinkham, *Introduction to Superconductivity: Second Edition*, Dover Books on Physics, Dover Publications, 2004.

[TKNTfd82] D. J. Thouless, M. Kohmoto, M. P. Nightingale, and M. den Nijs, *Quantized Hall Conductance in a Two-Dimensional Periodic Potential*, Physical Review Letters **49** (1982), 405–408.

[TSG82] D C Tsui, H L Stormer, and A C Gossard, *Two-Dimensional Magnetotransport in the Extreme Quantum Limit*, Phys. Rev. Lett. **48** (1982), no. 22, 1559–1562.

[TW05] Matthias Troyer and Uwe-Jens Wiese, *Computational Complexity and Fundamental Limitations to Fermionic Quantum Monte Carlo Simulations*, Phys. Rev. Lett. **94** (2005), 170201.

[VGRC04] F. Verstraete, J. J. García-Ripoll, and J. I. Cirac, *Matrix Product Density Operators: Simulation of Finite-Temperature and Dissipative Systems*, Phys. Rev. Lett. **93** (2004), 207204.

[Vid03] Guifré Vidal, *Efficient Classical Simulation of Slightly Entangled Quantum Computations*, Phys. Rev. Lett. **91** (2003), 147902.

[Vid04] Guifré Vidal, *http://link.aps.org/doi/10.1103/PhysRevLett.93.040502*, Phys. Rev. Lett. **93** (2004), 040502.

[VLE+14] Davide Vodola, Luca Lepori, Elisa Ercolessi, Alexey V. Gorshkov, and Guido Pupillo, *Kitaev Chains with Long-Range Pairing*, Phys. Rev. Lett. **113** (2014), 156402.

[vNH14] Evert P. L. van Nieuwenburg and Sebastian D. Huber, *Classification of mixed-state topology in one dimension*, Phys. Rev. B **90** (2014), 075141.

[VS13] Ashvin Vishwanath and T. Senthil, *Physics of Three-Dimensional Bosonic Topological Insulators: Surface-Deconfined Criticality and Quantized Magnetoelectric Effect*, Phys. Rev. X **3** (2013), 011016.

[VWIC09] Frank Verstraete, Michael M. Wolf, and J. Ignacio Cirac, *Quantum computation and quantum-state engineering driven by dissipation*, Nat Phys **5** (2009), no. 9, 633–636.

[WA58] Maier W. and Saupe A., *Eine einfache molekulare Theorie des nematischen kristallinflüssigen Zustandes*, Zeitschrift für Naturforschung A **13** (1958), 564.

[Wen91] X. G. Wen, *Non-Abelian statistics in the fractional quantum Hall states*, Phys. Rev. Lett. **66** (1991), 802–805.

[Wey29] Hermann Weyl, *Elektron und Gravitation. I*, Zeitschrift für Physik **56** (1929), no. 5, 330–352.

[WGS08] B Wunsch, F Guinea, and F Sols, *Dirac-point engineering and topological phase transitions in honeycomb optical lattices*, New Journal of Physics **10** (2008), no. 10, 103027.

[Whi92] Steven R. White, *Density matrix formulation for quantum renormalization groups*, Phys. Rev. Lett. **69** (1992), 2863–2866.

[Wil75] Kenneth G. Wilson, *The renormalization group: Critical phenomena and the Kondo problem*, Rev. Mod. Phys. **47** (1975), 773–840.

[Wil09] F. Wilczek, *Majorana returns*, Nature Physics **5** (2009), 614–618.

[Wit88] Edward Witten, *Topological sigma models*, Communications in Mathematical Physics **118** (1988), no. 3, 411–449.

[WS89] F. Wilczek and A. Shapere, *Geometric Phases in Physics*, Advanced series in mathematical physics, World Scientific, 1989.

[WTVS11] Xiangang Wan, Ari M. Turner, Ashvin Vishwanath, and Sergey Y. Savrasov, *Topological semimetal and Fermi-arc surface states in the electronic structure of pyrochlore iridates*, Phys. Rev. B **83** (2011), 205101.

[WZ84] F. Wilczek and A. Zee, *Appearance of gauge structure in simple dynamical systems*, Physical Review Letters **52** (1984), 2111–2114.

[WZ89] X. G. Wen and A. Zee, *Winding number, family index theorem, and electron hopping in a magnetic field*, Nuclear Physics B **316** (1989), 641–662.

[XAB+15] Su-Yang Xu, Nasser Alidoust, Ilya Belopolski, Zhujun Yuan, Guang Bian, Tay-Rong Chang, Hao Zheng, Vladimir N. Strocov, Daniel S. Sanchez, Guoqing Chang, Chenglong Zhang, Daixiang Mou, Yun Wu, Lunan Huang, Chi-Cheng Lee, Shin-Ming Huang, BaoKai Wang, Arun Bansil, Horng-Tay Jeng, Titus Neupert, Adam Kaminski, Hsin Lin, Shuang Jia, and M. Zahid Hasan, *Discovery of a Weyl fermion state with Fermi arcs in niobium arsenide*, Nat Phys **11** (2015), no. 9, 748–754.

[XBA+15] Su-Yang Xu, Ilya Belopolski, Nasser Alidoust, Madhab Neupane, Guang Bian, Chenglong Zhang, Raman Sankar, Guoqing Chang, Zhujun Yuan, Chi-Cheng Lee, Shin-Ming Huang, Hao Zheng, Jie Ma, Daniel S. Sanchez, BaoKai Wang, Arun Bansil, Fangcheng Chou, Pavel P. Shibayev, Hsin Lin, Shuang Jia, and M. Zahid Hasan, *Discovery of a Weyl fermion semimetal and topological Fermi arcs*, Science **349** (2015), no. 6248, 613–617.

[XCN10] D. Xiao, M.-C. Chang, and Q. Niu, *Berry phase effects on electronic properties*, Reviews of Modern Physics **82** (2010), 1959–2007.

[Yam09] Daisuke Yamamoto, *Correlated cluster mean-field theory for spin systems*, Phys. Rev. B **79** (2009), 144427.

[YLS+15] L. X. Yang, Z. K. Liu, Y. Sun, H. Peng, H. F. Yang, T. Zhang, B. Zhou, Y. Zhang, Y. F. Guo, M. Rahn, D. Prabhakaran, Z. Hussain, S. K. Mo, C. Felser, B. Yan, and Y. L. Chen, *Weyl semimetal phase in the non-centrosymmetric compound TaAs*, Nat Phys **11** (2015), no. 9, 728–732.

[YN03] J. Q. You and Franco Nori, *Quantum information processing with superconducting qubits in a microwave field*, Phys. Rev. B **68** (2003), 064509.

[Yos11] Beni Yoshida, *Feasibility of self-correcting quantum memory and thermal stability of topological order*, Annals of Physics **326** (2011), no. 10, 2566 – 2633.

[Zak89] J. Zak, *Berry's phase for energy bands in solids*, Phys. Rev. Lett. **62** (1989), 2747–2750.

[ZV04] Michael Zwolak and Guifré Vidal, *Mixed-State Dynamics in One-Dimensional Quantum Lattice Systems: A Time-Dependent Superoperator Renormalization Algorithm*, Phys. Rev. Lett. **93** (2004), 207205.